NASA-CR-193012

(NASA-CR-193012) NASA/USRA UNIVERSITY ADVANCED DESIGN PROGRAM FIFTH ANNUAL SUMMER CONFERENCE (USRA) 229 p

N94-71267
--THRU--
N94-71311
Unclas

Z9/12 0160626

Proceedings of the

5th Annual Summer Conference

NASA / USRA

University Advanced Design Program

Marshall Space Flight Center

June 12-16, 1989

NATIONAL AERONAUTICS & SPACE ADMINISTRATION

UNIVERSITIES SPACE RESEARCH ASSOCIATION

ORIGINAL [illegible] AND
COLOR ILLUSTRATIONS

NASA/USRA
UNIVERSITY ADVANCED DESIGN PROGRAM

PROCEEDINGS OF THE
FIFTH ANNUAL SUMMER CONFERENCE

Huntsville Marriott

Huntsville, Alabama

June 12-16, 1989

Cosponsor: American Institute of Aeronautics and Astronautics (AIAA)

NASA/USRA UNIVERSITY ADVANCED DESIGN PROGRAM
FIFTH ANNUAL SUMMER CONFERENCE

Cosponsor: American Institute of Aeronautics and Astronautics

The NASA/University Advanced Design Program is operated by the Universities Space Research Association (USRA) under a contract with NASA Headquarters (NASW-4435). Inquiries regarding the program may be directed to the Program Manager:

John Alred, Ph.D.
USRA
17225 El Camino Real, Suite 450
Houston, Texas 77058
(713)480-5939

PRIMARY

FOREWORD

The Program

The NASA/USRA University Advanced Design Program is a unique program that brings together NASA engineers, students, and faculty from United States engineering schools by integrating current and future NASA space/aeronautics engineering design projects into the university curriculum. The Program was conceived in the fall of 1984 as a pilot project to foster engineering design education in the universities and to supplement NASA's in-house efforts in advanced planning for space and aeronautics design. Nine universities and five NASA centers participated in the first year of the pilot project. Close cooperation between the NASA centers and the universities, the careful selection of design topics, and the enthusiasm of the students has resulted in a very successful program than now includes forty universities and eight NASA centers.

The study topics cover a broad range of potential space and aeronautics projects which could be undertaken during a 20-30-year period beginning with the deployment of the Space Station Freedom scheduled for the mid-1990s. Both manned and unmanned endeavors are embraced, and the systems approach to the design problem is emphasized. The student teams pursue the chosen problem during their senior year in a one or two semester capstone design course and submit a comprehensive written report at the conclusion of the project. Finally, student representatives from each of the universities summarize their work in oral presentations at the annual Summer Conference, held at one of the NASA centers and attended by the university faculty, NASA and USRA personnel, and aerospace industry representatives.

The Proceedings Volume

As the Advanced Design Program has grown in size, it has also matured in terms of the quality of the student projects. The comprehensive final reports are distributed through the National Technical Information Service. However, the results of the studies reach only a small audience, principally those who attend the Summer Conference. In order to broaden the distribution, a Proceedings volume which summarizes the project

results and roughly parallels the Conference presentations is published. The present volume represents the student work accomplished during the 1988-89 academic year and reported at the 5th Annual Summer Conference held at the Marshall Space Flight Center, June 12-16, 1989.

ACKNOWLEDGMENTS

This publication was made possible through the efforts of a great many people. First of all, we are grateful to the students, the university faculty, and their teaching assistants for the excellent technical work. Second, we are indebted to those individuals from NASA Headquarters and from the NASA centers who conceived the program in the beginning, have provided valuable guidance throughout, and through their keen interest in the student projects, are in large part responsible for the boundless enthusiasm of the students. Finally, we thank the staff at the USRA Advanced Design Program Office for the preparation of the manuscripts and the staff of the Publications Services Office of the Lunar and Planetary Institute for the excellent work in the preparation of the final Proceedings volume.

TABLE OF CONTENTS

SPACE PROJECTS

AERONAUTICS PROJECTS

INVITED TALKS

Space Projects

N94-71268

382666 1994004513

121

S1-18

160627

p. 12

ADVANCED DESIGN FOR ORBITAL DEBRIS REMOVAL IN SUPPORT OF SOLAR SYSTEM EXPLORATION

UNIVERSITY OF ARIZONA

This work continues to develop advanced designs toward the ultimate goal of a Getaway Special to demonstrate economical removal of orbital debris utilizing local resources in orbit. The fundamental technical feasibility was demonstrated last year through theoretical calculations, quantitative computer animation, a solar focal point cutter, a robotic arm design, and a subscale model. During this reporting period, several improvements are made in the solar cutter, such as auto track capabilities, better quality reflectors, and a more versatile framework. The major advance has been in the design, fabrication, and working demonstration of a robotic arm that has several degrees of freedom. The functions were specifically tailored for the orbital debris handling. These advances are discussed here. Also, a small fraction of the resources were allocated toward research in flame augmentation in scramjets for the NASP. Here, the fundamental advance has been the attainment of Mach numbers up to 0.6 in the flame zone and a vastly improved injection system; our current work is expected to achieve supersonic combustion in the laboratory and an advanced monitoring system.

INTRODUCTION

We can hardly improve upon the lucid descriptions of the Orbital Debris issue by science writers(1,2,3,4) and other popular news media coverage(5,6,7,8,9). Without doubt the problems of orbital debris have grown to be of serious concern to astronomers, space technologists, and terrestrial dwellers. The specific problems were presented at the XXXIX IAF Congress. The University of Arizona Space Engineering Design team is developing the design for economical removal of the larger debris pieces through local resource utilization. The fundamental idea is to concentrate solar energy into a point focus, cut the debris into precise shapes that can be added on to the "sweeper" craft, and robotically assemble the pieces into a manageable configuration. This will be followed by one of three disposal modes: (1) retrieval by a spacecraft (e.g., STS, HERMES, BURAN, etc.), (2) precise splashdown into the oceans, or (3) planned burnup during atmospheric reentry. The fundamental space technologies to be demonstrated are solar cutting of candidate space junk materials, robotic assembly, and accurate disposal. In 1988 the University of Arizona began participation in the USRA program and demonstrated solar cutting and a subscale model robotic arm. This year (1989), a full-scale robotic arm has been constructed, is operational, and the entire assembly is shown to be technically feasible. This report is a summary of the work and explains the details of the space engineering.

Consistent with the USRA philosophy, new undergraduate students were brought on board. This year, five new students were involved in the Autonomous Space Processor for Orbital Debris (ASPOD) design, two new students built a "target" spinning satellite, and two other students worked on advanced designs for the NASP. The project continues to draw worldwide attention, even from elementary and high schools.

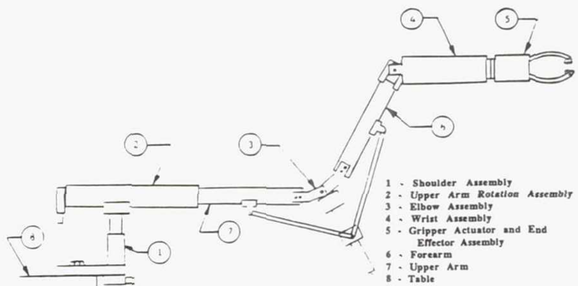

SPECIFICATIONS:

Degrees of Freedom	5
Approx. Weight	25 pounds
Max. Horizontal Reach	66 inches
Max. Vertical Reach	59 inches

Fig. 1. ASPOD Robot Arm Final Assembly

ROBOTIC ARM DESIGN

Design Specifications

The ASPOD design incorporates a solar-powered metal cutter to facilitate dead satellite processing in a cost-effective manner. In order to position debris at the focal point it is necessary that the ASPOD be equipped with robotic arms. The final spacecraft will require two arms to ensure that any final movement imparted to the debris will not cause the cut piece to move toward the key lenses and mirrors of the solar cutter. The task for this year's team, however, is the design and fabrication of one arm to be used in conjunction with the current solar cutter. The arm is to hold and move material to be cut in the focal plane of the solar concentrator. The design will have to meet several requirements. The movement of the arm should not interfere with the light being

PRECEDING PAGE BLANK NOT FILMED

PAGE 2 INTENTIONALLY BLANK

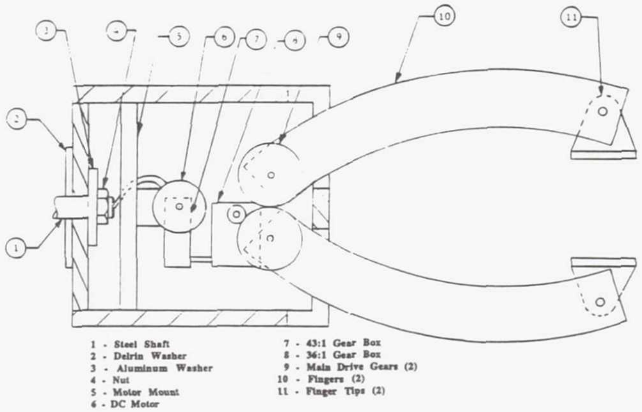

Fig. 2. Gripper Actuator and End Affector Assembly

concentrated by the focal point cutter. Hydraulic actuators cannot be used due to the fact that hydraulic fluid leakage would be difficult to control in the hard vacuum of space. The arm should be able to position curved and flat pieces of material so that the concentrated light is perpendicular to the surface being cut. To ensure accurate control of the arm, tight tolerances (0.002 in on all critical load-bearing members) are observed. This is evident in the lack of play in the arm.

All modes of operation of the arm, including deploy/stow, processing, and placement, require slow steady motion. The current solar concentrator will cut 0.005-in aluminum at approximately 5 in/min. This is the nominal speed at which the arm is designed to operate.

Final Design

A sketch of the arm is presented in Fig. 1 and shows major components and specifications. Each component is described in detail below. The design work was carried out in six coordinated sections: the end effector, the grip actuator, the wrist (both bending and rotation), elbow and forearm segment, upper arm rotation, and shoulder swivel.

End effector. The end effector is of a simple claw-type design. Two $5\frac{1}{8}$-in-radius arc-shaped fingers allow grasping of large objects of varying geometries. At the end of the fingers are knurled surface grips that swivel to allow objects with nonparallel faces to be grasped. The fingers and grips are made of $\frac{1}{16}$-in 6061-T6 aluminum and have hollow sections that give the strength needed as well as minimize the weight. Figure 2 shows finger and tip geometry. The fingers were designed based on the clamping force needed to hold a mock satellite. This mock satellite was sized in proportion to the current solar cutters heat flux vs. that estimated to be required for the full size solar cutter, approximately 1/10 scale.

Grip actuator. The grip actuator assembly is shown in Fig. 2. The fingers are designed to operate at a rotation rate of 0.105 rad/sec. Based on the force needed to hold the mock satellite, and the geometry of the fingers, the maximum torque required was determined to be 1.3 ft-lbs. The drive motor for the fingers, as well as the other arm joints, is a 24-V DC motor coupled in series to 43:1 and 36:1 reduction gearboxes.

Wrist assembly. The wrist has two degrees of freedom: rotation and bending. The wrist can rotate a full 360° and bend 90° in both directions. The wrist housing is made of linen phenolic composite and the inner component supports are composed of aluminum and polycarbonate. The wrist rotation assembly is shown in Fig. 3. It is powered by a 24-V DC motor coupled to two 36:1 reduction gearboxes with a 5:1 final pinion and spur, producing 474 in-oz at 1 rpm. The required torque was determined by assuming the wrist must counter a moment produced by the mock satellite if grappled at one end in a cantilever fashion. The bearings between the gripper and wrist housings are made of delrin, having a coefficient of friction comparable to teflon but with greater rigidity. Furthermore, delrin was selected over ball bearings because of the appreciable weight savings. The bearing shaft was attached to the grip actuator housing and was bored out to accommodate the wires for the grip actuator motor. To eliminate twisting of the wires when the wrist rotates, a slip ring mechanism is attached to the final spur gear.

Wrist bending is powered by a 24-V DC motor with a 550:1 reduction gear train contained in the wrist housing. The final

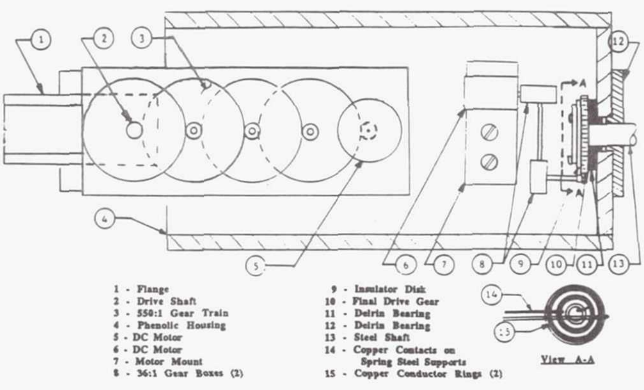

Fig. 3. Wrist Assembly

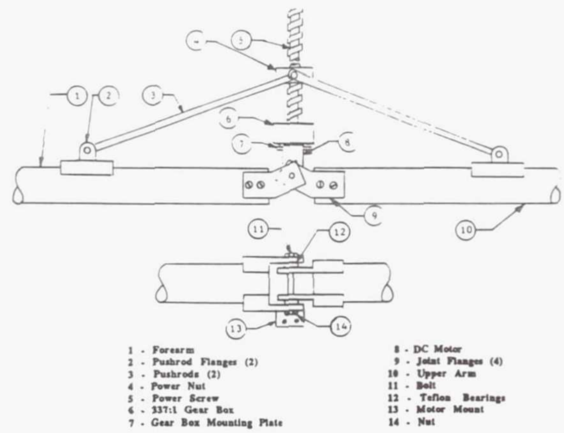

Fig. 4. Elbow Assembly

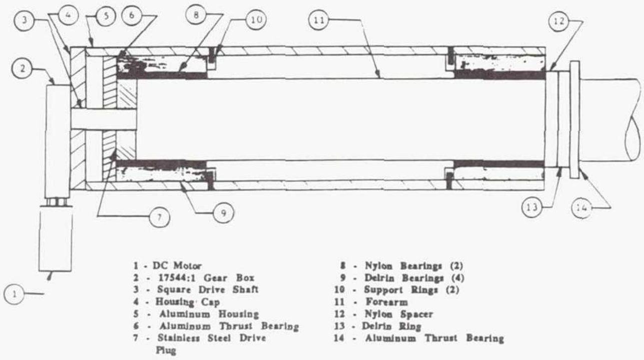

Fig. 5. Upper Arm Rotation Assembly

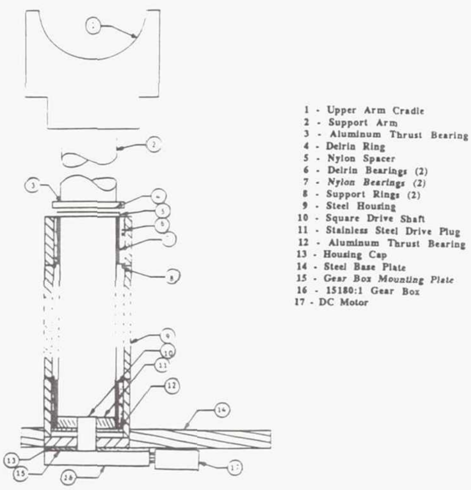

Fig. 6. Shoulder Assembly

drive shaft is attached to the forearm and is extended through both sides of the wrist housing.

Arm and elbow. The forearm and upper arm segments are made of 6061-T6 aluminum and were sized according to the mock satellite load described above. The elbow mechanism incorporates an aluminum square thread power screw as shown in Fig. 4. The power screw points outside the elbow, keeping the length to 8 in while still allowing 175° of forearm rotation about the upper arm. Movement is provided by a 24-V DC motor running through a 337:1 reduction gearbox. The collar power nut is machined from delrin, and is clamped between an aluminum collar operating pushrods connected to the upper and forearm sections.

Upper arm rotation and shoulder swivel. A sketch of the upper arm rotation assembly is shown in Fig. 5 and the shoulder swivel assembly is shown in Fig. 6. Similar designs are used for both that allow a full 360° of rotation. The inner tube extension is made of 1¼-in schedule 40 6061-T6 aluminum tubing. The loadings that this section must handle include torsional, bending, and compression and tension. Nylon is used as an inside bearing surface, and delrin-filled aluminum thrust washers were manufactured to reduce friction and power requirements.

The bearing housing consists of 2¼-in schedule 40 6061-T6 aluminum tubing. Delrin is used for the outer bearing

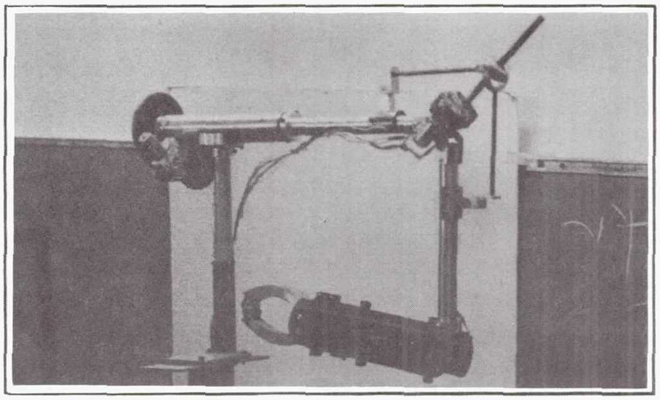

Fig. 7a. Assembled Arm

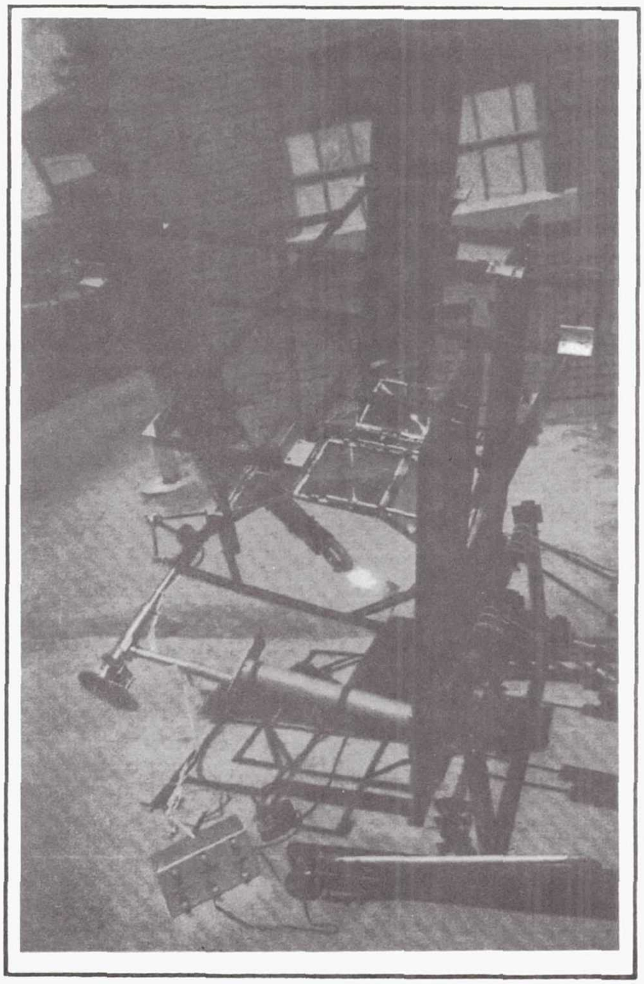

Fig. 7b. Assembled System Cutting a Piece of Metal at the Focal Point

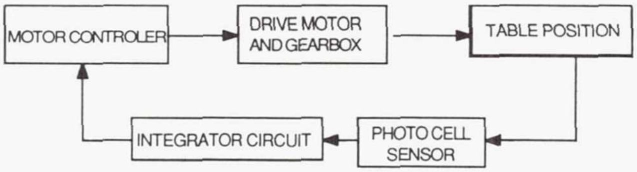

Fig. 8. Block Diagram of Tracker Components

surface, which mates with the above mentioned nylon bearings producing a low-friction, lightweight bearing assembly capable of handling large loads.

The gearbox assembly produces a 17,500:1 reduction and is driven by a 24-V DC motor.

Photographs of the assembled arm are shown in Fig. 7.

SOLAR TRACKER

The solar tracker consists of a custom-made mount and circuitry controlling two degrees of freedom. It provides directional positioning of the table-mounted focal-point-cutter during operation. There are two independent control/drive circuits, one for elevation, the other for azimuth. Figure 8 shows a block diagram of the major components.

The position of the sun is determined by a sensor composed of two photo cells mounted at 90°. This sensor is mounted facing the sun so that the bisector of the angle between the photo cells coincides with the optical axis of the focal-point-cutter. The sensor and integrator circuit are wired as shown in Fig. 9 so that when the cutter is pointing directly at the sun the sensor output is zero and the integrator circuit output (V_{out}) is constant. This constant voltage is input to a motor speed controller. When the cutter begins to drift off track the sensor output becomes nonzero, signaling the controller to decrease or increase motor speed accordingly. The solar tracker has been tested and maintains positioning accuracy to within approximately ±1°. Photographs of the components and assembled system are shown in Fig. 10.

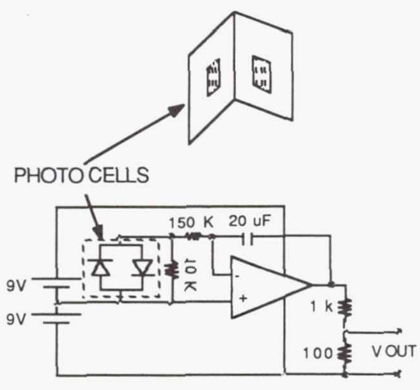

Fig. 9 Mounted Photo Cells and Arrangement in Integrator Circuit

MISSION SCENARIO SELECTION

ASPOD may be delivered to the rendezvous orbit via STS or an expendable launch vehicle. A schematic of the mission sequence is presented in Fig. 11. Once ASPOD has rendezvoused with a target, the question becomes: What to do with it? Several different debris disposal scenarios were looked at, including (1) retrieving and carrying along each debris, rendezvousing with shuttle for salvaging; (2) aerobraking, i.e., deploying large mylar sheets on debris to increase rarified atmospheric drag, thus lowering orbital lifetime; and (3) attaching a small solid rocket motor (SRM) to transfer debris to a lower lifetime orbit.

Two methods of orbital transferring were investigated: (1) ΔV for direct transfer between orbital planes and (2) using the natural orbital perturbations from the oblateness of the Earth, for nodal regression to synchronize orbital planes. These are discussed further in the Sample Mission section.

Some satellites now in Earth orbit may be worth bringing down for scientific studies or salvaging. Some debris might hold a wealth of scientific information concerning long-term satellite exposure to micrometeorites and small debris. Some satellites may contain expensive materials, parts, or top-secret data or machinery. Thus, for this particular type of debris, ASPOD would cut it with the solar cutter and store it in an onboard storage bin. With each retrieval, ASPOD will increase in mass, compared to other spacecraft that tend to decrease in mass. This will raise the propellant requirement considerably. However, with careful planning, a retrieval mission could still be quite successful and is considered in detail in the Sample Mission section.

Aerobraking uses the rarified atmosphere to cause drag on a satellite to lower its orbit or change its orbit in a hyperbolic planet flyby. Orbital lifetime is a function of altitude, eccentricity, mass, and area perpendicular to the direction of travel. Thus, if one were able to increase this area, it would be possible to decrease the orbital lifetime of a piece of debris, allowing it to disintegrate and burn up in the atmosphere upon reentry. To analyze this, a 1-yr lifetime was assumed and the necessary area was calculated for a typical 2000-kg piece of debris in a circular orbit of 750 km. This was found to be 2367 m^2, which corresponds to a sheet of mylar, 48 m × 48 m with composite structural supports behind to hold it rigid. In the lower atmosphere, the drag on a sheet this large will become very high, requiring a stronger and heavier structure. Due to the expected high mass, difficulties in attitude control, increased target area for smaller debris, and unreliable estimates of the upper atmosphere for aerobraking, this method was not analyzed further.

Small solid rocket motors are considered as a means of deorbiting debris after rendezvous and processing. The SRMs would be welded to payloads by the solar cutter and would be attached to boosters by inserting them into the nozzles of the rocket motors. ASPOD will then use its attitude control thrusters to orient and spin-up the debris for the SRM burn. This burn will result in a one ΔV orbit transfer (see Fig. 12). The point of this burn will become the apogee of a new

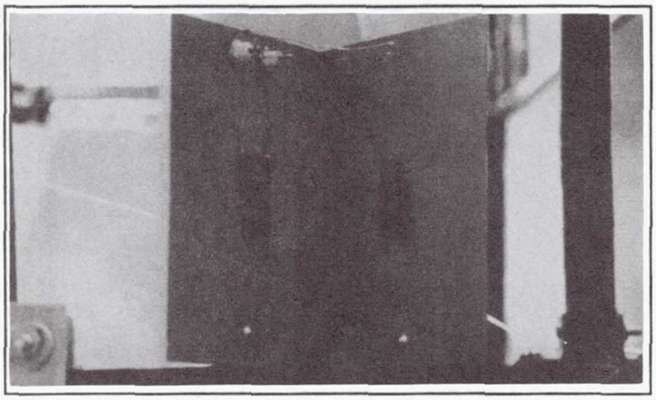

Fig. 10a. Photo Cell Sensor

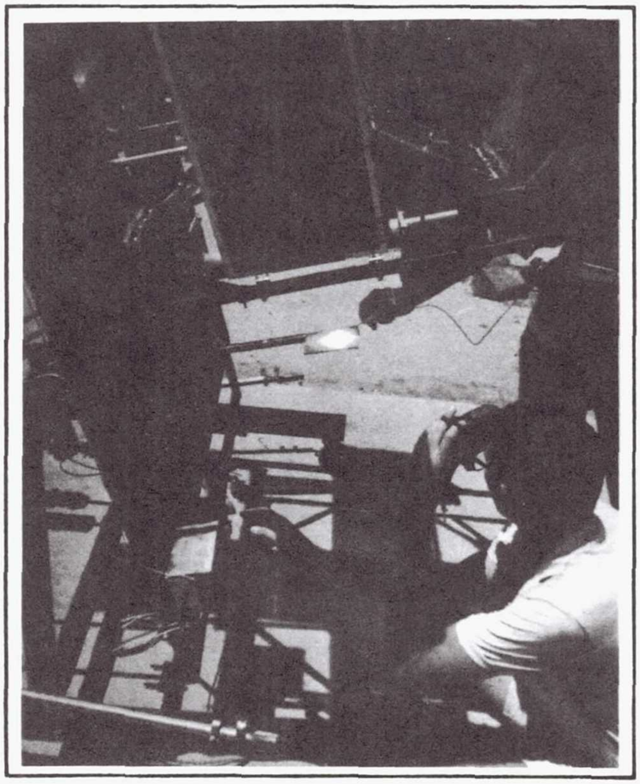

Fig. 10b. Measurement of Temperature at Focal Point

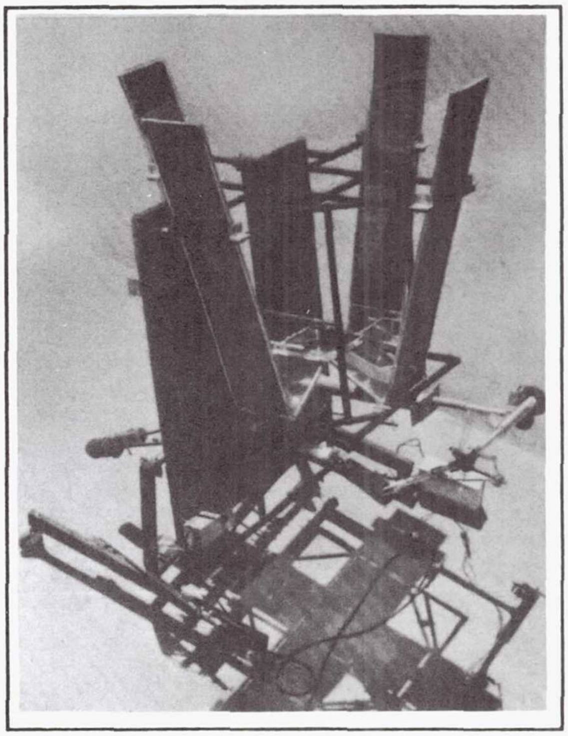

Fig. 10c. System Operating with Auto Tracker

elliptical orbit. The perigee altitude will be 350 km to allow for a reasonably rapid orbital decay.

For each piece of debris to be deorbited, an SRM has to be brought along. In addition, the propellant needed to transfer to each subsequent orbit must also be brought along. Thus, as the number of pieces of debris targeted increases, the launch weight of the satellite will increase exponentially. A numerical example is discussed in the Sample Mission section.

After all the chosen debris has been deorbited, ASPOD will fire its engine, consuming all remaining propellant for a reentry orbit. This prevents ASPOD itself from contributing to the debris problem.

BASELINE TARGET SELECTION

In choosing which debris to remove from orbit, there are many considerations. The most important are probability of collision, mass, orbital lifetime, and accessibility. Thus, the search concentrated on locating large pieces of debris with long orbital lifetimes. Since the majority of debris resides in altitudes between 700 and 1600 km[10], objects not in this range were ruled out. The search was also limited to objects with an angle of inclination below 50° to minimize propellant requirements. It would be possible to achieve a rendezvous with a target above this range, but with an abundant amount of debris below, such targets were not currently baselined.

Larger, more massive pieces of debris are bigger targets and have more kinetic energy. When they are struck, they scatter a greater amount of small debris. This small debris is what concerns NASA and NORAD the most. From studies done on hypervelocity impacts, a small piece of debris, on the order of 3% mass relative to the target, can turn the target into shrapnel[(10)]. Thus an exploding rocket booster or a satellite break-up from an impact could add to the debris in Earth orbit by the thousands. These small pieces are also very difficult to track. NORAD is currently capable of tracking debris larger than 10 cm at 1000 km[(10)]. Thus, it would be appropriate to remove a larger object before it becomes many small objects.

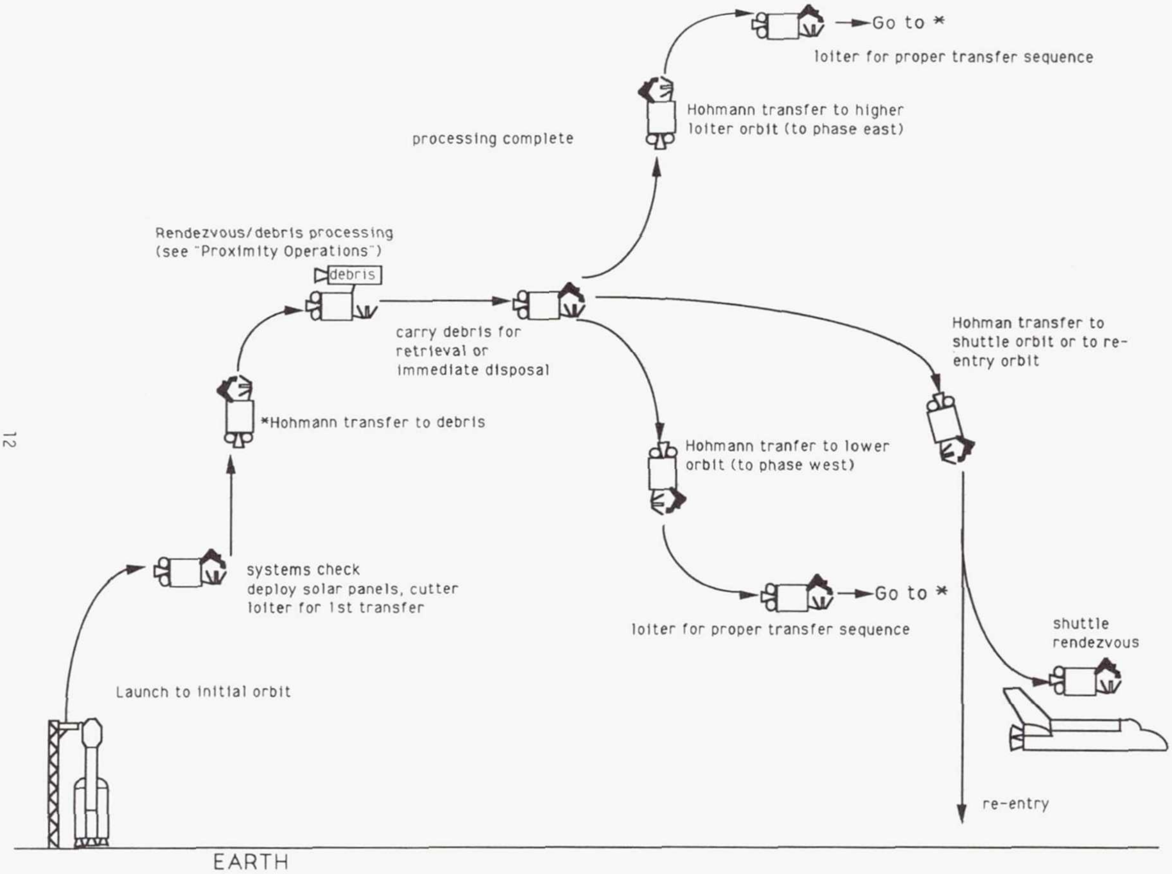

Fig. 11. ASPOD Mission Sequence

A simple yet important aspect in choosing the target debris was orbital lifetime. Some objects, because of their low altitudes, will soon reenter and burn up in the Earth's atmosphere. It was assumed that ASPOD will not be launched before the turn of the century. This led to the decision not to go after any objects that will reenter before the year 2025.

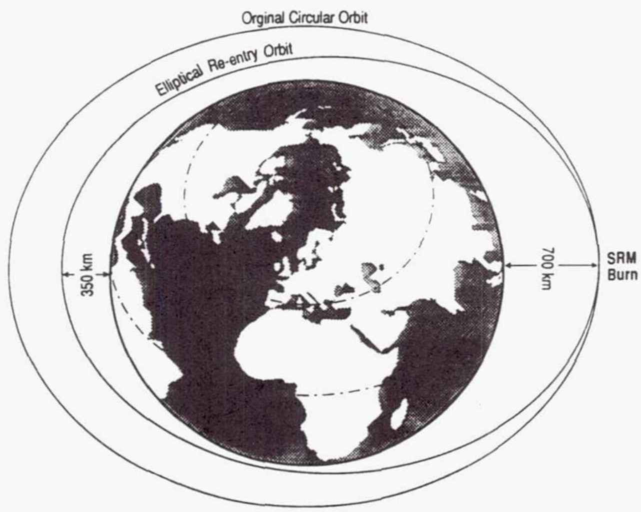

Fig. 12. Single Burn Re-entry Trajectory

Because of the extreme altitudes and low probability of collision of geosynchronous satellites, these were not included in the search for possible debris. These satellites actually present the least danger since they are significantly beyond most other satellites. At this time the debris population density at the geosynchronous altitude is still relatively low. Also, since objects in geosynchronous orbit are all at similar altitudes and inclinations ($i \sim 0°$), their relative velocities approach zero.

Using the above criteria, over 200 pieces of debris qualified as potential targets. Out of these, four were eventually chosen to perform mission feasibility studies. The four pieces are all U.S. contributions to the debris population and are orbiting at altitudes of approximately 750 km and inclinations of 35°. These are used for a representative sample mission in the following section.

ORBITAL TECHNIQUES AND SAMPLE MISSION

There are several inclinations in which a majority of the larger pieces of debris (roughly 2000 kg) are in orbit. The Soviet Union has put a large number of satellites into orbits with inclinations of 65°, 74°, and 82°, and altitudes ranging between 600 km and 1500 km. Most U.S. debris is located in orbits with inclinations of 21°, 28°, and 35°. The pieces of debris in the 21° and 28° inclinations often have apogees greater than 36,000 km, while the pieces in the 35° inclination

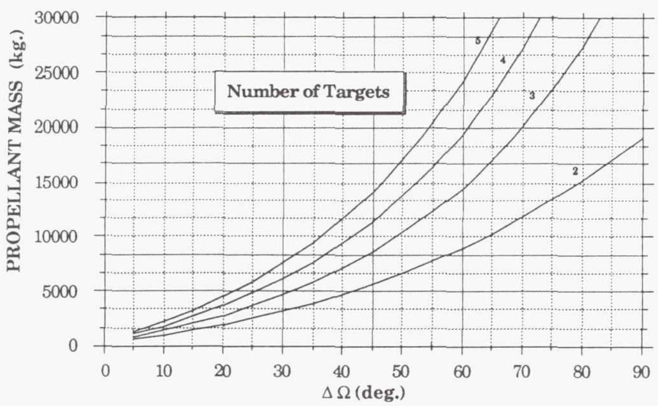

Fig. 13. Propellant Mass vs. ΔΩ and Number of Targets

have orbits with altitudes of approximately 750 km. Because a majority of the large pieces of debris are located in only a few inclinations, the opportunity exists to "clean up" space an inclination at a time. Over the past three decades, many thousands of satellites have been launched into Earth orbit, with most of these having unique ascending node locations. Thus, while many satellites may have common inclinations, they are not necessarily in a common plane. Therefore, a method of transferring longitudinal planes, while minimizing the total ΔV and the propellant requirement, must be found.

Two methods of transferring from one longitudinal location to another, while remaining in the same inclination, were investigated. The first method that was investigated utilized spherical trigonometry to calculate the angle between orbital planes with common inclinations and different ascending node locations. Knowing the angle between the planes and the velocities of the satellites at the line of intersection, allowed calculation of the ΔV's. As was expected, this transfer profile was very expensive in terms of propellant requirements. Figure 13 shows the propellant mass vs. total longitudinal difference

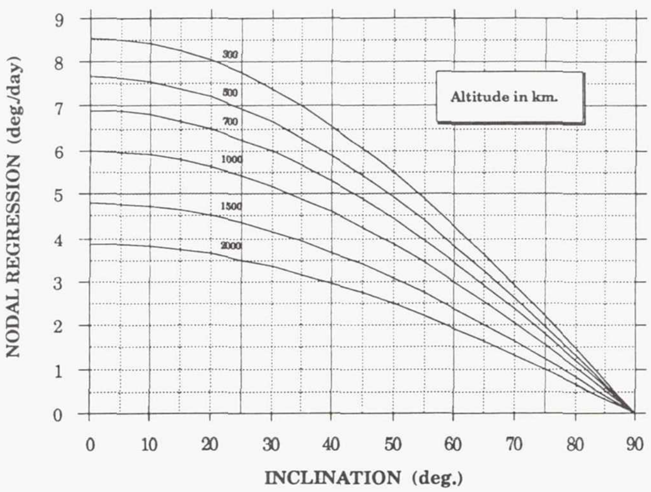

Fig. 14. Nodal Regression vs. Inclination and Altitude

(ΔΩ) curves for rendezvous and retrieval of 2-5 pieces of 2000-kg debris with inclinations of 35° and altitudes of 750 km.

As can be seen in Fig. 13, the propellant mass requirements become too great for even modest ascending node differences (maximum shuttle payload is approximately 16,000 kg). For all mass calculations an estimated dry mass of 526 kg (minus fuel tanks) was used with a main thruster specific impulse of 325 sec. Because the size of the fuel tank is a function of the amount of propellant used, the mass of the fuel tanks was not included in the dry mass estimate. To take into account the effect of the tank mass on the propulsion requirements, a tank-to-fuel mass percentage was used. With a main thruster chamber pressure of 145 psia, a percentage of 2.3% was found to give a factor of safety for aluminum fuel tanks of 1.5.

If the Earth were a perfect sphere, an ASPOD mission to remove a significant amount of mass from low Earth orbit (LEO) would be seriously limited to pieces of debris that have longitudes of ascending nodes extremely close together. Because of the oblate shape of the Earth and the nonuniform gravitational field, natural perturbations exist that, over time, significantly affect the orbital parameters of a satellite in LEO. The oblateness of the Earth particularly affects the ascending node of an orbit by applying perturbing torques on a satellite as it travels around the Earth[11]. This natural perturbation causes the locations of the ascending node to regress westward if the satellite has a direct orbit ($0° < i < 90°$), and eastward if the satellite has a retrograde orbit ($90° < i < 180°$). Figure 14 shows the nodal regressions per day as a function of altitude and inclination (for circular orbits).

The second method of orbital transferring that was analyzed takes advantage of the natural nodal perturbations. Since the nodal regression rate at a given inclination is primarily a function of altitude, by establishing an ASPOD orbit at a different altitude than the debris orbit, the planes of the two orbits will eventually coincide. Therefore, the need for a plane change maneuver is eliminated and a coplanar Hohmann transfer can be employed.

If a piece of debris is to the west of ASPOD, establishing an orbit at a lower altitude will allow ASPOD to eventually align itself in the same plane as the debris. Likewise, if a piece of debris is to the east of ASPOD, loitering in a higher altitude orbit will eventually align the orbit planes. If ASPOD's ascending node differs by 180° from that of a debris orbit, ASPOD has the choice of either decreasing or increasing the altitude of its orbit to initiate the transfer sequence. For purposes of this analysis the criterion was established to loiter at an altitude that will result in a difference in nodal regression rates between the ASPOD orbit and the target orbit of at least 0.5°/day. Thus, ASPOD will not have to loiter for more than one year before an alignment of orbital planes will occur. Figure 15 demonstrates the propellant mass requirements using nodal regression for the retrieval of 2-6 pieces of 2000-kg debris with inclinations of 35° and altitudes of 750 km.

Adhering to the criteria of a 0.5°/day minimum for nodal regression difference results in loiter orbit altitudes of 550 km and 950 km for a debris orbit of 750 km, or Δh's of -200 km and +200 km, respectively. Since the ΔV's are not dependent

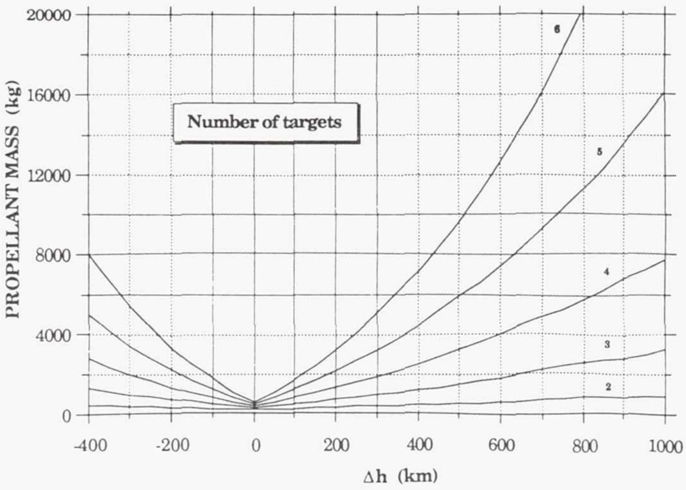

Fig. 15. Propellant Mass vs. Δh and Number of Targets for Debris Retrieval Mission

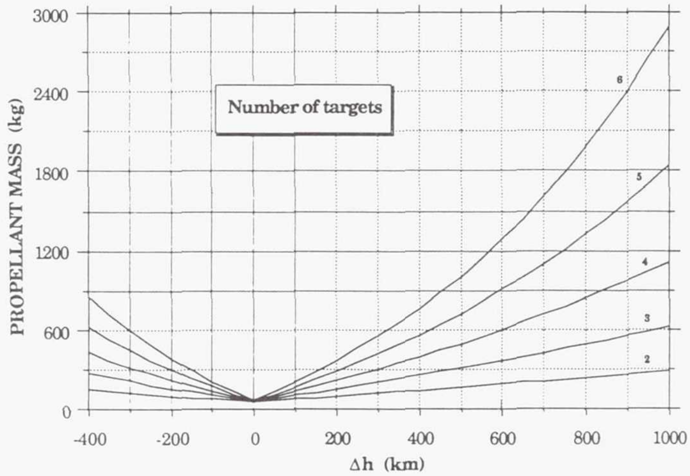

Fig. 16. Propellant Mass vs. Δh and Number of Targets for Deorbit Mission

on the longitudinal differences, the propellant masses were plotted against Δh. From Fig. 15, using an ASPOD dry mass of 580 kg and specific impulse of 325 sec, the required propellant mass to rendezvous with and retrieve four typical 2000-kg pieces of debris is approximately 1500 kg. For deorbiting with SRMs rather than retrieval, Fig. 16 shows the corresponding propellant mass for 2-6 pieces of large debris. From this figure, the necessary propellant to deorbit the chosen debris is approximately 200 kg. The four SRMs would add a total of 280 kg (70 kg each) to the initial dry mass of the ASPOD spacecraft.

The use of nodal regression to transfer orbits will now be applied to the retrieval of four actual pieces of debris. The orbital parameters and masses for the chosen debris as of February 8, 1989, are shown in Table 1[12] (longitude location of OAO-2 telescope is used as reference location).

The average altitude of the four pieces is 754 km and the average mass is 1956 kg. As mentioned, the expected propellant mass required for this mission will be roughly 1500 kg if a minimum loiter orbit is used. If the ASPOD satellite begins the mission by retrieving the OAO-2 telescope first (a west to east sequence), the minimum loiter orbit will be 950 km to allow the remaining pieces of debris to drift toward ASPOD. The total ΔV for this mission is 860 m/sec, with a propellant requirement of 1646 kg. The corresponding propellant masses to deorbit the four pieces of debris for the two sequences are 219 kg and 241 kg, respectively. The total longitudinal difference between the four pieces is 160°, thus the loiter time to accomplish the transfers is 320 days. Allowing time for the solar cutter to cut the debris into manageable pieces and store them on board, or for SRM attachment, the total mission time will be approximately one year.

Another possible mission scenario is a combination of the above approaches, that is, retrieving the telescopes for any valuable materials, but deorbiting the spent booster stages. The propellant necessary to deorbit the boosters first and continue on to the telescopes for retrieval is approximately 652 kg. The SRMs for retro firing added a total of 140 kg to the initial mass.

As mentioned before, a large quantity of debris is located at inclinations of 65°, 74°, and 82°, with varying altitudes. The use of nodal regression is a convenient method for retrieving debris with various altitudes. The most economical mission sequence is to rendezvous with the piece of debris that is at the highest altitude and work back down to the piece of debris in the lowest altitude. As the mission begins at the debris with the highest altitude, ASPOD is confined to a west to east sequence. Therefore, the mission may be on the order of 2-3 years. Since most of the debris in the 600 km to 1500 km altitude range have lifetimes of 100 years or more, a 2- or 3-year mission is not an inhibiting circumstance.

It is clear from the above analysis that the most fuel-efficient method for removing orbital debris is to attach an SRM to the debris and send it into an orbit that will quickly decay and burn up in the atmosphere. This is not to say that it is the best method. The technical aspects of attaching the SRMs and assuring that the debris is properly deorbited presents formidable difficulties. The opportunity will also be missed to

Table 1. Orbital Parameters of Baseline ASPOD Targets[12]

	Perigee (km)	Apogee (km)	i (deg.)	ω (deg.)	Ω (deg.)	Mass (kg)
OAO-2 rocket	7089	7189	35	239	160	1815
OAO-3 rocket	7067	7152	35	350	121	1815
OAO-3	7108	7116	35	293	10	2220
OAO-2	7137	7150	35	315	0	2012

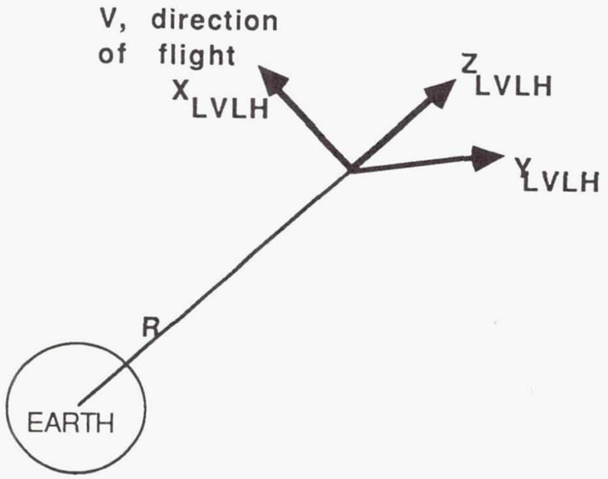

Fig. 17. Local Vertical, Local Horizontal Coordinate System

take advantage of the material resources that the debris population presents. Many thousands of kilograms of high-grade, "space-age" material may be salvaged by the abilities of the ASPOD spacecraft to cut up the debris and store it onboard for eventual recovery by the space shuttle or a controlled splashdown. Thus, the ASPOD spacecraft has two potential mission purposes: (1) to clean up the increasingly polluted LEO region and (2) to retrieve useful materials in orbit about the Earth for possible recycle or long-duration exposure study.

PROXIMITY OPERATIONS

This analysis will bring ASPOD within 50 m of the orbiting debris. A local coordinate system is defined and two approaching techniques are briefly explained[13].

The coordinate system used has its origin at the center of mass on the respective orbital vehicle. This system is the local vertical/local horizontal (LVLH). The x-axis (X_{LVLH}) lies along the velocity vector of the orbital vehicle, while the z-axis (Z_{LVLH}) lies along the radius vector between the Earth and the orbiting vehicle. The y-axis (out of plane) completes the coordinate system (Fig. 17).

Two approach trajectories ASPOD can use are (1) V-bar and (2) R-bar. For V-bar, the ASPOD approaches the debris along the X_{LVLH} axis. The advantage of this method is low fuel requirements for station keeping. However, since ASPOD would never "catch" the debris while along the same orbit, there are added fuel costs for "accelerating" ASPOD, then braking once the debris is reached. This has an additional side effect of plume impingement that could potentially tumble the debris.

The R-bar method uses an approach along the Z_{LVLH} axis. This approach is still an in-plane approach, but the orbit of ASPOD will be slightly greater than or less than the debris. One advantage of this method is plume impingement on the debris while station keeping is minimized. There will, however, be some station keeping required since velocities of the two orbits will be slightly different at any given time.

As previously discussed, nodal regression and Hohmann transfer techniques will be used for matching orbits. R-bar approaches are recommended for final approach to minimize plume impingement effects.

Once it has been determined that ASPOD is in the proper plane in order to rendezvous with the debris, ASPOD will fire its engines so that it may change to an orbit slightly larger than that of the debris. This new orbit should be less than 10 km higher than the debris so that the debris can be located by ASPOD's microwave radar. The rendezvous sequence is summarized in Fig. 18.

When ASPOD has achieved this orbit, it determines relative velocities and range between itself and the debris using its microwave radar and Doppler effect. If the orbit is on the outer limit of radar range (10 km), the orbit will be quickly adjusted so that ASPOD can be brought to within 1 km of the debris. One important reason for doing this is the relatively large amount of fuel that would be needed for station keeping with this altitude difference.

Assuming the debris to be in a circular orbit at 700 km, and ASPOD's initial orbit at 710 km, velocity differences are approximately 5.3 m/sec. This is a worst-case scenario since the orbits are somewhat higher than this, and therefore velocity differences are lower. The 10-km upper limit is chosen because it is the outer range of the microwave radar. It is probable that the initial orbit will be closer than 10 km, but no closer than 1 km. In any case, once orbit and radar contact are established, ASPOD will quickly fire its engines to come within 1 km. ASPOD will constantly be monitoring relative ranges and velocities between itself and the debris.

Once 1 km is reached, the TV/zoom lens can be used to locate the debris. At this point station keeping would require firing the engines for an approximate velocity deficit of 0.53 m/sec. The ASPOD can now determine orbital attitude of the debris and recheck range and velocity differences, and can begin to slowly move closer to the debris.

The ASPOD uses the onboard computer to analyze range and velocity, then fires its engines to orbit within 500 m of the debris. During this time, ASPOD is constantly being updated on the relative velocities and range between itself and the debris. Any deviation that could be considered catastrophic can

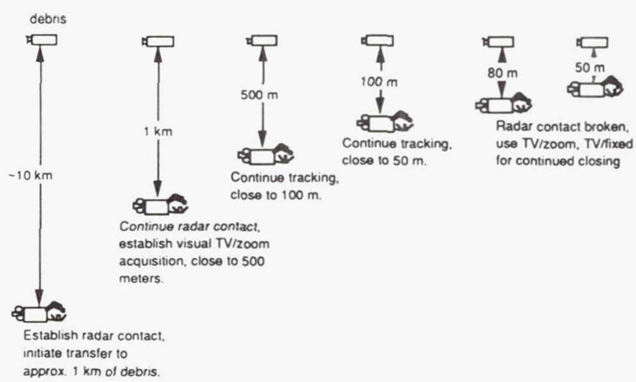

Fig. 18. ASPOD Proximity Operations Summary

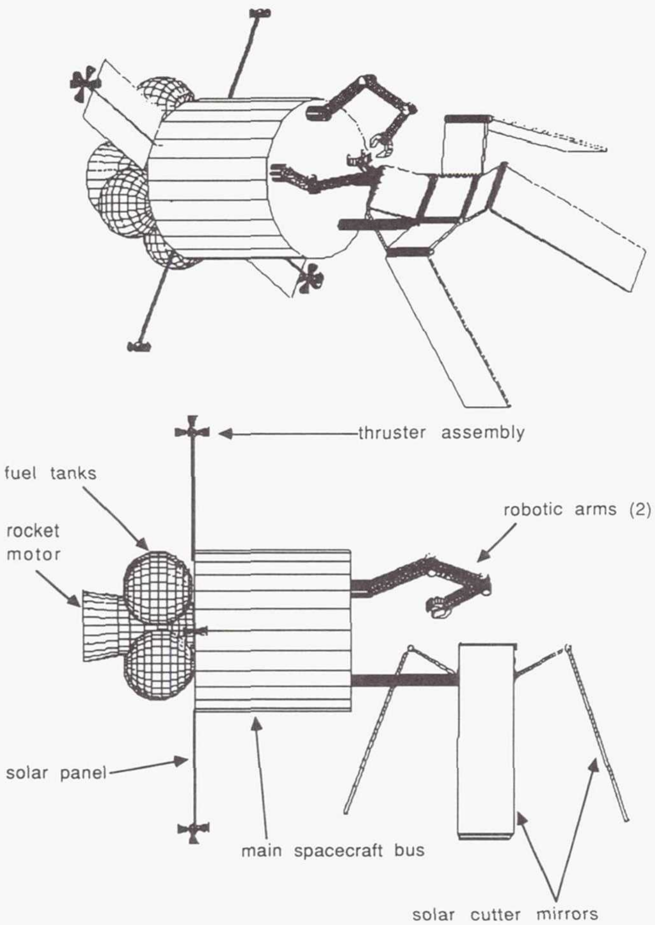

Fig. 19. Basic ASPOD Configuration

be corrected by firing the appropriate engine to compensate. Again ASPOD uses the radar to measure ranges and velocities while ground control can use the TV/zoom lens to observe the mission if required.

These same procedures are repeated to bring the orbiter to within 100 m, then 50 m of the debris. Each step is carefully analyzed and as the orbiter approaches the debris in each step, greater care and precision are required so as not to destabilize the debris any further. Once inside approximately 80 m the microwave radar is essentially useless, and a TV/fixed lens can be used in conjunction with the TV/zoom lens.

At 50 m above the debris, station keeping for ASPOD consists of an approximate velocity deficit of 0.03 m/sec in the X_{LVLH} axis. It may be decided to despin or detumble the debris from this range, or closer proximity may be needed in order to complete processing of the debris.

Once the debris is processed, ASPOD continues on its mission and the cycle is repeated. For nodal regression, ASPOD moves to a higher (or lower) orbit, then approaches the debris, in plane, using the R-bar method. For the first piece of debris using a launch from the space shuttle or ELV, the same R-bar approach may be used, except ASPOD approaches from a lower orbit (higher velocity) using similar techniques.

Whether or not a closer approach is needed to despin or detumble the debris is unknown at this point. An in-depth study is being conducted at this point to develop a method to despin and make contact with the debris.

SPACECRAFT CONFIGURATION

The ASPOD spacecraft is currently envisioned as consisting of a main cylindrical body section approximately 5 m in length by 3 m in diameter. Attached to the aft end of this central body are a main rocket motor, solar arrays, attitude thrusters, and tankage. A solar cutter device, two robot arms, and most spacecraft instrumentation are attached to the front of the spacecraft. Within the central body section is cargo space for the storage of orbital debris or other mission hardware, such as solid rocket motors for the deorbiting of debris not to be retrieved within ASPOD itself. The basic configuration for the ASPOD spacecraft is depicted in Fig. 19.

For the mission scenario investigated, the initial (wet) mass of the ASPOD spacecraft is approximately 2500 kg, with a dry mass of approximately 560 kg. The overall spacecraft mass is dominated by propellants, which account for the majority of the initial total.

The ASPOD system has been logically divided into 10 major subsystems, namely structure, electrical power, thermal control, propulsion, attitude control, communications, command and data handling, robotics, solar cutter, and

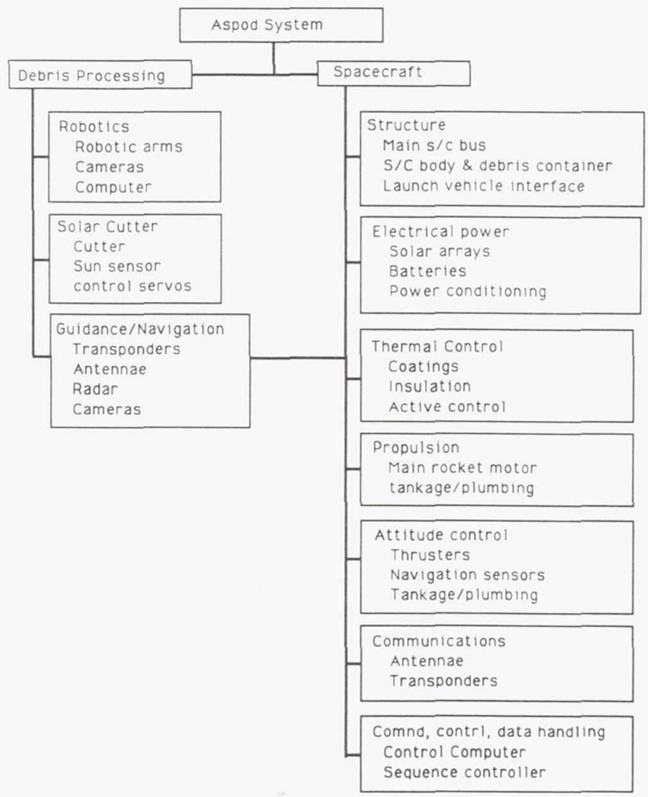

Fig. 20. Block Diagram of Main ASPOD Subsystems

guidance and navigation. These main subsystems are depicted in block diagram format in Fig. 20. The conceptual breakout of a spacecraft configuration is somewhat subjective as many functions overlap. The following sections describe the major ASPOD subsystems in greater detail. The overall ASPOD configuration and mass estimates are based on comparison with various other spacecraft and on technological forecasts contained in references 14-19.

Structure. The main ASPOD structure includes an approximately 300-kg main body with robotic arms, a solar cutter, and various sensors and spacecraft equipment attached to the front end. Within this main body is space for the storage of any orbital debris for which retrieval is desired. The front of the spacecraft body constitutes the main spacecraft bus and must provide mounting and power connections for various spacecraft sensors and instruments for navigation and debris processing purposes. The propulsion, attitude control, and electrical power subsystems are mounted to the rear of the ASPOD main body. Mounts and launch vehicle interfaces must also be provided here.

Electrical power. The average electrical load for ASPOD is estimated at approximately 50 W. Primary power is supplied to ASPOD from solar arrays deployed on booms at the aft end of the spacecraft. Power for peak activities and during periods of eclipse is provided by nickel-hydrogen-type rechargeable batteries, massing approximately 5 kg. The amount of time a spacecraft spends in and out of the sun varies with season, orbital inclination, and altitude. For the ASPOD mission scenarios investigated, the average time in the sun was approximately 67%, with a worst case of 27%. Thus, the solar panels must be sized to provide power in excess of the nominal spacecraft load to provide the batteries sufficient charge to operate the spacecraft during periods of darkness. For the spacecraft load of 50 W, a total collection area of approximately 1.7 m^2 is needed for the solar arrays (see Appendix), with a mass of 12 kg (based on expected array performance available by the mid-1990s)(16). It may also be desirable to place additional solar cells on the body of the spacecraft itself to allow greater flexibility of orientation during debris processing operations.

Thermal control. A detailed thermal analysis for ASPOD has not yet been conducted. However, the relatively low nominal power dissipation of ASPOD and the relatively short orbital periods of LEOs (compared to geostationary orbits) indicate that passive means of thermal control such as insulation blanks and absorptive/emissive/reflective coatings should be sufficient for most thermal control. The thermal control system is estimated to mass approximately 12 kg. Small electrical heaters will also be needed in choice locations to prevent propellants from freezing and to keep thrusters working properly.

Propulsion. The ASPOD propulsion system is designated as a pressure-fed hydrazine/nitrogen tetroxide bipropellant system. The main rocket motor weighs 8 kg and provides 2000 N of force with a specific impulse of approximately 325 sec. Propellants are stored in four pressurized tanks mounted at the aft of the spacecraft. The hydrazine propellant and nitrogen tetroxide oxidizer are storable liquids at room temperature, hence avoiding the refrigeration power consumption and other difficulties associated with cryogenic (hydrogen/LOX) propellants.

Attitude control. The attitude control system consists of 2 sets of 5 thrusters mounted at the ends of the solar array booms, as well as 2 additional sets of 2 thrusters on booms set perpendicular to the solar arrays, for a total of 14 thrusters massing 20 kg (1.4 kg net hardware each). Such thrusters are typified by the Marquardt Model number R-6C (used for the GOES satellite), which provides 22 N of thrust. The thrusters are arranged to provide six degrees of freedom (translation and/or rotation about all three principle axes), which will be necessary for proximity (i.e., to debris) operations. The attitude control thrusters use the same propellants and tankage as the main rocket engine and have a specific impulse of approximately 280 sec.

Communications. ASPOD will need to telemeter data to the Earth and receive commands from the ground. Transponders and antennae used for other spacecraft should be quite adequate for the needs of ASPOD. ASPOD should, however, have omnidirectional (low gain) communications capabilities to allow orientational freedom during debris processing.

Command and data handling. The ASPOD spacecraft will be largely autonomous and computerized, with computers controlling spacecraft operations and monitoring the health of various ASPOD systems. Functions will also include pattern recognition capabilities in conjunction with navigation sensors and cameras.

Robotics. ASPOD will be equipped with two robotic arms similar in concept to the space shuttle RMS system but smaller. Two arms are necessary to allow pieces of debris to be dismembered and stored, or to hold the debris with one arm while the other performs other operations, such as the retrieval and mounting of a solid rocket motor. Television cameras will be necessary to monitor the debris processing robotic activities, and the robot arms will be computer controlled.

Solar cutter. The ASPOD solar cutting system is currently envisioned as consisting of an assembly of gold-plated mirrors (to better reflect infrared) and fresnel lenses to focus sunlight to cut or weld debris. A sensor will track the sun and orient the cutter assembly for optimal cutting by means of a feedback servo-control system. The solar cutter system is estimated to weigh approximately 40 kg.

Guidance/navigation. The ASPOD spacecraft will be three-axis stabilized with inertial (gyroscopic) guidance referenced to an inertial measuring unit (IMU). Sensors including a horizon sensor, sun sensor, and magnetometer (to measure Earth's magnetic field) will be used to reset the inertial measuring unit from any gradual drift. Accelerometers will measure and verify spacecraft velocity changes for orbital maneuvers. Orbital debris will be tracked by onboard radar and camera systems. However, before the debris is close enough in promixity to ASPOD for the use of onboard tracking methods, ground tracking may be necessary. This can be made easier by providing the ASPOD spacecraft with a tracking transponder to facilitate more accurate tracking of ASPOD's position from the ground.

The ASPOD configuration presented above is not finalized and will become more refined as the concepts of an ASPOD mission mature. Still, it provides a good general idea of what sort of spacecraft might carry out the envisioned debris processing mission.

SUMMARY

The Space Engineering Design program has been on track. The ASPOD solar cutter, auto sun track mechanisms have all been built and are working satisfactorily. One (gathering) robotic arm has been built and is also operating satisfactorily. The second robotic arm for positioning/assembly of the cut parts is being built. The project has drawn considerable news media attention with many popular and science forums. It is expected that with continued progress, a hardware experiment can be conducted on a Getaway Special in 1991 or 1992.

ACKNOWLEDGMENTS

Principal authors were David Campbell, Bruce Carter, Leslie Donalson, Larry John, Dan Rodina, Jeff Brockmann, and Micky Marine. Faculty advisor was Professor Kumar Ramohalli, Aerospace and Mechanical Engineering Department.

REFERENCES

1. Beard J., "Sweeping Up Space Junk", *Discover,* December, 1988, p. 22.
2. Lechleitner H., *Raumpfleger Drigend Gesucht,* March, 1989, p. 154.
3. Beard J., "Verdens Forste Flyvende Skraldemand," *Danish Science,* December, 1988, p. 46.
4. Stewart D., "Eyes in Orbit Keep Tabs on the World in Unexpected Ways," *Smithsonian,* December, 1988, p. 70.
5. Erickson J., "Engineer Plans to Clean the Heavens," *Arizona Daily Star,* February 21, 1987.
6. Stiles E., "Space Junk," *Tucson Citizen,* February 27, 1987.
7. Hodge C. "'Sweeper' Would Gather Space Junk," *Tucson Citizen,* September 23, 1988.
8. Stiles E., "U of A Robot Will Collect Space Junk," September 23, 1988.
9. Turner M. H., "Trashed in Space," *American Way,* May 15, 1989.
10. John N. and McKnight D. S., *Artificial Space Debris,* Orbit, Malabar, Florida, 1987.
11. Kaplan H., *Modern Spacecraft Dynamics and Control,* Wiley, New York, 1976.
12. King-Hele D. G., Walker D. M. C., Pilkington J. A., Winterbottom A. N., Hiller H., and Perry G. E., *The R.A.E. Table of Earth Satellites 1957-1986,* Stockton, New York, 1987.
13. Johnson Space Center, *Proximity Operations Analysis,* NASA TM-81104, National Aeronautics and Space Administration, 1980.
14. Swensen et al., *A Conceptual Design Study of the Reusable Reentry Satellite,* NASA TM-101043, National Aeronautics and Space Administration, 1988.
15. Agrawal B. N., *Design of Geosynchronous Spacecraft,* pp. 1-4, 36-55, Prentice Hall, Englewood Cliffs, New Jersey.
16. Hord R. M., *CRC Handbook of Space Technology: Status and Projections,* pp. 53-65, CRC Press, Boca Raton, Florida, 1985.
17. Fimmell R., Colin L., and Burgess E., *Pioneer Venus,* NASA SP-461, NASA, Washington, DC, 1983.
18. Yenne B. (ed.), *Interplanetary Spacecraft,* pp. 16-82, Bison Books, New York, 1988.
19. Woodcock G. R., *Space Stations and Platforms,* Orbit, Malabar, Florida.

N94- 71269

382667

1994004514

S2-18

160628

P- ~~14~~ 20

DESIGN OF A SOLAR SAIL MISSION TO MARS

AUBURN UNIVERSITY

INTRODUCTION

A new area of interest in space vehicles is the solar sail. Various applications for which it has been considered are attitude control of satellites, focusing light on the jungles of Vietnam, and a Halley's comet rendezvous. Although for various reasons these projects were never completed, new interest in solar sails has arisen. The solar sail is an alternative to the rocket-propelled space vehicle as an interplanetary cargo vehicle, and manufacture of solar sails on the space station is a possibility. Solar sails have several advantages over rockets, including an unlimited power supply and low maintenance.

The purpose of this project is to design a solar sail mission to Mars. The spacecraft will efficiently journey to Mars powered only by a solar sail. The vehicle weighs 487.16 kg and will be launchable on an expendable launch vehicle.

The project includes an investigation of options to minimize cost, weight, and flight duration. The design of the sail and its deployment system are a major part of the project, as is the actual mission planning. Various topics researched include solar power, materials, space environment, thermal control, trajectories, and orbit transfers. Various configurations are considered in order to determine the optimal structure. Another design consideration is the control system of the vehicle. This system includes the attitude control and the communication system of the sail.

This project will aid in determining the feasibility of a solar sail and will raise public interest in space research.

STRUCTURES

There are many aspects of the solar sail vehicle to consider in the design of the actual structure of the vehicle, including sail configuration, stability, method of stiffening, and housing for the various systems.

Designing the sail of the solar sail vehicle included consideration of several configurations such as various separated panels as used in the helio-gyro vehicle considered for a Halley's Comet rendezvous, and uniform panels such as the square sail chosen for this project. The square sail, as seen in Fig. 1, was chosen for several reasons. The simplicity of deployment of the square configuration is a major advantage, as is its high area-to-mass ratio[1]. This design consists of four booms, 114 m in length, connected tangentially to a cylindrical bus measuring 1.4 m in diameter and 1 m in length. The sail has four triangular sections contained between the booms and has a total area of $25{,}992\ m^2$[2]. The weight limitation determined the final measurements of the sail and the total force, 210,040.00 N/m^2, on the bus determined the thickness of the bus at 1 cm. This thickness includes a large increase from the necessary thickness calculated to insure reliability.

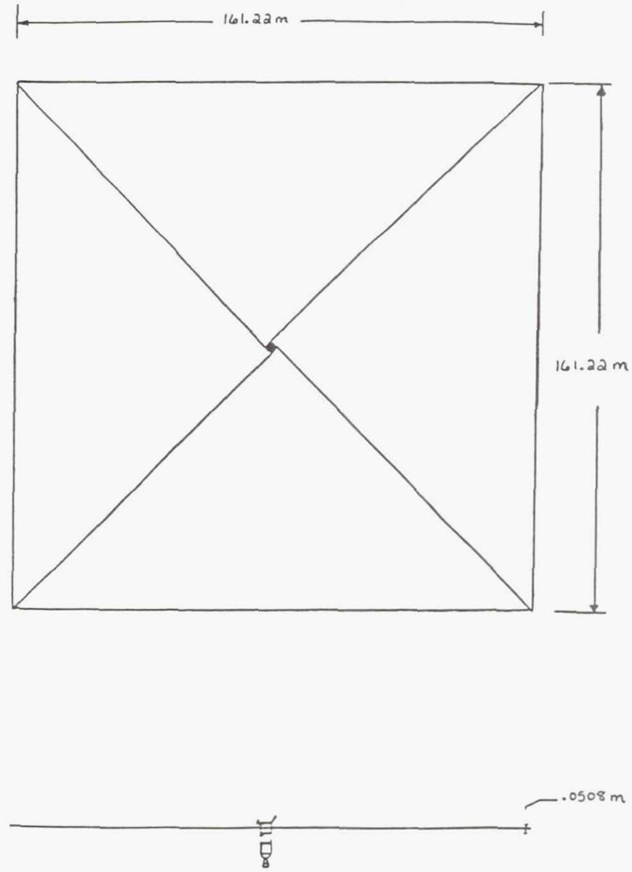

Fig. 1. Two-View Drawing of the Solar Sail

The method of stiffening the structure is also an important design consideration. Spinning the sail after deployment was not feasible because of complications in attitude control. Extendable booms were ruled out because of complexity and weight. A free sail without booms was considered but lacked sturdiness for such a long trip. Uncured booms were chosen for their flexibility and compactness in the uncured state; curing takes place after deployment[1].

DEPLOYMENT

One of the major design considerations for the solar sail vehicle is the method of deploying the sail. Minimizing weight and complexity of the deployment system are primary concerns in designing the method of deployment.

The sail folds accordion-style into a wedge shape between the booms. Both the sail and the booms will coil around the bus before deployment and be encased in an open-ended cylinder. The enclosed solar sail vehicle will be set into orbit spinning. The casing will slide off with the small rocket used to initially escape Earth orbit. The sail will then deploy due to the force of the spinning motion and the strain energy in the sail and boom material[2]. The attitude control system will stop the spin.

SPACE ENVIRONMENTAL EFFECTS

Several aspects of the space environment influence the solar sail, such as electromagnetic radiation, solar particle radiation, electrostatic charging, and micrometeors.

The most significant of these environmental phenomena is electromagnetic radiation, which consists of optical and ultraviolet radiation. Optical radiation is the sail's means of propulsion. As photons of light impact and reflect from the sail, they impart a momentum, causing an increase in pressure on one side of the sail resulting in acceleration. The main effect of ultraviolet radiation is to cure the sail booms after deployment.

A means of measuring solar radiation is the solar constant, the amount of energy from all wavelengths produced by the sun per second per square meter[3]. At Earth the constant is 1370 W/m^2 and decreases to 590 W/m^2 at Mars[4].

The force on the sail is obtained from this solar constant by multiplying the pressure increase on the sunside of the sail by the area of the sail. The force decreases from Earth to Mars and also as the sail is angled away from the sun. Acceleration and velocity are calculated to range from 0.0005650 m/sec^2 and 32.73 m/sec at Earth, to a velocity of 238.14 m/sec halfway between Earth and Mars, to an acceleration of 0.0002437 m/sec^2 at Mars[5]. The duration of flight, calculated assuming that the effective sail area is equal to the sail area, is 5.2 years; however, the sail will have to change its orientation to maintain its trajectory.

The rate of temperature increase is used to determine materials and thermal control requirements. The maximum temperature increase is 0.4466°C/sec-m^2 and is based upon the solar constant and the distance from the sun.

Solar particle radiation originates from the solar wind and consists of high-energy free electrons, positive ions, and neutral particles. Its density is dependent on the sun's 11-year emission cycle. At the peak of its cycle, known as the solar maximum, the sun is emitting several tons of particles per second. The next solar maximum will occur in 1992, which coincides with the start of the mission and makes particle radiation a potential hazard. There are not many materials that are effective against particle radiation, so the sail will use redundant electrical systems.

Electrostatic charging is the buildup of a potential difference between the sail and the plasma in which it is immersed in the space environment. The most feasible solution to this potential problem is to use as many conductive surfaces as possible and to cover nonconducting surfaces with a conductor.

The large surface area of the sail and its thin material make the problem of micrometeor collisions a concern. These particles, ranging from micrometer to millimeter proportions, present problems in the space environment due to the extremely high velocities of particles in space.

MATERIALS

The solar sail materials are classified into two parts: the actual sail materials, and all structures reinforcing the sail and bus. The sail itself consists of several thin layers, a film base with a sunside coating to increase both reflectance and emittance and a backside coating to increase emittance.

The film chosen for the solar sail is a 2.0 μm thickness of Kapton, a polyamide film made by Dupont. It can withstand temperatures up to 350°C, has a low thermal expansion, and a high resistance to tearing from micrometeors. Kapton is easy to metallize to resist radiation. Furthermore, Kapton will fold and crease well, making it easy to pack[6].

A metallic coating of the sunside is necessary for the effective transfer of momentum from the photons and for thermal control. A 1000 Å thickness of aluminum is chosen because it exhibits these qualities as well as being electrically conductive and able to give the sail protection from UV radiation. Aluminum will provide a high reflectance to reduce thermal absorption and a high reflectance component to help maximize the thrust while not adding significant weight to the sail. Furthermore, a 100 Å layer of chromium is chosen to coat the sail's backside for thermal control[7]. The solar sail film will also have a polyamide composite tape with unidirectional graphite fibers bonded to the sail's rearside to avoid "billowing" and therefore loss of force, and to help control rips from micrometeors.

Composite beams are chosen for the sail's reinforcing structure because of their strength, light weight, and versatility for packing. The booms will consist of the F263 Epoxy Resin, a high-temperature resin for aerospace applications produced by HEXCEL, combined with a UV activator and woven with carbon fibers into a fabric. The uncured boom is joined with the sail material with a polyester adhesive and wrapped around the bus for storage. Normally this resin system is cured by heat, but the addition of the activator will cause the curing by UV radiation after deployment[8].

The material for the bus, based on the density and minimum strength required, is a magnesium alloy sheet AZ313-H24. The rear side of the bus is coated with silvered Teflon for thermal control of the bus[9].

POWER SYSTEM

Various components of the power system to be chosen for the sail mission include an energy source, energy conversion, energy storage, and a power conditioning and control system. The energy source will be direct solar radiation, converted into power by a 0.75 m × 0.75 m flat solar sail array located on the bus (Fig. 2). The array is comprised of silicon cells that are well tested and reliable[7]. For energy storage, rechargeable nickel-cadmium cell batteries are used. They are charged by

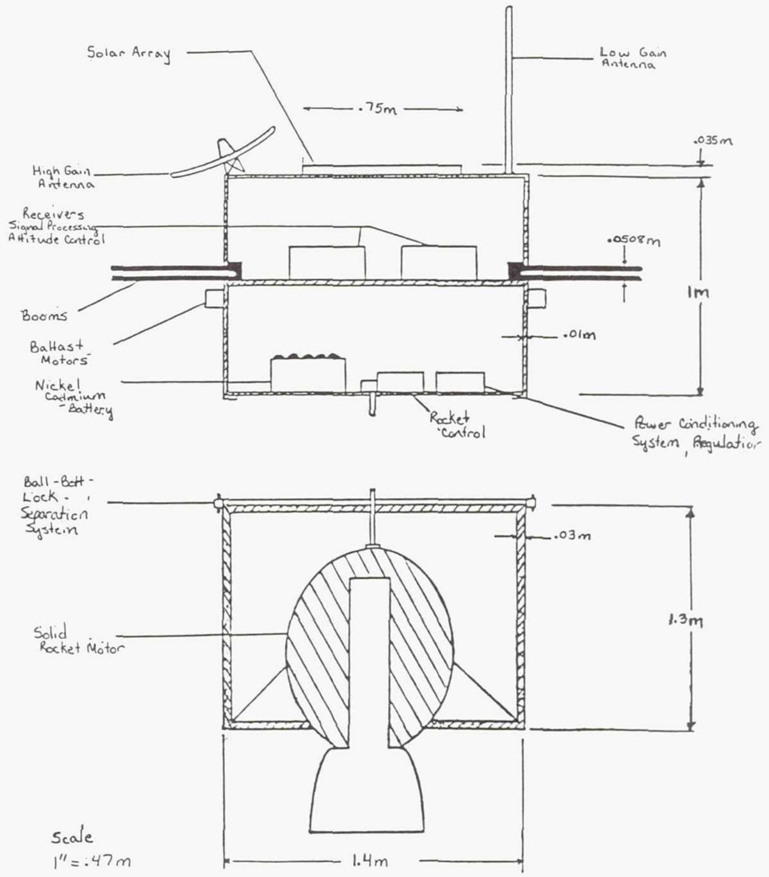

Fig. 2. Cross-Sectional View of the Sail Bus

the solar panels and used for energy storage and as a back-up.

The power conditioning and control system uses regulators, AC/DC converters, and control circuits to match the power produced by the solar cells with that required by the sail subsystems such as telemetry, control, and communciations. It will also control and regulate the charging of the battery.

ATTITUDE CONTROL

The attitude control system can be broken down into three different categories, the attitude sensors, computer system, and the motors used to move ballast masses. The attitude sensor system will consist of two star trackers. They will define the pitch axis and the yaw axis; the spin axis will be fixed at an angle of 35° with respect to the sun. A star tracker is locked onto a target star by focusing the image of the star on a photosensitive surface with an optical telescope(10). When the target star is not focused properly, an error signal is sent to the computer system, which will counter the improper rotation. The computer system will send a signal to the ballast motors, which will move the ballast masses to their necessary position.

The resultant force from the solar radiation is assumed to act through the center of the solar sail. When the ballast masses are moved from their equilibrium positions, the center-of-mass for the solar sail is changed, producing a moment-arm between the resultant force and the center-of-mass that causes the moment required to stop the unwanted angular velocity. The moment needed to produce critical yaw or pitch is much larger than that needed to produce spin. Therefore, the unwanted yaw and pitch due to inconsistencies in the sail material can be easily handled by the attitude control system. The spin due to these inconsistencies is not as troublesome since the orientation with the sun will not be affected.

COMMUNICATIONS

The main components in the communications system will consist of a low and high gain antenna, a transmitter, and a receiver. The main purpose of the communication system is to periodically transmit the coordinates of the solar sail to the Earth, about once a week. The power required by the communication system will peak at about 20 W over a short period of time.

THERMAL CONTROL

The solar sail will experience a wide range of temperatures along the trajectory from Earth to Mars. These temperature variations will affect not only the solar sail itself, but also the electronic equipment and the supporting structure of the sail. Excess heat due to heat dissipation of the solar arrays must be directed away from the electronic equipment since the electronics temperature range is -5°C to 65°C, the batteries 0°C to 20°C, and transmitter 10°C to 60°C[9]. Heat pipes will transport excess heat of internal components to an external radiator surface. Reducing the amount of heat radiated from the surface will protect the vehicle from very cold temperatures. The batteries and the bus except for the two ends will be wrapped in a thermal blanket to minimize temperature fluctuations[9].

TRAJECTORY

The solar sail is mounted on a launch vehicle (possibly the Titan IV) that will place it directly into a geosynchronous transfer orbit[11]. In order to overcome the gravity of Earth, a solid rocket motor will be fired. The correct phase angle for interception is 107.56°[9]. The heliocentric longitude of Mars is found in the *American Ephemeris and Nautical Almanac* and the possible launch times can be determined.

The logarithmic spiral trajectory was chosen for several reasons. From a mathematical point of view, it is the simplest to model and the necessary initial conditions can be met by the mission profile. These conditions include a hyperbolic excess velocity to establish the proper velocity direction required for insertion into the spiral trajectory[12]. Finally, the spiral trajectory is very effective when compared to more complicated optimal strategies[9]. The spiral trajectory is achieved by maintaining the velocity vector at a constant spiral angle and the sail's orientation with respect to the incoming radiation at a fixed value of 35°. The point of closest approach is 6087 km.

AUXILIARY PROPULSION

A solid rocket motor was chosen because it is easier to separate from the bus. A system capable of sustaining large loads, high reliability, minimum weight, good survival of temperature and radiation, minimum impulse, and no debris or contamination was essential to ensure that the sail is not damaged before deployment. For these reasons, the ball-lock-bolt separation system was chosen[12].

ACKNOWLEDGMENTS

Principal authors R. Eastridge, K. Funston, A. Okia, J. Waldrop, and C. Zimmerman were assisted by faculty advisor Dr. J.O. Nichols.

REFERENCES

1. Svitek T. et al., "Solar Sail As OTV/Solar Sail Concept Study- Phase II Report." *American Institute of Aeronautics and Astronautics Paper 83-1347,* Seattle, 1983.
2. Price H. W., "Solar Sail Engineering Development Mission," *American Institute of Aeronautics and Astronautics Student Journal, vol. 19.* Summer, 1981.
3. Trascione T. F., *Introduction to the Space Environment,* Orbit, Malabar, Florida, 1988.
4. Giancoli D. C., *General Physics,* Prentice-Hall, Englewood Cliffs, New Jersey, 1983.
5. Bate R. R., *Fundamentals of Astrodynamics,* Dover, New York, 1971.
6. Linden D., *Handbook of Batteries and Fuel Cells,* McGraw-Hill, New York, 1984.
7. Rowe W. M., "Thermal Radiative Properties of Solar Sail Film Materials." *American Institute of Aeronautics and Astronautics Paper 78-852,* Palo Alto, 1978.
8. Gross—Auburn University Aerospace Department, personal communication, 1989.
9. Chetty P. R. K., *Satellite Technology and its Applications,* Tab Books, Blue Ridge Summit, Pennsylvania, 1988.
10. Corliss W. R., *Space Probes and Planetary Exploration,* D. Van Nostrand, Princeton, 1978.
11. Van Der Ha J. C., "The Attainability of the Heavenly Bodies With the Aid of a Solar Sail." *International Aerospace Abstracts,* Germany, March 1980.
12. Modi W. C., "On the Maximization of Orbital Momentum and Energy Using Solar Radiation Pressure," *The Journal of the Astronomical Sciences, vol. XXVII, no. 1,* Jan.-March, 1979.

LOW EARTH-ORBIT RAIDER (LER) WINGED AIR LAUNCH VEHICLE CONCEPT

AUBURN UNIVERSITY

INTRODUCTION

The need to launch small payloads into low Earth orbit has increased dramatically during the past several years. The Low Earth-orbit Raider (LER) is an answer to this need.

The LER is an air-launched, winged vehicle designed to carry a 1500-lb payload into a 250-nautical-mile orbit. The LER is launched from the back of a 747-100B at 35,000 ft and a Mach number of 0.8. Three staged solid-propellant motors offer safe ground and flight handling, reliable operation, and decreased fabrication cost. The wing provides lift for 747 separation and during the first stage burn. Also, aerodynamic controls are provided to simplify first-stage maneuvers.

The air-launch concept offers many advantages to the consumer compared to conventional methods. Launching at 35,000 ft considerably lowers atmospheric drag and other loads on the vehicle. Since the 747 is a mobile launch pad, flexibility in orbit selection and launch time are unparalleled. Even polar orbits are accessible with a decreased payload. Most importantly, the LER launch service can come to the customer; satellites and experiments need not be transported to ground-based launch facilities.

The LER is designed to offer increased consumer freedom at a lower cost over existing launch systems. Simplistic design emphasizing reliability at low cost will allow the LER to be the industry leader in light payloads for years.

VEHICLE DESCRIPTION

The basic configuration of the LER is composed of four parts: the nose, body, wing, and tail. This configuration with dimensions is shown in Fig. 1.

The nose/payload area design chosen for the LER is a tangent ogive nose with cylindrical volume in the rear to increase payload area. The radius of curvature of the nose is 75 in and the payload volume is 92.04 cu ft.

The LER body is cylindrical in shape. The body has a diameter of 60 in and a length of 660 in. The cylindrical shape is structurally sound, has little drag, and is easily manufactured.

The primary lifting component of the first stage is the wing. All pertinent wing characteristics are given in Table 1. For stability reasons, the quarter chord of the wing is located at the center of gravity of the LER at launch.

The tail section consists of three equally sized, all moving fins. These fins, built of composites, are lightweight and easy to manufacture. They are of biconvex design, with the largest thickness occurring at the center of the chord. Table 2 lists all important fin characteristics.

The bulk of the LER weight is made up of the solid propellant. Table 3 lists some of the pertinent weight estimates.

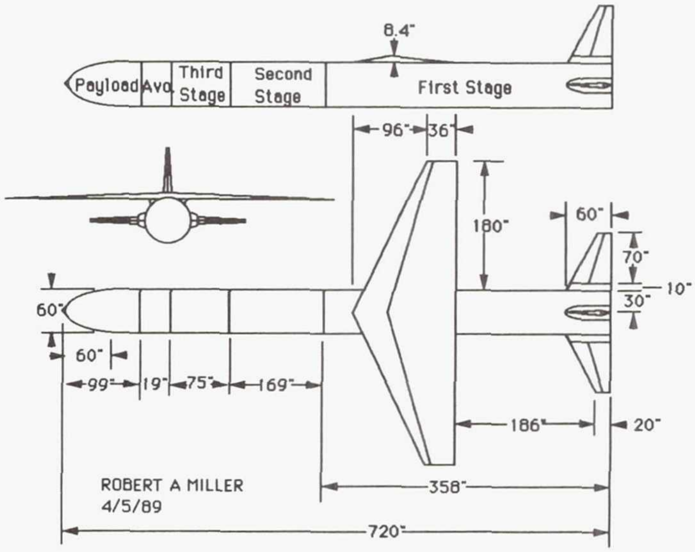

Fig. 1. Three-Dimensional View of the LER

Table 1. Wing Parameters

Item	Value
Wing span	35 ft
Root chord	11 ft
Tip chord	3.0 ft
Taper ratio	0.273
Aspect ratio	5.0
Sweep angle (leading edge)	25.75°
Planform area	245.0 ft^2
Wetted area	437.9 ft^2
Thickness to chord ratio	7.0%
Maximum thickness location	1/4 chord

Table 2. Tail Fin Characteristics

Item	Value
Fin span	5.833 ft
Root chord	5.0 ft
Tip chord	1.67 ft
Taper ratio	0.334
Sweep angle (leading edge)	29.75°
Wetted area	36.11 ft^2
Thickness to chord ratio	7.0%
Maximum thickness	1/2 chord

Table 3. LER Weight Estimates

Item	Weight (in lb)
Payload	1,500
Payload fairing	300
Avionics and thrusters	130
Third-stage propellant	5,023
Third-stage structure	556
Second-stage propellant	13,276
Second-stage structure	719
First-stage propellant	37,993
First-stage structure	1,937
Total	61,434

TECHNICAL ANALYSIS

Initial technical analysis and performance estimation has been accomplished for the LER project. The analysis work is broken into several distinct areas including mission profile, aerodynamics, propulsion, and structures and materials. A synopsis of the work performed in each area is presented.

Mission Trajectory

The LER will separate from the Boeing 747 at approximately 35,000 ft at a Mach number of 0.8 (see Fig. 2 for a complete trajectory schematic). Immediately after separation, the LER will pitch up to approximately 10° angle of attack, and the host aircraft will pitch down and execute a hard turn. The LER will coast 5-7 sec before the first stage booster ignites.

After first-stage ignition, the LER will pitch to approximately 34° flight-path angle. The first-stage burnout will be followed by a very short coast period (5-7 sec). The wing will be jettisoned with the first stage after burnout.

The second stage will ignite and burn for about one third of the total burn time of the mission. Payload fairing separation will occur during the second-stage burn period. Thrust vectoring will be used to control the attitude of the vehicle. Second-stage burnout will be followed by a long coast period.

Third-stage ignition will occur at the desired insertion altitude of approximately 250 nautical miles. The primary reason for the third stage is to boost the LER to the required velocity of 25,000 ft per sec.

Aerodynamics

The LER is a cross between a ballistic missile and an airplane. Therefore, the prediction of aerodynamic performance utilizes modern missile and aircraft theories. These two types of analysis are brought together to simulate the actual performance of the LER from launch to first-stage burnout.

In flight, the LER body will experience two primary types of drag forces. The first type of drag force is skin friction drag and is caused by air viscosity. The second type of drag force is pressure drag and is due to differences in pressure on the surface. Since the LER body is assumed to be nonlifting, induced drag is not present.

Estimation of skin friction drag is accomplished using the Blasius and Schoenherr solutions. The pressure drag is estimated using the methodology of E. R. C. Miles.

Wing analysis is conducted using the theories and prediction methods in the British Data Sheets, published by the Royal Aeronautical Society in 1957. Several assumptions are used during the analysis of wing performance. The major assumption used is flat wing theory. This assumption is justified since the wing has a low thickness-to-length ratio. Other assumptions used include a fully turbulent boundary layer over the entire wing and zero heat transfer. Mission profile considerations and the nonreusability of the structure deem such assumptions valid.

The tail analysis is greatly simplified by assuming a nonlifting tail. This assumption is considered valid for early proof-of-concept analysis. The coefficient of drag of each tail surface is equivalent to that of the wing using flat plate theory.

The total drag for the LER is determined by adding the body drag, the wing drag, the wing-induced drag, the wing wave drag, and the tail drag for each tail surface. Once this value has been determined, an extra 10% is added to include interference factors.

Propulsion

The LER utilizes three stages of solid propellant motors during ascent. The study of the propulsion system is split into two major disciplines: grain design and nozzle design.

The solid grain design for all three stages of the LER is a three-pointed star arrangement. Two types of propellant are in each motor. In the center of the motor is the propellant hydroxl-terminated polybutadiene (HTPB). This propellant burns quickly, 0.40 in/sec, and provides high thrust at ignition. Unfortunately, as the propellant burns, combustion chamber pressure increases to unacceptable levels due to the increasing burn area inside the motor. Therefore, polyurethane (PU), a slower burning propellant, is placed around the HTPB. The PU is ignited during flight as the last of the HTPB burns away. The burn rate for PU is 0.15 in/sec. This arrangement limits the chamber pressures to provide long, steady burns with a powerful ignition phase for each motor.

Conical nozzles of 18° half angles are used for each stage of the LER. This type of nozzle offers the best performance-to-cost ratio for solid propellants. Two major assumptions are utilized for the nozzle analysis: steady flow at chemical equilibrium, and frictionless, adiabatic flow. The calculated thrust values for each motor are decreased by 4% to account for the assumptions.

The material chosen for the nozzles is Udimet 500, a high-quality, high-strength steel particularly useful at extreme temperatures. The throat and portions of the converging section of the nozzles are lined with molded graphite to protect against throat erosion and excessive heat transfer. An ablative plastic coating protects the diverging portion of the nozzle from extreme temperatures.

Thrust vectoring on the second- and third-stage motors is achieved with movable nozzles. The basic design chosen for the LER is a flexible bearing design. With the use of two

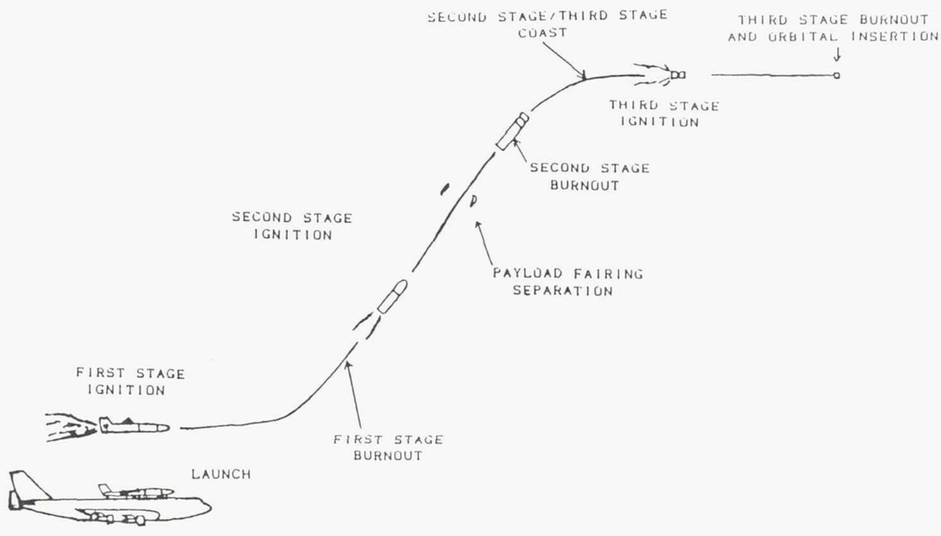

Fig. 2. LER Trajectory Schematic

actuators, each nozzle is capable of a vectoring angle of approximately 10°. Advantages of the flexible bearing design include reliable sealing around the joint and the elimination of sliding parts exposed to hot gases.

Structure and Materials

Ballistic vehicle structures require strict design requirements. Materials are required to be very strong and very light. Selecting materials to satisfy both requirements is difficult. The structure of a missile must be a container for propellant, and support loads such as those resulting from ground handling and transportation, flight conditions, staging, and thrust vectoring. Thus the design requires structural materials that can withstand high compression, shear, and bending stresses.

Materials with high specific stiffness and strength are needed for the LER. The material chosen for the motor casings is the composite Thornel-400. The composite has a large weight advantage over aluminum 7178-T76, another common material used for solid motor casing. The cost of procurement and fabrication of the Thornel-400 epoxy composite is comparable to that of aluminum. The composite casing is produced by applying a thin epoxy matrix to the Thornel-400 filament as it is wound at a 45° angle around a mold. Thornel-400 loses strength when exposed to high temperatures, so it will be necessary to thermally shield the solid rocket motor casing with a graphite-asbestos insulation.

Water damage is a major disadvantage to the use of composites. Most metals produce an oxidation layer that either protects the surface from further water damage or produces an easily noticed surface deformation. Water can seep into composites, though, without surface deformation. Thornel-400 epoxy gains very little water content if stored properly in low humidity conditions. The composite will weaken significantly as water content increases.

Large bending and shear stresses are produced by the aerodynamic loading and large accelerations of the second-stage trajectory, so it will be necessary to stiffen the structure. Aluminum box beam stiffeners will be bonded to the casing walls in order to prevent destructive bending and shear strains. The crossing of the graphite filaments at 45° will help minimize shear by giving maximum strength in the shear plane.

Honeycomb, corrugated, and waffle sandwich composite designs are being pursued for the construction of the wing and tail surfaces. These types of construction offer very high strength-to-weight ratios.

SUMMARY

The LER system developmental period is expected to take three years from the date of formal funding. Projected cost of the project is less than $60 million. The LER does not advance technology. This system uses proven, reliable technology to provide a low-cost launch service. Therefore, low system development time and cost add to profitability in fewer missions.

At present, no other system near production exists with the flexibility of mission of the LER. Initial studies have shown that the LER concept is sound. Although design work remains to be completed, trajectory studies show that the entire system works as advertised.

ACKNOWLEDGMENTS

Principal authors K. Feaux, W. Jordan, G. Killough, R. Miller, and V. Plunk were assisted by faculty advisor Dr. J.O. Nichols.

SPACE SHUTTLE II ADVANCED SPACE TRANSPORTATION SYSTEM

AUBURN UNIVERSITY

PROBLEM STATEMENT

The current Space Transportation System (STS), designed and constructed during the 1970s, faces an increasingly difficult challenge entering the 21st century. Its ability to provide safe, reliable, efficient, and economical transportation will become compromised as its operational life comes to a close. A number of disadvantages inherent in the present STS make it less than optimal as a launch vehicle for the future. These problems currently include: (1) 1970s base technology level; (2) high operational cost per launch; (3) long turnaround time; (4) low reliability level; and (5) not as safe as anticipated.

At some point, the current system will no longer be feasible from either an operational or economic standpoint. Consequently, some follow-up vehicle will be necessary to continue and redefine the role developed by the STS.

An Advanced Space Transportation System (ASTS), designed to enter service at the beginnning the 21st century, is the next logical step in the evolution of the space transportation program. Designed as a high-technology replacement to the STS, the Shuttle II offers the promise of lower operational costs and greater efficiency in manned missions and cargo deployment. Its design will take advantage of technological advances made during the past 20 years. These advantages include, but are not limited to, composite materials, automated control systems, propulsion, hypersonic aerodynamics, and the experience gained from the present STS.

INITIAL DESIGN REQUIREMENTS

Several critical factors will influence the final design configuration for the second-generation shuttle system. Because a number of features in the future system will be based on the present STS, valuable lessons gained from the current system will be incorporated into future designs. However, the potential for significant changes in mission design requirements is great. Several important design requirements are reliability, reusability, lower cost per launch, and cargo compatibility with existing systems. Other mission design considerations include a decreased turnaround time and a preprocessed payload system.

To more clearly define the requirements for designing a second-generation space transportation vehicle, NASA has established a number of ground rules to which the system must conform. First, the Shuttle II must be able to launch into the two standard orbits presently used by NASA. The first, a due-east launch from Kennedy Space Center, is a 270-nautical-mile orbit with an inclination of 28.5°. The second, a launch from Vandenberg Air Force Base, is a 150-nautical-mile orbit with an inclination of 98°. The final configuration was based on its ability to deliver payload into these two orbits.

The Advanced Space Transportation System must be fully air-transportable to be fully compatible with current NASA transportation systems used for the STS. A carrier aircraft much like the present refitted Boeing 747 would be used to deliver the Shuttle II from landing site to an operations site when needed. Also, to maximize safety and provide the greatest probability for a successful launch, the second-generation shuttle must be able to continue its mission even if one engine fails to operate during a launch. Finally, a thrust-to-weight ratio of 1.3 was established for the total configuration to insure the vehicle can be properly inserted into its orbit.

PROPOSED CONFIGURATION

To select the most practical and efficient configuration, a number of parameters governing the size, shape, and mission requirements of the system were assembled. Among the principal considerations were the extent of system reusability, burn staging and scheduling, and the type of propellant used in the system.

The general considerations were grouped into five unique variables: reusability, manned/unmanned booster, number of stages, propellant, and type of burn staging, which were then arranged in a number of ways to produce different families of configurations. These configurations therefore represented all of the possible designs that were considered. Forty-eight distinct configurations were reduced to 18 realistic, compatible configurations that were evaluated according to a set of criteria that reflected safety, performance, expense, and operating and support costs.

From the preliminary design studies, a fully-reusable system employing parallel burn from a manned orbiter and an unmanned fly-back booster were determined to be the most efficient and economically feasible arrangement for extended life cycles (see Fig. 1). It was further decided that the orbiter and booster would be designed to be as similar as possible to reduce development and production costs (see Figs. 2 and 3).

The booster and orbiter will have a common fuselage, wing, vertical tail, and avionics and control systems. They will differ in the size and number of fuel and oxidizer tanks, number and arrangement of engines, payload, and passenger compartments. Design and construction costs will be minimized by having a common structure into which components can fit corresponding to either the booster or orbiter.

A delta wing configuration was chosen for its significant advantages over conventional constant-taper wings in terms of both heat shielding during reentry and static stability. The horizontal tail may be eliminated by using a delta wing that is both swept and twisted. Furthermore, flight experience gained from the STS can be incorporated into anticipated Shuttle II wing performance. The wings on both the orbiter

PRECEDING PAGE BLANK NOT FILMED

PAGE 22 INTENTIONALLY BLANK

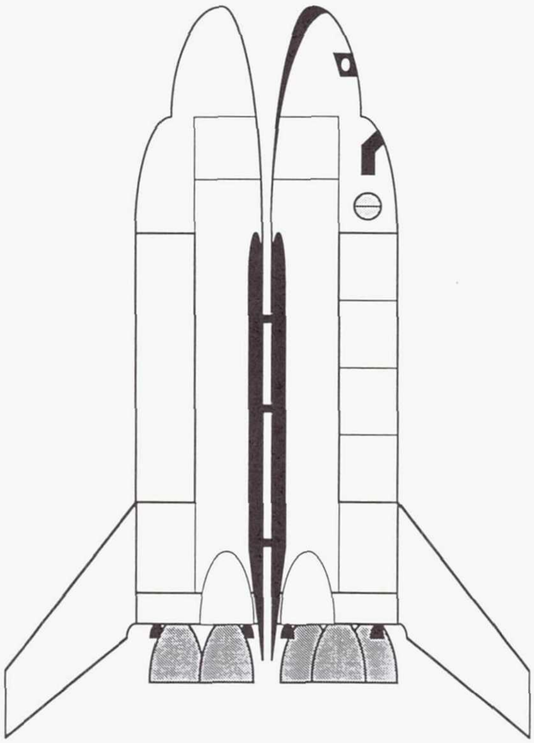

Fig. 1. ASTS Bimese Launch Configuration

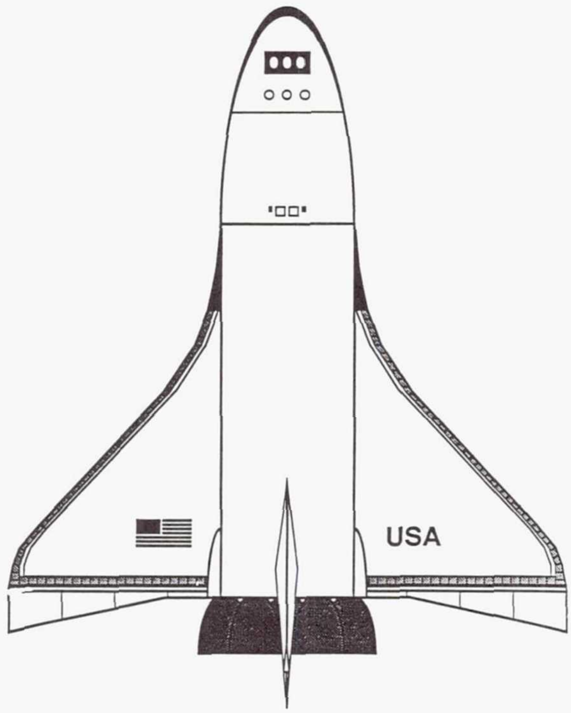

Fig. 3. Shuttle II Booster Vehicle

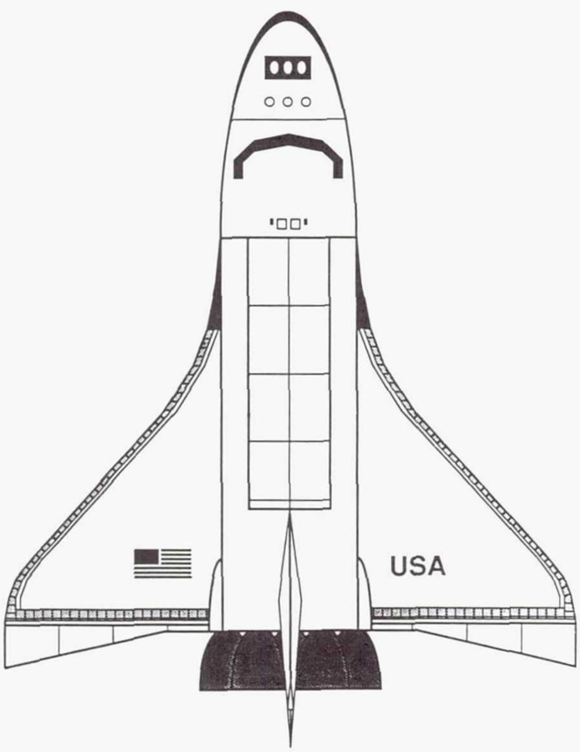

Fig. 2. Shuttle II Orbiter

and booster are similar to those used on the current STS, although they are larger to accommodate the greater weight and fuselage length of the ASTS. The wing loading does not differ significantly from that of the current shuttle orbiter.

A simple constant-taper vertical tail was chosen for both the orbiter and the booster. The only control surface incorporated into the tail is a combination rudder and speed brake. This design reduces both complexity and component weight, while not significantly impairing performance.

The first 50 ft of the fuselage constitute the forward section. The forward sections of the fuselage on the orbiter and booster are the most dissimilar parts of the two vehicles. The forward section on the booster is a shroud covering the upper section of the hydrogen tank. It is designed to be aerodynamically suitable for reentry, and it contains the avionics and control systems for the forward section. On the orbiter, the forward fuselage houses most of the complex mechanisms not related to propulsion. It contains the flight deck, crew compartment, life support systems, external access mechanism, cargo bay access mechanism, all flight avionics, forward reaction control systems, and the section of the orbiter with the heaviest thermal shielding.

The mid section constitutes the 60 ft of fuselage behind the forward fuselage. The section has a constant cross-sectional area. On the booster, it is featureless. On the orbiter, it consists exclusively of the cargo bay compartment, external doors to the cargo bay, and room for the hydrogen tanks and their

associated plumbing. The aft fuselage is the section that contains the oxygen tank and most of the plumbing for the main engines on both the booster and the orbiter. However, since the number of engines on the booster differs from that on the orbiter, the rear panel is completely different on the two vehicles.

The fuel and oxidizer tanks are the components that are most dissimilar between the booster and the orbiter. In the booster, which has a largely uniform cross-section available throughout its entire length, simple cylindrical tanks are used. In the orbiter, a more complicated arrangement is necessary to accommodate personnel and cargo. The location of the cargo bay immediately behind the flight deck and along the top of the fuselage leaves empty a large volume directly under the flight deck and cargo bay. The hydrogen tanks of the orbiter are located here to use available space most efficiently. The tanks are arranged symmetrically to insure proper weight distribution during ascent and landing maneuvers. The oxygen tank is located immediately aft of this section and just before the engine housing.

STABILITY AND CONTROL ANALYSIS

During ascent, the flight path of the ASTS can be modeled as a simple ballistic trajectory. However, during reentry and landing, both the orbiter and the booster are flown as conventional aircraft.

A stability and control analysis was performed for the ASTS in order to determine the feasibility of atmospheric flight for the proposed design. Analytical methods developed by Roskam, Etkin, and Smetana were applied to a geometrical approximation of the Shuttle II in order to obtain the necessary aerodynamic coefficients.

The proposed ASTS has demonstrated static stability. Estimates as to the weight and number of components in both the orbiter and the booster located the center of gravity sufficiently ahead of the neutral point of the configuration. This condition insures the negative pitching moment coefficient needed for static stability.

In addition to static stability, a flight vehicle should also demonstrate dynamic stability. In actuality, neither static nor dynamic stability is essential since fly-by-wire control systems can be implemented to account for any instabilities that may be present.

In order to determine the dynamic properties of a system, the equations of motion for both longitudinal and lateral motion must be written and analyzed. These equations are then transformed into matrices based on the values of key dynamic coefficients, which are, in turn, analyzed by determination of Eigen values that provide answers to the question of dynamic stability.

The Shuttle II system was modeled as a rigid aircraft with fixed controls. After determining the components of the dynamic matrices for the Shuttle II during its landing/approach sequence and determining their respective Eigen values, it was found that the Shuttle II was both longitudinally and laterally dynamically unstable. Therefore, the ASTS will implement a fly-by-wire control system.

MISSION PROFILE

The launch phase of the ASTS was subjected to the most intensive studies in order to evaluate the effectiveness of the ASTS in providing access to orbit. To this end, a launch simulation progam was written. The program approximates the performance of the ASTS with a fourth-ordered Runge-Kutta integration scheme. This simulation employed the following variables: (1) thrust variation with altitude (from STME performance study); (2) engine nozzle extensions from STMEs; (3) atmosphere variation as per 1962 Standard Atmosphere Table; (4) option for engine-out capability; (5) weight of the system as a function of time; (6) gravitational variations with altitude; and (7) pitch angle of the orbiter/booster system.

The results from this simulation were fine-tuned as part of the design process. The final estimate for the position and velocity of the ASTS at the end of the launch phase placed the orbiter at an altitude of 70.1 nautical miles in an elliptical orbit.

The NASA ground rules for the ASTS specified two orbits into which the orbiter must be able to launch. The first of these is a 270-nautical-mile circular orbit. Through the use of a minimum energy orbital transfer, the ASTS could transfer from its insertion orbit to this orbit with a total change in velocity of approximately 357 ft/sec. Using this same type of analysis, the ASTS may transfer into the polar NASA orbit (150 nautical miles) with a total change in velocity of only 61 ft/sec. Both these velocity changes fell well within the capabilities of the orbital maneuvering system. Hence, under the conditions set by the simulation, the ASTS meets the orbital insertion requirements specified by NASA.

The particulars of any given orbital mission are determined by the payload and crew carried into orbit. Missions will be designed for three-day to one-week periods, depending on their specific purposes. In general, enough provisions for 16 man-weeks will be standard on all missions. Thus, even missions that visit the space station will have the luxury of operating independently from external sources. Typical mission profiles include the launch and assembly of space station components, maintenance of and/or taking stores to the space station, performing experiments independently using the ESA Spacelab, shuttling personnel to and from the space station, launching satellites into both LEO and GEO, repair and/or retrieval of already-orbiting satellites, and rendezvous with other space facilities.

Once the orbital mission is completed, preparations must be made for reentry. The desired landing location dictates the point where the actual reentry sequence is initiated. An OMS burn, which slows the orbiter just enough to begin the reentry process, is performed and supplemented with small RCS adjustments to maintain the correct nose-up attitude as the orbiter continues on its reentry course.

At an altitude of approximately 250,000 ft, attitude control is exercised by means of the reaction control system. These adjustments will continue to be made by the RCS until at altitude of approximately 80,000 ft. From 80,000 ft until touchdown, the orbiter is controlled with the large body flap, speed brake, and elevons.

To minimize the effects of drag on the control of the orbiter, the landing gear is not deployed until the orbiter is approximately 250 ft from the ground and the wheels do not lock into place until 11 sec before touchdown. The Shuttle II touches down with a velocity of approximately 300 ft/sec.

Accurate guidance to the landing site is currently provided by a microwave scanning beam landing system that sends the necessary signals so that the orbiter can make the required adjustments on descent.

CONCLUSION

A time line for the proposed ASTS fleet of 6 orbiters indicates that the program will ultimately span a time frame of approximately 30 years. In this time, each of the six orbiters will be constructed, tested, and put into service. Initial cost estimates for this program indicate an initial total price of $22 billion (based on constant 1992 dollars). This cost estimate includes savings arising from the use of preexisting shuttle technology and facilities. The total operational cost per launch for the ASTS is estimated to be significantly less than that of the current STS. These savings coupled with the technological advances made during the past 20 years will enable the ASTS to provide a space transportation vehicle for the coming century.

ACKNOWLEDGMENTS

Principal authors J.N. Adinaro, P.A. Benefield, S.D. Johnson, and L.K. Knight were assisted by faculty advisor Dr. J.O. Nichols.

PRELIMINARY DESIGN OF A SHUTTLE-C AVIONICS RECOVERY SYSTEM

AUBURN UNIVERSITY

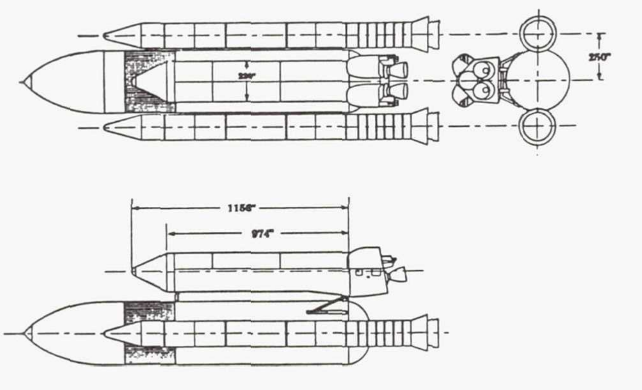

Fig. 1. Shuttle-C System

INTRODUCTION

The Cargo Shuttle or Shuttle-C is being designed as the next phase of the National Space Transportation System or NSTS (Fig. 1). This vehicle is designed to fill the gap between the space shuttle and heavy lift vehicles currently being developed.

Shuttle-C will consist of a space shuttle external tank and solid rocket boosters, as well as an expendable cargo vehicle that is a hybrid of the current orbiter. The cargo vehicle will be unmanned and will consist of a boattail that contains the propulsive systems, a cargo-carrying component, and a nose cone to house any necessary avionics. Large savings in cost and development time will be realized since the boattail and avionics are nearly identical to that of the current shuttle orbiter. In addition, the cargo carrying component is similar in structure to the body of the current orbiter with the wings removed.

The main objectives of the Shuttle-C program are to produce a vehicle quickly and cheaply that is capable of placing 100,000+ lb into low Earth orbit. To help fulfill this goal, the recovery of various portions of the Shuttle-C vehicle were studied. The design that was determined to be most economical and that best fit NASA's specifications was the recovery of the Shuttle-C avionics by using a reentry vehicle and an assortment of parachute decelerator systems (Fig. 2). As seen in the figure, this vehicle will comprise a reentry vehicle that forms the nose of the Shuttle-C cargo vehicle, an avionics module that separates from the recovery vehicle, and a parachute system for recovery of the avionics module.

A summary of the design of this recovery system is presented in the following sections. Specific areas addressed are:

1. Analysis of the loads and heating rates encountered by the conical reentry vehicle and optimization of reentry parameters to minimize these loads.
2. Design of an ablative thermal protection system to protect the reentry vehicle and its contents during reentry.
3. Design of the internal structure of the conical reentry vehicle to withstand reentry forces.
4. Design of a three-stage parachute system to guide the avionics package to a landing at Edwards Air Force Base.
5. Design of a module to house the avionics and guidance system.
6. Ability of the Shuttle-C with modifications for recovering the avionics to meet mission and payload specifications as dictated by NASA.

This design will reduce the cost of the Shuttle-C program by allowing the recovery of the avionics. It is estimated that the space shuttle avionics cost $150 million a copy. Recovering a portion of this cost will make the Shuttle-C program more economical.

REENTRY ANALYSIS

An important aspect in the design of the Shuttle-C avionics recovery system was the determination of the loads and heating transfer encountered during reentry. These factors defined the parameters necessary for the design of the heat shield and structure of the reentry vehicle.

The reentry vehicle will enter the atmosphere with the base of the conic toward the freestream flow since data about this type of reentry are readily available. Two reentry modes were studied. The first was a ballistic reentry with a lift-to-drag ratio (L/D) equal to zero. The second was a reentry with L/D in the range of 0.25 to 1.00. Of these two reentry modes, reentry with an L/D in the range of 0.25 to 1.00 was chosen.

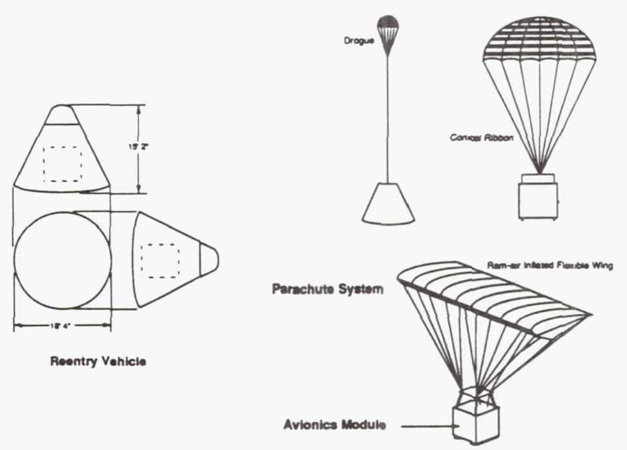

Fig. 2. Avionics recovery system for Shuttle-C. System includes reentry vehicle, avionics module, and parachute system.

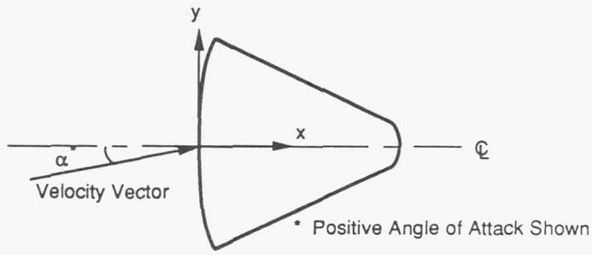

Fig. 3. Angle of Attack of Reentry Vehicle

Table 1. Reentry Parameters for Shuttle-C Avionics Recovery System

Initial flight path angle	3.000 deg
Lift/drag ratio (L/D)	0.250
Angle of attack	-14.000 deg
Maximum deceleration	4.000 g
Flight path angle at max deceleration	0.603 deg
Altitude density at max deceleration	0.0002869 slugs/ft^3
Maximum heat flow rate	4.040 Btu/s$\cdot$ft^2
Flight path angle at max heat flow rate	0.840 deg
Total heat	274,679.000 Btu

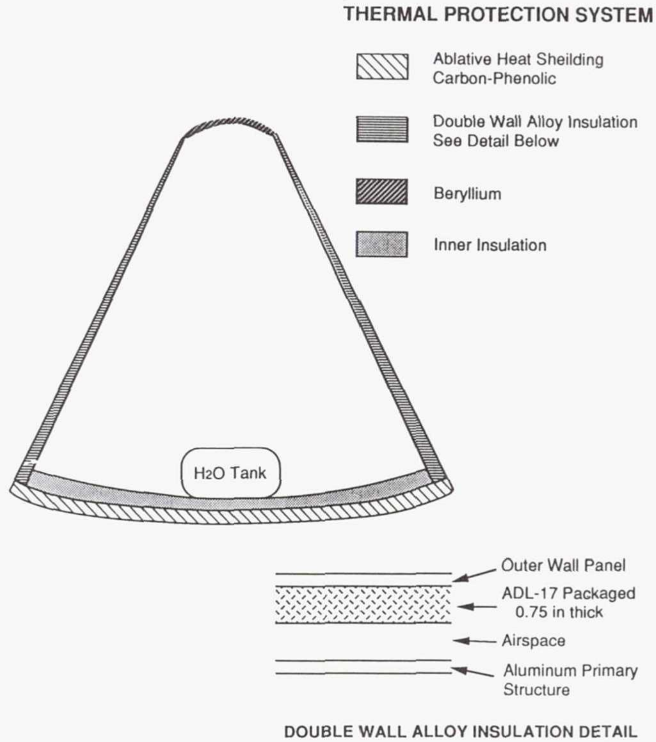

Fig. 4. Thermal Protection System

There are two primary reasons for this choice. The most important is that reentering with L/D in the range of 0.25 to 1.00 limits the maximum deceleration force to the range of 3 to 32 *g*, dependent on the initial flight path angle. For ballistic reentry maximum deceleration force would fall in the range of 14 to 161 *g*. Limiting the load on the reentry vehicle is desirable because a stronger, heavier vehicle would be required to survive a high *g* reentry.

Heat transfer was also considered when selecting the reentry mode. It is interesting to note that although entering at an L/D in the range of 0.25 to 1.00 limits the *g* loading on the reentry vehicle, it does not have a dramatic effect on the total heat or maximum heating rate of the vehicle if L/D is kept small. For this reason, an L/D of 0.25 was selected. To achieve this L/D, an angle of atack of -14° must be maintained. Angle of attack is measured from the centerline of the reentry vehicle as shown in Fig. 3. Other pertinent reentry parameters are given in Table 1. The reentry selected was deemed the best because it limited the *g* loading allowing for a lighter reentry vehicle without causing an unreasonable amount of heat flow.

THERMAL PROTECTION SYSTEM

The thermal protection system for the Shuttle-C avionics recovery system is divided into two basic parts. The first is the ablative heat shield that covers the base of the reentry vehicle and absorbs/dissipates the majority of the heating experienced during reentry. An ablative heat shield is an effective protection system for low lift reentry. The second is the secondary heat shield that covers the sides and the tip of the reentry vehicle. Figure 4 shows a detail of the heat shield.

For the ablative heat shield, carbon phenolic was chosen. Carbon phenolic has low thermal conductivity and leaves an insulating char layer as it burns away. These two characteristics make it desirable as a heat shield. It was determined that the base of the reentry vehicle should be covered with an average thickness of 0.32 in to withstand reentry conditions. Carbon phenolic has a density of approximately 0.085 lbm/in^3, and the base of the reentry vehicle is approximately 37,000 in^2. This results in an ablative heat shield weighing approximately 1000 lb.

The secondary heat shield is divided into two sections. The lower secondary heat shield covers the sides of the reentry vehicle. The upper secondary heat shield covers the tip of the reentry vehicle. The lower secondary heat shield is composed of a double wall alloy insulation. Figure 4 shows a detail of this system. The double wall alloy consists of a 0.0320-in outer wall of an alloy of coated molybdenum, 0.75 in of ADL-17 packaged powder, 0.75 in airspace, and the aluminum primary structure. In addition, this system is cooled by a circulating water system. The lower secondary heat shield has the ability to keep the inner structure of the reentry vehicle at or below 200°F.

The upper secondary heat shield is made of beryllium and utilizes the same water coolant system as the lower secondary heat shield. The upper secondary heat shield was designed from a different material than the lower secondary heat shield to save weight. Beryllium's density is approximately one sixth

that of molybdenum. This results in a weight savings in the upper secondary shield of approximately 630 lb. Beryllium was determined to be adequate for protecting the nose of the reentry vehicle since the temperature reached by this portion of the vehicle is only about 1200°F, or approximately one-half the 2300°F melting point of beryllium. Total weight of the secondary heat shield is 2727.4 lb. The lower secondary heat shield weighs approximately 2000.0 lb. The upper secondary heat shield weighs 154.4 lb. The water coolant system, including a holding tank for the water, weighs 573.0 lb.

REENTRY VEHICLE STRUCTURAL DESIGN

The design of the internal structure of the reentry vehicle is based upon a previous design used by the Apollo capsule. Since the Shuttle-C reentry vehicle is much larger than the Apollo capsule it contains more internal formers and bulkheads.

An example of the structural design is presented in Fig. 5. Shown in this figure is a section through the base of the reentry vehicle and a side view of the reentry vehicle. The spoked distribution of the formers is easily seen in the base view.

Sizing of the main formers in the reentry vehicle was accomplished through the plastic hinge method. This method determines ultimate moment by predicting the failure mechanism of the structure.

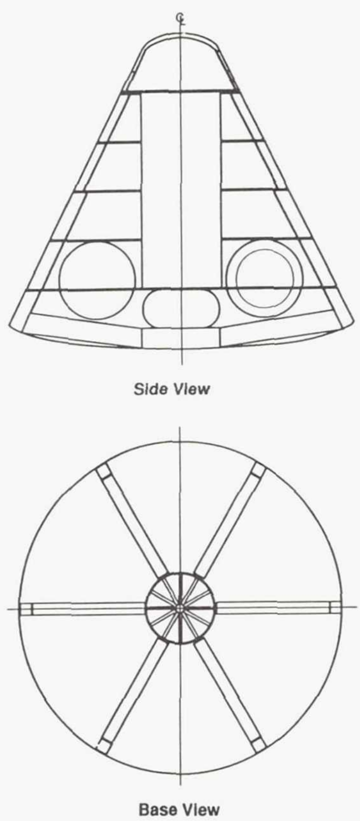

Fig. 5. Partial Structural Design—Slide View and Base Section

All structural materials in the reentry vehicle are made of aluminum alloy 7178-T6. This material was chosen because it has a high ultimate strength and is commonly used in the aircraft industry, thus making it readily available.

The total weight of the reentry vehicle's structure is approximately 2615 lb. The base plate and bulkheads comprise appoximately 1900 lb, the formers comprise another 360 lb, and the remaining 350 lb is used for miscellaneous parts.

THREE-STAGE PARACHUTE SYSTEM DESIGN

The final job of the Shuttle-C avionics recovery system after entry into the atmosphere is to provide a safe, self-reliant landing of the avionics module. This is accomplished through the use of a three-stage parachute system (Fig. 2).

The three-stage system is as follows: (1) mortar deployed ribbon hemisflow drogue; (2) conical ribbon; and (3) ram-air inflated flexible wing.

The first stage, the mortar deployed ribbon hemisflow drogue, is deployed at approxiamtely 65,000 ft. The main purpose of this parachute is to stabilize the capsule and to slow the speed of the capsule to below Mach one. The 6 ft drogue is made of 16 gores of high-tension nylon webbing, and is attached to the avionics module by a 180-ft bridle made of coreless braided nylon. The total weight of the drogue is 45 lb and the pack volume is 1.89 ft^3.

The second stage is the conical ribbon. This parachute is deployed at approximately 45,000 ft. During deployment of the conical ribbon, the avionics module is extracted from the reentry vehicle. The main purpose of removing the avionics module from the reentry vehicle is to reduce the landing weight, thereby reducing the size of the final stage parachute. The conical ribbon slows the descent of the avionics module to 135 ft/sec. The conical ribbon chute is 12 ft in diameter and is made of 16 gores of high tension nylon ribbon. The total weight of the conical ribbon parachute is 90 lb and the pack volume is 2.69 ft^3.

The third and final stage of the parachute system is a ram-air inflated flexible wing. This parachute was chosen for the final stage due to its high glide ratio and its ability to be maneuvered for pinpoint landings.

The ram-air flexible wing consists of a top and bottom skin separated by vertical cell dividers or ribs. At the rear of the decelerator, the top and bottom skins are sewn together. Air entering the front of the ram-air flexible wing pressurizes the inside of the parachute causing it to take the shape of an airfoil. The ram-air flexible wing then acts much the same way as a wing and generates lift.

The ram-air flexible wing in the Shuttle-C recovery system is activated at approximately 40,000 ft when it is extracted by the second-stage conical ribbon parachute. A guidance, navigation, and control system inside the avionics module controls the descent and glide path of the module until it is within visual range of the landing site. At this point, the avionics module is guided to a low vertical velocity landing by remote control.

The ram-air inflated flexible wing proposed for the Shuttle-C avionics recovery system measures approximately 87 ft by

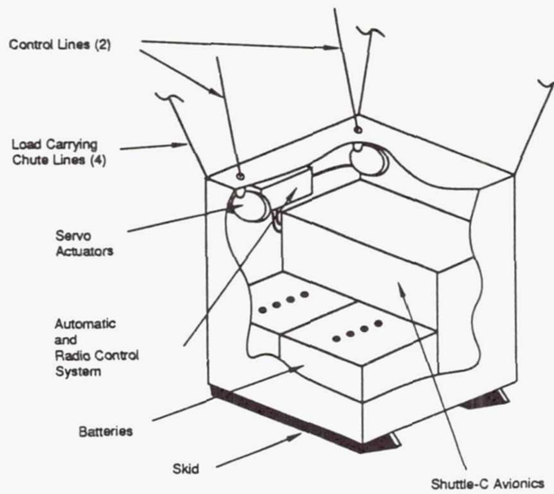

Fig. 6. Design Conception for Avionics Module

28 ft. It has a lift-to-drag ratio of 3.5:1. The ram-air flexible wing is made of Harris F-111 low-porosity nylon and has a weight and pack volume of 100 lb and 2.89 ft^3 respectively.

AVIONICS MODULE DESIGN

The primary purpose of the avionics module is to contain the avionics and cushion the landing so that the avionics can be reused for a future mission. Figure 6 shows a design conception for the avionics module.

The avionics module measures 5 ft tall by 4 ft square. It contains the shuttle avionics, a radio control, and an automatic guidance system, servo actuators for controlling the flexible wing, and four batteries for power. On the bottom are a pair of shock-absorbing skids to help absorb the forces encountered during landing. Projected total weight for the avionics module is 2150 lb.

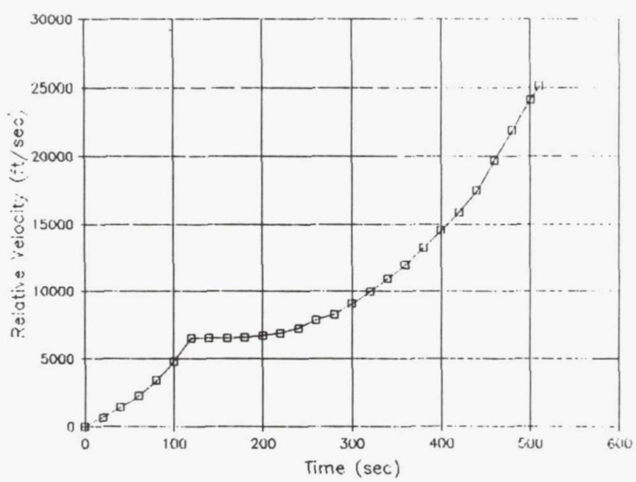

Fig. 7. Shuttle-C ascent velocity as a function of time. Final velocity at end of SSME burn is necessary orbital velocity.

CONFORMANCE OF AVIONICS RECOVERY SYSTEM WITH NASA SHUTTLE-C GUIDELINES

There are two primary guidelines for Shuttle-C presented by NASA in the Shuttle-C Design Data Book. These guidelines are the ability to achieve an early launch date by using existing technologies, NSTS components, and NSTS launch facilities, and the ability to lift a minimum of 100,000 lb to a 220-nautical-mile, 28.5° circular orbit. The addition of an avionics recovery system to the Shuttle-C can be shown to conform to these requirements.

The first requirement was satisfied by using only proven technology in the avionics recovery system. Examples of this are as follows: (1) The heat shielding system has been used on other space reentry vehicles—all manned space vehicles prior to the space shuttle used ablative heat shields; (2) reaction and control systems are the same as those utilized on the space shuttle; and (3) ram-air parachutes have been previously used for military payloads dropped from airplanes.

Although the design of a recovery system will take longer than designing a completely expendable vehicle, the use of proven technology should keep this design time to a minimum. In addition, an avionics recovery system can be developed in parallel with a fully expendable vehicle and implemented after the start of the Shuttle-C program.

By using dynamic equations, it can be shown that the second condition, a 100,000-lb lift capability, is met. For insertion into a 220-nautical-mile circular orbit, a velocity of 25,146.023 ft/s must be reached. Figure 7 is a graph of the velocity as a function of time. It can be seen from this figure that the Shuttle-C can easily reach insertion velocity. Calculations indicate that by using two solid rocket boosters and three space shuttle main engines, a lift capability of 150,000 lb can be achieved, well above that specified by NASA.

CONCLUSION

It has been shown that the recovery of the avionics from a Shuttle-C vehicle is consistent with NASA's guidelines for development of this vehicle. Although a Shuttle-C vehicle with an avionics recovery system will have an initial cost of development greater than that of a fully expendable Shuttle-C, this development cost will be returned quickly through the saving of the avionics package.

ACKNOWLEDGMENTS

Principal authors M. Brookfield, D. Decker, H. Gilbert, D. Moore, and M. Rist were assisted by faculty advisor Dr. J.O. Nichols.

PROPOSAL FOR A ZERO-GRAVITY TOILET FACILITY FOR THE SPACE STATION

AUBURN UNIVERSITY

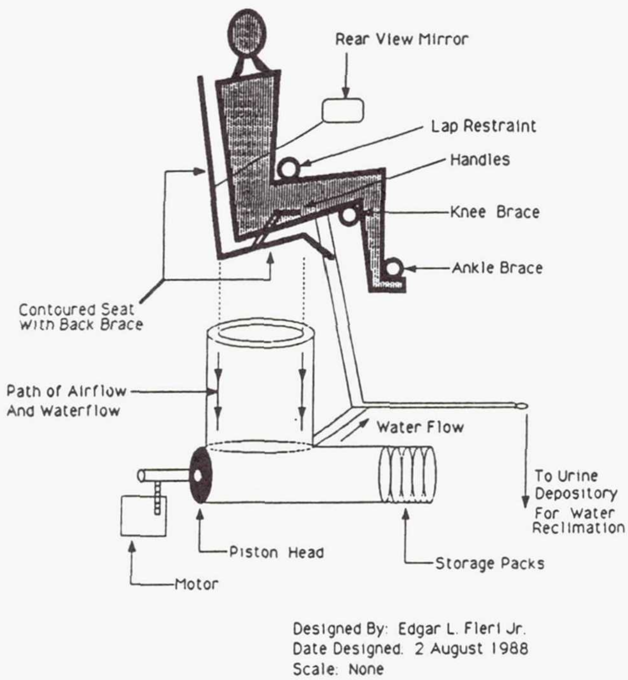

Fig. 1. Proposed Toilet Facility

INTRODUCTION

This proposed toilet facility (see Fig. 1) has a straightforward design. It has few moving parts and is easily maintained. Air and water flow provide sanitary movement of the waste. The toilet's chambers are coated with teflon that, along with the water flow, makes it self-cleaning. An added disinfectant called betadiene kills any bacteria that may form on the chamber walls. The chair is contoured to take into account the neutral body position and the necessary strain position for defecation. Restraints at the ankles, knees, and midsection hold the body in the chair. The waste is stored in disks of Gortex material that are inside a replaceable storage chamber. This chamber can be removed, capped, and stored until eventual return to Earth.

AIRFLOW

Since the space station operates in a microgravity environment, a force is needed to replace the role gravity serves in defecation. A moving airflow will provide this force (see Fig. 2).

There are two "vents" for the air to enter the fecal chamber. The details of the vents are further explained in the disposal and storage section and the corresponding figures. This air comes from the ambient air in the toilet compartment. The air is pumped by a fan that is powered by a brushless motor. After the air is exhausted from the storage chamber, it is channelled through a charcoal filter and out into the ambient space station air.

The primary vent directs air towards the base of the seat. This provides the necesssary excrement force. A secondary vent provides a directed airflow to help move the water flow. A sheet of air will be aimed almost parallel to the water flow. This will aid in keeping the water against the sides of the chamber.

The air is exhausted through three vents at the head of the storage chamber; these vents are equally spaced around the circumference of the chamber. Manifolds, sealed by silicone rubber gaskets, will be attached to the outside of the vents to provide the airflow. They will be attached by latches, allowing them to be removed easily when the chamber is full. The vents are each 9 in long by 1 in wide and are formed of a taut layer of Gortex heat-sealed to a rigid plastic screen. This will assure that no liquid can pass through the air vent. The tension in the material will prevent the squeegee on the disk from tearing the material. Since these vents are a part of the storage chamber, they are removed when the chamber is full. A cap that covers the entire head of the storage chamber,

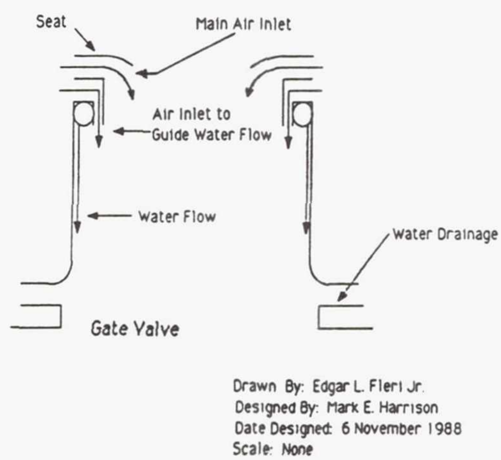

Fig. 2. Air and Water Flow Arrangement

including the vents, will be placed on the chamber preventing any possible biohazard.

WATER FLOW

This facility is unique in that it is self-cleaning. The major innovation is a dynamic water layer along the sides of the fecal chamber.

The space stations water supply will provide the water necessary to operate the toilet. Utility runs are located in the station's module. The amount of water used is not of paramount concern since the space station recycles used water. Even if it were a concern, the toilet only uses about two gallons a day.

The water will be injected at the head of the fecal chamber by an annular pipe. In the absence of gravity, surface tension will be the primary force acting on the layer of water and will keep the flow attached to the sides of the chamber. The airflow will drive the water down the length of the fecal chamber. Just above the gate valve, which separates the fecal chamber and the settling chamber, the water will be drawn off through a slot.

The sheet of water will be assumed to be $\frac{1}{16}$ in thick and travel down the fecal chamber at approximately 3 in/sec. This determines a flow rate for the water at 3.5 cu in/sec. To ensure proper drainage of the water, the drain slot will be $\frac{1}{8}$ in wide, and will turn the water by means of a curved surface to insure that the water continues to cling to the fecal chamber and does not separate and go down into the settling chamber. The fecal chamber widens below the slot to help prevent interference with waste transmission. The toilet will use approximately 0.9 gal of water per min. This should not be a major problem since the space station will recycle water.

For the normal flush mode, the water will run in the toilet for 5 sec, then the water flow will be diverted to the urinal for 5 sec. Once the water stops flowing, the air will continue to run for an additional 5 sec to guarantee that the water does not escape. When the air stops flowing, the gate valve will be closed. This will signal the piston to begin. The air will continue to flow in the urinal for the duration of the piston action. When the piston is fully retracted, all flows cease.

In the event of diarrhea, the water will be continuously flowing because it is needed for sanitation. A 5-min use of the facility will use approximately 4.5 gal of water. Given a 0.5% loss, this would come to approximately 3 oz. Any loss during the process will be driven down into the storage chamber. Since the Gortex is waterproof, this will not be a problem.

A single button will operate the normal flush mode. This will be connected to an electronic switching unit that will actually control the valves. A switch will be used to select the desired mode (Normal or Diarrhea). In the event that safety considerations preclude the use of the electronic switch, a mechanical system could be designed. Such a system would use a knob that would activate a timer. The knob could be locked into place for the diarrhea mode.

URINAL

A urinal for a microgravity environment is a simple device. It consists of a funnel at the end of a suction tube. However, there are several drawbacks to this type of system:

1. The best funnel design for the male is a conical funnel 3 inches long and $2\frac{1}{8}$ in in diameter, while the most favorable funnel for the female is an oval shape.
2. Air entrainment for the male urinal is directly through the open end of the funnel. In contrast, since female urination is less directed, the female funnel should use angled air openings to give a vortex action to the airflow.
3. Since female and male astronauts must have different funnel designs due to anatomical considerations, each crew member must have an individual funnel for hygiene reasons. These individual funnels must be connected to the suction tube before use, and after use they must be removed and cleaned out before being stored. This system has obvious drawbacks, primarily inconvenience and awkwardness.

The best solution is to optimize a design that can be used by both men and women with equal effectiveness: an egg-shaped funnel three inches deep. It will seal effectively against the female anatomy where angled air outlets will provide the necessary vortex flow. For male use, the funnel is moved forward and up along a track. Each crew member can optimally position the funnel. During male use, the urinal will not seal against the body and will allow air to enter along the sides of the funnel.

To provide adequate hygiene, the lip of the funnel will have an annular tube to inject a water and disinfectant mixture to clean the funnel. This arrangement is similar to that of the fecal chamber, but the urinal will require a flow rate of only 0.37 gal/min. During the flush process the water would be shut off to the fecal chamber and started in the urinal. This allows the possible use of a simple valve between the water line leading to the fecal chamber and the water line leading to the urinal.

DISPOSAL AND STORAGE

A disposal system has been adopted that uses preformed disks. These are plastic rings 0.233 in thick, with an outer diameter of 10 in and an inner diameter of 9.5 in with a Gortex sheet in the center of the ring. The rings will be manufactured in two pieces, the male coupler and the female coupler. The Gortex sheet will be heat sealed between the two, embedding it within the ring. The Gortex will have adequate slack to allow for large or odd-shaped waste products. The size of the storage disk is based on the waste volume criterion per person for a 24-hr period. Thus, an average use of once or twice per day ensures that the capacity is not exceeded. Also taken into consideration were vomitus and diarrhea. Since their volumes tend to be larger than that of a normal defecation, a special disk will be developed that is three times the thickness of the normal disk. Gortex is a breathable liquid-proof material used in the production of parachutes, waterproof clothing, and sleeping bags. The ring itself is made of rigid plastic.

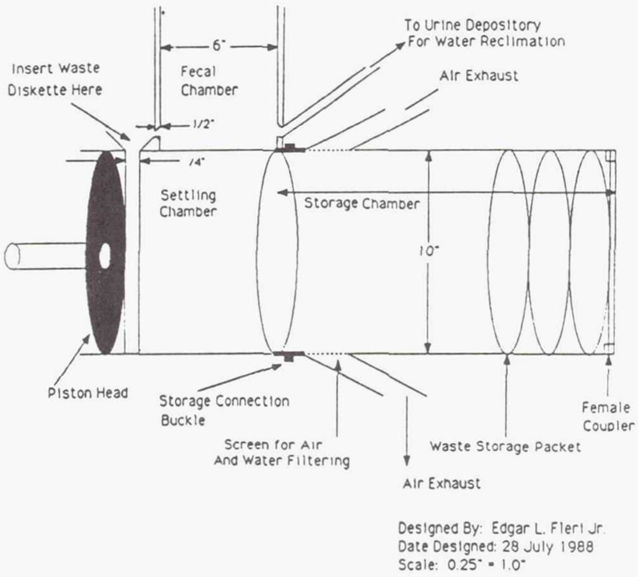

Fig. 3. Piston Arrangement

Each time the facility is used, one of these disks is manually placed in a slot behind the settling chamber (see Fig. 3). The piston pushes the disk into the storage chamber while the outer edge of each disk scrapes the cylinder walls for cleaning purposes. Each disk locks onto the previous one. These disks will be stored in a dispenser next to the facility. The last Gortex disk will be reinforced with a rigid plastic to prevent accidental tearing of the Gortex when the chamber is removed. An explosion-proof, alternating-current, 1-hp Baldor motor will be used to drive the piston. The motor will run on a 210-V line supplied by the space station in the utility runs. The motor will have no arcing, will be permanently lubricated, and will have casing on the wires. Any paint used on motor parts will be nontoxic. A motor will also be used for the air pump. It is specially designed with no brushes so that no sparks are emitted, and it is fail-safe.

A start switch on the side of the toilet activates the motor. The motor drives the piston by using a telescoping screw with three 12-in-long shafts contained within each other. A governor will sense the applied force. The basic idea of the motor is similar to that of a trash compactor; it will be reversible. At first the motor pushes the piston. When the governor switch senses a certain amount of resistance, the motor will shut off and reverse, retracting the piston.

The storage chamber is attached to the settling chamber so the disks can move in a flush fashion through both tubes. It has a seal between the two chambers and locks into place by a set of three latches similar to those on a tool box. Latches are used because they can be handled with only one hand and easily manipulated in space unlike a screw or a wrench. Once the storage chamber is full (i.e., when the precounted disks reach the end of the supply) removal procedures can begin. The space station rack can be rotated away for servicing allowing easy removal of the storage chamber. The user then unlatches the storage chamber and places a cover onto it. The cover latches to the storage chamber in the same fashion.

The cover will allow the free flow of air through a charcoal filter that will vent any decomposition gases such as methane into the logistic module's ambient atmosphere. The charcoal filter will insure that there is no odor problem, while the space station's air recycling system will remove the methane to prevent any hazard. Bacteria buildup is not perceived to be a problem since studies by Hamilton Standard showed no significant buildup for a 90-day period. The Hamilton Standard study used feces stored in a Gortex bag.

GATE VALVE

Between the fecal and storage chambers is a sliding assembly called a gate valve. This valve is basically two of the interfaces between the 7-in-diameter fecal chamber and the perpendicularly mounted 11-in settling chamber joined together. One of the interfaces has a 6.25-in diameter opening between the two chambers. This is used during defecation. The other interface has no opening. This seals the chamber and allows for smooth passage of the piston during its operation. The two connected interfaces slide along a rail from the opened to closed positions. When the toilet is not in use, the valve is kept in the closed position to prevent odors from escaping. When the assembly is closed, the "defecation interface" protrudes from the front of the toilet, allowing for easy cleaning.

ANTHROPOMETRICS

The absence of gravity in space on the space shuttle or space station creates a unique seating problem for defecation. Effective anthropometrics must be used to overcome this problem. Comfort, ease of use, and design simplicity are the three main parameters that were considered during the anthropometric design process.

In the zero-*g* environment the body assumes a position known as the neutral body position. This is the position that the human body will naturally tend to return to when displaced. Although the neutral body position puts the least strain on the stomach muscles in zero-*g*, this position is not conducive to the defecation process. The optimal position for defecation is a squatting or seated position that increases abdominal pressure. To overcome the body's natural tendency to remain in the neutral body position, several restraints are used to place the astronaut in the best position for defecation without straining the abdominal muscles.

Application of logical designs with applied concepts was used to narrow the choice of options. The current ideas were checked with earlier applied designs. The restraining system consists of a combination of handles, foot and lap restraints, and knee and ankle braces. The construction of these devices is based upon the construction principles of athletic

conditioning equipment (i.e., Nautilus) that similarly require support and restraint to maintain body positioning while in use. Utilization of these principles accounts for the simplicity of design and ease of use.

The restraint primarily responsible for holding the astronaut down on the seat is the lap restraint. Its design is very simple and straightforward. It consists of a curved lightweight bar hinged at one end with a nylon strap attached as shown in Fig. 1. The unhinged end is pulled down and secured with a latch positioning the nylon strap across the astronaut's pelvic girdle above the groin area where the urinal is positioned. This type of restraint already exists and is in use on amusement park rides. This restraint was chosen over the roller coaster lap restraint because it does not interfere with the use of the urinal. The restraint is very effective because it is comfortable and secure under the action of several negative *g*s and is therefore more than adequate for use in zero-*g*. The second major source of restraint is the combination of the knee and ankle brace. The knee brace acts in combination with both the lap restraint and ankle brace to provide support and position the buttocks for proper contact with the toilet seat. The knee brace is adjustable in the vertical position to accommodate persons of varying stature. The ankle brace is attached to the knee brace by a friction lock, which keeps the ankle brace locked down to keep the feet from floating up. This also helps to maintain proper contact with the seat.

The foot restraints and handles act as auxiliary restraints for the system. The foot restraints are used to aid in entering and exiting the facility. They are the main source of restraint during the clean-up period. The handles are used to enter and exit the facility as well as to position oneself when locking down the primary restraints.

The final anthropometric consideration is the seat itself. The backrest is contoured to fit the average person while the seat is a unique design. The seat consists of a doughnut-shaped ring partially filled with fluid. The density of the fluid inside the ring is such that when a person sits on it the buttocks will force the fluid forward to the groin region to assist in forming a tight seal with the toilet. This feature is advantageous for both males and females.

ACKNOWLEDGMENTS

Principal authors E.J. Fleri, Jr., P.A. Galliano, M.E. Harrison, W.B. Johnson, and G.J. Meyer were assisted by faculty advisor Dr. J.O. Nichols.

N94- 71270

1994004515
382669
53-18
160629
p. 8

SPACE STATION TETHERED ELEVATOR SYSTEM

UNIVERSITY OF CENTRAL FLORIDA

The optimized conceptual engineering design of a space station tethered elevator is presented. The tethered elevator is an unmanned, mobile structure which operates on a ten-kilometer tether spanning the distance between Space Station *Freedom* and a platform. Its capabilities include providing access to residual gravity levels, remote servicing, and transportation to any point along a tether. The report discusses the potential uses, parameters, and evolution of the spacecraft design. Emphasis is placed on the elevator's structural configuration and three major subsystem designs. First, the design of elevator robotics used to aid in elevator operations and tethered experimentation is presented. Second, the design of drive mechanisms used to propel the vehicle is discussed. Third, the design of an onboard self-sufficient power generation and transmission system is addressed.

INTRODUCTION

For years, America's journey into space has demonstrated the benefits associated with working in the unique environment of microgravity. Continuing in this tradition, man will soon launch an ambitious and far-reaching program to further the advancement of space technology. With the advent of Space Station *Freedom,* the United States will enter an era marked by a permanent presence in space. Moreover, the Space Station *Freedom* will allow continuous rather than intermittent operations to be conducted in orbit. The Station will open new doors to many new methods of research and experimentation. Furthermore, man will better explore the Earth on which we live and the solar system of which we are a part.

A permanent presence in space will allow a multitude of new and varied technologies to evolve. One of the technologies currently being developed is tether technology. The idea of tethers in space dates back to the mid 1800's. Now, as the idea is reaching technical maturity, tethers in space will be used in innovative ways for many applications. The objective of this report is to present an optimized spacecraft design that will complement the use of tethers in space, namely, the tethered elevator.

The Space Station Tethered Elevator has several uses. An elevator can serve as a remote laboratory platform, a transport system, or a service vehicle. This multifunctional capability will allow scientists to tap resources and environments which at the present time are inaccessible. Additionally, an elevator will provide basic elements needed to further explore the operating environments of both the Space Shuttle and Space Station.

Use of the elevator as a remote laboratory to access and control the gravity acceleration level is one of the most promising features offered by the system. By precisely positioning the elevator near the center of gravity (c.g.) on a tether system of fixed length, a minimum gravity acceleration level of $10^{-8}g$ could be attained[1]. Scientists can utilize this residual gravity level and clean environment provided by the elevator to perform highly sensitive experiments.

The elevator can function as an exchange vehicle between the Space Station and a tethered mass. In this role, the transporter will be used to deliver payloads from a shuttle to the Space Station. This allows an Orbiter to dock with a tethered mass at some distance from the station, thus saving fuel and increasing payload capacity. For example, the elevator could transport substances such as refuse requiring orbital deboosting[1]. This would be accomplished by lowering the elevator along the tether to a predesignated position and then releasing the transported item. Decreasing the tethered mass has the advantage of transferring momentum to the Space Station and boosting its orbit, with no expenditure of fuel[2].

Lastly, the potential for the elevator as a remote servicing vehicle exists. If repairs were needed on a tethered mass such as a spacecraft or satellite, the elevator could be deployed to provide assistance. The provision of robotics on board the elevator would enable manipulation of various articles such as mechanical and electrical umbilicals and orbital replacement units (ORUs).

DESIGN CONSIDERATIONS

Tether technology has not been fully tested in a space environment. The planned Tethered Satellite System (TSS) missions will be valuable in determining elevator feasibility. Moreover, a TSS flight will be significant as a means of validating mathematical models and describing the dynamics, control, and key design factors for a tethered system and its components[1]. Here, general design considerations for one of these components, the tethered elevator, are presented.

Dynamic disturbances induced by elevator motion are primary design issues. If uncontrolled, adverse effects to the acceleration environment of the Station or a tethered object may result. These disturbances may act laterally or longitudinally with respect to a tether. Lateral vibrations are induced by the Coriolis force acting on the elevator as it moves along the tether. The Coriolis force, depending on the magnitude of the elevator's velocity, is as controllable as the velocity is small[1]. Longitudinal modes of vibration act on a line through the tether axis. These vibrations are due to control forces exerted from the elevator to the tether while accelerating and decelerating. The longitudinal modes have short periods in the axial direction and should be easiest to control[1]. The overriding consideration is the elevator's velocity. To minimize Coriolis effects, the velocity of the elevator will be constant, not greater than 5 m/s, and compatible with required mission time.

In addition to control forces induced by elevator motion, the directional gravity acceleration along the tether will act on a line through the elevator's center of mass (c.m.). This gravity acceleration level can range from 10^{-8}g at the c.g. of the tethered system to as high as 10^{-3} at a tethered body[3]. The combination of drive and gravity acceleration forces could induce moments on the elevator causing additional longitudinal vibration in the tether. It is important to note that drive forces, however small, will always contribute to disturbances acting longitudinally, but moments created by an offset c.m. can be controlled by the elevator design.

Consideration of elevator mass is crucial to the elevator design. Cost, stability, and tether life are influenced by elevator mass. Minimizing elevator mass is advantageous for the following reasons: (1) Launch costs are great and increase with increases in payload mass; (2) mass moments of inertia about a tether are minimized; and (3) tether life is preserved because drive forces and frictional effects applied to a tether are minimized.

Once the mass of the elevator is determined, the acceleration of the elevator is limited by the tension in the tether. For example, an elevator mass of 10,000 kg, mounted on a ten-kilometer tether, will be limited to a maximum acceleration of 0.17 m/s^2. This acceleration dictates an 11.76 second rise time to a constant velocity of 2 m/s. If an acceleration greater than 0.17 m/s^2 were permitted, either slippage or kinking of the tether would occur. Moreover, the axial force subjected to the tether by an elevator drive mechanism would be greater than the maximum allowable force of the tether. The product of the elevator mass and the acceleration of the elevator is limited by tether tension.

An area requiring critical analysis is the hooking/unhooking operation of the elevator by means of an Orbiter's Remote Manipulator System (RMS)[4]. The driver mechanism(s) must be located in a position suitable for easy tether access, thus minimizing the time required for the maneuver. Though the driver mechanism(s) must be easily accessible, it would also be beneficial if the elevator structure could shield the driver(s) from the space environment once the elevator is attached to the tether.

Robotics on board the elevator have been considered to aid in hooking and unhooking operations, manipulation of equipment, and servicing of tethered masses. Location of the system must provide accessibility to equipment mounted on, as well as off, the elevator. Operation of robotics will only occur when the velocity of the elevator with respect to the tether is zero.

The self-sufficient power generation and transmission system is the final design consideration for the tethered elevator. This independent system will primarily power the drive mechanism(s), robotic, and computer systems of the elevator. Important factors to be considered in this system are the elevator's overall power requirement, power source mass, and volumetric capacity. The latter consideration addresses mounting requirements for the system hardware. The drive mechanism(s) and robotic subsystems will dictate the maximum available power to be supplied by the system.

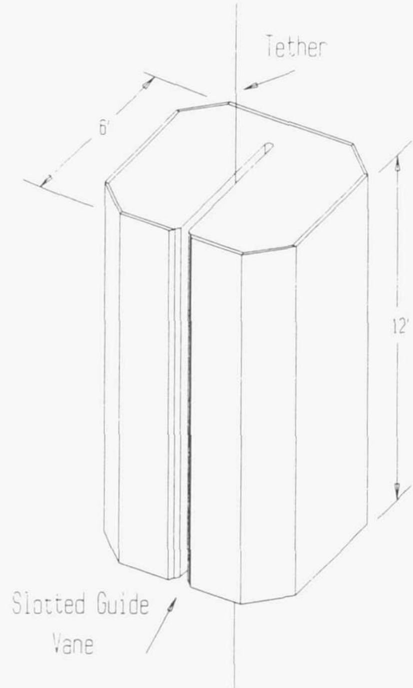

Fig. 1. Elevator Housing

DISCUSSION OF RESULTS

Proposed Configuration

Several designs for the tethered elevator were developed. These designs vary in their form and provide a variety of solutions to problems encountered during the design process. In this report, optimized subsystem designs have been united to form the proposed configuration of the tethered elevator system.

At the outset of the tethered elevator design, four areas of importance were identified. The design of the elevator structure was deemed the most critical aspect of the project. The three major subsystems of robotics, drive mechanisms, and power generation complete the list of significant design issues considered.

The structural configuration of the elevator will first be addressed. The hardware involved consists of a main unit, component shielding, a horizontal positioning mechanism, and a counterbalance system. The main unit shall house, support and protect all systems on board the elevator. Its shape, dictated by internal component dimensions, is best described as an elongated octagon (see Fig. 1). The octagonal shape occupies a 6×6×12 ft envelope and provides ample surface area for many unique hardware mounting capabilities. The volumetric capacity associated with this efficient shape also allows sufficient room for all internal subsystems. The four chamfered edges of the octagon were incorporated to minimize stress concentrations inherent in a rectangular

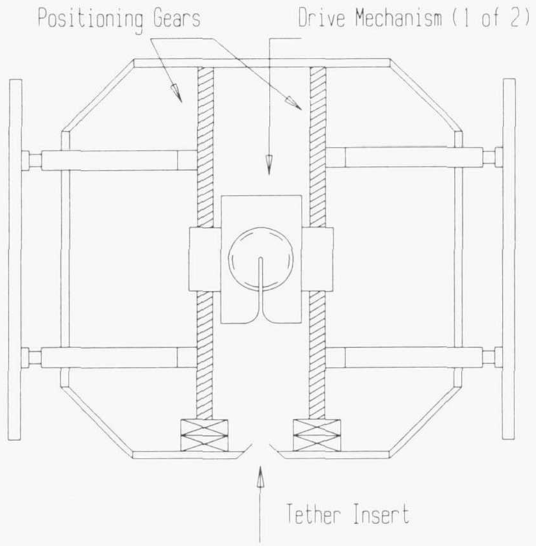

Fig. 2. Positioning Mechanism (Top View)

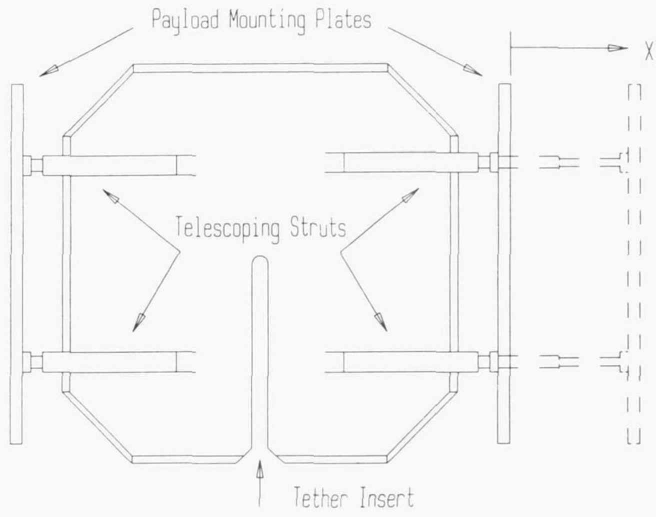

Fig. 3. Counterbalance Mechanism (Top View)

structure. These edges, angled at 45 degrees, eliminate sharp corners that may otherwise be unsafe to astronauts in the event of an extravehicular activity.

Shielding will be used to protect the internal components of the tethered elevator. Shielding will reinforce the structure and provide mounting surfaces for an array of elevator components. It will be insulated to isolate internal fixtures from the extreme temperature fluctuations present in low Earth orbit. Not only will the surface protect components from thermal radiation, but it will also act as a safeguard against atomic oxygen and micrometeoroid impact.

A horizontal positioning mechanism will be implemented to offset any moments created by an uneven mass distribution on the elevator. A counterbalance system will act in conjunction with the horizontal positioning mechanism to insure the center of mass of the elevator coincides with the tether axis. Both systems are used to perform the same function; however, each device operates in a slightly different fashion.

In order to offset elevator mass moments, the elevator and/or its payload must be moved relative to the tether. The horizontal positioning mechanism moves the elevator whereas the counterbalance system reconfigures the elevator payload. Horizontal positioning is accomplished through the interaction of two worm gears with each drive mechanism (see Fig. 2). Actuated by computer software, these worm gears rotate and simultaneously position both the tether and drive mechanism to the desired location. Because the tether is being moved within the confines of the elevator housing, a stationary slot will be built into the design. The slot will allow the tether and drive mechanisms to move with respect to the elevator. Additionally, the slot is used to "funnel" the tether into the drive mechanisms when the elevator is mated to a tether.

The counterbalance system manages the c.m. by extending a series of telescoping struts which connect an elevator payload to the elevator structure (see Fig. 3). Use of telescoping struts is favorable because: (1) They are structurally rigid; (2) they provide sufficient c.m. movement; and (3) they take up minimal volume within the elevator. The struts are affixed to a rigid plate on which payloads are connected. When the struts are extended, both the plate and payload are moved accordingly.

An integral function of the elevator is to provide transportation and support for a wide range of payloads. For this reason, the idea of using a shuttle-based pallet was utilized in the design (see Fig. 4). The pallets flown on the shuttle are designed to secure support equipment and experiments. The elevator must similarly perform this function on a tether deployed from the Space Station. The use of a shuttle-type pallet is therefore attractive for purposes of transporting and housing many types of payloads whether they be station, shuttle, or tether based.

Elevator Subsystems

The optimum design of the elevator configuration incorporates important features that satisfy a multitude of design considerations. The integration and design of elevator subsystems are also important and demand great attention. Three major subsystems are addressed to support the operation of the elevator on any given mission.

Robotics. It is envisioned that the elevator will provide a reliable means of transporting experiments, materials, and supplies to any point along a tether. These tasks can most efficiently be accomplished with the design of robotic

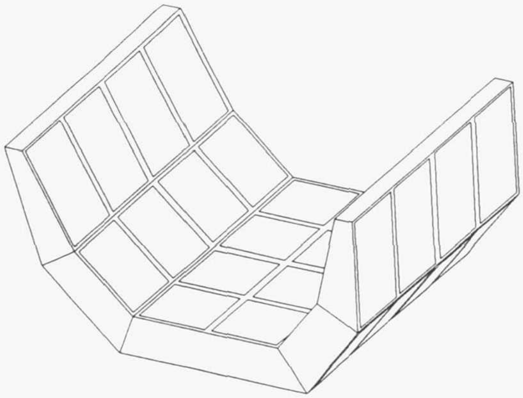

Fig. 4. Space Shuttle Pallet

implements to be affixed to the elevator structure. The Tethered Elevator Remote Manipulator Subsystem (TERMS) is therefore proposed to assist those operations in which mechanical manipulation of a tethered object is required. It will also aid in attaching the elevator to a tether at the outset of an elevator mission. The robotic subsystem will provide a mechanical linkage between the elevator and any object located on a tether. End effectors on the manipulators will provide a means of securing or servicing a broad range of devices.

Manipulators, in use and under development, were evaluated to gain insight into the design of a manipulator for space applications and to better define the operations that can reasonably be performed by the elevator manipulators.

The proposed design consists of two diametrically opposed arms which are 1:3.5 scaled versions of the shuttle's RMS. The shuttle RMS has been utilized to a great extent in the space environment and offers promising features that make it desirable for elevator implementation. The arms are approximately 4.4 m long. Both are three-jointed arms possessing six degrees of freedom. The arms perform in space while anchored to the elevator structure. A standard end effector attaches to the wrist of either manipulator and is used primarily for grappling and releasing payloads and for applying loads and/or motion to a payload. The capture mechanism is comprised of three cables that close around a standard grapple fixture(5). The manipulator arms, when equipped with a standard end effector, are capable of capturing a payload with a large misalignment and are dextrous enough to position a payload relative to the elevator's longitudinal axis with precision(6).

Specifics investigated in the manipulator design include mechanical and electrical elevator interfaces, end effectors, end effector tools, control systems, man-machine interfaces, and drive motors. Fixed mount, quick change mount, and track drive designs were considered for the mechanical elevator interface. The electrical interfaces considered were coaxial cone and multipin connections. End effectors researched were snare type, parallel jaw, and multiple fingers. End effector tool types evaluated included multiple arms and grippers. Teleoperation, telerobotics, and autonomous control were addressed. The man-machine interfaces were composed of master-slave, joystick, exoskeletal, and helmet types. Lastly, drive methods researched were electromechanical and digitally driven servomanipulators.

Final design analysis dictated use of the following choices for the TERMS: fixed mount elevator connection, standard snare type end effector, two-arm end effector tool, Langley intelligent gripper, telerobotic control system, joystick interfacing, and exoskeletal drive control.

The selection of computer hardware and data transfer devices completed the design of the robotic subsystem. The general purpose IBM AP-101 computer was chosen as the optimal computer system to coordinate various functions on the elevator. The primary reasons for the selection of the IBM AP-101 include physical dimensions, space worthiness, and reliability. Currently, five IBM AP-101s are employed aboard each space shuttle. Each computer is capable of handling a variety of tasks. The IBM has provisions for a ninety-five percent detection rate of hardware failure. With this capability, it is evident that a large degree of reliability is inherent in this system. Upon detection of hardware failures, the system immediately switches to a backup unit. This benefit, among others, makes employment of the IBM AP-101 an attractive choice for the tethered elevator.

Because the tethered elevator is a remote vehicle, a data transmission technique was chosen to relay computer commands to elevator systems. Packet radio data transmission has been chosen as the optimal solution for a data link between the Space Station and the tethered elevator. Packet radio techniques represent an evolution of wireless message switching methods. Information is assembled in short messages (packets) that are transmitted to a remote destination. Antennas for transmitting and receiving electromagnetic waves would be mounted on the elevator and Space Station. At microwave frequencies, relatively small antennas, on the order of one meter in diameter, are capable of directing energy in the form of electromagnetic waves into narrow beams of a few degrees of divergence(7). This is of paramount importance for the control of TERMS since the signals must be diverted to an intended coverage area which may exist at any location along a tether.

Drive Mechanism. The elevator drive mechanism is the most important subsystem addressed. Its design determines the mobile transporter's ability to traverse tethers in space. The drive mechanism determined to be the optimal design is the Bi-Wheel Friction Belt (see Fig. 5). It utilizes the same basic operating theory as the Tri-Wheel Friction Belt designed by E. Turci(8). However, the Bi-Wheel Friction Belt incorporates several changes which make this design truly unique.

The theory behind the Bi-Wheel Friction Belt is based upon the interaction of two endless, toothed belts which make direct contact with the tether to be traversed. The belts operate separately on two pulley wheels. One wheel is driven by a torque motor and one wheel is idle. When torque is applied by a drive motor, the belt is set in motion. The contact

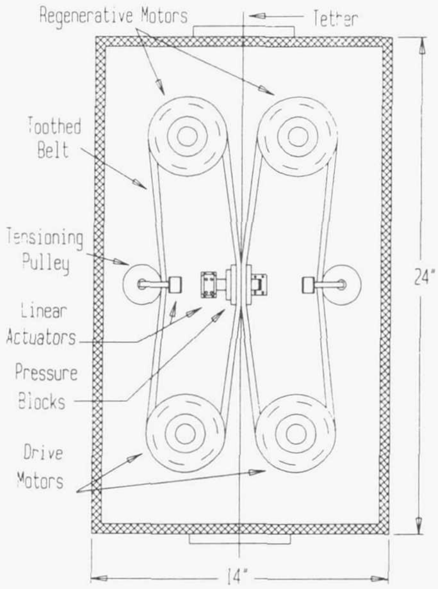

Fig. 5. Drive Mechanism (Side View)

between the belt and the tether then enables the elevator to move along the tether.

The Bi-Wheel Friction Belt mechanism will utilize two adjustable speed motors. These motors will be used to drive the two friction belts and, in turn, propel the elevator along the tether. The types of motors to be used are reversible, direct current, shunt-wound motors with field resistance control designed for a considerable range of speed adjustment[9]. Each motor will incorporate an automatic starter control to regulate the amount of current supplied to the motor. Automatic controls are essential to the drive mechanism's electric motors so that smooth acceleration with frequent starting and stopping may be obtained[10].

Tachogenerators will be used to control the speed of each drive motor. A tachogenerator consists of a small, permanent-magnet type generator coupled to the motor's rotating shaft. The resultant voltage induced on the motor's armature coil is directly proportional to the speed of the shaft. The tachogenerator receives this voltage signal and, through the use of a feedback loop to the drive mechanism's control link, controls the motor speed.

The Bi-Wheel Friction Belt drive mechanism will utilize a synchronous belt to overcome creep effects that are present in V-shaped belts and flat belts. A synchronous belt is a toothed belt which merges with a toothed pulley during operation. A synchronous belt eliminates slip by transmitting power through the positive engagement of belt teeth with pulley teeth. Synchronous belt drives have an advantage over gears and chains because they can reliably transmit high loads with low noise, and without lubrication. The shock absorbing characteristics of the rubber teeth against a metal pulley can also be beneficial. Yet another advantage is the synchronous belt's static tension which is less than that of V-shaped and flat belts, thus imposing lower static loads on shafts and bearings. This lower preload reduces starting load, an advantage in drives with motors that have low starting torques.

The drive mechanism's belts will be toothed only on the middle one-third of their width. They are 47 inches in length and 2.67 inches in width. The toothed portion of the belts will interface with the drive pulleys, while the smooth portion of the belts will interface with a flat plate. The plate is self-lubricating, contains no moving parts, and maintains constant pressure over the entire surface area of the pressure block. It is attached to a linear actuator which maintains proper pressure on the toothed belts and tether. The design keeps the tether positioned in the middle of the belt and minimizes friction between the pressure plate and drive belts with use of DuPont's Delrin 500AF, a material which is nonwearing and has a low coefficient of friction[11].

A torque transducer assembled on each drive wheel will measure the dragging force to provide proportional control of the pressure block's pushing force. The transducer will convert a change in the pulley wheel's torque into a signal which adjusts the linear actuator's pressure force. If slipping occurs, the torque transducer will recognize the event and an increase in pressure will be commanded to the linear actuator. The torque transducer signal is incorporated in a feedback loop with linear actuator control.

Braking the elevator will be carried out by a rotor/caliper combination similar to that used in automobiles. Rotors located at the ends of each drive motor shaft will be grasped by calipers during braking. This design excels in the areas of safety, controllability, and efficiency.

Regenerative braking will be used on the elevator. A total of four 1.7 hp DC shunt-wound motors are used. The motors are connected to the two idle pulleys of each drive mechanism. During braking, the motors are engaged and act as generators which convert rotational energy into electrical energy.

The components of the drive mechanism will be housed in a rectangular case of 14×26×24 inches. Two drive mechanisms will be utilized in the elevator design. When the elevator is placed on a tether, shuttle or station robotics will mate with a standard grapple fixture on the elevator and approach the tether. At this point, the linear actuator of each driver will be in its open mode to insure space between the friction belts is available for tether insertion. The tether will be "funnelled" into a stationary guide slot. Remote optics will visually confirm that the tether is properly inserted. The linear actuator will then be signaled to close the pushing blocks, applying a predetermined pressure. The tether will then be trapped between the friction belts of the two drive mechanisms. Rotating disks affixed to the drive mechanisms will "capture" the tether by rotating ninety degrees about the tether axis (see Fig. 6). Once the elevator has been positioned on the tether, it is ready to perform its intended mission. Upon completion of the mission, the rotating disks will be returned to their open position to facilitate removal of the elevator from the tether.

Power Generation. The final subsystem to be described is the power generation and transmission system. Because

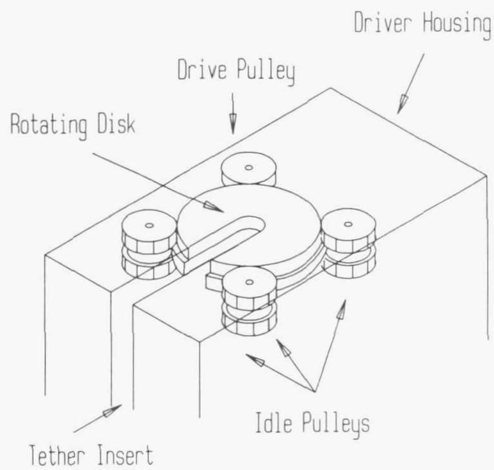

Fig. 6. Capture Mechanism

Space Station users will demand a large percentage of the total station power available, the elevator has been designed to operate independently of Station power systems. Major designs considered for power generation include solar, radioisotopic, electrodynamic, and fuel cell systems.

The idea of using the sun as a power source is an age-old concept. One modern method of extracting the sun's energy involves the use of solar cell arrays. Solar cells are ideal for use in space because they do not consume fuel, they do not exhaust themselves, and they have no adverse effect on the surrounding environment. However, the use of solar cells requires surface area proportional to power needs. This is one consideration that makes solar power unattractive for use on a tethered elevator. Whether panels are mounted on the elevator body or on externally attached wings, the required surface area and associated drag will interfere with elevator operation. Also, positioning of panels and/or the elevator towards the sun poses a major problem during operation. Though the use of solar power has many advantages for space applications, elevator requirements indicate an alternate means of power generation is needed.

Radioisotopic power generation is another means for fulfilling power requirements in space. Radioisotopic generators are compact, highly reliable, and capable of producing electrical power for extended periods of time. Through the selection of radioactive isotopes and energy converters, the problem of power generation in many space applications can be solved. Unfortunately, concern in the areas of human safety, heat dissipation, and power/weight ratios indicates the system may be unfeasible for elevator applications.

The geomagnetic power generation system offers both challenging and promising features. This system utilizes an electrodynamic tether which travels through the Earth's magnetic field and ionospheric plasma to induce an appreciable voltage across a conducting tether. Plasma-motor generators are specified to promote contact with the ionosphere and ambient plasma so that a sufficient current can be made to pass through the tether. This effectively closes an electrical circuit and ultimately provides power to the tethered elevator.

Four plasma-motor generators (PMGs) could be used in this design, one at each end of the tether and one on both the top and bottom of the elevator structure. This configuration allows two separate circuits to be created. One circuit exists between the elevator and Space Station, and the other exists between the elevator and the tether end. As the elevator traverses the tether, the electrical potential varies with elevator position. Maximum power capacity becomes available at the point of maximum power requirement since the voltage delivered is proportional to tether length. PMGs allow automatic switching of current direction. This enables the elevator to travel in either direction along the tether.

The electrodynamic tether has great potential for many space applications. This power medium is particularly well suited for the elevator because it requires no surface area and enables full use of the elevator structure to fulfill its primary functions in a microgravity environment. The major disadvantage of a conducting tether is its lack of proven use. The principle of generating electricity with a tether has been shown, but converting this power and transmitting it to a device, such as the tethered elevator, has not been tested in space.

The use of fuel cells on the tethered elevator appears to be the best solution for the production of power. Fuel cells offer a means of energy conversion that eliminates high temperature combustion and subsequent processes found in nearly all schemes designed to produce electrical power. A fuel cell is an electrochemical device that continuously converts the chemical energy of a fuel and oxidant into electrical energy. Since the conversion cycle is electrochemical, rather than thermal, fuel cells are not subject to Carnot cycle limitations, thus leading to high efficiencies(12).

Fuel cells have been used in several spacecraft including Apollo, Gemini, and the space shuttle orbiters. Due to their small size and modularity, they can be configured to meet virtually any power requirement without sacrificing efficiency. Fuel cell power is continuous in nature so long as oxygen and hydrogen can be supplied. Fuel cells produce very little noise or noxious emissions.

The proposed fuel cell power system for the tethered elevator consists of a single power plant utilizing three oxygen and three hydrogen tanks. The system has been designed to provide 2 kW minimum, 7 kW continuous, and 12 kW peak power. The fuel cell stack will be equipped with an accessory package to handle reactant management, thermal and electrical control, and water removal. This accessory package is located at one end of the power plant stack and can be separated from the cell stack for easy maintenance.

The hydrogen and oxygen required for the fuel cell must be cryogenically stored in a supercritical condition (97°K or -285°F for oxygen and 22°K or -420°F for hydrogen)(13). For

this type of storage, double-walled, Dewar-type spherical tanks are necessary. The oxygen tanks will be 7.87 inches in diameter and hold 183 lbs of oxidant. The hydrogen tanks will be 15.2 inches in diameter and hold 22.9 lbs of fuel. Coupled together by a simple fuel regulator system, these tanks will provide 168 hours of continuous operation.

A secondary fuel cell will serve as a backup for purposes of redundancy. Fuel from the primary fuel cell will be rechanneled to the secondary fuel cell through a series of regulator valves in case of primary fuel cell failure. In the case of regulator valve failure the secondary fuel cell will also be equipped with two emergency fuel tanks capable of powering the vehicle under maximum loads. Each tank will be equivalent in size to that of the primary fuel cell and capable of 56 hours of continuous operation.

A second source of power was considered in the unlikely event of a primary system failure. Nickel-cadmium batteries have traditionally been used as storage systems on spacecraft. However, the latest and most efficient battery configuration involves the use of hydrogen in place of cadmium. Nickel-hydrogen batteries will therefore be used to back up the fuel cell power generation systems.

METHOD OF ANALYSIS

The optimum design for the tethered elevator configuration, including subsystems, was achieved by analyzing evaluated design considerations and parameters (see Fig. 7). The analysis was conducted using decision matrix theory. Numbers ranging from zero to twenty are inserted into a matrix that relates each design consideration to individual design parameters. The parameters are given a weighting factor to represent their relative importance to each other. The weighting factor ranges from one to ten with the latter signifying a relatively more significant parameter. To compute the results, a summation of the applicability numbers, multiplied by the weighting factors, is performed. This yields a numerical representation for each design and is used for determining the optimal design.

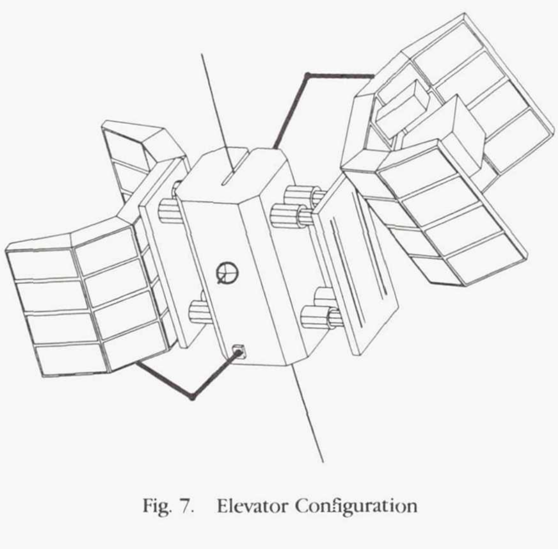

Fig. 7. Elevator Configuration

CONCLUSION

The tethered elevator concept, still in its infancy, holds great promise for future implementation on the International Space Station. Besides its ability to traverse a deployed tether of fixed length, the elevator will be capable of providing robotic support to tethered objects, tapping variable gravity levels, and generating self-sufficient power.

Assessment of the elevator's operation in microgravity will be critical in determining its feasibility. The tether dynamics, elevator stability, and control of elevator motion are all important areas for further study and experimentation in the advanced development of this spacecraft. The conceptual engineering design of the Space Station Tethered Elevator System has been carried out to demonstrate the potentialities of a device that may soon revolutionize space operations.

ACKNOWLEDGMENTS

The authors, Michael H. Haddock and Loren A. Anderson, wish to acknowledge NASA and the Universities Space Research Association for providing the opportunity to work on this advanced space design. Thanks are also extended to the University of Central Florida students of Engineering Design (1988-89) who contributed to the design of the Space Station Tethered Elevator System. Principal authors were K. Hosterman, E. Decresie, P. Miranda, and R. Hamilton. Faculty advisor was Dr. Loren Anderson; teaching assistant, Michael H. Haddock.

REFERENCES

1. Merlina, P., Bogo, W., and Ciardo, S., "Tethered Elevator and Pointing Platform Demonstrations: A Shuttle Flight Test of Scaled Engineering Models," *Proceedings of the NASA/AIAA/PSN International Conference on Tethers in Space,* 1986, pp. 1-15.
2. Ionasecu, R. and Penzo, P.A., "Space Tethers", *Spaceflight,* Vol. 30, May 1988, pp. 200-208.
3. Bekey, I., "Tethers Open New Space Options," *Proceedings of the Workshop on Applications of Tethers in Space,* Vol. 1, 1983, pp. 18-30.
4. Aeritalia, "Tethered Elevator and Platforms as Space Station Facilities: System Studies and Demonstrative Experiments," *Proceedings of the Second Workshop on Applications of Tethers in Space,* 1985, p.40.
5. Daniell, R.G. and Sachdev, S.S., "The Design and Development of an End Effector for the Shuttle Remote Manipulator System," *Proceedings of the 16th Aerospace Mechanisms Symposium,* 1982, p. 46.
6. Thring, M.W., *Robotics and Telechirs: Manipulators with Memory; Remote Manipulators; Machine Limbs for the Handicapped,* IFS Publications, Ltd., United Kingdom, 1986, p. 258.
7. Kamilo, F., *Advanced Digital Communications: Systems and Signal Processing Techniques,* Prentice-Hall, Inc., Englewood Cliffs, N.J., 1987, p. 10.
8. Turci, E., "Tether Pointing Platform and Space Elevator Mechanisms Analysis of the Key Concepts for SATD," *Proceedings of the Second Workshop on Applications of Tethers in Space,* 1985, pp. 287-324.
9. Oberg, E., *Machinery's Handbook,* 21st Ed., Industrial Press, New York, 1984, pp. 2363-2364.
10. Avallone, E., *Mark's Handbook for Mechanical Engineers,* 9th Ed., McGraw-Hill Co., New York, 1987, pp. 15-32-15-36.

11. *Design Handbook for DuPont Engineering Plastics: DELRIN,* E. I. duPont de Nemours & Co., Inc., Wilmington, Del., 1989.
12. Angrist, S.W., *Direct Energy Conversion,* 3rd Ed., Carnegie-Mellon University, Allyn and Bacon, Inc., Boston, 1982, p. 353.
13. "Space Shuttle News Reference," National Aeronautics and Space Administration, Washington, D.C., GPO 341-570/3256, 1983.

N94- 71271

1994004516 382670

54-54 160630 P. #4

ELECTROCHEMICAL CELL FOR OBTAINING OXYGEN FROM CARBON DIOXIDE ATMOSPHERES

CLEMSON UNIVERSITY

INTRODUCTION

For manned missions to Mars to become a reality, an efficient and reliable means of obtaining oxygen from the carbon dioxide-rich atmosphere will be required. Otherwise, the high cost of transporting the oxygen needed to sustain the astronauts will severely restrict the expedition to the martian surface(1).

Recently, the use of electrochemical devices has been explored as a means of obtaining oxygen from the carbon dioxide-rich atmosphere. In these devices, oxygen ions diffuse through solid oxide membranes, thus separating oxygen from the other gases present(1,2). This phenomenon has only recently been explored as a means of obtaining large quantities of oxygen from toxic atmospheres, although first observed by Walter Nernst in 1899.

Nernst observed that stabilized zirconia will conduct oxygen ions when an electrical potential is applied across metallic electrodes applied to the ceramic membrane. Diatomic oxygen molecules are dissociated at the positive electrode/electrolyte interface. The oxygen ions enter the ceramic body due to the ion density gradient which is produced by the electrical potential across the electrolytic membrane. Once the ions have diffused through the membrane, they reform diatomic oxygen molecules at the anode.

The separation of oxygen from carbon dioxide is achieved by the combination of thermal and electrochemical processes. The thermal decomposition of carbon dioxide (at 1000°C) results in the production of carbon monoxide and oxygen by the reaction:

$$2CO_2 \rightarrow 2CO + O_2 \qquad (1)$$

The oxygen produced by this reaction is then electrochemically separated from the toxic gases.

The electrolyte most often employed in solid state electrochemical devices is eight mole percent yttria (Y_2O_3) stabilized zirconia (ZrO_2). The addition of the yttria to the zirconia structure induces oxygen vacancies by the solid state reaction:

$$Y_2O_3 \xrightarrow{ZrO_2} 2Y_{Zr}^{-1} + O_O + [V_O^{+2}] \qquad (2)$$

The reaction indicates that as yttrium atoms take the place of zirconium atoms in the atomic structure, a concentration of oxygen vacancies results. The oxygen vacancies $[V_O^{+2}]$ serve as charge carriers for the oxygen ions separated from toxic atmospheres(3).

PRODUCTION OF ZIRCONIA ELECTROLYTES

To produce an electrochemical device, one must first determine the variables influencing oxygen transport. Recent studies have shown that the thickness of the membrane, the grain size, and the electrode thickness are the most influential variables in these devices(1,2,4).

Thin membranes are necessary because they allow oxygen ions to be transported through the ceramic body faster than thick ceramic bodies.

Additionally, the use of small particles in manufacturing the ceramic membranes is also important. Once fired, ceramic bodies made from small particles possess many small grains, and consequently many grain boundaries. A high quantity of grain boundaries is important in electrochemical devices, as some of the diffusion of oxygen occurs along grain boundaries present in the body, as well as through the atomic structure.

Finally, a porous coating of the electrode material will be required. To obtain thin coatings (~20 μm), a process similar to silk screening is often employed. The coating must be extremely thin to prevent the loss of active area on the surface of the electrolyte.

To produce thin membranes, a ceramic forming process known as tape casting was adopted. This process is used in the production of ceramic substrates, multilayer capacitors, and other electronic materials. In this procedure, fine particles are suspended in a mixture of organic solvents and binders. The suspension is passed under a blade held at a constant height, thus producing a thin membrane with a uniform thickness(5,6).

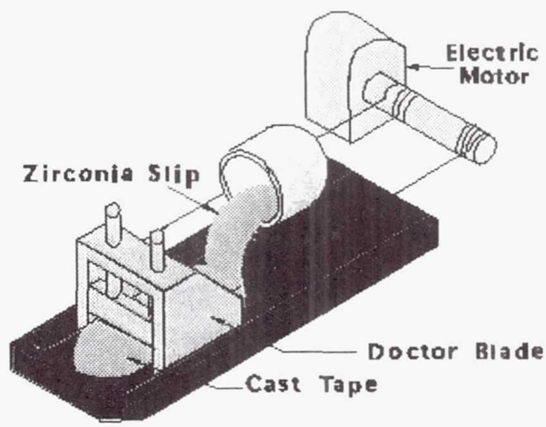

Fig. 1 Tape Casting Process

Table 1. Tape Cast Batch Constituents (in grams)

Zirconia	100
Trichloroethylene	39
Ethyl alcohol	15
Menhaden fish oil	2.3
Butvar(B98)*	5
Santisizer 161*	10

*Monsanto products

Industrially, this process is done on a continuous basis; however, for this project a batch process was employed.

The batch process used involves pulling a doctor blade over zirconia slip (Fig. 1). Once cast, the tapes were allowed to dry and then were removed from the casting surface. Several batch recipes and casting surfaces were tested to determine the optimum conditions for tape casting zirconia. The initial trials involved the adoption of a tape casting recipe used industrially in the production of Al_2O_3 substrates. The slip ingredients are shown in Table 1.

Each ingredient serves a specific function in the formation of the membranes. Trichloroethylene is employed to dissolve the deflocculant and the ethyl alcohol dissolves the binder. The deflocculant (Menhaden fish oil) is used to chemically disperse the zirconia powder in the solvents. The binder (Butvar B98) and plasticizer (Santisizer 161) are included in the batch to give the cast tapes strength and flexibility.

To produce the zirconia slip, the zirconia powder, solvents, and the deflocculant were mixed together and ball milled for 24 hours. The binder and plasticizer were then added, and the constituents were milled for an additional 24 hours.

Once the batch was prepared, it was cast and allowed to dry. Several casting surfaces were tested during the course of this study; however, most were found to be unsuitable for this application (Table 2). The majority of the casting surfaces tested were plastics. Of these, only polyethylene was unaffected by the presence of the organic solvents. The other plastics tested were attacked by the solvents, which prevented the tapes from drying uniformly. The differential shrinkage associated with the non-uniform drying process resulted in the cracking of the cast tapes as they dried.

A glass surface coated with a thin layer of Menhaden fish oil also had limited success as a casting surface. The problems associated with casting on a liquid film were reproducing the thickness of the coating and obtaining uniform coatings.

The problems associated with the use of this tape casting system caused another binder system to be implemented. The binder is a commercially available composition (binder 73171 from Metoramic Sciences, Inc.). The product is a gel-like substance that, when mixed with an equal quantity of trichloroethylene, forms the liquid part of the slip. The zirconia powder was then added to the mixture, and ball milled for one hour. The milling process is needed to mix the suspension and break up any agglomerates present in the powder.

Table 2. Casting Surfaces

Successful	Unsuccessful
Polyethylene	Mylar
Fish oil on glass	Untreated glass
	Polyolefin
	Teflon
	Aluminum foil

Once mixed, the slip was cast in the same manner as before and allowed to dry. This binder system did not react with any of the casting surfaces tested (polyethylene, glass, or Teflon), and high quality tapes resulted. Teflon was used as the casting surface to produce the membranes necessary to assemble the cell.

The next step in producing the ceramic membranes is firing. The firing of thin membranes requires that the temperature be raised slowly through the lower temperature region to allow the binder to burn out evenly. Otherwise, the fired product will not be flat. Three sintering temperatures (1500°, 1550°, and 1600°C) were initially examined in this work; however, no significant difference in the shrinkage, density, or handling strength of the tapes was evident. A 25% shrinkage was associated with each firing temperature, indicating that all of the shrinkage occurred at low temperatures, and was due to the binder burn out.

The fired tapes possessed greater than 95% of theoretical density. The density of the final product is important, as voids in the ceramic body will not permit the transport of oxygen ions through them. Additionally, dense tapes are generally easier to work with due to their relatively high strength.

The handling strength of the fired tapes is also dependent upon the thickness of the tapes. Extremely thin tapes (<0.2 mm), when fired, possessed very little strength; whereas, tapes with a thickness of more than 0.4 mm were easier to handle. Therefore, thicker tapes (0.3 to 0.4 mm) were cast to construct the electrochemical cell.

The next phase in the development of the electrochemical cell is the application of the electrode to the electrolyte. Platinum was chosen as the electrode for this device due to its stability and high electrical conductivity at elevated temperatures. To produce the thin coating necessary for this application, platinum paste was applied to the electrolyte with a process similar to silk screening.

The final step in the production of the cell is the actual cell assembly. The entire cell is made from cast zirconia membranes, so the material used to seal the plates must possess the same thermal expansion as that of zirconia. With this in mind, a zirconium phosphate solution was produced and used to "glue" the cell together. The zirconium phosphate solution was obtained by mixing stabilized zirconia powder with phosphoric acid. The zirconium phosphate solutions was produced by the following reaction:

$$3ZrO_2 + 4H_3(PO_4) \rightarrow Zr_3(PO_4)_4 + 6H_2O \qquad (3)$$

To ensure that the crystal structure of the bonded region is identical to that of the cast membranes, a phosphate solution was cast in a thick layer upon an alumina substrate and cured at 500°C. The cured material was then analyzed with X-ray

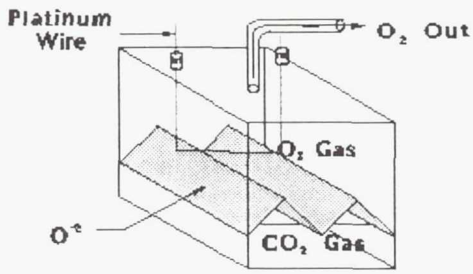

Fig. 2 Cell Design

diffraction, and was found to possess the same crystal structure. This verification is important, because if other compounds were present, the thermal expansions of the substrates and bonding agents would not match. A thermal expansion mismatch would ultimately result in the degradation of the cell's structural integrity.

CELL DESIGN

Once all of the processing difficulties associated with the production of thin membranes were overcome, the cell could be assembled (Fig. 2). To eliminate the need for a complex manifold system, the cell was designed to have as few gas inlets and outlets as possible. For this reason, the cell possesses an open bottom to allow the free flow of carbon dioxide into the system. The carbon dioxide entering the system would first have to be filtered to eliminate dust, and circulated to maintain a high level of oxygen in the feed gas. The atmospheric circulation and filtering systems were not considered in the design of the electrochemical cell.

The series of intersecting, slanted membranes provides the high surface to-volume-ratio necessary for an electrohemical cell. This ratio should be high so that as large a quantity of oxygen gas as possible can be obtained from as small a volume as possible.

The voltage needed to split the diatomic oxygen molecules is supplied by a platinum wire that touches the top of each peak of the electrolyte. An additional amount of platinum ink was painted along this ridge to ensure that no voltage losses occurred at the interface between the voltage source and the electrode.

The cell is operated in a furnace at 1000°C to ensure that the carbon dioxide gas is completely decomposed, thus producing carbon monoxide and oxygen. The continuous circulation of the gases will keep a high concentration of oxygen near the electrolytic membrane, and thus a continuous flow of oxygen through the electrolyte.

CONCLUSION

To maintain the lives of astronauts on the martian surface, an efficient and reliable means of supplying oxygen to them will be required. These needs can be meet through the use of an electrochemical device.

To obtain large quantities of oxygen from the atmosphere, thin membranes will be required. A ceramic forming process known as tape casting was employed to produce membranes as thin as 0.1 mm. Thicker membranes were also produced to compose the body of the cell.

To construct the cell, a zirconium phosphate solution was developed to serve as a "glue." The use of this sealing agent provides a gas-tight seal that possesses a thermal expansion identical to that of the zirconia membranes. Thus, the cell will not lose its structural integrity due to thermal cycling, and the useful life of the cell will be increased.

ACKNOWLEDGMENTS

Design team members M.W. Hooker, H.E. Rast, and D.K. Rogers were assisted by faculty advisor Dr. T.D. Taylor, Department of Ceramic Engineering.

REFERENCES

1. Richter, R., "Basic Investigation into the Production of Oxygen in a Solid Electrolyte Process," AIAA 16th Thermoplastics Conference, Palo Alto, CA, AIAA-81-1175, June 1981.
2. Erstfeld, T.E., Mullins, O., and Williams, R.J., "Carbon Dioxide Electrolysis Using a Ceramic Electrolyte," Fourth Princeton AIAA Conference on Space Manufacturing Facilities, Princeton, NJ, AIAA-79-1375, May 1979.
3. Kingery, W.D., Bowen, H.K., and Uhlmann, D.R., *Introduction to Ceramics,* John Wiley & Sons, New York, 1976, pp. 126-176.
4. Dueker, H., Friese, K., and Haecker, W., "Ceramic Aspects of the Bosch Lambda-Sensor," Transactions of the Society of Automotive Engineers, Paper Number 750223, 1975.
5. Mistler, R.E., Shanefield, D.J., and Funk, R.B., "Tape Casting of Ceramics," Onada, G.Y. and Hench, L.L., (eds.), *Ceramic Processing Before Firing,* John Wiley & Sons, New York, 1978, pp. 411-448.
6. Reed, J.S., *Introduction to the Principles of Ceramic Processing,* John Wiley & Sons, New York, 1988, pp. 395-399.

N94- 71272

382671

19940045I7

CISLUNAR SPACE INFRASTRUCTURE: LUNAR TECHNOLOGIES

UNIVERSITY OF COLORADO

S5-12
160631
P-12

Continuing its emphasis on the creation of a cislunar infrastructure as an appropriate and cost-effective method of space exploration and development, the University of Colorado explores the technologies necessary for the creation of such an infrastructure, namely (1) Automation and Robotics, (2) Life Support Systems, (3) Fluid Management, (4) Propulsion, and (5) Rotating Technologies. The technological focal point is on the development of automated and robotic systems for the implementation of a Lunar Oasis produced by Automation and Robotics (LOAR). Under direction from the NASA Office of Exploration, automation and robotics have been extensively utilized as an initiating stage in the return to the Moon. A pair of autonomous rovers, modular in design and built from interchangeable and specialized components, is proposed. Utilizing a "buddy system," these rovers will be able to support each other and to enhance their individual capabilities. One rover primarily explores and maps while the second rover tests the feasibility of various materials-processing techniques. The automated missions emphasize availability and potential uses of lunar resources and the deployment and operations of the LOAR program. An experimental bio-volume is put into place as the precursor to a Lunar Environmentally Controlled Life Support System. The bio-volume will determine the reproduction, growth and production characteristics of various life forms housed on the lunar surface. Physicochemical regenerative technologies and stored resources will be used to buffer biological disturbances of the bio-volume environment. The *in situ* lunar resources will be both tested and used within this bio-volume. Second phase development on the lunar surface calls for manned operations. Repairs and reconfiguration of the initial framework will ensue. An autonomously initiated, manned Lunar Oasis can become an essential component of the United States space program. The Lunar Oasis will provide support to science, technology, and commerce. It will enable more cost-effective space exploration to the planets and beyond.

LIST OF SYMBOLS

A/R	Automation and Robotics
DIPS	Dynamic Isotope Power System
EPV	Experimental Bio-Volume
ECLSS	Environmentally Controlled Life Support System
ELV	Expendable Launch Vehicle
FTIR	Fourier Transform Infrared spectral analyzer
ICP	Inductive Coupled Plasma analyzer
ISPV	Specific Impulse delivered in Vacuum
LECLSS	Lunar Environmentally Controlled Life Support System
LEL	Lunar Expendable Lander
LEO	Low Earth Orbit
LH_2	Liquid Hydrogen
LO	Lunar Orbit
LOAR	Lunar Oasis produced by Automation and Robotics
LOX	Liquid Oxygen
LPO	Lunar Polar Orbiter
LRAT	Lunar Remote Access Technology
LRV(s)	Lunar Robotic Vehicle(s)
LS	Lunar Surface
MR	Mass Ratio of initial to final mass of rocket
RTG	Radioisotope Thermoelectric Generator
XRF	X-Ray Fluorescent spectrometer
WETOX	Wet oxidation

INTRODUCTION

The United States Space Program must have a safe and cost-effective means of enabling missions in the space environment. *Pioneering the Space Frontier* and the *Leadership Report* both emphasize the need for activities that will catalyze future mission scenarios such as the "Exploration of the Solar System" and "Humans on Mars"[1,2]. The development of a cislunar infrastructure has been proposed as the foundation for implementing such future space missions[3] (Fig. 1).

A key element in the development of the cislunar infrastructure will be a habitable manned outpost on the lunar surface. Implementation utilizing automation and robotics will develop the framework for the lunar outpost and will have immediate benefits to U.S. industry. Manned activities will be supported by the Lunar Oasis produced by Automation and Robotics (LOAR) program and will provide an enhanced level of capability to the overall infrastructure (Fig. 2).

The success of the Apollo missions, due in part to the lunar Surveyors and Rovers, has shown the feasibility and desirability of coupling automated and manned missions. The LOAR project will demonstrate the enduring value of advanced robotics missions followed by manned missions. Automation and robotics (A/R) coupled with manned operations are a lower cost yet safe and effective means for implementing many elements of the space program.

A Lunar Oasis by definition must provide respite from the rigors of the harsh lunar environment. A secure habitat with the capability to sustain an atmosphere, to store both delivered and lunar-recovered consumables, and to support communication would be of high value. Full deployment or even partial completion of the Lunar Oasis will enable more productive and innovative human missions on the lunar surface. Automation and robotic technologies would be used to deploy a primitive oasis on the lunar surface prior to human presence. Upon arrival, humans could finalize the oasis, deploy science experiments, explore along robotically prepared trails and initiate higher level lunar processing activities.

PRECEDING PAGE BLANK NOT FILMED

PAGE 46 INTENTIONALLY BLANK

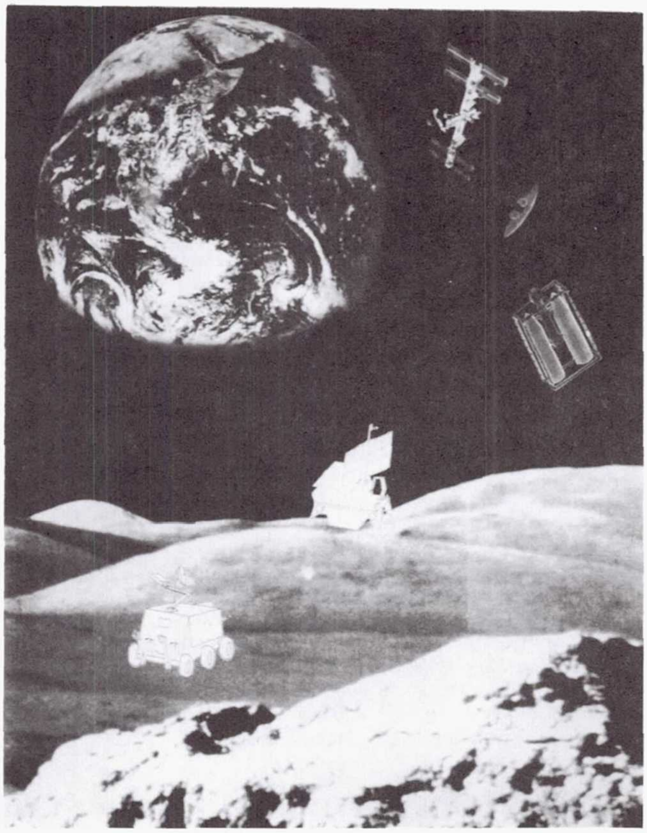

Fig. 1. The cislunar infrastructure, showing its key elements the Space Station *Freedom* at LEO, the L1-Station and an Orbital Transfer Vehicle. Robotic Vehicle, LRV, and Experimental Bio-Volume, EBV, pictured on the lunar surface.

Ground-based topographic maps and resource deposit location maps created by the robotic vehicles and Lunar Remote Access Technology (LRAT) will verify and enhance the maps generated using LPO remote sensing information. Prescribed vehicle interactions with the environment coupled with the field testing of a variety of processing and resource recovery techniques will provide the experimental data necessary to develop detailed resource recovery and processing operations. The resource and operations databases will enable manned use of the LOAR to enable efficient and effective lunar science, technology and commerce activities.

The continuous long-term support of life in the nonterrestrial lunar setting establishes confidence in subsequent use of the bio-volume as a safe manned habitat. The support of life on the Moon will stimulate public interest in the exploration and development of space as a future habitable environment. The experimental bio-volume is envisioned as a novel but highly useful prelude to manned habitation on the lunar surface. The EBV will provide quantitative data on the life cycles of biological systems in the lunar environment. It will field test key technologies for the implementation of a LECLSS. The EBV will further provide on-site testing of a refittable module suitable for fulfilling the immediate life support requirements of the LOAR project. A unique opportunity to characterize an environmentally controlled system with respect to remote terrestrial performance should be attained, and the use of biological interactions in extracting and using *in situ* resources can be evaluated. The tandem mission scenarios of the LRVs and EBV will provide the ground-based verifications and databases necessary to establish the feasibility and baseline technologies required for the development of manned habitation, leading to full lunar surface access for science, technology and commerce.

To initiate the LOAR project three major hardware elements are to be delivered to the Lunar surface: two robotic vehicles and an autonomous bio-volume (Fig. 3).

The development of two Lunar robotic vehicles (LRVs) and an experimental bio-volume (EBV) provides the requisite conditions for implementation of the LOAR. The LRVs will develop the preliminary information and hardware deployment framework required for the establishment of the lunar outpost. Implementation requires that specific remote-sensing information be gathered by the Lunar Polar Orbiter (LPO). Databases on regolith composition and location, resource and volatile availability, and navigable terrain will be crucial to search strategies utilized by the automated vehicles. Continuous monitoring via telemetry will enable ground-based verification of Lunar activities. Manned teleoperation is anticipated only in the case of "unrecognized" circumstances and emergencies. The vehicles will systematically search the lunar surface for valuable resources and will carry out the deployment of hardware and scientific experiments. The bio-volume will be set up to provide information on lunar life-support systems. It will be convertible to an interim habitable module for the LOAR supporting early manned sorties to the lunar surface (Fig.4).

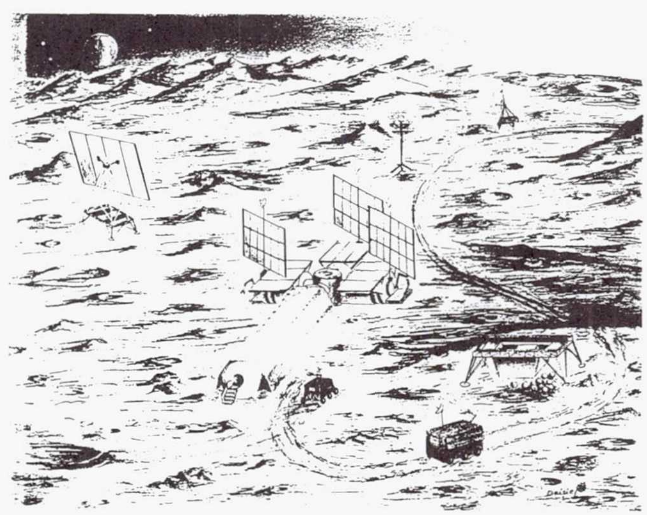

Fig. 2. The envisioned LOAR following manned operations. Shown are the three combined EBVs, together with an additional habitation module. The two LRVs are shown in the foreground.

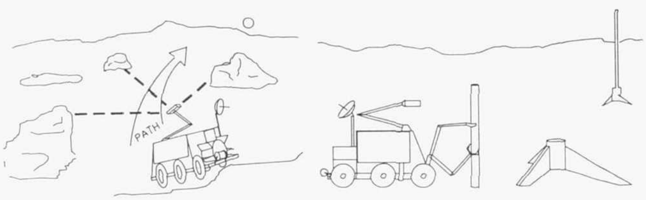

Fig. 3. The Lunar Rover Vehicle, LRV. Vehicle on left is shown utilizing pulsed-laser ranging and its neural network for navigation on the lunar surface. Vehicle on the right is shown deploying one of the triangulation beacons.

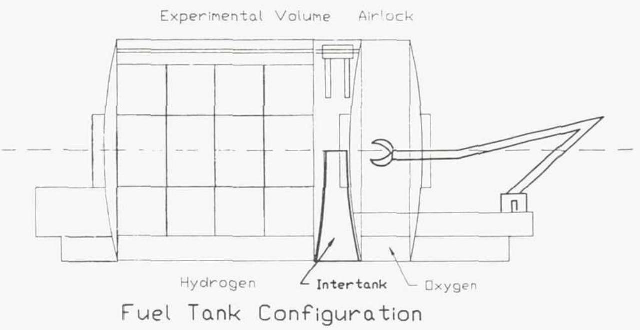

Fig. 4. The experimental bio-volume, EBV, is shown prior to reconfiguration. Used as the propellant tanks during delivery, it will be reconfigured into the experimental bio-volume.

RATIONALE

The LOAR is envisioned to be a critical element in a practical space infrastructure. It is a rudimentary resource storage and accumulation site, an exploration base on the lunar surface and a near-Earth technology demonstrator. Preparation for such an oasis as a prelude to manned presence can be achieved using a variety of automation and robotic technologies. These high-impact technologies in turn can have immediate positive influences on the automation and robotic capabilities of U.S. industry. Initial costs and public investments can be kept relatively modest without safety risks, high reliability costs, and time-sensitive concerns (Fig. 5).

Using automation prior to manned missions offers a number of advantages. The LRVs and LRAT can be utilized to implement the remote-sensing verification and resource availability studies. The automated mission scenarios take advantage of the fact that A/R hardware is inexpensive to transport, does not require life-support systems, and is insensitive to unanticipated mission delays and constraints. Manned presence following implementation via automated and robotic systems provides a logical step forward in LOAR development. The processing techniques and biological system databases can be used in the design and certification of life support requirements necessary for man-rated missions. Starting with autonomously demonstrated resource recovery and processing techniques, manned operations can capitalize on the initial framework established by the LRVs and EBV. Scientific and technological spin-offs such as advanced robotics could be utilized by industry, even during the initial Earth-based testing of LOAR technologies. Commercial interests in low-volume, low-power food production and waste handling systems would benefit almost immediately from LOAR technologies. Controlled environmental research would provide valuable clues to the dynamic alterations that appear to be occurring on Earth.

The implementation of lunar activities beginning with the LRVs and EBV will provide the field testing and initial development of the LOAR project for utilization within the cislunar infrastructure. As seen in Fig. 5, the LOAR plays a critical role in providing both immediate and long-term returns from the public investment. As described below, the activity can become a major focal point for precursor missions that enable a more productive, less risky human activity in the space environment. As a programmatic matter, the precursor mission may be more dependent on academic and industrial support than a manned, NASA mission support.

Mission Goal is to explore space in an effective and low cost manner.

Interim Objectives are to (1) Establish a continuous progression of programs leading to space exploration,

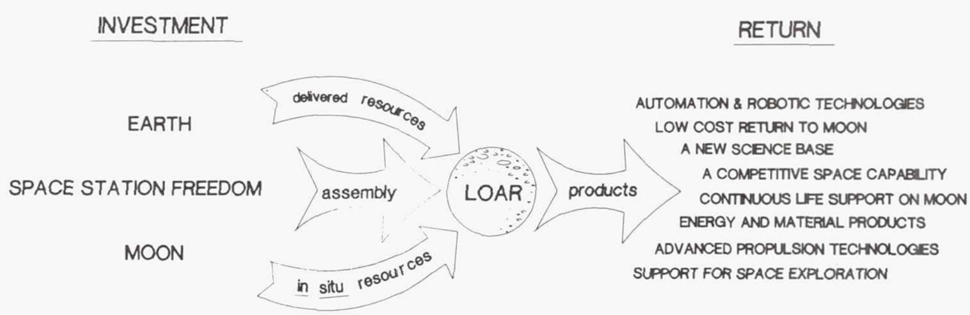

Fig. 5. The investment and anticipated returns from the LOAR program.

utilization, and eventually habitation; (2) Develop space science, technology, applications, and commerce for the benefit of humans on Earth; and (3) Utilize space activities as the focus for industrial, technological and commercial growth for future generations in the United States.

Mission Scenario. The LOAR mission scenario focuses on a phased automated and manned activity to be undertaken on the lunar surface. Robotic and automated systems provide a starting point for the development of enabling technologies, and the establishment of an operational lunar framework. The EBV supports and evaluates biological systems such as plants, primitive unicellular life forms, and invertebrates on the lunar surface. Interactive physicochemical systems are used to provide environmental buffers and to aid in *in situ* resource use. LRV activities include ground-based verification of remote sensing topography. Gas chromatography, X-ray fluorescent spectrometry (XRF), Fourier transform infrared spectral analysis (FTIR), and inductive coupled plasma analysis (ICP) of recovered soil samples will aid in the detailed quantification of remote sensing information. Candidate locations for the recovery of volatiles are searched both by the LRVs and LRAT. The LRAT can be used for the exploration of spatially restrictive craters, caves, and lava tubes. Manned operations take advantage of the information gathered on the effectiveness of resource recovery methods for lunar regolith. Initial automated evaluations can be done for rock cooking, ilmenite reduction by hydrogen, and centrifugal separations of the lunar soil into baseline components. The production of materials such as lunar composites, concrete and fiberglass for use in fiberglass winding technologies for making "utility" volumes or for the construction of lunar buildings is explored. A general database on space-based LECLSS is established and used to satisfy future manned mission requirements. Scientific locations of interest are mapped and scientific apparatus, such as the darkside synthetic-aperture radio observatory are deployed. Manned operations will utilize any resources that have been recovered, and will instigate any repairs and modifications necessary for the conversion of the bio-volume to a man-rated habitation module. Manned operations complement the LOAR project with the establishment of a habitable, manned outpost on the lunar surface and the development of a key element in the cislunar infrastructure. A permanently manned lunar base may arise from these initial infrastructure developments.

MISSION IMPLEMENTATION

1. Prototype Field Testing

The first step in the implementation of a phased, automated and manned scenario should involve extensive prototype field testing. Development of the vehicles is envisioned to start in 1994, leading to prototype demonstrations in 1998. Crater National Park (Arizona) has been chosen as the site where the functional operating characteristics of the robotic vehicles will be determined. Bio-volumes can be developed at university centers. Both activities are to be fully completed prior to delivery on the lunar surface. The natural breakpoint for manned operations will be determined based on such testing.

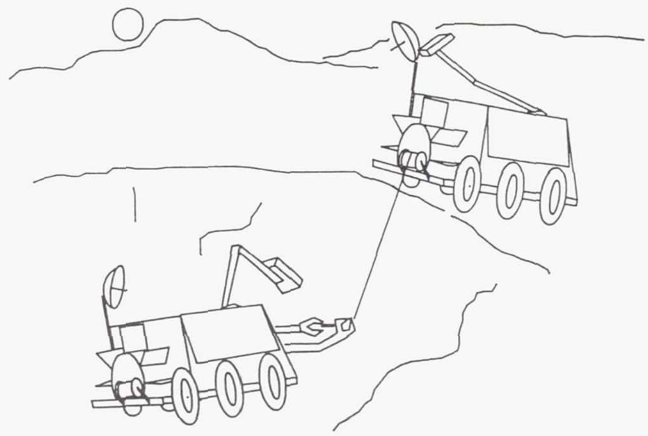

Fig. 6. The "Buddy System": Utilizing 'Manual Override' through teleoperation, the two vehicles can assist each other when required.

Paradigms and control systems for LRV remote sensing verification, resource exploration and recovery, and resource transport will be tested. The functional operating parameters of the subsystems to be utilized in remote sensing verification will be defined. Topographic maps can be verified using pulsed-laser ranging. Soil calibration can be accomplished through sample retrieval, gas chromatography, XRF, FTIR, and ICP. The available sensor systems for monitoring both the internal state of the vehicles and external interactions with the environment can be field-tested. A determination can then be made on the completeness of available sensory information. System upgrades can be implemented to fill any voids in the required sensory information. Field testing of control system integration with pulsed-laser ranging and infrared proximity sensing will document the operational accuracy of spatial localization for both the LRVs and robotic arms. Strain gauges and magneto-resistive systems utilized in the robotic arms will be tested to determine the quality of cutaneous and kinesthetic information, respectively. The functional control algorithms of all subsystems will be updated based on information gathered during field testing. The power requirements for the vehicles and subsystems will be determined for a broad range of mission scenarios. Extensive field testing will allow the operational capabilities of the LRVs and LRAT to be defined, and an appropriate manned intervention scenario to be chosen. The extent to which automated control can be utilized will be determined, and functional manual override systems tested. Teleoperation will be utilized for repairs and control of the LRAT during exploration and remote sensing verification. The completion of field testing in 2000 will define the degrees of freedom available for autonomous interactions with the environment and the capabilities of teleoperation.

Model crisis situations can be contrived in a highly-monitored environment in order to determine the extent and effectiveness of a "buddy system" operating protocol (Fig. 6).

Classically the "buddy system" is an arrangement in which two individuals operate individually but may work together as

a team in critical situations. In this scenario an otherwise disabling or dangerous situation can be avoided by the intervention and support of the other team member. Field testing of manned intervention will enable hands-on human training. Estimates on the capabilities of manned teleoperated repairs will be elucidated, and programmed crisis recognition routines will be experimentally verified. Nominally, teleoperated intervention, communication constraints withstanding, are anticipated for most repairs. Manned intervention on the lunar surface during the automated missions would occur only in the event of LRV failure or "unrecognized" circumstances. The "buddy system" should not only enable more complicated tasks to be undertaken, but should also provide an effective manner in which to perform these tasks. The implementation of the "buddy system" via teleoperated links could, for example, allow a wheel to be changed using the manipulator arms. Similarly, a towline could be utilized if one vehicle became stuck, or a jumper cable could be installed to supplement the power of a single vehicle. Further, the quantity of information gathered during the mission will be doubled, and memory dumps will provide redundancy in the stored information as well as shared information between vehicles. The teleoperated "buddy system" should play a crucial role in the effective initiation of lunar activities utilizing automation and robotics.

Field testing of the bio-volume will evaluate life-support system hardware and show balanced compatibility of plants, fish and primitive life forms. The role of physicochemical systems and storage volumes will be assessed. The experimental field testing will provide the necessary control studies and experimental verification of the operating systems to compare earth-based to lunar-based biological experimentation. The types of plants, fish, algae, bacteria, and fungus to be utilized can be determined. The volumes and power dedicated to each subsystem should be determined such that an optimal balance between the biological and physicochemical systems is attained. Subsystems can be monitored to determine power requirements, water and nutrient requirements, and growth rates. Further, the extent of interactions with the vehicles will be determined, and the potential degree of local resource utilization defined. Manned interactions and modifications of the EBV necessary to provide habitat modifications of the LOAR can be extensively planned and structured. Modular designs will be essential in the development of the subsystems in order to permit rapid manned upgrades of system technologies. Information gathered will impact the LOAR program, Space Station *Freedom* and terrestrial-based ECLSS programs. Extensive earth-based testing of fully controlled life-support systems will allow the baseline capabilities of the EBV to be defined. A detailed scenario for manned re-configurations can then be determined.

2. Lunar Polar Orbiter (Remote Sensing)

The site chosen for the implementation of the LOAR project relates directly to the initial missions and future development scenarios. The LPO information will be crucial in order to determine the areas of maximum sunlight, resource availability, and navigable terrain. The polar regions offer the possibility of nearly continuous lighting. Continuous satellite monitoring of the lunar poles will enable the determination of the variable lighting and power use schedules. The thermal and lighting characteristics available at a polar site should play a major role in determining a landing site. The north pole has been more extensively mapped, while the south pole faces the scientifically intriguing galactic center. A polar site offers the advantage of at least 6 months continuous sunlight (maximum elevation above the horizon is 1.5 degrees). Areas continuously shadowed, caves and lava tubes, are sites for the potential existence of volatiles. Maximum sunlight is likely to be the most applicable for manned outposts, since at least some portion of the power requirements will be fulfilled utilizing solar voltaic arrays. The availability of natural sunlight for growing plants would also reduce the power requirements of the EBV. Potentially a site can be located that will provide continuous sunlight throughout the year[4].

The implementation of lunar activities will begin with the launch of the Lunar Polar Orbiter (LPO) scheduled for 1994. High resolution (1 meter) topographic maps coupled with candidate identification of available resources will provide the initial world models (maps) upon which the automated exploration and search strategies will be built. Each mission scenario will require a particular database of sensory information. High resolution topographic maps (1 meter or less) will provide the information for creating internal maps and markers for autonomous navigation of the lunar surface. Further, elevation changes and the relative hardness or softness of the lunar regolith will be estimated in order to develop safe and efficient navigable routes on the lunar surface. Gamma-ray, X-ray, IR and neutron spectrometers will provide the initial mapping of candidate areas for deposits of both volatiles and recoverable *in situ* resources. The information obtained by remote sensing will determine not only the initial landing site, but also the operating characteristics and mission scenarios undertaken at each of the various exploration sites. The availability of local information or "ground truth" will allow more detailed and accurate remote sensing to be accomplished; therefore, more detailed and accurate world models can be developed. Periodic updates of the robotic systems should increase the efficiency and safety of progressively more ambitious missions. A/R coupled with the LPO will enable manned missions to take advantage of accurate topographic maps and resource locations.

3. Surface Delivery

Following the evaluation of remote-sensing data from the LPO, the LRVs and EBV will be delivered to the selected landing site on the lunar surface by Lunar Expendable Landers (LEL). Initial deployment is scheduled for the years 2000-2001. The unique features of the LEL includes the maximum use of all hardware and consumables delivered with the payload. Cryogenic propellants, liquid hydrogen (LH_2) and liquid oxygen (LOX), rather than existing storable propellant technology have been selected due to potential use in the LOAR. Leftover propellants will be combined into water for use in regenerative fuel cells. The attitude control jets, fueled

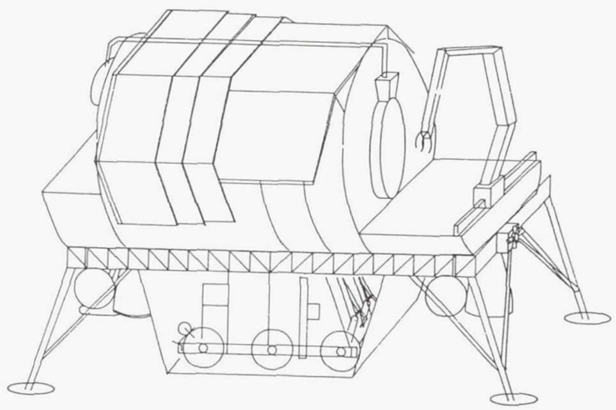

Fig. 7. The landing configuration of the proposed Lunar Expendable Lander (LEL).

by nitrogen, will be scavenged and used as the inert gas in the bio-volume. The principal advantage of this propulsion system is its suitability for reconfiguring and using the tank structures in the bio-volume. The hydrogen tank is equipped with rack-type structures for the biological experiments and the ceiling track for the robotic arms. The oxygen tank will serve as the airlock for bio-volume operations. The intertank section is a safety buffer between the LOX and LH_2 tanks and serves as a storage volume for the temperature-sensitive equipment and biological experiments. The robotic arms utilized in the bio-volume will have to remove the hydrogen bulkhead in order to gain access to the hydrogen tank. The landing configuration of the LEL includes an approximate dry mass of 8770 kg (lander structure, engines, tank, bio-volume support equipment, and LRV). With the characteristics given for the chosen propellants and the mission, a total wet mass of 33,300 kg to be launched into Low Earth Orbit (LEO) (Fig. 7).

A breakdown of the mission and mass assumptions are as follows:

Δ-V from LEO to LO	4100. m/s
Δ-V from LO to LS	1900. m/s
Total Δ-V	6000. m/s
$I_{sp\ vac}$	4500. m/s
Dry Mass on LS	8770. kg
Propellants LO to LS(MR=1.52)	4600. kg (Δ-V 1900 m/s)
Wet Mass in LO	13,370. kg
Propellants LEO to LO (MR=2.49)	19,900. kg (Δ-V 4100 m/s)
Total Mass Delivered to LEO	33,270. kg

The propellant tanks (with the bio-volume support equipment attached on the outside) and the lander structure (with the LRV payload bay, engines, and LRV) will be launched in the Shuttle-C (D-4.5m × L-22m, → 35,000 kg payload into LEO). In orbit the lander and tank module will be reconfigured into the lunar transfer and landing configuration as shown in Fig. 7. The LEL consists of a truss structure with landing gear, two cryogenic engines (20 kN thrust each, restartable, and with variable thrust) and distributed attitude-control jets. Trans-lunar shipment and the lunar landing sequences for the LEL will be controlled via automated computer systems. The solar arrays, heat radiators, and external robotic arm are permanent installations on the outside of the tank. The LEL assembly will be protected from dust during landing by a removable cover. Micrometeorite "bumper" shielding is built into the individual components. Beginning activities on the lunar surface will require that the LRV deploy solar arrays and heat radiators. Remaining propellants will be combined into water for storage.

4. Remote Sensing Verification

Utilizing the mobile search routines developed during field testing, the groundtruth of remote sensing information will be determined using the first LRV. The vehicle will establish a home base at the landing site by deploying a set of triangulation beacons. Starting from this central hub, gas chromatography can be utilized for the calibration testing of lunar soil, and pulsed-laser ranging can verify the topographic maps. Pulsed-laser ranging should also allow the vehicle to determine relative position to known landmarks and the triangulation beacons. Stereoscopic television cameras will provide earth-based verification of search and movement strategies, as well as the capability for teleoperated intervention and control of both the vehicles and robotic arms.

Navigation strategies will take advantage of the world model developed from the remote-sensing topographic maps. Determination of the routes and search orders will be made via neural network computation. A three-dimensional version of the two-dimensional Hopfield model[5] should allow for rapid, accurate calculations of shortest routes and pathways. The sites and topographic markers would form the nodes of such a model. A two-dimensional model solves the traveling salesman problem on the order of 1000 times faster than conventional computer systems. A three-dimensional architecture should provide real-time strategies. Verification of the pathway integrity would rely on expert system diagnostics that compare the defined routes to available topographic maps.

Sample retrieval can be done via robotic arms utilizing infrared proximity sensors and a sample coring device. The robotic arms should be able to place the samples inside a closed module containing a number of separate storage compartments on a rotating track. The analyzer package onboard the LRVs must be capable of providing information on the chemical and mineralogic composition of the lunar soil and volatiles.

An important mission driver is the search for and retrieval of volatiles trapped within the soil and recoverable by heating. The analyzer package should consist of the following: (1) X-ray fluorescent spectrometer (XRF) for analysis of trace elements; (2) Gas chromatography for analysis of heat released gases from rock samples; (3) Fourier transform infrared spectral analyzer (FTIR) for volatile searches; (4) Inductive

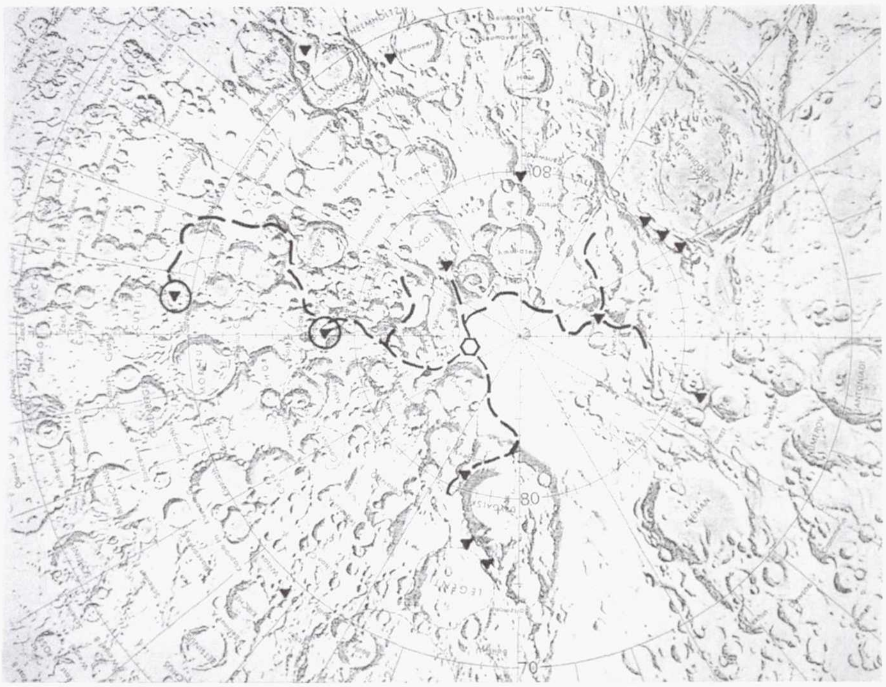

Fig. 8. Possible map of the lunar South Pole showing the Lunar Oasis (hexagon), volatiles and resources identified by the LPO (triangle), verification of LPO information by LRV (circle/triangle) and navigable pathways (dashed line).

coupled plasma analysis for analysis of bulk chemistry; and (5) X-ray diffraction for mineralogic analysis of soil.

Teleoperated LRAT tethered to the main vehicles will provide access to craters, caves and lava tubes in the search for volatiles during the verification of remote sensing. Information on soil hardness and spectrographic analysis information will also be obtained both for calibration and verification of remote-sensing information. By 2004 the more detailed lunar topographic and resource maps should provide manned missions with the databases required for a more effective and efficient development of a habitable manned outpost on the lunar surface (Fig. 8).

5. Volatile Availability/Recovery

Following remote sensing calibration by the LRVs and LRAT, the question of volatile availability at the lunar poles in shadows, caves, craters and lava tubes will be reasonably well resolved. Areas indicated as potential resource deposits via remote sensing will be searched. These sites can be located using the same search and navigation strategies as utilized for verification of the remote sensing, and will in all likelihood parallel such efforts. Gas chromatography of samples taken from the sites can not only serve as verification, but should provide an estimate of the quantity and recoverability of the resources. Available resources of interest are expected to be water, carbonaceous meteorites, metal deposits, and regions of regolith high in ilmenite, silicon dioxide, or iron. Exploration for volatiles and resource availability in less accessible areas will have been carried out by the teleoperated LRAT. Utilizing existing high-survivability cart designs and tethers for connection with the main vehicles, areas several hundred meters from the main vehicles will be explored. The LRAT are anticipated to provide science information on the interior of craters, caves and lava tubes. Highly accessible local resources will be collected utilizing specialized digging appendages and a 10-meter core drill. Recovered volatiles will be transferred into a trailer-towed N_2 tank for transport to the Lunar Oasis and EBV for storage. The collection and mapping of high-quality resource deposits should enhance future manned missions. Manned missions should be able to plan on the *in situ* resources available to the LOAR, as well as on consumables which must be shipped to the lunar surface.

6. Experimental Processing

Experimental processing will be carried out by both a robotic vehicle designated for processing and the bio-volume facility. The LRV will perform small-scale tests on experimental processing techniques such as material separation, fiberglass, concrete, and composite production from lunar regolith. A 0.05-m^3 silicon-carbide ceramic furnace, (1500°C) powered by the vehicles and RTG waste heat, will test "regolith cooking" for volatile extraction. Vibratory screens and electromagnetics are anticipated to be the separation techniques employed to increase the expected yield from raw materials (e.g., ilmenite separation for reduction by hydrogen to water).

In addition to feasibility testing, the LRVs will produce one specific lunar composite. The LRVs will collect lunar rocks and, utilizing an earth-derived resin poured onto the rocks, should be able to create a composite material. To protect the polymers from ultraviolet radiation, the composites will be coated with a UV resistant paint. The composites can then be utilized in the exploration of building techniques for use on the lunar surface. The EBV will perform moderate-scale regolith cooking for volatile recovery. Zonal centrifugal acid separation techniques should be explored for the recovery of other valuable components of the regolith such as the silicates and metal oxides. The high grade materials can be stockpiled and/or utilized in the EBV as inputs to the life-support system. For example, ilmenite might be reduced utilizing the methane produced in the bioreactor. Outputs from this process would be carbon dioxide and water which could be stored and/or utilized in the biological experiments. Microbial acidification of lunar regolith into the soil components suitable for higher plant growth will also be explored. Such microbial action can be considered a first step in microbial resource recovery such as carbon extraction from carbonaceous meteorites.

7. Biological Experimentation

The utilization of local resources and the viability of primitive life forms will be tested on the lunar surface. Information relevant to the development of life-support systems should be gathered not only for space-based operations but also for potential utilization on the Earth. A percentage of the EBV will be dedicated to a higher plant growth chamber, a dark box for the growth of fungus, spores, and sprouts, a soil composter, a Wet Oxidation (WETOX) digester, an aquaculture chamber, and a bioreactor. Outputs from the higher plants will include transpired water, oxygen, and biomass. Outputs from the fungus, spores, and sprouts can potentially be fed into the bioreactor. The bioreactor will test waste processing by bacteria, algae, and primitive animals such as worms. The worms should perform soil conditioning and serve as a digestive mechanism for plant biomass. The bacteria and algae should remove the gaseous, liquid, and small solid contaminants from the plants. The outputs of the bioreactor will include carbon dioxide, nitrates, and other chemicals which can be used to nourish the higher plants. The physicochemical systems working in concert with the biological systems must produce an atmosphere capable of sustaining life. Atmospheric control in the EBV coupled with plant growth and waste processing should provide valuable information in the development of LECLSS technologies (Fig. 9).

HARDWARE

1. Surface Support Equipment

Prior to manned missions to the LOAR, the following requisite equipment is envisioned to be in place: (1) Power Supply, (2) Heat Rejection System, (3) Storage Volume, (4) Airlock Access to EBV.

2. Vehicles

The vehicles will be designed and built using many existing technologies with proven success rates and reliability. Advanced robotic and automated system designs will be utilized, such that the next generation of robotic systems will no longer simply observe and interact passively with the environment. Rather, these systems will be capable of autonomous interaction with, and manipulation of, the environment.

Design Guidelines

1. Highly redundant: Multiple sensors, effectors and control systems.

2. Self-similarity: Modular components and functional exchanges.

3. Existing technology: Reliability tested, low cost, accurate integrations.

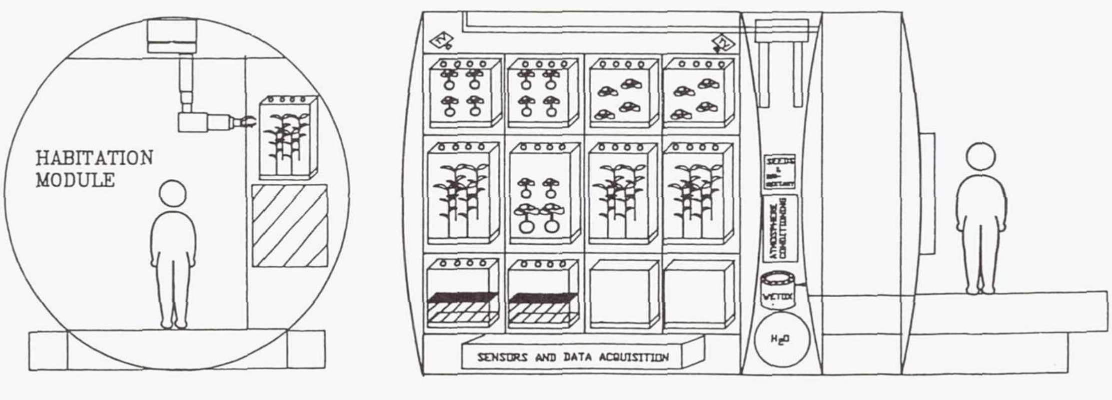

Fig. 9. The Experimental Bio-Volume (EBV) following reconfiguration and implementation of the biological systems. Shown are the higher-plant growth chambers.

4. Simple mission profiles: Planned, mapped, structured tasks.

5. Environmental and situational predictability: Extensive sensing, internalized maps, "learning."

6. Modular system upgrades: Phased technology demonstrations.

7. Common power bus, standard hardware templates, standard mechanical and electrical connectors.

General System Recommendations

1. The baseline models in space robotic development were the Lunar Roving Vehicles of the Apollo era, as well as the Mars Viking Lander. The LRV weight of 1500 kg each is twice that of the Lunar Rovers. Each vehicle should be capable of towing/winching approximately 1.5 times the vehicular weight and manipulating 250 kilograms. The vehicles are anticipated to be six-wheeled flat platforms of approximately 10.5 m^2 (4.2 m length, 2.5 m width), with attachment sites for the modular components. Advanced materials such as aluminum alloys and composites should be utilized to increase the strength to weight ratio. Composites can be made highly resistant to general wear and laminated to minimize their coefficients of expansion.

2. The vehicles will be similar and modular in design. Specialized components will be utilized for specific tasks. Functional overlap between the following subsystems is anticipated: power supply systems (RTG and DIPS, battery back-up), thermal control systems (heat rejectors, 5 to 10 times the electric power), meteoroid protection shields, the guidance and control systems, antennas, the electric drive motors (3 kW each, 4 hp total), onboard computers for autonomous operation (maneuvering, geological analysis) and the manipulator arms for self-maintenance as well as for surface operations. Robust systems with an emphasis on parallel delivery of information, sensory input, power, and computation through multiple pathways will provide redundancy in all levels of operation.

3. Task and mission scenarios will be designed to place minimal requirements on the computational systems. Accordingly all mission scenarios and tasks should be designed in a fashion conducive to robotic implementation.

Specialized Subsystems will include: (1) Materials processing and (2) Geologic/Soil analysis. For geologic analysis, the modular packages include drilling equipment for core samples and automated laboratory equipment (see Geologic Analysis Systems). For materials processing, the modular packages include mechanical separators for material sorting and mechanical testing rigs for material evaluations (see Materials Processing Systems).

Geologic Analysis Systems

Sample collection:	Drill, manipulator arm, teleoperated LRAT
Sample preparation:	Core-drill, cutter, polisher
Physical properties:	Density, hardness, temperature, thermal conductivity, melting point, magnetism, solubility (consumables water and acids)
Optical analysis:	Polishing facility, microscope
Composition:	Gas chromatography/thermal release of volatiles
	X-ray fluorescent spectrometer for analysis of solids
Geophysical data:	Magnetometer, gravimeter, vibrator, seismometers

Materials Processing Systems

Pre-processing:	Sieves, separator, storage, transportation
Sample analysis:	Strength tests, loading/bending, outgassing, hardness
Materials processing:	Lunar composites, aggregate binding, environmental endurance, fiberglass, fiberglass winding technologies

Additional Requirements

(1) consumables for analyzer laboratory
(2) spare parts for vehicles and modules
(3) manipulation of landed volumes/material-crane

Vehicle Specifications

Total mass with payload	1500 - 3000 kg
RTG for 5 kWe	800 kg (2 m × 2 m × 0.25 m)
DIPS for 5 kWe	500 kg (1.32 m × D 0.65 m)
Structure	500 kg
Scientific Instruments	300 - 2000 kg
Radio/communication	100 kg
Computer/navigation	100 kg
Computer/analyzer/data processing	100 kg
Propulsion power	3 kW (4 hp) for electric motors
Payload power	2 kW
Max. slope	20° or 36%
Max. speed	10 km/h

3. Bio-Volume

The reconfigurable bio-volume will consist of two major parts: the airlock and the experimental volume. The airlock (previously the oxygen tank) will provide access to the pressurized interior (see Bio-volume Atmosphere Control). The experimental volume (previously the hydrogen tank and the intertank section) will provide space for experiments as well as control and monitoring equipment. During the automated phase of the LOAR operation, biological experiments for a Lunar ECLSS will be conducted. Manned sorties starting in 2004 can utilize the volumes to provide temporary shelter and life-support consumables. The proposed mission scenario requires three LEL landings prior to any human mission. Each of the three bio-volumes will provide reconfigurable volumes for the development of life supporting modules, a laboratory area and control centers. Activities

within the experimental volume will include plant growth, biological waste treatment (bioreactor) and small-scale animal experiments (aquaculture and soil processing). The use of lunar soil as a growth medium and the recovery of trace elements from the soil via microbial acidification and extraction will be investigated. The EBV will provide the first non-terrestrial ECLSS capabilities. Plants, animals and microorganisms will live in a physicochemically buffered symbiosis. Robotic arms will provide internal manipulation of hardware for all experiments. Buffer volumes will be maintained for carbon dioxide, oxygen, nitrogen and water. Capitalizing on local resources (trapped volatiles such as water, carbon from carbonaceous meteorites) the buffer volumes can potentially be increased prior to human visits. Results obtained from the experiments will elucidate important questions in the design of a LECLSS (see Bio-volume Specifications).

Design Guidelines

1. Highly redundant growth chambers.
2. Autonomous: self-contained power and regulatory systems.
3. Multiple sensors and experimental monitoring systems.
4. Phased technology demonstrations: lunar processing, *in situ* resource recovery.
5. Utilization of available *in situ* resources: volatiles, carbon, ambient temperature, light.
6. Modular adaptability for manned habitation.

Bio-volume Specifications

Module:	recycled from cryogenic propellant tank
Airlock (oxygen tank):	L = 1 m, D = 4.5 m, volume = 12.5 m^3
Bio-volume (LH_2 tank):	L = 5 m, D = 4.5 m, volume = 60 m^3
Total mass:	3500 kg (empty tank = 1250 kg, equipment = 2000 kg, buffer = 250 kg)
Total power:	10 kWe (30 m^2 solar array), regenerative fuel cell back-up
Heat rejection:	30 m^2 solar radiator

Bio-volume Atmosphere Control

Volume:	3 m^3 (intertank)
Mass:	300 kg
Power:	2 kWe
Atmosphere:	Control temperature, humidity, composition, temperature, pressure, nitrogen 75-95%, oxygen 5-25%, carbon dioxide 25-5000 ppm

Physicochemical systems

CO_2 absorption:	Solid amine process
O_2 absorption:	Salcomine process
CO_2 conversion into H_2O:	Sabatier
Oxygen generation:	Electrolysis (H_20 into O_2 and H_2)
Humidity/Temperature control:	cold-plate condenser, heat exchanger

The contents of the bio-volume consist of multiple-start, stored biological systems including complex, "wild-type" lyophilized cultures of microorganisms. Adapted soil and water cultures will range from N_2 and CO_2 fixing organisms to soil acidification/digestion organisms. Higher plant seeds will be maintained in sufficient amounts to employ a variety of reseeding technologies. Using "batch mode" operations, materials will periodically be changed-out between growth and production environments. Human consumables will be stored for subsequent manned missions. The net N_2 fixation losses will be restored from cold jet tankage supplies and carbon fixation losses from derived lunar carbon resources. Lunar soil exhausted of carbon reserves by composter activities will be returned to the lunar surface. Other bio-volume contents and systems are listed (see Bio-volume Systems).

Bio-volume Systems

Higher plants
Bioreactor - algae, bacteria
Fungus, spores, sprouts
Aquaculture
WETOX digester
Atmospheric control system/humidity control
Hydroponic nutrient delivery system - for higher plants
System controller and data acquisition system
Buffers - gases, liquids

The bio-volume uses the buffer and process rate mixes arising from five major systems. The composter and WETOX systems focus on long-term and short-term, respectively, elemental extractions and bio-conversion. The bioreactor provides rudimentary gas release and fixations. Finally, the higher plant and aquaculture systems provide consumable products, most of which are candidates for storage (see Bio-volume Commitments).

Bio-volume Commitments

Higher plants:
Volume: 8 m^3 growth space
Power: 0.7 kW/m^2 = 5.6 kWe
Temperature: 20-25° C
Hydroponic growth media
Lighting - red and blue LED
Transpiration water recovery (centrifugal, dew point precipitator)
Lunar soil (processed)
Bioreactor:
Volume: 2.0 m^2
Temperature: 20° C
Algae, bacteria, microorganisms
Gas fixation/release
Filtered recoveries/separation of species
Aquaculture:
Volume: 0.5 m^3
Temperature: 15-25° C
Eggs, brine shrimp, live cultures
Bacteria, micro-algae
Controlled P_{CO_2}, P_{O_2}

Composter:
Volume: 1.0 m^3
Temperature: 10-30° C
Pressure: 300 kPA
Mixing: Auger
Atmosphere: High O_2
WETOX:
Volume: 0.5 m^3
Temperature: Ambient to 700° C (microwave heat)
Pressure: Ambient to 7 MPa
Buffer volumes:
Gases, liquids (approx. 10 m^3, total)
Plant materials such as seeds, spores, lyophilized algae and bacteria (1 m^3)
Carbon sources (CO_2, recovered meteorite carbon)

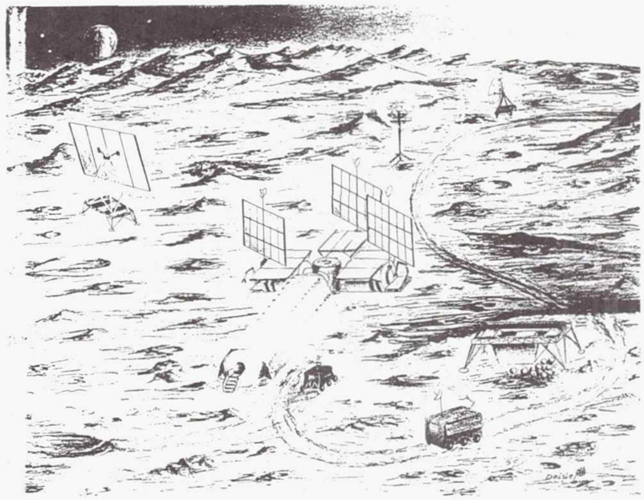

Fig. 10. The completed and operational Lunar Oasis, LOAR, after return of humans to the lunar surface.

CONCLUSION

The initiation of lunar activities via automation and robotics will enable effective low-cost implementation of the LOAR project prior to manned operations. Databases containing the topographic features of the lunar surface and the availability and recoverability of volatiles and lunar resources are completed. Future manned missions spanning the period of 2004-2010 finish and elaborate the fully manned LELCSS. Utilization of available resources should be optimized. Potentially, the shipment of consumables from the lunar surface to supplement the cislunar infrastructure can be undertaken. This might be a commercial activity. The propulsive system utilized in the delivery of lunar resources is projected to be a mass launcher. The far side synthetic aperture radio observatory as well as remote seismic and gravitational experiments should be enhanced. Manned reconfiguration of the experimental bio-volumes into the habitable LOAR should allow manned sorties to complete the deployment of scientific apparatus or repair and service them as necessary. The development and growth of an effective cislunar infrastructure is anticipated to rely heavily on A/R and manned projects such as LOAR (Fig. 10).

Preliminary data from the EBV will allow a quantitative comparison between the capabilities of a terrestrial life-support system and a lunar life-support system. Information gathered will not only impact space-based life-support systems, but also should impact on the development and implementation of ECLSS technologies on the Earth. Commercial interests in life-support systems and advanced robotics will stimulate the design of these systems, as well as provide potential earth-based industrial utilization of the technologies developed. The phased mission scenario emphasizes a shift in space-based operations to a more cost-effective, efficient system in which automation and robotics coupled with manned missions can play a crucial role in the development of the cislunar infrastructure. The LOAR program highlights the possibilities of this cooperative type of endeavor for future activities in the space environment.

To permit implementation at modest cost and with maximum technical impact, the LOAR is projected to cost $5 billion. Technical manpower will be leveraged through academic involvement, and international business/industry competition will be assured by corporate involvements. The LOAR will be implemented by these entities and subsequently interfaced with the NASA manned space program elements.

ACKNOWLEDGMENTS

Authors W. Faller, A. Hoehn, S. Johnson, P. Moos, and N. Wiltberger were assisted by faculty advisor Professor Marvin W. Luttges.

REFERENCES

1. National Commission on Space, *Pioneering the Space Frontier,* Bantam Books, New York, 1986.
2. Ride, S.K., *Leadership and America's Future in Space,* U. S. Government Printing Office, 1986.
3. Buck, C.A., Johnson, A.S., McGlinchey, J.M., Ryan, K.D., Luttges, M.W., "The Development Of A Cislunar Space Infrastructure," *Proceedings of the 4th Annual Summer Conference,* NASA/USRA University Advanced Design Program, 1988, pp. 75-83.
4. Burke, J.D., "Merits of a Lunar Polar Base Location," Mendell, W.W. (ed.), *Lunar Bases and Space Activities of the 21st Century,* Lunar and Planetary Institute, Houston, 1985.
5. Hopfield, J.J., Tank, D.W., "Computing With Neural Circuits: A Model," *Science 233*:625-633.

382673 **N94-71273**

1994004518

DESIGN OF A LUNAR TRANSPORTATION SYSTEM

FLORIDA A&M UNIVERSITY/FLORIDA STATE UNIVERSITY

S6-37
160632
P. 8

INTRODUCTION

The development of a good transportation infrastructure is a major requirement for the establishment of a permanent lunar base. Transportation is characterized by the technology available in a specific time frame and the need to transport personnel and cargo between Earth and Moon, and between lunar bases. In our study, attention was first focused on developing a transportation system for the first generation lunar base. As a first step, a tracked-type multipurpose lunar transportation vehicle was considered as a possible mode of transportation and a detailed study was conducted on the various aspects of the vehicle. Since the vehicle is composed of many moving parts, exposing it to the environment of the Moon, where fine dust particles are prevalent, can cause problems associated with lubrication and friction. The vehicle also posed problems concerning weight and power. Hence, several modifications were made to the above design ideas conceptually, and a Lunar Articulated Remote Transportation System (Lunar ARTS) is proposed as a more effective alternative with the following objectives:

(1) Minimizing the transportation of construction material and fuel from Earth or maximizing the use of the lunar material;

(2) Use of novel materials and light-weight structures;

(3) Use of new manufacturing methods and technology such as magnetic levitation using superconducting materials; and

(4) Innovative concepts of effectively utilizing the exotic lunar conditions, i.e., high thermal gradients, lack of atmosphere, lower gravity, etc.

To achieve the above objectives of designing transportation systems from concept to operation, the project was planned in three phases: Phase I: conceptual design; Phase II: detailed analysis and synthesis; and Phase III: construction, testing, evaluation, and operation.

In this project both phases I and II have been carried out and work on phase III is in progress. In this paper the details of the Lunar ARTS are discussed and the future work on the vehicle are also outlined.

VEHICLE DESIGN

Before addressing the specific design problem, it is assumed that there is a lander with the capability of delivering the required payload to the surface of the Moon and the vehicle is to support lunar base operations in the years 2000-2005. The conceptual design of Lunar ARTS is shown in Fig. 1, and the details of each component are discussed in the following sections.

The design criteria for the vehicle include the following:

- Reliability and simplicity of operation

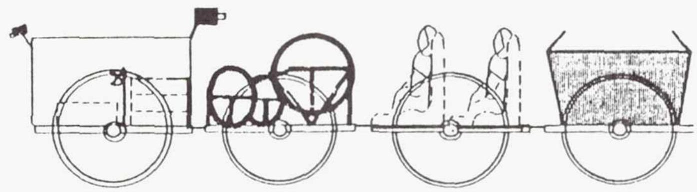

Fig. 1. Modular Vehicle Design

- Maximum payload capacity
- Ease of operation
- Ease of maintainability
- Ease of mobility
- Emphasis on modularity

It is also emphasized that the latest available technology be used at all levels of construction of the vehicle. In order to meet the aforementioned goals, it was decided to design the vehicle in a modular format as follows: (1) control and power cart, (2) energy cart, (3) personnel carrier, and (4) materials carrier.

The multiple module design extends flexibility in terms of size and weight control, expandability, mobility, power, and design efficiency.

Power Requirement

The power and energy requirements for the Lunar ARTS varied between mission configurations. Differences in peripheral equipment, vehicle weights, and the expected terrain to be covered were the primary causes of these variations. The vehicle is powered by a fuel cell system, as shown in Fig. 2.

They are durable, dependable, and may be sized acccording to power requirements. The portion of the vehicle that houses the energy source consists of a power cart and a fuel cell cart. The power cart contains the fuel cells and necessary control equipment and the fuel cells would be made available for any power level. Any number of cells can be operated to provide the total energy requirement.

Fuel cell system description. The fuel cell system consists of the following subsystems: (1) reactant storage; (2) stacks, including water storage; (3) radiator; and (4) fuel replacement.

The complete reactant and by-product storage system includes the following components: tanks for reactant and by-product storage, piping for fluid flow, and control equipment. Much of this design is based upon the current space shuttle system. Hydrogen and oxygen are stored in thermally insulated spherical tanks. Each tank has a vacuum annulus between the

58 INTENTIONALLY BLANK

PRECEDING PAGE BLANK NOT FILMED

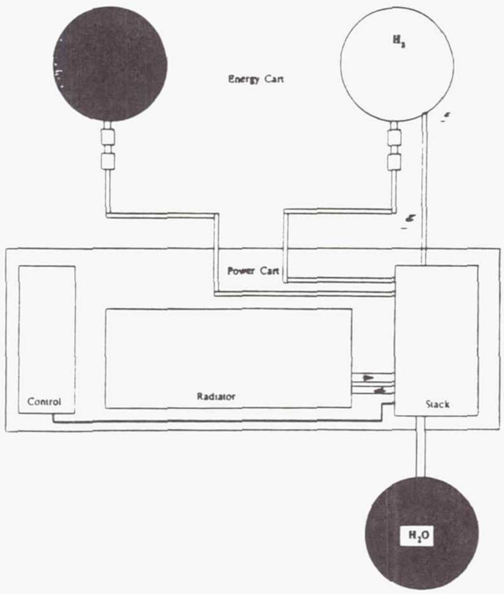

Fig. 2. Fuel Cell System

inner pressure vessel and the outer shell of the tank. This tank configuration allows the reactants to be stored at supercritical conditions for long periods of time. The by-product of the reaction in the fuel cell system is water that can be used for human consumption. The inner pressure vessel temperatures are maintained by minimizing conductive, convective, and radiant heat transfer. Twelve low-conductive supports suspend the inner vessel and outer shell, and convective heat transfer is minimized by maintaining a vacuum between the vessel and the outer shell.

Hydrogen tanks will have one heater probe with two elements, while the oxygen tank has two heater probes with two elements on each probe. As the reactants are depleted, the heaters add energy to maintain a constant pressure in the tank. The heaters operate in an automatic mode.

Each tank is equipped with level detectors, quantity sensors, and pressure sensors. These are controlled by the hydrogen/oxygen control box located in the power cart. All other equipment needed to monitor, maintain, and feed the system is contained in the fuel cart.

The reactants from the tanks flow through two relief valve/filter modules and valves, then to the fuel cells through a common manifold. The pressure of the reactants will be essentially the same at the fuel cell interface as it is in the tanks since only a small decrease occurs in the manifold. The relief valve/filter modules contain the tank relief valve and a 12-micron filter. The filter removes reactant impurities that could degrade the fuel cell stack. The valves relieve excessive pressure that builds up in the tank. A manifold valve relieves pressure in the manifold lines. The reactants then flow through four valve modules. Each module contains a check valve for each tank line coming in, a manifold valve, and a fuel cell reactant valve. The check valve in each tank line prevents reactants from flowing from one tank to another in the event of a tank leak. The fuel cell reactant valves allow reactants to flow into the fuel cells from the manifold or isolate the reactants from the fuel cell. In the case of dual fuel carts, the manifold valve isolates one reactant system but allows reactants from the remaining supply system to reach the fuel cell.

Stacks. The central part of any fuel cell energy system is the stack. This is where the chemical reaction takes place to produce energy. One of the main reasons for choosing a fuel cell energy system is its flexibility to meet changing power requirements. Fuel cell stacks can be selected to produce energy in varying degrees and can be combined to give maximum energy when required. The stacks can also be shut down individually if a problem occurs so the remaining system can operate. Typical fuel cell stacks consist of a power section, where the chemical reaction occurs, and an accessory section, which controls and monitors the power section performance. For this particular design the power section consists of 62 small cells contained in 2 substacks. Manifolds run the length of these substacks and distribute hydrogen, oxygen, and coolant to the cells. The cells contain electrolytes consisting of potassium hydroxide (KOH) and water, an oxygen electrode (cathode), and a hydrogen electrode (anode).

Hydrogen is routed to the cell's hydrogen electrode, where it reacts with hydroxyl ions in the electrolyte. This electrochemical reaction produces electrons (electrical power), water, and heat with the electrons being routed through Lunar ARTS subsystems to perform electrical work. Oxygen is routed to the cell's oxygen electrode, where it reacts with the water and returning electrons to produce hydroxyl ions. The hydroxyl ions then migrate to the hydrogen electrode, where they enter into the hydrogen reaction at the electrode. The oxygen and hydrogen are reacted (consumed) in proportion to Lunar ARTS electrical power demand.

Excess water vapor is removed by an internal hydrogen system. Hydrogen and water vapor from the reactants exit the cell stack, are mixed with replenishing hydrogen from the storage and distribution system, and enter a condenser, where waste heat from the vapor is transferred to the fuel cell coolant system. The resultant temperature decrease condenses some of the water vapor to water droplets. A centrifugal water separator extracts the liquid water and pressure-feeds it to a potable tank on the fuel cart. Water from the potable tank can later be used for human consumption and cooling of the Freon-21 coolant loops. The remaining circulating hydrogen is directed back to the fuel cell stack.

The fuel cell coolant system circulates a liquid fluorinated hydrocarbon (FC-40) and transfers the waste heat from the cell stack through the fuel cell heat exchanger of that fuel cell power plant to the Freon-21 coolant loop system in the power cart. Internal control of the circulating fluid maintains the cell stack at a normal operating temperature of approximately 93°C (200°F). The lifetime of each stack is approximately 2000 hr.

Fuel replacement system. In order to make Lunar ARTS a more efficient vehicle, refueling time of the fuel cells is to be kept at a minimum. In order to decrease this time,

it was decided to integrate the fuel storage and by-product tanks onto the chassis of the fuel cart. The entire system can then be removed and replaced as necessary. The removed set may then be refilled at a later time.

Suspension Design

Several designs for the suspension system were investigated for the Lunar ARTS using DADS (Dynamic Analysis and Design System) software.

DADS analysis. The DADS software is a set of general computer programs that can be used to model and predict the motion of a variety of real-world mechanical systems. Using a set of data that describes the machine to be modeled, DADS builds a mathematical model of the various parts of the mechanism, as well as resultant forces that act in the system. By using such a program for analysis, the designer can simulate the behavior of a wide range of alternatives prior to building and testing the prototypes. The DADS software can be modified for different gravitational effects, rigid and flexible body motion, etc. The constraints in the suspension design include the weight or load per wheel, the ability to traverse a one-foot bump, environmental protection, and the minimization of oscillations.

The methods of analysis used to observe the behavior of the suspension systems were kinematic and dynamic. These methods are summarized in the sections below.

Kinematic analysis. Kinematic analysis is used to calculate the motion of the various bodies in the mechanism, disregarding both their mass properties and any forces in the system. All degrees of freedom must be eliminated from the mathematical model by specifying a "driver." The results of kinematic analysis are the positions, velocities, and accelerations of all the bodies in the model, for each time step in the analysis.

Dynamic analysis. In dynamic analysis, the model may have any number of degrees of freedom. The motion of the bodies is calculated from the forces acting upon them and the mass properties of the bodies. The program requires that the initial position be specified at the start of the analysis. The results of the dynamic analysis are the positions, velocities, and accelerations of all the bodies in the model for each time step. Internal reaction forces in the joints and constraints can also be calculated.

Analysis output. Two types of design were analyzed by using the DADS program. These were the modified monoshock design and the double wishbone design. The double wishbone system (Fig. 3) was selected as the final design. The double wishbone allows for a constant vertical motion of the wheel and also provides better load distribution (3 points vs. 2).

From this selected design, four cases were then analyzed: (1) fuel cart, (2) power cart, (3) personnel cart, and (4) materials cart.

Several aluminum alloys were considered, and aluminum 2025-T6 was selected as a possible material for the suspension. From the analysis, the maximum forces on the revolute (ground) joint were obtained. The axial and bending stresses were calculated and compared with the yield stress of Al 2025-T6. Details of the analysis are given in the annual report. These values were found to be considerably less than the yield and it was decided that Al 2025-T6 would be a suitable material for the suspension system.

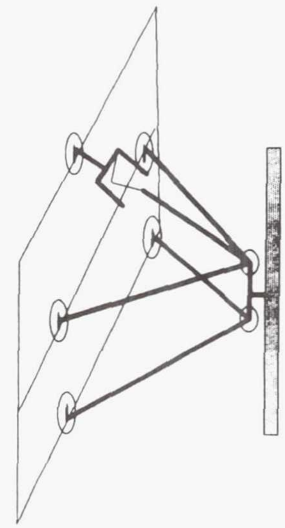

Fig. 3. Double Wishbone Design

Gear System

The gear system designed for the Lunar ARTS consists of two parts. The first is the analysis and design of a planetary gear system for a derived reduction ratio; the second step is the gear system assembly.

Planetary gear system. The assumptions in this section relate to values assigned to the variables used in typical spur gear analysis. After a detailed study it was determined that the best design utilized motor and drive shafts consisting of Titanium Alloy 38644, which provides the strength required. The pinion gear is to be made of high strength steel (AISI 4142). The design selected minimized the required diameter, while allowing for enough strength to withstand the forces applied through vehicle operation.

Gear system assembly. The initial assumption for this section is that the gear assembly chosen must relate to the double-wishbone suspension system selected for the vehicle. Also, the size selected for the drive shaft was used as a constraint.

Design option 1. The first option proposes the use of a spline gear to allow for the change in drive shaft length caused by the movement of the wheel. This design option consists of a stationary motor connected to the chassis. The drive shaft is then connected to the wheel through a universal joint. The other end of the shaft is connected to a spline gear that, in turn, is connected to the motor gear through a universal joint. The primary constraint of this design option

appears to be the requirement of lubrication for the spline gear in addition to all the joints.

Design option 2. A second proposal consists of a motor and drive-shaft, configured as a single unit, mounted on a sliding and rotating track, and connected directly to the wheel. The sliding track arc will match the arc produced by the vertical movement of the wheel, while the rotating track will correspond to the turning of the wheel. The track mounts, which will attach to each side of the motor casing, and the tracks themselves will consist of a layer of Kevlar at the contact areas to reduce friction while eliminating the need for a lubricant. A primary constraint for this option is the force acting on the track systems due to the implementation of the single-unit motor, shaft, and wheel system.

Analysis. To limit the requirement for lubrication, the second option was selected and analyzed. This analysis consisted of an estimation of the forces acting upon the entire assembly, and the selection of the materials necessary to withstand such forces. This was done to determine the shear forces and bending moments on the drive shaft. The materials were chosen that could withstand them. It was found that the Titanium Alloy 38644 is strong enough to withstand the resulting forces. Therefore, this alloy was confirmed as the selection for the drive shaft because of its high-strength and low-density characteristics.

Wheel Design

The design of any wheel is unique given a vehicle's weight and performance requirements. The main objective in this wheel design is to optimize the drawbar pull (DP). The DP is defined as the thrust a wheel is capable of producing minus the total motion resistance of the wheel. Despite the different weights supported by each wheel, only one size wheel has been designed. This was decided on so that in case of a wheel failure, a wheel from another cart may serve as a replacement. This produces a wheel that may not be optimized for the specific cart but will be optimized for the vehicle as a whole. The following sections discuss the lunar parameters that will have an effect on the Lunar ARTS performance.

Lunar surface characteristics. This section defines the terrain parameters that affect the wheel design and in turn the surface propulsion requirements and capabilities. The Lunar ARTS is assumed to be able to perform at any of the four recent areas of interest for future landing sites. Data for these sites has been accumulated from previous landings (Apollo 15 and Apollo 17) and unmanned probes such as the Lunar Orbiter IV. Two sites are on relatively flat mare surfaces (Taurus Littrow and Lacus Veris) enclosed by mountains. The third is located solely on a smooth mare (Nubium) and the fourth lies in a rugged highlands region (South Pole). Areas range from a sloped severely cratered surface to smooth craterless mare. During the exploration phase of operations, the vehicle capabilities will be decided by its own performance limitations. Physical obstacles include steep slopes, boulder fields at rims of newly formed craters, fault scarps, and walls of rills.

Surface slope distribution. The slope distribution varies on the lunar surface from 0 to 0.1745 rad (0-10°) on the average. This does not include crater rims nor uniquely steep areas. Slopes over 20° make up less than 2% of even the most rugged terrains.

Lunar soil mechanics. The lunar vehicle should possess the capability of producing sufficient thrust independent of its terrain or of the soil characteristics. The lunar surface varies from highly cratered and rocky to smooth and powdery. On a rocky or low sinkage surface, it is most likely that the tread design will grip the solid surface providing the required thrust. However, for areas in which the wheel continues to sink until soil compaction pressure equalizes wheel exertion pressure, the amount of thrust that may be produced will rely on the contact area. The soil consists of finely grained particles, a major portion of which is finer than 0.05 mm (0.002 in). The first few centimeters of regolith is a porous zone that produces a progressively increasing compactness and supporting capability with depth. For reference, an astronaut boot or the Apollo lunar module both placed a stress on the surface of about a pound per square inch (0.69 N/cm^2 or 6.9 kN/m^2). Such stresses result in penetration of the lunar surface of less than a centimeter to a few centimeters. Soil characteristics vary by only small amounts. Soil mechanics values for selected soil properties were taken from various sources (given worst-case scenario) and averaged to obtain the following: Soil angle of friction, $\phi = 39°$; soil cohesion, $c = 0.017 N/cm^2$; frictional modulus of soil deformation, $k_\phi = 0.81 N/cm^3$; cohesive modulus of soil deformation, $k_c = 0.35 N/cm$; and exponent of soil deformation, $n = 1$.

Design. The main objective of our wheel design is to optimize the DP. Secondary objectives include weight consideration, energy/power requirements, dynamic flexibility, transportation, and slope-climbing capabilities. Dynamic flexibility is the ability for the wheel to flex when load is applied. This will increase the ground contact area, which leads to a lower motion resistance value. Initially, three types of dynamic wheels were investigated. The first is the Boeing wire mesh wheel, which is the original LRV wheel. The second is designed by Grumman and the third by Bendix. The data obtained indicated the Bendix wheel as the superior selection. However, with actual desired loads being over twice that of the design load, a long life cycle and soil cohesion problems prompted the selection of a simpler Grumman type wheel. The idea of combining the Grumman rim with the tread of the Bendix proposed a possible solution. The design of a solid, yet flexible rim led to a hollow hemispherical design as shown in Fig. 4. A stress analysis is currently under investigation. The selection of the wheel diameter and tread width will be further discussed below.

Analysis indicates the wheel total motion resistance decreases rapidly while the thrust capability increases very slowly with increasing radius. For maneuverability reasons, the wheel should be less than each segment's length of 2.13 m (7 ft). Based on the drawbar pull only, it is theoretically advantageous to have a wheel diameter larger than the vehicle. However, other parameters limit the wheel diameter. Weight must also be taken into consideration in sizing the wheel. A heavier wheel requires larger motors to produce rolling torque, a heavier suspension, and stronger brakes. This adds undesirable weight to the vehicle. Indirectly, transportation

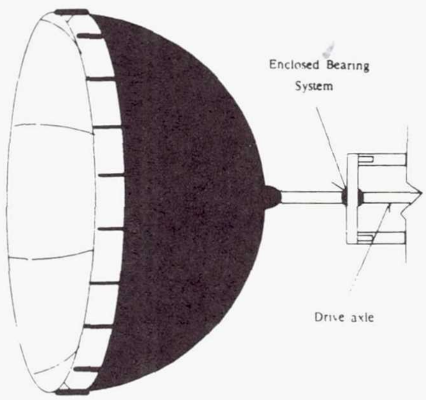

Fig. 4. Hemispherical Dome-type Wheel

also limits the wheel size. The cargo bay of the space shuttle can accommodate a diameter of 180 in. Doubling the 3-in static safety margin, a vehicle with 1.6-m-diameter hemispherical wheels will still fit into the cargo bay. This diameter was increased from the original 1.52 m (5 ft) to gain extra pulling capability. Using this diamater wheel will also reduce the weight to 56% of a 2.13 m wheel. DP also increases as width increases. However, for the same reasons as above, the tread width was selected as 31 cm (12.2 in). The geometric shape indicates the 1.6-m-diameter value. Slope climbing capability is based on the exploration cart. The present design will presently climb only a 17° slope; greater slopes may be ascended with an added fuel cart to increase DP. This not only increases the climb capability but also lengthens the exploration range.

Material selection will be from the composite family. Fiber-reinforced composites such as Devlar 49 may be used for the hemispherical rim section, provided it is shielded from solar radiation to prevent cross linking. A thin film of aluminum would provide this required protection. Tread material would perform exceptionally well with a high impact, light weight, wear resistant plastic such as polysulfone or polycarbonate. However, solar radiation will rapidly destroy the chemical bonds. Unless a suitable coating is found that is highly wear resistant, a fiber reinforced metal is suggested.

In conclusion, optimizing the DP with the limitations of weight and size, analysis produces a 1.6-m-diameter wheel with a 31-cm tread width. Although analysis indicates low drawbar pullslope climbing capability, actual physical testing must be performed in order for the exact capabilities to be determined.

ADDITIONAL DESIGN PROJECTS

This design project is supplemented with additional conceptual design projects for later consideration and integration with the Lunar ARTS. They were prompted by specific requirements of Lunar ARTS in the present design and future needs for expanding its capabilities. These systems are briefly described below. Also discussed is another project called the Lunar-lift Transportation System, which can supplement Lunar ARTS in meeting some of the needs on the Moon.

Heat Rejection System

A heat rejection system, as shown in Fig. 5, was designed to effectively remove the heat generated by the fuel cells during the operation of the Lunar ARTS. Two designs are under consideration for implementation in the Lunar ARTS vehicle. This system is to be placed on the same cart that holds the fuel cell stacks, and the stacks are to remain at a constant temperature of 96° for optimum performance. Important to the design of the heat rejection system is the cycle of 14 lunar days followed by 14 lunar nights.

Fuel cell coolant system—Design option 1. The fuel cell coolant system consists of two main components: the Absorptive/Storage Unit (ASU) and the Refrigerant/Radiative Unit (RRU). The ASU circulates Freon 21 through fuel cell stacks and transfers the waste heat to an insulated storage unit. This unit is segmented into three units and is filled with solid sodium. This heat can be used later if the temperature of the fuel cell stack drops below its optimum operating temperature.

As a possible radiator that would operate in the day (where the temperature of the Moon is hotter than the fuel cell stacks) the RRU was introduced. The RRU channels water through the sodium storage region by means of a pipe. This absorbs the

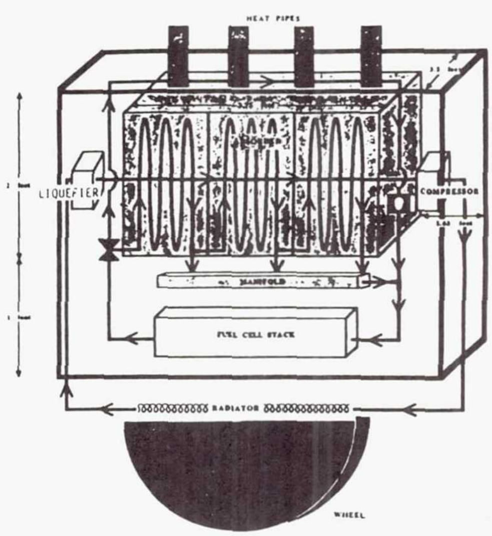

Fig. 5. Heat Rejection System

heat and changes the water to steam. The steam exits the storage unit, is channeled into a compressor where the temperature of the steam is hotter than the temperature of the Moon's surface and thus will radiate outward. The steam becomes cool as it radiates its heat outward from the fuel cell stacks. A liquefier then changes the steam back to water.

At night when the temperature of the Moon is much less than the fuel cell stacks, heat pipes are proposed as a means of removing heat from the ASU or the fuel cell stacks to the radiator unit where the excess heat is radiated outward. Since heat pipes require no external work to operate (they operate on the basic phenomena of condensation, evaporation, and surface tension pumping in a capillary wick), these were chosen as the most efficient means of transferring heat away from the fuel cell stack. The pipes are designed to be unidirectional (transferring heat from the fuel cell stacks to the radiator) since wick dryout will occur if they try to transfer heat the opposite way from which they were intended. Methyl alcohol was the working fluid of choice since it seemed to be one of the very few fluids that could operate within the temperature gradients located on the Moon.

Double loop system—Design option 2. This design consists of a double loop system. The primary loop that comes from the fuel cells goes through a heat exchanger and then back to the fuel cells; if the outside temperature is too high to radiate heat then the heat is placed in storage material. The second loop goes through the heat exchanger, a radiator, and the storage material.

The storage material will incorporate the latent heat of fusion. As the heat is added to the material, the solid melts, and the heat is absorbed in the solid. This heat will be transported to this solid material when the radiator cannot reject all the heat generated by the fuel cells by means of the radiator. The solid material that was chosen was sodium because of its large specific heat and fusion temperature.

The heat exchanger is designed to be a counterflow heat exchanger and the radiator was chosen to be a flat plate fin-tube radiator having central fin-tube geometry (see Fig. 3). The radiator is to be placed both on top and on the sides of the cart. Louvers are to be placed on top of the radiator during the days when the temeprature of the Moon's surface is above that of the radiator, keeping unwanted heat from entering the system. The louvers also keep dust from the radiator when it is not in use. Parts of both systems will be integrated in the ARTS vehicle. Future calculations will also be done to provide a more suitable day radiator (e.g., providing a shading above the radiator unit decreasing the surrounding temperature of the Moon's atmosphere with respect to the fuel cell stacks).

Remote Vision Monitoring System

Control of the Lunar ARTS may be performed on the vehicle or at a remote control base. There are three objectives that are employed within the vision system: (1) environmental sensor system capable of three-dimensional vision, (2) optimum method of transferring data both to and from a remote base, and (3) actual system used for processing the information at the base.

Environmental sensor. The purpose of the environmental sensor is to monitor the environment surrounding the vehicle. A camera will be used to give a two-dimensional image, and an electromagnetic radar will be used to provide a third dimension (depth) to the vision system (electromagnetic radar requires no medium within which to travel). A radar gun will emit electromagnetic waves at a radar frequency that would rebound off objects and return back to the sensor on the gun. This would be used to focus the lens on the camera to the nearest focal point available. A light will be mounted directly on the camera since the only area that requires lighting is where the camera is pointed.

Data transmission. For this to be possible, a continuous data relay with minimal time delays will have to be incorporated. A distance of no more than 100 km (round trip) is assumed to be the maximum traveling distance of the ARTS vehicle.

Relay antennas will be used for linear transmission between the base station and the rover. Approximate height for each antenna is 30 m for a base antenna and 15 m for a remote antenna. Using three remote antennas, a distance of 50 km for the base may be covered for transmission between the base and the rover. A telescopic design will be used for transferring the mast since a telescopic design is more easily integrated into the robotics of the lunar rover. By using electromagnetic waves as a means for transferring data and vision control, a remote vision monitoring system for the ARTS vehicle may be employed. More in-depth calculations will be done regarding integration between the Lunar ARTS vehicle and the vision monitoring control system.

Lunar-Lift Transportation System

As an alternative to the Lunar ARTS vehicle as a means of transportation for men and materials on the Moon, a thermocouple-powered cable trolley system was designed. Using this cable system that runs above the surface of the Moon allows transport of men and materials while avoiding the rough terrain of the surface of the moon. This design consists of a carriage support system, intermediate support stations, and end stations.

Carriage support systems. The method that is chosen to transport the carriage is a mono-cable. This mono-cable is inexpensive and is sufficient for the lunar terrain and expected loads. The material of choice is Invar.

Intermediate support system. A three-link structure is used for the intermediate support system. This structure eliminates the need for nuts and bolts (these small objects are cumbersome for the astronauts while wearing their gloves). The trolley system will cover one mile with a suggested load of 700 Moon pounds. The safety factor of the structure would be 2.11.

The three-link structure can be folded easily for transportation. Since Moon surface preparation is minimal, only a small amount of surface material needs to be removed to form a trench parallel to the path of the cable. Flotation support plates are in the trench, and the legs of the structure are slipped into the support plate boots. After filling the trench, optional tie-

down lines can be attached for further support. The end clamps are then locked to secure the structure. The choice of material for the supports is Al 6061. This three-link structure is designed for easy installation of the cable support assembly.

End stations. End stations are used to drive the carriage as well as provide the tension for the cable. These end stations are also used for loading and unloading cargo. This station consists of large pulleys to drive the cable and change direction and a system to disconnet and reconnect the car for loading and unloading.

The station is supplied with power by a thermo-module heat pipe bank of 249 thermo-modules. The car unhooks from the cable as it comes into the station in the same way it traverses the intermediate support station. Tension is maintained in the cable at all times by a dead weight that is hung from a tension pulley hanging in a shaft. The dead weight consists of Moon boulders and can be variable such that tension can be maintained at all times (regardless of the temperature gradients). As an alternative to the Lunar ARTS vehicle, a lunar lift transportation system allows for transportation of men and materials without being subjected to the rough terrain of the Moon. This lift tansportation system is limited in its transportation ability because it can only operate between the two points at which end-stations are located. This system would be very useful, however, for transportation to and from an excavation site.

SUMMARY AND CONCLUSION

The report summarizes the detailed design of Lunar Articulated Remote Transportation System (ARTS). The system is in a modular form to increase its reliability and extend its applicability in various timeframes and activities. The detailed design of components includes fuel cell system, suspension, wheel, gear, and the cart itself. Additional projects including heat rejection systems, cart interconnection system, and vision system have been conceptually designed and will be eventually integrated into the Lunar ARTS.

ACKNOWLEDGMENTS

Participants included A. Sankaravelu, graduate assistant; H. Goddard, R. Gold, S. Greenwell, J. Lander, B. Nordell, K. Stepp, and M. Styer. They were assisted by faculty advisors, Drs. N. Chandra, P. Hollis, and A. Krothapalli

REFERENCES

1. Faymon K. A., *Power System Concepts for Lunar Surface Mobile Equipment,* NASA-Lewis, Lunar Base Symposium; Houston, Texas, April 1988, LBS-88-009.
2. Alred J., *Development of A Lunar Outpost: Year 2000–2005,* NASA Johnson Space Center, Houston, Texas, LBS-88-240.
3. Shigley J. E. and Mitchell L. D., *Mechanical Engineering Design, 4th ed.,* McGraw-Hill, New York, 1983.
4. Eagle Engineering, Inc., *Lunar Surface Transportation Systems Conceptual Design, Lunar Base Systems Study Task 5.2,* EEI Report 88-188, NASA Contract Number NAS9-17878, 1988.
5. *Dynamic Analysis and Design System Software, "DADS."* Computer Aided Design Software, Inc.
6. Baumestier T., *Standard Handbook for Mechanical Engineers.* McGraw-Hill, New York, 1987.
7. Chandra N. and Arun S., *Design of a Lunar Transportation System,* Proceedings of the NASA/USRA Summer Conference, Kennedy Space Center, June 1988.

N94- 71274

19940004519

382674

S7-51

160633

P. 10

DESIGN AND IMPLEMENTATION OF COMPONENTS FOR A BIOREGENERATIVE SYSTEM FOR GROWING HIGHER ORDER PLANTS IN SPACE

UNIVERSITY OF FLORIDA

This report summarizes the efforts of the NASA/USRA Advanced Design Program during the 1988-89 scholastic year. The primary goal was to address specific needs in the design of an integrated system to grow higher order plants in space. The initial phase of the design effort concentrated on studying such a system and identifying its needs. Once these needs were defined, emphasis was placed on the design and fabrication of devices to meet them. Specific attention was placed on a hand-held harvester, a nutrient concentration sensor, an air-water separator and a closed-loop biological system simulation.

INTRODUCTION

Man's exploration of space on long-term missions is dependent on a reliable, self-supporting life-support system capable of operation in microgravity conditions. The Advanced Design Program of the University of Florida in conjunction with the National Aeronautics and Space Administration (NASA) and Universities Space Research Association (USRA) is working on a prototype closed-loop life-support system designed to grow high order plants in space. The generic Closed-loop Life Support System (CLLSS) concept addressed in the following report is loosely based on the Closed Ecological Life Support System (CELSS) designed by NASA. While the research being performed by NASA at Kennedy Space Center (KSC) revolves around a prototype plant growth unit, the focus of the design class centers on the needs of a successful, real-time CLLSS.

The CELSS program is a long-term research and development effort that addresses the future needs of NASA for recycling and regenerating materials needed for human sustenance during extended space missions. Ideally, this closed system will provide basic life-support requirements such as food, potable water, and breathable atmosphere for space crews on long-term space missions or during extraterrestrial habitation. This involves a "bioregenerative system" where the products of the producer are the nutrients of the consumer and vice versa.

To ensure the success of a completely independent bioregenerative system, precise sensing and control strategies are warranted. The aim of the 1988-89 design class was to surmount some of the obstacles in the development of these strategies. The following paper summarizes the achievements in each of the four task areas identified by the design class.

ION CONCENTRATION SENSOR DESIGN

Introduction

In a system such as CLLSS, where the products of the producer are the nutrients of the consumer, the containment of all nutrients in the system is vital. In the prototype CLLSS considered in the 1988-89 Design Project, plants are the primary food source of the crew. Therefore, plant health is a major interest. The particular concern is how to evaluate and monitor plant health. One of the most important parameters controlling plant health is the concentration of the macro- and micro-nutrients in the nutrient solution. However, present methods do not allow for precise, real-time measurement of ion concentrations. An ideal ion concentration sensor would require little space, be non-destructive to the sample being tested, would be fast and accurate, and would produce real-time results.

The design concept of the ion concentration sensor is based upon thermal changes that could be induced in the solution according to Beer's Law which states that electromagnetic absorption depends only on the number of absorbing molecules through which the radiation passes. Since energy is absorbed at ion-specific wavelengths of light and then released as heat, temperature change in the solution should correspond to the concentration of the specific ion. If light of a specific wavelength is incident upon a solution containing its corresponding ion, the higher the ion concentration in solution, the greater the temperature change in the solution.

Design Requirements

To design an effective and useful sensor, certain criteria must be met:

1. The sensor must use a method that is nondestructive to the sample. The sample must be returnable to the stock solution.
2. The sensor must be compact and easily adaptable to various nutrient delivery systems.
3. The sensor must be accurate and reliable over long periods of time.
4. The sensor must produce realtime results.
5. The sensor should be totally automated, not requiring continual monitoring by crew members.

These criteria were developed in hopes of producing a sensor that would offer more benefits than present sensing technology.

Design Strategy

This design would divert a small portion of the nutrient solution to the concentration sensor just before and after the

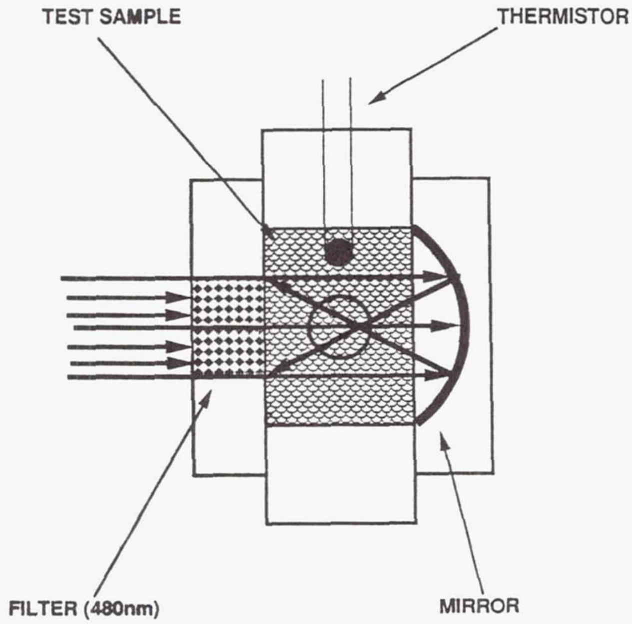

Fig. 1. Test Chamber

plant growth trays. By determining the ion concentrations as the solution enters and exits the plant trays, not only the exact concentrations of nutrients, but also the amounts taken up by the plants will be known. This can aid in monitoring plant health.

The sensor is composed of a light source, a series of lenses, an insulating chamber, a test chamber, and a computer. The light first passes through a piece of heat glass which filters out the infrared and thus minimizes temperature change due to thermal radiation. The light proceeds through two lenses which focus it on the filter located outside of the test chamber.

The test chamber, constructed of acrylic, contains the actual solution sample (Fig. 1). It consists of a subchamber that contains the test sample, a light filter, a parabolic mirror, and a thermistor.

The light filter allows only light of 480 ±3.5 nm, specific to the absorbing wavelength of the chloride ion, to pass into the chamber. By limiting testing to one ion, variables in the system design were reduced to allow errors or necessary changes in the physical system to be more apparent. To maximize the amount of light incident on the sample, a parabolic mirror is attached to the back of the test chamber. The thermistor is used to measure the temperature changes within the chamber. The thermistor is interfaced via an analog-to-digital (A/D) board to a computer that records the temperature changes at desired time intervals.

The entire test chamber is suspended in an outer chamber made of an insulating foam board (Fig. 2). Because of the sensitivity of the thermistor, conditions surrounding the test chamber should remain as stable as possible. The insulating chamber serves to eliminate as many of the fluctuations in the chamber's immediate surroundings as possible.

Results and Conclusions

Control tests were run on samples of distilled water, with and without incident light (Figs. 3 and 4). For both sets of control experiments, results were the same. There was no appreciable heating of the distilled water with or without incident light.

The next set of results displayed the effects of the incident light on different salt solutions (Fig. 5). Consistent with expectations, there were definite temperature changes in the solutions containing the chloride ion. These changes increased with the concentration of the solution.

The 25 g NaCl in 375 g water experiment showed a 30-ohm change in resistance while the 50/375 g and the 100/375 g yielded changes of 90 ohm and 120 ohm, respectively. These results demonstrate that higher concentrations of salt in solution do correspond to greater temperature change.

Although the research and design was limited to the chloride ion, experimentation substantiated the specific-wavelength absorption model. The concept should be applicable to any ion in solution. Therefore, with simple physical modifications to the system, the concentration of any ion in solution could be measured using the same method.

AIR/WATER SEPARATOR DESIGN

Introduction

The concept of a CLLSS is based on growing high-order plants in space. This environment introduces limitations on traditional air-water separation equipment. Therefore, new equipment must be developed to maintain conditions desirable

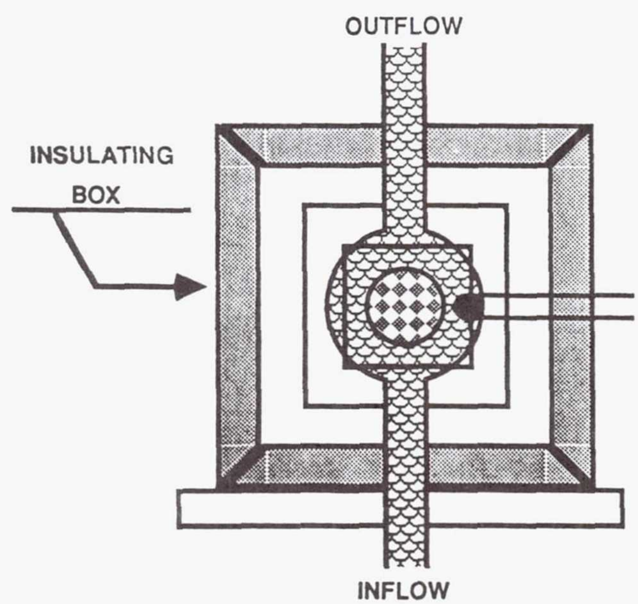

Fig. 2. Test Chamber Contained in the Insulating Box

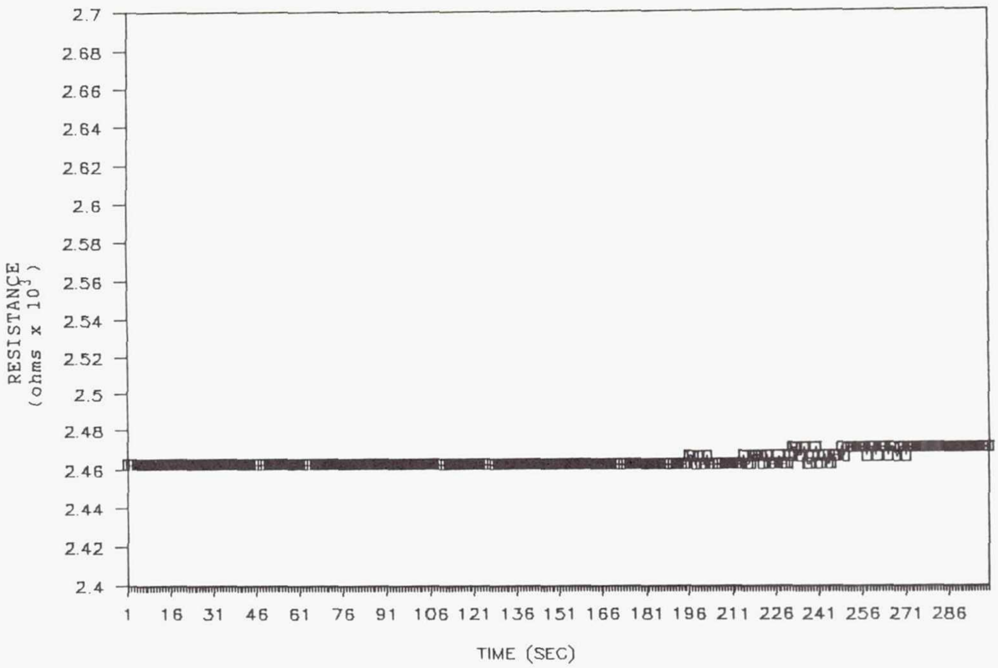

Fig. 3. Distilled Water with Incident Light

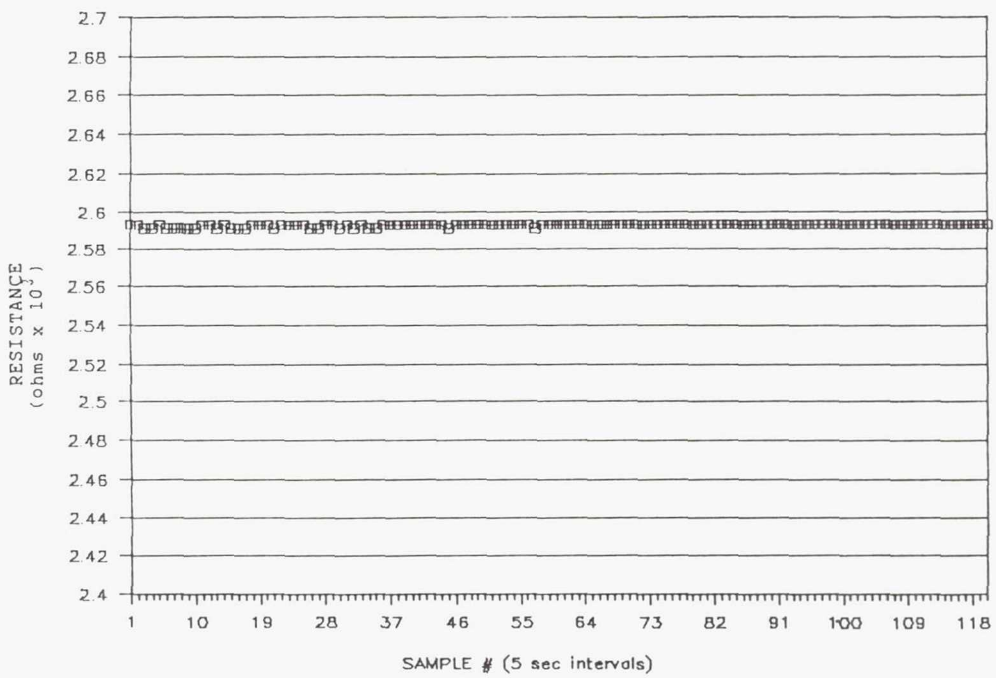

Fig. 4. Distilled Water without Incident Light

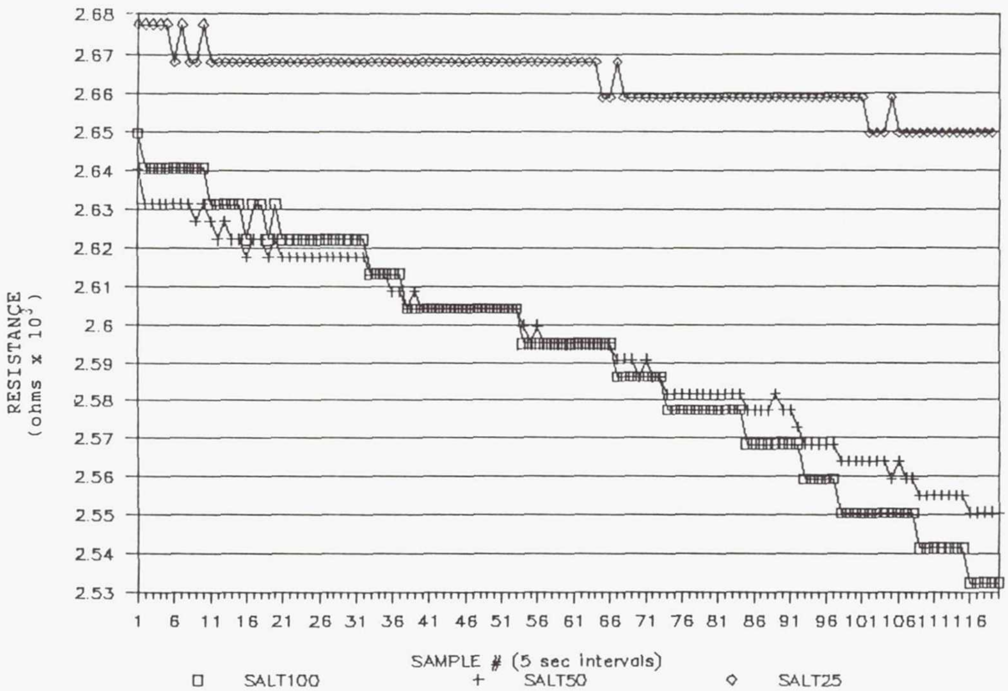

Fig. 5. Salt of Varying Concentrations with Incident Light

for optimal plant growth. Humidity is a major concern in maintaining an environment ideal for plant growth. Condensers are commonly used to separate water or water vapor from the air; however, these are gravity dependent. This section describes the design of a dehumidifier capable of operation in microgravity.

Design Requirements

The design specifications of the prototype dehumidifier developed and tested were as follows:

1. The system must be able to separate a sufficient amount of water from air to obtain the specified humidity level.
2. Materials should be easily obtainable, reasonably inexpensive, durable, and easily replaced.
3. The system must be able to operate under the worst case scenario (i.e., against gravity).
4. The system must be able to withstand the high wind velocity generated by the blower.
5. The main pipe must be cooled below the dew point temperature of water in order for condensation to occur.
6. The system must be sealed to prevent infiltration of outside air or water.
7. The system must have temperature and pressure indicators with simple access and easy visibility.
8. The system must have emergency water ports at the base of the system in the event that all the water must be removed to prevent damage to the system.

Design Strategy

The system (Fig. 6) is designed to stand in an upright position requiring the humid air to move against gravity (the worst case scenario). The dehumidifier consists of a five-foot-long, four-inch-diameter steel pipe surrounded by a six-inch-diameter PVC pipe. The PVC pipe holds ice to cool the steel pipe. Air is run through the steel pipe by a blower at a rate of 300 cfm. An annulus is created by placing a metal pipe of smaller radius within the outer metal pipe. The annulus accomplishes two tasks: It increases both the cold surface area in contact with the flowing air and the velocity of the air. The increased velocity is able to force the water droplets taken from the system upward inside the pipe.

The inner pipe has a series of eight 1.0-inch-long, 0.5-inch-wide vertical slits at the top. These slits allow air to flow through the system, but the water is retained by two collecting collars. The collecting collars, short cylinders with water troughs cut to catch the water, are located between the metal pipes. Both collecting collars are offset beneath the vertical slits. The outer collar is placed lower than the inner collar for optimal streamline flow. The condensate, driven into the collars by the air velocity, is drawn out by a series of eight thin tubes. The air exits the top into an accordion-like plastic pipe. This pipe directs the air into a humidity chamber from which it is drawn back into the bottom of the system by the vacuum end of the blower.

The dehumidifier operates by cooling air below its dewpoint temperature. This causes the water vapor to condense on the

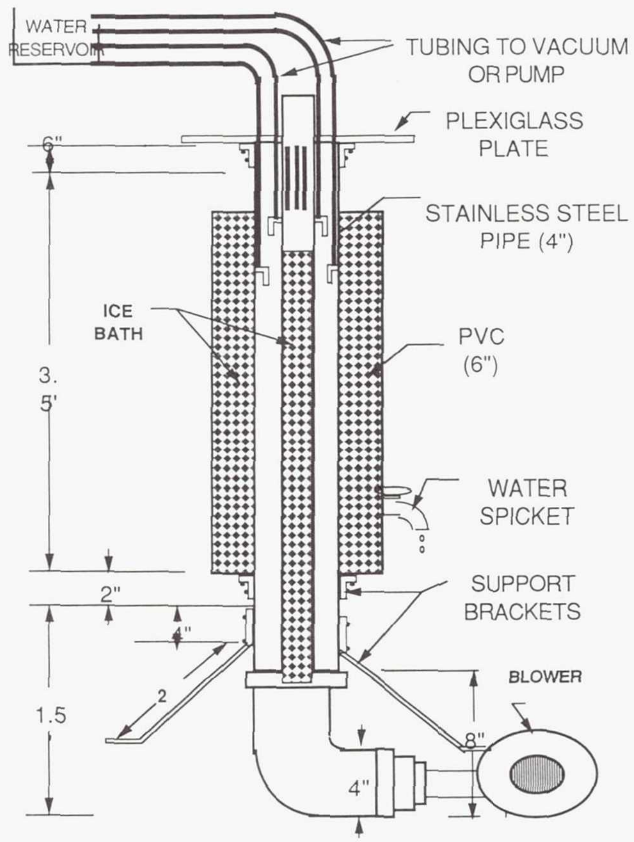

Fig. 6. Air/Water Separator

cold surfaces of the outer and inner pipes. A high airflow rate is provided by the blower to move the condensate to the collector collars. At these collector collars, the air flows in such a way as to create a dead zone. The condensate collects at this point and is drawn from the system by a pump.

Results and Conclusions

The results obtained for the prototype established that the principles of the system were correct. For testing, a fine spray of water was introduced directly into the steel pipe until the air was completely saturated. The water droplets were then forced up, against gravity, into the collection collars by air from the blower. The system continued extracting water until the humidity level became too low. The appearance of water droplets in the extraction tubes demonstrated that the principles of the system were valid.

MICROGRAVITY WHEAT HARVESTER DESIGN

Introduction

This project involves the harvesting of wheat. The wheat heads must be removed from the stalk to be further processed into an edible form. This leads to the need for a mechanical harvester capable of performing such a function in microgravity.

Design Requirements

The requirements of a working harvester model are as follows:

1. The unit must be hand-held (disregarding weight).
2. It must be capable of removing wheat heads from live, rooted plants.
3. The heads should remain intact (for study purposes).
4. No stray particles should be introduced into the plant growth unit.
5. The heads should be contained for further processing and study purposes.

These criteria were used to assess possible methods of cutting, transporting and containing the heads.

Design Strategy

A gentle method must be employed to remove the wheat heads without damaging them. This is accomplished by a slow-moving rotating drum (Fig. 7). As the drum rotates, nylon rings grab the wheat stalks. The nylon rings, normally held apart by compression springs and riding on two outer axles, are forced together to pinch the wheat (Fig. 8). This pinching is activated by two collars opening and closing at precise locations during rotation of the drum (Figs. 9 and 10). The collars are thin aluminum strips which ride on a center axle. A wire placed between the collars, on either side of the center axle, controls the motion of the collars. Attached to each wire is a steel roller which rides along a variable diameter steel function plate (Fig. 11). This function plate is located at midpoint on the center axle. Both the function plate and the axle remain stationary while the drum rotates. The steel rollers are located such that they contact the plate at all times during rotation. A stationary metal blade is located adjacent to each set of nylon rings. These blades shear the wheat stalks as the stalks are across them.

Located 180 degrees from the front of the drum is an opening to the vacuum bag. The bag and vacuum source are located in the upper rear portion of the harvesting unit, below the handle. An acrylic channel leading to the opening of the vacuum bag aids in directing the wheat into the bag.

The driving motor is located below the handle and vacuum bag. It consists of a modified power drill with variable rotation speed. Electronic feedback maintains a constant rotation of the chuck regardless of the load being applied. The chuck is replaced with an alloy sprocket enabling it to drive a light chain. The power control to the drill doubles as the power control to the harvester unit.

The drum is connected to a sprocket which is, in turn, connected to the motor sprocket by a chain. As the motor sprocket turns it forces rotation of the connected sprocket and drum. The drum's sprocket and chain combination is separated from the nylon rings by a circular sheet of acrylic. The entire unit is contained in an acrylic box with an upper handle, a

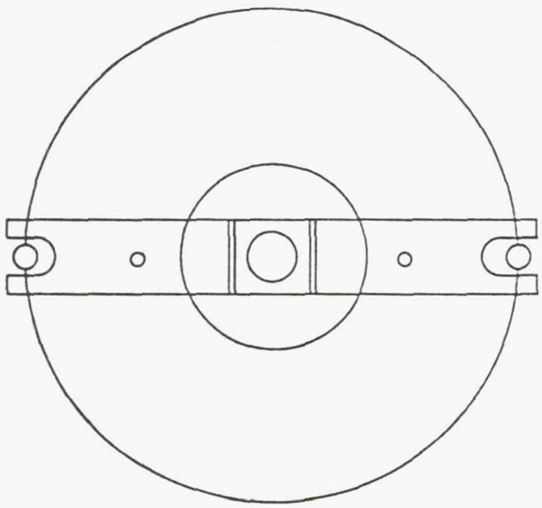

Fig. 7. Cross-Section View of Rotating Drum without Nylon Rings

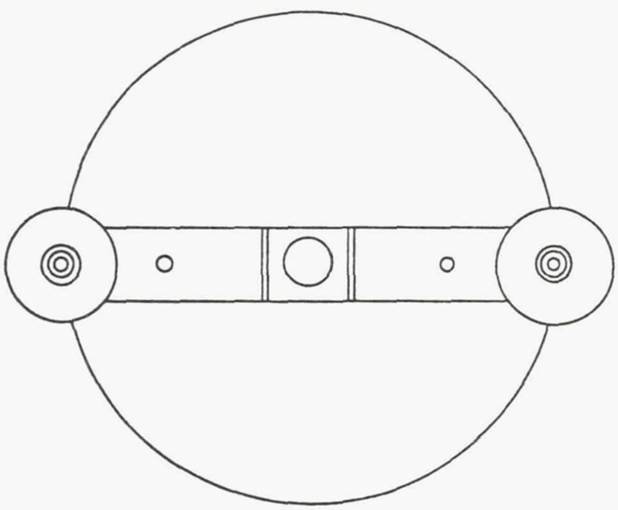

Fig. 8. Cross-Section View of Rotating Drum with Nylon Rings

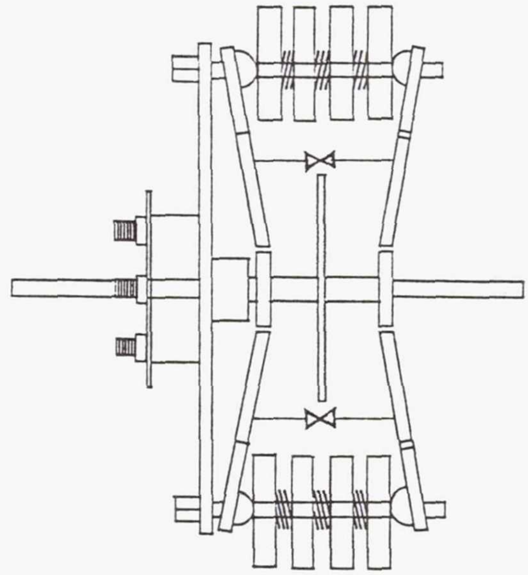

Fig. 9. Rotating Drum in Open Position

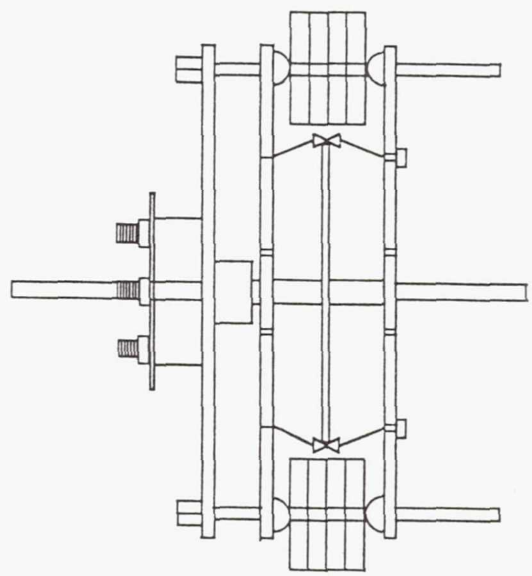

Fig. 10. Rotating Drum in Closed Position

side handle/power controller and a hood to direct any loose wheat.

Results and Conclusions

Passive wheat head removal is a viable method of microgravity harvesting. Gentle pinching, cutting and transporting of the wheat heads meets all of the original design criteria. The design concept presented can be manually operated or automated. This hand-held wheat harvester does not require a skilled operator.

SIMULATION AND CONTROL SYSTEM DESIGN

Introduction

The future of long-term manned space missions is dependent on many factors. In order to better understand and predict some of the problems that will be encountered while designing such a system, a simulation of a closed-loop plant growth system with control was developed. The closed-loop system was modeled using system dynamics and simulated using the DYNAMO simulation language. The simulation

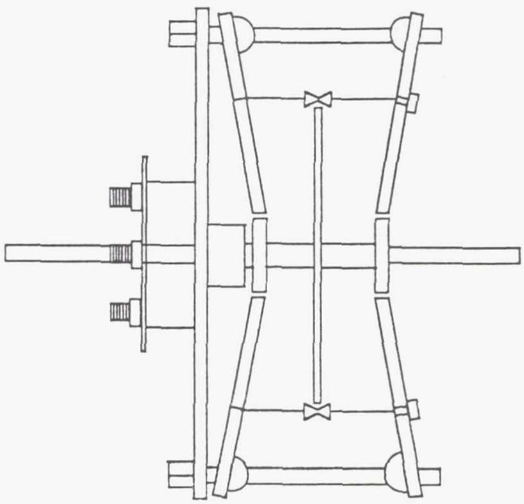

Fig. 11. Rotating Drum in Open Position without Nylon Rings

consisted of three sections. A plant/chamber loop was developed to model some of the basic physiological cycles of the plant (such as photosynthesis, respiration, and transpiration). An energy loop was developed to model energy flow in the system. A controller was implemented to maintain balance in the system.

The plant and energy loops modeled do not yet represent all of the complicated processes which would actually take place in a closed loop system. Their purpose, however, is to predict roughly some of the major trends of the system. This rough model serves as an abstract test environment for proposed sensing and control systems. Therefore, the simulation provides a preliminary testbed for various controllers of the modeled system.

Design Requirements

Several design criteria were established to develop a model and simulation of a plant growth chamber. First, the system was divided into three sections: a plant loop, an energy loop and a control loop. Then, constraints were placed on each of these sections of the model. Once a reasonable model was established and a simulation was developed, system variables were manipulated to allow study of system behavior.

Plant/Chamber Requirements. To obtain a working model of a plant growth chamber within the limited time available, several simplifying assumptions had to be made. The model's purpose was to represent generic processes that take place in a plant growth chamber. The processes represented were photosynthesis, transpiration, and respiration.

Simplifying assumptions were made in the plant physiology equations. The photosynthesis equation was modeled to be a function only of carbon dioxide level and the light in the chamber. Similarly, transpiration was limited to being a function of photosynthesis, temperature, and humidity. Finally, respiration was modeled only in terms of photosynthesis and maintenance respiration.

Energy Requirements. The requirements for a simplified energy model for a CLLSS system are numerous. The energy flows should be related to the mass flows of the rest of the system. The temperature of the growth chamber should be an integral part of the entire model and should be monitored and controlled. Heat should be easily added or removed from the growth chamber as well as the atmosphere processor. Finally, the total energy flow into the system should be monitored to ensure that the total energy requirement is reasonable and practical.

Control Requirements. Many internal parameters of a CLLSS system have a tendency to grow rapidly, exceeding acceptable ranges. This tendency demonstrates the need for automatic control. A control system should limit the parameter values of the system while providing them with a degree of stability. Stabilizing the individual parameter values contributes to the stability of the overall system. The design of such a controller was completed in stages, beginning with an elementary control system and increasing in complexity. At this stage, a controller which limits the parameter values, but does not achieve the necessary degree of stability, has been designed.

Design Strategy

Initially the system had to be modeled. Both the plant/chamber and the energy models were developed using system dynamics modeling notation (Fig. 12). The system consists of state variables or levels. These levels, such as oxygen or humidity, are changed by variables. There are two types of rates in the system. Plant physiological rates, such as transpiration and photosynthesis, cannot be directly controlled. However, they are controlled indirectly by rates associated with control equipment, such as humidity. The solid lines represent material flow in the system. An example of this is water moving from the plant into the atmosphere through transpiration (Fig. 13). Information flows are represented by the dashed lines. For example, because photosynthesis is directly dependent on the carbon dioxide in the chamber, there is an information flow from the CO_2 level to the photosynthetic rate.

Once the system was modeled, its behavior could be simulated. The simulation is designed to run at minute time intervals. Because of the versatility of the simulation language used, several of the system parameters may be changed before each execution. These parameters include system constants and initial values of state variables. Therefore, initial system conditions may be varied to compare the effects of different starting levels on the operation of the chamber. In addition, the simulation length and time step intervals are variable parameters. The state of the system is evaluated at each of these time steps and may be plotted or tabulated. The choice of run length and saved step interval is dependent on the desired output.

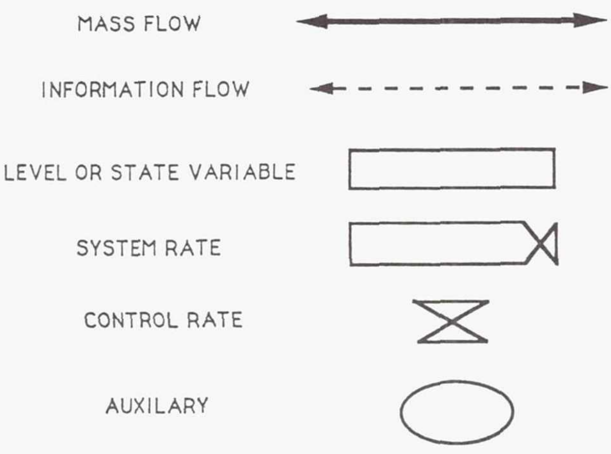

Fig. 12. System Dynamics Modeling Notation

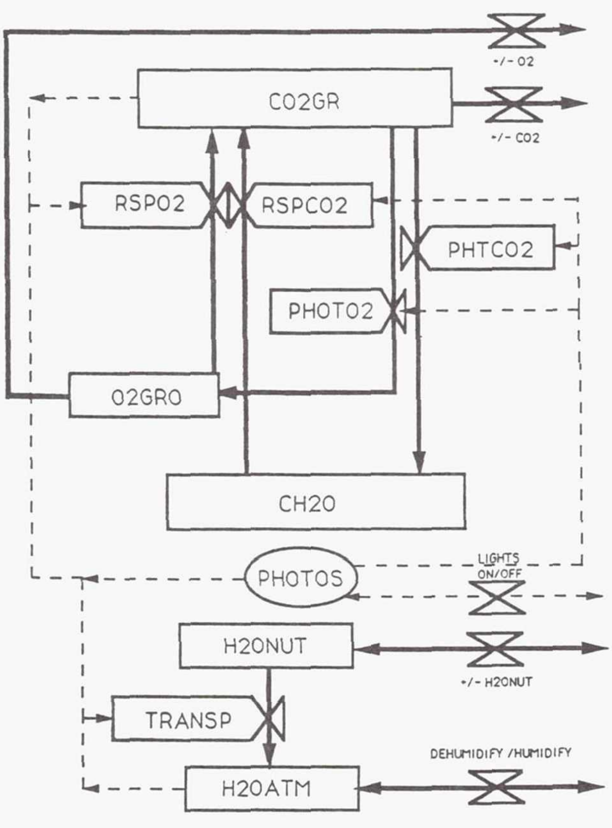

Fig. 13. Plant Chamber Mass Model

Plant/Chamber Operations. The first version of the simulation is used to observe the trends of an uncontrolled system. The behavior of an uncontrolled plant growth chamber can provide valuable information regarding the sensing and control needs of the system. An uncontrolled version of the simulation also provides a basis for comparison.

Without control, the system changes rapidly in the first few hours but reaches an equilibrium in approximately two hours. The system equilibrates because the plant physiological rates saturate or deplete critical state variables. Good examples of the uncontrolled system behavior are the transpiration rate and water level in the atmosphere (Fig. 14). Transpiration is the only factor affecting the humidity, while at the same time it is dependent on the humidity. Once the air becomes saturated with water the plants can no longer transpire. Therefore, the transpiration rate becomes zero and the humidity equilibrates. Similarly, the photosynthetic rate approaches zero when the carbon dioxide level is depleted. Unfortunately these rates would kill the plants.

Another version of the simulation is designed to run with a controller. Instead of the system stabilizing to a nonproductive equilibrium stage, the system remains relatively stable. To affect the plant rates, the controller changes the state variable which, in turn, influences the physiological rates. By maintaining the optimum range for each critical state variable the plant growth equations (photosynthesis, respiration, and transpiration) remain finite rates. A good example of system control is the photosynthetic rate and carbon dioxide level in the system (Fig. 15).

Photosynthesis is directly proportional to the level of carbon dioxide in the system. As the plants take in CO_2, the controller adds CO_2 to the atmosphere and the level of CO_2 in the chamber stays within a specified range. This, in turn, keeps the photosynthetic rate within a productive range.

Energy Loop Operations. The operation of the energy loop is based on several levels and rates. An imaginary source of energy is created to represent the energy source of the entire system, such as a generator. This level steadily decreases with time, showing a continuous draw of power from the source.

Another level models the energy present in the plant growth unit (PGU), and is given an arbitrary initial value. The lights in the PGU and a heater increase this energy level, while a cooler and heat leakage from the PGU decrease the energy level. A temperature variable is calculated from the energy level in the PGU. If the temperature is too high, a cooler is switched on by the controller. If the temperature of the growth chamber is too low, a heater is turned on.

An atmosphere processing system is described to contain the heating and cooling devices for the atmosphere in the PGU. The atmosphere processor level is monitored to establish its effect on the energy level of the entire system. Consequently, energy added, in the form of heat, to the energy level of the PGU would result in a decrease in the energy level of the atmosphere processor. Cooling of the PGU would result in the reverse effects on the energy levels.

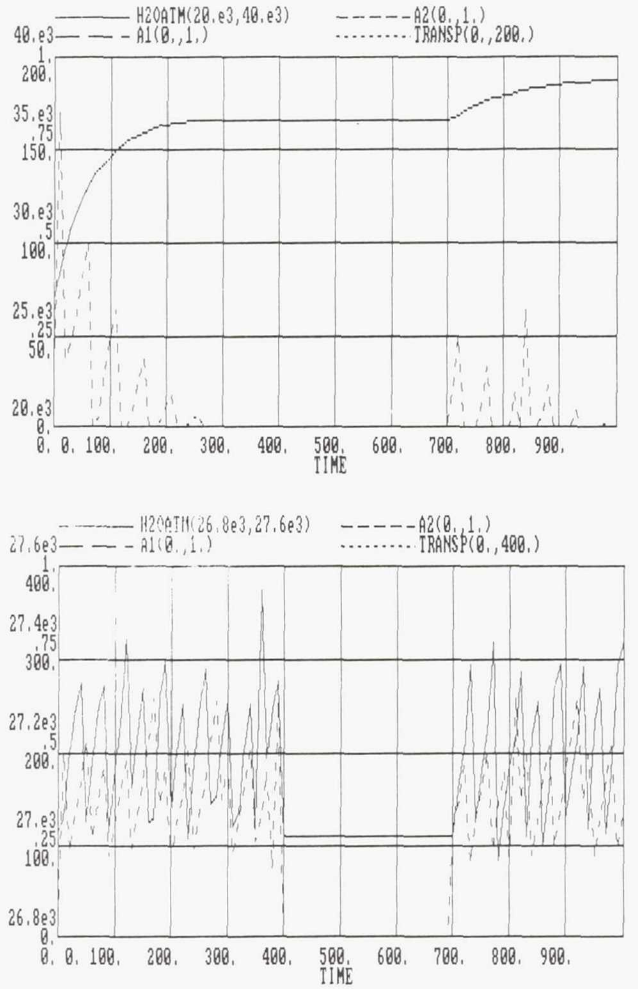

Fig. 14. Uncontrolled (Top) and Controlled (Bottom) Examples of System Behavior

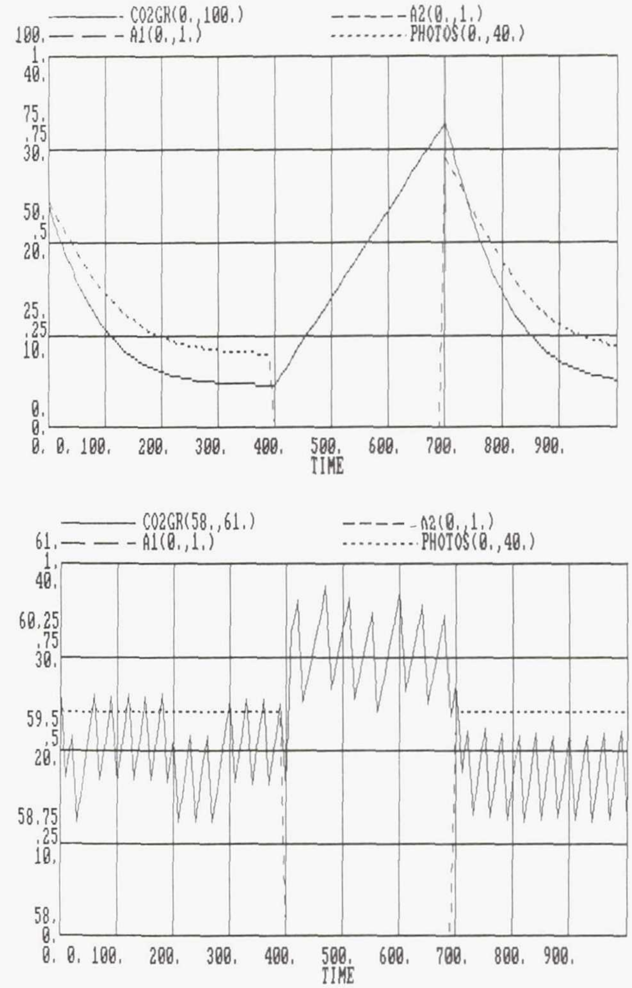

Fig. 15. Uncontrolled (Top) and Controlled (Bottom) Examples of System Behavior

The controller turns on or off the heater or cooler depending on the temperature of the PGU. This allows the DYNAMO user to specify a desired temperature range for the PGU.

Control Loop Operations. The process of designing a controller for the CLLSS simulation was rather intuitive. The initial system response criteria involved the maintenance of various levels within specified ranges. The most logical way of effecting this type of control was to design a series of controllers. Each controller would add to or subtract from a specific level when that level exceeded its acceptable range.

A "clip" statement proved to be very useful in the design of the additive-subtractive controller. The clip statement appears as follows: RATE = CLIP(W, X, Y, Z). This is interpreted as: When Y ≥ Z, let RATE = W or else RATE = X. Clipping at the lower bound of a range may be achieved by negating Y and Z or by setting W = 0. The variable RATE represents a rate into or out of the level Y. RATE was designed to represent a rate of operation of a piece of control equipment such as an air processor or a pump. Similarly, the clip equation also serves as a simulation of a sensor. It "senses" the present value of level Y when the computer checks to see if Y ≥ Z.

The additive-subtractive control is achieved by setting W = a constant and X = 0. Thus when Y ≥ Z, the clip equation "turns on" and RATE = W. This rate is used in evaluating the new value of the level Y. This use of the clip equation simulates the operation of a constant-speed motor such as a water pump.

If it is assumed that variable-speed equipment will be used, then a conditional negative feedback loop may be employed. This loop also uses the clip equation, but with a subtle difference. Instead of letting W = constant, W is assigned the value of a percentage of the output level. (Example: $W = k \times Y$, where $0 \leq k \leq 1$).

This control, however, does not yet increase the stability of the system. The simulation still remains in constant oscillation

within the appropriate boundaries. The choice of the feedback constant, k, will increase or decrease the number of oscillations in a given period of time, but will not cause the system to stabilize about a designated value.

Results and Conclusions

As feedback constants were varied, the response of the mass model was visually evaluated. Regardless of the feedback constants the system would continually oscillate. An attempt was made to find a constant which would generate the fewest oscillations per unit time. The constant also needed to cause the values of the level to fluctuate somewhat uniformly about the setpoint (initial level value). After much trial and error, the approximate "best" value for the feedback constant, k, appeared to be 0.3. This constant provided the least volatile system response of all the values tested. If too small a constant was chosen, the level would merely oscillate slightly about the high or low end of its range. Conversely, if too large a constant was chosen, one process would overcompensate to the extent of initiating the reverse process.

In addition, it was determined that the plant model was operating correctly due to the tendency of the system to almost shut down during the lights-off period.

The energy input level to the entire energy system increases linearly with time, indicating relatively smooth system behavior. The temperature of the growth chamber, using a simplified control system, remains between 16°C and 28°C. This is close to the setpoint temperature of 23°C. The energy and temperature of the atmosphere processing system are not as stable as those of the growth chamber. The temperature fluctuates over a wider temperature range. Some of the fluctuation may be due to mass flows in other parts of the system since the energy level of the atmosphere processor is dependent on them. Considering the limitations of the energy model, the response of the mass model to the energy model is acceptable.

By varying the control parameters of the simulation, it was possible to determine which state variables were the most sensitive to parameter changes.

The most critical variable to sense and control proved to be humidity because it varies in magnitude more quickly than any other variable. Humidity needs to be sensed continuously and controlled frequently, if not constantly.

Of less critical importance is the level of CO_2 in the chamber. This level causes variations in the transpiration rate of the plants and requires periodic sensing and control. The O_2 level tends to vary even less than that of the CO_2 level. With a range of 9400 ± 94 moles, O_2 does not require control over periods of time less than a day. Similarly, the nutrient solution level changes very slowly requiring less frequent sensing and control.

ACKNOWLEDGMENTS

Principal authors were B. Brakman, L. Dioso, D. Parker, L. Segal, C. Merriman, I. Howard, H. Vu, K. Anderson, S. Riley, D. Amery, C. Buckels, J. Larson, P. Brachhold, and C. Rhoads. Faculty advisor was Dr. Gale E. Nevill.

The design team of the 1988-89 Engineering Sciences Design class would like to thank the following people for their help in making this project a success: Mr. Kip Cooper of Pugh-Roberts Associates, Inc. for the contribution of Professional DYNAMO Plus and Mr. Ralph Prince, Dr. Bill Knott, and Dr. John Sager of Kennedy Space Center.

S8 N94- 71275
AB: 160634 77
P 1
1994004520
382675

LUNAR LANDING AND LAUNCH FACILITIES (COMPLEX 39L): GUIDANCE SYSTEMS AND PROPELLANT SYSTEMS

FLORIDA INSTITUTE OF TECHNOLOGY

After a general, overall definition of Complex 39L during the previous two years, the 1988-89 projects were chosen to focus on more specific aspects, specifically, guidance systems and propellant systems. Six teams or subtasks were formulated: (1) Cascade refrigeration for boil-off recovery of cryogenic storage vessels; (2) Lunar ground-based radar system to track space vehicles; (3) Microwave altimeter for spacecraft; (4) Development of a computational model for the determination of lunar surface and sub-surface temperatures; (5) Lunar cryogenic facility for the storage of fuels; and (6) Lunar lander fuel inventory tent for the storage of cryogenic vessels.

At the present time, a cascade refrigeration system for a cryogenic boil-off recovery system has been designed. This is to serve as a baseline system. The ground-based tracking system uses existing technology to implement a reliable tracking radar for use in the lunar surface. A prototype has been constructed. The microwave altimeter is for use on lunar landers. It makes use of the Doppler effect to measure both altitude and the vertical velocity component of the spacecraft. A prototype has been constructed. A computational model that predicts the spatial and temporal temperature profiles of the lunar sub-surface was formulated. Propellant storage vessels have been designed. A support for these vessels which minimizes heat leaks was also designed. Further work on the details of the Fuel Inventory Tent (FIT) was performed. While much design work on the overall Complex 39L remains to be done, significant new work has been performed in the subject areas.

N94- 71276

160635 79
p. 1
1994004521
382676

LUNAR DEEP DRILL APPARATUS

GEORGIA INSTITUTE OF TECHNOLOGY

INTRODUCTION

Proposed as a baseline configuration, this rotary drill apparatus is designed to produce 100-mm-diameter holes in the lunar surface at depths up to 50 meters. The drill is intended to acquire samples for scientific analysis, mineral resource location, calibration of electronic exploration devices and foundation analysis at construction sites. It is also intended to prepare holes for emplacement of scientific instruments, the setting of structural anchors, and explosive methods in excavation and mining activities. Defined as a deep drill because of the modular drill string, it incorporates an automatic rod changer. The apparatus is teleoperated from a remote location, such as Earth, utilizing supervisory control techniques. It is thus suitable for unmanned and man-tended operation.

Proven terrestrial drilling technology is used to the extent it is compatible with the lunar environment. Augers and drive tubes form holes in the regolith and may be used to acquire loose samples. An inertial cutting removal system operates intermittently while rock core drilling is in progress.

The apparatus is carried to the work site by a three-legged mobile platform which also provides a 2-meter feed along the hole centerline, an off-hole movement of approximately .5 meters, an angular alignment of up to 20° from gravity vertical and other dexterity required in handling rods and samples. The technology can also be applied using other carriers which incorporate similar motion capabilities. The apparatus also includes storage racks for augers, rods, and ancillary devices such as the footplate that holds the down-hole tooling during rod changing operations.

INTERFACE AND STRUCTURE

A three-point mechanical interface attaches the main structure of the drill to the walker. The drill has its own fuel cell for power (2-12 kWe) and its own control and communications system. The structure supports the rod racks which store the rods generally radially outward and upward between the walker legs. Also attached to the structure is the rotary drive motor and the rod handling arm.

ROD HANDLING ARM

Each auger, rod, and downhole tool is 2 meters long and is grasped by a clamp at the end of the arm. The arm has 2 degrees of freedom; rotational movement about the string centerline and rotational movement in a vertical plane. It selectively removes a rod from the rack and adds it to the string and vice versa.

FOOTPLATE

The footplate is carried to the drill site attached to the rotary spindle. At the site, the walker squats toward the surface while the rotary motor spins it slowly. Radial blades form a conical seat for the footplate base in line with the hole centerline. The local slope and surface irregularities are thus compensated for.

BIT AND CORE RETRIEVAL

The rock coring bit produces a 50-mm-diameter core. The bit is attached to a 2-meter-long rod which includes the first section of the inertial cutting removal device. Configured for dry drilling, it is composed of 30-per-carat diamonds in a centered tungsten carbide matrix. Three horizontal discs are used to sever and hold the macro core until the rod is inverted by the rod changing arm.

MICRO-CORING

Another 2-meter-long down-hole tool is a self-contained micro-coring device. It is designed to cut and retrieve a 5-mm-diameter by 25-mm-long core from the main hole wall. Thermal and foreign matter contamination avoidance are prime design drivers for this device.

CONCLUSIONS

This conceptual design serves to outline the task of drilling holes and acquiring core samples from lunar boulders and bedrock. It is far from being complete or certified but indicates the technologies expected to be required. Additional effort is needed to simplify the system and to advance significantly the bit technology.

PRECEDING PAGE BLANK NOT FILMED

PAGE 78 INTENTIONALLY BLANK

N94- 71277

S
160636
P. 7
1994004522
382677

PARTIAL GRAVITY HABITAT STUDY

UNIVERSITY OF HOUSTON

INTRODUCTION

General

The purpose of this study was to investigate comprehensive design requirements associated with designing habitats for humans in a partial gravity environment, then to apply them to a lunar base design. Other potential sites for application include planetary surfaces such as Mars, variable-gravity research facilities, and a rotating spacecraft.

Design requirements for partial gravity environments include locomotion changes in less than normal Earth gravity; facility design issues, such as interior configuration, module diameter and geometry; and volumetric requirements based on the previous as well as psychological issues involved in prolonged isolation.

For application to a lunar base, it was necessary to study the exterior architecture and configuration to insure optimum circulation patterns while providing dual egress; radiation protection issues were addressed to provide a safe and healthy environment for the crew; and finally, the overall site was studied to locate all associated facilities in context with the habitat. Mission planning was not the purpose of this study; therefore, a Lockheed scenario was used as an outline for the lunar base application, which was then modified to meet the project needs.

Goal

The goal, or purpose of this report was to formulate facts on human reactions to partial gravity environments, derive design requirements based on these facts, and apply the requirements to a partial gravity situation which, for this study, was a lunar base.

Scope

The scope of this study was to investigate architectural and humanistic design criteria in partial gravity environments. Therefore, the decisions and results of this study were based on human safety and comfort for extended stays in isolated space environments. Results have yielded human requirements for partial gravity based on physical and psychological criteria.

Assumptions

A Heavy Lift Launch Vehicle (HLLV) must be available that can lift a module size of 22' (6.7 m) by 57.5' (17.2 m) and a weight of approximately 77,000 lbs (35,000 kg).

A Space Operations Center (SOC) needs to be in operation in LEO to support a planetary base.

If a planetary base is the application, a lander that can land a module weighing 35 metric tons, 6.7 m by 17.2 m, as well as a vehicle that can maneuver the module on the surface must be available. Without these two vehicles, this concept cannot be implemented.

An assumption has also been made that radiation protection for a lunar application is desirable for at least part of the base[1]. The portion of the base that is covered would act as a safe haven for the rest of the base, while the remainder of the base is only thermally shielded.

For a lunar base, a liquid oxygen (LOX) plant will probably be the major function; therefore, the mining equipment needed for the plant can be shared to aid the construction process.

PARTIAL GRAVITY DESIGN REQUIREMENTS

Locomotion

For design in a partial gravity environment, the issue of human locomotion becomes very important. A partial gravity environment is different from normal Earth gravity (1 g) in that human walking and running gaits change, posture changes, and the level of traction changes. The following discusses the differences that are known and speculates as to how these differences will affect design of a partial gravity habitat.

Humans are designed to walk in a normal 1-g environment and have adapted to a certain force and traction due to that gravity level. A change in the gravity level changes the forces and traction acting on the human body and, therefore, changes the gait. A comparison of Earth gravity and partial gravity walking and running gaits is shown in Fig. 1.

Human posture in a partial gravity environment differs from posture in a 1-g environment. In a partial gravity environment, as the speed is increased, the forward inclination of the body gets progressively larger. For example, the inclination of a sprinting gait on the lunar surface is 60°, while the same gait on the Earth is only 10°[2]. Figure 1 shows, visually, the differences between body inclinations in 1 g and 1/6 g.

The reduction of traction can make human balance and locomotion hazardous in any environment. With a reduction in gravity, a human experiences a reduction in the friction between himself and the surface of the ground. Another constraint affecting locomotion is that the inertial force required to start moving from a complete stop is the same as it is in 1 g; therefore, the subject must overcome the same inertial force in partial gravity as in 1 g utilizing less traction.

Some of the adverse effects of low traction can be reduced through effective design. Traction effects in partial gravity could be offset by using high-traction floor surfaces, hand/foot mobility aids and increased corridor volume for starting and stopping.

PRECEDING PAGE BLANK NOT FILMED

PAGE 80 INTENTIONALLY BLANK

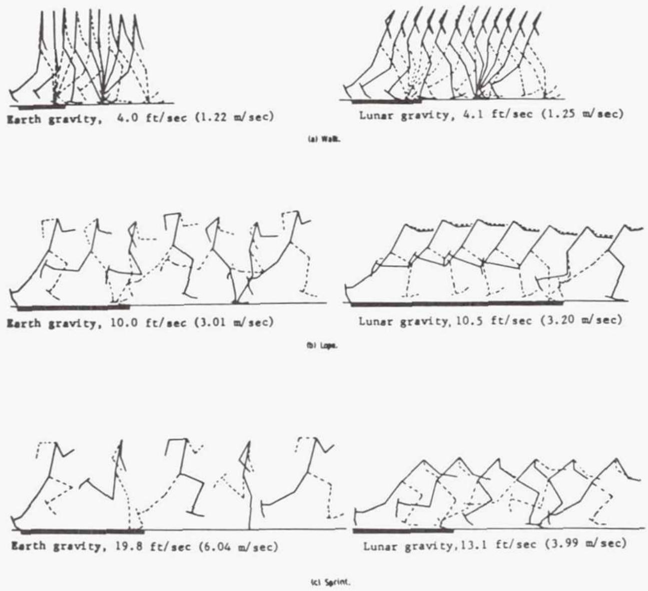

Fig. 1. Body Inclinations[2]

In conclusion, human locomotion in partial gravity is quite different from that of a 1-*g* environment. In general, a person would lean forward more, whether walking or running, and adjust to the new environment. This can be offset somewhat by good design.

Facility Design

Partial gravity habitats are affected by mission parameters as well as the varying gravity level. Mission parameters that affect the design of partial gravity habitats include mission length and activity level as well as architectural issues, such as the functional layout and geometry required to make the habitat function properly.

Mission length is determined by factors such as destination and planned operations, which affect the design of facilities directly in the form of crew habitat volumes and comfort levels. The requirements of the crew increase as the length of the mission increases[3].

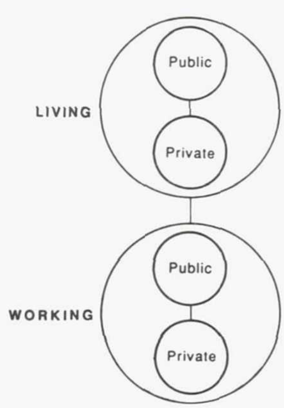

Fig. 2. Concept Diagram for Functional Layout

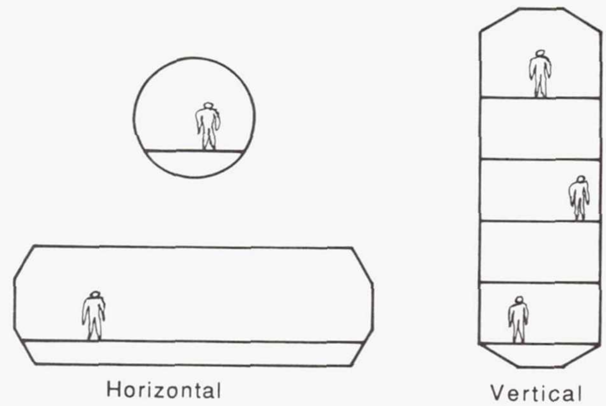

Fig. 3. Configuration Options

A change in activity level would also have an effect on the crew design requirements. A high activity level could demand shift work, resulting in more shared facilities and less volume. A low level of activity could demand more volume for leisure activities.

The most logical way to subdivide a habitable volume is on the basis of function. By their nature, various functions dictate adjacency or separation from each other. The connections between these functions must accommodate each function's specific constraints. Four functional units can be derived from typical crew activities during a mission: (1) Private Unit (personal quarters), (2) Public Unit (dining, recreation and exercise), (3) Work Unit (mission operations and management), and (4) Living Unit (habitation).

A diagram of these breakdowns can be seen in Fig. 2. The separation and adjacencies of these four functions are based on factors such as noise, mechanical issues and privacy. Separation could either be psychological (visual separation) or physical (wall or door). Optimal design should have separations between functions that have different noise, lighting, vibration, or privacy requirements.

Inherent in the design of space hardware is the fact that all habitable spaces must occur within pressure hulls. Another given is that the most efficient geometry for a pressure hull is the circular section. Although structurally efficient, the circle is not efficiently fitted to the linear design of the human figure, which traditionally has orthogonal patterns for design. However, the circular section is a geometry that we must use, for efficiency reasons, in the design of habitable spaces.

The two configuration options considered for the Space Station *Freedom* were the vertical, with the long axis of the module parallel to the long axis of the body, and the horizontal, with the long axis perpendicular to the long axis of the body (Fig. 3). In microgravity, these two configurations present a closer trade study than in a partial gravity environment. In partial gravity, height, egress, and vertical circulation problems inherent to the vertical configuration make it impractical. We, therefore, chose to look at horizontal configurations.

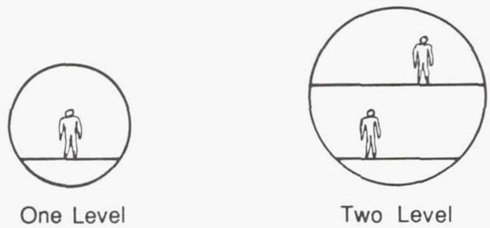

Fig. 4. Interior Configuration Options

The next trade-off to be studied lies between having a one- (one "story" or floor) or two-level (two "stories" or floors) interior configuration (Fig. 4). Considerations in this trade-off are the overall module size being considered (which is determined by transportation and handling requirements), and the internal circulation requirements (corridor, ladders, etc.).

From an internal architecture standpoint, the two-level module configuration is more efficient for long duration missions because the equipment to circulation ratio is minimized. The two-level module is more space efficient than a one-level configuration. It also affords the possibility of creating higher, two-level spaces as required.

Another aspect of geometry is the need for a partial gravity habitat to be reconfigurable as well as expandable. Internal structure must be designed so that, if the need arises to reconfigure the internal layout, the task can be accomplished without great effort. The modules should also be standardized so that expansion is just a matter of bringing in another module and attaching it to the existing configuration.

Volume Study

The volume study investigates volumes required for human habitation in a partial gravity environment. The volumes calculated are space efficient yet psychologically acceptable for long duration isolation. These volumes are applicable to a partial gravity environment for places such as a lunar base, martian base, or an artificial gravity space habitat. The volumes calculated and recommended for long duration space settlement are a galley, dining/wardroom area, recreation hall, exercise area, health maintenance facility, personal quarters, personal hygiene/waste management facilities, laundry, EVA storage, laboratory/work space, maintenance, circulation, ECLSS, and safe haven.

Partial gravity volume requirements differ from the Space Station *Freedom* in that there is a certain level of gravity which restricts the use of space due to inherent needs and the reach envelope in a gravity environment. In other words, crew members cannot use the area in the ceiling and floors and cannot sleep on the walls and ceiling in partial gravity as they can in microgravity. However, similarities are that the equipment sizes and design (in a "rack" system) will be basically the same. Therefore, the volume study investigates volumes for a partial gravity habitat using the Space Station *Freedom* equipment and "rack" system as a standard, and adapting it to a partial gravity situation.

Table 1. Lunar Base Habitation Volume

Function	Volume ft^3	Volume m^3
Galley	830	23.5
Contingency Food & Trash	378	10.7
Dining/Wardroom	1,600	45.0
Recreation	4,080	115.0
Exercise	700	20.0
Health Maintenance Facility	480	14.0
Personal Quarters (250 $ft^3 \times 12$)	3,000	85.0
Personal Hygiene/Waste Management (3)	495	14.0
Laundry	256	7.0
EVA Storage	636	18.0
Maintenance/Work Area	660	19.0
Circulation	4,070	115.0
ECLSS	275	7.8
Total	17,460	494.0

APPLICATIONS TO LUNAR BASE DESIGN

Volume Calculations

The following shows the volumes necessary for habitation space in a lunar base (Table 1). The volumes calculated investigate the amount of habitat space, excluding laboratory, needed for a crew of 12 that will eventually expand to a crew of 36.

When the crew of 12 expands to a crew of 36, the volume of the habitat space will triple to bring the total habitat volume to 53,580 ft^3 (1518 m^3). The crew can be housed in three modules that are 22 ft (6.7 m) by 56.5 ft (17.2 m), with a total volume of 58,125 ft^3 (1650 m^3).

If Space Station *Freedom* sized modules are used for a lunar base, the number of modules required will increase by about a factor of three. The Space Station *Freedom* modules are approximately 15 ft (4.5 m) diameter by 45 ft (13.7 m) in length, with a volume of approximately 7,000 ft^3 (200 m^3).

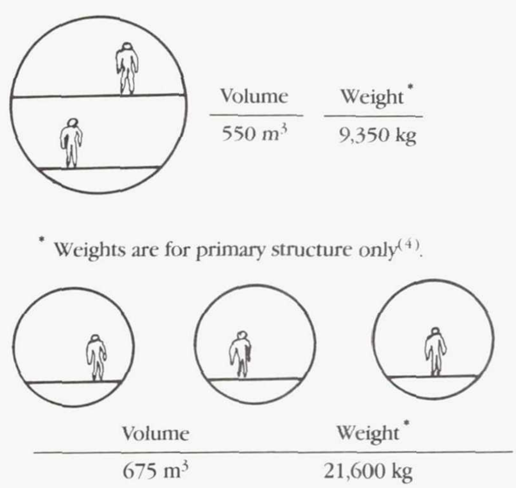

Fig. 5 HLLV vs. Space Station *Freedom* Modules

Since the volume required for circulation is about 1620 ft^3 (46 m^3), three modules would probably be required for the same crew of 12 (Fig. 5), thus increasing the weight of the habitation modules. Therefore, the crew of 36 would require approximately nine Space Station *Freedom* sized modules for habitation.

There is added difficulty in landing and maneuvering an HLLV module on the lunar surface, which is why we have assumed availability of vehicles and landers which can accommodate this.

Interior Architecture

The interior architecture is derived by determining the interior configuration of the human habitation areas (i.e., one-level like Space Station *Freedom* modules, or two-level HLLV-sized modules), studying the circulation patterns within and outside of the modules, and finally, arriving at a functional layout based on the previous as well as functional adjacencies. The interior architecture will become optimum if the proper volumes are coupled with the process of deriving the interior architecture, therefore creating an interior arrangement that works functionally as well as psychologically for the crew.

The sectional configurations are evaluated based on size, circulation patterns, and overall space efficiency. From a module study conducted by our group in the fall semester, 1988, it was concluded that a 22 ft (6.7 m) diameter module with two levels would be the most space efficient size and arrangement.

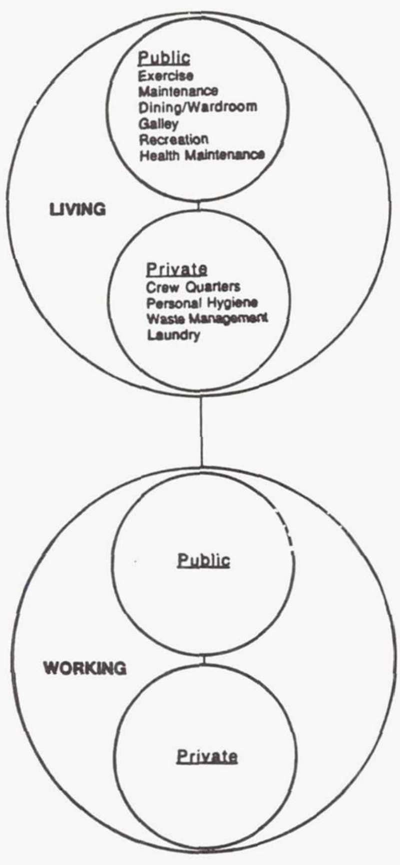

Fig. 6. Functional Layout Breakdowns

Circulation patterns are very important to the efficient functioning of the human habitation areas. Circulation should be clear and uninterrupted to allow for easy travel from one place to another. Dual egress, which allows two means of exit from anywhere, should also be provided as a safety precaution.

Finally, the functional layout must be derived from functional adjacencies. In other words, the public areas should be isolated from the private areas, the work areas from the living areas. These separations allow for efficient use as well as psychological acceptance from the crew. Figure 6 shows further breakdowns of the public, private, work, and living areas. The attached drawings show the final design concept for the human habitation area of a lunar base to accommodate a crew of 12.

Exterior architecture

For practicality, the configuration must lend itself well to growth and expansion as well as ease of installation and construction.

The modules must be functional in configuration due to the harsh and extreme conditions of the Moon. Because of this, dual egress became an issue of concern. Dual egress means that there is always a safe area to escape to in the event of an emergency, and that no "dead ends" are created as a result of the layout. This issue was stressed in meetings we had with Colonel Gerald Carr, commander of the third Skylab mission.

Since the initial base is to house roughly 36 crew members, and is to be built primarily from Earth-launched goods, it was necessary to save weight wherever possible without hindering the functionality of the base; therefore, the design must be very flexible within its own constraints to provide optimum functionality.

The most important issues in the module configuration study were dual egress, phased growth, and modularity. To determine what type of configuration would best suit our purposes, studies of four basic geometric forms were made. Geometric forms were studied because the modules to be used are all uniform; therefore, geometric growth is preferred.

Two-dimensional configurations were the only ones studied because in trying to erect, stabilize and support vertical configurations, it became difficult, time consuming, and expensive, requiring much additional structure and extensive Extra Vehicular Activity (EVA) time to achieve the task.

The following are studies of four potential configurations (Figs. 7-10). The configurations are based on geometric forms utilizing modules of equal size to keep the geometry simple and basic. Each study is then evaluated via pros and cons to determine which is the most practical to be used as the lunar base configuration.

As a result of the configuration study, the grid base configuration was chosen for the lunar base. It was chosen primarily for the following advantages: (1) dual egress; (2) uniform growth; (3) planetary application benefit; (4) easily

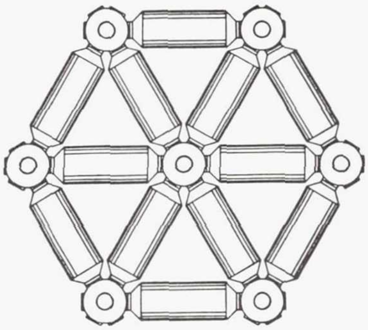
Fig. 7. Triangular Configuration

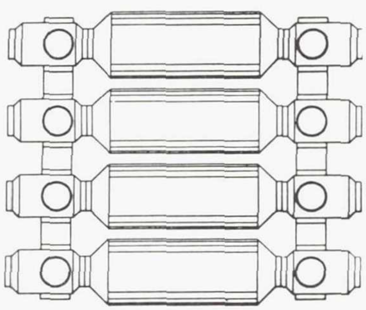
Fig. 8. Raft Configuration

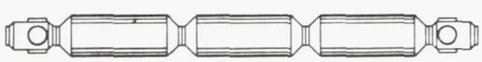
Fig. 9. Linear Configuration

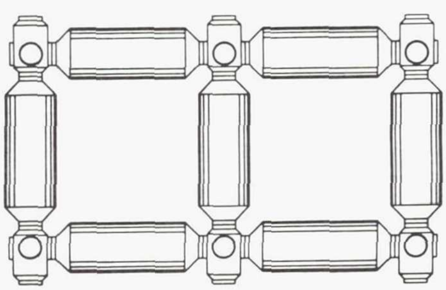
Fig. 10. Grid Base Configuration

implemented structure; and (5) standard-sized nodes. Its disadvantage is that four modules are needed to complete the configuration.

Radiation Protection

The major concerns in designing the lunar base were the harsh conditions on the Moon. Temperature, lack of atmosphere, radiation, and surface constraints are the issues of most importance, with radiation having the most serious effects.

Unlike the Earth, the Moon has no atmosphere or magnetic fields to protect it from harmful or deadly doses of radiation that bombard it constantly. Radiation shielding on the Moon could be achieved by placing a predetermined amount of mass between the radiation source and the crew living inside the base. Since mass is the key issue in radiation shielding, it would make sense to use *in-situ* materials wherever possible, and save the great expense of bringing thousands of metric tons of material from the Earth.

Permanent dwellers on the Moon can spend roughly 20% of their time without any significant shielding, providing they spend the rest of their time under at least 400 g/cm^2 of shielding(1). This amount protects the inhabitants from cosmic radiation, but to protect against gigantic solar flare events, a shield of at least 700 g/cm^2 is necessary.

The following is a study of three different methods for achieving radiation protection using the lunar regolith as a mass between the source and the crew (Figs. 11-13).

Contained regolith was chosen as the method for radiation shielding for the lunar base. It was chosen based on the following advantages, as well as the flexibility of the system, ease of deployment, and ease of achieving the end result. Advantages include: (1) allowance for easy growth; (2)

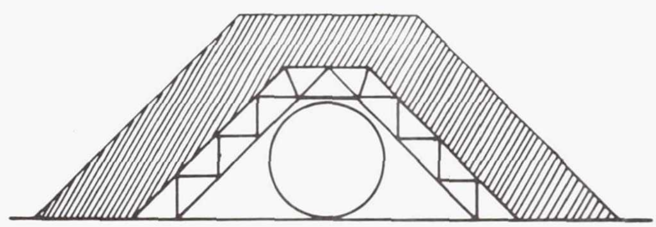
Fig. 11. Regolith Support Structure

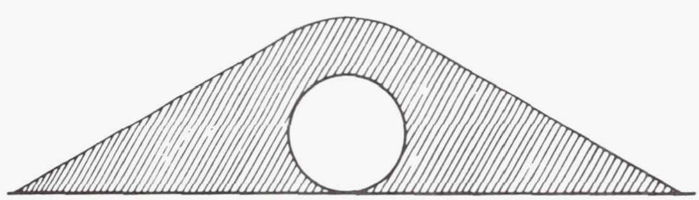
Fig. 12. No Regolith Support


Fig. 13. Contained Regolith

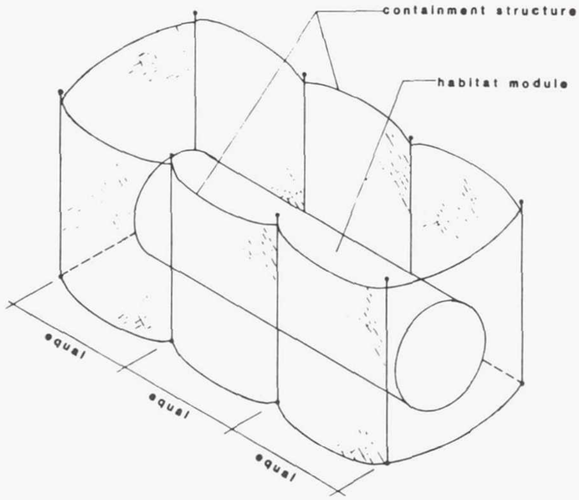

Fig. 14. Regolith Containment System

containment of regolith in a defined area; (3) relative ease of deployment; and (4) possibility for other uses of system. It has the disadvantage of adding mass through LEO due to its structure.

Contained regolith can be obtained by a number of different methods, but the principle remains the same. There is a structure that acts as a form or a mold to contain the regolith in a defined area so there is no overspill to hinder circulation around the exterior of the modules. The structure can be arranged on a grid system so that the module coverage and unearthing can be a controlled activity. Access to the hull can be gained by removing one wall, causing the regolith to spill away. This ensures ease of access to the hull for both expansion of the base and emergency repair (Fig. 14).

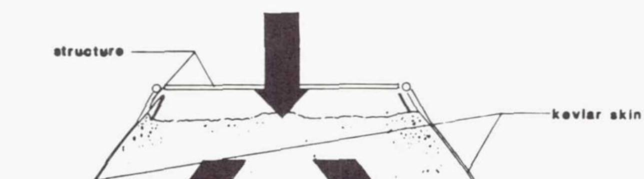

Fig. 15. Loading Diagram for Regolith Containment

The method for achieving contained coverage chosen by the design team is a tensile structure loaded internally with regolith. The lateral forces exerted on the structure, which put it into tension, are a result of the weight of the regolith trying to force itself out horizontally against the structure as it is poured into the structure from the top (Fig. 15). The system consists of composite graphite and high-tensile aluminum-alloy, tube-section members on a 4.5-m grid spacing.

The frame has multi-layered Kevlar suspended in the areas which are to receive the regolith. This Kevlar is held off the structure by a track system which is also used in the deployment sequence of the Kevlar. In the areas which do not receive regolith, a substitute material, thin multi-layered Mylar with a highly reflective outer surface, is used to reflect the intense solar bombardment and act as a thermal barrier. Figure 16 shows the deployment of the Kevlar and Mylar in the system. The system was designed to fold and unfold to make the deployment sequence as easy as possible, thus decreasing the amount of EVA time necessary.

Facility Planning

All facilities were shown in context with the habitat facility so that a complete analysis of the lunar base could be performed. Before any planning could be done for the lunar base, it was necessary to determine the purpose and functions to be served. The design team felt that the base should be the beginning of man's colonization away from planet Earth, a station for scientific study, and a testing ground for advanced technologies. The main industrial products of the facility will be Lunar Liquid Oxygen (LLOX) for fuel and human consumption, and the production of construction materials.

It was important to determine the needs of each facility for machinery and equipment as well as storage and physical space requirements. As a result, it was found that all of the required facilities could be grouped into four categories: industrial, transportation, living, and science and utility. Within each of these categories, the functional breakdown is as follows: industrial— mining, power plants, manufacturing and processing; transportation— landing, launching, vehicle storage, and maintenance; living— habitat and agricultural facilities; and science and utility— solar arrays and observatory sciences.

Site selection was an important issue because the site must be as versatile as possible. Access to and from the site needs to be as easy as possible; therefore, a site within a few degrees plus or minus latitude of the equator would be ideal. The base should be located on the nearside of the Moon to minimize communications problems as well as to provide a psychological link with Earth. It should offer a rich mineralogical and geological composition, providing access to mare and highland regions. A mare region is a good location for the facility because it provides flat terrain for construction and living areas, materials processing plants, solar arrays and telescope fields, and landing facilities. The highlands are good for mining, geological study, and natural shielding from incoming low angle projectiles (natural and manmade). Therefore, a site on a mare with near access to the highlands would be ideal.

C-2.

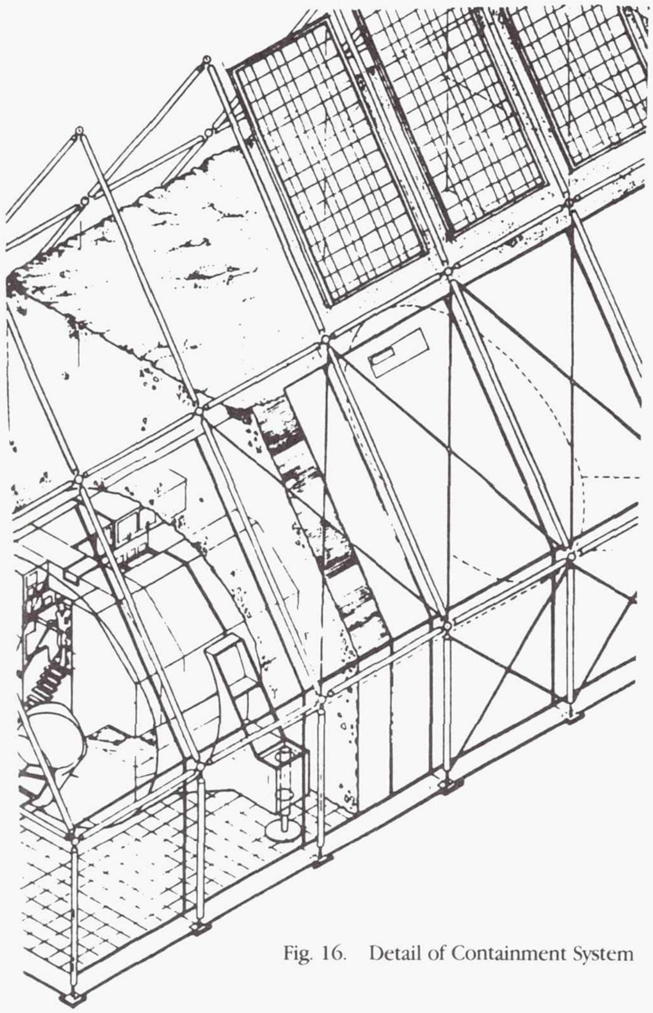

Fig. 16. Detail of Containment System

CONCLUSIONS

Lessons Learned

The goals of this study were to formulate facts on human reactions to partial gravity environments, derive design requirements based on these facts, and apply the requirements to a partial gravity situation. The approach was to compare partial gravity with Earth gravity (1 *g*) and microgravity to derive design differences.

Partial gravity is similar to Earth gravity except for human locomotion; however, it differs greatly from microgravity in that astronauts cannot sleep on walls and ceilings and are restricted to a 7 ft (2.13 m) usable height. Locomotion differences in partial gravity cause the human body to have a much greater forward body inclination as well as to "bounce" higher than in Earth gravity. Walking and running speeds are slower in partial gravity and it is harder to stop because of reduced friction.

It was also determined that a two-level interior configuration is the most efficient use of volume and minimizes the weight/volume ratio. Separation of working and living areas as well as public and private areas is the most efficient functional arrangement.

Radiation protection is desirable for at least part of a lunar base to protect humans from radiation. Lunar regolith coverage of the modules was determined to be the best method of radiation protection. Lunar regolith can also be a very good source of liquid oxygen (LOX) and can produce construction materials for structures (cast basalt), paved surfaces (sintered basalt) and cables (spun basalt).

Outstanding Technology

Research into the long-term effects of partial gravity on the human body is much needed to determine how the environment changes humans, which in turn will affect design.

A Heavy Lift Launch Vehicle (HLLV) must be developed to carry the modules into LEO, where a Space Operations Center (SOC) must be in place. The HLLV must be able to carry a module 22 ft (6.7 m) by 57.5 ft (17.2 m) that weighs 77,000 lbs (35,000 kg). From the SOC, there must be an Orbital Transfer Vehicle (OTV) that can carry the module to an orbit around the Moon. A lander that can deliver the module to the surface of the Moon must also be developed. Once the module is on the surface there must be a vehicle that can carry the module to its final destination. This fleet of vehicles is essential to bring this concept to reality.

We assume that the mining equipment can also be used to cover the modules with regolith for radiation protection. However, this seems to be a laborious process that might require additional equipment.

ACKNOWLEDGEMENTS

Team members were research assistants Stephen Capps and Jason Lorandos, along with Eval Akhidime, Michael Bunch, Denise Lund, Nathan Moore, and Kiosuke Murakawa. Faculty advisor was Professor Larry Bell.

REFERENCES

1. Silberberg, R., "Radiation transport of cosmic ray nuclei in lunar material and radiation doses," *Lunar Bases and Space Activities of the 21st Century*, Mendell, W.W., (ed.), Lunar and Planetary Institute, Houston, TX, 1985.
2. Hewes, D.E., Spady, Jr., A.A., and Harris, R.L., "Comparative measurements of man's walking and running gaits in Earth and simulated lunar gravity," NASA Technical Note, NASA/Langley Research Center, D-3363, 1966.
3. Man-Systems Integration Standards, NASA-STD-3000, Vol. I, 1987.
4. Duke, M.B. and Keaton, P.W. (eds.), Manned Mars Missions: Working Group Summary Report, NASA M001, Los Alamos National Laboratories, May 1986.

N94-71278

1994004523

LOGISTICS RESUPPLY AND EMERGENCY CREW RETURN SYSTEM FOR SPACE STATION FREEDOM

S11-66

UNIVERSITY OF ILLINOIS AT URBANA-CHAMPAIGN

160637

P 9

INTRODUCTION

Sometime in the late 1990s, if all goes according to plan, space station *Freedom* will allow the United States and its cooperating partners to maintain a permanent presence in space. Acting as a scientific base of operations, it will also serve as a way station for future explorations of the Moon and perhaps even Mars.

Systems onboard the station will have longer lifetimes, higher reliability, and lower maintenance requirements than seen on any previous space flight vehicle. Accordingly, the station will have to be resupplied with consumables (air, water, food, etc.) and other equipment changeouts (experiments, etc.) on a periodic basis. Waste material and other products will also have to be removed from the station for return to Earth. The availability of a Logistics Resupply Module (LRM), akin to the Soviet's *Progress* vehicle, would help to accomplish these tasks.

Riding into orbit on an expendable launch vehicle, the LRM would be configured to rendezvous autonomously and dock with the space station. After the module is emptied of its cargo, waste material from the space station would be loaded back into it. The module would then begin its descent to a recovery point on Earth.

Logistics Resupply Modules could be configured in a variety of forms depending on the type of cargo being transferred. If the LRMs were cycled to the space station in such a way that at least one vehicle remained parked at the station at all times, the modules could serve double duty as crew emergency return capsules. A pressurized LRM could then bring two or more crewpersons requiring immediate return (because of health problems, system failure, or unavoidable catastrophes) back to Earth. Large cost savings would be accrued by combining the crew return function with a logistics resupply system.

PROJECT BACKGROUND

This is the fourth year that the University of Illinois has participated in the NASA/USRA Universities Advanced Engineering Design Program. Sixty-one undergraduate students, divided into eight groups, were enrolled in the spacecraft section of Aeronautical and Astronautical Engineering (AAE) 241 in the Spring 1989 semester. This paper summarizes the work of six of the student groups as submitted in their Final Design Reports.

The **Logistics Resupply and Emergency Crew Return System for Space Station Freedom** was selected for this year's project and was approved by Frank Swalley, the University's USRA contact at Marshall Space Flight Center (MSFC), early in the Fall 1988 semester.

Several studies have reviewed the independent need for a logistics resupply vehicle and an emergency crew return lifeboat. The space station's anticipated downmass requirements have been predicted to exceed the shuttle fleet's capability. In light of the *Challenger* tragedy, the need for an available means of returning from the space station in the event of an unforeseen emergency calls for an auxiliary spacecraft to handle the load.

PROJECT OBJECTIVE

The project objective was to develop a conceptual design for the system required to perform a logistics resupply mission to the space station. In addition, the design had to allow for the use of a logistics module as a crew emergency return capsule to bring astronauts back to Earth from the space station. An optional, attachable orbital transfer propulsion subsystem would be used to carry supplies/crew/equipment to various orbiting platforms.

Performance, weight, and cost are very important to the acceptance of a combined system, so approaches were taken to optimize these parameters in design tradeoffs. The system had to be reliable, easily operated, and reusable. It also was required to use off-the-shelf hardware where available, but use of materials or techniques expected to be available after 1994 was prohibited.

SYSTEM REQUIREMENTS

A thorough preliminary design study was conducted by the students to determine major design issues as well as establish the size of, define subsystems for, and describe the operation of a logistics resupply and emergency crew return system that satisfied the following requirements:

1. The system will consist of three primary components: logistics resupply capsule(s), space station docking adapter, and orbital transfer propulsion subsystem.
2. The following subsystems are identified for the purposes of system integration:
   a. Reentry and Recovery System
   b. Structure (including docking adapter, materials, design)
   c. Power and Propulsion
   d. Attitude and Articulation Control
   e. Command and Data Control (including automated rendezvous and docking)
   f. Life Support and Crew Systems
   g. Mission Management, Planning and Costing

PRECEDING PAGE BLANK NOT FILMED

PAGE 88 INTENTIONALLY BLANK

Table 1. Ninety-Day Logistics Resupply Requirements

	Upmass(kg)	Downmass(kg)
Pressurized		
(Crew/Station)	4148.56	3497.99
(Customer)	4954.14	4757.39
Unpressurized		
(Crew/Station)	513.01	513.01
(Customer)	4152.18	4152.18
Fluids		
(Crew/Station)	360.61	0.00
(Customer)	365.14	173.73
Propellants		
(Crew/Station)	45.36	0.00
(Customer)	1681.92	0.00
Total	16220.92	13094.30
	Up volume (m^3)	Down volume(m^3)
Pressurized		
(Crew/Station)	14.78	11.50
(Customer)	13.92	13.75
Unpressurized		
(Crew/Station)	4.53	4.53
(Customer)	32.64	32.64
Fluids		
(Crew/Station)	0.45	0.00
(Customer)	0.50	0.17
Propellants		
(Crew/Station)	0.57	0.00
(Customer)	1.68	0.00
Total	69.07	62.59

3. The system's components and payload will be delivered to orbit on an expendable launch vehicle. The extent of shuttle support should be identified and minimized. Vehicle components must be returnable to Earth in the space shuttle bay.

4. Nothing in the system's design should preclude it from performing several possible missions, carrying vastly different payloads to the space station.

5. The system will have a design lifetime of six years, but nothing in its design should preclude it from exceeding this lifetime.

6. The vehicle will use the latest advances in artificial intelligence where applicable to enhance mission reliability and reduce mission costs.

7. All vehicle components will operate under positive space station control at all times.

8. The design will stress simplicity, reliability, and low cost.

9. For cost estimating and overall planning, it will be assumed that four logistics resupply modules will be built. Three will be flight-ready, while the fourth will be retained for use in an integrated ground test system.

RESULTS SUMMARY

Logistics and Crew Module Sizing

The student groups typically divided the resupply mission design problem into six tasks: payload identification, vehicle sizing, expendable launch vehicle (ELV) selection, space station rendezvous and docking, and resupply component unloading and storage. Using data available from several sources, the groups compiled a set of up and down totals for logistics resupply mass and volume. Table 1 details an averaged set of logistics requirements given to the students.

The students then calculated the volume and mass required to support the emergency crew return mission. Figure 1 illustrates the enclosed volume required to support crews of various sizes (2-8 persons) for various mission lengths (0-2 days). In the event of an emergency return, a logistics module sized to handle the entire 90-day up-volume requirement would be able to sustain the largest anticipated crew (8 persons), to be returned from the space station, for more than 2 days. If the logistics supplies were divided into two equally sized payloads, it was found that an 8-person crew could be comfortably contained for up to 40 hours. Correspondingly, the mass required to return a full complement of crew was found to be significantly less than the driving logistics return requirement.

Launch Vehicle Selection

Given the up-mass and up-volume requirements the students reviewed the capabilities of available expendable launch vehicles to fulfill the mission requirements. All six groups selected the largest available booster, the Titan IV, with a 18,000-kg capacity to low Earth orbit. With a 16,220-kg payload and less than 2000 kg left over for the module's structure and support equipment, several groups correctly chose to split the payload into two launch packages (8110-kg logistics payload each).

Crew Support

The students identified several threats that would require an emergency return from the space station. These included crew injury or illness, depletion of consumables, and several threats

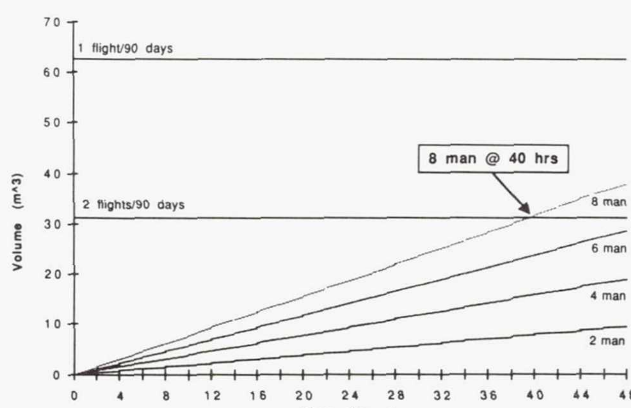

Fig. 1. Crew Volume vs. Logistics Resupply Requirements

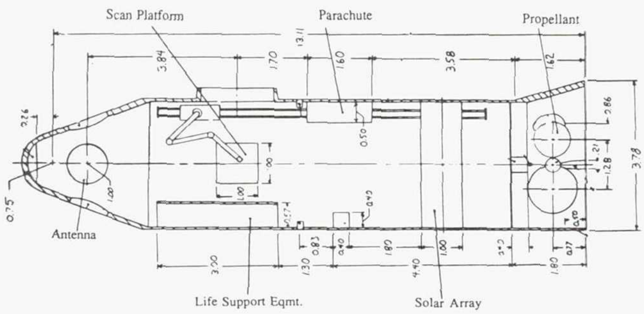

Fig. 2. Biconic Logistics Resupply Module Internal Layout

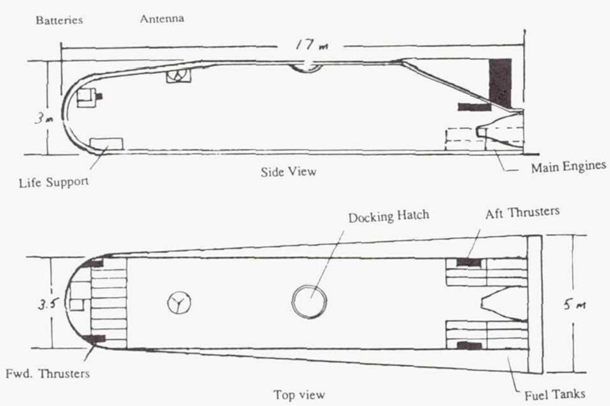

Fig. 3. Lifting Body Logistics Resupply Module Internal Layout

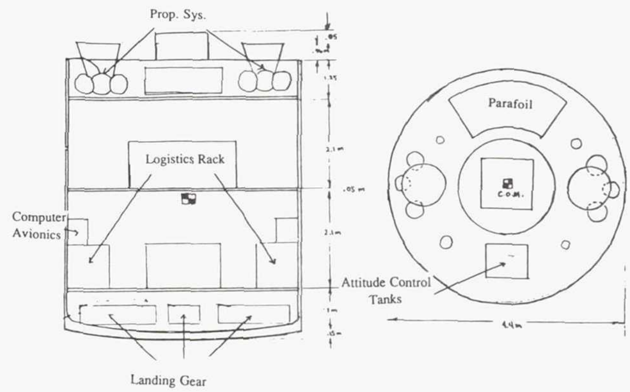

Fig. 4. Oblate Cylindrical Logistics Resupply Module Internal Layout

coming under the heading of "Acts of God," such as explosions, fire, or a collision with space debris.

In the event that a single crewperson needed medical attention beyond that available at the space station, the injured crewperson would be accompanied by at least one other crewperson for the return to Earth. With these constraints in mind, three groups retained an eight-person maximum crew return configuration, with either vehicle still capable of carrying a full space station crew. Two groups settled on a capacity of six persons for their vehicles, which would be able to return two if required and still handle the remaining six if required by a second emergency. One group designed for a four-person configuration specifying a minimum returning crew complement of four for any emergency return.

An open-loop environmental and life support system was dictated by the short return mission duration (less than 40 hr). Lithium hydroxide was employed by all of the groups to remove carbon dioxide from the crew cabin. A cold-water loop was used to remove cabin heat and provide humidity control. One group used two-phase wax blankets to transport internal cabin heat to an external heat exchanger system.

Given the nature of the logistics and resupply mission, crew piloting requirements were minimized by the groups. Several systems were identified by the students for use in an automated rendezvous and docking sequence. They included cameras and guide beacons, optoelectronic systems, and some form of artificially intelligent controller. All groups also employed communications packages capable of relaying information through the TDRSS system to ground-based controllers as well as to the space station itself as required by different mission profiles. Figures 2-4 exemplify the internal layout of three of the student group's designs.

Power and Propulsion

All of the student groups selected bipropellant propulsion systems based on the required on-orbit storability of propellants and the ability to throttle the main engine in response to various mission profiles. Five groups used a MMH/NTO-based system, while one group used a hydrazine/LOX system. Propulsion system mass ranged from 1496 kg to 3688 kg supplying ΔV's ranging from 152 m/s to 422 m/s.

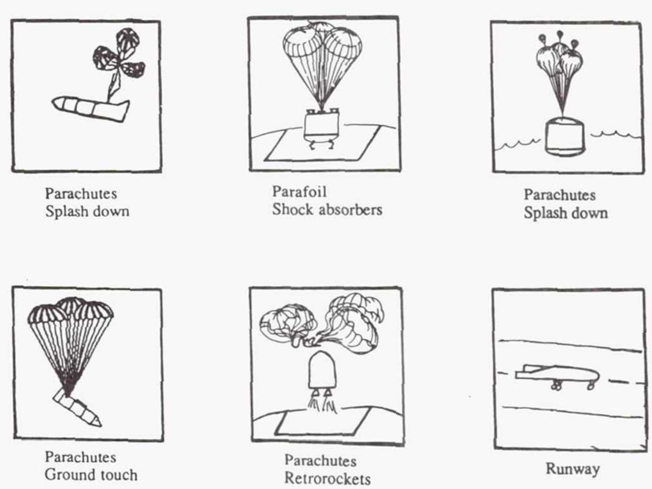

Fig. 5. Logistics Resupply Module Reentry Configurations

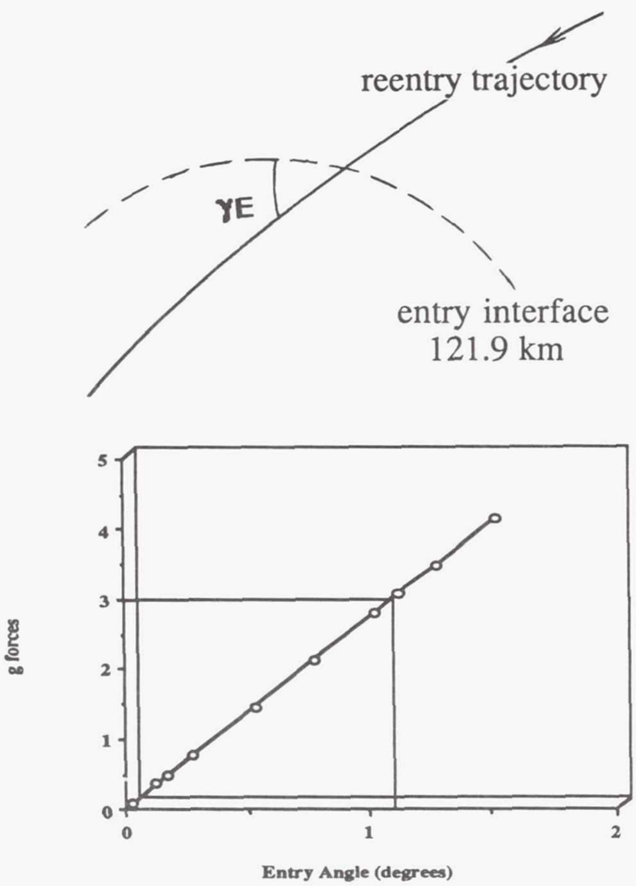

Fig. 6. *G*-limited Reentry Angle Calculations

Power supplies for the LRM designs included fuel cells (one design), solar arrays and batteries (two designs), and battery-only systems (two designs). The solar array systems were deployed by the LRM when docked to the space station to insure a fail-safe and independent power supply for the crew emergency return function. Available energy for these systems ranged from 30 kW-hours to 96 kW-hours.

Reentry

External vehicle shape was dictated by logistics volume requirements, crew accommodations, and chosen reentry method. Six different reentry vehicle configurations, encompassing lifting bodies, biconic shapes, and oblate cylinders, resulted from the students' work. Figure 5 illustrates the variety of shapes and reentry methods employed. For the biconics and oblate cylinder, parachutes and retro-rockets were employed for the terminal descent phase of the mission. The student groups typically employed reusable space shuttle-like outer surfaces, relying on carbon-carbon composites to protect the vehicle from the high temperatures of reentry.

To protect a possibly injured crewperson from high *g* forces during reentry, a 3-*g* limit was imposed on the reentry trajectory design. Using an analytical expression for maximum encountered *g* forces, the students calculated an acceptable entry flight path angle of a little over 1.1°. Figure 6 defines the entry flight path angle and illustrates the results of these calculations.

CONCLUSIONS

Because the LRM combines both logistics resupply and crew emergency return capabilities into one vehicle, the cost of the student group systems would be roughly half that of the two independent systems proposed by NASA to support space station operations. Total cost per vehicle was estimated by the student design groups to vary from $514 million to $1100 million.

In addition to gaining valuable insight into the spacecraft design process, the University of Illinois undergraduate students participating in the NASA/USRA design program have designed six potentially viable, cost-effective alternatives for the Logistics Resupply and Emergency Crew Return functions.

ACKNOWLEDGMENTS

This paper summarizes the work of six student groups: D. Ahne, D. Caldwell, K. Davis, S. Del Medico, E. Heinen, S. Ismail, and C. Sumner; J. Bock, B. Buente, R. Gliane, S. Hermann, Michael Le Docq, M. Mueller, and J. Selmarten; B. Baird, C. Helfrich, C. Martin, K. Powers, S. Staats, S. Thakar, and G. Wagner; J. Berg, R. Gianvecchio, J. Hedrick, E. Janensch, D. Quinn, D. Quitno, and R. Villalobos; J. Beirne, G. Fermoyle, J. Fittanto, E. Goletz, S. Murphy, D. Schafer, and S. Woods; and A. Fundich, S. Greenfield, J. Kane, H.S. Kim, J. Rauwolf, K. Stevens, and C. Higgins. Professor K. Sivier was the faculty advisor.

N94- 71279

1994004524
382679 S12-18
160638
4

A DUAL-ARMED FREE FLYER

UNIVERSITY OF MARYLAND

INTRODUCTION

In this summary, we present the main conclusions and results of the design studies conducted by a group of 13 students at the University of Maryland. The students, all participants in the spring 1989 course ENEE418 in the Electrical Engineering Department, met weekly in a two-hour class to discuss and evaluate design alternatives. The main problem considered was the design and control of a planar testbed simulating a free-flying space robot for applications in satellite servicing.

This project grew out of the 1988 class where a dual-armed free flyer (DAFF) was designed and partially built. This year, a group of six students continued the development of the DAFF, and after making several major improvements and additions, achieved computer-controlled motion of the DAFF's arms. All fabrication and testing of the DAFF is being conducted in the Intelligent Servosystems Laboratory at the University of Maryland.

While the work related to the design and development of the DAFF is the main subject of our report, we should point out that other students in the ENEE418 class have investigated additional issues related to manipulation in space. For example, one group studied a new parallel linkage based manipulator for fine motion applications such as in assembly operations in space. They investigated the mechanism's kinematics and its reachable workspace, and precision of applying forces and torques. In yet another project, a student set out to measure and map the friction characteristics of the actuators used in the Modular Dextrous Hand, which has been recently developed in the Intelligent Servosystems Laboratory. His results are expected to help compensate for this friction, which is a highly nonlinear disturbance and presents significant problems in high-precision, low-speed operations. This summary continues with the discussion of the results obtained by the group of students who have been working on developing the DAFF testbed.

LABORATORY TESTBED

The DAFF is built as a simulation for one of the realizations of the flight telerobotic servicer (FTS). The aim is to extend our knowledge about automation in the weightless environment. In particular, the controller developed would be able to operate more optimally in this kind of environment. For the FTS, the arms will be a significant proportion of the mass, therefore the torques generated by their movement will have a noticeable effect on the craft's attitude. This represents a unique problem in robotic control. In the case of most Earth-based robotics, large arms are usually fixed to the Earth or a large structure, which can absorb almost any torques that result. One method for compensating for these torques inherent in the FTS is to turn on the attitude control system, pretending that the robot is attached to something massive like the Earth. A more elegant and less wasteful system would understand the weightless environment enough to operate in it without the crutch of the attitute control system thrusters. In some ways, this environment can be turned to our advantage. For example, we believe the DAFF will phase shift as its arms move about. This could be used to orient the craft. With this in mind, the hardware simulation group set about to design and build a simulation so it can act as a testbed for the control ideas proposed.

Zero-G is simulated by floating a two-dimensional version of the DAFF on an airtable. In design, the main criteria kept in mind was accurate simulation. A tether would introduce significant torques to the body which would have little to do with the actual DAFF. A tether would therefore be limited only to testing, programming, and debugging uses. We chose DC servo motors for the arms over other methods because the proposals for the actual DAFF used them. Propulsion and attitude control is achieved using cold gas jets and a gyro, chosen for the same reason as the arm motors. The configuration and proportions are based on an optimality study conducted the semester before the design began.

ARCHITECTURE FOR THE DAFF

A secondary design criteria for the DAFF design was flexibility. Because it was to be an experimental testbed for many concepts we needed to be able to change and add to both the hardware and control software. The key to making the robot flexible lies in the choice of the control system. For flexibility all of the control loops were run through a computer. Having a computer do everything may be flexible, but it does require a lot of computer time. To alleviate this computational bottleneck, the tasks were divided up and distributed in a hierarchical fashion. The tasks that required constant monitoring, in particular the control loops, were placed onboard. Other parts of the control, such as decision algorithms and path planning, are offboard. A radio link is used to transfer information between the onboard and offboard algorithms, at the point where the lowest rate of communication is needed. The computer chosen for processing the control loops is a Mizar 8115, which is a 68000-based half-height board (Fig. 1). This computer has a great deal of power and expandability via the half-height VME bus it plugs into. This standard bus allows for expansion later, if we need the extra I/O or even an extra computer board. The onboard computer has an operating system, called PDOS, which allows easy software development. PDOS is multitasking as well, which is similar to the operating system proposed for the real system.

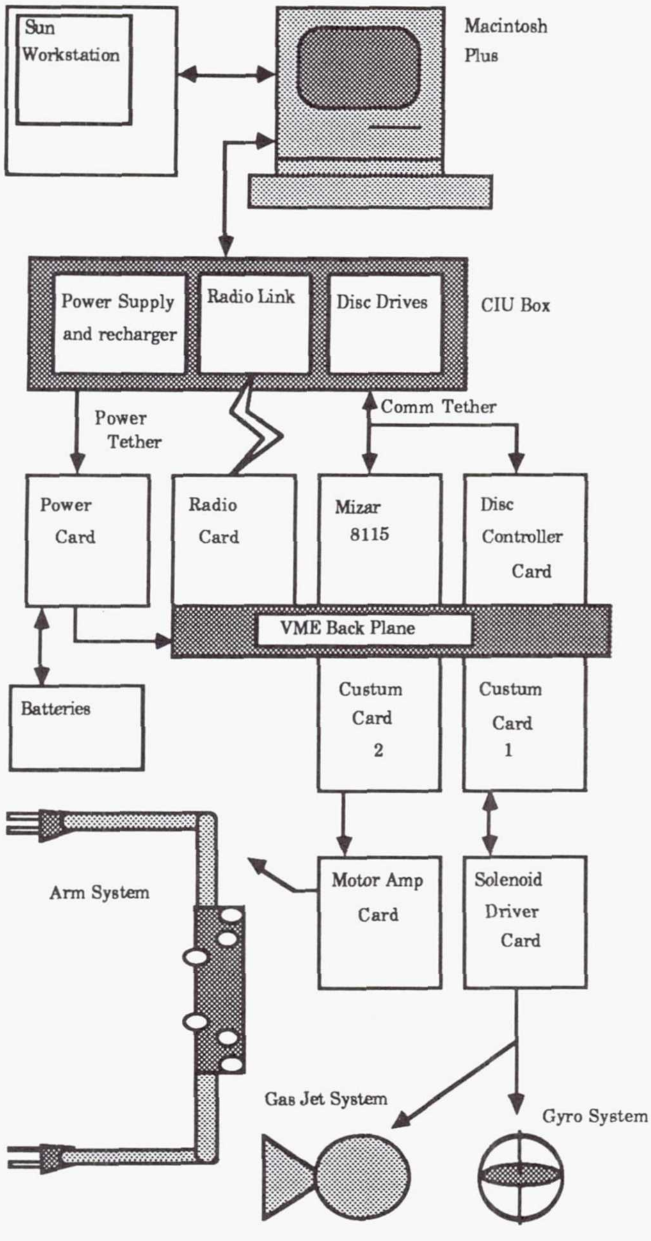

Fig. 1. DAFF Architecture Plan

ARCHITECTURE PLAN

The card cage includes the VME bus, the Mizar 8115 computer board, a disc controller for the Mizar, a card containing the radio link, and two custom I/O cards that handle the bus arbitration and interface the DAFF hardware to the computer. In addition, there are three cards held in the rack that do not plug into the bus: they are the motor amplifier card, the power distribution card, and the solenoid/gyro/hand driver card.

The offboard computer chosen is a Macintosh. The choice of computer here is not so critical; it was chosen because it was available. Mostly it will serve as a doormat for the more powerful Suns in the lab, which can communicate via the net. The Suns are being used to run simulations of the DAFF. The higher levels of the control system will be developed on these machines. Right now, the Macintosh serves only as a terminal for the Mizar.

MECHANICAL SYSTEM

Mechanically, the DAFF can be cut into four chunks. The heart of the system is a simple, rigid aluminum chassis, made of slotted u-channel so mounting thrusters would be flexible. The computer subrack, also made primarily out of aluminum, mounts on the rear. The shoulders, which the arms connect to, mount on its front. Lastly, a Plexiglas wash plate provides a flat surface toward the airtable (Fig. 2).

The arms themselves have three degrees of freedom each, allowing positioning and orientation in the plane. The end effector is a simple two-fingered pincer. Power is transferred to the joints of the arms by a toothed-belt transmission system. All of the motors are mounted in the shoulders with the exception of the hand motors, which are mounted directly on the end effectors. This shoulder mounting redistributes the arm mass so the air table can support the motor weight directly. The gyro acts primarily to stabilize this air-suspended platform, although it may be used to orient the DAFF in the future. The gyro, driven by a two-phase motor, is mounted directly behind the shoulders. The gas jets will be controlled by eight normally closed solenoids, which are driven by the onboard Mizar. Firing time for each jet can be varied from 0.25 to 25 seconds. The DAFF weighs a hefty forty pounds, and whether or not this current thruster design has enough power awaits testing with the airtable.

GRAPHICS AND REAL-TIME SIMULATION

A significant proportion of the first spring semester's work was devoted to the design of a real-time control system as an operating system and a graphical animation environment for the study of sophisticated motion-planning algorithms. The current version of the operating system runs on a Sun 3/260 and the animation runs on Silicon Graphics workstations.

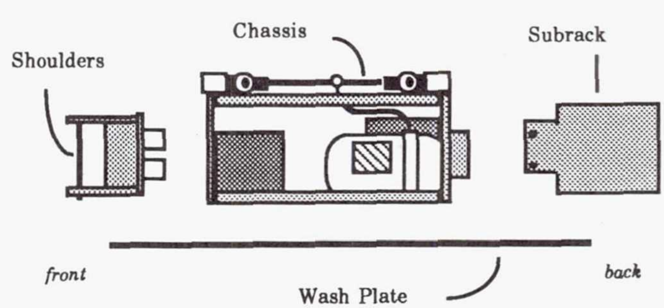

Fig. 2. DAFF (Side View)

ACKNOWLEDGMENTS

Design team members D. Beck, B. Das, C. Dickson, B. Douglas, L. Long, K. Middour, S. Reid, J. Uber, G. Walsh, and L. Wang were assisted by faculty advisor Dr. P.S. Krishnaprasad.

N94-71280

1994004525

S13-66
382680/60639
P. 6

THE DESIGN OF A COMMERCIAL SPACE INFRASTRUCTURE

MASSACHUSETTS INSTITUTE OF TECHNOLOGY

INTRODUCTION

Space Services and Logistics, Inc. represents the complete engineering design of a technically and financially viable commercial space company. The final proposal offers an economically sound program of space vehicles and systems designed to substantially affect a variety of space markets and produce a vertically integrated structure within the next 20 years. Throughout this design process, particular stress has been placed on attaining the highest possible levels of safety and reliability. The final program financial design requires a considerable initial outlay, but promises a relatively quick return on invested capital, culminating in large annual profits by the end of the 20-year scope of the cost outlook. The overall design has been extensively researched and was primarily driven by the present and near-term projected market demands for services uniquely or competitively offered only by space-oriented operations. Heretofore, available capabilities, rather than these market demands, have determined the degree and type of commercial market access. Removing this limitation through extensive use of modularity and reconfigurability allows our company to gear itself to the market, while still remaining extremely competitive with existing systems. The markets that we have identified as lucrative, and that have governed much of our design requirements, are:

1. Low-cost launch services to LEO over a wide range of payload masses and inclinations.
2. Upper stage payload delivery from LEO to GEO.
3. Manned space operations and human transport to and from orbit.
4. EVA assembly and maintenance of large space structures.
5. Satellite servicing and repair by both humans and telerobotic operations.
6. A line of customized satellites designed for extended life and capable of reconfiguration or technology upgrade on orbit.
7. Small-scale microgravity experimentation and manufacturing supported by spacecraft retrieval capabilities for experimental specimens and manufactured goods.
8. A full-range of payload integration, testing, design, and support services before launch and once in orbit.

Each of the systems designed as a coherent part of this proposal is based not only on detailed engineering analyses, but also on the current or anticipated market demands, economic modeling of the manufacturing and operational costs of the unit, and anticipated unit lifetime expectancy and reliability, all of which are viewed in the light of the profit margin of the market that the system is designed to impact. Additionally, the effects of cost discounting over the lifetime of the company and system are incorporated into this economic model of net present worth and net future worth, as well as the effect of the "learning curve" on the reduction in manufacturing costs for units that can be mass produced. It is worth noting that several other systems were developed, only to be determined economically, technologically or operationally infeasible, and are not included in the final program.

The overall *SSL, Inc.* organizational structure has been broken down into three major elements: a launch vehicle division charged with providing inexpensive access to LEO for a wide variety of payload parameters, a manned spacecraft group to provide human access to orbit, and an orbital operations division to handle all on-orbit operations not covered by the other groups. Each of these divisions was designed to work together, as well and as closely as possible, thus creating a highly integrated approach to commercial space activity. However, each division is independent enough to retain viability should unforseen difficulties arise. A division-by-division overview of SSL's systems follows.

ORION LAUNCH VEHICLE

The "Orion" class will be the primary launch vehicle for both SSL and commercial missions, covering both the "light" and the "medium" payload ranges of 500-12,000 kg to low-earth orbit (LEO), as well as conducting suborbital flights. Since these missions require vastly different payload capacities, the Orion can be reconfigured to meet specific launch goals and needs. This flexibility in configuration is made possible by the use of standardized, interchangeable modules. These modules are virtually complete launch vehicles in and of themselves, but are easily integrated through both vertical and horizontal staging to produce the desired launch vehicle. Thus, by the addition or subtraction of these modules an extensive range of lift capabilities can be provided.

The four configurations in Fig. 1 are known as the Orion 0 (also called the Sirius), Orion I, Orion II, and Orion III. The distinguishing feature that defines each vehicle is its payload mass capacity to a LEO altitude of 200 km. The Orion I is designed to lift 5850 kg to LEO, accessing a major share of present market demand. Orion II launches 8600 kg, a capability governed by the DaVinci Manned Spacecraft requirements, and Orion III provides for heavier payloads by lifting 12,000 kg to LEO. The Orion 0 is designed to handle suborbital flights and light payloads of slightly better than 1500 kg to LEO. The specific configurations were chosen based on careful analyses of module dimensions, mass, number of modules, and overall costs vs. the performances dictated by the market.

The modules use a bipropellant system of liquid methane and liquid oxygen, producing a sealevel thrust of 164,000 N. The fuel tanks are made of graphite-epoxy and are designed to be manufactured using a filament-winding technique that minimizes production costs through automation. The main engine of each module is cooled by a straightforward regenerative cooling system, and is constructed entirely out of

PRECEDING PAGE BLANK NOT FILMED

PAGE ____ INTENTIONALLY BLANK

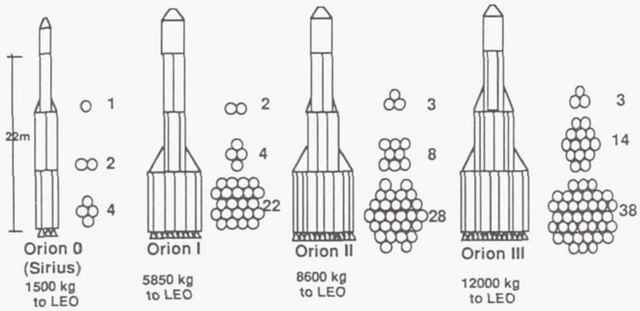

Fig. 1. The Orion Class Launch Vehicles

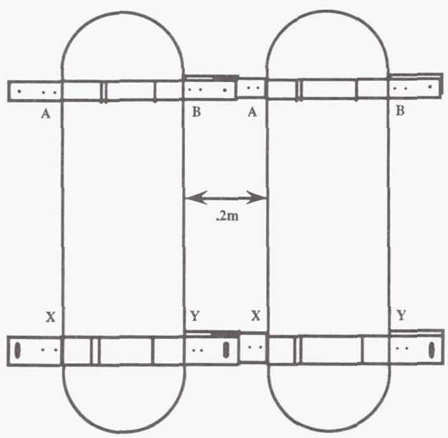

Fig. 2. Side View of Two Fastened Modules (Not to Scale)

thin stainless steel tubes running the length of the thrust chamber and nozzle. Each module has 375 kg of inert mass and 5375 kg of propellants for a total mass of 5750 kg.

By producing thousands of module units (in contrast to the previously most-produced rocket, the McDonnell Douglas Delta with its maximum production run of only 200 rockets for a given design), SSL takes advantage of true mass production. Also, since each of these reusable modules is identical, they are interchangeable within all positions on all possible configurations of the launch vehicle. After parachute-based aquatic recovery of the first stage modules, the modules are inspected and refuelled for future reuse. (The second- and third-stage modules will be damaged by atmospheric effects during the descent following burn-out and will not be reused.) Using an ingenious and yet simple interconnect design, shown in Fig. 2, the modules can be quickly integrated to form a launch vehicle, thus minimizing labor and integration time before the next launch.

DaVINCI MANNED SPACECRAFT

The DaVinci class spacecraft fleet is designed not only to support SSL's own operations by transporting humans into space, but also to target key profit centers, present and future, that require a manned presence in space. An effort was made to limit the role of the manned spacecraft and its crew to those tasks that absolutely require human expertise, since placing humans and the associated life support equipment in orbit clearly entails more cost and risk than an equivalent unmanned system. The selected missions are (1) human transport to and from orbit; (2) EVA assembly of large space structures; (3) satellite servicing and repair; (4) conduct of small microgravity experimentation requiring extensive tending; and (5) retrieval of small or fragile manufactured and experimental goods from orbit to Earth.

Each vehicle in the fleet of three reusable spacecraft is designed to be small and light enough to be vertically staged on top of several commercially available launch vehicles as well as on SSL's own Orion system. Based on a modified half-cone design, the vehicle exterior is shown in Figs. 3a and 3b.

In order to capture a part of the lucrative Space Station *Freedom* assembly and crew transport markets, the DaVinci spacecraft must be nominally operational by 1994, before SSL's launchers are designed and tested. During this time the manned spacecraft must rely on commercially available launch vehicles to operate. The substantial cost of these launchers requires a flexible spacecraft design incorporating two basic configurations, in the interest of minimizing mass and therefore cost, for the specified missions.

The two baseline configurations for the DaVinci are the Servicer configuration (for orbital assembly, repair, and servicing) and the Transport configuration (for human transport missions). The small experimentation and payload return missions are designed to be performed simultaneously with either of these primary missions. The Servicer configuration of DaVinci includes a six degree of freedom remote manipulator system (RMS) as well as either equipment for satellite servicing/repair or tools for orbital assembly. A crew of four operates on orbit with two astronauts in EVA and two inside the spacecraft. The total weight for the fully equipped and fuelled Servicer configuration is 8600 kg, requiring the use of an Orion II or Titan IV to achieve an altitude of 200 km, from which the spacecraft can climb as high as 525 km to rendezvous with satellites before performing its deorbit boost for atmospheric entry. The Transport configuration is equipped with six acceleration couches allowing a two-person SSL crew to transport up to four passengers. The manipulator is detached from the spacecraft and orbital maneuvering fuel is decreased to provide only for station rendezvous and deorbit burn. The associated mass reduction allows the DaVinci to launch on an Atlas IIs until the Orion family is functional.

Two hydrazine thrusters comprise the orbital maneuvering system and a combination of cold nitrogen thrusters and reaction wheels form the reaction control system. The power plant, nominally supplying 7.7 kW of power, is a set of three cross-strapped hydrogen-oxygen fuel cells. All fuels and life support gases are pressure-fed with nitrogen to increase system reliability by eliminating the possibility of pump failures. The avionics system is designed to require minimum interface with ground stations, and the computing system is based on a

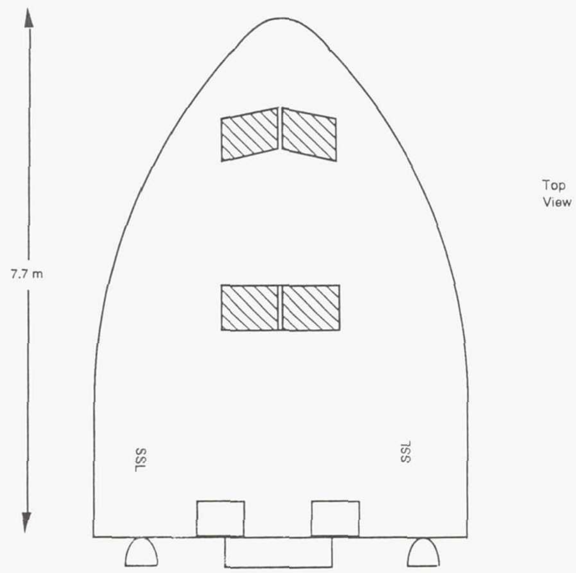

Fig. 3a. DaVinci Spacecraft External View (Top)

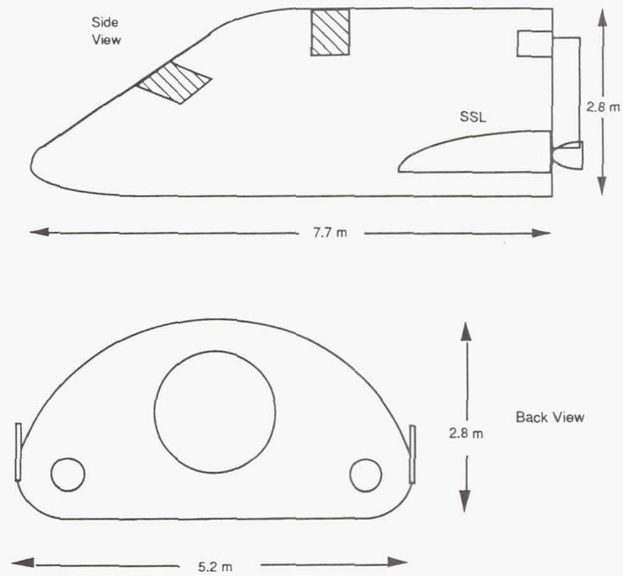

Fig. 3b. DaVinci Spacecraft External View (Side and Back)

transputer architecture. Navigation and guidance use an inertial measurement unit as well as GPS and ADS to determine position and attitude. The thermal system is embedded in the craft's structure and deploys radiators on the doors of the craft's two external storage bays. All spacecraft systems are designed for a mission length of seven days.

The spacecraft is also designed with the requirements that accelerations during ascent will not exceed 5 g and decelerations during descent should never exceed 3 g, a limit imposed by the return of injured crew or fragile manufactured goods. The vehicle's lifting body geometry provides it with a lift-to-drag ratio of one, minimizing entry decelerations until landing approach. To allow a dry landing (desirable to minimize operational and refurbishment costs) below 3 g, a high-glide parafoil system has been designed to deploy when the spacecraft reaches an altitude of 2 km, allowing the vehicle to fly in and land on gravity-deployed skids.

ORBITAL OPERATIONS

The majority of operations that are performed in space are accomplished without manned presence, for reasons detailed previously. SSL enters these markets through the development of the Prometheus Payload Delivery System (PDS) and the Altair Commercial Satellite, as well as the Satellite Servicer. Through these vehicles SSL has the capability to deliver customer payloads to GEO and, additionally, to launch and service its own satellites.

An expendable Payload Delivery System has been designed to serve as an upper stage for LEO to GEO transfer. The Prometheus PDS can be found in two models. The first is the SSL configuration composed solely of the Standard Propulsion Module (SPM). The cryogenically-fueled SPM uses the avionics on board the SSL satellite and needs little navigation and attitude control of its own. When launching third-party payloads, the Attitude Module, consisting of GNCI avionics and specialized attitude thrusters must be added (Fig. 4).

The capabilities of the PDS are compared to its competition in Fig. 5 in terms of payload to GEO and upper stage wet mass needed. The PDS clearly outperforms the Centaur G and IUS through reduced mass and vehicle cost, while retaining the liquid-fuel advantages lacking in the PDS.

The SSL Altair Commercial Satellite offers more flexibility than any other orbital system to date. By again employing a modular design, SSL has created a new generation of satellites designed for extended lifetimes, simple on-orbit upgrades to replace obsolete technology, retention of desired GEO slots,

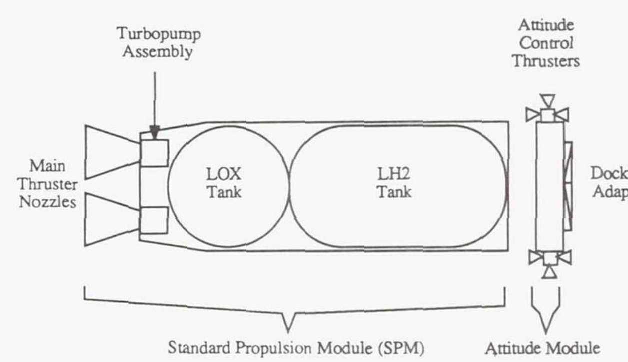

Fig. 4. Prometheus Payload Delivery System Configuration

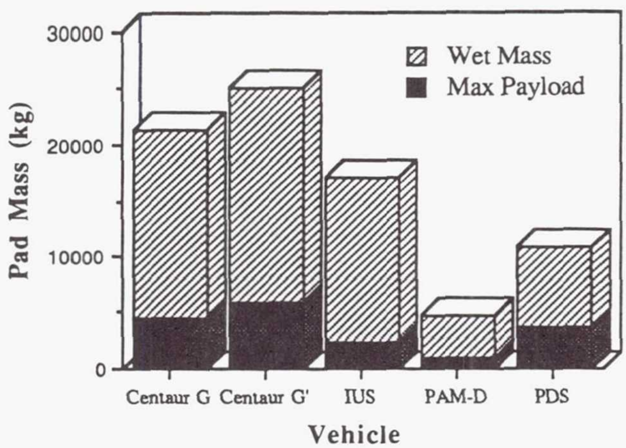

Fig. 5. Comparison of Payloads and Launch Mass

and easy repair in the event of failure. As shown in Fig. 6, the satellite is designed around a central common satellite bus (again to be mass produced for cost effectiveness) that serves as the housing for up to eight interchangeable Orbital Replacement Units, or ORUs. This bus also provides power (via solar photovoltaic cells), attitude control/station keeping, communication support, and thermal control to each of the ORUs. The GEO version of the satellite has the Standard Propulsion Module added to provide GEO boost. The SPM is dropped once the orbital change is complete.

Several different types of standard SSL-manufactured ORUs have been designed. Additionally, SSL will be able to manufacture customized ORUs should a customer have needs that are not met by any of the standard units. Table 1 illustrates three configurations. The ORU interface with the satellite bus will also allow customers to design their own ORUs or allow SSL to develop newer models of each of the standard ORUs.

The ORUs, as implied by their names, are designed to be switched-out or replaced on orbit. This can be used for either replacement of a damaged unit, an upgrade to a more effective module or one using newly developed technology, the addition of an ORU to a bus slot left empty when the satellite was launched, or the complete reconfiguration of a satellite for a new purpose.

By designing an orbital infrastructure and support network for our satellite system, SSL can offer its customers higher reliability and utility than any other company can hope to. Although the DaVinci manned spacecraft is capable of performing the orbital switch-outs of ORUs, the modular interface to the bus has been specifically designed to allow SSL to utilize telerobotics as a more cost-effective means of repairing and upgrading our own satellites. A robotic orbital satellite servicer has been designed to be placed in orbit carrying the ORUs required to service a number of satellites. The servicer is derived from the satellite and has added telerobotics and storage for replacement ORUs (Fig. 7).

The servicer is thus nothing more than a module that sits atop a standard satellite. It uses the subsystems of the satellite and controls the telerobotic arms through extra avionics placed within the ORU slots of the base satellite. The upper cage thus provides room for up to eight replacement ORUs.

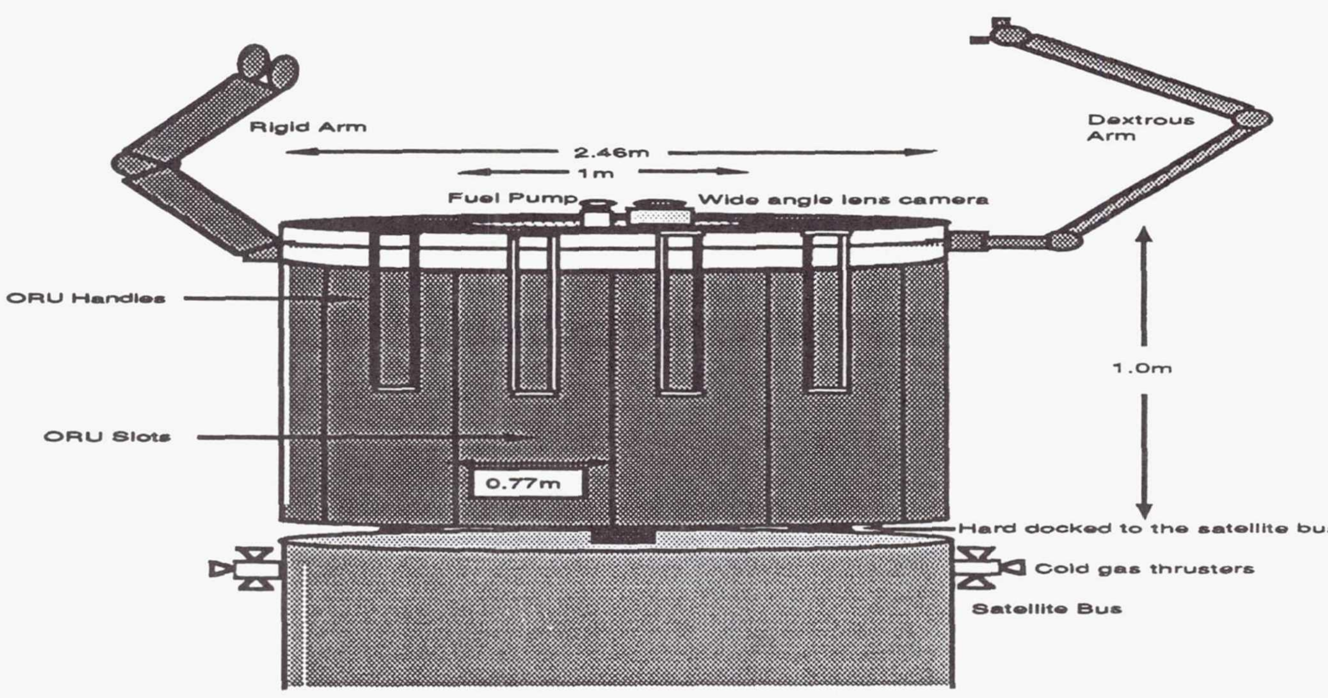

Fig. 6. Altair Satellite LEO Configuration

Table 1. Satellite Equipment Options

Standard Satellite		
Standard bus with 5 kW solar panels and 8 ORU slots	$15M	
SPM Orbital Transfer	$9M	
Flight Computer: Sensors, Experiment Coordination	$1.8M	slot 1
Guidance and Nav. System	$2.0M	slot 2
Communications	$3.0M	slot 3
Batteries (2)	$2.5M ea.	slots 4,5
TOTAL	$36M	
Communications Satellite		
Upgraded computer	+$1.8M	slot 1
Upgraded communications	+$3.0M	slot 3
Additional communications	+$6.0M	slot 7
Additional batteries	+$2.5M	slot 6
TOTAL	$53M	
Observational Satellite		
Upgraded computer	+$1.8M	slot 1
Upgraded communications	+$3.0M	slot 3
Additional batteries	+$2.5M	slot 6
Camera #1	+$4.0M	slot 7
Camera #2	+$4.0M	slot 8
TOTAL	$51M	

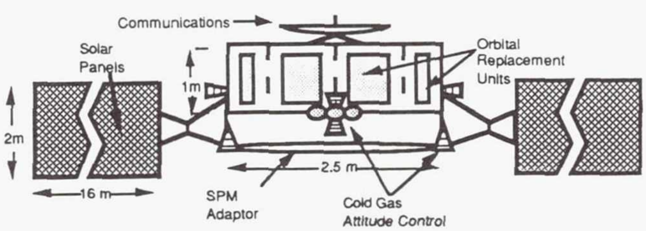

Fig. 7. The Servicer Configuration

The design efforts of the Orbital Operations group also extend far into the future of the company. Space platforms that also incorporate removable modules were developed, as well as a manned module providing extended duration manned presence for biological or manufacturing experiments. Although not included in the scope of our presented program, details on these projects are included in the full report.

SCHEDULING AND COST ANALYSIS

In order to develop a viable program from the vehicles presented above, a careful analysis of costs and scheduling was performed. A major component of this analysis was the development of needed ground facilities and the associated costs. To minimize this outlay, unused launch facilities at Kennedy Space Center will be refurbished as allowed under the Commercial Space Law. This will still entail a bill approaching $600 million, not including the $75 million annual operating expense. To bring this down to a manageable level, the facilities will only be developed as needed, bringing the first pad into operation in 1994-1995 and the second pad in 1998 when projected launch volume requires it.

To further cut costs and develop a financially sound program, the manned spacecraft development was delayed over another year. This sets first launch for 1995, and the loss of some market, but reduces the initial annual investment to a manageable amount. Two other programs, the platform and manned module, have been slated for future production and thus postponed entirely, as indicated before. If market demand increases greatly and profits allow, these two programs can be implemented at a later date. These decisions produce the following schedule (Table 2) and cost profile (Fig. 8).

The profiles in Fig. 8 reveal the performance of the SSL program. Initial investment is at a rate of about $100 million

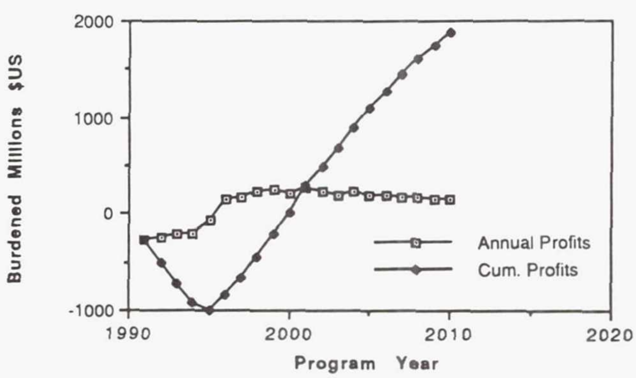

Fig. 8. SSL Profit Profile

Table 2. SSL Final Schedule

Year	Facilities	Launch Vehicles	Manned Spacecraft	Orbital Ops
1991	KSC R&D	Module R&D Begins	MSC R&D Begins	PDS R&D Begins
1992				Satellite R&D
1993				
1994		Module Tests	MSC Aerodynamic Tests	
1995	First Pad	Sirius Test	MSC Flight Test/Assembly	
1996		Orion 1 Test		PDS/Satellite Test
1997		Orion 2 Test		Servicer R&D
1998	Second Pad	Orion 3 Test	Transport Configuration	
1999				
2000			Servicer Configuration	
2004				Servicer Ops

a year for four years (all values account for devaluation, i.e. are burdened). This is a very large sum, but is offset by the quick return of profits by year six (1996). These profits average $150 million a year after this, offsetting the maximum cumulative debt of nearly $1 billion by 2001. The profits that follow represent a $2 billion capital mass that can be used for dividends, reinvestment, and upgrade, as well as allowing for the development of new systems and advanced capabilities for well beyond 2010.

N94- 71281

382681

1994004526

PROJECT ARGO: THE DESIGN AND ANALYSIS OF AN ALL-PROPULSIVE AND AN AEROASSISTED VERSION OF A MANNED SPACE TRANSPORTATION VEHICLE

S14-16
160640
p. 8

UNIVERSITY OF MICHIGAN

The Senior Aeropace System Design class at the University of Michigan undertook the design of a manned Space Transportation Vehicle (STV) that would transport payloads between low Earth orbit (LEO) and geosynchronous Earth orbit (GEO). Designated ARGO after the ship of the Greek adventurer Jason, two different versions of an STV that would be based, refueled, and serviced at the Space Station *Freedom* were designed and analyzed by the class. With the same 2-man/7-day nominal mission of transporting a 10,000-kg payload up to GEO and bringing a 5000-kg payload back to LEO, the two versions of ARGO differ in the manner in which the ΔV is applied to insert the vehicle into LEO upon return from GEO. The all-propulsive ARGO (or CSTV for Chemical STV) uses thrust from its LH_2/LOX rocket engines to produce the ΔV during all phases of its mission. While the aeroassisted ARGO (or ASTV for Aeroassisted STV) also uses the same engines for the majority of the mission, the final ΔV used to insert the ASTV into LEO is produced by skimming the Earth's atmosphere and using the drag on the vehicle to apply the required ΔV. This procedure allows for large propellant, and thus cost, savings, but creates many design problems such as the high heating rates and decelerations experienced by a vehicle moving through the atmosphere at hypersonic velocities. The design class, consisting of 43 senior Aerospace Engineering students, was divided into one managerial and eight technical groups. The technical groups consisted of Spacecraft Configuration and Integration, Mission Analysis, Atmospheric Flight, Propulsion, Power and Communications, Life Support and Human Factors, Logistics and Support, and Systems Analysis. Two committees were set up with members from each group to create the scale models of the STVs and to produce the final report.

SPACECRAFT CONFIGURATION AND INTEGRATION

The Spacecraft Configuration and Integration group (SC&I) was reponsible for integrating the various subsystems into a single, cohesive design configuration for each of the vehicles. SC&I worked closely with all the technical groups to ensure efficient integration of each subsystem into the overall design.

Unconstrained by atmospheric flight, the CSTV was developed with modularity and expandability as the main factors governing the design (see Fig. 1). The CSTV is divided into three modules: payload and servicing, command, and propulsion. Each module can be replaced with an expanded or specialized package for off-nominal missions. The payload and servicing module, normally configured for holding a single satellite, can be replaced with modules capable of supporting multiple satellites. If a satellite requires nonstandard mounting or support equipment, a specialized payload module can be developed for that satellite.

The command module, normally capable of supporting two people for seven days, can be replaced with a larger module for extended duration missions or for missions requiring extra personnel. The command module can even be replaced with an automated control package allowing for unmanned, autonomous missions that are hazardous or do not require human presence.

The propulsion module can be exchanged with another module with larger propellant tanks or an extra set of propellant tanks can be attached to the propulsion module for missions requiring a larger ΔV such as a lunar mission or one necessitating an increased payload capacity.

The front-end-loading configuration was chosen over a middle-loading design where the payload is placed between the command and propulsion modules, because of the virtually unconstrained space available for payload geometry allowed by the attachment of the payload at the front end of the CSTV. Thus, large bulky satellites or satellites with nonconventional geometries are easily accommodated.

The ASTV was designed to meet special requirements created by the hypersonic flight of the vehicle through the upper reaches of the Earth's atmosphere during each mission. As the ASTV passes through the atmosphere, a flow cone is created by the aerobrake. Allowing for a factor of safety, an impingement cone was defined such that all components of the vehicle, including the returning payload, must be placed within the cone so that no elements are burned up in the superheated flow. In order to maintain aerodynamic stability and control, the center of mass of the vehicle was constrained to a restricted area behind the aerobrake. This requirement physically translated into packing the components of the vehicle, e.g., command module, propulsion tanks, engines, etc., as close to the face of the aerobrake as possible.

After meeting the above requirements, three possible configurations of engine placement were considered. The first buried the engines inside the aerobrake with the thrust pointing through the brake itself. Due to the complex and massive mechanisms involved in opening and sealing a door in the aerobrake structure and to the catastrophic effects in the event of a failure of the seals, this configuration was rejected. Another configuration placed the engine behind the aerobrake with the thrust vector perpendicular to the plane of the brake. This idea was discarded because engine placement would have substantially reduced the usable volume within the impingement cone for payload storage.

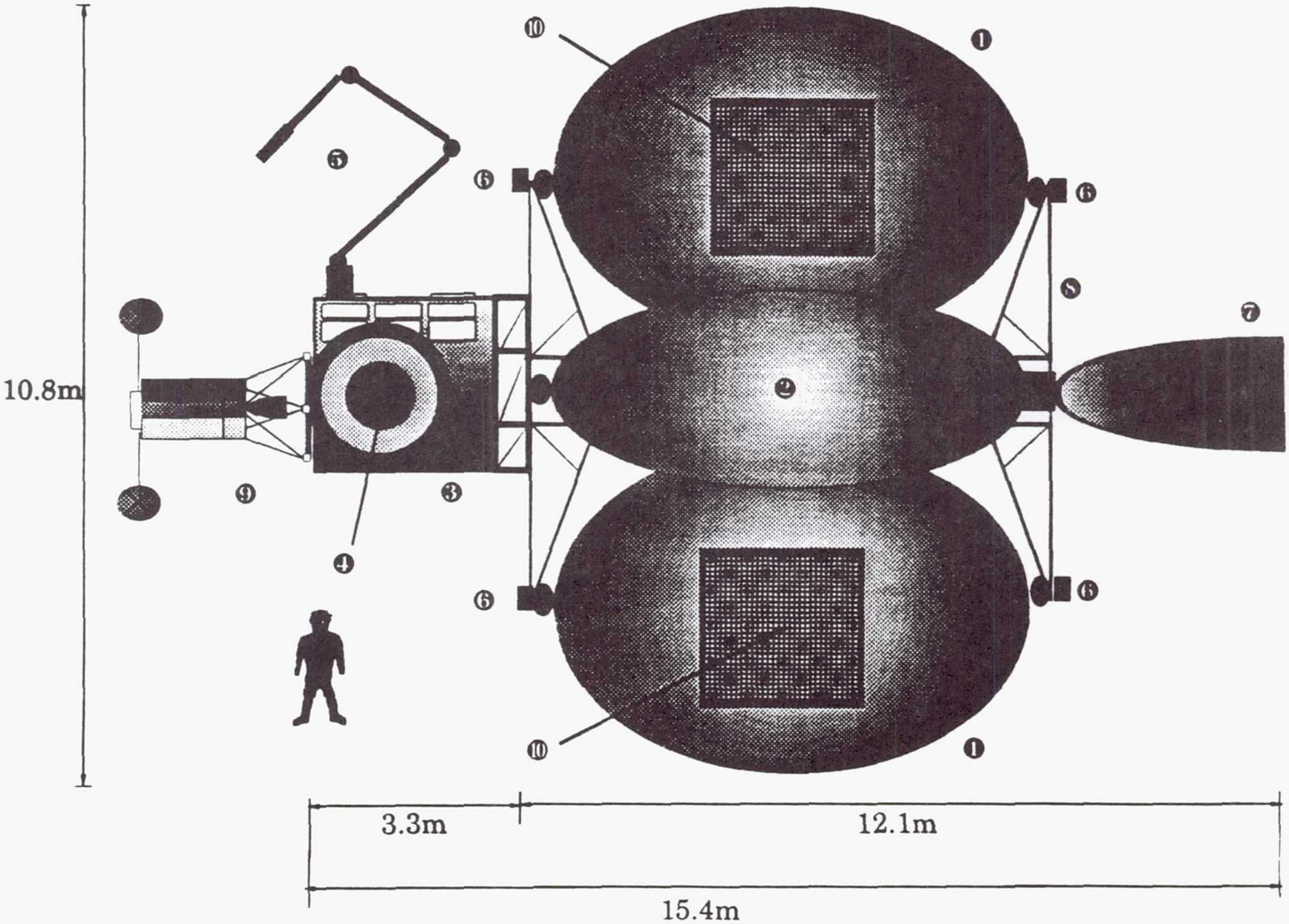

SPECIFICATIONS

Crew: 2
Mission Duration: 7 days
Dry Mass: 6341 kg
Gross Mass: 86,566 kg

Payload up: 10,000 kg
Payload down: 5000 kg

Engine: Rocketdyne RS-44 (2)
Thrust: 67,000 N each
Fuel: LH2/LOX

LH2 Tank: 4.5 x 8 m Elliptical
LOX Tank: 3 x 7 m Elliptical

Propulsion Mod.: 12.1 x 9 x 10.8m
Crew Mod.: L = 3.3m, D = 2.5 m

INDEX

1. Liquid Hydrogen Tanks (2).
2. Liquid Oxygen Tanks (2).
3. Command Module.
4. Airlock/Storm Shelter.
5. Remote Manipulator Arm.
6. RMS unit (4).
7. RS-44 Engines (2).
8. Thrust Structure/Tank Supp.
9. Payload mounted on pallet.
10. Radiators.

Fig. 1. All-Propulsive Space Transportation Vehicle (CSTV)

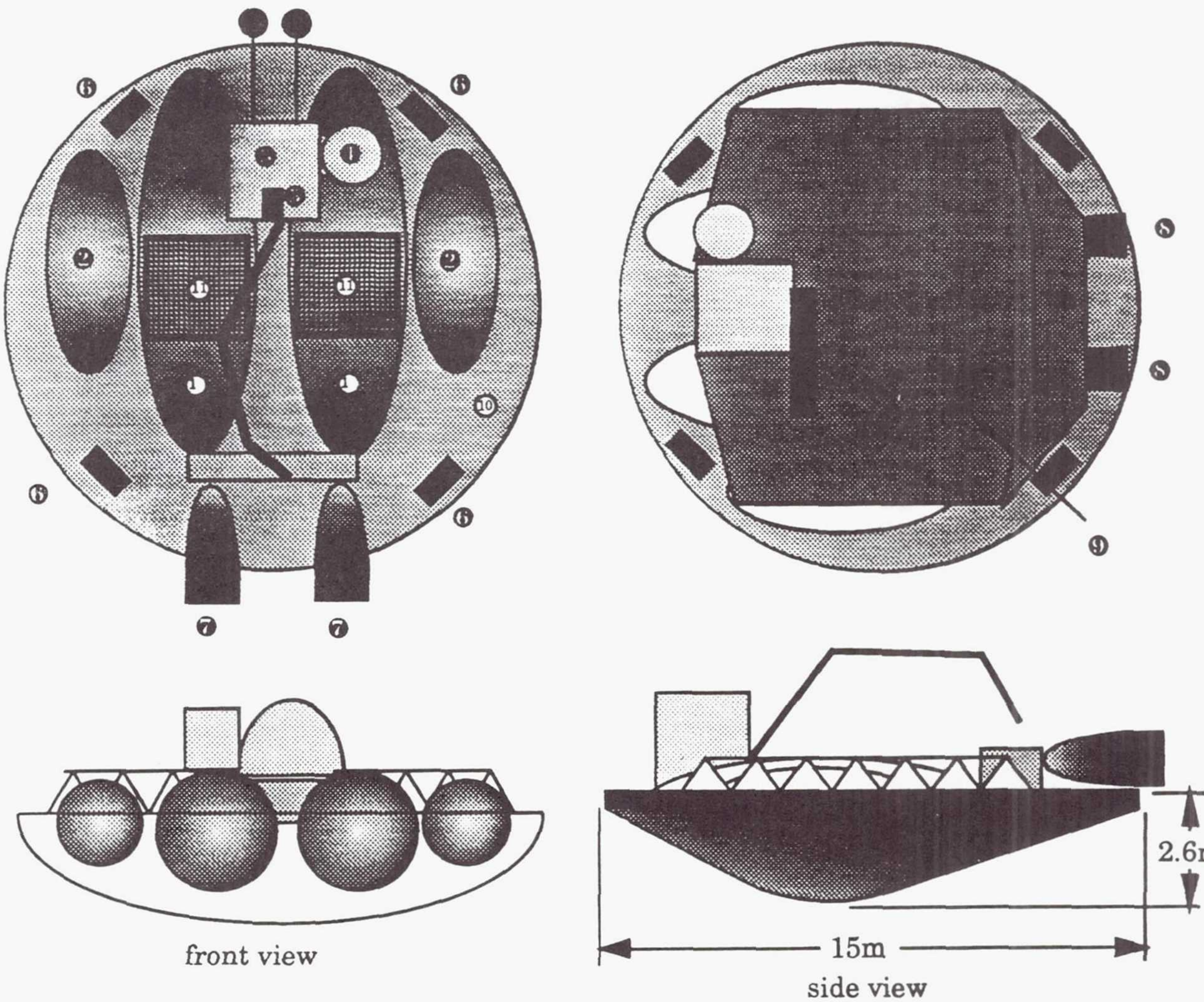

SPECIFICATIONS

Crew: 2
Mission Duration: 7 days
Dry Mass: 7841 kg
Gross Mass: 66,321 kg

Payload up: 10,000 kg
Payload down: 5000 kg

Engine: Rocketdyne RS-44 (2)
Thrust: 67,000 N each
Fuel: LH2/LOX

LH2 Tank: 3.4 x 11 m Elliptical
LOX Tank: 2.5 x 7 m Elliptical

Aerobrake: 15m dia., 2.6m deep
Crew Module: 3 x 2.6 x 2.6 m

INDEX

1. Liquid Hyrdogen (LH2) tank.
2. Liquid Oxygen (LOX) tank.
3. Crew Cabin.
4. Airlock/Storm Shelter.
5. Remote Manipulator System (RMS).
6. Reaction Control System (RCS) (4).
7. Rocketdyne RS-44 Engines (2).
8. RS-44 Engines. Retracted position.
9. Payload Plate.
10. Aerobrake.
11. Radiators.

Fig. 2. Aeroassisted Space Transportation Vehicle (ASTV)

Our final configuration of the ASTV consisted of rear mounted engines, firing in-line with the plane of the aerobrake, a raised command module in the front end of the vehicle with good visibility of the payload area, and a platform in between the module and engines capable of handling large-sized payloads (see Fig. 2).

MISSION ANALYSIS

The Mission Analysis group planned the trajectories and orbital maneuvers for both nominal and specialized missions. The only portion of the nominal mission that was different between the two versions of ARGO was the GEO-to-LEO return phase. Three methods were studied to transfer from the space station orbit (LEO), assumed to be at 278 km from the Earth's surface, to a target point in GEO, at about 36,000 km. The first and most energy efficient method examined was the simple Hohmann transfer. Although the Hohmann transfer requires the least amount of propellant, this method was rejected because it does not allow for targeting of an arbitrary point in GEO at a given time.

While the Three Impulse Transfer allows for targeting of arbitrary points in GEO, this transfer can take up to 23.9 hr, which limits the time that the STV can work in GEO. Also, the Three Impulse Transfer requires starting the main engines three times, which decreases the service life of the engines. The method chosen is a Direct Elliptical Transfer. This method allows for arbitrary targeting with a reasonable transfer time, 7.21 hr maximum, and only requires two main engine startups. The penalty associated with this transfer method is an increase of 25-249 m/sec of ΔV. However, we have the capability of targeting any point in GEO, twice a day.

To minimize the propellant required for a change from the plane in which the space station orbits and the equatorial plane where the GEO satellites reside, all of the 28.5° of plane change required to move into equatorial GEO is accomplished when the STV reaches GEO. At GEO, the STV is capable of targeting three points within an 180° arc. To move from point to point in GEO, conventional orbit walking maneuvers are used. A typical mission may require the STV to deploy two satellites at separate points in GEO and retrieve a satellite from a third point.

Returning to the space station from GEO is where the mission profiles of the CSTV and ASTV differ. The CSTV uses a simple Hohmann transfer to reach a point below and behind the station where the main engines are started to apply the ΔV required to insert the CSTV into the orbit. Mission Analysis found that if the plane change is effected in two steps, partially at GEO and the rest at LEO, the ΔV required for this maneuver is minimized. Once in LEO, the CSTV completes a terminal phase maneuver to reach and dock with the space station.

The ASTV also starts with a Hohmann transfer that places it into an elliptical orbit that enters the atmosphere at a predetermined angle. In the atmosphere, the ASTV receives the ΔV necessary to insert the ASTV into the same orbit as the CSTV, below and behind the space station. The same terminal phase maneuver is used for final docking.

The total ΔV required for the vehicles to complete their nominal missions is 9395 m/sec for the all-propulsive version (CSTV) and 7354 m/sec for the aeroassisted version (ASTV). Mission Analysis also explored the capability of the STVs for missions beyond nominal. They found that the STV will be able to target points in polar GEO orbits with a minimal reduction in payload capacity and, with modifications to increase mission duration, the STV should be able to reach and return from lunar orbits.

ATMOSPHERIC FLIGHT

Atmospheric Flight analyzed the hypersonic trajectory of the ASTV through the upper portions of the atmosphere and, from calculations of heating and deceleration rates, determined the size and shape of the aerobrake. With a computer model, the heating and aerodynamic loads were calculated at various points throughout the trajectory. The effects of different lift-to-drag ratios (L/D) and ballistic coefficients (m/CD^*A) were analyzed. The analysis constrained the group to choose a low L/D design with a small ballistic coefficent for reduced heating rates and deceleration loads, a constraint set by the Life Support and Human Factors group for crew safety.

Of the three types of low-lift aerobrakes, the spherical raked-cone was chosen over the ballute and truss configurations due to its superior stability characteristics and greater mass efficiency. A low ballistic coefficent translates physically to a raked-cone of a large diameter. Since the ASTV is to be lifted into orbit by the heavy lift launch vehicle (HLLV), not yet developed, the size of the aerobrake was limited by the estimated diameter of the payload bay of the HLLV of 15 m. Thus the size and shape of the aerobrake for the ASTV was determined.

The Atmospheric Flight group then proceeded to examine the materials required for the aerobrake structure and for the thermal protection system (TPS). They chose a graphite polymide honeycomb structure over titanium and aluminum after weighing mass vs. temperature resistance factors. For the TPS, they chose advanced shuttle-type silicon tiles called Fibrous Refractory-Composite Insulation (FRCI) tiles. FRCI-40 can withstand temperatures up to 2600 K and has a maximum heat transfer rate of 130 W/cm^2. This material is scheduled to be tested by the Aeroassist Flight Experiment, an experiment to be flown by NASA on the shuttle in the near future.

PROPULSION

Upon consideration of the high cost of launching STV propellant into orbit, the Propulsion Group decided that high efficiency of the engines used to provide primary thrust was required in order to reduce the amount of propellant consumed for each mission. Electric propulsion systems, energized by solar and nuclear power plants, have very high specific impulse (I_{sp}) and are therefore very efficient. Unfortunately, they do not produce the level of thrust required to complete our mission in a reasonable amount of time. In chemical propulsion, rocket engines using liquid hydrogen (LH_2) and liquid oxygen (LOX) as propellants have the highest I_{sp} and produce the thrust required by the mission.

The group decided, therefore, to focus on LH_2/LOX engines that were currently being manufactured or developed. The

Rocketdyne RS-44 engine, scheduled to be in production in the 1990s, was chosen for the main propulsion system. With a thrust of 67,000 N, it had the highest I_{sp} (192 sec) of all of the engines considered and also had two additional features required by the STVs. The RS-44 can gimbal 6° in any direction. This feature is required to adjust the thrust vector so that it passes through the center of mass of the vehicle, which changes as the mission progresses.

For the ASTV, the engine can be fitted with a retractable nozzle. Because of the limited space behind the aerobrake, a retractable nozzle is an attractive feature because it allows us to mount the engine close to the edge of the aerobrake, leaving more room for the payload. The nozzle will project over the side of the brake when the engine is in use and will be retracted behind the brake during the atmospheric portion of flight. The all-propulsive STV will not need this feature, and some mass can be saved by eliminating the retraction system.

To optimize the safety/cost tradeoff, two engines will be used on each vehicle. This configuration should provide a reasonable safety margin while keeping the production and maintenance costs as low as possible. Due to the increased burn time for the all-propulsive mission, the engines on the CSTV will only have a lifetime of 25 missions while the ones on the ASTV will have a lifetime of 35 missions.

The STV will also have an attitude control system (ACS) to provide pitch, yaw, and roll control as well as to perform maneuvers that do not require the thrust levels of the main engines. These maneuvers will usually involve proximity operations around the space station or satellites. While a compressed gas ACS with its noncorrosive exhaust would be very desirable for proximity operations, the high mass of such a system makes it impractical. Instead the Propulsion group chose to use smaller, lighter, and more efficient LH_2/LOX thrusters. Thirty-two of these engines, each producing 111 N of thrust, will be mounted in clusters to provide attitude control of both the CSTV and ASTV. These thrusters must be operated in a "low Z" mode during proximity operations to carefully avoid impingement of the exhaust on any station or satellite surfaces.

The propellant tanks are designed to be prolate ellipsoidal in shape, which has the property of orientating the liquid contents at the ends of the tank. Thus, in zero-g, the location of the propellants in the tanks is guaranteed to be at a propellant line outlet. The ellipsoidal shape also reduces the sloshing of propellant during maneuvers. A light and yet strong aluminum-lithium alloy, Al-Li 2090, will be used to construct the tanks. To protect the cryogenic propellant from heat, 8.75 cm of Dacron tuft insulation manufactured by the TRW Corporation will cover the tanks. For the nominal mission, the CSTV will require 77,926 kg of propellant, while the ASTV requires 56,280 kg.

POWER AND COMMUNICATIONS

Power and Communications handled the data management and guidance and navigation, as well as the power and communication aspects of the STVs. Both versions of the STV have nominal power requirements of 3.7 kW, with a maximum of 5.7 kW during times of operation of the remote manipulator system and a minimum of 1.9 kW for life support only. A nuclear power source was immediately eliminated from consideration due to the massive shielding required to protect the crew and nearby structures from radiation. In addition, if a catastrophic accident occurred during the atmospheric flight phase of the ASTV's mission, highly radioactive material could be spread over a large area.

A power system using solar dynamics was considered briefly but discarded because of the massive nature of such a system and because of the infancy of the technology. While solar photovoltaic power systems are a proven technology, there are some problems associated with their use. Since solar photovoltaic arrays only provide power during times when they are exposed to the sun, a secondary power source, e.g., batteries or fuel cells, must be used when the vehicle is in the Earth's shadow. This substantially increases the overall mass of the system. The solar array must also track the sun within 3-4° of the sun, potentially limiting the maneuverability of the STV. Also, the radiation environment in space slowly degrades the efficiency of the array by as much as 10% a year, thus necessitating sizing the array for use at the end of its lifetime, increasing its overall size and mass.

Subsequently, a hydrogen/oxygen fuel cell system was chosen as the power source for the STV. Mass analysis shows that for the length of our mission and the level of power required, the fuel cell system is more mass efficient than a solar array. The fuel cell technology is well-developed and reliable, and it provides potable water as a by-product that is supplied to life support as its only source of water. Three redundant fuel cell systems are packaged in the command module of the STVs. Only one cell is required to provide the necessary power.

The fuel cells supply electricity in 150 V DC; this voltage was chosen primarily because of distribution efficiency considerations. The power management system will automatically control the rate of power production, increasing the rate during times of heavy use and decreasing during periods of inactivity. The management system also monitors the system for failures in the distribution system or in the devices connected to the system. Devices can be automatically switched to one of three independent power buses or be isolated from the buses through direct current switches and circuit breakers.

The heat generated by the power system, communications and navigation equipment, computers and other avionics, and by human metabolism is removed either directly, using cold plates, or by a heat exchanger that cools the cabin air. The cooling loop inside the command module uses 30 kg of water for crew safety considerations. Outside the module, the heat is transferred to a Freon loop that passes through radiators where the heat is expelled into space.

The STVs will not nominally support direct communication with an Earth-based antenna system. Instead, the Tracking and Data Relay Satellite System (TRDSS) will be used to communicate with ground stations or with the space station. Hence most of the communications equipment onboard the STVs is designed to be compatible with TDRSS. Both S-band and K-band signals are supported. In addition, the K-band communications system can serve as a radar tracking unit. The K-band

radar will be used during rendezvous with satellites and the space station.

The data management system (DMS) provides command, control, and data processing for all systems on the STV. The DMS consists of computer processors, memory storage devices, connecting networks, workstations, and software programs. Three central computers form a triply redundant system that coordinates the actions of all of the STV subsystems. Each subsystem will have its own standard data processor that controls the real-time computations required to run the subsystem. A network interface unit connects each subsystem processor to the fiber optic ring network that links all of the systems as well as the central computers.

Erasable optical disks were the obvious choice for mass storage due to their high capacity, reliability, and resistance to radiation and electromagnetic interference. Because of the high radiation environment of space, especially beyond LEO, all electronic equipment must be shielded from radiation or be radiation qualified. Workstations will be the main interface between the crew and the vehicle. Color liquid crystal displays will be used because they use less power and take up less room than conventional cathode ray tube displays. Expert systems and other forms of artificial intelligence will aid the crew in routine operations, satellite repair, and planning. A voice control option will be included for use during labor-intensive tasks where the crew members have no free hands.

Guidance and navigation of the STV will be performed through the computer systems. The STV position, velocity, and attitude are automatically acquired and updated through the use of the Global Positioning System (GPS). GPS consists of 18 satellites in 12-hr-period orbits that continuously broadcast beacon signals. Processing of signals from four GPS satellites results in the determination of the STV's position and velocity. Star trackers update the attitude of the STV. Inertial measuring units (IMUs) will keep track of the navigational data between updates from the GPS and star tracker systems.

Guidance of the STV is accomplished entirely through software. The crew inputs the desired state of the STV, e.g., attitude and/or velocity, and the computer applies the control commands to the main engines or attitude control system after calculations using the navigational and mass property data stored in the system. The center of mass, moments of inertia, and total mass of the system are determined by applying a series of moments to the STV and measuring the response of the vehicle. The guidance software automatically corrects for errors and uncertainties and also optimizes the maneuvers to use minimal fuel.

LIFE SUPPORT AND HUMAN FACTORS

The Life Support and Human Factors group was responsible for creating a safe and comfortable environment for the crew. An Earth-like atmosphere (79% N_2, 21% O_2) at sealevel conditions (101 kPa) was chosen for the command module primarily for maintaining compatibility with the space station. The two gas system at 1 atm will also reduce the risk of fire and possible oxygen toxicity in a low-pressure, oxygen-rich environment. Prior to an extravehicular activity (EVA) phase of a mission, the cabin pressure will be slowly lowered to 55 kPa, which is the same pressure that is used by the space suits carried by the STV. Lowering the pressure will eliminate the pre-breathe procedure used by shuttle astronauts preparing for an EVA.

Enough oxygen and food is carried for the nominal seven-day mission plus a four-day emergency reserve. Three carbon dioxide removal systems were investigated: lithium hydroxide (LiOH), molecular sieves, and electrochemical depolarized carbon dioxide concentrator (EDC). Both the molecular sieve and EDC were eliminated due to mass considerations. Thus the STV will use the LiOH system that is currently being used by the space shuttle orbiter. Since LiOH is not regenerable, it must be replaced after every mission.

The cabin atmosphere will be continuously circulated through the air revitalization system (ARS). The ARS removes the carbon dioxide, humidity, odors, and excess heat from the air. The condensate is dumped into a waste water storage tank, where it is periodically vented into space.

Each crew member will be provided with an average of 2900-3000 calories per day. Meals will be integrated with the space station so that the nutrition and diet of the crew matches that of crew of the space station. Food will be brought onboard in dehydrated or semidehydrated form to save mass. The meals will be rehydrated in the galley, which will also contain an oven.

Five kg of water per day is allocated for each crew member for drinking, food preparation, and personal hygiene. This water will be solely supplied by the fuel cell system, which produces 34 kg per day. The excess water will be stored in waste tanks that are periodically dumped into space.

An advanced commode system based on the shuttle design will process and store human wastes. This system will be serviced upon the return to the space station. Other wastes such as used food containers and paper towels will be stored in trash bins that will be emptied at the station.

Simple elastic devices will be provided for the crew to use for exercise to counter the muscular atrophy problem of living in a zero-g environment. Heavy shielding of the command module will be required to protect the crew from the hazardous radiation environment of the Van Allen belts and of orbits outside LEO. The Van Allen radiation belts are regions of energetic charged particles trapped by the Earth's magnetic field. The STV must pass through this belt while traveling between LEO and GEO. At GEO, the environment is characterized by a high flux of energized electrons and cosmic radiation.

Both active and passive shielding were examined to protect the crew from this environment. Active shielding systems were considered too massive or impractical for the needs of the STV. Simple aluminum mass shielding of 2 g/cm^2 was the final choice for protecting the crew from the nominal environment. There are times, however, when this shielding will not be enough to protect the crew. Solar flares, although rare, can emit lethal doses of radiation. In LEO, the Earth's magnetic field deflects this radiation and thus protects the orbit. However, in GEO an extra massive radiation shield must be used to protect the crew of the STV. The STVs airlock was designed to serve as a "storm shelter" in the event of a solar flare. Limited control and communications will be available in

the shelter. In the event of a solar flare, the crew will reconfigure the airlock into the storm shelter and remain within while the STV escapes to the protection of the LEO environment.

Living in a zero-*g* environment reduces the human tolerance for acceleration or deceleration. The mission profiles of both STVs must be such that the crew is able to fully function while under the loading of main engine burns or of passage through the atmosphere. By examining centrifuge data and the experience of previous space missions, we scaled and set a maximum *g*-loading level of 4 *g*. In addition, the crew should not experience a loading over 1 *g* for over two minutes. Both of the all-propulsive and aeroassisted flight profiles fell well within our defined limits.

The interior design of the crew cabin was constrained by making sure that the command couches are placed in a position so that the crew is protected during times of maximum loading. The remote manipulator work station was placed to allow for direct visual observation of the payload area.

Extravehicular activity (EVA) will be required on missions to retrieve or repair satellites. Advanced hard shelled suits with an internal pressure of almost double that of the space shuttle model will be used. The high internal pressure, along with lowering the pressure of the cabin, will eliminate the need for a pre-breathe procedure. The suits will also be shielded for the radiation environment of GEO. A telerobotic remote manipulator system, similar to the one on the shuttle, will be used to maneuver payloads. A manned maneuvering unit (MMU) will also be carried.

LOGISTICS AND SUPPORT

The Logistics and Support group designed the elements that the STV would need to support its mission. They also considered the impact of a STV on the space station. The STV will be docked directly to the docking modules attached to the pressurized habitats of the space station. A "berthing" procedure will be used to softly dock the STV. This procedure consists of using the Mobile Remote Manipulator System (MRMS), based on the station's main truss, to grapple the STV and gently bring it into contact with the docking interface. The docking/berthing interface that we employed is an androgynous interface identical with the space shuttle/space station interface. Power and data buses, air, water, and other utilities will be integrally connected through the interface.

Two hangar designs were created to fully enclose both versions of the STV. While the hangar will protect the STV from the space environment, the hangar's main function is one of providing work platforms, hand holds, lighting, and storage areas for the astronauts to use while performing routine maintenance and service operations on the STVs. The hangar will be constructed of aluminum and covered with a multilayered insulation designed to protect the STVs from micrometeroids and thermal stresses.

The storage of the cryogenic propellants was a major impact on the station. A 115,000-kg-capacity storage tank will be mounted above the habitat modules on the main truss. The tank will hold enough hydrogen and oxygen for two nominal missions for the ASTV and 1.5 nominal missions for the CSTV. The tank system is purely passive with the hydrogen and oxygen boiloff stored in high-pressure accumulators, where the gases can be used by the space station. The passive system was chosen over a reliquefaction system because of the excessive power demands of such a system. Propellant transfer through a complex capillary acquisition system will eliminate problems with vapor-liquid separation found in zero-*g* environments. Periodically, the storage tank will be refilled by a transfer tank launched by a heavy lift launch vehicle.

STV maintenance will be simplified by using modular units that will be easily removed and replaced. The most costly maintenance activity will be the replacement of the main engines, every 25 missions for the CSTV and every 35 missions for the ASTV. Satellites brought to the space station for repair or deployment will be serviced and checked out in a satellite servicing hanger mounted on one of the keels of the station. These hangers will provide the tools and equipment necessary to repair a satellite.

SYSTEMS ANALYSIS

Systems Analysis estimated the cost for development, production, and operation of each of the vehicles. A quantitative and qualitative analysis was then performed to highlight the advantages and disadvantages of each configuration.

The initial costs of the vehicles, from design to launch, are estimated to be \$933 million and \$1359 million (1989) for the CSTV and ASTV, respectively. The additional \$426 million required for the development and construction of the ASTV reflects the cost of developing aerobraking into a usable technology. The operational costs of each vehicle are \$2115 million and \$1485 million per year for the CSTV and ASTV, respectively. The difference of \$630 million per year reflects the savings afforded by the use of aeroassisted technology.

For the nominal mission, the ASTV saves 21,000 kg of propellant per mission. At a launch cost of \$1500 per kg, over a period of 8 years at 15 missions per year, \$5 billion can be saved using the STV. If cost were the only factor under consideration, the ASTV would clearly "win," but other factors must be examined, many of them difficult to quantify.

The CSTV has the advantage of a lower initial cost and the use of well-developed technology. The time to design, build, and launch the CSTV will be subsequently shorter. The CSTV is expandable on a greater scale. The use of exchangable modules allows us to reconfigure the CSTV for missions for which it was not nominally designed. There is less risk to crew and payload by using known technology and by not traveling through the atmosphere at hypersonic velocities.

The ASTV has the aforementioned advantage of a lower operational cost, but the technology used in aeroassisted vehicles has yet to be developed. Additional maintenance will be required to take care of the aerobrake, and fatigue life of the structure will be decreased due to repeated cycling of the vehicle through thermal and aerodynamic loads. Significant risks are involved in passing through the atmosphere at hypersonic speeds. The stability and control of the ASTV

depends greatly on the accuracy of our model of the upper atmosphere. Unfortunately, unpredictable variations, especially in air density, will make each flight through the atmosphere different than every other flight. We must note, however, that the development of aerobraking into a known and safe technology is, perhaps, inevitable. The use of aeroassisted technology will greatly benefit the long-term exploration of the solar system and beyond. So whether the technology is developed now or later, aeroassisted vehicles will be used in the future.

ACKNOWLEDGMENTS

Principal author H. Wang was assisted by D. Seifert, J. Waidelich, M. Mileski, D. Herr, M. Wilks, G. Law, and A. Folz in the preparation of this report. Project manager M. Tillman and assistant project manager K. Pahl were assisted by group leaders D. McKinnis, M. Beer, S. Malhotra, G.T. Tomaich, K. Gordon, D. Schatt, M. Guenther, and I. Hutchison. The Models Committee included chairman D. McKinnis, G. Agresar, C. Beebe, C. Chu, M. Gawronski, I.E. Wegryn, and M. Wilks. Faculty advisor was Professor Harm Buning; teaching assistant, D. Schumacher.

N94- 71282
382684
1994004527

515-18
160641
p. 12

PETITE AMATEUR NAVY SATELLITE (PANSAT)

NAVAL POSTGRADUATE SCHOOL

BACKGROUND

The Naval Postgraduate School's (NPS) Space Systems Academic Group (SSAG) is designing and developing a small communications satellite for launch aboard the Shuttle as a Complex Autonomous Payload (CAP). The objectives of PANSAT are three-fold. First, PANSAT will provide an ideal educational tool for the officer students at NPS supporting Space Systems Engineering and Space Systems Operations with hands-on hardware development. Second, the satellite will provide digital store-and-forward communications, or Packet Radio, for the amateur radio community. The third objective is to provide a low-cost, space-based platform for small experiments.

PANSAT will be launched from the shuttle at a nominal altitude of 200 n.m. and an inclination of at least 37°. The satellite weight is 150 lbs. Since there is no attitude control, eight dipole whip antennas will be used to provide isotropic ground coverage for communications. FM digital communications will be used with up-link and down-link on a single frequency in the amateur band of 437.25 MHz. A maximum 50 kHz of bandwidth is envisioned for the satellite. The expected lifetime of the satellite is 1 1/2 to 2 years before atmospheric reentry. The PANSAT design consists of the following: (1) communications subsystem (COMM); (2) computer, or data processor and sequencer (DP&S); (3) power Subsystem; (4) structure subsystem; and experiment payload.

DESIGN SUMMARY

Much of the design and analysis has already been completed on PANSAT in the areas of the computer subsystem and structure subsystem. Further detailed design of the power and communications subsystems will naturally follow with an assigned frequency. The initial design and detailed specifications of the subsystems follow.

Communications (COMM)

The COMM design began with an application for a frequency allocation within the amateur band of 144 to 146 MHz through the Naval Electromagnetic Spectrum Center (NAVEMSCEN). Pursuant to the NAVEMSCEN response, formal coordination with the Radio Amateur Satellite Corporation (AMSAT) was made in the form of a proposal for PANSAT as an amateur satellite. The proposal is currently under review.

The amateur frequency bands are desirable for PANSAT because atmospheric attenuation contributes very little to path losses associated with the link equations. For example, a 144 MHz signal received at 0° elevation (line-of-sight) from a satellite in a 200 n.m. circular orbit has a free space loss of 142.5 dbW, whereas the atmospheric attenuation is only 1.06 dbW. In working with the amateur community, PANSAT will support the AX.25 communications protocol, a standard for amateur digital communications. In addition, exercising up-link and down-link on a single frequency is hoped to reduce ground coverage interference, which is a major regulatory concern.

Data Processor & Sequencer (DP&S)

Design issues for the processor include commonality, upward compatibility, and a real-time clock. Commonality deals with choosing a processor that is currently available and in extensive use. In addition, high-level language compilers must be available. The processor should be upwardly compatible for ease of expansion for more demanding future missions, including multiple processor configurations. A real-time clock is required for specific scheduled events in the satellite's mission.

Although PANSAT will be in a Low Earth Orbit (LEO), prime consideration is given for a microprocessor that is available in a radiation hardened version. This is important in the concern for upward compatibility as well as to guard against single event upsets (SEU). The processor selected is based on the Intel 8086 processor which is available in a CMOS radiation hardened version (the Harris 80C86RH). Processor interfaces will be required with the communications subsystem, power subsystem, experiments, and structure subsystem for available space. The mission requirements of PANSAT allow the processor to run in the minimum mode utilizing a single processor and fewer support chips, as well as having direct control over read and write signals.

As stated earlier, the AX.25 communications protocol will be implemented to support the standard for amateur digital communications. The AX.25 protocol is a bit-oriented protocol and is a variation of the X.25 protocol, but has additional address bits to accommodate the user call signs and any repeaters. AX.25 uses go back N format, where N is eight. The throughput, ρ, for this format is given by:

$$\rho = \frac{1-P}{1 + \frac{2Tp}{Tf}P}$$

P: Frame error probability given by: $P = 1 - (1 - Pb)^{Nb}$
Pb: Probability a single bit is in error
Nb: Number of bits in a frame
Tf: Time required for transmission of a frame
Tp: Propagation and processing delay

Assuming a 10% overhead, a minimal AX.25 frame will have 20 bytes of overhead and 1600 bits of information. As bit error

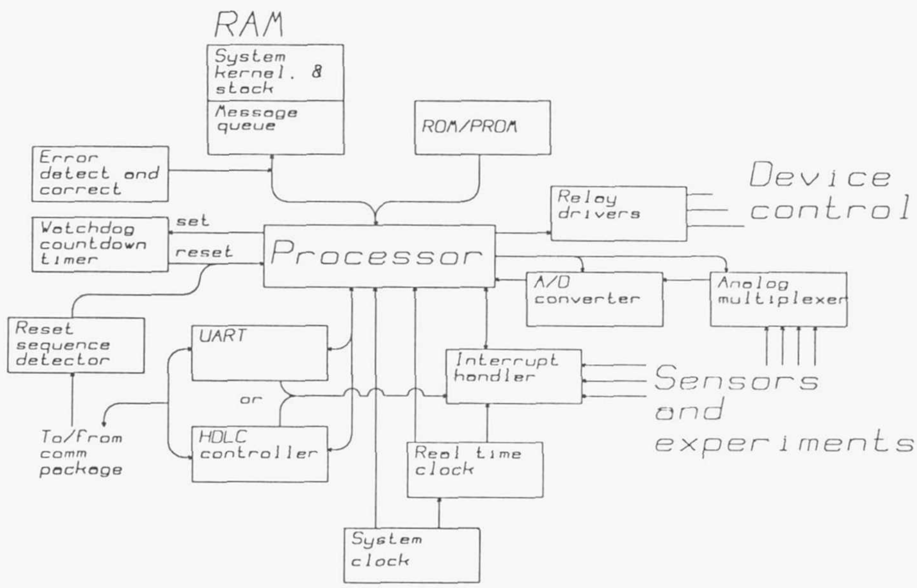

Fig. 1. PANSAT DP&S System Concept

rate increases, throughput drops rapidly. Frame error probability for AX.25 can be reduced by decreasing frame size; however, the 20 byte overhead cannot be avoided. Overhead could actually increase to as much as 76 bytes if addressing through repeaters is used. As long as single bit error probability remains below 3×10^{-4}, throughput for AX.25 is acceptable. Implementation of the AX.25 protocol can be done using a CMOS serial communications controller (SCC) (Zilog Z80C30 or Z85C30) chip that requires low power and is expected to be released late 1989 in a high-reliability JAN version.

Communication tasks required of the processor include adding messages to the buffer, retrieving messages from the buffer, listing buffer messages, issuing satellite commands or loading a program, and transmitting telemetry data. The DP&S must also have positive control of the transmitter. This is a necessary function to eliminate RF ground interference should the transmitter fail in the transmitting mode. Housekeeping duties will include monitoring such things as the voltage on battery packs, charging current, power supply current draw, and bus voltage.

Memory for the DP&S is divided into three sections. The first section is the fixed storage (PROM) holding the operating system kernel. The other two sections are the vital RAM, which holds system-vital data, and non-vital RAM, which holds the messages and telemetry data. The PROM and vital RAM will be high-reliability versions if not radiation hardened.

A watchdog timer will be used to safeguard against processor failure and subsequent transmitter keying. The timer will be reset by the processor in periodic intervals during normal operation. A completed countdown of the watchdog timer will initialize the processor and secure control of the transmitter. The periodic timer count reset will not be an interrupt function but rather a normal function of the operating system. The watchdog timer circuit can be accomplished by using an 82C54RH programmable interval timer. Other peripherals in the DP&S include analog/digital (A/D) converters and parallel input/output (I/O) capability. Fig. 1 shows the DP&S system concept.

Software requirements for PANSAT include developing the operating system kernel and device drivers. Programming will be done in the Ada language, which is the Department of Defense standard. Development of the kernel includes creating the interrupt routines and user interface shell. Device drivers will be responsible for controlling mass storage, radio communications, experiment(s) and sensors, and power control. Software testing will be an important consideration for breadboarding the DP&S hardware. Development of software flow charts will begin in the summer quarter 1989.

Power

Power will be provided by a 12-V unregulated bus from solar cells and batteries. Seventeen exposed panels will permit thirty-two 2 cm × 4 cm cells per panel, or 256 cm^2 per panel for solar energy collection. Terrestrial-type batteries will be used to lower costs. This will require housing the batteries in a sealed container for safety and accommodating the environmental specifications of the batteries. Using lead-acid batteries, six battery packs of six (2-V, 5 Ah) cells each can fly on PANSAT having a total of 360 W-hr capacity. Lead-acid batteries have been flown on the GLOMR satellite and a number of shuttle Get Away Special (GAS) payloads as a matter of record. Terrestrial type nickel-cadmium batteries are also being investigated since they have shorter recharging times. Long cycle life is an important factor for charge and discharge periods while surveying applicable batteries. Some of the data

requirements for battery use are as follows: (1) discharge voltage as a function of time under actual loads; (2) charge voltage and current as functions of time under actual conditions, (or required for particular cell if conditions are as yet unavailable); (3) overcharge current requirements; (4) quantity of electrical energy available from the battery at critical points in the mission and assurance that availability exceeds requirements at all other times; (5) rate of heat evolution as a function of time under the actual charge and discharge conditions expected, and a complete temperature profile of the battery as a function of time; (6) impedance and phase-shift characteristics of the battery as a function of frequency; (7) efficiency of the battery's energy storage and its associated electronics; (8) probability of battery failure as a function of time and conditions of use; and (9) battery voltage transients for critical load changes.

Orbital characteristics affect the power subsystem mainly in establishing the thermal environment the satellite will face and the amount of solar energy flux. For the satellite in a circular orbit at 200 n.m. (370 km) altitude, the approximate time of eclipse is 36.2 min. (2172 sec), or 39.4% of the period (ignoring inclination). Since the satellite is in LEO and will be tumbling, the thermal environment may not be a great concern. However, an analysis will be needed to determine the range of temperatures the satellite will encounter in order to select subsystem components or allow for active thermal control where applicable.

While in the sun, the average power is expected to be about 19.5 W assuming a tumbling rate of 0.1 rad per sec and solar cell efficiency of 12%. This should be more than adequate for normal operation. While in darkness, PANSAT will need to rely on power from its batteries. The power budget and further detailed design will proceed when the communications frequency has been assigned and communications components have been selected.

Structure Subsystem

The PANSAT structure will be of aluminum 6061-T6 and fabricated at NPS. The design incorporates modularity to ease fabrication. Five structural elements are used, as well as two plates, eight support structures, four plate supports, four lower support struts, and two end blocks. A wooden mock-up of the structure has been completed showing allowable subsystem envelopes. The total weight of the structure will be about 45 lbs.

A finite element analysis of the structure was done using GIFTS interactive software to show that PANSAT will survive loads of $\pm 9g$, translational accelerations in the X (and X+Y) direction, and $\pm 14g$ in the Z direction (see Fig. 2). The loads prescribed are found in the GAS Safety Manual for a GAS payload. Results show that the structural deflections remain in the linear regime. Stress concentrations occur in the corners of the frame-like support structures. Because of the magnitudes of those stress concentrations the lower struts were added.

Future work for the structure subsystem includes fabrication of the actual flight structure and performing dynamic and vibration testing. Structural testing will begin in early 1990 at NPS. Currently, test plans are being developed within the capabilities of NPS facilities. The major portion of testing will deal with qualification testing. Additional testing may be required and can be done at the Naval Research Laboratory. The test plan will need to include test objectives, type and number required, data required from each test, degree of confidence required, duration of each test, test sequence relative to design schedule, and facilities required.

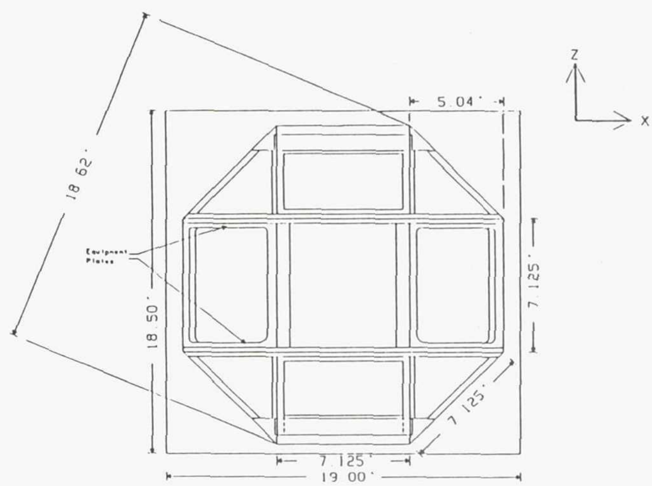

Fig. 2. PANSAT Structural Configuration

Experiment Payload

PANSAT will be designed to support small experiments that have minimal power, weight, and space requirements. The major experiment will test on-orbit annealing of radiation damaged solar cells. Solar cells show recovery (or annealing) of radiation damage when heated to extreme temperatures. By using a process called forward biased current annealing, the temperatures required for annealing can be lowered appreciably. This gives hope for extending the life of solar cells resulting in considerable cost savings for future space systems. Silicon, gallium arsenide, and indium phosphide have been identified as candidate solar cell types.

The experiment has already been developed and is currently in the testing phase. Modifications have already reduced size and weight of the experiment since its initial testing. The payload is an autonomous Motorola 68701-based experiment with 64K of static RAM and 16K of ROM. Fifteen cells will be tested with a sixteenth cell used as a sun sensor. A novel circuit design for calculating current-voltage (I-V) curves will be used with curve accuracies within 2 mV from 12 bit analog to digital converters.

An additional experiment that may fly aboard PANSAT will test the new technology of Ferroelectric memory. This technology is attractive for space applications since it is inherently radiation tolerant, non-volatile, and has high density. An actual experiment is still in the conceptual phase, however.

The major concerns for Ferroelectric memory devices are retention and endurance. If these issues can be overcome, Ferroelectric memory devices promise to be the unequivocal choice in solid state memory for space applications.

CONCLUSION

PANSAT development has begun with the satellite processor design and structural design. The groundwork for the other subsystem designs has been established concentrating on initial design requirements. The total cost of hardware is expected to be $100,000 with a delivery date of July 1991. PANSAT was ranked fourteenth of 19 experiments at the Navy Space Test Program (STP) call for experiments in May 1989. As an academic exercise, PANSAT promises a wealth of knowledge and experience for the student officers involved. PANSAT also will provide a valuable asset for low cost access to space.

ACKNOWLEDGMENTS

Principal authors D. Sakoda and J.K. Hiser were assisted by faculty advisor Dr. R. Panholzer.

APPENDIX

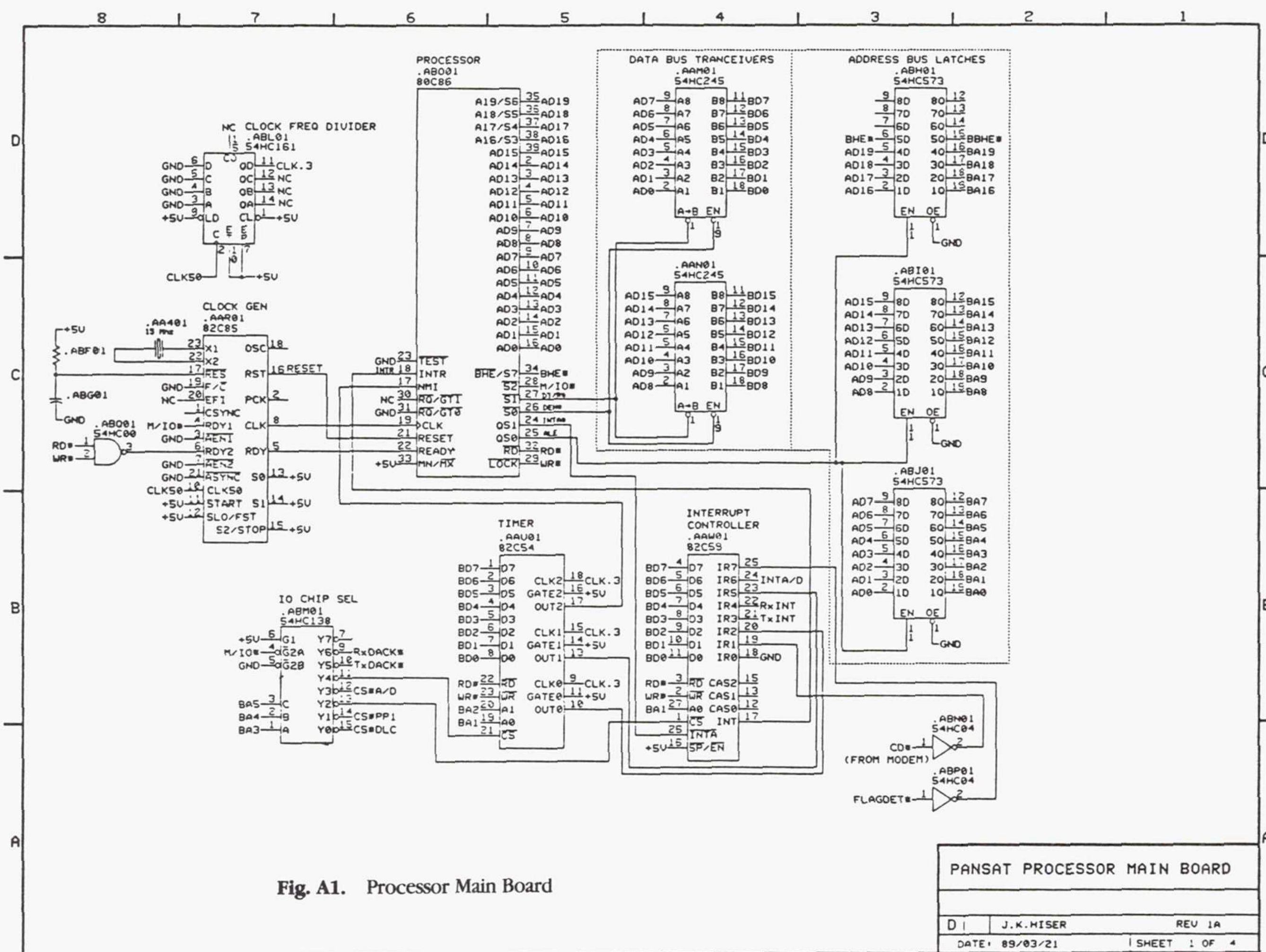

Fig. A1. Processor Main Board

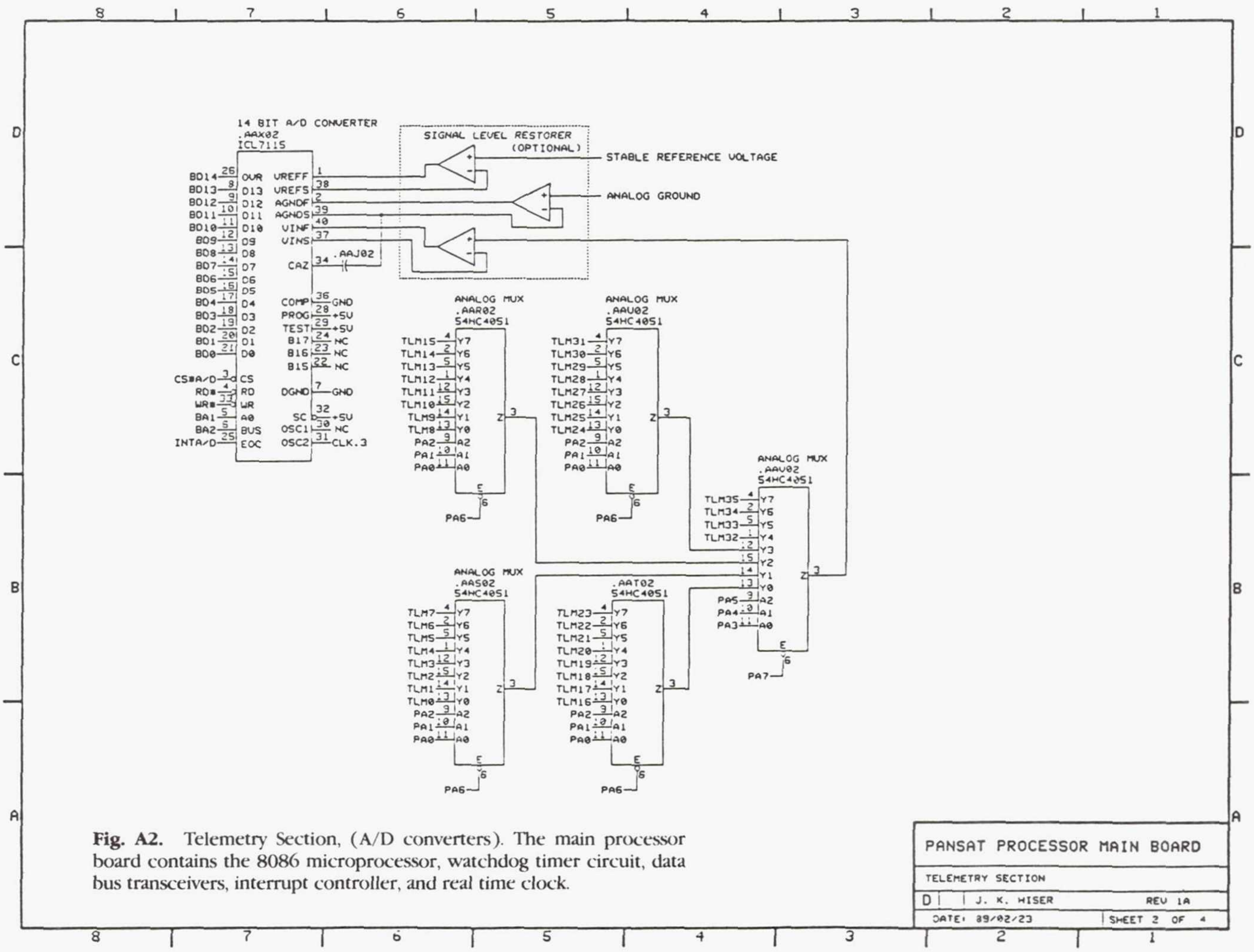

Fig. A2. Telemetry Section, (A/D converters). The main processor board contains the 8086 microprocessor, watchdog timer circuit, data bus transceivers, interrupt controller, and real time clock.

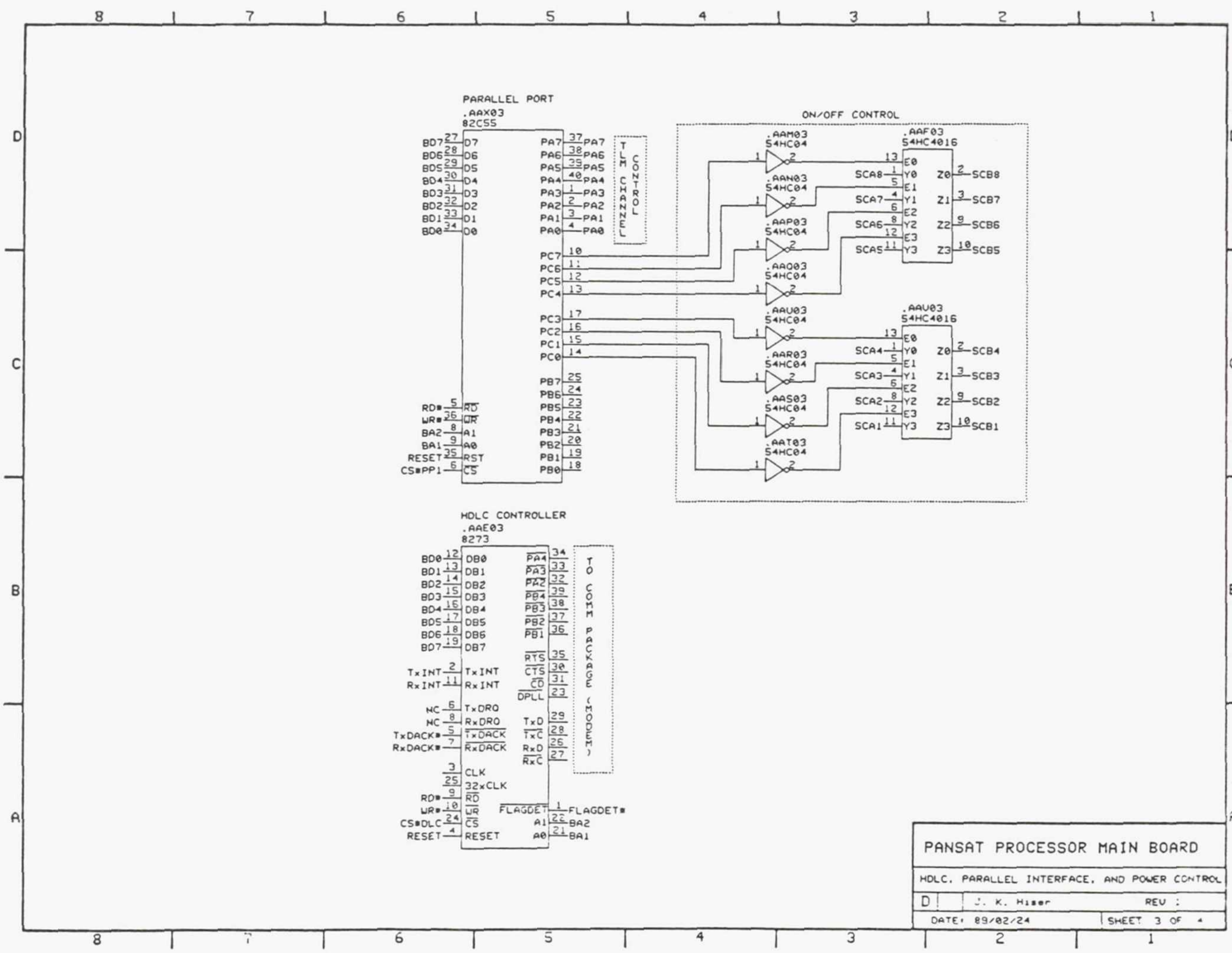

Fig. A3. HDLC, Parallel Interface, and Power Control. The HDLC 8273 protocol controller will be replaced by a CMOS version, SCC chip.

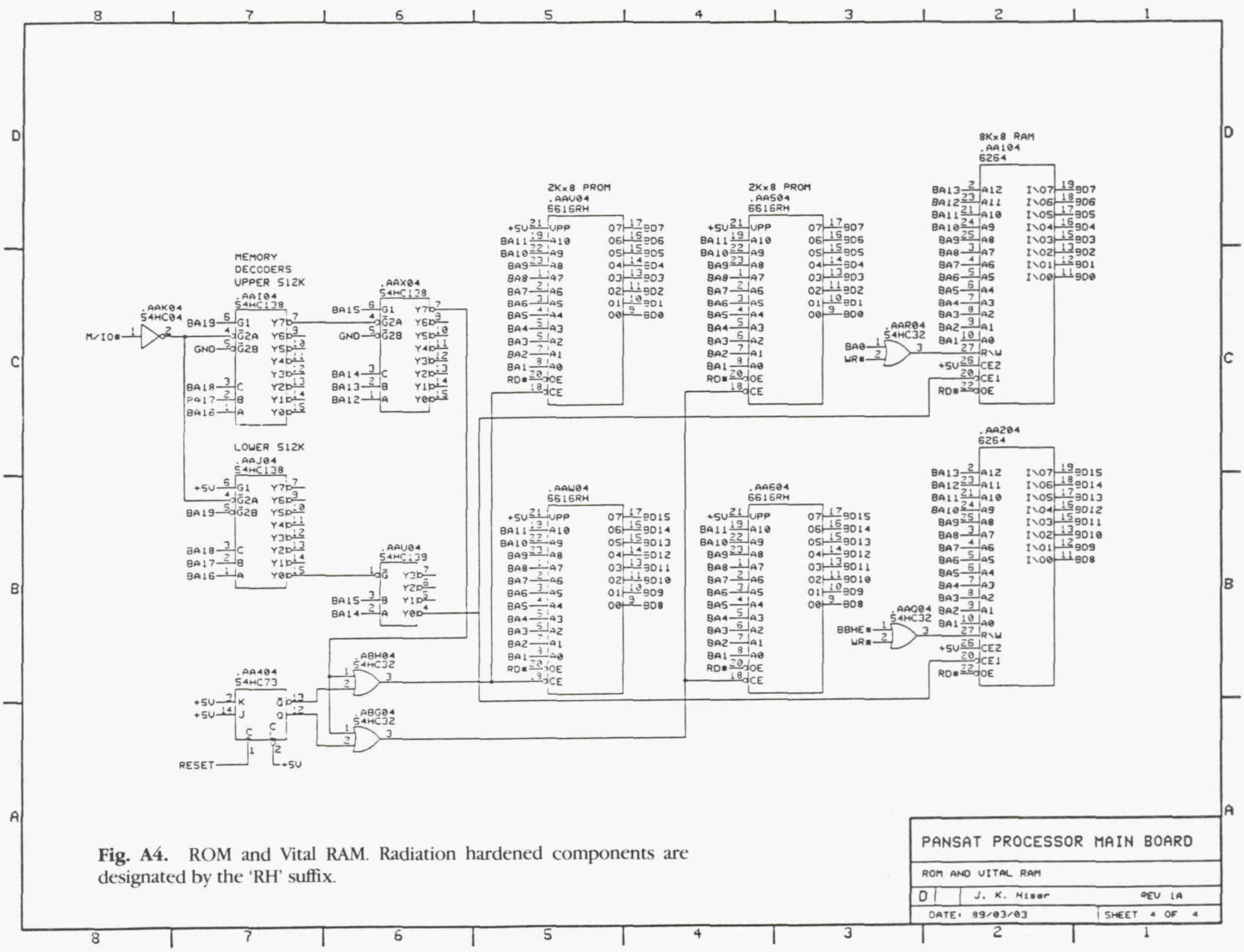

Fig. A4. ROM and Vital RAM. Radiation hardened components are designated by the 'RH' suffix.

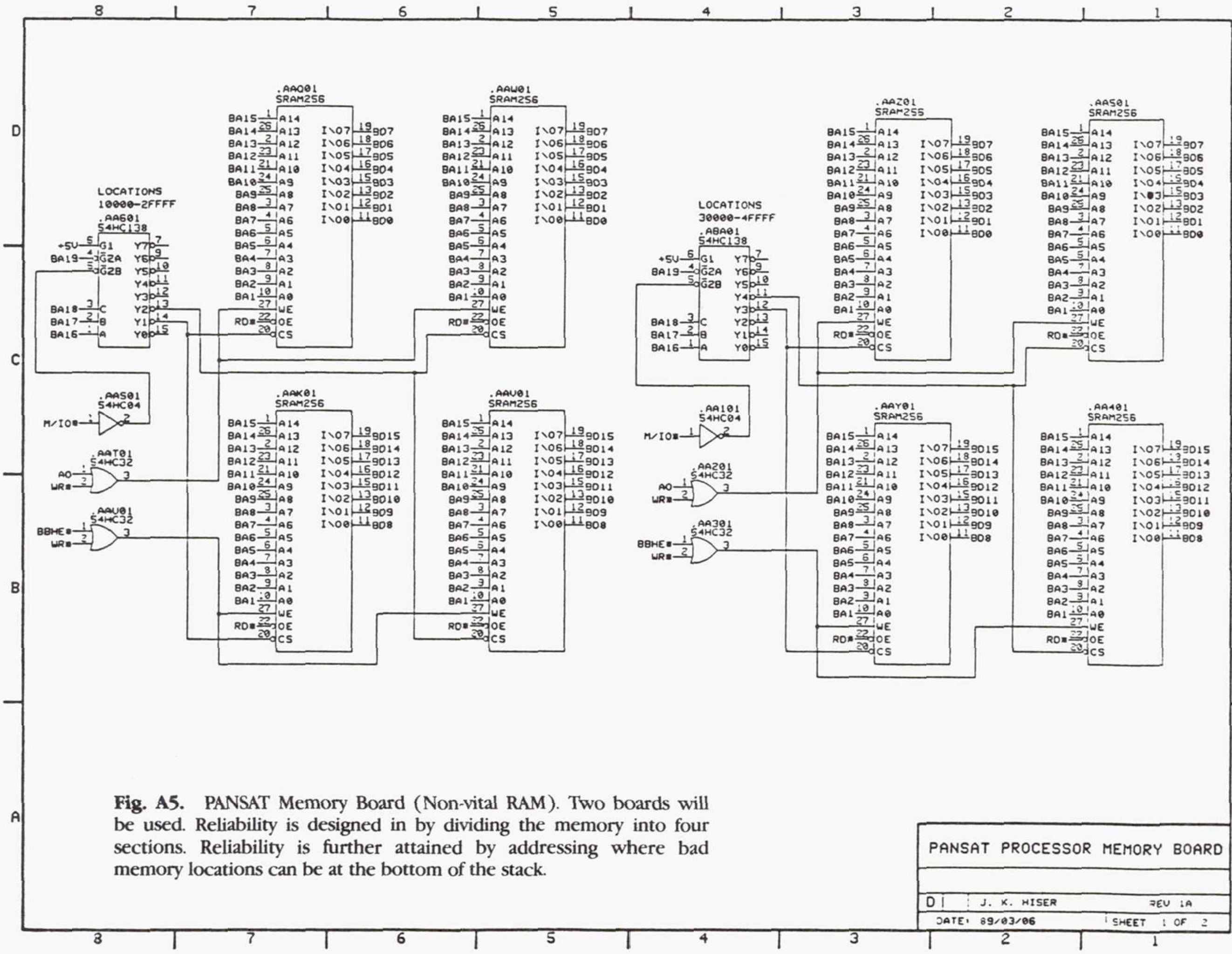

Fig. A5. PANSAT Memory Board (Non-vital RAM). Two boards will be used. Reliability is designed in by dividing the memory into four sections. Reliability is further attained by addressing where bad memory locations can be at the bottom of the stack.

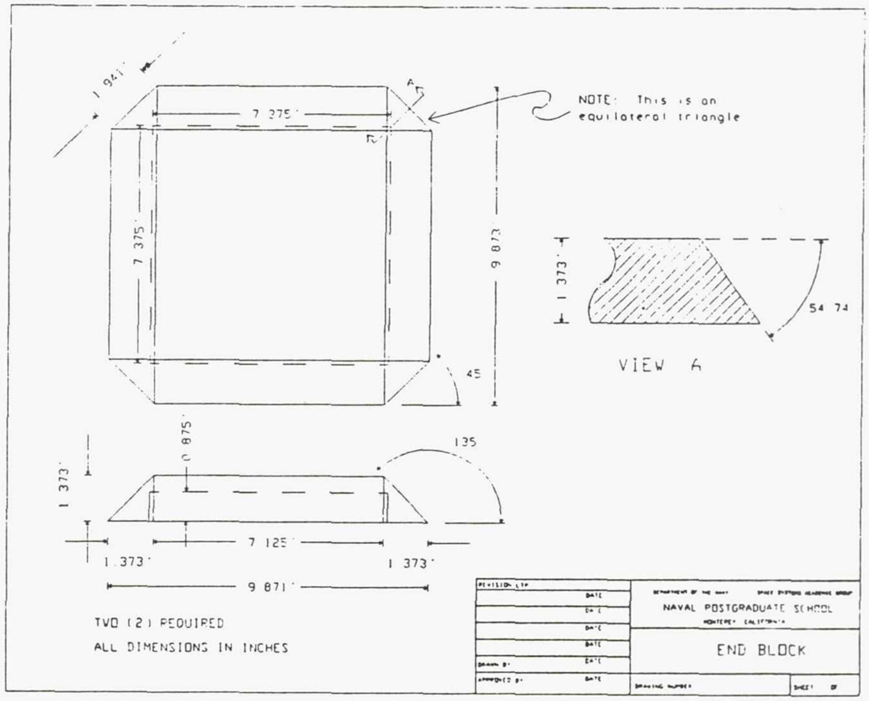

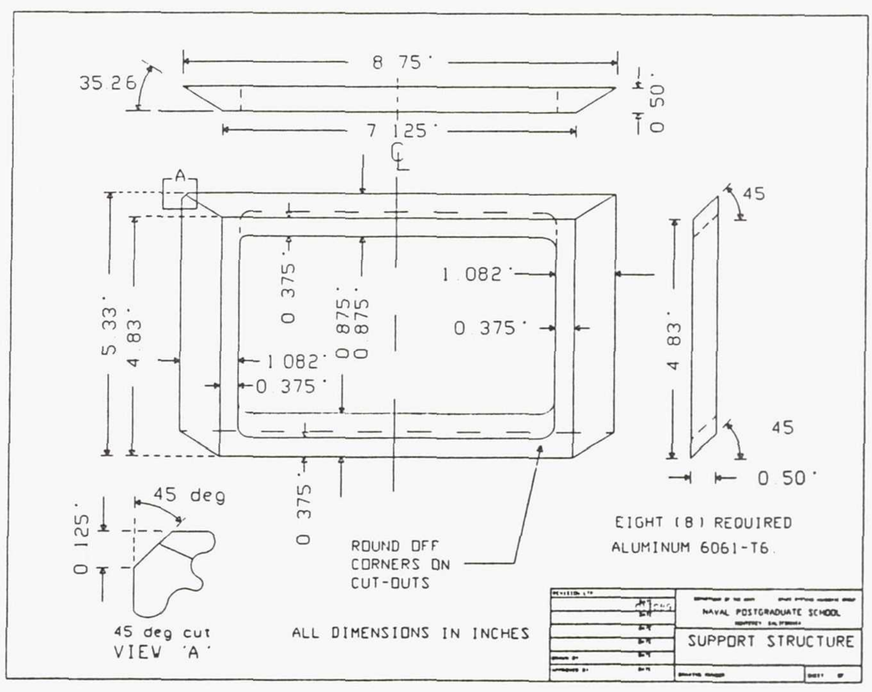

Fig. A6. PANSAT Structural Elements.

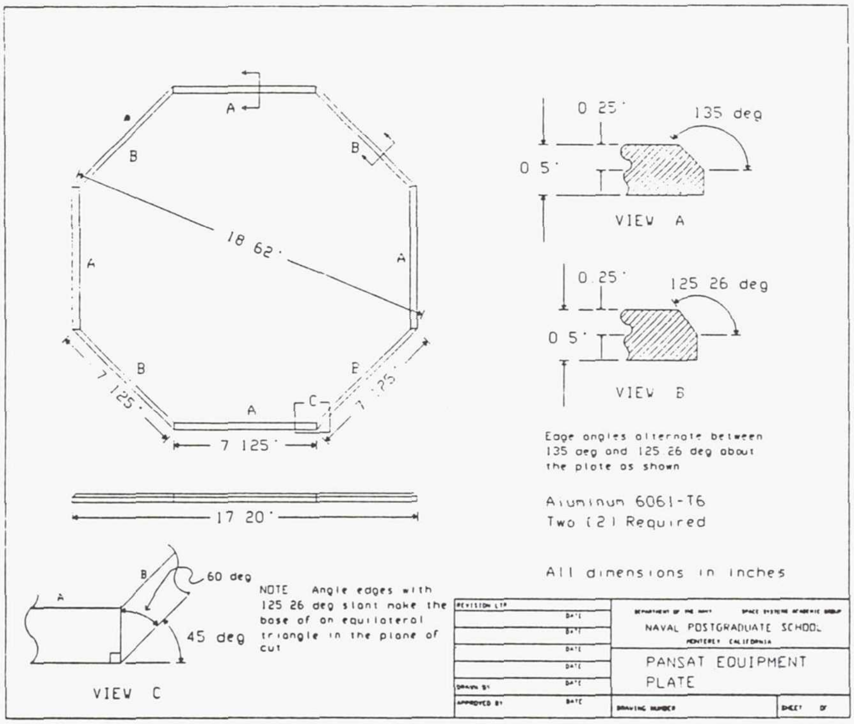

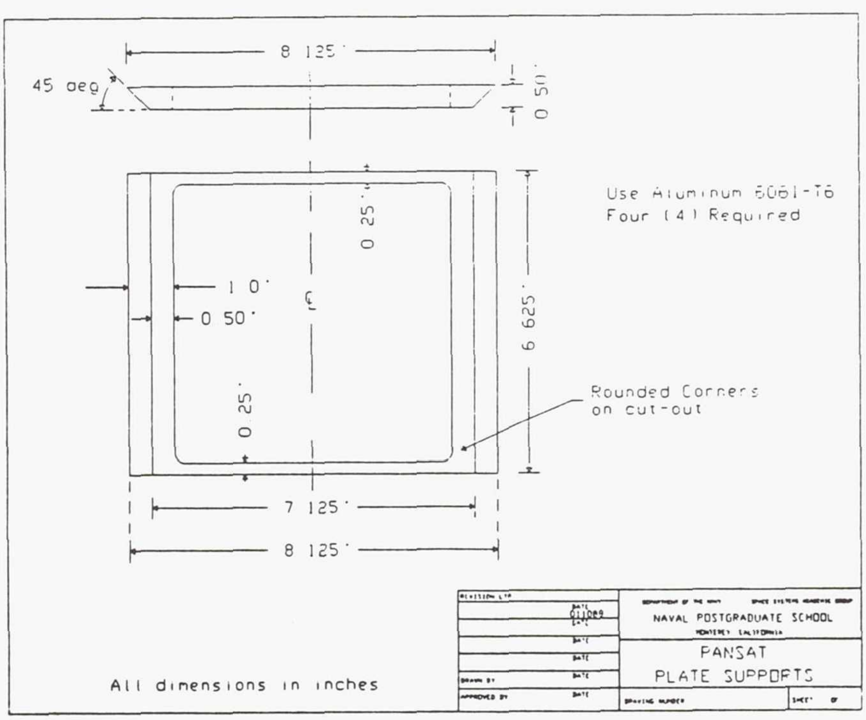

Fig. A7. PANSAT Structural Elements.

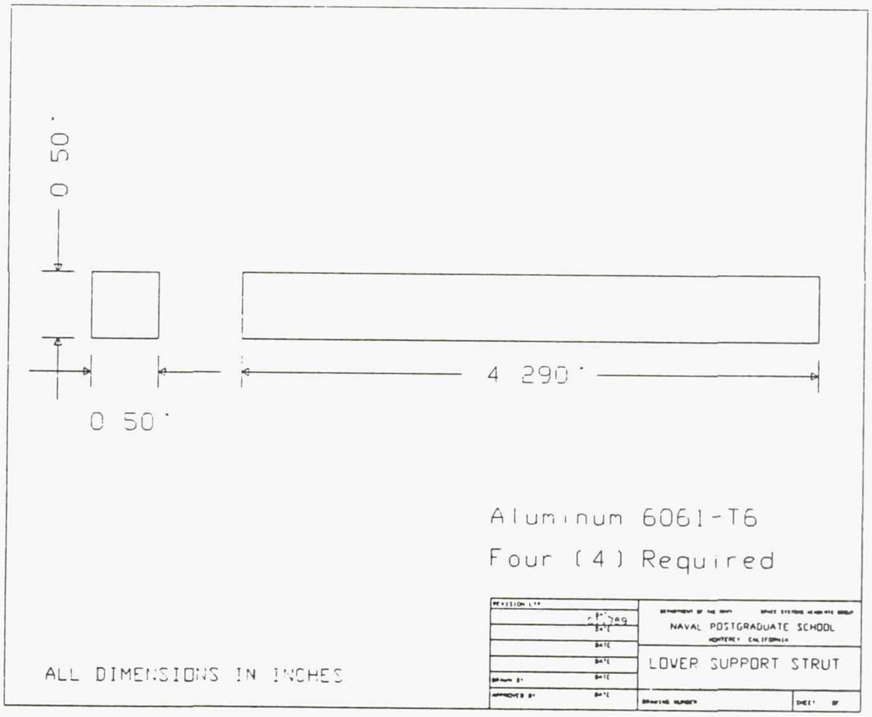

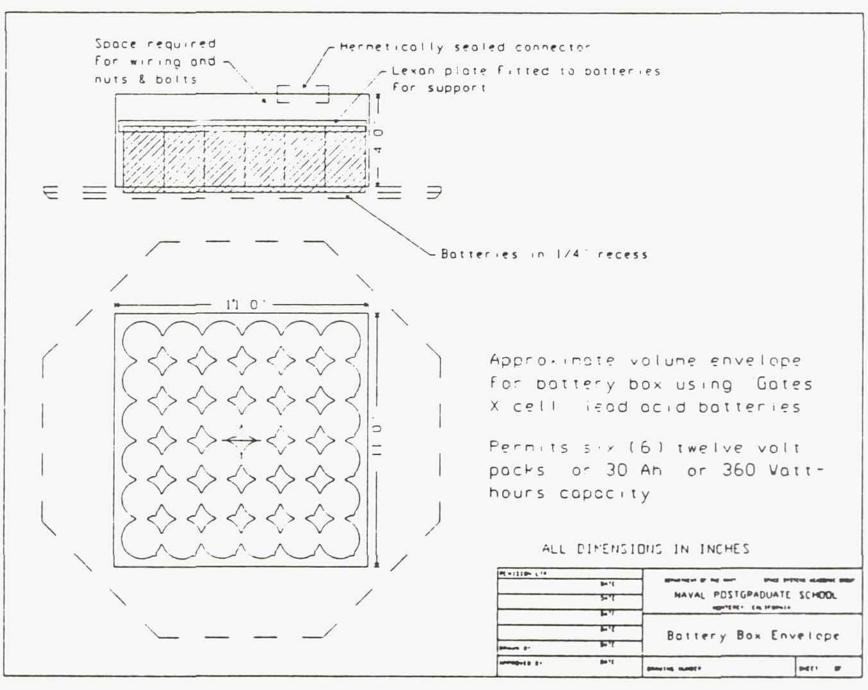

Fig. A8. PANSAT Support Strut and Battery Volume.

N94-71283

1994004528
382687
516-31
160642
p-18

LUNAR MINING EQUIPMENT

UNIVERSITY OF NORTH DAKOTA

INTRODUCTION

Definition of Topic

This document contains preliminary concepts for mining and beneficiation of lunar regolith from a 50-metric-ton-per-day mine. Assumptions for the design are outlined below.

Student Background

This work was done in the Department of Space Studies at the University of North Dakota by 6 students as part of the coursework for SpSt 405 - Advanced Space Mission Design, building upon work done by 19 students in SpSt 305 - Introductory Space Mission Design. The Instructor for these courses is Dr. Dick B. Parker. These courses are taken by undergraduate students in the Space Studies Minor program and the students have a wide variety of majors, therefore the designs are conceptual only.

Assumptions

Lunar regolith is the material to be mined. Since it is already a fine-grained material, the two steps of crushing and breakup from a rock surface are eliminated. The size of the operation was set at 50 metric tons of regolith per day for a three-year period. Operations will occur around the clock to make most efficient use of equipment, thus we assume 24 hr/day. For simplicity we have assumed that the lunar regolith has a uniform density of 1.68, and that it can be mined to a depth of 6 m. No research was done on power supply or distribution. It was left to others to consider the various trade-offs between nuclear and solar power, and to design the needed utility system.

DIGGER/LAUNCHER

Introduction

This section contains preliminary ideas for a lunar mining machine that will extract regolith from the lunar surface and will use a mass launcher to transport it to a processing plant.

Assumptions

The digger/launcher (DL) is a remotely controlled vehicle able to mine areas near the processing plant. It will consist of a digging apparatus and a mass launcher for the transportation of the regolith. The area of mining will be circular, with the processing plant at the center.

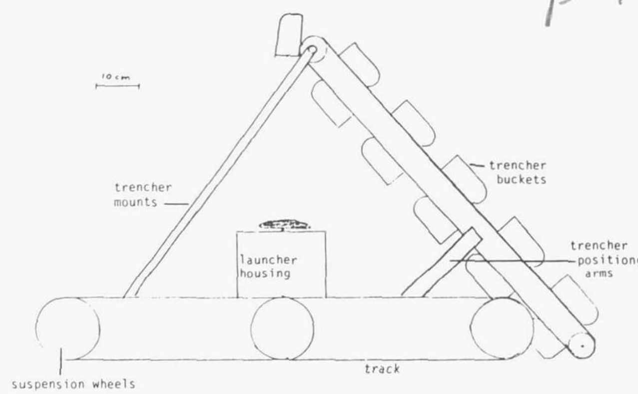

Fig. 1. Digger/Launcher (Side View)

Design

The design is a dual-tracked vehicle with a continuous excavator digging apparatus mounted on the front of the vehicle. On the platform of the vehicle between the tracks is mounted the mass launcher, aiming system, drive motor for tracks and digger, and control computer. A laser positioning system will be used to find range and direction of the processing plant (Fig. 1).

The excavator will be used for digging the regolith and loading the bucket of the mass launcher at a rate of 600 g/sec. The system will load, fire, and reset the mass launcher once per second. Given that the maximum distance from the vehicle to the processing plant will be 50 m, the maximum velocity needed will be 11 m/sec. The maximum acceleration needed of the mass launcher will be about 125 *g*.

Mass launcher. The mass launcher is an electromagnetic linear motor that consists of a row of drive coils through which the bucket magnet will be pulled as current is applied to the coils. This accelerates the magnet/bucket assembly in a linear fashion (Fig. 2). Once the bucket has reached maximum velocity, the remaining coils produce a decelerating magnetic field that stops the bucket. The inertia of the regolith will cause it to continue at the maximum bucket velocity toward the processing station in an arced path. Since the mass launcher has no friction-causing parts (the magnet/bucket assembly is suspended magnetically), there are very few wear surfaces. This will provide good system lifespan.

The bucket will be the site of the most wear in the mass launcher system. It must be a rigid structure capable of withstanding 125 *g* of acceleration force, and three years of

PRECEDING PAGE BLANK NOT FILMED

PAGE 122 INTENTIONALLY BLANK

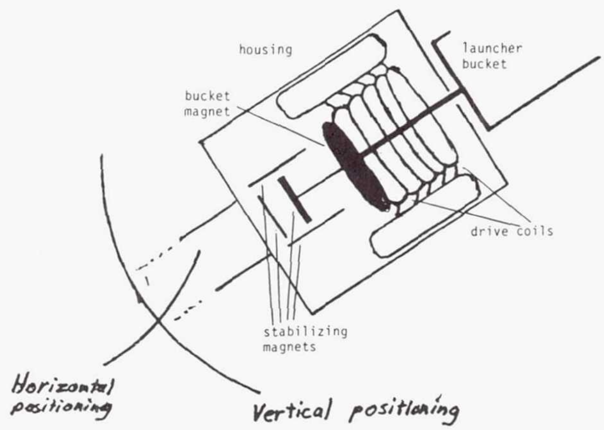

Fig. 2. Launcher

wear without replacement. High-strength, low-wear material is required.

Coils will be made from wire and mounted in a casting of high-strength, nonconducting material such as epoxy. The total number of coils, their spacing, and diameter are undetermined.

The magnet attached to the bucket could be either a permanent magnet or electromagnet. It is mounted on a rod attached to the bucket.

A capacitor storage system is required for the high-current bursts of power needed. These capacitors would be mounted on the DL vehicle.

A two-degree-of-freedom mount capable of withstanding 400 kg shocks is used to mount the mass launcher to the DL vehicle and to aim the launcher.

Aiming system. Positioning data accumulated from the laser range and targeting systems is fed to an onboard microcomputer, which aims the mass launcher at the processing plant.

Continuous excavator. The continuous excavator consists of a series of buckets mounted on a continuous oblong track powered by a drive motor. It was chosen because it offers periodic loading of the mass launcher, multiple (rather than single) wear surfaces, several low-wear surfaces in each bucket digging edge, and simple control.

Vehicle. The DL vehicle consists of a body that houses the drive motor, capacitors, computer, laser range finding system, and related hardware. The body is mounted on tracks, since tracks provide maximum traction and a stable base, and spread out the force of the mass launcher firing better that wheels. Power will be supplied to the vehicle via a power cable, which the machine drags behind it as it moves. Alternative energy sources are a beamed microwave energy system or solar cells mounted on the vehicle.

DRAGLINE SYSTEM

Introduction

Dragline mining systems are efficient and used to a great extent on Earth. This section will present a system for use in lunar mining.

Design

The dragline will consist of a single bottomless bucket that consists of two sides, angled back, long flat teeth that will span the entire width of the bucket, and a partially enclosed top. Kevlar cables will be attached to the bucket in three locations, one on each side near the top of the bucket and one to the rear of the bucket. The cables will be run by a two-drum winch system located at the processing plant. One drum is used in conjunction with a tracked crawler equipped with a pulley around which the rear cable runs to move the bucket away from the processing plant. When the bucket has reached the end of its outward run, this drum is declutched, and the second drum starts pulling the bucket back towards the plant. The bucket fills with regolith on the return trip, and is emptied into the plant at the end of this run (Fig. 3). Movement of

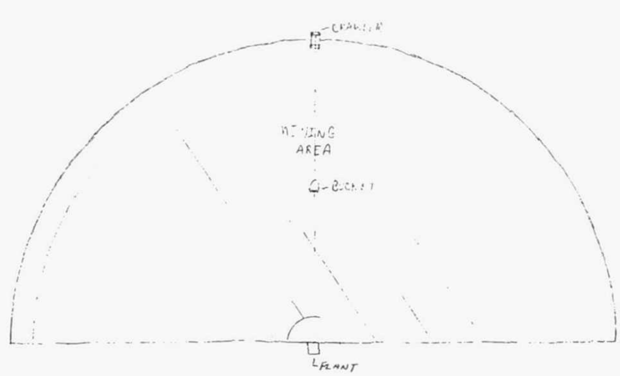

Fig. 3. Dragline System

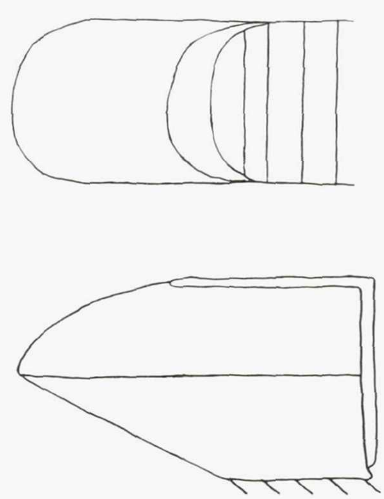

Fig. 4. Bucket Design

the crawler at the perimeter of the mining site changes the area that the bucket passes over, making it possible to mine a semicircular area. The crawler vehicle has a pulley mounted on a mast, which serves as the out-haul anchor for the bucket. The crawler also has out-rigger arms similar to those of a backhoe that are extended to provide additional stability.

Bucket Design

The bucket (Fig. 4) is bottomless and designed to allow the bucket to be lifted in a near-vertical fashion by the in-haul cables without spilling any regolith. It is emptied by hooks that catch the bottom lip of the bucket and cause it to tip forward and dump its cargo.

Crawler Design The crawler (Fig. 5) serves as a self-mobile anchor for the bucket out-haul. If the processing plant were placed by an unmanned vehicle, the crawler could exit the plant and station itself with no outside help. The continual movement of the crawler in a back and forth motion during mining would allow the terrain that the bucket must transverse to stay relatively level, making it less likely for the bucket to tip over. The extension arm on the crawler is extended when the crawler is not moving to provide a wide, stable base for the pulley located on the mast.

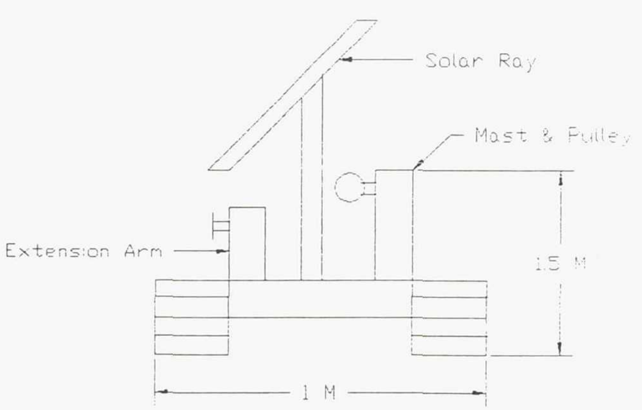

Fig. 5. Remote Crawler (Front View)

BENEFICIATION OF LUNAR REGOLITH

Introduction

This section describes a design for a lunar regolith beneficiation plant. The system is integrated into a complete mining system. Since the concentration of certain minerals varies with particle size, it was decided that methods for separating regolith into a spectrum of particle sizes was advantageous.

Lunar Conditions

The systems are designed to operate in the hard vacuum and low gravity of the lunar environment. Earth-based systems for separating particles the size of those in lunar regolith generally use a fluid medium of some type, but this is clearly impractical on the Moon.

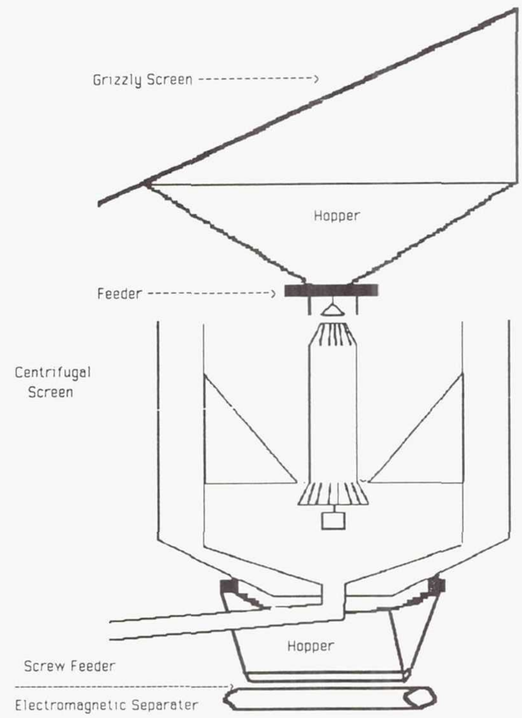

Fig. 6. Lunar Beneficiation Plant

Design

The design consists of three stages:

Grizzley screen. The first stage is an interface unit, made up of a grizzly screen and a hopper (Fig. 6). A grizzly screen is a set of parallel bars that screen out oversized particles but allow smaller particles to go through. The screened material is then fed into a hopper equipped with a flow regulator for temporary storage.

Centrifugal screen. The material then enters the second stage, the centrifugal screen (Fig. 6), which is made up of a cylindrical section of screen, inside which is a rotor. When the rotor is spinning, the material fed from the top of the system falls and strikes the edge of the spinning rotor. The rotor throws the material against the screen, with the small-sized particles going through the screen openings, and the oversized particles falling back into the machine. To improve efficiency (small particles may strike the wires of the screen and not go through), the process is repeated at the bottom of the device.

Electromagnetic separator. The small particles are then fed into the third stage of the system, an electromagnetic separator, which passes a strong magnetic field across a stream of falling regolith particles. The path of the particles is affected by the field according to their magnetic properties.

Electrostatic separator. An alternative to the electromagnetic separator is the electrostatic separator (Fig. 7). The

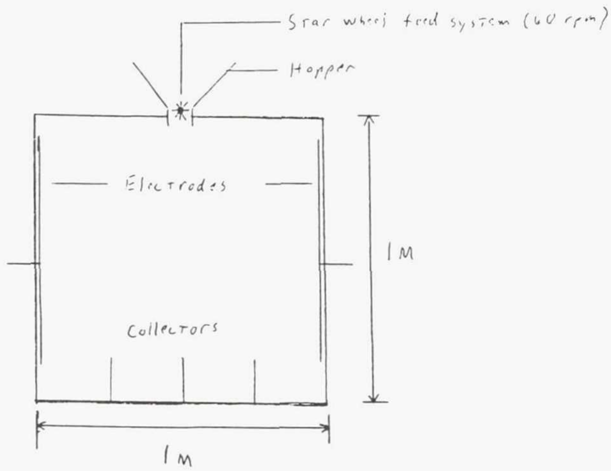

Fig. 7. Electrostatic separator. Height = 1 m; width = 1 m; length = 4 m; power required = 0.3 W; throughput = 600 g/sec, 50 tons/day.

electrostatic separator passes an electrostatic field across a stream of falling regolith. The particles' paths are affected according to their electrical charge. The charge is imparted mechanically to the particles by the rotor of the centrifugal screen device, or could be provided by an electron beam.

Product

The beneficiated material will provide a selected fraction of regolith for chemical processing.

VARIABLE GRAVITY RESEARCH FACILITY POWER AND TETHER SYSTEM

UNIVERSITY OF NORTH DAKOTA

VGRF POWER SYSTEM

Introduction

The goal of this section is to design a power supply system for the Variable Gravity Research Facility (VGRF). The VGRF is designed to be placed in a low Earth orbit (LEO) to study the effects of various gravity levels on the physiology of the human body. This design is concerned only with the supply of power; any required processing or storage facilities were deemed outside the scope of this project.

The design constraints were as follows: the system must supply 8.8 kW of continuous power for the eight-month mission duration and the design must follow a minimum mass criteria.

Three possibilities for powering the VGRF were investigated. Solar voltaic arrays with battery storage, fuel cells, and nuclear power were the options that seemed to have the most viable chance of success based on today's technology.

Nuclear power was eliminated on the basis that it would probably not be politically acceptable. Fuel cells require transporting a mass of fuel to LEO that is too large to make such a system desirable. In addition, storage during the eight-month mission is a problem. Thus, solar voltaic arrays were selected. The design developed at the University of North Dakota utilizes two assemblies of three rotating solar panel subassemblies to achieve the design specifications. This design saves size and hence, mass, by utilizing a configuration that tracks the sun during the rotation of the VGRF itself.

System Options

Nuclear power. The system examined as a potential option to power the VGRF was the SP-100 nuclear reactor. This particular design can generate 30 kW of continuous electricity, which is three times the amount required for this mission. The SP-100 has a mass of 14,000 kg resulting in a mass-to-power ratio of 467 kg/kW when the 30 kW is needed. This design uses Plutonium-94 as its reactor fuel and is being designed to be safe enough for use in a manned space station.

The major factor that prevents this design from being accepted is its lack of political acceptance in LEO.

Fuel cells. The Allied Signal Corporation fuel cell provides 10 kW of continuous power by converting hydrogen and oxygen to water to provide electricity. According to manufacturer's specifications, the fuel cell requires 5.0 kg/hr of fuel made up of both H_2 and O_2 for an average output of 10 kW. For each eight-month mission using 8.8 kW with 5% reserve fuel, the shuttle will be required to take an additional 26,600 kg of fuel for the VGRF. This yields a mass-to-power ratio of 3024 kg/kW for the eight-month period.

One problem associated with this option is that the VGRF rotates at approximately 3 rpm to achieve an artificial gravity. This requirement negates the possibility of off-system storage. Also, the habitation module (HM), to be utilized in the design of the VGRF, certainly has no provisions for the storage of this amount of fuel. Another option considered was utilization of the external tank (ET), which acts as a counter weight to the system, to store this fuel. A problem with this is the long-term storage of LH_2. By far the biggest problem faced by this option, however, is the cost of placing this huge mass into LEO.

System Choice

Since the overall system size is regulated by the size requirements of the arrays to output the 8.8 kW continuous power, it seemed logical to first determine array size. The solar panel specifications used to determine this size were taken from the NASA publication "Space Station Specifications"[1].

The total power reduction factor for the system has four contributors. In addition to shading by the Earth during the rotation of the VGRF about itself, the panels will also be shaded by the ET and by themselves as they track the sun. Sun angle is not always perpendicular to the panels because they rotate in only one plane rather than two. A program utilizing the University of Texas Mission Planning Subroutine Library was used to help determine the percentage of exposure time lost due to these factors. Totaling all the power reduction factors results in an average of only 44% of peak power production.

Sizing of the panels. Utilizing the information cited above on the solar arrays and the values achieved through our own calculations, the 8.8 kW of continuous power could be achieved by 610 sq m of array with a mass of 5700 kg giving a mass-to-power ratio of 648 kg/kW. (This mass includes rotational equipment and support structure.) These values are approximately ⅓ that required by a fixed (nontracking) array.

Design of the panel assemblies. In this design, the 610 sq m would be split into two panel assemblies, one located on each side of the HM, extending perpendicular to the plane of rotation of the VGRF. Both panel assemblies consist of three sections (see Fig. 1) 4.33 m × 24 m that could be assembled in space, resulting in a 13 m × 24 m solar panel subassembly resulting in a panel area of 624 sq m.

Each of the six sections, therefore, consists of two rotating panels 4.33 m by 12 m and a support truss 9.20 m in length. The support trusses utilize a four-point bearing at each end to support the rotating panels. These bearings not only provide for rotation of the panels but also provide structural strength in the axis normal to the HM. They will also resist transient sideward loading.

The support structure for the assemblies is made up of the aforementioned support trusses, a rigid mast attached to the

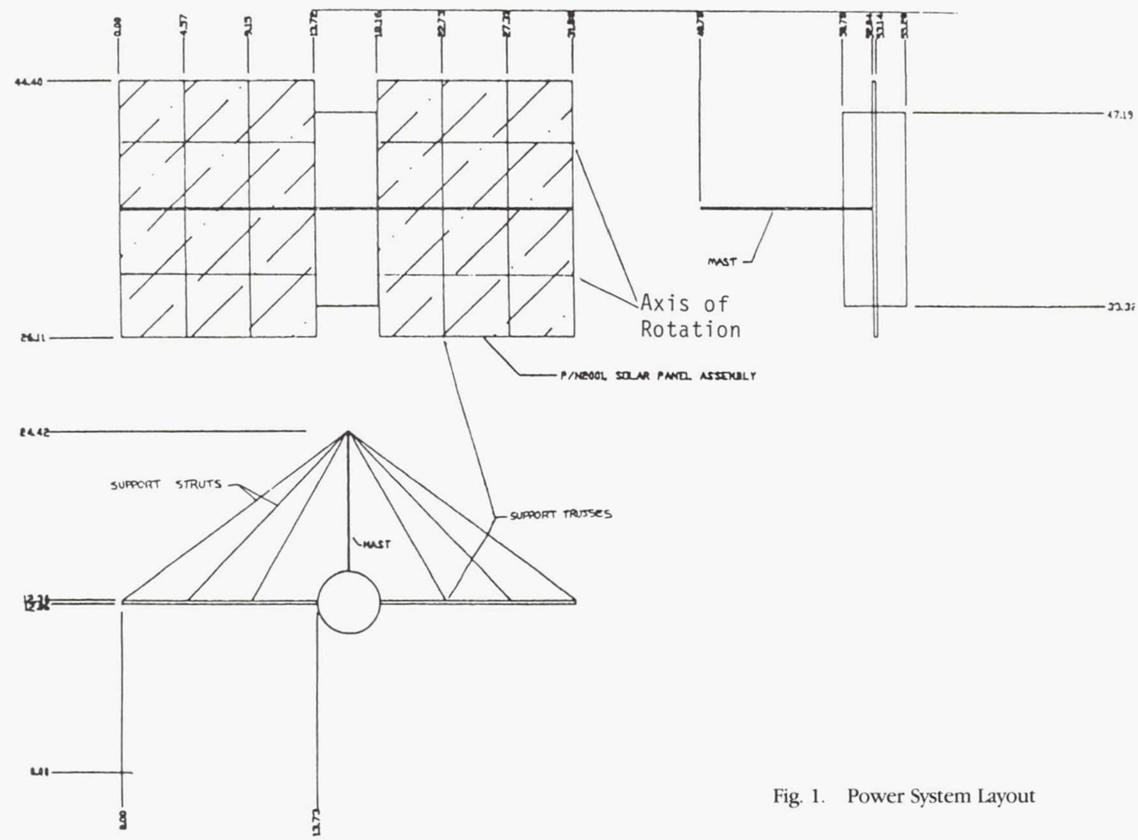

Fig. 1. Power System Layout

HM, and six support struts that have one end fixed to the center of their respective support trusses with the other end meeting at the tip of the mast (Fig. 1). The mast will be mounted on top of the HM towards the center of rotation of the VGRF. This will place the mast in compression and the struts in tension. Each of the two solar panel assemblies will attach to the HM at points located on its pressure bulkhead. By placing the struts and the mast in the center of the HM, they will not interfere with the rotation of the panels or the tether configuration used to join the HM and the ET.

The mast is fixed to the surface of the HM by a saddle designed to fit the curvature of the HM and adequately distribute the force over its surface.

Discussion

The deployment of this system is a simple one. The panel sections are joined on Earth to form the panel assemblies and folded in the manner shown in Fig. 2. On orbit they need only be removed and extended utilizing the space shuttle remote manipulator arm and a minimal amount of EVA. This EVA is required to attach the panels to the HM and assemble the mast and struts.

This system will require a variable speed motor to drive the panels to allow tracking of the sun. This motor can be configured so that it drives only the panels closest to the HM. Subsequent panels can be driven by a positive locking mechanism between panel subassemblies, which becomes engaged when the panels are erected. In this way, rotational torque is transmitted to all panels.

An important feature of this design is its ability to allow expansion. If power requirement estimates increase, additional sections can be added.

VGRF TETHER SYSTEM

Introduction

The objective for this section is to design a stable, flexible, tether configuration for the VGRF. The system requirements include a maximum artificial gravity level of 0.64 *g* on the floor of the HM at a rotational speed of 3 rpm.

To simulate the actual system, a scaled model was constructed and tested using a scaled rpm. A test procedure was used to evaluate a number of different configurations based on both a visual and a computer force analysis on each of the tethers for a given configuration.

A number of different types of instabilities can be expected in a flexible cable system such as this. The three main areas of instability under consideration here are rotating, twisting, and skewing.

Two methods of data acquisition, visual and a force analysis, were achieved using a test apparatus designed and constructed

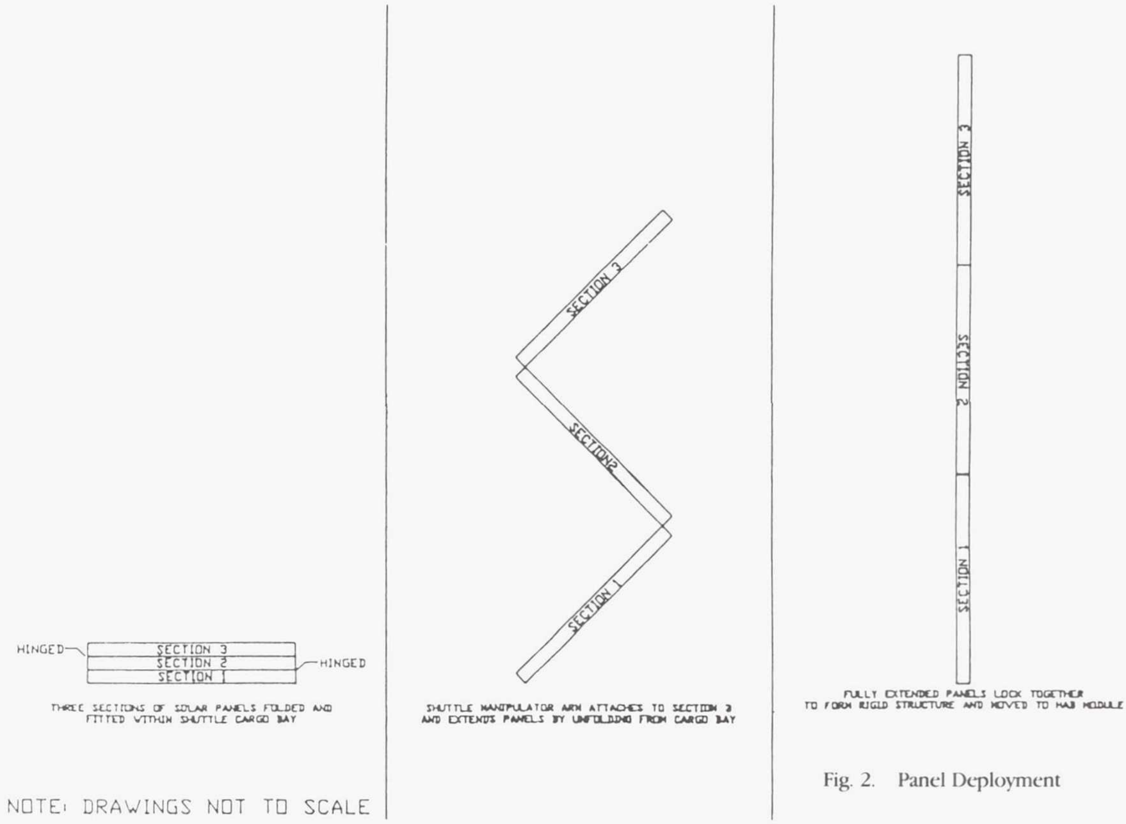

Fig. 2. Panel Deployment

for this purpose. This apparatus allowed the test model to be filmed using a pair of camcorders. In addition, "real-time" force analysis output to a computer during each test was obtained.

The eight-tether configuration shown in Fig. 3 is a configuration that best suits the criteria of stability.

Types of Disruptions

The three types of disruptions are twisting, skewing, and rotating. The first type of disturbance, twisting, occurs when the ET and HM maintain the same horizontal plane but pivot left and right parallel to the tether configuration, one end of either the HM or the ET leading the opposing end. Skewing occurs when the ET and HM do not remain in the same horizontal plane but pivot up and down normal to the tether configuration. Rotating is induced when the ET and the HM remain in the same horizontal plane but tend to rotate on their central axis perpendicular to the tether configuration.

Configuration Analysis

Each proposed tether configuration was initially evaluated in a research team meeting. If accepted, a static analysis of the forces present in each tether of the configuration was performed. Promising configurations went into the lab and were evaluated using the following methods.

Visual data acquisition. After preparation of the model, which included building the scaled tether configuration from Kevlar cable donated by Cortland Cable Company, the model was placed in the test apparatus shown in Fig. 4. The visual data acquisition system consisted of two video camcorders and

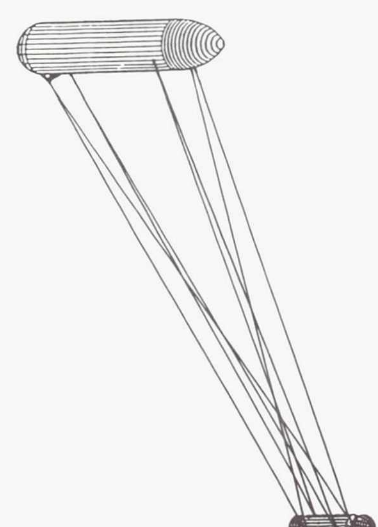

Fig. 3. Eight-Tether System

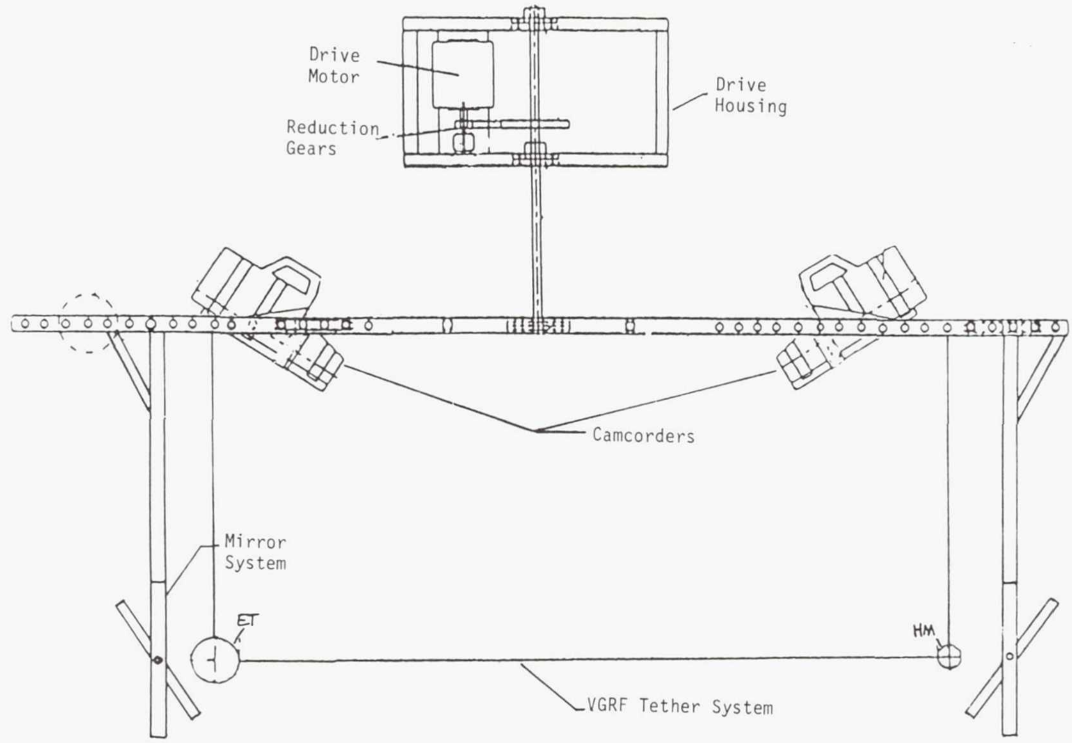

Fig. 4. Test Apparatus

a mirror system. As can be seen from the illustration, this type of system allows the camera to view the tether configuration from a wide range of angles.

Computer force analysis. The computer force analysis system recorded real-time data and provided a real-time graphical representation of the tether configuration during testing as well as a stored data file. Tether forces were acquired by connecting the ET tether ends to slide-pot potentiometers located inside the ET model. As the force on a given tether changed during the test procedure, a different reading would be measured by the potentiometer. This information was passed through an A/D conversion board on a real-time basis and evaluated by a computer program written by the design group.

A configuration could be rejected based on either visual data or computer force analysis data.

Tether Configurations

Configuration options. Many configurations were evaluated. Of those, 12 went through static analysis. Configurations containing 2 to 12 tethers were evaluated. Several configurations were reevaluated after slight modification to better understand how a particular tether affected the stability of the configuration as a whole. Elimination criteria included (1) large deviation of force measurement from the precalculated values based on a static analysis; (2) periodic change in the tensile force in a given tether suggesting a wave motion; and (3) lack of symmetry of forces where this should have been realized. The selected configuration consisted of eight tethers and, based on our evaluation, satisfied the stability criterion outlined in the mission of this project.

System choice. The selected configuration is shown in Fig. 3. The visual analysis of this configuration permitted the initial conclusion of a stable system. The effects of twisting, skewing, and rotating seem to be adequately eliminated.

Further evaluation of the configuration using the force analysis showed that the tether forces were evenly distributed between the tethers and that the desired symmetry was present. The forces on each tether differ from each other by less than 1%.

A total of 922 m of 22.3-mm-diameter Kevlar-29 cable would be required to construct the actual tether configuration for the VGRF producing 0.64 *g* at 3 rpm. Center-to-center separation of the ET and HM is 117.4 m. The overall simplicity of this configuration would allow easy implementation on the actual system. Another feature that this configuration had that others did not is its lack of intermediate tether-to-tether connections, which reduce the tensile strength of the cables by 15%. Adding such connections would not be a serious difficulty as the cable diameter could be slightly increased. The designed system has a factor of safety of 9 at 0.64 *g*. The eight-tether configuration also provides stability if a tether is severed by space debris.

Discussion

The model was subjected to aerodynamic forces during the test procedure. Although every precaution was taken to minimize the effects of this, some error may have been induced by it. We believe that this error was small enough to be

assumed zero, for our purposes. Vibrations induced by the test apparatus itself had an effect on testing until the apparatus was allowed to stabilize at a constant rpm. For this reason the spin-up/spin-down data gathered by both data acquisition methods were ignored for all the configurations evaluated.

Force analysis was not as sensitive as desired due to the friction in the potentiometers and in the tether entry into the model. This prevented useful data from being acquired by activation of stability disruption devices that were built and placed in the HM.

A more detailed version of this report is available from the Department of Space Studies, University of North Dakota, Grand Forks, North Dakota.

ACKNOWLEDGMENTS

Design team members S. Bekkedahl, T. Breidenbach, M. Brown, C. Francis, J. Freeman, M. Scharnott, and R. Thon were assisted by project managers T. Nordtvedt and Dr. D. Parker.

REFERENCES

1. National Aeronautics and Space Administration, *Space Station Specifications,* vol. 1, April 1988.

N94-71284

1994004529

6P

PRELIMINARY DESIGN OF A LUNAR CONSTRUCTION UTILITY VEHICLE

3 826888

OLD DOMINION UNIVERSITY

S17-31

160643

P. 5

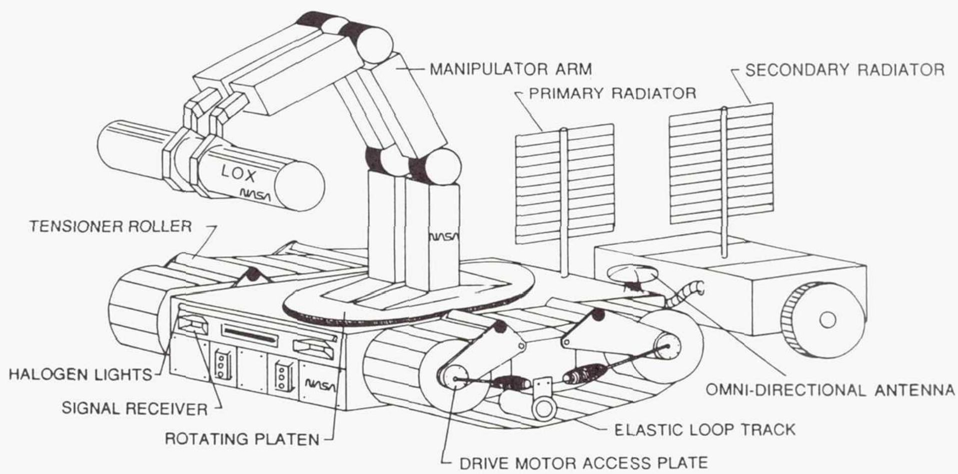

Fig. 1. Artist's representation of an LCUV

INTRODUCTION

Construction of a lunar base, prior to manned occupancy, is one of the most demanding technological challenges facing space system designers today. A flexible lunar construction machine is needed that can be operated remotely and that can perform a variety of construction tasks over a wide range of lunar conditions. A preliminary lunar construction utility vehicle (LCUV) design has been developed as part of a capstone design course at Old Dominion University and is described in this summary report. The design requirements are taken from a 1988 USRA Summer Design Report entitled *The Lunar Split Mission: A Robotic Constructed Lunar Base Scenario*(1), and from the proceedings of a workshop hosted by United Technologies Corporation entitled *Report of the In Situ Resources Utilization Workshop*(2). The first report describes a bootstrap base concept in which a minimum of essential surface elements are delivered and configured such that minimum EVA is required to bring the initial base on-line. The base is to be built in three phases, the first of which will be unmanned, while the second and third will be manned. The key to these concepts is the development of a semiautonomous, telerobotic lunar construction utility vehicle (LCUV).

The tasks required of this robotic vehicle during the Phase I build-up are (1) surface element transportation, handling, and assembly; (2) soil excavation and movement for site preparation; (3) radiation protection and materials processing; and (4) repair and maintenance of surface elements.

In order to meet the requirements of reference 1, the LCUV must be (1) transformable to perform a wide variety of tasks; (2) self supporting (as a minimum during Phase I); (3) designed to allow for telerobotic control as well as autonomous operation; (4) able to transport one fully configured space station common module (SSCM); (5) upgradable to allow for future growth; and (6) easy to maintain.

This work is the result of a single semester design course. Three competing design teams were asked to develop an initial design to accomplish the overall objectives for the LCUV. A design competition was held at the end of the semester in which the entire design class and representatives from industry judged the results. The overall objective of this strategy was to obtain as many ideas as possible in this initial phase of the design. The best ideas of each design have been incorporated into the present report. Since this design is partly conceptual and partly detailed, the work will continue next semester by a single group of Advanced Space Design students who will address the problems brought to light in this initial work.

OVERALL CONFIGURATION

An artist's sketch of the LCUV is shown in Fig. 1. The vehicle is considered to have three functional elements. There is a pair of elastic-loop tracks for locomotion(3), a main body that houses all support subsystems, and a remote or towable radiator for use during maximum power operations.

SUBSYSTEMS

Within the main body there are three major subsystems: (1) power; (2) thermal control; and (3) navigation, communication, and intelligence.

PRECEDING PAGE BLANK NOT FILMED

PAGE ___ INTENTIONALLY BLANK

On the top surface of the main body there is a circular rotating platform that supports two robotic arms. Also on the top are four cameras, a primary radiator, communications antenna, lighting, and an area for various support equipment. These systems will now be briefly discussed.

FRAME AND BODY

A truss frame is employed to provide for light weight and ease of construction. The main objective of the frame system is to support internal subsystems and overhead robotic arms while allowing direct connection to the drive system. With the large variety of loading conditions, environmental considerations, and physical requirements, it was decided that a computer-aided design (CAD) was necessary. The model, which consisted of a network of truss elements shaped into a rectangular box configuration, was analyzed using PATRAN Plus and NASTRAN.

The design truss must take into account the effect of the variation of temperature on the lunar surface over the range of -170°C to +150°C. Consideration must also be given to the presence of solar and cosmic radiation and its corrosive effects on materials. Finally, the high vacuum of up to 1E-14 mm Hg must also be considered along with its adverse effects on the structure. The frame must function without failure during repetitive operations of each component and combinations of operations of more than one component at a time. This involves modeling working scenarios by applying equivalent forces to the frame that will be imposed by the various components.

The four loading subcases that were simulated in this analysis included applied forces of 12 kN (each applied in opposite directions to the mounting points of the arm base) to simulate an actual material off-loading operation. The second loading case included loading the track mounts to the maximum force that can be put out by the track motors (12 kN each) while constraining the mounts on the opposite side of the vehicle. The third criterion included the simulation of pushing a load of 32 kN in front of the vehicle such as that incurred by a blade. The final loading cases included a combination of both pushing and carrying simultaneously.

The loading conditions analyzed showed stresses and deflections to be within acceptable limits; however, thermal loads and several other loading configurations need to be investigated to finalize the design.

LOCOMOTION SYSTEM

Wheeled, walking beam, and track systems were considered initially as locomotion systems for the LCUV. The walking beam was eliminated due to mechanical and control complexity. Wheeled systems were discounted in favor of tracked systems due to limited surface contact area, since surface contact area is vitally important under heavy load conditions.

In the past there has been criticism of tracked systems due to the high number of mechanical parts; however, this design, based on Lockheed's Elastic Loop Mobility system, eliminates much of that criticism.

The tracks incorporated into this design are an elastic loop design that features one continuous elastic loop in place of a conventional multipiece track. Much of the suspension load is taken up by the elastic loop, minimizing the overall number of suspension parts. The drive drum for the elastic track system houses a DC motor that turns the drum via a planetary gear set. The drive drum is essentially a large spur gear in which the gear teeth transfer motion to the track via equally spaced drive lugs. The brushless DC motors that are installed inside the drive drums can be removed easily by accessing an external cover plate. A centrally located frame structure connects to the drive drum by a pivoting plate that is also used to support a tensioning device located over the top of the elastic loop. A set of shock absorbers absorb road shock. For ease of maintenance and to obtain variable track surface contact angles, a single pin connection will attach each track to the LCUV body. In this way the LCUV robotic arm can disconnect a damaged track by releasing a single pin. A frictional damping shock is attached transversely between frame and track by jointed ends to absorb horizontal track shock. The elastic loop track with single pin connection offers a very simple design that is easy to maintain yet covers a large surface contact area.

CONSTRUCTION PACKAGE

The construction package will utilize two mechanical arms that are derivatives of the Shuttle Remote Manipulator Arm System (SRMS) technology. There will be three booms totaling 50 ft in length with three degrees of freedom. They will utilize an electrical actuation system using DC brushless motors to provide virtually maintenance-free actuation. Since the initial construction tasks are to be telerobotically controlled, all motions of the mechanical arm must be fully predictable. To accomplish this continuous path, servo control will be implemented.

The three basic continuous path controls that will be used are as follows:

Conventional servo control. This control uses no information about where the path goes in the future. The controller may have a stored representation of the path it is to follow, but to determine the control signals to the arm's DC motors, calculations will be made based on the past and present tracking error.

Preview/feedforward control. This control uses some knowledge about how the path changes immediately ahead of the robot's current location. This is in addition to the past and present tracking error that will be used by the servo controller.

Path planning/trajectory calculation. This control involves using an available description of the path the manipulator should follow from one point to another.

There will be several attachments to the end effector of the robotic arm that will aid in construction. A one-cubic-yard bucket will attach to the end of the manipulator arm and be utilized for digging. The bucket design was chosen to minimize horizontal forces that are present on front-end loaders. Heavy lifting will be accomplished by specialized end-effector clamps and a cable-hook system. For site preparation there will be

front-end attachments consisting of grading blade, tiller, and roller.

Preliminary design analysis has shown the manipulator arm to be one of the most challenging aspects of the LCUV design. Clearly, more effort is required to finalize the design. The most difficult task that needs to be addressed is that of heat dissipation of the large DC brushless motors that are utilized. A combination of both passive and active thermal control must be used to remove excess heat loads. Preliminary design analysis indicated that the manipulator arm structure can serve for heat dissipation purposes. The drawback of this concept is that a major redesign of the existing structure must take place. On the other hand, the structural design of the manipulator arm must change to allow the large loading that will be experienced in the presence of lunar gravity. This has yet to be addressed.

POWER SYSTEM

The power required for the LCUV is derived from rather arbitrary yet meaningful constraints. A worst case scenario has been developed in which the vehicle must operate. A maximum vehicle speed of 2.4 m/sec is used, which accounts for the time delay of telerobotic operations from Earth. Also, in the event an LCUV gets caught in very "weak" soil, a maximum slippage of 30% should be tolerated. Finally, if an LCUV should become disabled, a separate LCUV should be able to tow the disabled vehicle up a 30° slope.

The following list estimates the total system power requirements.

- Propulsion:
  4-10 kw Brushless DC Motors, 90% efficiency
  Maximum load: 35 kw

- Manipulator Arm:
  (Based upon 5 × SRMS)
  Maximum load: 20 kw

- Housekeeping:
  Communications controls, coolant pumps, etc.
  Maximum load: 2 kw

In designing this power system, several goals were identified. The system should have inherent high power and high energy density, low maintenance, long life, high reliability, and the ability to operate in the lunar environment.

With this in mind, several power sources were considered, i.e., batteries, photovoltaic cells, radioisotope generators, and fuel cells. Photovoltaics and batteries were eliminated due to weight and space limitations and due to the length of the solar night. Radioisotope systems require additional shielding mass for man rating, and the environmental effects are not known. On the other hand, fuel cell technology offers a high power-to-weight ratio. It is safe, reliable and a fully developed space technology. Of the number of types of fuel cells in use, an alkaline Raney-nickel hydrogen/oxygen fuel cell was chosen for the LCUV design. This material was selected since it is relatively inexpensive, has high mechanical strength and is a highly active nonnoble metal catalyst. There are several areas that need to be addressed that are also areas for further research. One concern is the effect of the temperature extremes on a nonactive fuel cell. Secondly, an effective heat rejection technology is required for fuel cells operating under full load.

NAVIGATION AND COMMUNICATIONS

The basic configuration of the navigation and communication systems are shown in Fig. 2. All subsystems feed information to two parallel redundant central processing units. Each central processing unit is outfitted with analog-to-digital (A/D) and digital-to-analog (D/A) converters, and power conditioning interfaces. The lunar base receives the Earth-based FM signals through a Cassegrain parabolic antenna that relays the signal to a Yagi-Uda omnidirectional antenna mounted on the LCUV. The CPU interprets these signals and sends the proper control commands to the respective subsystems. Physical feedback, i.e., position, velocity, and visual data, are transmitted back to Earth-based operations. During the initial phases of base construction, the LCUV will be required to perform many complex communication commands and control tasks without astronaut assistance. Some of these tasks include navigation between lunar lander and lunar base sites, mapping the lunar base and augmenting the map during base construction, control of the manipulator arm for positioning and assembling of lunar base modules and connectors, unloading the lunar lander, and controlling the regolith handling equipment for site excavation, preparation, and construction. The control system must monitor the state of the LCUV, compensate for environmental changes (i.e., temperature, radiation, and terrain), and manage system data. To accomplish these tasks, the LCUV requires a very complex navigation and control system. Currently, two techniques have been investigated for navigation and control of the LCUV. They are telerobotic and semi-autonomous control.

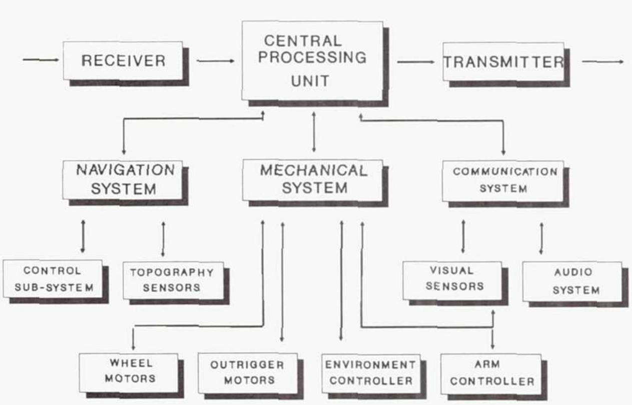

Fig. 2. Block Diagram of Navigation and Communications Systems

A telerobotic LCUV uses a technique called Computer-Aided Remote Driving (CARD) for navigation and control. This concept requires a direct Earth-to-LCUV communications link and possibly an orbiting relay satellite. Using state-of-the-art camera equipment, the LCUV transmits a stereo picture of the vehicle's forward view back to Earth where the picture is analyzed by a vehicle control operator. From these pictures, direction and distance commands are transmitted to the vehicle to provide for a safe path of travel. In case of transmission problems, the commands can be repeated. The path designated by Earth command is carried out by stored on-board computer programs that control the motors and actuators of the mobility system. Other functions such as regolith handling, material handling, and base module assembly are performed by Earth operators through the use of CARD. Thus, operators control both regolith handling equipment and manipulator arms by viewing a monitor that receives the picture from cameras located on the LCUV.

Some advantages of the telerobotic LCUV are (1) possibility for Earth command to directly control the vehicle; (2) more flexibility for controlling and navigating the LCUV during complicated base construction; and (3) less need for navigation sensors or controls.

Disadvantages of the telerobotic system are (1) time delay of 3 sec between the transmission and reception of signals; (2) need for the vehicle operator to analyze the data on the monitor before sending commands, thus adding to the time delay; (3) need for dedicated personnel to operate the vehicle; and (4) difficulty with depth perception at times other than sunrise and sunset.

The semiautonomous system requires knowledge of surface terrain to perform its tasks automatically. A global map of the lunar terrain can be provided from an orbiting satellite that photographs the lunar base area. The LCUV analyzes the surrounding terrain through an LCUV camera for local path planning. Given a destination, the LCUV compares the camera view to a global map to plan a safe path towards its destination. The LCUV proceeds along its planned path without Earth command intervention unless the LCUV cannot plan a safe path or is abruptly deviated from its path (i.e., unforeseen holes, extremely soft soil, steep cliff, etc.).

On the plus side, this system allows mapping of the lunar terrain during base construction. If need be, the map may be revised. Programmable capabilities allow for repetitive operations that do not require dedicated personnel to operate.

Its disadvantages include the need for extensive programming to allow the vehicle to perform operations, artificial intelligence to process camera pictures, and extensive navigation and control routines.

An LCUV equipped with both the telerobotic and semiautonomous features could more readily meet mission requirements. The advantages of the semiautonomous LCUV offset disadvantages of the communication cycle time, night operation, and repetitive tasks. On the other hand, telerobotic operation allows for additional flexibility in handling complex tasks and operations, possibly reducing the complexity of converting the LCUV to a human-operated machine. Therefore, it is concluded that the combination of both techniques will fulfill the requirements of the LCUV.

THERMAL CONTROL

Thermal control is accomplished by the use of a relatively thin, flat primary radiator panel and towable secondary panels. The panels feature two active sides and are constructed from 6061-T6 Aluminum alloy. They will be coated with a highly reflective zinc-oxide pigment and measure 4 ft wide by 10 ft high. Ethylene glycol will be pressurized to 1 atm and circulated to the fuel cells, DC motors, robotic arm, and to the electronics section. The primary radiator panel is oriented with its length extending upward and with its active sides radiating from the sides of the vehicle. It is positioned in the center along the rear edge of the vehicle to allow a maximum working envelope for the robotic arms. During peak loads, the secondary or auxiliary radiator panels will be required due to the additional heat generated by the DC motors. The details of extracting these heat loads from the motors is a technology that needs to be further developed.

CONCLUSIONS

In the development of a robotically constructed lunar base, a telerobotic, semiautonomous construction vehicle will play a vital role. This preliminary design utilizes available technology and indicates that a practical design is feasible. Two areas where current technology needs to be developed are the integration of structural and heat transfer elements as in the manipulator arm and the development of DC motors with heat transfer capabilities. This design, conceptual in part, did not go into the details to the extent of developing overall mass estimates with accuracy. The dual-arm, multiple-end effector design allows for a variety of tasks to be accomplished including unloading of base modules and regolith handling. The single loop elastic track with single pin connection and drive motors mounted inside the drive drum provides for a locomotion system that is simple and easy to maintain. This project will continue for another year with the goal of developing more fully the concepts presented herein.

ACKNOWLEDGMENTS

The authors wish to thank Dr. O. Gonzales and Dr. J. Hibey of the Old Dominion University Electrical and Computer Engineering Department for their help in the area of navigation and communications; Mr. B. Hobson Shirley of Lockheed Missiles and Space Company's Huntsville Research and Engineering Centers, and the senior mechanical engineering students of Old Dominion University, spring class of 1989.

Principal authors were C.A. Bryant, graduate teaching assistant, D. Alcorn, R. Bentley, B. Campbell, T. Coulson, J. Jacobs, and P. Stiles. Chairman and faculty advisor was Professor R.L. Ash.

REFERENCES

1. Davis G., "The Lunar Split Mission: A Robotic Constructed Lunar Base Scenario," NASA/USRA Advanced Space Design Report, August, 1988.
2. Fairchild K. and Mendell W. W., "Report of the In Situ Resource Utilization Workshops," *Workshop Proceedings,* United Technolo-

gies Corporation, NASA Conference Publication 3017, Lake Buena Vista, Florida, 1987.
3. Trautwein W., "Design, Fabrication and Delivery of an Improved Single Elastic Loop Mobility System," Lockheed Missiles and Space Co., Executive Summary Report, NASA-CR-123840, June 1972.

N94-71285
382696
19940004530

MARS SURFACE-BASED FACTORY: COMPUTER CONTROL OF A WATER TREATMENT SYSTEM TO SUPPORT A SPACE COLONY ON MARS

PRAIRIE VIEW A&M UNIVERSITY

S18-54
160644
P. 6

In a continued effort to design a surface-based factory on Mars for the production of oxygen and water, the Design Group at Prairie View A&M University made a preliminary study of the surface and atmospheric composition on Mars and determined the mass densities of the various gases in the martian atmosphere. Based on the initial studies, the design group determined oxygen and water to be the two products that could be produced economically under the martian conditions. Studies were also made on present production techniques to obtain water and oxygen. Analyses were made to evaluate the current methods of production that were adaptable to the martian conditions. The detailed report (Phase 1—Mars Surface-Based Factory: A Preliminary Design) was contained in an Interim Report submitted to NASA/USRA in August of 1986. Even though the initial effort was the production of oxygen and water, we found it necessary to produce some diluted gases that can be mixed with oxygen to constitute "breathable" air. In Phase II—Task 1A, The Prairie View A&M University team completed the conceptual design of a breathable-air manufacturing system, a means of drilling for underground water, and storage of water for future use. The design objective of the team for the 1987-1988 academic year (Phase II—Task 1B) was the conceptual design of an integrated system for the supply of quality water for biological consumption, farming, and residential and industrial use. The design has also been completed. Phase II—Task 1C is the present (1988-1989) task for the Prairie View Design Team. This is a continuation of the previous task, and the continuation of this effort is the investigation into the extraction of water from beneath the surface and an alternative method of extraction from ice formations on the surface of Mars if accessible. In addition to investigation of water extraction, a system for computer control of extraction and treatment was developed with emphasis on fully automated control with robotic repair and maintenance. It is expected that oxygen- and water-producing plants on Mars will be limited in the amount of human control that will be available to operate large and/or isolated plants. Therefore, it is imperative that computers be integrated into plant operation with the capability to maintain life support systems and analyze and replace defective parts or systems with no human interface.

INTRODUCTION

The Design Group at Prairie View A&M University designed a computer control system for a water treatment plant to support a colony on Mars. The system was developed with emphasis on fully automated control, and robotic repair and maintenance. It is expected that the water-producing plant on Mars will be limited in the amount of human control that will be available to operate the plant, so computers must be integrated into plant operation with the capability to maintain the water system and analyze and replace defective parts or systems with no or limited human interface.

Also methods to extract water from beneath the surface of Mars were investigated. It is believed that water exists on Mars in polar ice deposits and in permafrost layers (ground ice). There is also evidence that water exists underneath the permafrost zone. The Prairie View Design Team is investigating ways of extracting and treating the water for human consumption and protein production. To carry out the described task, teams were formed to investigate and design necessary equipment and implementation procedures for the four areas of drilling for water, plant control, computer interface, and maintenance. Continuation of this project will be the production of proteins for human consumption. This continuation will be for the 1989-1990 academic year.

DRILLING FOR WATER

The success or failure of any attempt to colonize Mars will largely depend on the availability of the most important life sustainer, water. Not only is water important for life but also any meaningful self-sustained technological advancement on Mars will be based on water as a process fluid. It is therefore imperative that every attempt be made to locate adequate supplies of water on Mars.

Mars is presently too cold to support oceans or any form of stable liquid water on its surface. Mars' mean ambient temperature is -25°C. It is believed that there are ice deposits or permafrost beneath the surface of Mars. The thickness of the zone containing ground ice is about 10 to 30 cm. More water may exist underneath the permafrost zone.

In order to accurately assess the amount of water on the planet, some form of drilling must be done to establish the existence of water on Mars. The study of the composition of the martian soil is very important in determining its drillability. A survey of the martian soil conducted through the exploration by the Viking landers found that the soil is composed of different elements such as silicon, iron, phosphorus, calcium, aluminum, thallium, and sulfur. The debris analyzed by the Viking landers showed silicon oxides in abundance of approximately 45% by weight.

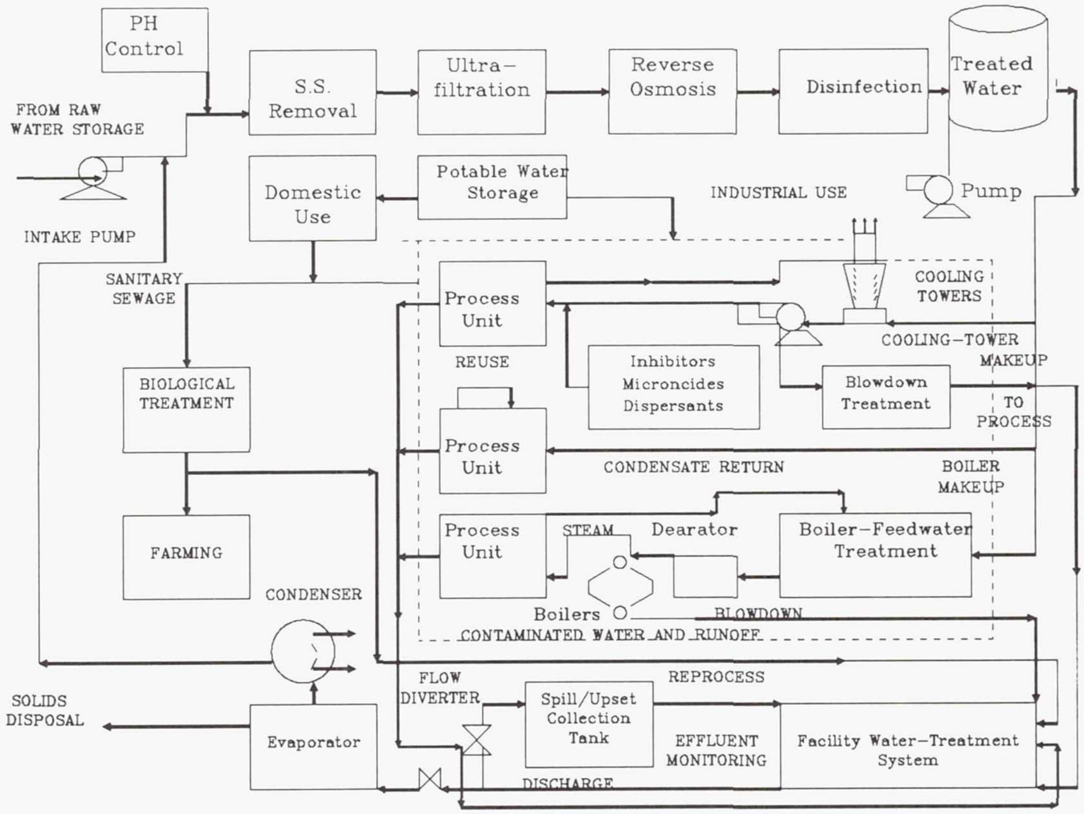

Fig. 1. Simplified Plant Water Circuit

One other important factor to consider in the design of the drilling unit is the drilling rate. The drilling rate is a function of several variables, the most important of which are the rock drillability, the weight on the bit, and the extent of cleaning the hole. The effect of the weight on the bit is of great importance to our design since the gravity on Mars is substantially less than that on Earth.

The drilling process will involve boring a hole by using a rotating bit to which a downward force is applied. The bit is supported and rotated by a hollow stem composed of high-quality steel, through which a drilling fluid is circulated. The fluid leaves the stem at the bit, thereby cooling and lubricating the cutting structure. By flowing across the cutting surface, the drilling fluid drags cutting from the hole stem annulus. This process formed the basis for the design of the drilling unit.

PLANT CONTROL AND COMPUTER CONTROL

The integrated water treatment plant consists of several processes, such as a suspended solids removal unit, ultrafiltration unit, and reverse osmosis unit, (Fig. 1), that have parameters that need to be monitored or controlled. These parameters include flow rate, temperature, pressure, and conductivity. Therefore, devices such as sensors, transmitters, and control valves must be employed.

To facilitate automated control, a personal computer would be used to maintain and run the entire water system. The electronic sensors, transmitters, and control valves, along with analog-to-digital and digital-to-analog converters, will communicate with the personal computer, an IBM PC. Through the use of one or more microprocessors, RS-232 serial cables, analog-to-digital converters, and/or fiber optics, the above devices will be integrated. By using an external bus product, we can configure virtually any size system, the system can be placed close to the field signals, and the system can off-load some of the data-collecting task from the host computer. Figure 2 shows a simplified block diagram of how the data acquisition and control system will communicate with its host computer. Communication through RS-232 requires the data acquisition system to have its own internal microprocessor. This local microprocessor also facilitates remote operation and helps achieve the reduced load on the host personal computer. The system will be a box that contains space for the microcomputer, power supplies, and analog and digital input/output hardware. The microprocessors that were investigated are the Intel 8088, Motorola 68000, and the Zilog Z80.

The Intel 8088 microprocessor was chosen because it is used with the IBM PC and because of a large availability of software on the market. The Intel 8088 is a 16-bit microprocessor with an 8-bit memory bus. Its instructions are

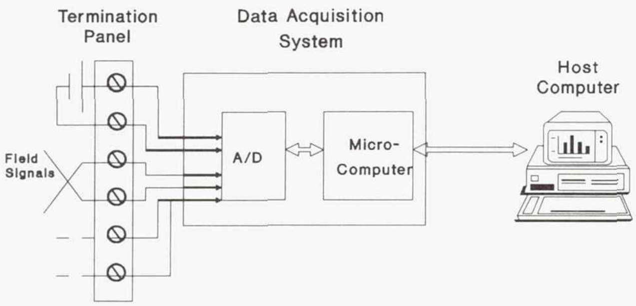

Fig. 2. External Bus DA&C System

fetched and written to memory 8 bits at a time. The 8088 has the ability to address up to 1 megabyte of memory, which can contain either data or programs. The 8088 will also support the functions of interrupts and direct-memory access. These are of particular value when interfacing to the PC.

In the PC implementation, the clock circuit of the 8088 is run at a clock rate of 4.77 MHz. This results in a system clock time of approximately 210 nanosec. Since most bus cycles are 4 clock cycles long, a typical memory cycle in the PC is 840 nanosec long.

The major functional components of the system board are tied to the 8088 microprocessor by the system bus. This bus is made up of several types of signal lines: data bus, address bus, control, timing, interrupt requests, and direct memory access control.

The 8088 microprocessor is a derivation of the Intel 8086 microprocessor, with the major difference being the data bus width. The 8086 has both an internal data path of 16 bits and an external memory data-bus width of 16 bits, whereas the 8088 has an internal data-path width of 16 bits but its memory interface is only 8 bits.

Some of the highlights of the 8088 microprocessor are 16-bit internal architecture; supports 1 megabyte of attached memory; 8- and 16-bit signed and unsigned arithmetic in both binary and decimal notation, including multiply and divide; 14 words of 16-bit registers; maskable and nonmaskable interrupt capability; 24 operand addressing modes; direct memory access capability; and supports on local bus co-processors[1].

The transducer is the most vital element in the data acquisition and control system, which must be able to handle a variety of field signals. This device is the link between the physical and electrical world[2]. When the signal is sent from the plant, the first element it reaches will be the transducer. Data acquisition and control involves both input and output signals. Input signals can represent temperature, flow, displacement, speed, level, and pH. The electrical equivalents produced by input transducers are most commonly in the form of voltage, current, charge, resistance, or capacitance. In order for the data acquisition and control system to operate, these signals will have to be conditioned and converted to a voltage signal.

Analog signals will be transformed into a digital representation by the systems analog-to-digital (A/D) converter. When analog outputs are required, they will be generated by the system's digital-to-analog (D/A) converters.

The purpose of the A/D and D/A converters will be to interpret the analog signals being sent from the sensors and convert them to digital signals to be analyzed by the computer. If an adjustment needs to be made within a process, the computer will send a signal to a valve (actuator) to make the proper adjustment.

Analog inputs usually come from some type of preamplifier where the primary sensor signal has been conditioned and amplified for presentation to the data acquisition system. Most preconditioned signals are of a relatively high amplitude, in the range of ±1 to ±10 V. However, many primary sensors, such as thermocouples, photovoltaic cells, piezoelectric sensors, and biomedical sensors, produce small signals that may have a full scale range of only 10 mV. A quality data acquisition such as this will be able to handle both high- and low-level signals with equal ease and accuracy.

Signal conditioning may be considered as comprising all those operations that are ancillary to the functioning of the transducer itself, and that are necessary in order to extract a signal from it related to the physical quantity being measured. Figure 3 shows a block diagram of the signal conditioning process. There are two categories of signal conditioning. Active signal conditioning includes amplification and isolation, and passive signal conditioning includes voltage division, surge suppression, current-to-voltage conversion and filtering.

The maximum signal amplitude that can be applied to an amplifier or A/D converter is usually ±10 V. In order to scale voltages down to this level, a resistive divider can be used. Scaling voltages down is a very important function of the signal conditioning process because if signals greater than 15 V were sent to the components of the data acquisiton and control system, the electronic components would be damaged.

Of all the categories of signal conditioning, filtering is the most widely needed and used. Filtering is used to separate desired signals from undesired signals. Undesired signals include noise, AC line frequency pick-up, and signal frequencies above half the sampling frequency. The low pass filter is

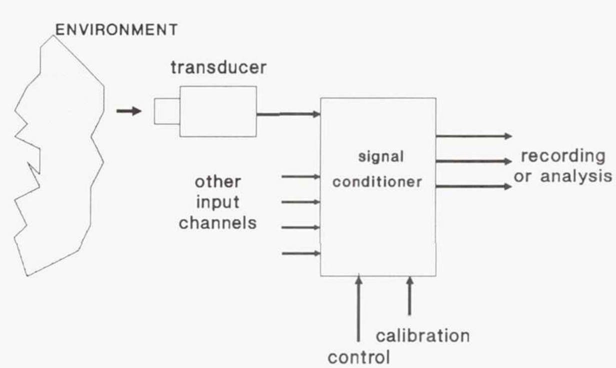

Fig. 3. Signal Conditioning Process

generally used to control these unwanted sources of error by excluding the portion of the frequency spectrum where desired signals do not exist.

Signal conditioning can be physically installed at a number of locations, including at the signal source, at the input to the amplifier, at the A/D, etc. The most convenient and hence most common location is on the signal termination panels.

In order to communicate with a digital computer, signals must be in a suitable format. Most real world signals are analog signals. Because these signals cannot be readily accepted by the computer, they must be converted. It is the data acquisition system that performs this conversion. Internal to the data acquisition unit, there is a variety of data acquisition components that facilitate the translation operation. These include A/D and D/A converters, multiplexers, sample/holds, amplifiers, counter/timers, and some specialized functions.

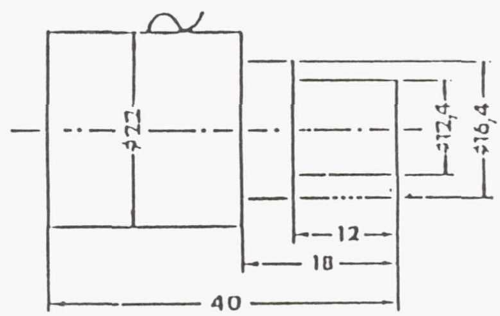

Fig. 5. Sample Work Piece

MAINTENANCE

The initial habitation of Mars will require machining and maintenance for space applications. Machining and maintenance on Mars is complicated due to the following factors: the absence of atmosphere, light is not diffused or scattered, the natural space environment consists of intensive light and dark periods, few people, and the lack of machining parts. The factory communication network system consists of an industrial microcomputer cell control, computer interface units, a robotic controller, vision, and a computer numerical control machine (CNC lathe)[3].

Robotics for space applications have been proposed for increased productivity, improved reliability, increased flexibility, higher safety, and for automating of time-consuming tasks. If a malfunction takes place within the system, it takes almost 20 minutes to receive a signal from Earth. This signal instructs the machine on how to recover from the fault, so it is necessary to have an emergency plan that can start automatically right after the shutdown of the plant.

Vision/sensing is projected to include the fusion of multisensors ranging from microwave to optical with multimode capability to include measuring capability for position, attitude, recognition, and motion parameters[4].

The objective of using a CAD/CAM system on a CNC lathe machine is to produce machine parts on Mars instead of loading parts on board a mission, and it is planned to modernize the CNC lathe by developing a software system on a personal computer. The CAD/CAM system is able to take all the data from design programs and convert the information to numerical control (NC) programs that are used on the CNC lathe.

The design programs are written in BASIC language on a personal computer. The CAD/CAM software system is developed in FORTRAN language. By using software packages, the need for punched tape for the CNC lathe and blueprints of the design drawings are eliminated. As a result, the complete automation from design to manufacturing for the CNC lathe is achieved. The sample design program is shown in Fig. 4, the sample of a manufactured work piece is shown in Fig. 5, its horizontal tool-path cutting is shown in Fig. 6, and its NC program is shown in Fig. 7.

The computer graphics method using BASIC to generate CNC program offers the following advantages:

1. It is safer. A problem, such as the cutting tool colliding with the chuck of an engine lathe, would provide a genuine hazard to a user trying out a CNC program. With the CAD/CAM program, the problem is eliminated.

2. It is economical. Besides saving all the scrap work that would have been produced in the actual situation, CAD/CAM program allows the limited machine tools to be utilized.

3. It is psychologically more satisfying. The major advantage of using this CAD/CAM system is to generate a CNC program[5].

```
10 'PIECE OF IRON
20 SCREEN 1,0 :CLS: KEY OFF: DEFINT A-Z
30 LINE (48,39)-(132,39), 1
40 LINE (48,39)-(48,121),1
45 LINE(48,121)-(132,121),1
50 LINE (132,39)-(132,121),2
60 LINE (132,50)-(155,50),2
70 LINE (132,110)-(155,110),2
80 LINE (155,50)-(155,110),2
90 LINE (155,57)-(199,57),3
100 LINE (155,57)-(199,57),3
110 LJNE (155,103)-(199,103),3
120 LINE (199,57)-(199,103),3
122 LINE (132,39)-(132,50),1
124 LINE (132,121)-(132,110),1
126 LINE (155,110)-(155,103),1
128 LINE (155,50)-(155,55),1
130 LET X1=48 : X2=199
140 LET Y=80
150 FOR I=X1 TO X2 STEP 21
160 LINE (I,Y)-(I+10,Y),1
170 LINE (I+15,Y)-(I+16,Y),2
180 NEXT I
190 END
```

Fig. 4. CNC Lathe Program

RECOMMENDATIONS FOR FUTURE RESEARCH

The following are recommended areas for future development.

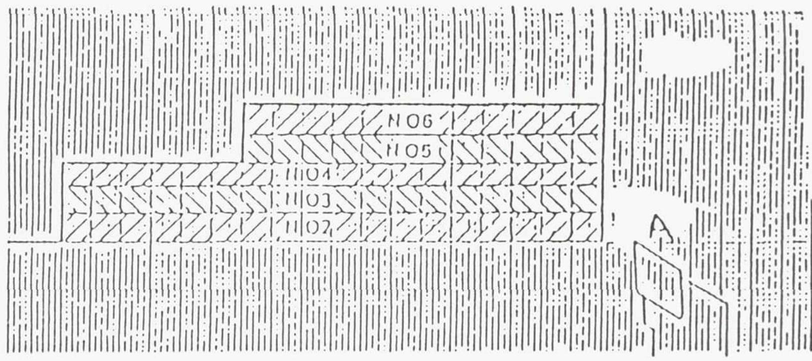

Fig. 6. Horizontal Tool-Path

1. Develop the CAD/CAM software package of the CNC lathe for threading operation.
2. Comprehend all errors and malfunctions that can take place between the personal computer and the CNC lathe.
3. Test the system by a set of design programs to produce mechanical parts.
4. Design a plant prototype with simulation of all system parameters.
5. Study the martian moon, Phobos, as an alternate source of water.
6. Raise fish on Mars for life support.

ACKNOWLEDGMENTS

Design group members were R. Brice and J. Mosley, Drilling; D, Willis, K. Coleman, C. Martin, and L. Shelby, Plant Control; U. Kelley, E. Renfro, and G. Griffith, Computer Control; A. Warsame, O. Davis, and T. Harrison, Maintenance, Project advisor was Dr. John Fuller.

REFERENCES

1. Eggegrecht L. C., *Interfacing to the IBM Personal Computer,* Howard W. Sams & Co., Indianapolis, Indiana, 1983.
2. Beauchamp K. G. and Yuen C. K., *Data Acquisition for Signal Analysis,* George Allen and Unwin, London, 1980.
3. *EMCO-5 CNC Lathe Manual,* pp. 4-39, Fabrik fur Spezialmaschingen, Emco Maier & Co., Friedman Maier Strasse 9, Hallein, Austria, 1982.
4. Krishen K., "Space Robotic Vision System Technology," *Proceedings of the ISA 88 International Conference and Exhibit,* pp. 1527-1537, Houston, Texas, October 16-21, 1988.
5. Ali W., "Development of a CAD/CAM System on An EMCO-5 CNC Lathe," p. 22, Master's Thesis, Prairie View A&M, 1988.

N	G	• X (BLU)	Z (BLU)	F (mm/min)
00	00	-300		
01	01	00	-600	
02	84	-100	-1900	600
03	84	-200	-1900	600
04	84	-280	-1900	600
05	84	-380	-1300	600
06	84	-480	-1300	600
07	22			

BLU=0.01 mm

Fig. 7. NC Program for Tool-Path

N94- 71286

J19-54
160645
P. 12
1994004531
382692.

CAMELOT III: HABITABILITY CRITERIA

SPACE RESEARCH AND DESIGN STUDIO

SCHOOL OF ARCHITECTURE
UNIVERSITY OF PUERTO RICO

RATIONALE

Acknowledging the importance of human beings on a mission to Mars, the University of Puerto Rico studied both psychological and physiological aspects. Different conditions necessary for human health and well-being were considered. As a result, habitability criteria were developed.

When we speak of habitability, we refer to the state of equilibrium that results from the interaction between the components of the complex "individual-architecture-mission," that allow the person to sustain physiological homeostasis, adequate performance, and acceptable social relationships.

On several occasions the relation of "man-machine-mission" has been referred to as the system that governs actions in space travel. Probably that has been the dynamic within the missions accomplished thus far. However, the mission should not be conceived as a "great machine" that is to be expected to perform an assignment, because humans are not machines, but living beings who react positively or negatively according to the environment that surrounds them. For this reason they should not be treated as objects or pieces of a system, but rather as key figures within it, in keeping with the objectives of the mission, acknowledging the physical and technical aspects that must be taken into account in space travel. This could be compared to a "bee hive" (colmena) that scientists describe as a "living organism" in the whole, because of the mutual dependency and interaction among each of the components of the "colmena." Ultimately it is not possible to really conquer space if the appropriate means are not attained to make it possible for humans to develop there, beyond the level of mere survival.

Thus, architecture as an art-discipline of creation of environments that promote good physical and psychological performance for humans, whatever their needs or activities, must be recognized for its primordial role in the design of the vessels that will become the habitats of space travelers, especially those who will stay there for prolonged periods. Obviously the success of such a mission will be highly influenced by the quality of the architectural design of such a habitat.

It should be pointed out also that the environment in these travels will be made up by the physical (material and technological) parts of the vessel and by the nonphysical and psychological aspects that must harmonize and complement each other. That is, in order to develop the design of the physical habitat, first the nonphysical and psychological aspects of the environment to be created for prolonged travel in space must be studied, to identify and reinforce those desirable conditions that are found, and to repress or eliminate completely those negative aspects that may come out. This endeavor will allow the designer to stay within a correct frame of reference or context, which will guide him as he develops architectural form and as he makes design decisions.

After studying psychological conditions and physiological effects associated with prolonged space travel, we have established a list of intangible psychological aspects that must be considered in the architectural design process to create a realistic physical environment that is to be a positive contribution to the quality of life—not mere survival—of space travelers. These we have called habitability criteria, which later on will be tested or better yet, demonstrated in the architectural development of a specific habitat.

HABITABILITY CRITERIA

In the design of habitats for prolonged space travel the following must be considered:

1. *Personal identification.* Travelers in space actually realize they cross the threshold of space, leaving the Earth behind, as soon as the environment and everything they sense become unfamiliar. From writings and expressions of astronauts and cosmonauts we have learned that they refer to the immediate physical surrounding envelope to establish a sense of identity and relationship to ensure security and as much comfort as possible within such a new, strange, and hostile environment. Many space travelers have expressed their sense of alienation within the surrounding envelope, but also have developed a "sense of belonging" as soon as they are within the vessel. To satisfy such a need, habitable places must be able to be "personalized" with objects and arrangements of family photos, souvenirs, etc. Some degree of flexibility in furniture and equipment arrangement within the specific area in which each traveler is to relate to as his/her dwelling place is also advantageous.

2. *Social interaction.* To be able to share and to feel the presence of others seems to be very important in prolonged space travel. The sensation of knowing companions are nearby promotes a sense of security, of not being alone, and of mutual confidence and trust among travelers. Therefore, it is necessary that within the vessel there be areas designed in such a way that they promote positive group dynamics and good social interaction, since to a great degree that will enhance the inhabitants' sense of being humans.

3. *Unpredictable conditions.* Many of the astronauts and cosmonauts who have had the experience of prolonged stay in space have expressed their profound appreciation for positive surprises, whenever they would find something new, something unexpected that was nonthreatening, or something

PRECEDING PAGE BLANK NOT FILMED

PAGE 144 INTENTIONALLY BLANK

was discovered from a hidden condition. There is a deep need to escape routine and tedium. Elements of surprise were incorporated in many special occasions to celebrate and commemorate events, seasons, birthdays, holidays, and anniversaries. In such a confined lifestyle one begins to understand the necessity of major and minor festivals to enhance the liturgical acts of ordinary days. This suggests that besides the specific required areas in the architectural program of the vessel there must be allowed to exist areas without a specific or rigidly defined use, or better yet, areas of universal use that could change surprisingly according to the festivity. On the other hand, elements within the design of the vessel (ceilings, walls, "windows") could be programmed to change unpredictably to impart a sense of variety within the habitual routine of having to live in a very confined envelope. After billions of years of development in the "terrestrial vessel," humans have learned to consider it a punishment to constrict themselves to an unchanging restricted environment. Here it should be viewed, rather, as a protective, friendly, and motherly womb, capable of sustaining as well as entertaining human life in a style of quality.

4. *Contact with nature.* It must be understood that the environment in such missions has two additional key elements: the individual and the architectural. It is necessary to create a system that would maintain equilibrium between them. In such a relationship the greatest contrast exists between the person and the machine-artifact, which we have called "architecture," of the enveloping vessel. For billions of years humans have developed relating to a "natural" environment that is not an artifact or a machine. Thus, prolonged space travel will put humans in a completely artificial relationship with nature, which is important to consider. A different sense of "indoors" and "outdoors" must be developed. Even though it is important that the surrounding universe be perceived through windows that permit vision beyond the limits of the vessel, it is also important, even within such limits, that contact with natural objects be kept and promoted. This contact with nature could be attained through the presence of plants, animals, or aquariums, which may or may not be part of the environmental life support system of the vessel. Besides the scientific value that such a contact may have, it has the practical value of the pleasure and enthusiasm that it gives the travelers as they work with and observe the natural processes taking place: growth, blooming, harvesting, and all the natural processes of life. A great fascination and enjoyment has been reported by astronauts and cosmonauts as they got involved in the observation of such processes that entail changes from the routine. It seems to be a very enjoyable and important contact that can also be coordinated with the life support of the vessel.

5. *Mental landscapes.* When in the study of psychology reference is made to enclosed spaces, such as we find in vessels traveling in space, they are called "acute places." It is important that these acute places contain symbolic elements that would evoke diverse memories and sensations. This is termed "a mental garden." Such gardens and even landscapes help a person to transcend his or her immediate physical reality through images, photos, forms, spatial sensations, colors, textures, and materials.

6. *Privacy.* Even though positive group dynamics must be promoted, and a lot of social interaction between passengers on such vessels should be encouraged, a certain degree of privacy should also be provided. Lack of privacy has been demonstrated to be the most irritating factor to humans in confined and restricted environments. This is true of every culture, although it varies to the degree in which the extension of personal space or territorial dominion is and has been expressed in history and in different socioeconomic strata. It seems reasonable and important as well to assign to each person traveling on the vessel an area that can be made "private," that he or she could call his or her own, so that he or she could arrange and accommodate to a certain degree to his or her taste, needs, or will. Once this is established then the question is how large or how much area is adequate for fulfilling the need for privacy of a person traveling for prolonged periods in space?

This is a difficult question, since its answer is dependent on culture, sex, age, duration of the mission, and the general background of travelers in the vessel. Previous studies such as that published by the architectural firm of Warner, Burns, Toan and Lunde (New York) have concluded that the minimum acceptable volume for a dormitory would be 350 cubic feet. That is approximately the cubage generated by an erect human figure with arms extended.

7. *Equalitarian conditions.* Research performed in Antarctic stations regarding social behavior tend to disfavor strict hierarchical systems of personnel. Such stations were originally organized in strict rank hierarchies of personnel. Later the system was relaxed and emphasis was placed on purpose, rather than rank. Interpersonal relations became more relaxed, group morale was boosted, and group work became easier and more productive. Research by Warner, Burns, Toan and Lunde showed that even though social dynamics vary, a space station would work better under equalitarian conditions among crew and passengers rather than strict hierarchical ranking orders. Architecturally this could be reflected, for example, in the quality, size, and location of the rooms of the travelers. Differences should reflect purpose and functions, as well as individual preferences, rather than rank or hierarchy.

8. *Variety.* Psychological studies suggest that similar elements and repetitive features in the interior of an acute place are boring, and cause irritability and environmental stress. It is important that in the habitable places of the vessel there be a degree of variety in elements, shapes, furniture, partitions, decor, and color.

9. *Functionality.* For a place to be considered "habitable," in the qualitative sense, it must perform well as a dwelling or abode for humans. It must meet physical as well as psychological needs for the sustenance of human life, individually and collectively, supported by all the technical means that aid in the fulfillment of the mission. It must contribute positively to the success of the mission by providing a proper stage or proscenium for the drama of human life to develop appropriately.

10. *Sensory stimulation.* Travelers in space must not be deprived of sensory stimulation. It is fundamental that they have as close to normal and as varied as possible a range of sensory stimulation. Such sensations are the primordial matter

of human experience, and through them the learning process takes place. Surfaces of the vessel should be treated with color, which stimulates the visual sense in a meaningful coding system, as well as texture, which will stimulate tactile sense and would help solve acoustic and friction problems under microgravity. Smells within the vessel must be controlled, since unpleasant odors due to oxidation or other biological processes do not contribute to a positive environment. Food must not only be nutritious, but also should be appetizing to the eye and the sense of taste. The acoustic system should not only guarantee satisfactory communication among the travelers, but also provide for privacy, even in the profound silence of space. Standing waves, flutter echoes, and unpleasant resonances should be eliminated. The atmospheric pressure and gas composition may alter the frequencies in which sound is perceived; thus a voice change will be noticed first, as well as a shift of the musical notes for the discriminating amateur or the professional musician.

11. *Music and environmental sound.* The most critical acoustical problem of the travelers on a vessel moving inertially through space without engines on is that of silence. They would be able to listen to all their visceral movements, would be startled by very minor sudden noise, and would be listening to all the conversations that they may not desire or be entitled to hear. Electronic sound masking and environmental music is a possibility. The air conditioning system could be so designed to produce enough "white sound" to attain a masking effect.

12. *Stability and security.* Stability refers to that tendency or inertia that resists forces that cause motion or distortion. Human reflexes and muscle tone developed in the surface of Earth under normal gravitation will find alien an environment in which there is artificial gravity or a gravitational gradient and a significant Coriolis effect. Thus, the environment must offer means to compensate for the sense of instability and insecurity that will result from being subjected to such conditions.

13. *Comfort.* This includes conditions such as illumination, temperature, humidity, pressure, and atmospheric compositions, which can be accurately determined according to standards that must be objectively applied to the design for the habitable places in the vessel.

14. *Sense of orientation.* In space the sense of up and down as we perceive it on the surface of Earth is absent. In an artificial gravity vessel, up would be toward the center of rotation and down would be away from it. As passengers move toward the center, even that gravity will diminish. The orienting sense of a horizon will not exist and the line formed by the two eyes that provides our sense of stereoscopic vision will become a very subjective personal reference. The architectural design of such places could contribute to reinforce a common sense of orientation for all the travelers rather than ignoring it. It is conceivable that treatment of the surfaces could be such that it would differentiate similar parameters as on Earth, such as floors as surfaces designed to walk on, ceilings as vertical limits of volumes, and walls as work surfaces and area definitions. Colors, texture, light sources, materials, and symbols could order or reinforce an agreed-upon convention, which will create a different sense of orientation to be shared by the travelers.

ARCHITECTURAL DESIGN CONSIDERATIONS

Having established the habitability criteria above, we will use them as a frame of reference or context to develop the habitat for a specific mission and group of travelers on a prolonged stay in space. Architectural design here must translate the habitability interior into a proposal for a physical reality and analyze the following data regarding the mission itself.

Design Factors

Nature of the mission. It is important that the mission objective be restated in terms of its architectural implications, since it is on such a basis that the design process will have its point of departure. The design of the vessel and its habitable places should be done in a way that will promote the fulfillment of the objectives of the mission.

Duration of the missions. Time spent within the interior of the space vessel is a vital component in the understanding of the psychological picture that will arise within the habitat environment. This will serve as guide and context for the design process.

Size of crew and/or number of passengers. This factor will serve as a guide to decide the nature, number, and type of areas and places listed as architectural program requirements for the vessel, as well as its minimum requirements for the vessel and its minimum required dimensions.

Size of the crew and passenger characteristics. The success of a mission in space depends to a great extent on the type of dynamics of interaction that is generated or developed between the sidereal travelers. It is very important to analyze the characteristics of this kind of people, and ensure that the architectural design of the habitable places contribute positively to the development of good group dynamics. For example, group recreation areas, meeting rooms, leisure facilities, as well as individual quarters should take into consideration factors such as age, sex, physical conditions, interests, and purpose of the crew and passengers.

Flexibility for change. There always exists the possibility that the number of crew members and/or passengers can change according to circumstances. Nevertheless, design of the habitable areas, as well as the psychological group dynamics, will place constraints and will limit such a possibility in the design of space vessels.

Gravitational force. It has been demonstrated that the absence of gravitational force in prolonged stays in space promotes deterioration in the physiological and anatomical characteristics of humans, particularly if they intend to return to an environment subjected to gravitational force. Thus, artificial gravity by rotation becomes a must, since physiological conditions will be altered by its presence or absence. In a mission to Mars it may suffice to have 0.4 g by and large, since it will serve as training and conditioning on the travel towards the planet. Therapeutic actions will have to be taken for the returning crew and passengers as they approach Earth. Measures will have to be taken to provide for security and

stability of motion of people due to the presence of a gravitational gradient in every "up" or "down" movement (in or out from the center of rotation) and also in every sideways movement due to the Coriolis effect. The rotation to induce artificial gravity would have to be sufficiently large to offset motion by humans in the opposite direction of rotation so that there is no significant reduction in the centripetal force that creates the gravity effect. The human, being such an adaptable creature, subjected to such conditions for some time, would modify conduct and reflexes in accordance to such an environment. Nevertheless, the architecture should be expected to be of aid in such an adaptative period, as well as the time after the travelers have become familiar with such an alien environment.

Activities. Habitable places must respond to the activities and events in which crew and passengers will get involved during travel. Thus a program of activities has to be developed and the architectural design of the vessel must include a degree of flexibility to satisfy and support such activities.

Technology. Obviously, and in all humility, such vessels cannot be designed by architects. The aerospace engineer, the scientist, and the technician must come into the process before the architect. Specialization must provide the answers to prolonged travel in space before the architectural design can effect its integrating function and the imposition of aesthetic orders, social, psychological, and other quality-of-lifestyle considerations. Space vessels must have operational systems, both interior and exterior, which have a greater priority in the sustenance of life.

ARCHITECTURAL TRANSLATION OF HABITABILITY CRITERIA

Strategies

Having established habitability criteria and the factors that will serve as design parameters for space vessels and their habitable places, we should consider the strategies for developing architectural concepts in such a design process. This way the habitability criteria can be translated from a conceptual to a physical reality. An explanation of the way we conceive such a strategy follows.

Fixed Volumes

When the interior areas or volumes of a space vessel are to be designed, in our case CAMELOT III, it should be decided what type of system is to be utilized in order to define such volumes. The system can use furniture, as well as vertical and horizontal plane divisions (using terrestrial parameters of horizontal, meaning along the circumference of rotation, and vertical, meaning toward the center of rotation, to create artificial gravity). These can be fixed or flexible, modular, or a combination thereof. Whichever option is selected, it must reflect the habitability criterion related to functionality. Nevertheless, each possibility has positive and negative aspects that must be weighted. Fixed volumes provide security and stability, since each area would be designed for a specific use or uses. However, since there would be no flexibility and no possibility of change, this can cause a decrease of motivation and excitement in the travelers and be boring after a while.

Modular Volumes

A system of furniture and vertical partitions that are modular can be utilized to organize the habitable areas of the vessel. All its elements are designed in such a way that forms and dimensions are congruent, but each is potentially capable of existing in formal terms alone or combining with each other to form a greater complex. Such a system requires a coordinated relationship between parts and the total design of the vessel, since the whole and the parts must complement and fit each other. This system can provide certain varied possibilities limited by its inherent characteristics. Thus, according to the manner in which elements are combined, there could be variety in the habitable areas, since configuration could be altered according to design. This type of system fulfills the criterion of variability, as well as that of equalitarian conditions among travelers by providing the potential for all to develop the quality of places. However, the possibility of making changes allows space travelers to rearrange certain areas according to their preference aiding their personal identification with such habitable areas.

Flexible Areas and Volumes

A flexible volume is that which can have its configuration completely altered. This means ceiling heights, movement of walls, movement of furniture, lighting changes, and even use change. Such a system has its advantages, since it reinforces the following habitability criteria: variability, functionality, personal identification, and social interaction. Travelers can program such changes in volume through the use of computers including random variables in order to fulfill the criterion of unpredictable conditions. Floors and walls could be made of a moldable material that could change its configuration at the proper command. If it is decided that the habitable places in the vessel have to be flexible, then rules and parameters must be established to guarantee that the objectives and the mission can be fulfilled and also that the common welfare of the travelers can be assured.

Combined Volumes

A combination of the aforementioned alternative systems is one of the better options that the designer has for the solution for these volumes. Some areas, such as kitchen, bathrooms, laundry, etc., lend themselves to a fixed system because of the hardware and fixtures involved. These should be considered first. Then modular volumes could be considered, since changes here can be affected with constraints. Finally, the flexible areas will be considered as stages on which many things can happen. This combination has the advantages of all the previous and also reinforces all the individual criteria of habitability that each fulfills separately. The criteria included are variability, functionality, unpredictable conditions, personal identification, social interaction, and equalitarian conditions.

Concepts

Besides deciding the design strategy to be utilized in reference to fixed volume, modular, flexible, or combined volumes, architectural quality must be considered. For such consideration we should point out the following concepts:

Spatial sensations. Each one of the habitable places in the vessel must possess a proper identity according to its use and the way it was designed. In each of the habitable places space sensations and the way they are perceived will depend on the use of color, texture, materials, size, utilization of the furniture, and the kind of impression that is to be made on the user of the place. These sensations on the user can be termed as privacy, intimacy, monumentality, pleasure, security, etc. Habitability to be enhanced with these sensations will depend on the effect to be attained. Obviously all could be fulfilled in general, or some specifically, but it becomes clear that no matter what kind of spatial sensation is accomplished by the design, there would be a generous sensory and perceptual stimulation.

Sense of scale. It is important that the design of the vessel and its habitable places take into account the physical dimensions of the human body and proportion the sizes of the volumes of the places to be created accordingly. This is termed in architecture as "sense of scale." The human would fit comfortably in places that correspond adequately to his physical dimensions. This does not mean that all spaces must be of a specific or standard dimension, but that there be a correlation between the elements utilized or the strategies followed that reflect or refer to the user—the space traveler, in this case. The sense of scale will depend also on the furniture, equipment, fenestration, ceiling heights, materials, etc. Among the habitability criteria reinforced by this factor are personal identification, privacy, orientation, and comfort.

Gardens. Architects have always harmonized their designs (artifacts) with nature, and the use of the interior gardens has been one of the resources with which such an intention has been accomplished. Obviously, by virtue of the conditions of the extraterrestrial vessel, contact with nature through interior gardens is very important. Such resources must be used in strategic places within the configuration of the vessel, so that they would positively contribute to the activities programmed to occur in such places.

Appropriate technology. Architectural design of such a vessel must be able to incorporate the latest available technology to attain functionality, psychic comfort, variability, unpredictable conditions, and variety in spatial sensations. To that end, it should utilize holography, videos, computer resources, cybernetics, chemotecture, biotecture, cryotecture, etc.

Lighting. Illumination is one of the most important elements that a designer has to enhance habitable places. In this case all lighting is artifical or manmade. It should correspond to the kind of volume, the use that it must respond to, and the spatial sensations that are to be created in it. The type of illumination utilized will also influence the physical and psychological reaction of the travelers and will contribute directly or indirectly in all the habitability criteria. Unpredictable variations could be introduced so that lighting can have a degree of variability similar to the terrestrial environment.

Interior design. Selection and design of equipment and furniture must also reflect good design to reinforce the fulfillment of habitability criteria. Dimensions of the humans, proportions of the body, and the alien conditions of microgravity or artificial gravity will have to be taken into account.

Other considerations. Symbolism relating to culture will aid in creating mental gardens and landscapes to enhance the quality of life in the vessel; form and traditional vocabularies that make reference to terrestrial life and the history of the Earth, and the enjoyment of the peak artistic accomplishment of humanity through recordings in fields such as the performing arts, and in the visual arts by means of holography, will all contribute to the quality of life during travel in the vessel.

ACKNOWLEDGMENTS

Principal authors F. Arroyo, O. Budet, A. Garcia, J. Lee, R. Lopez, R. Lugo, A. Mateo, R. Mellado, H. Mendez, N. Ortiz, L.A. Rivera, M. Rivera, O. Rodriguez, J. Toucet, H. Velez, E. von Gundlach, and teaching assistant A. Diaz. They were assisted by faculty advisors Professor A.F. Andino and Associate Professor E. Sobrino.

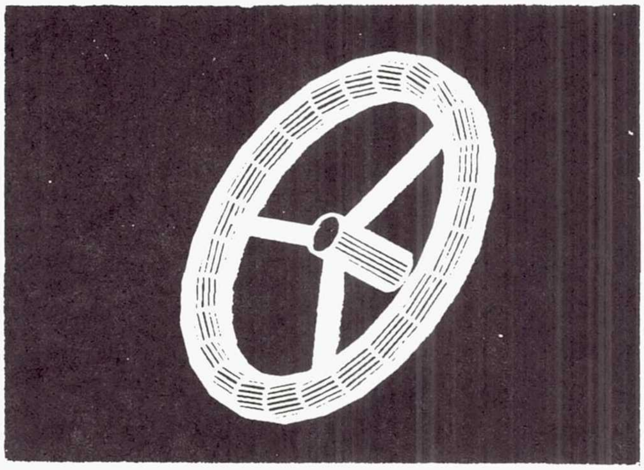

Apollo Workstation Views of Camelot III.

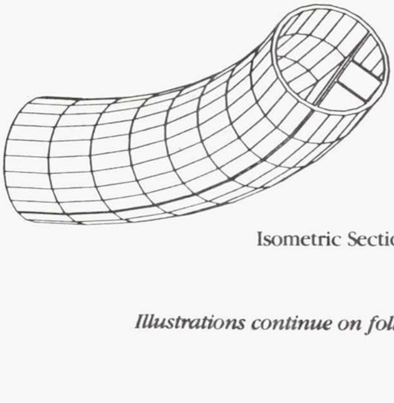

Isometric Section.

Illustrations continue on following pages

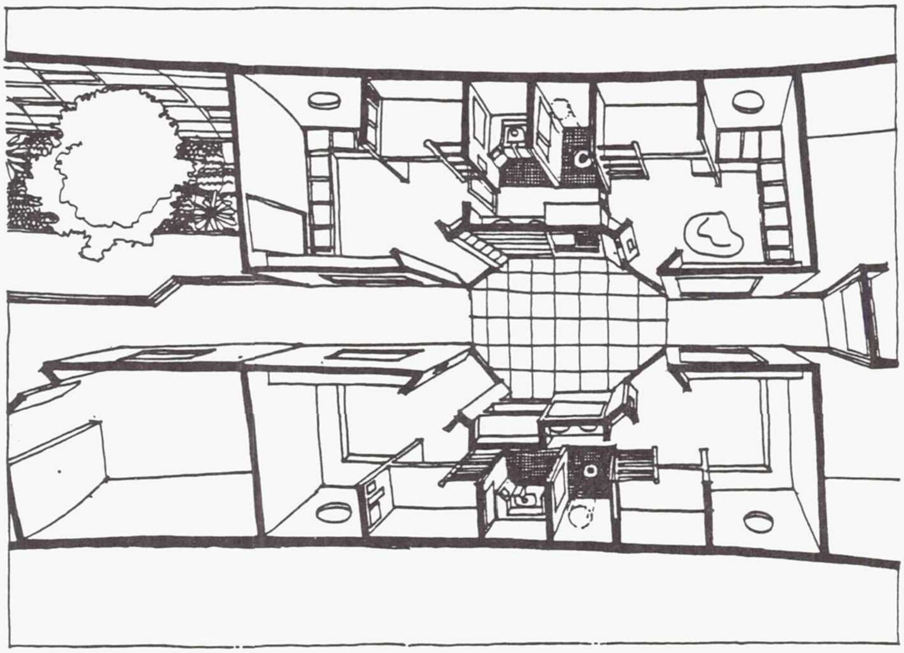

Bedrooms (3.04 m × 3.04 m): The cabin arrangement for passengers allows the individual users to have a private place. It has a sleeping area in the left and small living area, work space, or small office. Each room shares a bathroom/toilet with the adjacent room, except in the case of crew who have individual bathrooms and a large area. The organization of these cabins took communal relations into account. Rooms were aligned along a hallway where trees and plants that are parts of the CELSS development, creating a sense of contact with nature and a feeling of "outdoors" and vegetation. There is a communal area in the center with a small lounge and a laundry.

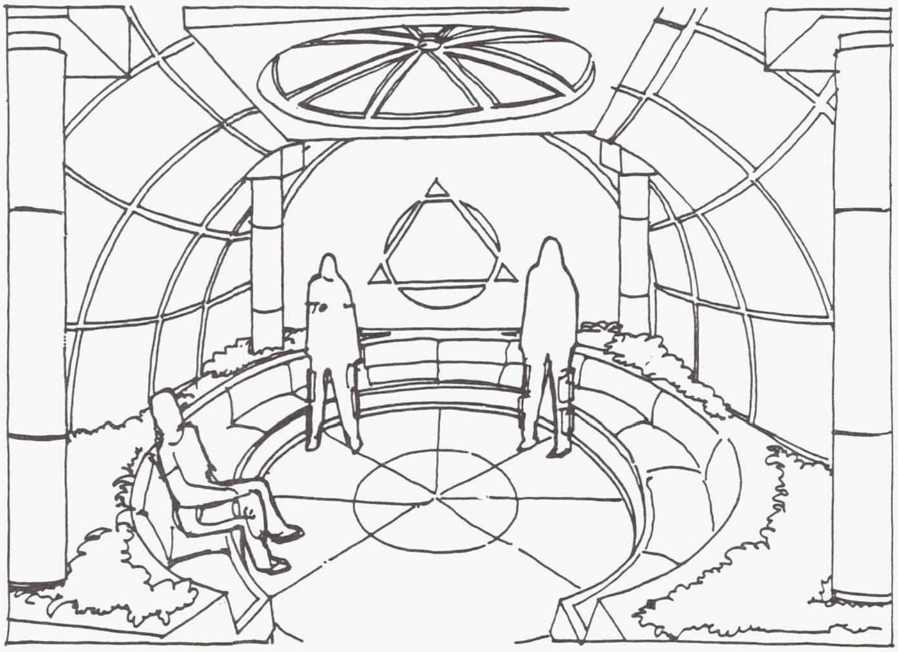

Chapel (8.23 m × 7 m): This is a place for quiet meditation that can alter its environment through light effects and holographic projections. It should lend itself to individual prayer, as well as corporate acts of worship. It will have a quiet and ecumenical character, so that it can serve all faiths.

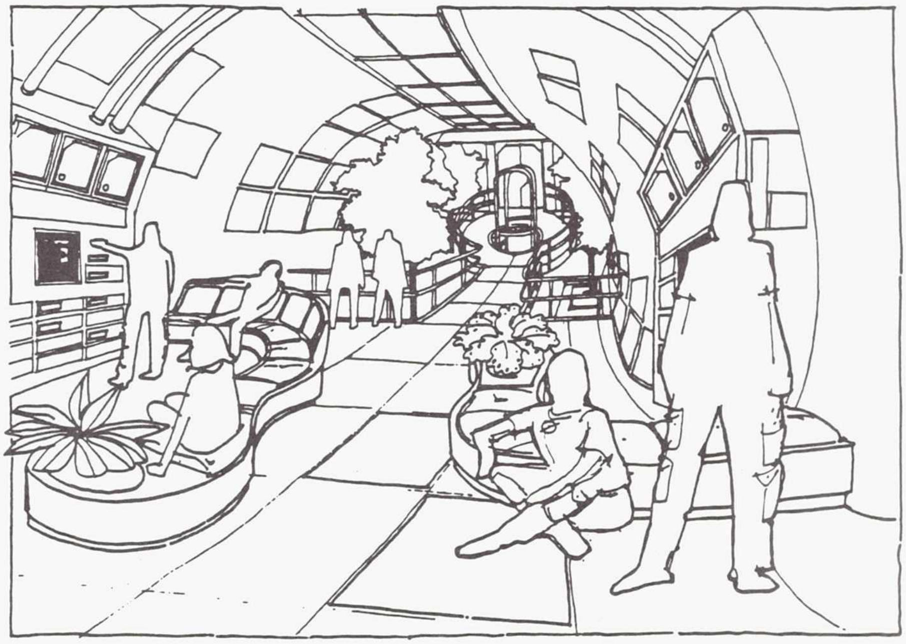

Lounge (12.8 m × 7 m): An area for passive recreation, conversation, and sharing. It will have video system, sound systems, books, and microfiche, in areas with individual as well as communal seating.

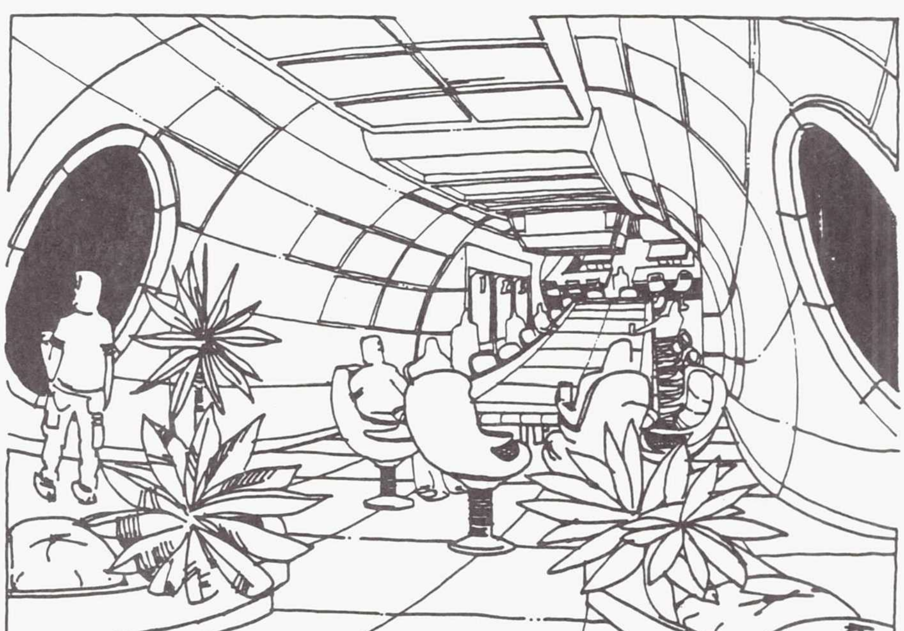

Conference/Dining (14.63 m × 7 m): An area with two main purposes: one for eating, the other for meetings of all passengers and crew or special occasions and/or emergencies. It houses a large conference table, a counter area, and is adjacent to the kitchen, freezer, and a small lounge area.

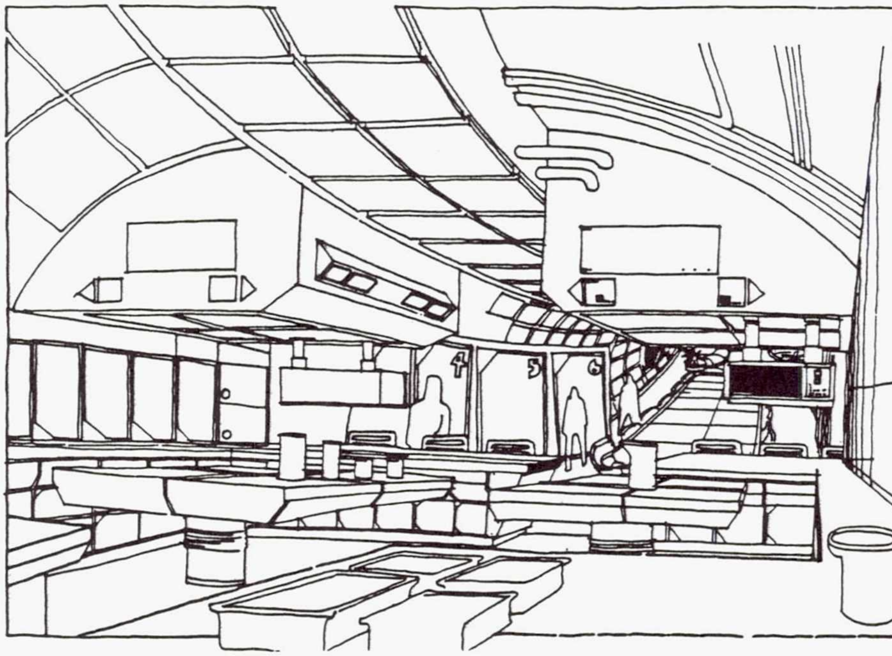

Kitchen (4.57 m × 7 m): The kitchen is totally automated for greater flexibility and convenience. Food will generally be programmed, even though customized food preparation should be possible on occasion. Each person will have free access to storage cabinets, counters, and seating, and will be able to prepare his or her own meals using microwave ovens, etc.

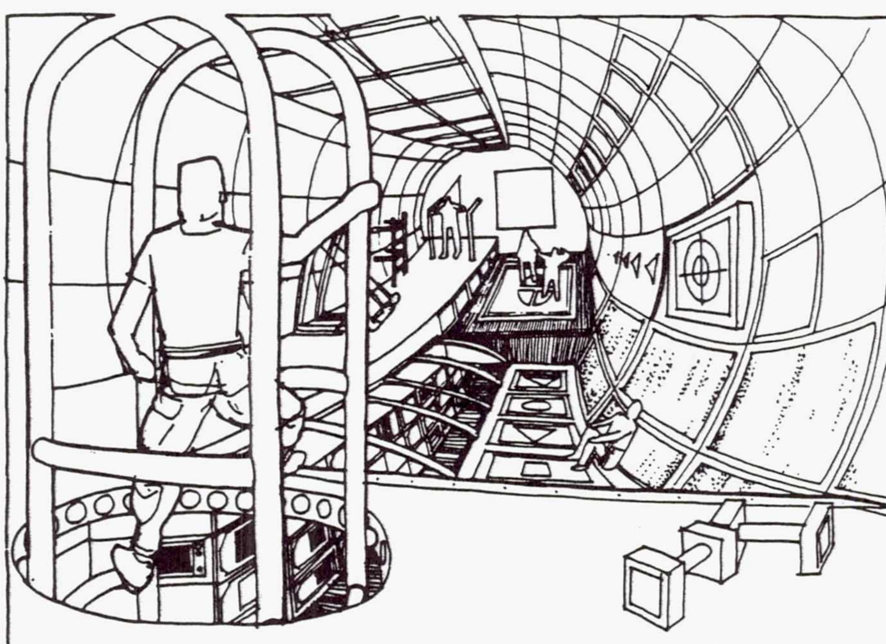

Gymnasium (9.14 m × 7 m): This is a place to ensure muscle tone, physical well-being, and general satisfaction and enjoyment of the passengers and crew. Exercise and activities will be programmed and designed taking into account the artificial gravity conditions with special machines for exercise calisthenics and aerobics. Some parts will have double height to take advantage of the 0.4 *g* gravity.

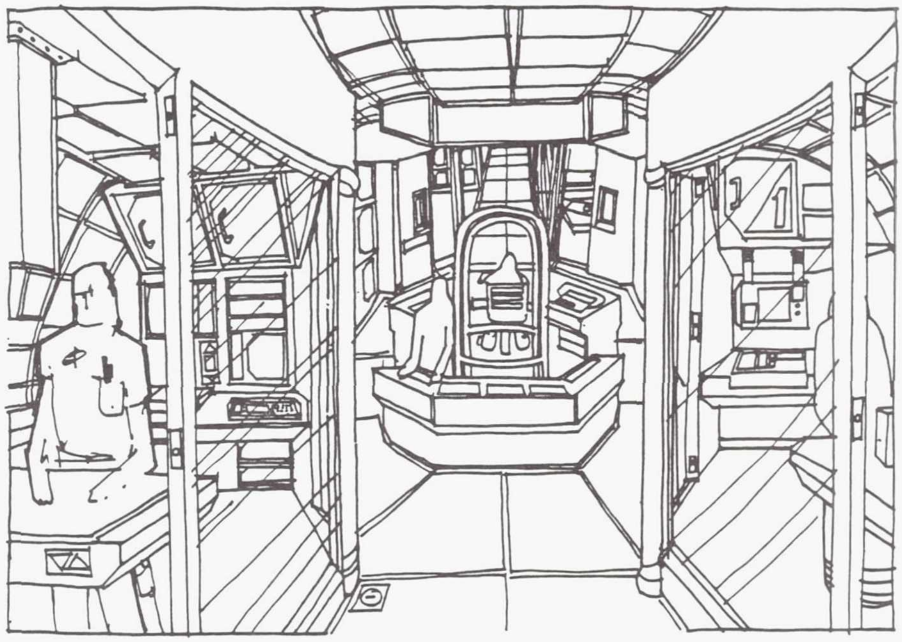

Laboratories (24.69 m × 7 m): There is a central control area in the laboratory complex from which all the work could be monitored. It is surrounded by six laboratories for scientific work on the vessel, as well as support for the Medical Center. Circulation is similar to that of the Medical Center itself, thus providing access through a hatchway and connection to the circumferential transport. Laboratory areas could also be customized according to the specific needs of individual travelers on each mission.

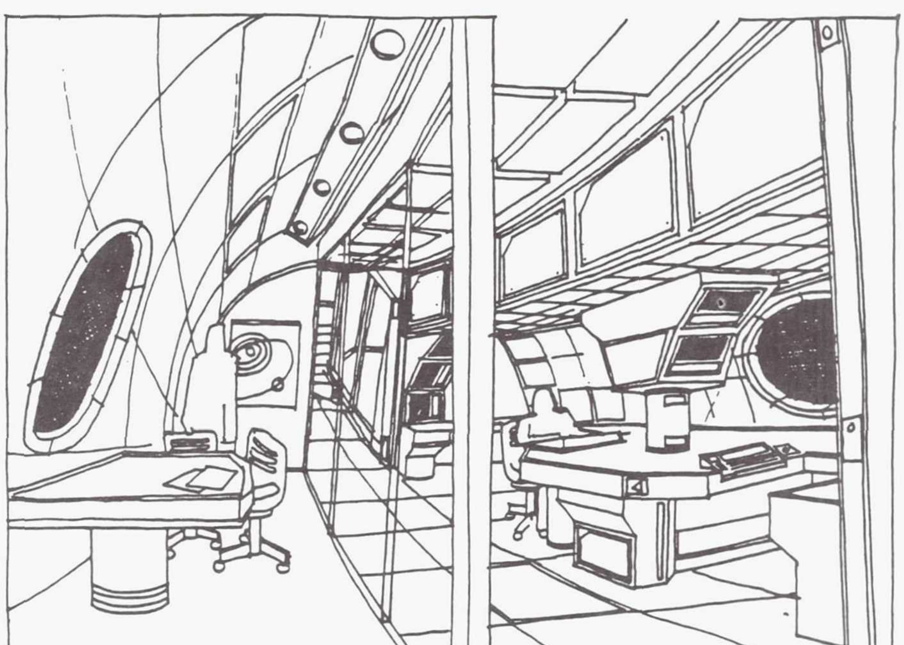

Torus Control Room (4.87 m × 7 m): This is an area within the Torus that will allow the crew to control and monitor all systems on the vessel without having to go to the Central Hub, where there is a similar facility (but under microgravity conditions). It is adjacent to a small office for meeting with individuals and is located within the work sector of the vessel, which also includes laboratories, the Medical Center, and the Master CELSS. It should be considered an auxiliary and subservient facility to the Hub Control Room, which is the main command bridge of the vessel.

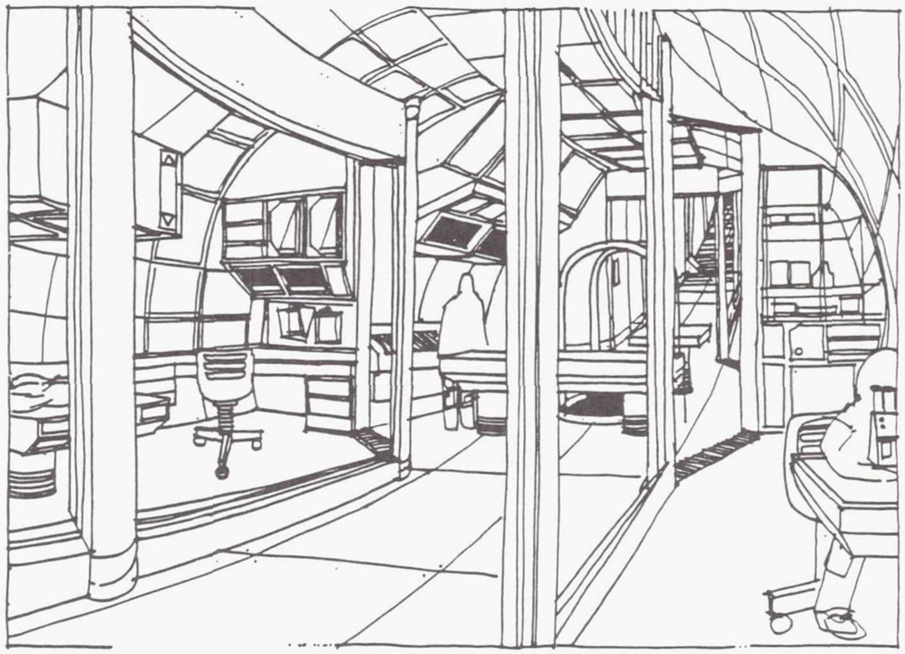

Medical Center (8.53 m × 7 m): This is conceived as a place for the attention and treatment of medical emergencies, illnesses, and routine check-ups of passengers and crew. It has a vertical access as well as a circumferential transport that can move a patient from any place on the vessel along the main corridor. It features four main areas: surgery, control, bathroom, and convalescence areas.

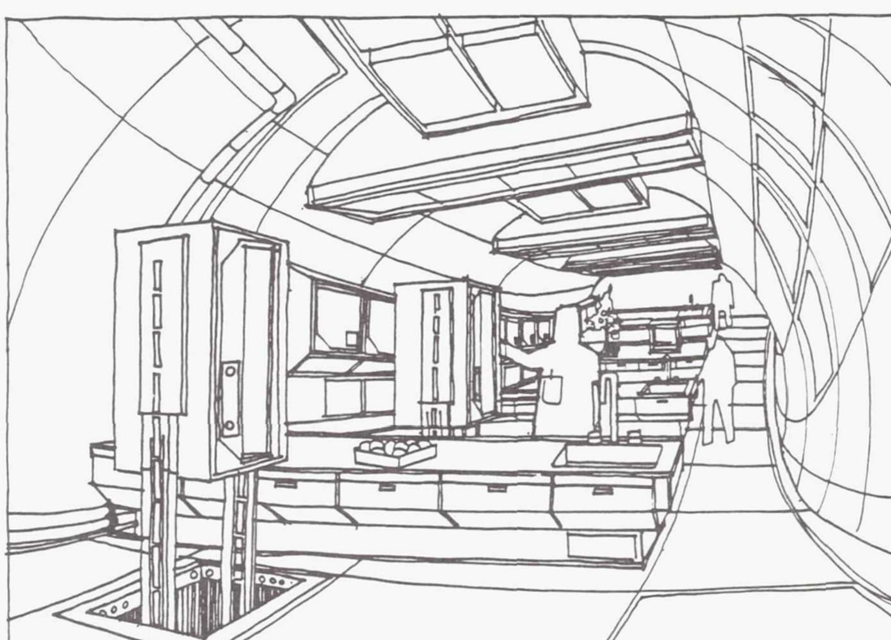

Master CELSS (201 m × 2.74 m): This is a control and inventory area for the "Controlled Environmental Life Support System" (CELSS). The system takes advantage of all the minor spaces throughout the vessel, especially those that do not have suitable shape or proportions for human habitation just as cargo compartments work in an airplane. The whole system is operated or monitored from here. It is accessible also through the circumferential transport as well as the appropriate hatchways. It has work tables besides the controls and indicators that monitor the life and chemical processes of the plants and animals of the system. This is the place in which the carousel drawers containing plant life can be pulled up for cultivation.

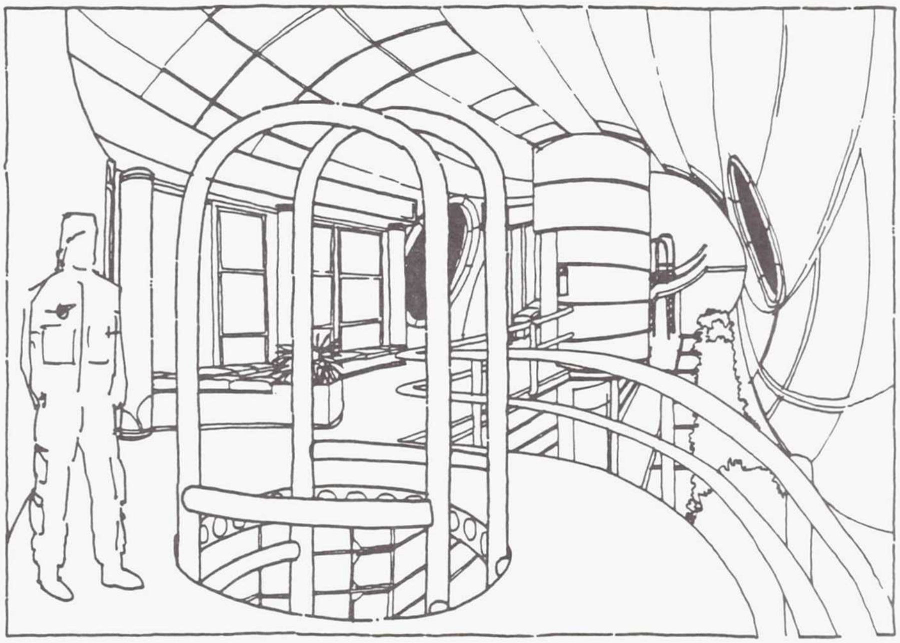

Spoke Elevator (12.19 m × 7 m): This provides access from the Central Hub to the Torus habitable spaces that feature artifical gravity of 0.4 g by rotation of 3.22 rpm in three different locations. It features a reception lounge and area of double height with vegetation. It has two access hatchways to the main corridor and windows to permit a view of the outside of the vessel.

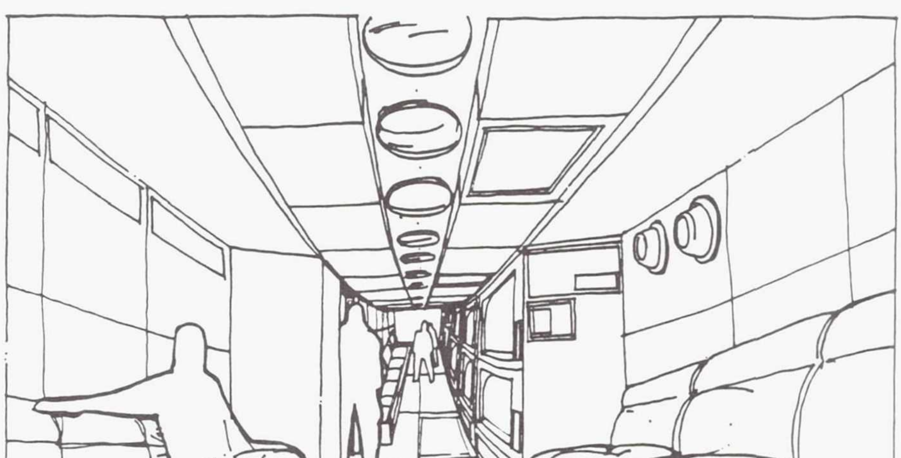

Safe Haven (20.12 m × 7 m): This is a shelter on the vessel for emergencies and protection from radiation of solar flares. There will be 3 of these, but each is capable of housing the 20 occupants of the vessel, since they may not have enough time to distribute themselves along the vessel once an emergency alarm signals the need for shelter. The individual niches provided for each person are similar to the facilities of a Japanese Hotel that provides enough space for lying down and individual entertainment.

N94-71287

19940015532
S20-31
160646
382693
p. 22

LUNAR BASE AND MARS BASE DESIGN PROJECTS

THE UNIVERSITY OF TEXAS AT AUSTIN

The space design classes at the University of Texas at Austin undertook seven projects in support of the NASA/USRA advanced space design program during the 1988-89 year. A total of 51 students, including 5 graduate students, participated in the design efforts. Four projects were done within the Aerospace Engineering (ASE) design program and three within the Mechanical Engineering (ME) program. Both lunar base and Mars base design efforts were studied and the specific projects were as follows:

- Lunar Crew Emergency Rescue Vehicle (ASE)
- Mars Logistics Lander Convertible to a Rocket Hopper (ME)
- A Robotically Constructed Production and Supply Base on Phobos (ASE)
- Robotic Construction of a Permanently Manned Mars Base (ASE)
- A Mars/Phobos Transportation System (ASE)
- Manned Base Design and Related Construction Issues for Mars/Phobos Mission (ME)
- Health Care Needs for a Lunar Colony and Design of Permanent Medical Facility (ME)

LUNAR RESCUE/MEDICAL OPERATIONS

The lunar base related projects focused on care of seriously injured or medically impaired astronauts. The first design was for a Lunar Crew Emergency Rescue Vehicle to evacuate injured personnel from the Moon to adequate medical facilities on Earth. An enlarged Apollo-type vehicle capable of returning a patient and an attendant astronaut was the final design. The vehicle included the capability of carrying a pressurized litter module. The second lunar project was for construction of a health maintenance facility as a part of a bootstrap lunar base.

Lunar Crew Emergency Rescue Vehicle

The construction of a permanently manned base on the Moon will require adequate medical care for the base crew[1]. However, during the initial development of the base, construction of a fully capable health maintenance facility may not be feasible due to initial costs of transportation, as well as the medical facility's power, thermal control, and maintenance requirements. With only a limited medical infirmary in place at the bootstrap base, it may be necessary to evacuate injured personnel to the Earth's surface. The Lunar Crew Emergency Rescue Vehicle (LCERV) will serve as a safe, quick, and efficient method for returning medically infirm personnel from a lunar base to adequate medical facilities on Earth. This study presents a preliminary design of an Apollo-like vehicle to meet the rescue requirements of a lunar base. The vehicle is capable of returning an injured astronaut with one attendant to Earth in approximately 48 hours. The vehicle will weigh approximately 52,000 lbs and its command and service modules are depicted in Fig. 1.

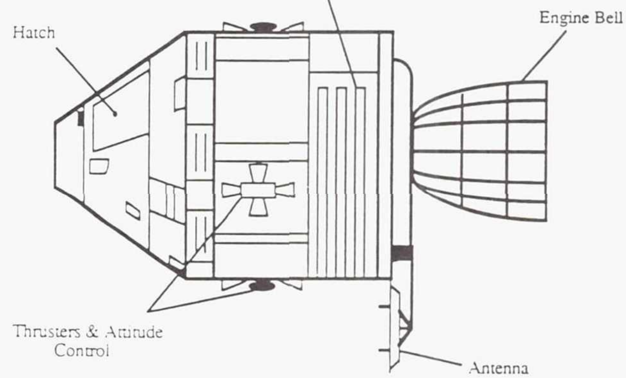

Fig. 1. LCERV Command and Service Modules (Sketch from Texas A&M - "Escape to Odyssey" presentation)

Three major areas were covered — vehicle design, trajectory analysis, and vehicle integration. The study assumed the construction of a lunar base would follow the Lunar Split Mission scenario developed by the NASA/USRA Summer 1988 Design Group at JSC[2]. This scenario uses robots for the construction of the preliminary lunar base prior to the return of astronauts to the Moon. This approach reduces the risk of human injury during the construction of the lunar base. In this scenario, the rescue vehicles can be delivered to the base when the required launch facilities have been robotically constructed. Thus, the rescue vehicles will be fully operational prior to the return of manned crews to the Moon.

We made the following assumptions:

1. After preliminary robotic construction of the lunar base, the base will be manned by crews of 4 to 8 astronauts for surface stay times of 30 to 90 days.
2. Mission technology for the scenario will be baselined in the year 2000.
3. The lunar crew will have a minimum of three personnel cross-trained in LCERV piloting and emergency medical procedures.
4. Heavy lift launch vehicles, orbital transfer vehicles, and Space Station will be operational.
5. The patient will be able to survive the Moon-Earth trip in microgravity.
6. The service module of the LCERV will aerobrake into LEO for future recovery.

A two-staged, Apollo-type configuration was chosen for the rescue vehicle. The vehicle will be propelled by a service

PRECEDING PAGE BLANK NOT FILMED

PAGE 156 INTENTIONALLY BLANK

Table 1. LCERV Subsystems

Subsystem	Function
ECLSS	Supply a breathable atmosphere, humidity control, thermal control for the crew and on-board equipment, post-landing ventilation, and consumables.
Medical	Support the medical concerns of an incapacitated astronaut while maintaining an average equipment life of 5 years.
Structures	Minimize structural mass while assuring structural integrity.
Power	Provide power to avionics, medical equipment, ECLSS, and the propulsion system.
Propulsion	Supply an adequate, flexible system that will meet the needs of multiple trajectories.
GNC	Give reliable position establishment along the trajectory and adequate and effective control over this state.
Communication	Establish and maintain reliable communications between LCERV, Space Station, Earth, and lunar base.

module, and the patient and attendant will be located in the command module. The service module will provide all propulsive requirements prior to re-entry. The subsystems studied are shown in Table 1. Fig. 2 depicts the crew compartment with the pressurized litter module installed. The vehicles are expected to reside at the lunar launch facility for extended periods of time and must be shielded from excessive amounts of radiation, thermal cycling, and debris from launch or landing of other vehicles. Consequently, the rescue vehicles will remain in a partially buried hangar when not in use. Fig. 3 shows the hangar configuration.

Either land or water landings are options for the rescue vehicle returning to Earth. The vehicle can be accurately maneuvered to land within 1½ miles of its desired target. It is suggested that proposed water landing sites be located as near as possible to land to allow for the airlift of proper medical equipment to the patient or the patient to proper medical facilities. The benefit of a land site is that the patient can easily be taken to medical facilities without the delay that may occur with water landings. Both landing methods will cause a high *g*-force on impact, but this can be corrected by reducing impact forces with a propulsive braking system and/or a hydraulic support for the patient.

Because of the mass of the rescue vehicle and the need for at least two such vehicles, the design team recommended that a cost comparison be made between the LCERV and a permanent health maintenance facility at the lunar base.

Health Care Needs for a Lunar Colony and Design of a Permanent Medical Facility

The overall goal of this project was to develop creative, conceptual breakthrough ideas for the health maintenance facility for a future lunar base[3]. Through extensive research and interviews with medical professionals, this design team has developed a Permanent Medical Facility for the first manned phase of a lunar base. This includes: determining the equipment, supplies, and astronaut training required; reviewing possible injuries and illnesses and their probability of occurrence; and developing a conceptual, physical layout for a medical facility serving 4 to 8 people on missions up to 27 days in duration. Additionally, the team outlines the future health concerns for the medical facility as it develops from a small mining and research base to a self-sufficient lunar colony. Finally, the design team makes nine major recommendations for further study, specifically in the areas of remote area bases already in existence, safety programs, equipment redesign for low mass, and emergency contingency plans in case of life support and power failure.

The design criteria placed upon the design team were:

1. The facility shall be designed to minimize total mass sent to the Moon.

2. The facility will be expandable.

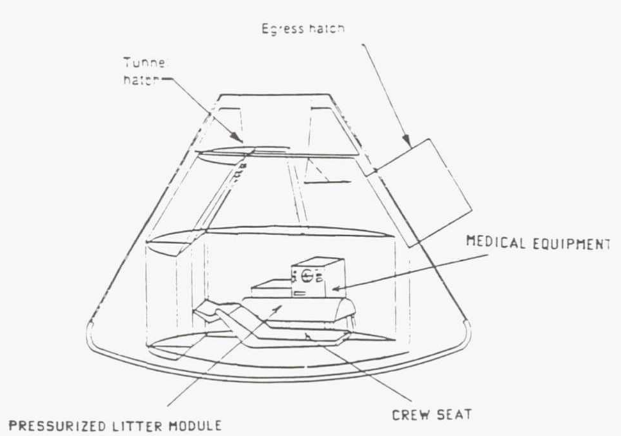

Fig. 2. Crew Compartment Configuration (Adapted from NASA-JSC Contingency Return Vehicle for Space Station)

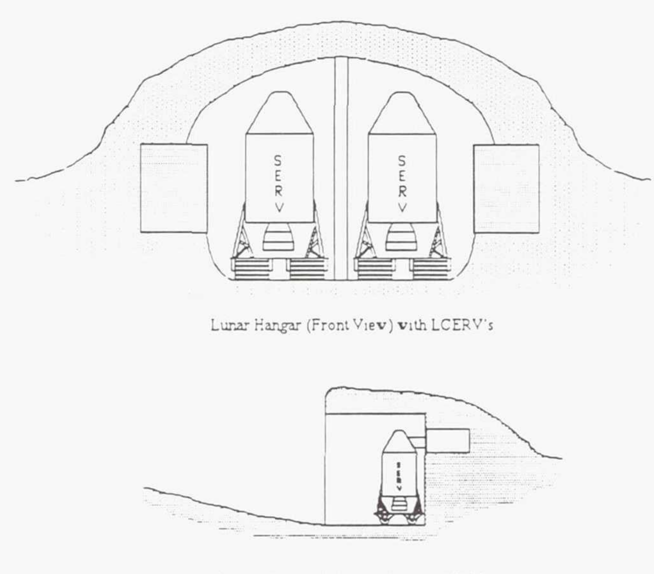

Fig. 3. LCERVs in Lunar Hangar

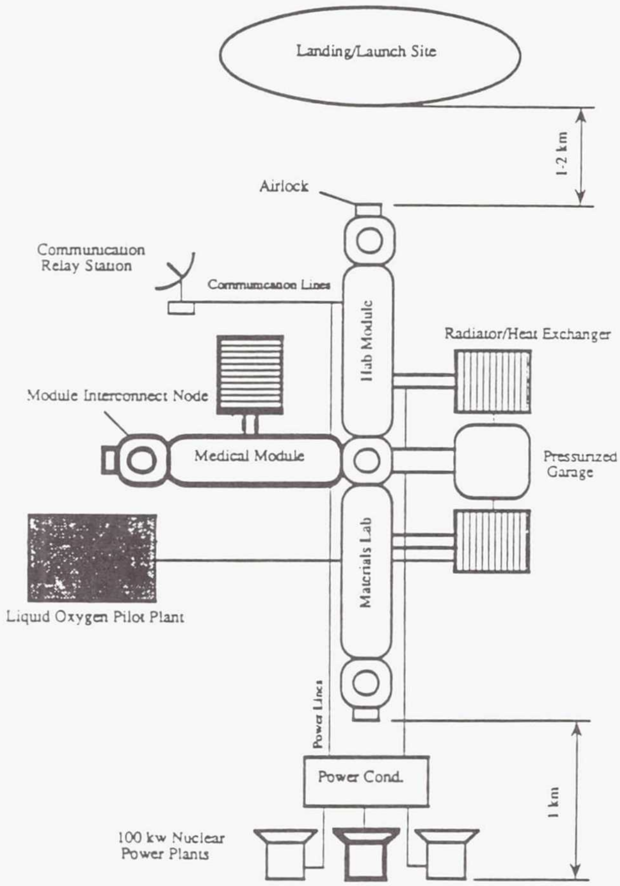

Fig. 4. Medical Facility in Axial Base Configuration

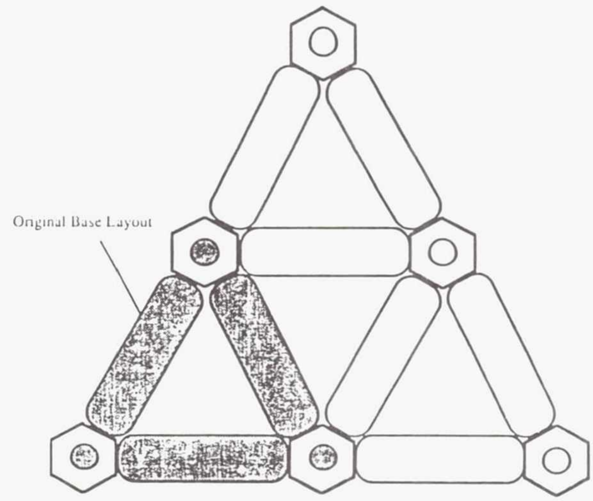

Fig. 5. Base Expansion in Triangular Layout

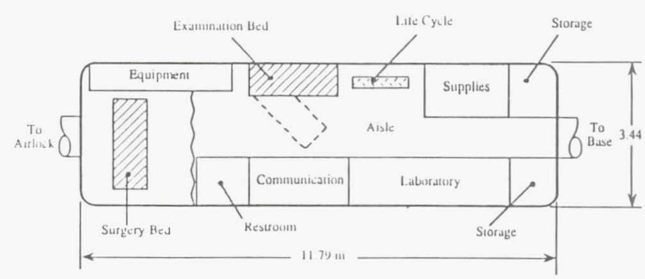

Fig. 6. Possible Interior Layout of Medical Module

3. The facility shall have means to minimize the waste heat generated by both human activity and equipment operation.

4. The facility shall be equipped with a back-up power and life-support system.

5. The facility will meet both routine and emergency health care requirements of the crew.

6. The facility shall provide adequate protection from radiation exposure for its occupants.

7. The facility will be designed to make the most efficient use of power.

The design team gathered information from both print and verbal sources. Current information on health care in remote areas proved valuable. The team also consulted Austin area doctors and hospitals to discuss both procedures and the equipment needed to treat common injuries and illnesses. Based on this information the team developed a conceptual health care facility for the first manned phase, which will support 4 to 8 astronauts, 3 to 4 missions per year, and up to 27 days per mission. Fig. 4 shows the Permanent Lunar Medical Facility in axial base configuration.

The team recommends using a triangular rather than axial layout of the modules to save mass and allow for easier expansion of the base. Fig. 5 shows expansion capability in the triangular layout, and Fig. 6 shows the possible interior layout of the medical module. The mass of the medical module alone is estimated at 42,525 lbm. Table 2 lists the mass of each component of the medical module.

Table 2. Mass of Medical Module Components[2]

	Mass (lbm)
1 Module (including equipment and supplies)	38500
1 Node	2050
1 Airlock	1700
1 Flexible Tunnel	275
Total	42525

Injuries account for about 74% of medical emergencies on Earth. Accounting for the exceptional health of astronauts upon arrival at a lunar base, the design team feels that injuries will account for about 85 to 90% of the emergencies on the Moon, making their treatment the single most important aspect of a lunar medical facility. Fig. 7 lists specific possible injuries which the team considered to be representative or most critical at a lunar base.

Although injuries are expected to account for the majority of emergencies on a lunar base, illnesses can have an equally

	Equipment	Pharmaceuticals	Supplies
FRACTURES			
bones	X-Ray	analgesics	splints &
spine/cranium	"	"	bandages
DISLOCATIONS, STRAINS & SPRAINS			
joint dislocations	X-Ray	analgesics	N/A*
back/muscle strain	N/A	muscle relaxants	elastic bandages
muscle attrition	Life Cycle	"	N/A
HEAD INJURY (not face)	X-Ray	analgesics	ice
LACERATIONS & OPEN WOUNDS			
open wounds	N/A	analgesics &	bandages
cuts due to fracture	"	antibiotics &	"
skin irritations	"	ointments & salves	"
skin abrasions	"	"	"
eye injury/irritation	ophthalmoscope	"	eye wash
CONTUSIONS & CRUSHING			
bones	X-Ray	analgesics	splints
spine/cranium	"	"	"
BURNS			
First/Second degree	N/A	ointments & slaves &	bandages
Third Degree	"	antibiotics	"
Electrical	"	"	"
Chemical	"	"	"
SUPERFICIAL INJURY	N/A	ointments & salves	bandages
POISONING			
gas inhalation	respirator	antidotes	oxygen
drug overdose	stomach pump	"	N/A
RADIATION EFFECTS			
burns	flow cytometer	ointments & slaves	bandages
poisoning	"	N/A	N/A
PRESSURE EFFECTS			
air embolism	Pressurized	N/A	N/A
decompression sickness	Litter Module	"	"

Fig. 7. Selected Treatment for Representative Injuries

	Equipment	Pharmaceuticals	Supplies
ALLERGIC, METABOLIC, NUTRITIONAL			
tonsillitis	microscope &	antibiotics	various lab tests
strep	flow cytometer	"	"
fever	"	"	"
MENTAL			
depression	biofeedback	anti-depressants	N/A*
nervous breakdown	"	sedatives	restraints
psychosis	"	"	"
NERVOUS SYSTEM & SENSE ORGANS			
shock	multi-purpose scopes	anti-shock medicines	blankets
VASCULAR LESIONS			
strokes	respirator	TBD+	N/A
CONVULSIONS	N/A	anti-convulsants	restraints
CIRCULATORY SYSTEM			
profuse nose bleed	N/A	clotting drugs	ice & bandages
leukocyte loss	flow cytometer	various	N/A
appendicitis	surgical table	"	"
heart attack	defibrillator	"	"
RESPIRATORY SYSTEM			
cold outbreaks	flow cytometer	antibiotics	various
respiratory ailments	respirator	pulmonary drugs	various
DIGESTIVE SYSTEM			
motion/space sickness	N/A	anti-nausea drugs	N/A
renal failure	dialysis machine	antibiotics	various

*N/A: Not Applicable +TBD: To Be Determined

Fig. 8. Selected Treatment for Representative Illnesses

severe effect on the health and the performance of the astronaut. Figure 8 lists certain illnesses of concern and suggests equipment and consumables to handle each emergency. One of the largest concerns will be the mental health of the astronauts. Although actual debilitation due to mental illness is unlikely during the short missions of the first manned phase, depression or lethargy could hamper the success of the busy first missions.

MISSIONS TO MARS

Four projects addressed the construction of bases on Phobos and Mars, a transportation system supporting the robotic construction of bases on both Phobos and Mars, and a Mars lander which transforms into a ballistic hopper for martian exploration.

A Robotically Constructed Production and Supply Base on Phobos

Phobos, the Interplanetary Gas Station. For voyages from the Earth to the outer planets, this moon of Mars, Phobos, stands out as a prime site for resource utilization. A small, craggy, oblong chunk of rock, this body bears little resemblance to Earth's moon. Its density indicates that the planetoid contains large quantities of water, probably locked up as water of hydration. Phobos' water could be mined and processed into liquid hydrogen and liquid oxygen, the prime fuels for chemical rockets. The low mass of Phobos means it has approximately one-thousandth of the Earth's gravity. Finally, since Phobos is locked to the orbit of Mars, the outermost terrestrial planet, it provides the ideal gateway to the outer planetary bodies.

The Manned Outpost. Phobos can serve as a stepping stone for the manned exploration of Mars. Due to the moon's lack of atmosphere and low gravity, it is easier and cheaper to send astronauts to Phobos than to Mars. In addition, the cost of manned missions could be reduced even further by using propellent mined ***in-situ*** for the return voyage to Earth. On Phobos, manned crews could explore the martian system from a natural space station, and also assist in the construction of a martian base using telerobotics. A manned mission to

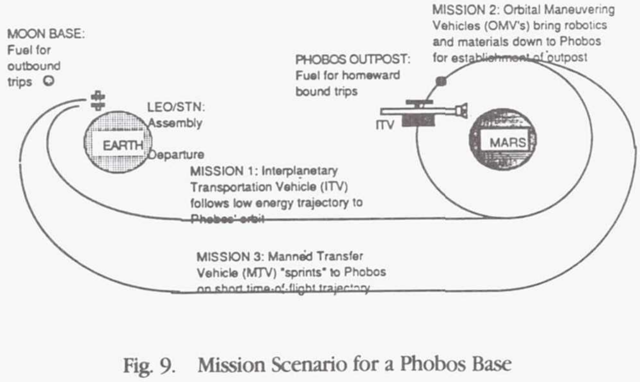

Fig. 9. Mission Scenario for a Phobos Base

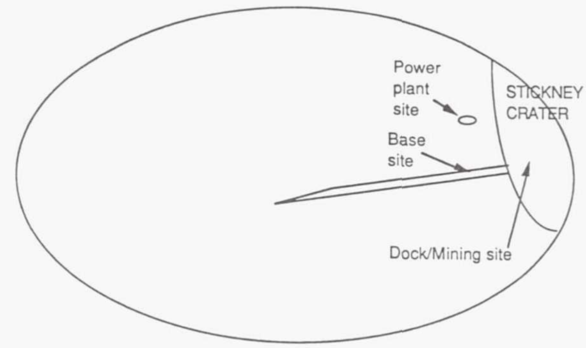

Fig. 10. Preliminary Site Locations

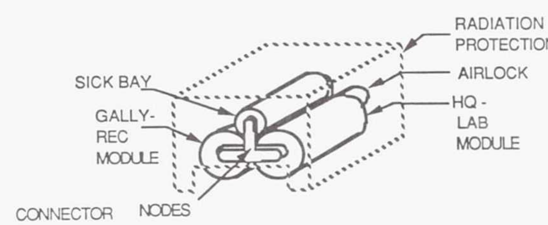

Fig. 11. Phobos Base Configuration

Phobos could be accomplished sooner than a corresponding Mars mission, establishing early leadership in the exploration of the martian system[4]. The establishment of a manned outpost on Phobos would provide a base for the first detailed exploration of an asteroid-type body. This outpost would serve as a base for the operation of telerobotic probes on Mars, martian weather observations, and eventually telerobotic construction of a manned base on the surface of Mars. Once the Mars base is established, some of the equipment and facilities required for the Phobos base could be sent down to Mars, reducing the cost of constructing the planet-side base. At this stage, the Phobos outpost would become a man-tended facility with autonomous, automated mining and fuel production capability. It would be capable of serving as both a temporary habitat for crews sent up from the Mars base and as a safe-haven for passing spacecraft or for the Mars base.

Autonomous Automated Assembly, the Key to Phobos. The construction of Space Station *Freedom* in the 1990's will pioneer the technology of space-based robotic construction. If an evolutionary expansion approach into space is implemented, the space station will be followed in the next century by a robotically-assembled base on the Moon. The construction of such a base will require that a great deal of autonomy be given to the robots, due to time lags on the order of several seconds for Earth-based monitoring and communications. When the construction scenario is shifted to Phobos, however, fully autonomous robots are a necessity. Time lags on the order of forty minutes preclude any direct supervision

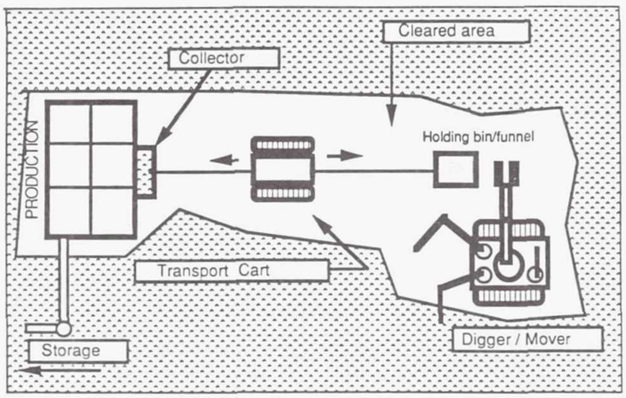

Fig. 12. Surface Mining Layout

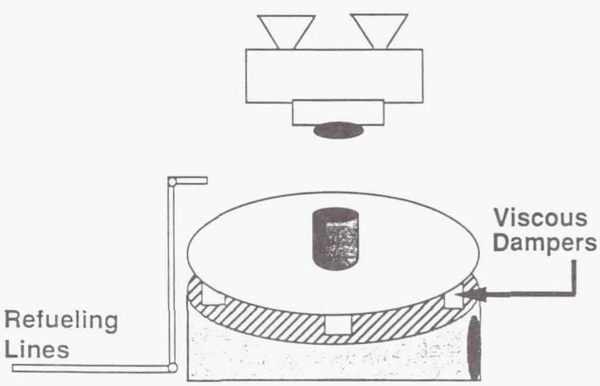

Fig. 13. Refueling Dock

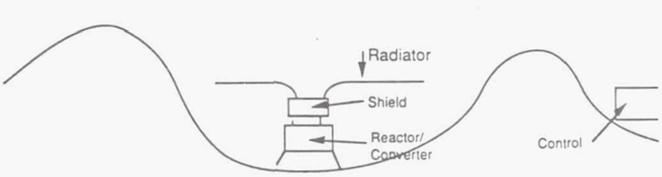

Fig. 14. Nuclear Power Source Shielded in a Crater

and control from Earth. With the expected advances in artificial intelligence and the experience gained through previous robotic construction missions, an autonomous, automated assembly scenario for the Phobos base seems plausible(5).

The following groundrules were established by the design team for the robotic construction of a base on Phobos:

1. Human activities shall not affect the structural integrity nor the orbital motion of Phobos, and shall not substantially detract from its scientific or aesthetic value.

2. The first manned expedition to Phobos will use fuel produced *in-situ* for its return trip; however, it will carry enough fuel in a backup capacity for a safe and timely return to Earth.

3. Subsequent return trips from the martian system and martian space transportation systems will use phobian fuel.

4. Robotic construction activities are to be monitored by Earth stations.

5. Human crews do not depart Earth until completion and checkout of habitation on Phobos.

The construction of base is considered to occur approximately 30 to 40 years from the present, in the neighborhood of 2020 to 2035. This timeframe allows adequate time for the establishment of a lunar base and an Earth-orbiting space transportation node, both of which are considered necessary for the development of the Phobos base. Figure 9 shows a schematic of the mission sequence.

The Phobos outpost will have three major functions: (1) providing a fuel station for spacecraft undertaking missions to the outer planets; (2) providing a base for the exploration of Phobos and Mars; and (3) serving as the command center for subsequent telerobotic construction of a bootstrap base on the surface of Mars.

The outpost will consist of three sites; the docking and mining site within Stickney Crater, the base site within a trench extending from Stickney Crater, and the power plant site approximately 1 km from the base site. Fig. 10 shows the preliminary site locations, Fig. 11 the base configuration, Fig.12 the surface mining layout, Fig. 13 the refueling dock, and Fig. 14 the nuclear power plant layout.

Key to the construction of the Phobos base are the autonomous robots. The robots must be capable of manipulating and connecting large structural components, as well as detailed work such as drilling and soldering. These tasks can be accomplished with maximum flexibility through the use of modular effector packages, which attach to a legged chassis. Each effector package contains several modular end effectors to increase further the flexibility of the design. Each chassis will contain fuel cells which provide power for both the chassis and the effector package. Fig. 15 shows the construction effector package.

Control of the construction robots will be accomplished through a division-of-labor scheme. The chassis will contain the locomotion programs, and the effector packages will be programmed to accomplish their own tasks. All robotic tasks will be directed by a "foreman," which is a separate, immobile unit containing the bulk of the artificial intelligence codes. For mining operations, the major robotic activity will be digging and transporting the phobian regolith, a fairly repetitious

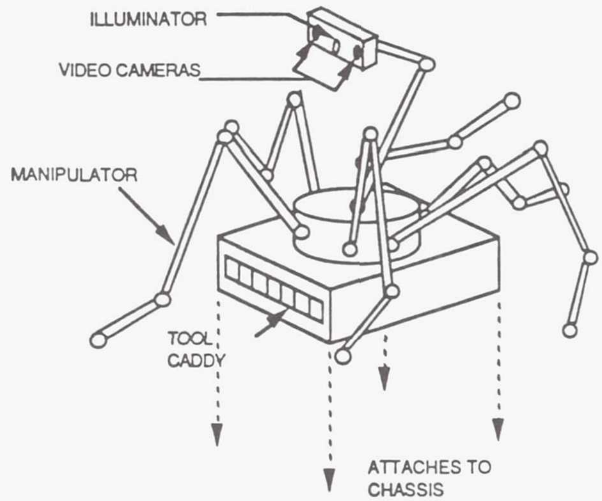

Fig. 15. Construction Effector Package

chore. Therefore, a more robust, but less flexible design is required.

The design included a failure modes and effects analysis table on the major components of the Phobos base. This qualitative method was used to explore possible modes by which components of the base may fail and to determine the consequences and criticality of each mode of failure on the system as a whole.

Robotic Construction of a Permanently Manned Mars Base

The objective was to design a permanently manned robotically constructed base on Mars[6]. The reasons for establishing a permanently manned Mars base are numerous. Primarily, human presence on Mars will allow utilization of new resources for the improvement of the quality of life on Earth, allowing for new discoveries in technologies, the solar system, and human physiology. Such a mission would also encourage interaction between different countries increasing international cooperation leading to stronger unification of mankind. Surface studies of Mars, scientific experiments in multiple fields, the search for new minerals and natural resource production are more immediate goals of the Mars mission. Finally, in the future, colonization of Mars will insure man's perpetual presence in the universe.

Robotic construction is a feasible alternative to human construction of the martian base (Fig. 16). The martian atmosphere does not provide adequate radiation protection, and the harsh environment makes it extremely difficult for humans to work efficiently and safely. Bulky space suits are not suitable for construction tasks. Robots can easily operate under these martian conditions and would also be more efficient at large-scale construction activities. Robots don't require the life support and are capable of repairing each other.

A set of ground rules and assumptions have been established to narrow the scope of the design effort.

1. A fully operational lunar base will be a major assumption of this design effort. A lunar base is necessary to study the variety of technological problems of man in space.
2. Long-term living in space will be assumed to have been studied over the course of Space Station, Moon Base, and Phobos missions, thereby answering most questions on human habitation in space. These known solutions can then be easily applied within the framework of the Mars base.
3. Precursor accomplishments, such as the existence of a Heavy Lift Launch Vehicle, a Space-Docking facility in Low Earth Orbit, and efficient Orbit Transfer Vehicles are likewise presumed. Additionally, following the evolutionary expansion into space, the design will assume that a man-tenable facility is in existence at Phobos.
4. Manned missions to the martian system have starting dates ranging from an optimistic 2020 through a pessimistic 2045. This timeframe, 30 to 50 years into the future, allows for huge gains in technological development which may facilitate the design effort.
5. Construction of the manned facility will be completed almost exclusively through the use of advanced robotics. If unforeseen problems do arise, human supervision will be available from the Earth, the lunar base, or Phobos for reprogramming or teleoperation.
6. The Mars base will utilize components of the Phobos base, such as the sick bay and exercise equipment. The base will also be designed to allow for unlimited expansion to achieve the objective of a permanently-manned facility.
7. Necessary teleoperations will be undertaken from the operational Phobos base. Communications satellites positioned as a part of the Phobos installation will be used for Phobos-Mars and Earth-Mars communications.
8. All martian equipment should be thoroughly tested in a simulated martian environment on Earth.

The base layout is shown in Fig. 17 and will consist of the following components: two nuclear power plants, communication facilities, a habitat complex, a hangar, a garage, recreation, and manufacturing facilities. The power plants will be self-contained nuclear fission reactors placed approximately 1 km from the base for safety. The base communication system will use a combination of orbiting satellites and surface relay stations. This system is necessary for robotic contact with Phobos and for future communications requirements.

As stated previously, Mars base construction will begin only after the Phobos base has become operational. A team of

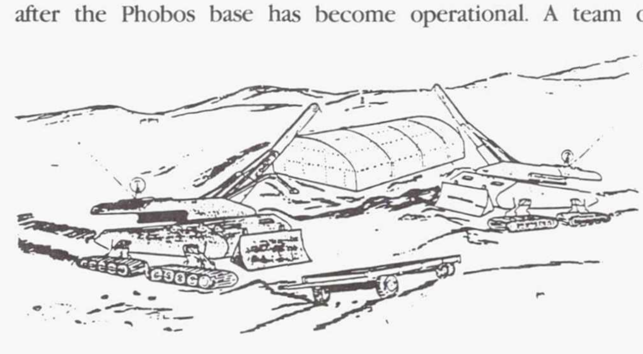

Fig. 16. Robotic Construction of a Permanently Manned Mars Base

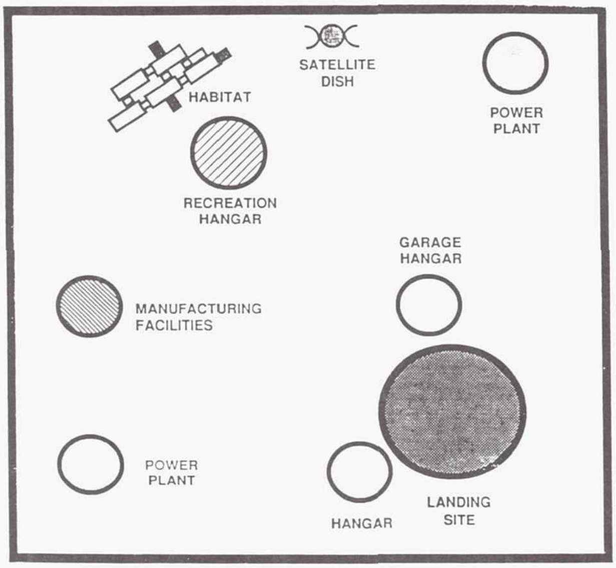

Fig. 17. Mars Base Layout

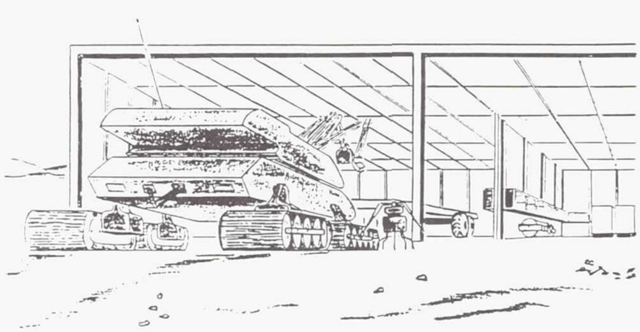

Fig. 18. Mars Robots Entering Garage

specialists will be present on Phobos during the entire construction period monitoring progress and providing teleoperation assistance as necessary. However, unless serious problems arise, men will not be going to the surface of Mars until the base is entirely completed.

The automated construction process will be completed within a maximum time period of 60 days, which is a design safety limit of human stay-time on Phobos. Due to the modularity of the design, each step can be extensively tested and improved upon prior to Earth launch through multiple test scenarios by the construction team and the robots. This will insure that each robot is capable of completing its required tasks. To correct problems encountered by the robots or faults in the design, a period of up to two years may be required for simulated test cases on Earth before actual mission engagement.

The complete base complex will be built by autonomous, artificially intelligent robots (Fig. 18). The robots incorporated into our design are as follows: Large Modular Construction Robots (Fig. 19) with detachable arms capable of large scale construction activities; Small Maneuverable Robotic Servicers (Fig. 20) capable of performing delicate tasks normally requiring a suited astronaut; a trailer vehicle with modular type attachments to complete specific tasks; and finally, Mobile Autonomous Rechargeable Transporters (MARTs) (Fig. 21) capable of transferring air and water from the manufacturing facility to the habitat complex.

The habitat complex is shown in Fig. 22 and its module construction is depicted in Fig. 23. The habitat complex will consist of six self-contained modules: core, biosphere, science, living quarters, galley/storage, and a sick bay which has been brought from Phobos. The complex will be set into an excavated hole and covered with approximately 0.5 m of "sandbags" to provide radiation protection for the astronauts (Fig. 24). The recreation, hangar, garage, and manufacturing facilities will each be transformed from the four one-way

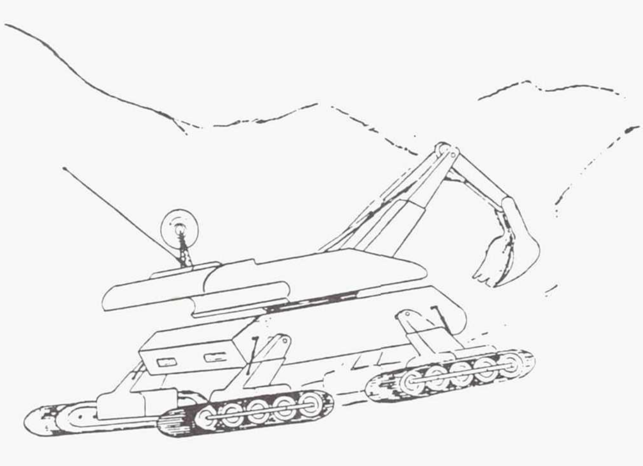

Fig. 19. Large Modular Construction Robot

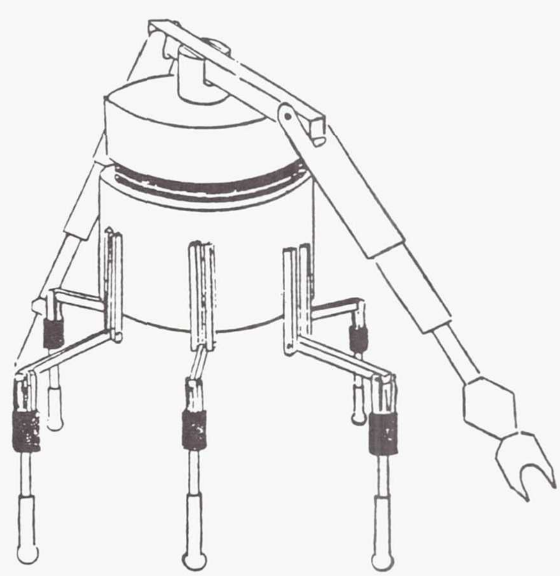

Fig. 20. Small Maneuverable Robotic Servicer

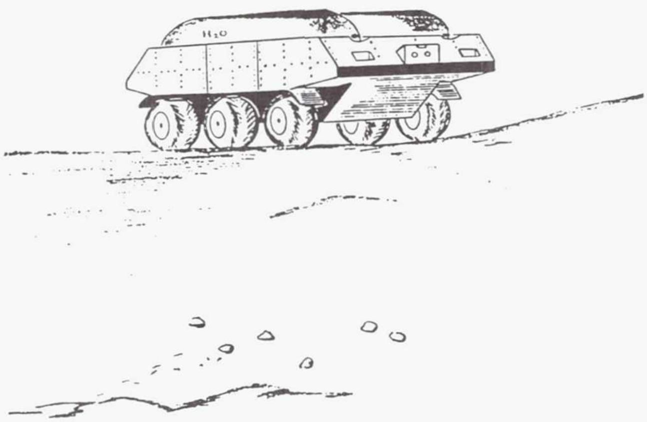

Fig. 21. Mobile Autonomous Rechargeable Transporter (MART)

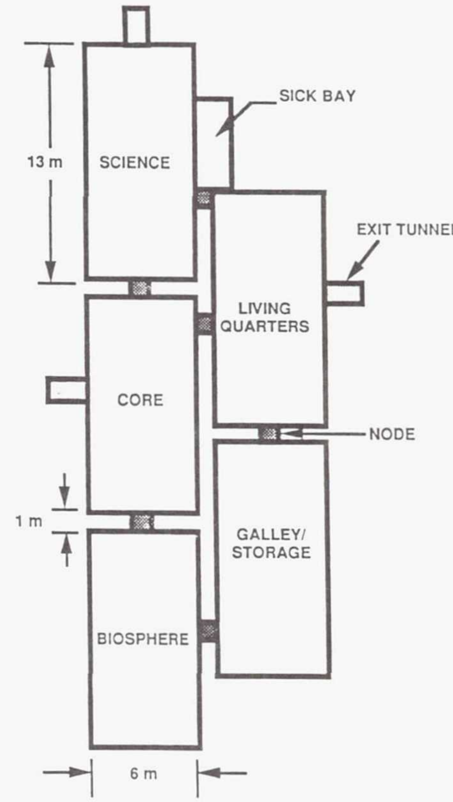

Fig. 22. Layout of Habitat Complex

landers which are detailed in the study by the Mars/Phobos Transportation System design group.

It is assumed that the fuel production for transportation needs will take place on Phobos, although some fuel for local or emergency needs should be manufactured on Mars. Fuel produced on Phobos will be stored on Mars in pressurized vessels underground. These vessels will be old lander fuel tanks buried near the landing/launch area. If liquid oxygen is the primary propellant of spacecraft at the time of base operation, a facility for its production can be designed from similar technology applied at the lunar and Phobos bases. Another possibility for fuel is methane, which could be used for Mars operations (rovers, MARTs, manufacturing processes, heating, etc.). The essential elements for producing methane, which are water and carbon dioxide, are believed to be easily accessible on Mars.

Three possible base locations were explored, with the primary location at -5° to 5° latitude and 65° to 75° longitude. The main advantage to this location is its proximity to the equator, making access from a low-martian orbit and communication with Phobos easier. This area, on the east edge of the Tharsis Bulge, is close to interesting geography such as the Lunae Planum and Valles Marineris.

Several areas were identified as needing future research or investigation. Since one of the goals of this project was to determine and highlight driving technologies, the following sections outline the recommendations from each group within the Mars base design team.

Environmental Group. One of the goals before the Mars base is constructed should be the miniaturization of the equipment for the base. The robots' tasks would be greatly simplified if the mass and size of subsystems could be significantly reduced from what today's technology would require. Equipment subsystems, such as the manufacturing facility, should be designed as easily-joined modular structures. Furthermore, with the lower mass, payload demands aboard interplanetary transport vehicles would be reduced.

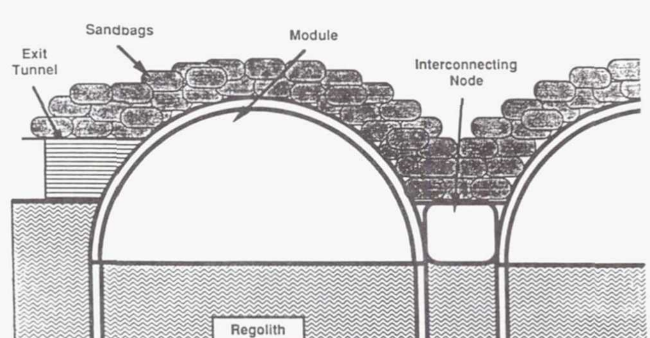

Fig. 23. Side View of Module Construction

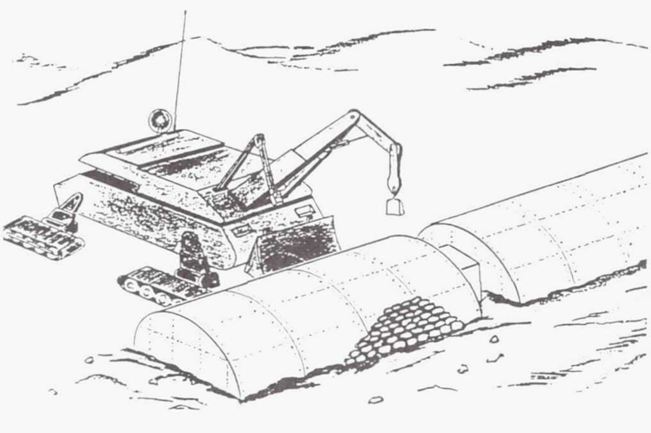

Fig. 24. Construction Robot Laying Sandbags

Another topic which must be examined concerns the construction of a permanent landing site for spacecraft. At this time, the use of concrete in this task is not workable. Because of the near-vacuum pressures and low temperatures of Mars, concrete as we know it could not be mixed or poured onto the desired surface before its water froze or evaporated. An alternative that should be explored is the use of ceramic, thermal insulating tiles laid out over a flat surface to provide a landing pad. The production of the ceramic-like material could be a long-term goal of the manufacturing facility. Another option that should be investigated is the use of polymer concrete which is currently being developed.

Robotics Group. The conditions on Mars will have significant impact on robotic operations. Any mechanical equipment used on Mars will have to overcome the effects of reduced gravity, increased radiation, friction, and evaporation of volatiles due to low atmospheric pressure. The robots should be composed of lightweight materials possibly taking advantage of newly discovered composites in the future. In addition, advanced seal technology should be developed in order to protect all mechanical equipment from the martian environment.

Advanced power systems should be investigated to power the robots. High-energy regenerative fuel cells and batteries should be further developed along with research and development of a compact nuclear power source.

Simulations should be accomplished on Earth prior to the mission. In addition, the robot tasks should be designed for simplicity, taking advantage of ideas such as adhesive connectors, twist locks and levers, surfaces that provide automatic indexing, guides, and self-aligning parts.

Habitation Group. Research should be directed at more efficient, closed life-support systems. Waste, oxygen, and water regeneration systems should be extremely efficient and reliable. A Closed Ecological Life Support System should definitely be expanded to accommodate a large crew community. Additional biosphere modules should produce food for the entire crew. The biosphere modules should be able to regenerate the air and waste water without relying on other systems.

Human mobility on the surface of Mars is also a very important factor for research. Buggies, carts, or monorails should be developed to make it easier for the crew to travel around the base. A transportation system for the exploration of Mars by humans or robots needs to be developed to better utilize martian resources. This would also allow for further investigation of the martian surface and related technologies.

A Mars/Phobos Transportation System

A transportation system will be necessary to support construction and operation of bases on Phobos and Mars beginning in the year 2020 or later. This study presents an approach to defining a network of vehicles and specifying the types of vehicles that may be used in the system. The network will provide convenient, integrated means for transporting robots and material for robotically constructing bases on Phobos and Mars. All the technology needed for the planned system is expected to be available for use at the projected date of cargo departure from the Earth system. The modular design of the transportation system provides easily implemented contingency plans, so that difficulties with any one vehicle will have minimal effect on the progress of the total mission.

Before specifying the objectives of the transportation system, the long-term goals of a manned presence in the martian system will be addressed. Idealistically, establishing bases on Mars and Phobos will provide a source of national pride and international cooperation, a technology catalyst, and scientific knowledge. Commercially, these bases will provide fuel and material production sites, a proving ground for life support systems, and a refueling point enroute to the asteroid belt and outer planetary system. Eventually, a Mars base could support life independent of Earth's resources.

The bases will be transported as prefabricated units by a low-thrust Interplanetary Transfer Vehicle (ITV) (Fig. 25) to the martian system and assembled by robots. In this way, humans will not be exposed to the harsh radiation environment during construction. In addition, these unmanned vehicles will use a slow, low-energy transfer orbit to Mars, reducing the fuel consumption. Furthermore, using unmanned vehicles simplifies the vehicles by reducing the redundancy

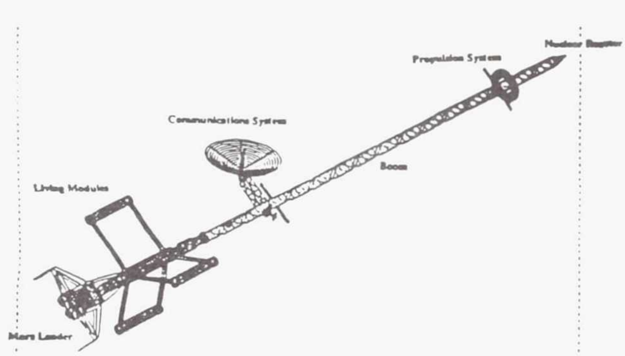

Fig. 25. Kepler Interplanetary Transfer Vehicle[8] (from University of Michigan "Project Kepler")

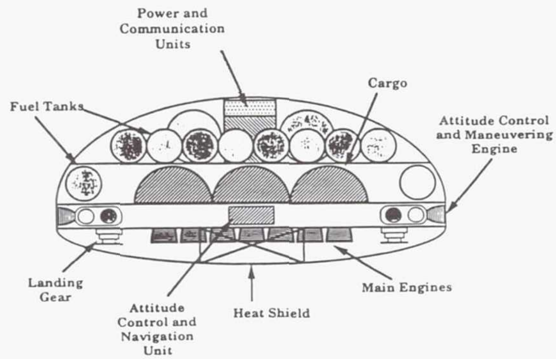

Fig. 26. Mars One Way Lander (OWL-200)

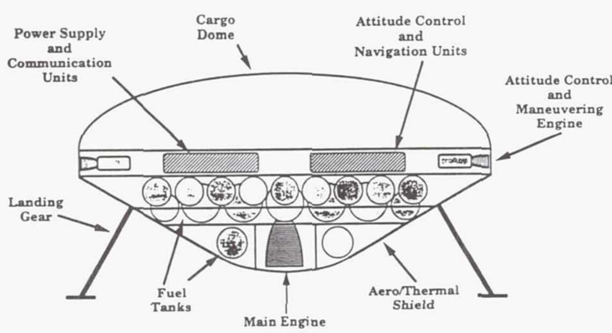

Fig. 27. Mars Ascent/Descent Vehicle (ADV-50)

requirements. However, these autonomous missions will require highly sophisticated technology that either currently exists or is being developed within the following areas:

- Cryogenic Fluid Management
- Automated Proximity Operations
- Autonomous Rovers (Telerobotics)
- Aerocapture
- On-orbit Assembly and Construction
- Surface Power
- Advanced Propulsion
- Propellant Production
- Advanced Life Support Systems
- Vehicle Maintenance Facilities

The main objective is to design a fleet of vehicles to transport base components, cargo, and personnel between martian parking orbit and the base locations. This fleet will include a combination of vehicles, the designs of which depend on the specific functions to be served. The proposed vehicles include: Mars one-way landers (OWL) (Fig.26), Mars ascent/descent vehicles (ADV) (Fig. 27), orbital maneuvering vehicles (OMV) (Fig. 28), orbital transfer vehicles (OTV) (Fig. 29), and a transportation node in martian orbit (MarsPort). In addition, satellites will be deployed to provide communications.

In order to define the scope of the transportation problem, the following assumptions have been made.

1. Year of initial cargo departure from low Earth orbit (LEO) and or low Lunar orbit (LLO) will be between 2020 and 2030.
2. A space station suited for vehicle assembly will be operational in LEO and/or LLO.
3. A lunar base will be operational and producing liquid oxygen.
4. Elements of the Phobos and Mars bases, along with equipment needed to assemble the bases will be delivered to the martian system from the Earth system by a single ITV or a series of ITVs.
5. Each ITV will enter martian orbit in the vicinity of Phobos. It will carry base equipment, satellites, and elements of the transportation system. MarsPort (a truss structure, similar to the delta-truss space station proposed for Earth orbit) could be the backbone of the vehicle or just another payload.
6. OMVs and OTVs will be operational (with one generation of experience).

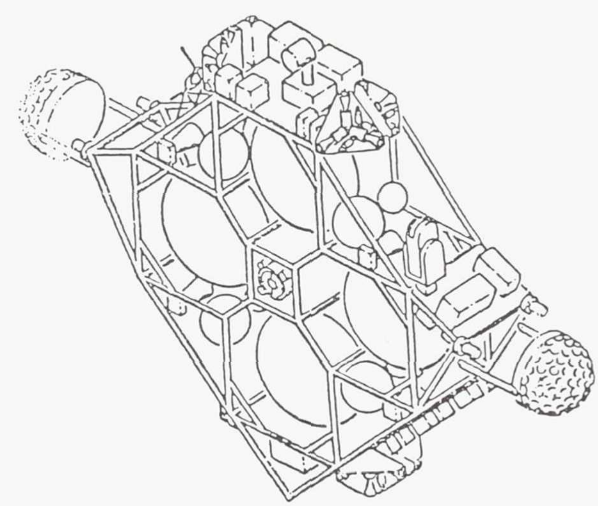

Fig. 28. Orbital Maneuvering Vehicle (OMV) (NASA-Los Alamos)

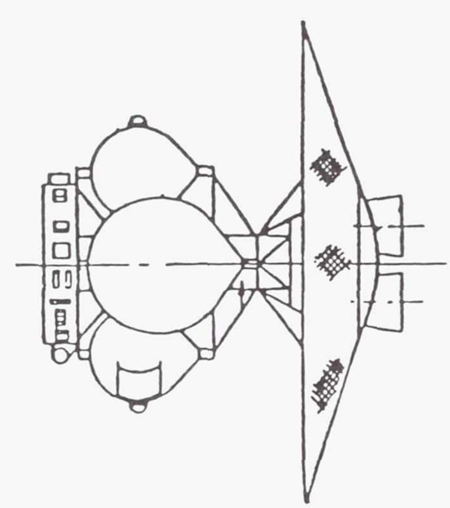

Fig. 29. Orbital Transfer Vehicle (OTV) (Martin Marietta)

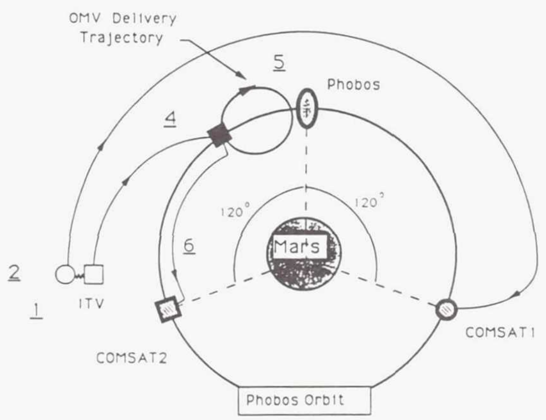

Fig. 30. Mission Scenario for Phobos Base Delivery

7. An inspection team will travel to Phobos to verify base construction. After the initial inspection, the Phobos base will be crew-tended.

8. Mars base construction will begin after the Phobos base is completed and operational.

9. Data from precursor missions of cooperating nations will be available.

10. Accurate models of the martian atmosphere will be available.

11. Before the ITV carrying the Mars base arrives, the Phobos base will have produced fuel to support vehicle flights as required by mission scenarios.

The transportation operations scenario covers two missions which will occur during different time frames: Phobos base

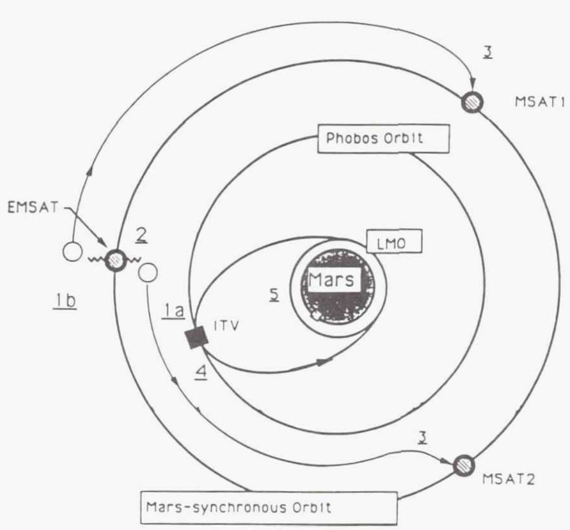

Fig. 31. Mission Scenario for Mars Base Delivery

construction and, later, Mars base construction. One or more ITVs will be dedicated to each mission, and as each ITV approaches its parking orbit, the communication satellites on board the ITV will be deployed. The ITV will then proceed to co-orbit with Phobos. After each ITV is positioned in orbit near Phobos, the other vehicles, base components, cargo, and the MarsPort will be removed by an OMV and transported to their respective locations by the OMV or an OTV. Fig. 30 depicts the Phobos base delivery scenario. Phobos cargo will proceed directly to the surface, and landers bound for the martian surface will receive fuel from Phobos before OTVs transfer them to low Martian orbit. Fig. 31 depicts the Mars base delivery scenario.

An upside scenario is discussed which assumes that the political and economic environments favor the development of a large-scale program. It assumes that all advanced technologies critical to the program can be developed within the specified context and time frame. This report emphasizes the upside scenario because it describes a more efficient and adaptable transportation system. This requires a larger initial investment, but the long-term benefits of a more sophisticated vehicle fleet will better prepare man for a permanent presence on Mars. All vehicles mentioned above are used in the upside scenario. The first ITV will insert into a chaser orbit with Phobos, and the OMVs will then be used to deliver the Phobos base elements.

OTVs and the MarsPort will not be used during the Phobos mission, but the MarsPort will be delivered on this cargo mission to alleviate the cargo mass requirements on the subsequent Mars base mission. Years later, another ITV with the Mars base cargo will insert into Phobos orbit. Since fuel production and vehicle service facilities will be available at Phobos, the ADVs, the OWLs, and OTVs will be transported from Earth without fuel, thereby reducing the payload mass.

The tanks of MarsPort will also be fueled at Phobos prior to delivery of the MarsPort to low Martian orbit by the OTVs. At that time service and refueling facilities will be available at MarsPort and Phobos. The OTVs will then begin transporting the Mars landers to MarsPort where the OTVs will assist the OWLs with de-orbit burns. Since this maneuver will require large amounts of fuel, the OTV will refuel at MarsPort prior to the burn. Further study is recommended on the efficiency of refueling in low Martian orbit at MarsPort since this imposes rendezvous constraints.

All vehicles in the transportation system will be equipped with compatible docking mechanisms. Each vehicle will be equipped with two docking mechanisms located on opposite sides of the vehicle. This configuration will allow simultaneous attachment to the OMV and ITV. The docking system is shown in Fig. 32. The base will be attached directly to the vehicle while supporting the attenuators and capture frame.

The vehicle referred to as "active" is the maneuvering vehicle and the "passive" vehicle is the maneuvered one. Upon initiation of the docking procedure, the active vehicle will have its attenuators extended while the passive vehicle's attenuators will be retracted. The attenuators will act as shock absorbers to reduce the impact forces of docking and also allow for minor misalignment of the vehicles upon capture. Once the

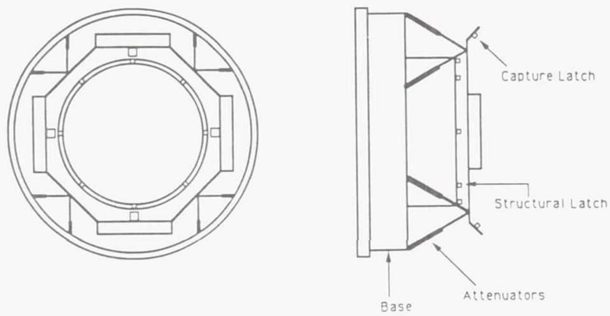

Fig. 32. Phobos Docking Mechanism

capture latches have been engaged, the attenuators will retract to realign the mating vehicles. Finally, the structural latches will be engaged and the procedure will be completed.

In order to explain some of the orbital vehicle requirements, two orbital mechanics studies were undertaken. The first examined the minimum ΔV required for insertion into a Mars parking orbit from an Earth-to-Mars transfer orbit. The second studied the minimum ΔV required to transfer within the Mars system. A simplified analysis was performed using circular orbits and Hohmann transfers incorporating a plane change. It was assumed that the computed ΔV was strictly a function of inclination and orbit radius, and that launch windows were not time critical. A TKSolver™ model was used for these studies. The optimal parking orbit radius is at approximately 3.5 Mars radii, which is very near the Phobos orbit radius of 2.8 Mars radii.

The differences between ΔV requirements for the two orbits were negligible, so the Phobos orbit was chosen as the parking orbit for the ITV. Parking in a Phobos chaser orbit is favorable because it minimizes the ΔV required for Phobos cargo delivery, and it simplifies operations. Orbit transfer, hence fuel consumption and operations associated with OTVs, is eliminated in this scenario. In addition, incoming vehicles can be serviced and refueled at or near Phobos.

MarsPort will be placed in low martian orbit at an altitude of approximately 100 km with an inclination that equals the latitude of the Mars base. It is recommended that the Mars base be located as close to the equator as possible to reduce the ΔV required for the plane-change for the transfer between Phobos and the Mars base.

A Mars Logistics Lander Convertible to a Rocket Hopper

A manned mission to Mars is a prominent objective of NASA's space exploration plans. The purpose of this mission is to establish a permanent martian base for research, exploration and industrialization. It is assumed in this study that the base will be established in two phases. First, unmanned landers will deliver to the surface of Mars the construction hardware and heavy support equipment for the base. Shortly afterwards, astronauts will arrive at the base site. The astronauts will construct the Martian base and begin planned mission operations. To facilitate research and exploration of the planet, surface transport vehicles will be required. Therefore, a transportation system must be designed to establish the base and provide the astronauts with surface mobility. One component of the transportation system will be a fleet of three logistics landers. These logistics lander are unmanned vehicles which deliver payloads from the Martian moon Phobos to the surface of Mars. The second component is a manned rocket hopper vehicle which will be used for surface point-to-point excursions. The purpose of this project is to develop a conceptual design for a Mars Logistics Lander that is convertible to a rocket hopper vehicle[9].

The following design criteria were specified for the logistics landers:

1. There will be three logistics landers. Each lander must be capable of delivering a payload from Phobos to the base site on the surface of Mars. The logistics lander is an unmanned, single-mission vehicle.

2. Each lander must be transformable into some device or part of a device which is needed for the support of the base.

3. Each lander must be capable of a precision landing within 25 meters of the selected base site.

4. The design should include different descent braking options to minimize the mass of the lander.

5. Lander touchdown speed should be no more than one meter per second.

6. The mass allocations for each lander are:

Mass at Phobos	75 metric tons
Propellant capacity	20 metric tons
Mass at Mars touchdown	55 metric tons
Dry mass (engines, structure,etc.)	10 metric tons

7. The landers will use liquid oxygen/liquid hydrogen engines with specific impulse of 470 seconds and a 7:1 fuel ratio.

Design criteria for the rocket hopper:

1. The hopper can be constructed of components from one, two, or all three of the logistics landers.

2. The hopper will carry a crew of two or three astronauts.

3. The hopper must carry the space-suited crew, three days of supplies, and a small rover vehicle. The hopper crew cabin will serve as the vehicle airlock.

4. The hopper capacity must be 500 kilograms of cargo plus the crew of suited astronauts and life-support systems.

5. The hopper will have three or four engines with an engine-out capability.

6. The hopper will traverse most of its trajectories ballistically with initial and final powered flight segments.

7. The hopper fuel and oxidizer may be hypergolic (propellants which spontaneously ignite on contact) or liquid oxygen/liquid hydrogen.

8. The hopper range must be at least 1000 kilometers with return fuel carried outbound. Fuel reserves of ten percent must be carried onboard.

Alternative designs were proposed for the logistics lander and the rocket hopper. Design alternatives were also developed for the lander and hopper subsystem components, such as landing gear and aerobraking devices. The advantageous

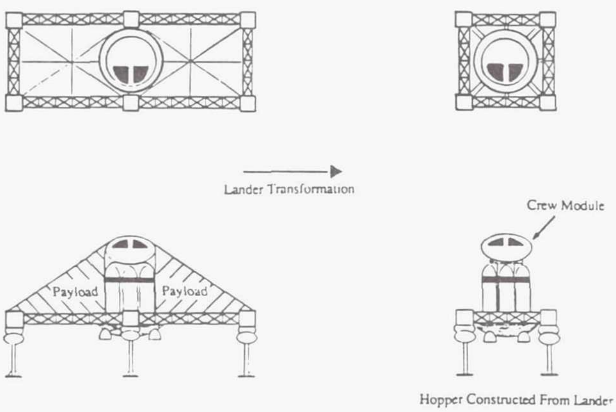

Fig. 33. Tinker Toy Lander Alternative Design

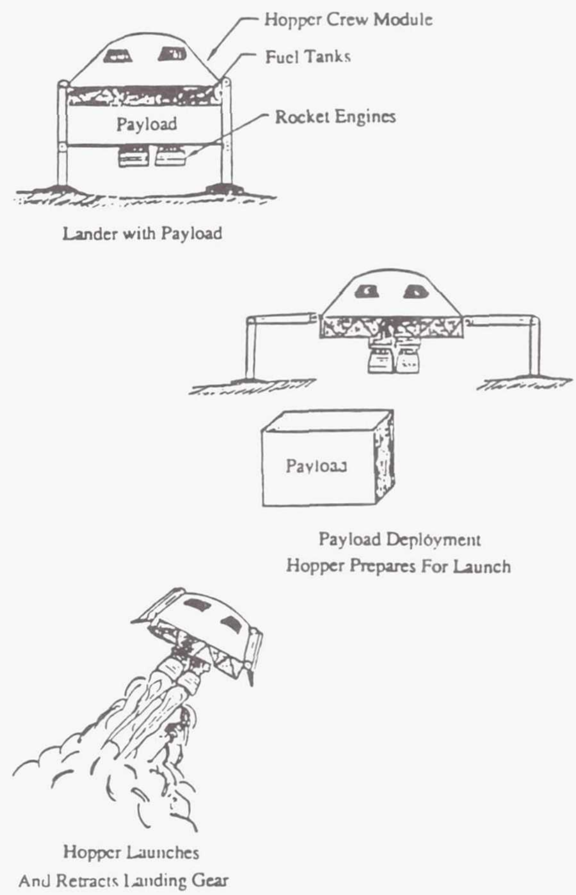

Fig. 35. All-in-One Lander Alternative Design

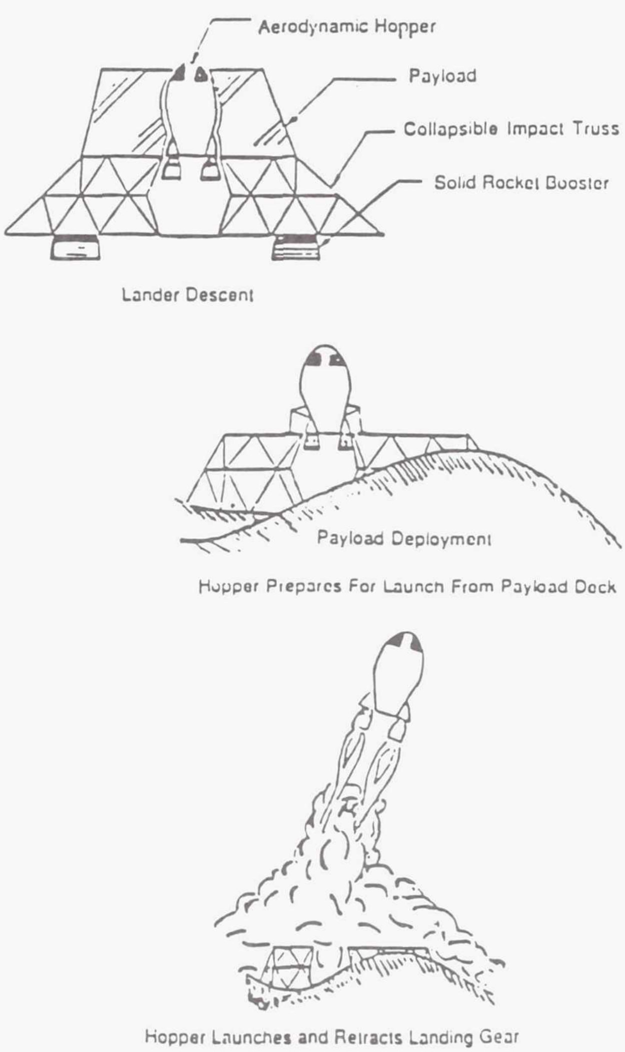

Fig. 34. Filled Doughnut Lander Alternative Design

features offered by individual subsystems were combined to produce an optimum final vehicle configuration. The three alternative designs for the conversion of the logistics lander into the rocket hopper are shown in the Figs. 33, 34, and 35.

The final conceptual design of the Mars Logistics Lander was selected from the proposed alternative designs by a Method of Pairs analysis. The Tinker Toy alternative design accumulated the highest overall rating and was adopted for development as the final design for the lander. The lander can be described in terms of five major components of its design: (1) Truss Frame and Payload Decking, (2) A Modular Propulsion Unit, (3) A Crushable Landing Pad, (4) A Cone and Skirt Heat Shield, and (5) A Central Navigation and Control Module.

The frame of the Mars Logistics Lander consists of six 5-meter-long square truss beams connected to form a hexagonal perimeter. The circumferential beams are supplemented by six 4-meter-long trusses. These trusses radiate from the centrally located modular propulsion unit as seen in Fig. 36. All truss beams are one meter on a side and are made from rods of graphite epoxy. The circumferential and radial trusses are

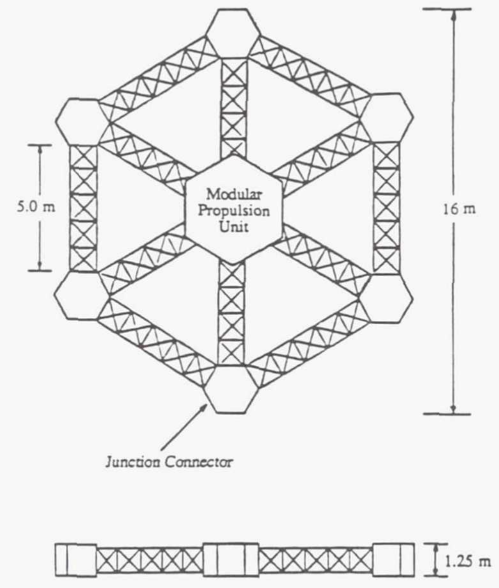

Fig. 36. Truss Frame of Mars Logistics Lander

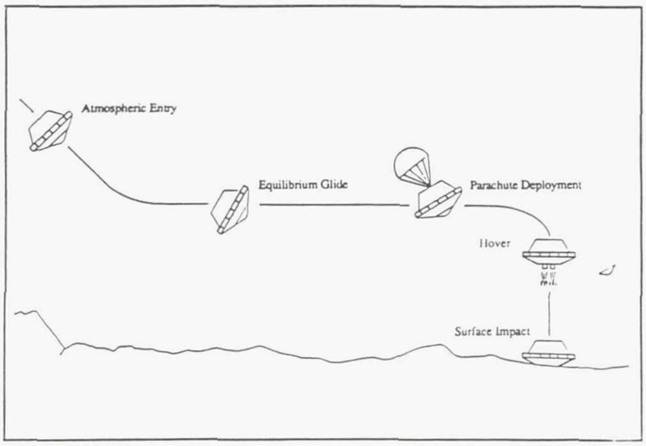

Fig. 38. Entry and Descent Scenario for Logistics Lander

joined at their ends by six hexagonally shaped junction connectors. Each connector has a cluster of reaction control thrusters mounted on its outboard surface. Fig. 37 shows a schematic of a single junction connector.

The truss frame supports the payload of the lander during the transfer from Phobos. The payload will be mounted directly on the trusses, either above or slung below. Decking made from composite material can be added to the truss frame for payloads which require planar supporting surfaces. The truss frame and payload decking can be modified to fit a wide range of payload mass distributions. After the lander has completed its mission, the truss beams and decking will be used as structural elements in the construction of the martian base.

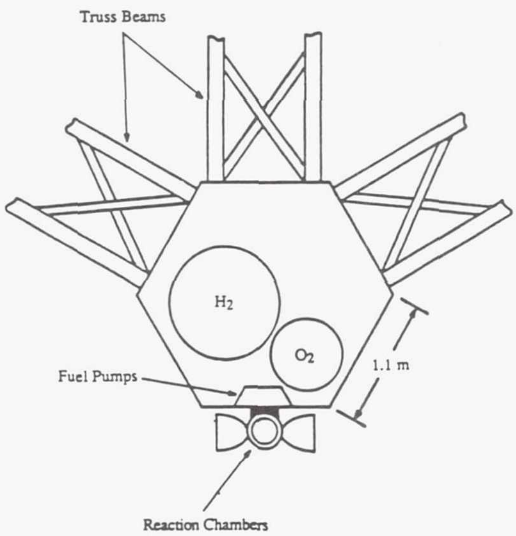

Fig. 37. Hexagonal Junction Connector

The propulsion, aerobraking, and landing gear systems of the lander are also mounted to the truss frame. This arrangement gives the lander the flexibility to accommodate a wide range of transport mission requirements. Fig. 38 depicts atmospheric entry and descent of the lander.

Lander Design. The characteristics of the logistics lander follow.

1. It is a one-way, unmanned vehicle.
2. It delivers a 45,000 kilogram payload from Phobos to Mars.
3. Modular truss elements support the payload. Two modular engine propulsion units provide a combined thrust of 400 kN. The lander's total dry mass is 12,097 kg.
4. Liquid oxygen/liquid hydrogen propulsion system with a 6:1 fuel mixture ratio and a specific impulse of 492 seconds. The lander carries 20,000 kilograms of fuel and its initial wet mass is 75,000 kilograms.
5. An ellipsoid hardshell ACC heat shield is placed at the critical heating areas and a fabric heat skirt protects the subcritical lander areas during descent.
6. A crushable torus of T-22 styrofoam serves as the lander's landing gear.

Rocket Hopper Design. The final design for the rocket hopper is a modified version of a ballistic low-profile hopper and a gliding lifting-body hopper (Figs. 39-42). The hopper design characteristics are:

1. A manned vehicle for point-to-point excursions on the martian surface.
2. The hopper body is constructed from the modules of the logistics lander. The modular propulsion unit forms the main body of the hopper. The command module is brought down as payload on the lander and is attached to the propulsion unit. The hopper wing sections are delivered as payload and attached to the modular propulsion unit to form the hopper body.

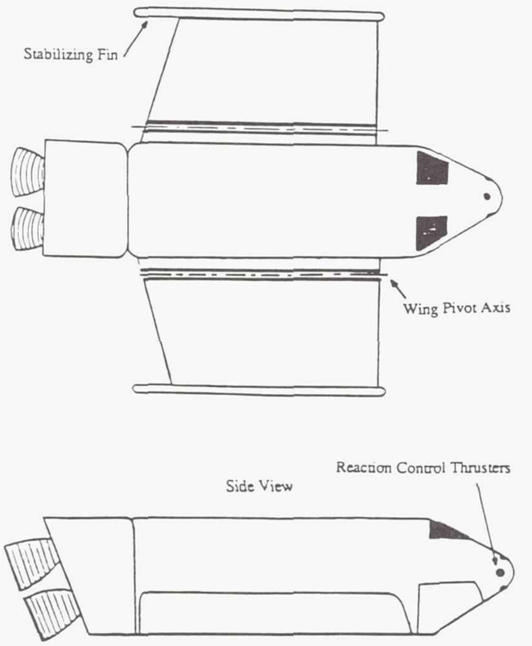

Top and Side View of the Mars Ballistic Hopper Using a Modified Low Profile Design. Wings are added to provide lift, drag, and stability at the high Mach numbers existing throughout the aerobrake phase of the trajectory. The wings also pivot down to serve as a component of the landing gear.

Fig. 39. Mars Ballistic Hopper Design

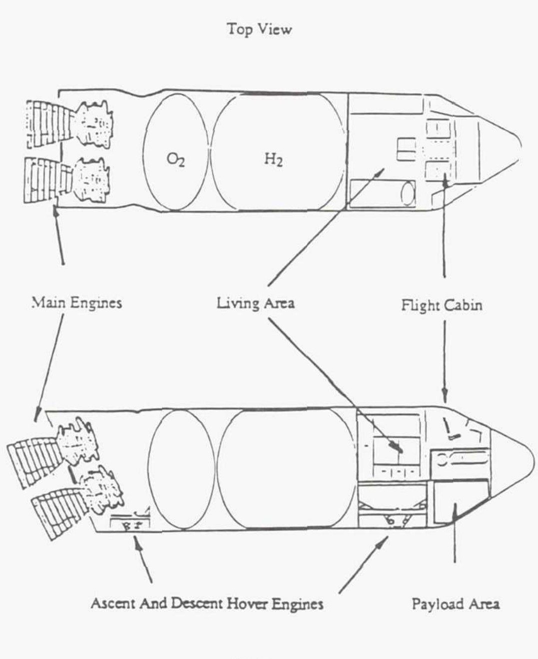

Fig. 40. Cut-Away View of Hopper Interior

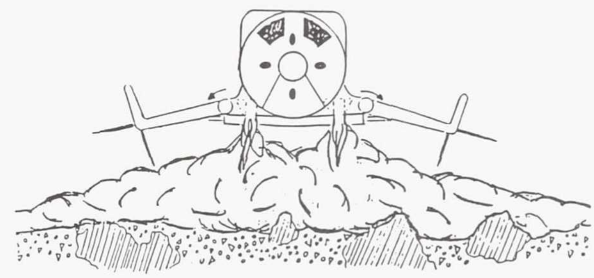

Fig. 41. Hopper Hovering Prior to Landing

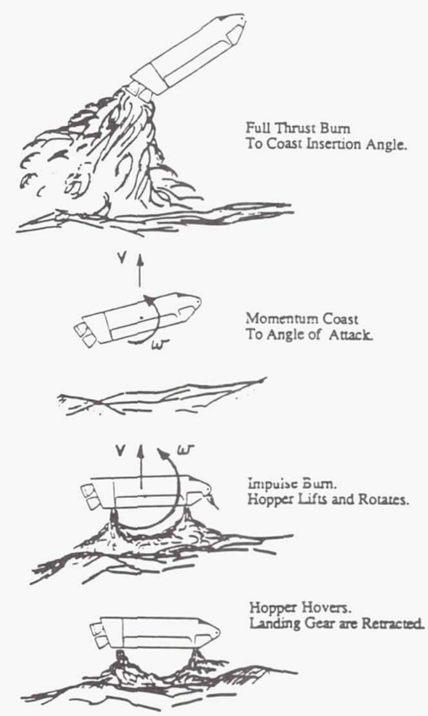

Fig. 42. Launch Maneuvers for the Ballistic Hopper

3. The hopper is a winged vehicle with a lift to drag ratio of 1.5, a ballistic drag coefficient of 500, and a ballistic lift coefficient of 1000.

4. The hopper has a cylindrical shape, 12 meters in length and 3 meters in diameter and has an initial wet mass of 15,000 kilograms.

5. The hopper's trajectory has initial and final powered-flight segments separated by a projectile coast at a constant thrust attitude of thirty-five degrees from the horizontal.

6. The hopper uses its aerodynamic shape and rotofoil parachutes to aerobrake in the Martian atmosphere.

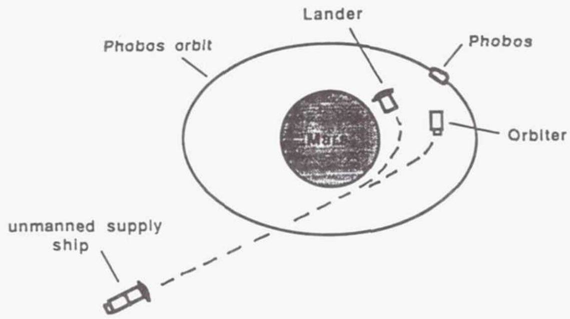

Fig. 43. Mars Mission Scenario

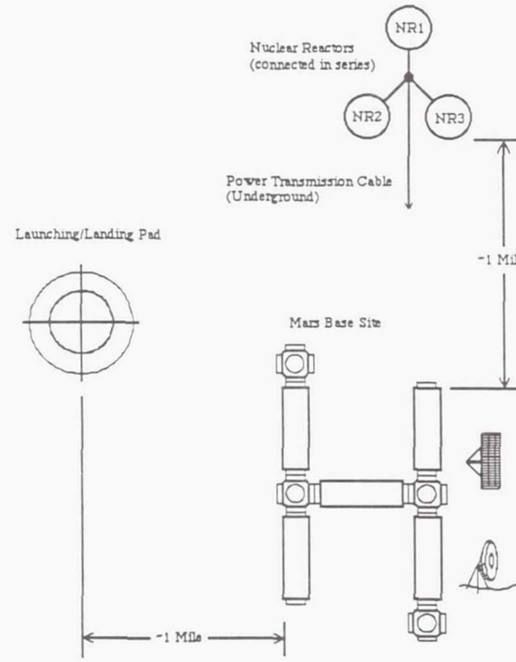

Fig. 44. Mars Base Layout

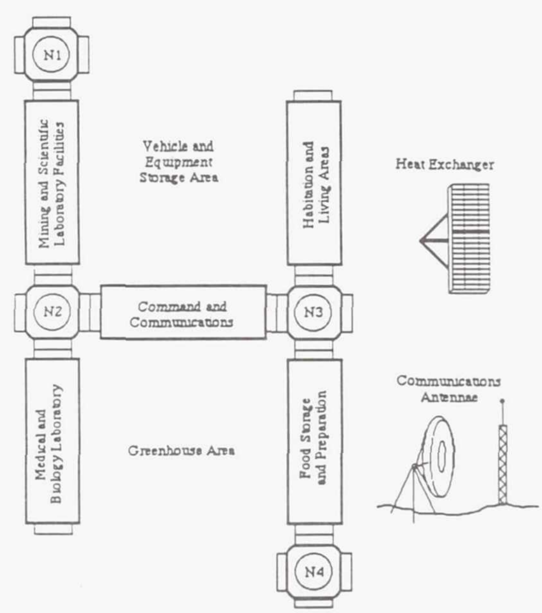

Fig. 45. Top View of Martian Base in 'H' Configuration

7. The wings of the ballistic hopper serve as flight stabilizers, aerobraking devices, and landing skids.

Manned Base Design and Related Construction Issues for Mars/Phobos Mission

Construction and operation of distant planetary bases involve unusual problems. Conventional construction and operations techniques are considered inefficient due to the communication time delay between the Earth and Mars and the prohibitive cost due to the large mass of construction equipment needed. Additional factors such as low gravity fields, harsh environments, and high levels of solar and galactic radiation may complicate conventional methods. Innovative techniques for the remote construction of a base on Mars or one of its moons are sought. The design team formulated a variety of conceptual designs that could meet the safety, habitability, ease of construction, and reliability parameters required for such a facility[10].

The general mission scenario chosen for this design project is depicted in Fig. 43. The mission consists of an unmanned supply ship which has both a lander and an orbital vehicle. The lander contains one experimental facility designed to house 4-5 people. This base would be responsible for conducting research on factors related to the establishment of a permanent base. This base would also contain the heavy mining experiments (possibly including a large core drilling system to look for life in the water table as well as take various core samples). The lander would also contain 3-4 rovers for use when the astronauts arrive on a later mission.

The orbiter will do extensive high-resolution imaging of Mars to pick a landing site for the lander. For Phobos exploration, the orbiter, minus some possible communications satellites, will land itself inside a crater on Phobos. This orbiter would be capable of anchoring itself to Phobos as well as initiating a mining procedure. It will also be able to house several people for periods of up to a week.

Mars Base Design. Figure 44 depicts the proposed Mars base layout. When viewed from above, the main section of the fully deployed base will resemble an 'H' and Fig. 45 gives details on the function of each module and the joining areas.

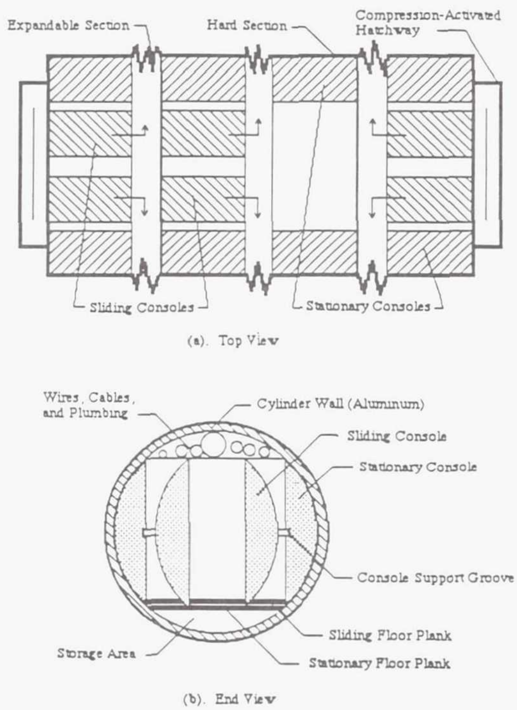

Fig. 46. Cross-Section of Packed Accordion Module

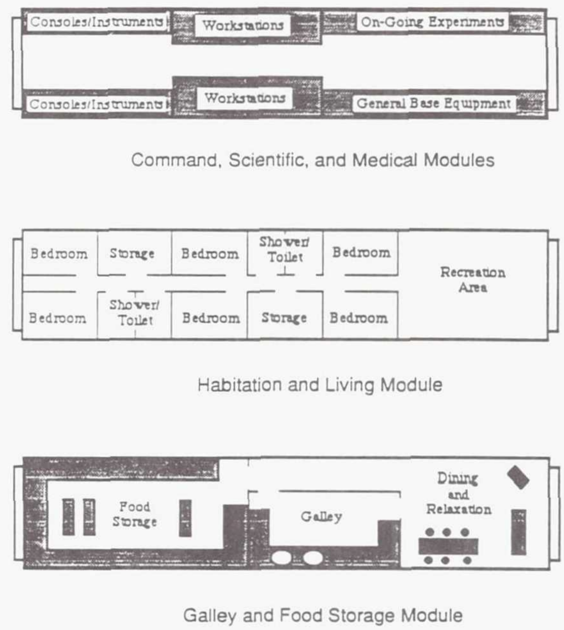

Fig. 47. Interior Layouts of Base Modules

Peripheral items such as the nuclear reactor, the thermal dissipaters, and the landing area will be located at areas surrounding the pressurized modules. The chosen construction concept for the Mars base modules is the use of an accordion design shown in Fig. 46. The accordion design incorporates expandable modules that each have four 6-foot-long hard sections with expandable sections between the hard sections. When expanded, the total module length will be 45 feet. The expandable sections are constructed of two layers of inflatable fabric which remain folded during transport to Mars. Once on Mars, the module is expanded, allowing the fabric to form concentric layers. During expansion, the inflatable sections of the module are injected with a liquid mixture. This mixture hardens upon drying to form a hard cylindrical shell which is similar in size to the hard sections. When dry, the hardened sections will provide additional structural support for the module so that it will withstand the weight of the 4 meters of regolith shielding under which it will be buried. This shielding is to protect the base from both galactic cosmic and solar radiation.

The size of the compressed module is 27 feet long and 15 feet in diameter. This size will enable the modules to be launched from Earth in a variety of launch vehicles including the shuttle. The compressed module will contain 4 hard sections which are each six feet long. Three sections of the inflatable fabric will be packed between these hard sections. When expanded the module size will be 45 feet in length. The

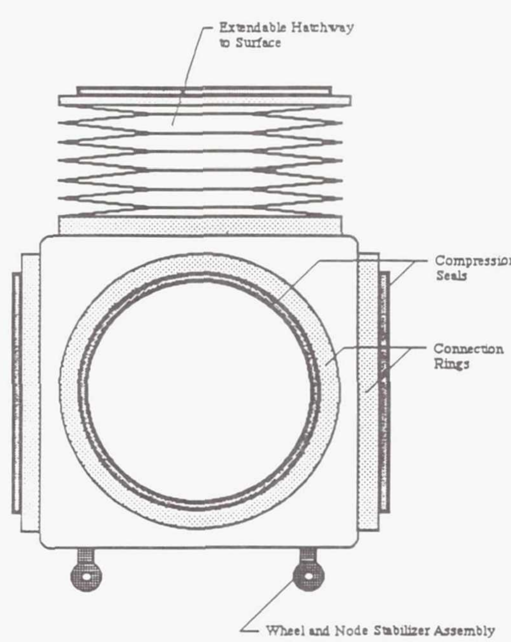

Fig. 48. Generic Configuration of Connection and Airlock Nodes

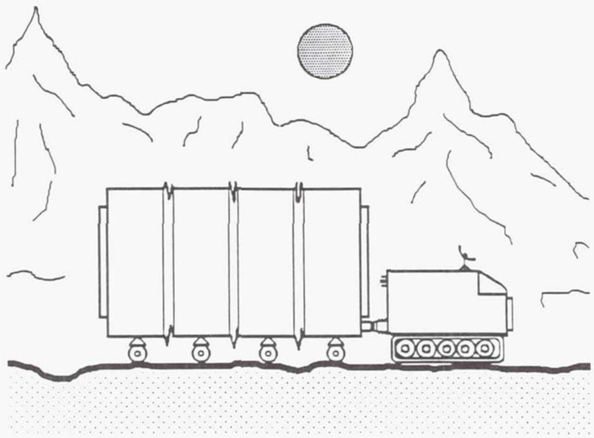

Fig. 49. Martian Utility Vehicle Towing an Accordion Module

ends of the modules will house hatchways and connections which will be used to join the modules to the nodes. Specific module interior layouts and functions are shown in Fig. 47.

Module sizing is dictated by the amount of space needed by humans to function relatively comfortably. The importance of human factors and ergonomics in an extended mission in

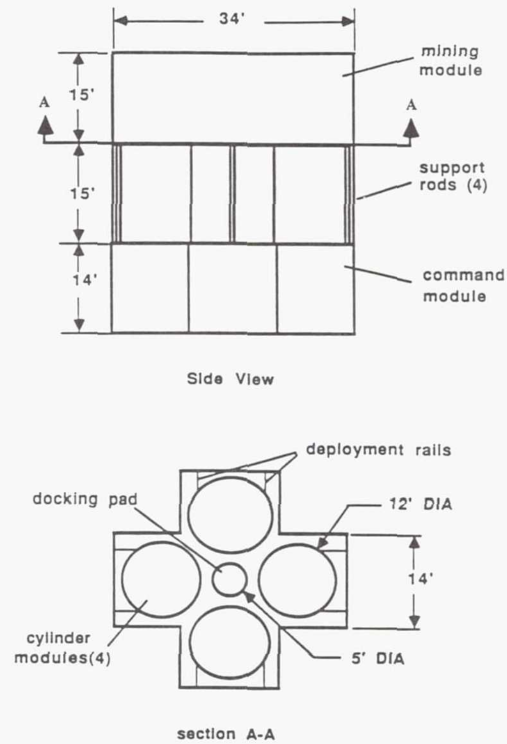

Fig. 51. Phobos Base Packed for Transport

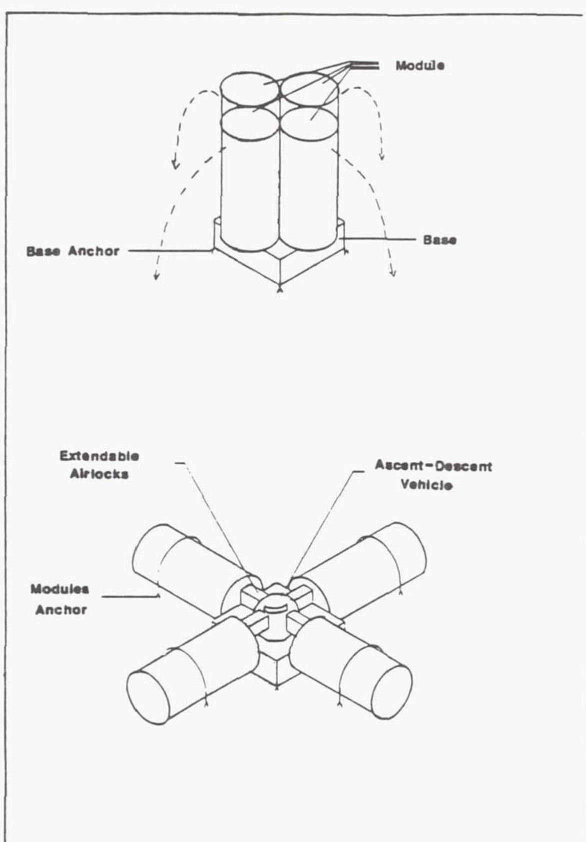

Fig. 50. General Star Design

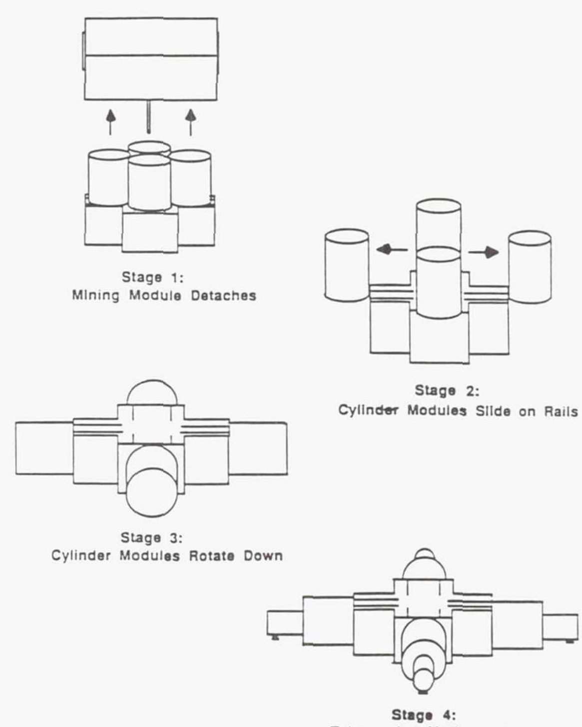

Fig. 52. Four Step Base Deployment

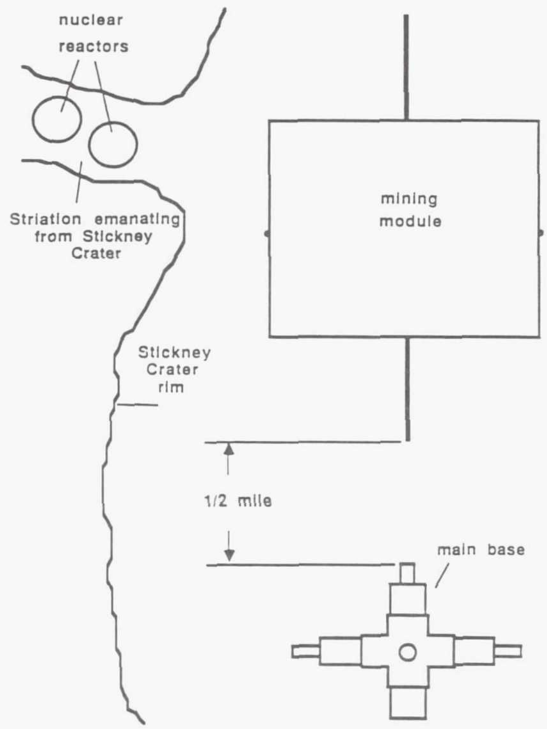

Fig. 53. Final Phobos Base Layout

reduced gravity is significant. The 7 × 7 foot open interior space extending the length of the working modules allows two humans wearing environmental suits to pass each other reasonably easily if an emergency should arise. It also allows for enough space to avoid crowding if people are working at adjacent work stations. The living areas such as the galley and the bedrooms do not have this walkway but are designed for the specific tasks accomplished there. The semicircle between the removable floor planks and the bottom of the cylinder will provide storage space, and the space above will contain wiring, plumbing, etc. The placement of the wiring and plumbing above the working areas will also provide further radiation protection. This module design will allow a comfortable "shirt-sleeve" environment throughout the base.

Figure 48 shows the design of the connection nodes. These nodes resemble cubes with hatchways built into each of their four sides and on the top. These hatchways serve as windows, airlocks, or connection points for the addition or joining of modules. When connected, the nodes will hermetically seal the base. For base uniformity, all hatches on the base will be standardized, allowing a variety of base configurations.

Phobos Base Design. The Phobos base will utilize a Star Design for the base configuration. The star design makes use of cylindrical, pre-built modules (Fig. 49). Attached to the bottom of the cylinders is a disk-shaped base which contains an anchoring system. Once the entire structure lands on the surface of Phobos, the anchors will be released into the

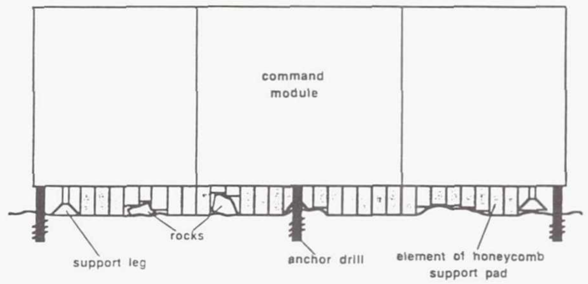

Fig. 54. Honeycomb Pad Conforming to Surface

Phobian regolith. Figs. 50-52 depict the star design and Fig. 53 gives the final base layout.

The command module of the base resides in the center section of the star and will house a docking facility for small spacecraft, a "safe haven" from radiation, the main computer facilities, and much of the base control systems. The docking port will be 5′ in diameter and will be centered on top of the module. It will connect to an airlock which will provide access to the bottom level of the two level command module. This airlock will also be shielded well enough to serve as a refuge from the 1 to 2 hour radiation storms caused by the sun. The remaining portion of the command module will contain equipment necessary to sustain base functions and to provide computer information and control to various base equipment.

The four cylinder modules will be used for habitation, science labs, storage, etc. Three of the four cylinders will contain telescoping tubes which will be 5½ feet in diameter. These tubes will telescope out of the vehicle and be used for storage as well as "shirt-sleeve" access to a Phobos rover. Access to the rovers would be through a 2¾-foot-diameter crawlway down the center of the tube. This crawlway would lead to a small hatch which would connect to a rover vehicle. The remaining cylinder will be a surface access module and will contain an airlock and a work area.

To assist in leveling the base, the design includes a one-foot, crushable pad under the command module as well as 11 adjustable support legs (four on the command module, one on each cylinder, and one on each telescoping section). The crushable pad will consist of a honeycomb network of material which will collapse when it encounters a sufficient force. The outside of the honeycomb pad will be made of a slightly harder material which will support the honeycombs during transit to Phobos. This harder material will also be selected such that it will puncture when a certain pressure is exerted against it. Note that the pad will also help in steadying the base while the drill anchors are being set to permanently anchor the base. Figure 54 shows the honeycomb pad and drill anchoring system.

ACKNOWLEDGMENTS

Principal authors included J. Amos, J. Campbell, C. Hudson, E. Kenny, D. Markward, C. Pham, and C. Wolf. They were

assisted by teaching assistant G. Davis and faculty advisors Drs. G. Botbyl, W. Fowler, and S. Nichols.

REFERENCES

1. The University of Texas at Austin, "Final Design for a Lunar Crew Emergency Rescue Vehicle," NASA/USRA Design Project, December 1988.
2. Davis, G.W., et al. "The Lunar Split Mission: A Robotically Constructed Lunar Base Scenario," NASA/USRA Summer Design Project, JSC Advanced Programs Office, August 1988.
3. Campbell, J., Engel, J., and Yazdani, M., "Analysis of Health Care Needs for a Lunar Colony and the Conceptual Design of a Permanent Medical Facility," NASA/USRA Design Project, The University of Texas at Austin, Spring 1989.
4. NASA, "Beyond Earth's Boundaries," 1988 Annual Report to the Administrator, Office of Exploration.
5. The University of Texas at Austin, "A Robotically Constructed Production and Supply Base on Phobos," NASA/USRA Design Project, May 1989.
6. Amos, J., et al., "Robotic Construction of a Permanently Manned Mars Base: Final Report," NASA/USRA Design Project, The University of Texas at Austin, May 1989.
7. The University of Texas at Austin, "Final Design Review Report for a Mars/Phobos Transportation System," NASA/USRA Design Project, May 1989.
8. University of Michigan, "Project Kepler: Manned Mars Mission," NASA/USRA Design Project, Winter 1986.
9. Wolf, C.V., Dierks, J.M., and Valdez, A.M., "Conceptual Design of a Mars Lander Convertible to a Rocket Hopper," NASA/USRA Design Project, Fall 1988.
10. Kenny, E.M., Bhaskaran, S., and Feng, V.C., "Conceptual Study of Manned Base Design and Related Construction Issues for Mars/Phobos Mission," NASA/USRA Design Project, Spring 1989.

N94- 71288

1994004533
382694
521-66
160647
P. 8

MISSION: PHH_2O

TEXAS A&M UNIVERSITY
AEROSPACE ENGINEERING

The purpose of this project was to design a mission and spacecraft capable of retrieving 120,000 kg of water from Phobos, a martian moon. There were no restrictions on the types of propulsion or power systems used. The duration of the mission was not defined, but a factor influencing the length of the mission was the statement that it would be cyclic in nature and the spacecraft could be manned or unmanned. The only assumptions provided were that a pumping and refueling station existed on Phobos and that a base existed on the Moon. The technology used for this mission was to be of the year 2007 and beyond.

The first option to be considered was a manned vs. unmanned spacecraft. The advantages of a manned spacecraft are: man's ability to investigate unexpected events, to detect and correct errors, to adapt to unknown situations, to change response characteristics, and to display logic gained from specialized training. Experiments could be performed on the ship during the journey; the ship could also replace crewmen stationed on Mars or Phobos. However, these advantages are far outweighed by the disadvantages. The disadvantages are: the sensitivity of humans to the stresses of spaceflight, the demands for a livable environment, the need to provide sustenance and waste removal, and the increase in complexity of the spacecraft design. Also, the presence of man on the spacecraft and the life-support systems would add tremendous mass to an already considerable amount, therefore the unmanned spacecraft was deemed more practical.

Another design option was the type of thrust production required for the mission. All options of thrust were theoretically possible, high, low, and some combination. Although a purely high-thrust mission was possible, the fuel requirements would be extraordinarily high. A purely low-thrust option would present mission length difficulties; Since the mission was thought of as cyclic in nature, the spacecraft needed to deliver the water expeditiously. The difficulty in meeting the mission time constraint was more critical than fuel savings, therefore, a hybrid mission was chosen. High thrust would be required to escape the Earth-Moon or martian system, while low thrust would be used for heliocentric travel.

The mission plan originates with the spacecraft in a lunar orbit. A high-thrust ΔV will be applied to escape the Earth-Moon system. During the heliocentric orbit transfer to Mars, constant low thrust will be applied. After Mars arrival, a minimal ΔV will be required to transfer the spacecraft from martian orbit to Phobos. The return leg does not involve any additional requirements; therefore the propulsion system for the entire mission needs the capability for both high and low thrust.

Four types of propulsion systems were studied to see if the mission requirements could be satisfied. The first studied was the chemical rocket engine. The fuel requirements needed for the chemical rocket engine were excessive due to the low specific impulse and the mission duration. Solar-powered propulsion systems were considered, but rejected since the technology for their development would probably not be feasible by 2007. Fusion-powered systems would provide a high specific impulse and low propellant mass; however, they were rejected. Realistically, fusion-powered systems will not have reached the production stage in the next 25 years. If, however, the technology did become available, fusion engines would be a viable option. Nuclear electric engines are primarily of low thrust providing a high specific impulse but maximum thrust of only 5 N. This low thrust would not meet mission time constraints; therefore, nuclear electric engines were rejected.

The first hybrid system considered was a single magnetoplasmadynamic (MPD) engine. The engine produces a high specific impulse at small mass flow rates. The MPD engine is primarily designed for low-thrust applications, but is capable of producing the high thrust needed for escape trajectories. The engine generates large amounts of power using relatively small amounts of propellant, which may allow the option of using the MPD as a power supply. At the current state of development, MPD engines have high cathode erosion rates. The high erosion rate leads to the failure of the engine at a comparatively short lifetime, a maximum of 3600 hours. The MPD engine was rejected because of the high cathode erosion rate.

The second hybrid system considered was direct nuclear propulsion using a single nuclear reactor. A nuclear reactor operates similarly to a chemical rocket engine in that they both use heat to expand a gas for propulsion. The propellant mass is significantly lower compared to the chemical rocket because the nuclear reactor is more efficient. Only one propellant is needed for the nuclear reactor compared to the fuel and oxidizer used for the chemical rocket engines. Also, the nuclear reactor generates much higher chamber temperatures that result in higher specific impulses. A nuclear reactor can be throttled by various means to provide any desired mass flow rate and thrust. The specific reactor considered was the Nuclear Engineering for Rocket Vehicle Applications (NERVA) reactor. The NERVA reactor has already been tested and has demonstrated its usefulness. A benefit of the NERVA reactor is the low mass of the reactor itself. The NERVA reactor and the mass of the pumps and the other system hardware was a small fraction of the mass of the water and fuel. The problem with using only one reactor was that the reactor would experience changes in the mass flow rate of order of magnitude three (i.e., kilograms down to grams/second) due to the high/low thrust requirements of the mission. The system

C-3.

N

Table 1. Dimensions and Performance Values for the Small and Large NERVA Reactors

Engine Characteristics	Small Reactor	Large Reactor
Core Diameter (m)	0.50	1.00
Core Length (m)	1.00	2.00
Engine Mass (kg)	1000.00	2200.00
Specific Heat Ratio	1.30	1.30
Chamber Temperature (K)	2700.00	2700.00
Gas Constant (J/kg-K)	4124.20	4124.20
Exhaust Velocity (m/s)	10000.00	10000.00
Max Mass Flow Rate (kg/s)	0.01	30.00
Thrust Force (N)	50.00	300000.00
Specific Impulse (sec)	1020.00	1020.00

was not considered feasible due to the unknown effects on the reactor caused by the large fluctuations in the mass flow rate.

The hybrid propulsion system chosen for the mission consisted of three NERVA reactors in order to meet the high and low thrust requirements. Since one NERVA reactor cannot handle the large changes in mass flow rate, combinations of small and large reactors would yield a propulsion system capable of handling a hybrid mission (see Table 1). The design consists of a small reactor with a maximum of 10 g/sec mass flow rate in combination with two large reactors capable of a maximum of 30 kg/sec mass flow each. For the high thrust at the begining of the mission, the two large reactors would be utilized. After the escape ΔV of 3.723 km/sec is achieved, the two large reactors would be shut down. The small reactor would then provide the low thrust for the heliocentric orbit trajectory to Mars. The NERVA reactors would contain cores comprised of subcritical masses of uranium carbide (UC) fuel. A system of reflectors would be used to activate the reactors by reflecting the neutrons back into the core causing radioactive reactions to begin. The NERVA reactors are cylindrical with a shield around the core (see Fig. 1). Since the NERVA reactor is an open cycle system, the heat and particles produced during the nuclear reaction are expelled along with the propellant through the exhaust. This process requires that the nozzle be kept cool by regeneratively flowing liquid hydrogen around the nozzle area.

The propellant used for the propulsion system was hydrogen. Hydrogen has the lowest molecular weight of possible propellants, thereby providing the best engine performance. Two methods were considered for storing and providing the hydrogen.

The first method would be to dissociate the hydrogen from water. The water would be broken down as propellant was needed; the oxygen could be stored for delivery to the lunar base or simply expelled. The reactions involved in the breakdown are often impure, leading to extraneous byproducts. This method would also require a considerable amount of power to break up the water. The dissociation of water was determined to be impractical.

The second method for obtaining and storing hydrogen was to transport the hydrogen in a cryogenic system. Hydrogen, in order to be kept in a liquid state, must be stored near absolute zero. The standard cryogenic-fluid vessel is the Dewar vessel, a double-walled container with insulation between the walls.

The power required to operate the spacecraft could be provided in several ways. One way is to utilize the exhaust of the propulsion system. In the case of a nuclear reactor, the exhaust gases would have to be channeled off. Any such method of drawing from the exhaust flow was determined to be unsatisfactory. Another method for providing power is to use the excess heat generated by a closed cycle reactor. Thermionic plates surround the reactor, converting the heat directly into electricity. The problem is that the Thermionic plates are only 10% efficient; thus leaving 90% of the heat to be removed via radiators. Due to the fluctuating heat intensity, power cells would have to be used to provide a steady power supply to the spacecraft. Since an open cycle reactor was chosen, no excess heat is generated and therefore negates the use of Thermionic plates.

The power system chosen was to use an existing power source for interplanetary missions, radio isotope thermoelectric generators (RTGs). The RTGs are comprised of a fixed amount of plutomium 238 in a small container. The amount is based on the required life of the power supply (calculated from the half-life of plutonium). Two Thermionic plates surround the container converting the radioactive decay into electrical power using the temperature differential between the Thermionic plates. The spacecraft has eight RTGs, four being utilized for power while four are for backup. Each RTG produced 500 watts of continous power. (The RTGs are continually being improved, so by 2007 they should be one of the best power sources available.) Two RTGs will be used simultaneously to provide 1 kW of power for the central control and guidance system. The other two RTGs will provide 1 kW of power for the other three systems: (1) the heaters and circulation pumps for the water; (2) the cryogenics system and flow values for the hydrogen; and (3) the valves and heaters for the reaction control system.

The communications system is composed of two systems, long range and short range. The long-range "update" system keeps in contact with the lunar base to indicate mission status or problems that have arisen and how the spacecraft is correcting the situation. The short-range system will be on a

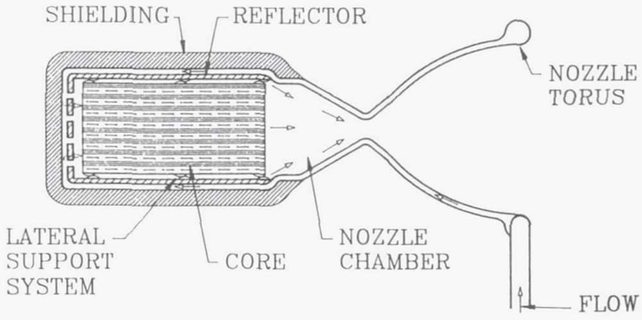

Fig. 1. Schematic of a NERVA Reactor

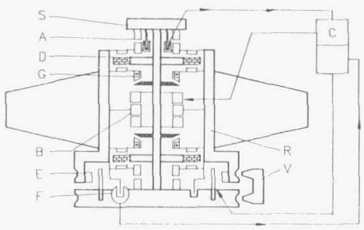

Fig. 2. Schematic of a Single-Axis Magnetic-Bearing Momentum Wheel

different wavelength and is used for the teleoperation of the spacecraft during docking procedures. Should a problem occur beyond the range of the short-range system, the spacecraft could be controlled through the long-range system using transmitted control programs. The receiving station for the long-range system is located at the lunar base. An automatic feedback system will return a signal to the spacecraft while the lunar base is receiving a signal from the spacecraft. If the signal stops, the spacecraft will have an override program to redirect the antenna to an alternate receiving location. Should the spacecraft lose its pointing and position sensors, it will automatically cease all relative motion and adjust the antenna to transmit a signal with four degrees of arc. The spacecraft will then proceed to send an emergency signal for 30 minutes per sector in a prescribed pattern of 3284 sectors over 68 days to cover the surrounding sphere. When the spacecraft receives a signal, a feedback signal is returned to the lunar base and the spacecraft can lock on and corrective procedures can be implemented. (The communication system contains data for planetary eclipses, so corrective maneuvers will not be initiated at that time.)

Central control and guidance of the spacecraft are provided by a computer system housed in the inner corridor. The computer receives information from two 3-axis, magnetic-bearing momentum wheels and two star scanners (Fig. 2). The momentum wheels provide rotation and acceleration information while the star scanners provide position and pointing information. There are also sensors located throughout the spacecraft to update the status of the various onboard subsystems. Each of the subsystems has its own artificial intelligence (AI) unit, but the central control system monitors all subsystems and can override them if necessary. The subsystems that are controlled by the central control system are: the heaters and circulation pumps for the water, the cryogenics system for the hydrogen, the inlet valves for the water and hydrogen, the valves and heaters for the attitude control system, the communication system, the guidance system, and the nuclear reactor control systems.

In order to maneuver the spacecraft about its three primary axes, a reaction control system (RCT) was needed (Fig. 3). The spacecraft must be able to rotate to decelerate for the approach to Mars and Earth. The system chosen is the one currently used by the space shuttle. The RCTs are comprised of primary thrusters used for vehicle reorientation and vernier thrusters used for fine adjustments. Both thrusters operate by using monoethylhydrazine (MMH) as fuel and nitrogen tetroxide (N_2O_4) as the oxidizer. The fuel and oxidizer are hypergolic; that is, they are capable of spontaneous ignition. Since the propellants run the risk of freezing while inoperative, heated lines circulate around the thruster feed lines.

The fuel and oxidizer for both thrusters are stored in spherical tanks utilizing a gas pressure feed system. Helium expands into the fuel and oxidizer tanks, forcing the liquids into the combustion chamber. Thirty-six RCTs are located around the spacecraft such that the spacecraft can be oriented about any of the three axes of symmetry. Each primary thruster produces 3800 N of thrust and each vernier thruster produces 100 N.

The design of storage vessels has an enormous impact on the overall thermal energy storage capabilities of a spacecraft. The vessel must seal the storage medium from the prevailing external conditions while minimizing any undesired thermal losses or gains. Mass and/or heat exchange must be allowed for during both charging and discharging operations. The vessel must also resist any pressure exerted by the stored fuel while maintaining dimensional stability. Finally, corrosion resistance should be provided in the event that there are chemical reactions with the storage medium.

The final geometry of the vessel must be determined by analyzing many factors and realizing that some trade-offs must be made. Some of the factors that must be considered are as follows:

- Total volume required
- Optimum material usage to minimize system mass
- Optimum surface area to control heat loss/gain to the ambient
- Shielding for meteorite protection
- Redundancy of system to provide backup against failures
- International design criteria if pressurized
- Special considerations, such as cryogenics
- Construction process
- Cost

Thus, by analyzing the many factors that are involved and carefully weighing the various trade-offs, a suitable storage vessel may be designed.

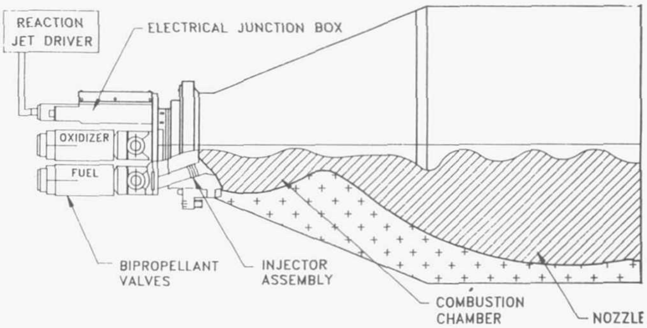

Fig. 3. Reaction Control Thruster

Table 2. Possible Materials for the Water Storage Tanks

Material	Stainless Steel	Al7075-T6	Ti-8AL-IMO-IV	Graphite/Epoxy*
Yield Strength ($10^8 N/m^2$)	2.07	5.03	8.27	7.65
Density (kg/m^3)	7806	2796	4373	1323
Mass (kg)	1670	246	236	78
Temperature (C)	<400	<250	<535	<150
Minimum Wall Thickness (mm)	3	2	1	1

*This is composed of 70% epoxy, 15% high modulus graphite, and 15% high-strength graphite.

One of the most important design considerations involved is the selection of the best possible material. The material must be able to withstand the anticipated stresses, exhibit the desired thermal properties, and be resistant to corrosion. Once a list of materials has been established that meets the above criteria, the best can be selected based on both density and cost (see Table 2).

The storage tanks must be protected from damage by meteorites on the mission to and from Phobos. Since any additional mass decreases the payload capacity, it is desirable to minimize the shielding mass while still maintaining an adequate amount of protection for the spacecraft. By using the existing vehicle components as much as possible to provide the maximum inherent shielding capacity to the payload, only a small amount of supplementary shielding will be required to provide sufficient protection. This can be accomplished by surrounding the water storage tanks with the propellant tanks and related spacecraft structure. Each of the propellant tanks was designed to be completely shielded from meteorites, so only the gaps between the propellant tanks and the front end of the spacecraft are to be covered by supplementary shielding. This additional shielding has a surface area of approximately 150 m^2 and a mass of 2381 kg.

A well-protected tank is useless if it cannot be charged and discharged both effectively and efficiently. A set of charging pipes will be routed from each tank to the front end of the spacecraft. After the spacecraft docks at Phobos, the front meteorite shield will be opened to expose both the charging pipes for easy access.

After the front meteorite shield has been opened for charging pipe access, a small auxiliary cargo area (2 m × 2.6 m × 2.6 m) will also be exposed. This cargo area is completely shielded from the environment and will not experience temperatures greater than 100° C. The maximum mass of material that can be transported in this space was determined to be 4900 kg.

Since the mission to Phobos is to retrieve a large supply of water for the lunar base, the water storage system is of extreme importance. Two tanks will be utilized instead of only one in order to ensure that a major portion of the water will arrive safely at the lunar base even in the unlikely event of a tank rupture. Assuming that adequate pumping facilities are present, two tanks will also allow for faster charging and discharging operations since both may be filled or drained simultaneously. The liquid state was chosen to simplify the charging and discharging procedures and as a means to absorb any excess heat generated by the fuel cells and automated systems. Circulation pumps and electrical heaters will also be installed to ensure that the temperature is relatively uniform and remains at 20°C. This temperature was chosen since that is the design temperature of the cryogenic propellant storage system. Sensors will monitor the water temperature to control the use of both the pumps and heaters. The electrical heaters will also be used to ensure that the tanks are at the correct temperature just prior to loading the payload of water. Since the quality of the Phobian water is not known, filtering devices will be installed to ensure that the circulation pumps are not damaged. The inside of each water tank will also be coated with a thin layer of material that is resistant to any anticipated corrosive agents that might be present in the Phobian water. Each water storage tank will be cylindrical with hemispherical ends, have an internal volume of 60 m^3, and be 10 m long with a diameter of 2.6 m (see Table 3). Since the highest anticipated temperature experienced by the water storage tanks will be less than 100°C, the best material for their construction was determined to be the epoxy/graphite composite. Combined, they have a mass of 160 kg and provide a total storage capacity of 120,000 kg.

Hydrogen is the propellant that will be used by the nuclear propulsion system and it must be stored cryogenically. A total of 150,000 kg is necessary for the return leg of the mission. This corresponds to four tanks with a volume of 1205.25 m^3 each. The largest vessel that has been used to date is from the Apollo program and it had a storage capacity of 3200 m^3, so the size of the proposed tanks is practical. The tanks that are proposed in this design are simply a scaled-up version of tanks designed to be carried into low Earth orbit by the shuttle. It was assumed in the design of this mission that a manufacturing facility would be available at either the space station or the lunar base for the construction of the spacecraft, so none of the spacecraft components were designed within the limits of the shuttle payload bay. The exposed surface area of each tank will be shielded by a series of three-layered panels. A thin coating of thermal insulation will be covered by a lightweight composite meteorite shield. The outer layer will consist of a reflective coating to minimize the effects of solar heating. In addition, the spacecraft is rotated slowly about its axis to ensure that not just one tank is constantly exposed to the sun. Damaged panels can be replaced when the spacecraft returns

Table 3. Water and Liquid Hydrogen Storage Tank Characteristics

Type	Water	Liquid Hydrogen
Number Required	2	4
Volume (m^3)	60	1205
Mass (kg)	80	1660
Surface Area (m^2)	82	632
Diameter (m)	2.6	6.7
Length (m)	10	30

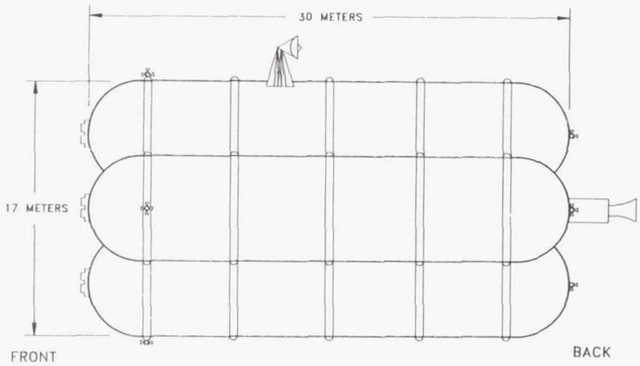

Fig. 4. Cargo Vehicle (Side View)

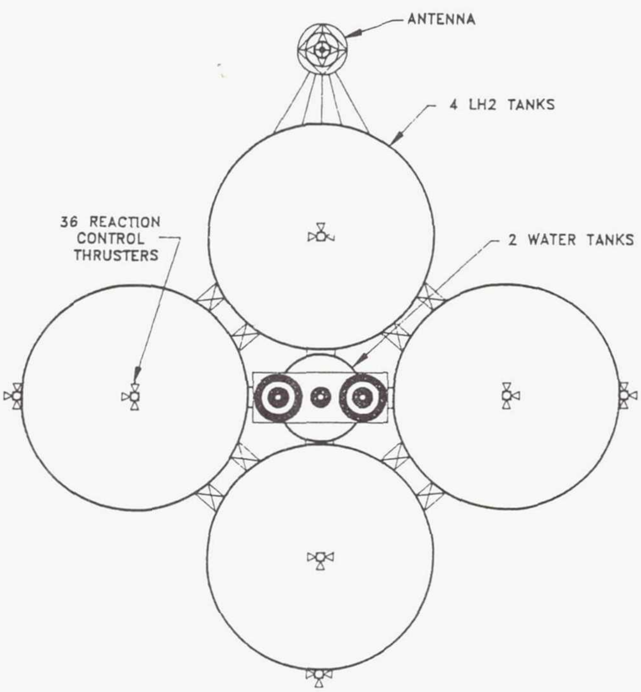

Fig. 5. Cargo Vehicle (Rear View)

to its lunar parking orbit and is inspected. The propellant tanks are also cylindrical with hemispherical ends and have a diameter of 6.7 m and a length of 30 m (see Table 3). The combined mass of all four tanks is 6640 kg.

Figures 4 and 5 illustrate the side and rear views of the spacecraft. An example mission profile for the return leg of the mission provides the determining factor for the spacecraft configuration (see Table 4). The determining factor was the maximum amount of propellant, dependent on the length of time for low thrust. Due to the large volume requirements of the liquid hydrogen and water, a multiple tank system was used for each. Since the liquid hydrogen was less dense than the water, four hydrogen tanks were needed compared to two water tanks. By keeping the water tanks along the line of thrust,

Table 4. Total Mass Breakdown of the Spacecraft

Component	Estimated Mass (kg)
Propulsion System	8,000
Automation, Controls, and Communication	10,000
Storage Tanks, Pumps, and Piping	10,000
Auxillary Shielding	2,400
Extra Cargo Capacity	4,900
Contingency Mass (10%)	3,530
Structural Mass (20%)	7,060
Total Structural Spacecraft Mass	45,890
Maximum Payload Mass	120,000
Maximum Propellant Mass	150,000
Total Spacecraft Mass	315.890

the mass moment of inertia was kept to a minimum. This configuration also provided additional protection from meteorites and solar radiation. The RTGs are placed between the water tanks so that any excess heat could be dissipated by the water. The automation and propulsion systems also were placed in the corridor, both for protection and minimum mass moment of inertia, as shown in Fig. 6.

Connections at the front of each hydrogen tank provided access for refueling while pipes extending through the corridor served to load/unload the water. The antenna was placed on the outer surface of one hydrogen tank so that communication in could be maintained. The RCTs are placed on the hydrogen tanks such that the spacecraft could be oriented about all three axes of symmetry. The number of hydrogen tanks is dependent on the propellant requirement. The longer the mission, the more propellant would be required. The rest of the spacecraft configuration would remain basically the same.

Due to the conceptual design of the spacecraft, the structural members should be a lightweight composite material that will enable the spacecraft to resist expected acceleration forces.

Before a decision could be made on what type of orbit transfer should be used from Earth to Mars, the mission parameters had to be defined. Assuming that the mission would be performed on a cyclic basis, the availability of conditions necessary to perform the mission and the required total trip time were the two most important considerations.

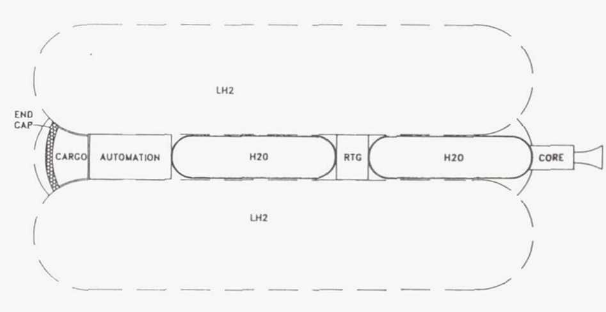

Fig. 6. Cargo Vehicle Corridor Layout

To duplicate a mission trajectory, the ephemeris of the planets must be the same. Since the ephemeris repeats itself approximately once every two years, the mission cycle was initially chosen to be two years. Accounting for the time necessary at Phobos to fill the tanks, and the time necessary at the Moon for unloading and refurbishing, the total transit time for the mission was initially approximated at 1.0 year. Although the mission was designed to be fully automated, a trip time this short would also allow for a manned mission, provided the necessary ECLSS could be incorporated into the spacecraft design.

In choosing the type of orbit transfer to be used, time and efficiency were considered. Although it is more efficient to use low thrust, the time required to break free of the gravitational attraction of the Earth/Moon system made this choice incompatible with the constraints. On the other hand, while the high thrust could meet the time constraint, efficiency would be lowered considerably. Given the mission constraints and objectives, a combination high/low thrust trajectory was chosen for the orbit transfer from Earth to Mars. The hope was that a hybrid mission would maximize the benefits of each.

To do an analysis of the trajectory a patched-conic approximation was used. In effect, the trajectory was divided into six sections, and then patched together using the final conditions of the previous leg as the initial conditions for the next. This was done in order to have only one body acting as the primary body of attraction on the spacecraft at one time. By doing so, each individual part of the trajectory could be treated as a two-body problem. For the first leg, the Earth and Moon were treated as one system with the center of mass located 4671 km from the center of the Earth. Once the spacecraft reaches the edge of the sphere of influence of the Earth-Moon system, the sun becomes the primary body of influence. The second leg begins here and ends once the spacecraft reaches the sphere of influence of the martian system. The return leg was approximated in the same manner. The gravitational parameters (μ's) used for each leg and the radii of the spheres of influence are listed in Table 5.

Other assumptions also were made to simplify the problem. Low thrust was used only for the heliocentric trajectory, and other than this no other perturbations were included in the analysis. The orbits of all the planets were assumed to be coplanar, the orbit of the Moon about the Earth was assumed to be circular, and gyroscopic effects generated by the rotation of the spacecraft were assumed to be negligible.

Since each leg of the problem was simplified to a two-body problem, the reduced first order system of equations in polar coordinates to be integrated for each leg with respective μ's is

$$\dot{r} = u \tag{1}$$

$$\dot{\theta} = \frac{v}{r} \tag{2}$$

$$\dot{u} = \frac{v^2}{r} - \frac{\mu}{r^2} + \frac{T}{M}\sin\phi \tag{3}$$

$$\dot{v} = \frac{-uv}{r} + \frac{T}{M}\cos\phi \tag{4}$$

where r and θ define the position of the vehicle, and u and v are the radial and tangential velocities, respectively. In these equations T refers to the low thrust provided. It will be nonzero only for the heliocentric portion of the analysis. The mass, M, will be approximated at 200,000 kg for the first leg of the trajectory, and at 320,000 kg for the return leg. The control to be optimized is ϕ.

Since the vehicle would be carrying an additional 120,000 kg of payload on the return leg from Mars, the problem of optimizing the mission was simplified to optimizing just the return leg. Once the return leg is defined, the stopover time and the desired trip time from Earth to Mars need be chosen only to define the first leg of the mission. The resulting trajectories may not correspond to the most optimal solution; however the degree of simplification achieved in the analysis warrants this assumption.

For the preliminary analysis of the return leg, the mean radius of Mars was chosen as the initial radius. The initial tangential velocity was the velocity necessary for the vehicle to be on a Hohmann transfer orbit to Earth. These conditions start the vehicle out on the most efficient, but least expedient high-thrust orbit transfer. The philosophy behind this choice is that by starting off in a Hohmann transfer and then optimizing the direction of the low-thrust vector during the trip, the ΔV required at Earth could be minimized. By doing so, it was hoped that the propellant required for the mission would be less than that for an all high-thrust mission.

Two methods were used to try to determine the control and the trip time needed to achieve the position and velocity of the Earth, given the initial conditions mentioned above and the available thrust to mass ratio.

The first method utilized a subroutine called VFO2AD given to us by George Davis, a graduate student at the University of Texas. The purpose of this subroutine is to calculate the least value of a function of several variables subject to general constraints on the values of the variables. The program is given an initial guess for a specified number of values used to define the control function. These values are spaced at even intervals during the return trip. The program linearly interpolates between the values to find ϕ at any given time. An iterative method is employed to determine the optimal control. For each iteration a quadratic approximation to the Lagrangian function subject to linear approximations to the specified

Table 5. Gravitational Parameter and Radius of the Sphere of Influence Used for Each Section of the Trajectory

Primary Body of Attraction	μ(km^3/s^2)	Sphere of Influence Radius (km)
Earth-Moon system	4.035e+05	923,738.2
Sun	1.327e+11	∞
Mars	4.305e+04	574,520.1

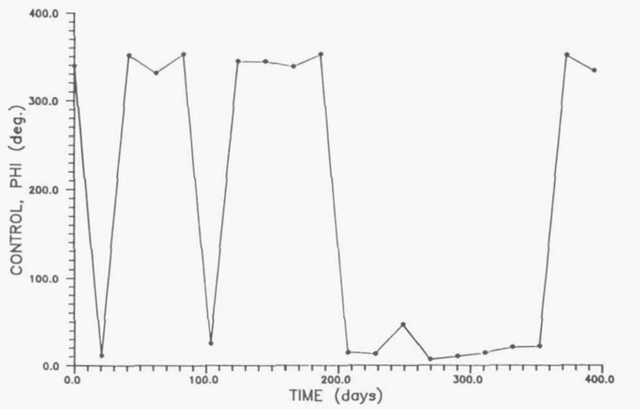

Fig. 7. Control time history for thrust/mass = 1.56 (10^{-4}) N/kg found using VFO2AD. Trip time of 394 days with a radial velocity of 3270 km/day.

constraints is minimized. The subroutine automatically estimates the second derivative matrix of the Lagrangian function. A line-search procedure is used to force convergence when the initial values of the variables are far from the solution. This method is also sometimes called suboptimal control, or a parameter optimization technique.

From a sample runstream that utilized VFO2AD to solve one of George's homework problems, several different programs were generated to solve the present optimization problem. The first approach to this problem was to find the minimal trip time necessary to meet the constraints. The constraints restricted the radial velocity at t_f to be zero, and the tangential velocity at t_f to equal the velocity for a circular orbit with the minimized final radius. Since our thrust-to-mass ratio was fixed, the minimum propellant required for the transfer will correspond to the shortest trip time. For the second approach, since the desired return-trip time was known, the program was written such that the variable to be minimized was the final radius of the orbit.

The second method utilized a program written for an AERO 623 project by Michael Niestroy, a graduate student at Texas A&M University. This program uses a first order gradient method to solve an optimal control problem with constraints specified at a fixed final time. Section 2.4 of *Applied Optimal Control*[1] by Bryson and Ho gives a more indepth description of the method used to solve this two-point boundary value problem.

Unfortunately, VFO2AD had difficulty converging given the minimum time problem, even for various initial guesses. For a thrust-to-mass ratio of 1.56×10^{-4} N/kg, the program could not come close to achieving a final radial velocity of zero. However, for a thrust-to-mass ratio of 8.33×10^{-4}N/kg, the program did not converge, but a final radial velocity of 3270 km/day was achieved. This number may appear large, but the units make the magnitude of the value deceiving. The control time history for the solution to this problem is shown in Fig. 7. The program written to solve the radius-minimization problem was not successful either. After a single iteration, VFO2AD gave an error stating that the new predicted guess was too large, greater than 10^6.

The second method produced much better results. For a thrust-to-mass ratio of 1.56×10^{-4} N/kg the return trip time was 401 days. The control time history for this solution is shown in Fig. 8 and a graph of the orbit transfer is shown in Fig. 9. The control distribution is smooth with a switch after approximately 46 days, or one-eighth of the return trip time. By increasing the thrust to mass ratio to 8.33×10^{-4} N/kg the return time was decreased to 187 days. Figures 10 and 11 show the control time history and the orbit transfer for this case. Again, the resulting control time history is very smooth, but for this case the switch occurred at about 85 days, or at a little less than half the return trip time.

Once the results for the second method were obtained, the control history was used as the initial guess for the first method with the hope that the program would converge better. For the smaller thrust-to-mass ratio the program still did not converge, and for the larger thrust-to-mass ratio the results were only a little better.

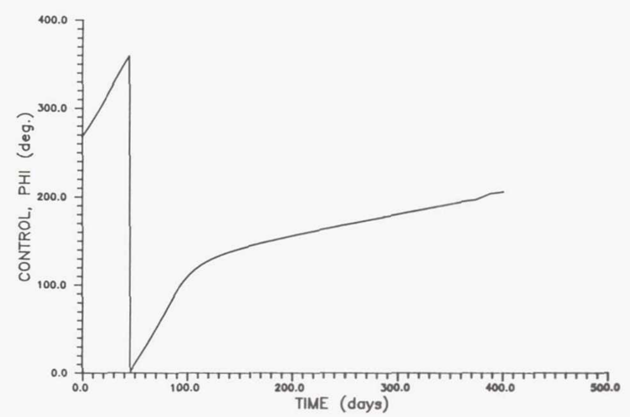

Fig. 8. Control time history for thrust/mass = 1.56(10^{-4}) N/kg found using Mike Niestroy's program.

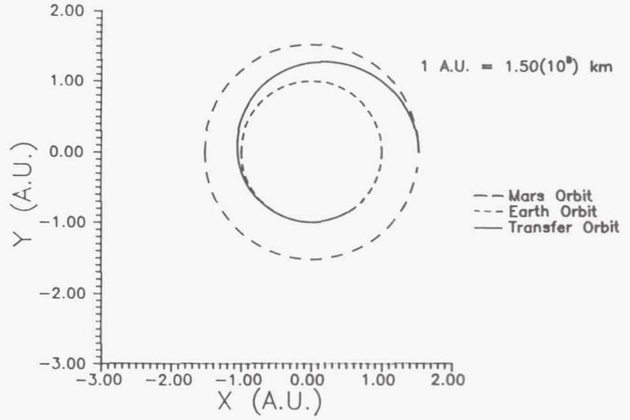

Fig. 9. Return trip transfer orbit in heliocentric coordinates for the control time history shown in Fig. 8 with a trip time of 401 days and $\Delta\theta = 290°$.

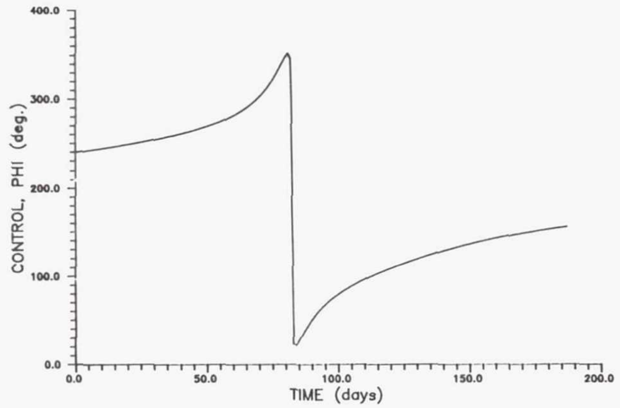

Fig. 10. Control time history for thrust/mass = 8.33 (10^{-4}) N/kg found using Mike Niestroy's program.

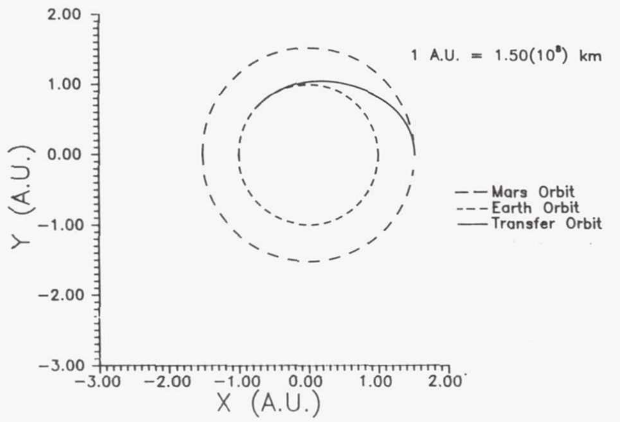

Fig. 11. Return trip transfer orbit in heliocentric coordinates for the control time history shown in Fig. 10 with a trip time of 187 days and $\Delta\theta = 135°$.

The first method was found to be very sensitive to the initial guess. The line-search procedure used by the program to force convergence was very unpredictable. The number of values used for the initial guess also affects the control function considerably. This is because the problem solution is sensitive to the switch time of the control. The more values used to define ϕ, the better the chances are that one of the ϕ's will be defined close to the switch time. The results obtained for the control function using this method are too erratic to be considered seriously as a control for the low thrust of a spacecraft.

For the second method, although the control time history obtained was much smoother, the results do not necessarily provide a feasible solution for this problem. The cyclic mission requirement could still be met by changing the cycle time from two to four years, but at a fuel consumption rate of 432 kg/day, this solution is not practical. The results found using the higher thrust-to-mass ratio produced an acceptable trip time, but at a thrust-to-mass ratio that is not attainable any time in the near future.

Although the initially proposed mission scenario was found to be impractical, this does not mean that the mission itself is impractical. Several different approaches could be used to find an appropriate scenario to perform the same function. One recommendation is that the quantity of water brought back from Phobos be reduced. This recommendation is the most obvious; however, cost-effectiveness is the bottom line. Another possibility is using a full high-thrust mission. This option would require further trajectory and cost analysis. If the technology necessary to provide substantially higher thrust at the same mass flow rate is developed, the hybrid mission concept would then be feasible.

ACKNOWLEDGMENTS

Principal authors D. Adams, J. Bays, G. Kronschnabl, J. McCutchon, E. Minier, and P. Rush were assisted by faculty advisor Professor Stan H. Lowy.

REFERENCES

1. Bryson A. E. and Ho Y. *Applied Optimal Control,* Hemisphere Publishing Corp., Washington, 1975.

N94-71289

1994004534
382696
522-17
160648
p-8

FEASIBILITY STUDY OF A SINGLE, ELLIPTICAL HELIOCENTRIC EARTH-MARS TRAJECTORY

TEXAS A&M UNIVERSITY

DEPARTMENT OF AEROSPACE ENGINEERING

The initial intent of this design project was to evaluate the existence and feasibility of a single elliptical heliocentric Earth/Mars trajectory. This trajectory was constrained to encounter Mars twice in its orbit, within a time interval of 15 to 180 Earth days between encounters. The single ellipse restriction was soon found to be prohibitive for reasons shown later. Therefore, the approach taken in the design of the round-trip mission to Mars was to construct single-leg trajectories which connected two planets on two prescribed dates. Three methods of trajectory design were developed in this report. Method 1 is an eclectic approach and employs Gaussian Orbit Determination (Method 1A) and Lambert-Euler Preliminary Orbit Determination (Method 1B) in conjunction with each other. Method 2 is an additional version of Lambert's Solution to orbit determination, and both a coplanar and a noncoplanar solution were developed within Method 2. In each of these methods, the fundamental variables are two position vectors and the time between the position vectors. In all methods, the motion was considered Keplerian motion and the reference frame origin was located at the sun. Perturbative effects were not considered in Method 1. The feasibility study of round-trip Earth/Mars trajectories in this report maintains generality by considering only heliocentric trajectory parameters and planetary approach conditions. The coordinates and velocity components of the planets, for the standard epoch J2000, were computed from an approximate set of osculating elements by the procedure outlined in an ephemeris of coordinates[1].

METHOD 1

Method 1 was *initially* based on the assumptions that the motion of the planets was two-body Keplerian motion and that the orbit of Mars was coplanar with the ecliptic. Another important assumption in the development of Method 1 was that the sphere of influence of Mars had no net effect on the calculated spacecraft trajectory. It was assumed that whatever deviation from the proposed trajectory occurred (due to the gravitational sphere of influence), the spacecraft could effectively maneuver back to the original trajectory.

For possible departure dates, a complete synodic period of Mars was arbitrarily selected to be between December 5, 1988, and February 5, 1992 (J2447500.5 - J2448658.5). For each departure date, the position and velocity of Earth and Mars were calculated using Ref. [1]. It was determined that if the departure velocity direction was coincident with the Earth's tangential velocity, the resulting orbit would encounter Earth's orbit at only one point. This restriction was unacceptable. In the velocity space of Fig. 1, V_h represents the hyperbolic excess velocity in the direction of Earth's tangential velocity. The dashed circle represents a velocity magnitude of $20V_h$. The speed range of V_h to $20V_h$ encompasses minimum energy transfer speeds and speeds large enough to escape the sun's sphere of influence.

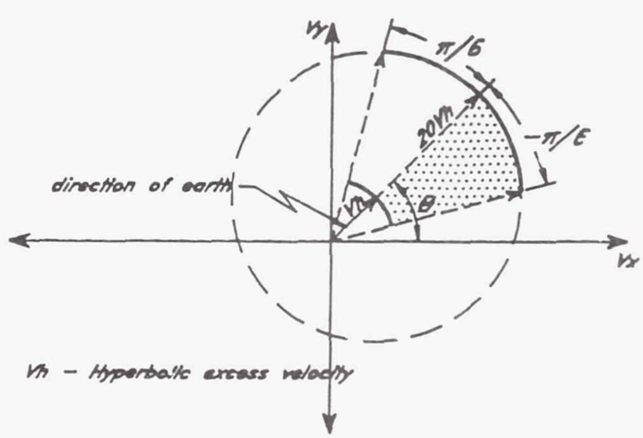

Fig. 1. Hodograph Plane

The velocity direction was initially allowed to range between $\pm\pi/6$ radians from the Earth's tangential velocity. However, for velocity directions greater than θ in Fig. 1, the spacecraft would be injected back into the Earth's sphere of influence. Therefore, the velocity direction was allowed to vary only between θ-$\pi/6$ and θ (note that θ is not the direcion of the spacecraft, but only a representative angle in the Hodograph Plane). Thus, for each departure date, the direction and magnitude of the spacecraft's initial velocity were allowed to vary within the limits of a complete range of possible velocity magnitude/direction combinations.

To establish the initial position of the spacecraft, it was assumed that the initial position was at the edge of the sphere of influence in a direction away from the sun and perpendicular to the velocity vector of the Earth at that point. The unit vector in the direction of the Earth's velocity was calculated by dividing Earth's velocity vector by its magnitude. The spacecraft was then displaced to the edge of the sphere of influence by multiplying each component of Earth's unit velocity vector by its opposite position component (resulting in displacement perpendicular to the tangential velocity).

To verify that the proposed orbit was elliptic, the eccentricity and semimajor axis were calculated. If the trajectory was not elliptic, the velocity magnitude was incremented, thereby establishing a new trajectory.

At this point, the spacecraft's initial position and velocity were known and the trajectory could be determined by use of the Lagrange F&G solution. The F&G solution was chosen as opposed to the classical solution because of the assumption of coplanar motion of the planets. The step size of the points calculated was based on the ratio of the distance to the edge of the martian sphere of influence for one point, compared to the next point. If this ratio was greater than two, the step size was decreased since at that step size, the next point would be past the sphere of influence. For each point, the difference between the spacecraft position and the martian sphere of influence was calculated. If there was agreement to over six significant figures, it was determined that a first encounter had occurred, and all essential data was written to an output file. If, however, the spacecraft missed Mars or spent an excessive time before an encounter, a new trajectory was started.

This method was successful at finding a trajectory to Mars; however, the following problems were encountered: (1) the method was very slow since points on every possible orbit were calculated; (2) the method missed possible trajectories completely because the velocity could only be increased in fairly large steps; and (3) the results produced were not categorized and very hard to analyze.

Therefore, it was decided to abandon Method 1 and attempt orbit determination given two position vectors and the time between the position vectors. Two different methods (Method 1A and Method 1B) were used in conjunction with each other and are similar to Method 2.

Method 1A: Gaussian Orbit Determination

Referring to Fig. 2, the Gaussian Method is an iterative scheme which iterates the eccentric anomaly difference until the correct sector to triangle ratio is converged upon. This uniquely determines the ellipse that must pass through r_1 and r_2 over time τ. This method was used when the angle between position vectors was small. The method converges automatically from an initial guess. The convergence becomes unstable at spreads close to or greater than 90°; therefore it was used in conjunction with Method 1B. The semiparameter of the ellipse can be written as

$$P = r^4 \dot{v}^4/\sqrt{\mu}$$

The angular momentum is

$$h = r \times \dot{r}/\sqrt{\mu}$$

where $/h/ = \sqrt{\mu p}$. So by substitution

$$\sqrt{\mu p} = x_w\dot{y}_w - y_w\dot{x}_w = 2dA/d\tau \qquad (A1)$$

where $dA/d\tau$ is the "areal velocity." The area of sector ABC can then be calculated by

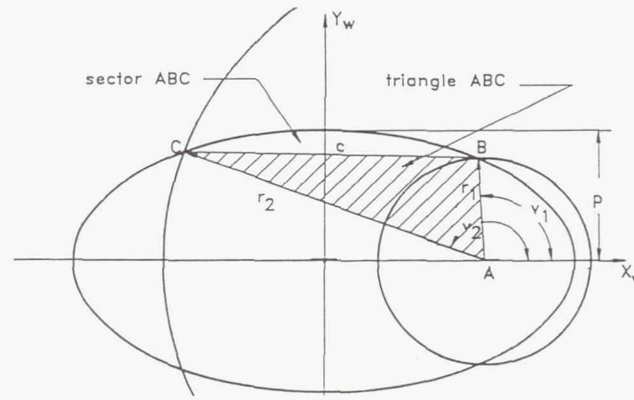

Fig. 2. Relationships in the Transfer Plane

$$A_S = \tfrac{1}{2}\int_0^{\tau} \sqrt{\mu p}\, d\tau = \tfrac{1}{2}\sqrt{\mu p}\,\tau \qquad (A2)$$

The area of the triangle ABC is simply

$$A_t = (\tfrac{1}{2})/r_2//r_1/\sin(v_2 - v_1) \qquad (A3)$$

Therefore by combining the two areas to get the ratio of sector to triangle

$$y = \sqrt{\mu p}\,\tau/[r_1//r_2/\sin(v_2 - v_1)] \qquad (A4)$$

where τ is the modified time $\tau = k(\text{delt})$ and ($k =$ the gravitational constant).

With y known, it must be related to the difference in eccentric anomalies. Using the equation of a conic section, $r = p/(1 + e\cos v)$, write the equation twice, once for each time τ_1 and τ_2, and add them together to obtain

$$P[(1/r_1) + (1/r_2)] = 2 + 2e\cos[(v_2 + v_1)/2]\cos[(v_2 - v_1)/2] \qquad (A5)$$

Using the half-angle identity to eliminate $e\cos[(v_2 + v_1)/2]$

$$\sqrt{r}\cos(v/2) = \pm\sqrt{(r/2)(1+\cos v)}$$

$$\sqrt{r}\sin(v/2) = \pm\sqrt{(r/2)(1-\cos v)}$$

This derivation becomes restricted to an ellipse with the introduction of $r = a(1 - e\cos E)$, $r\cos v = a(\cos E - e)$. The half-angle formulas can now be written as

$$\sqrt{r}\cos(v/2) = \sqrt{a(1-e)}\cos(E/2)$$

$$\sqrt{r}\sin(v/2) = \sqrt{a(1+e)}\sin(E/2)$$

and combined with the polar equation of an ellipse, equation (A6) is obtained

$$P[(1/r_1) + (1/r_2)] = 2+(2P/\sqrt{r_1r_2}) \cos[(E_2-E_1)/2]\cos[(v_2-v_1)/2] -2\cos^2[(v_2-v_1)/2] \quad \text{(A6)}$$

From equation (A4), P can be solved for, resulting in

$$P = [y^2 r_2^2 r_1^2 \sin^2(v_2-v_1)]/\mu\tau^2 \quad \text{(A7)}$$

Substitute this expression for the semiparameter of the ellipse into equation (A6) to obtain an equation relating the sector to triangle ratio (y) to the difference in eccentric anomalies

$$y^2 = \mu\tau^2 \sec^2[(v_2-v_1)/2]/2r_1r_2 \{r_1+r_2-2\sqrt{r_1r_2}\cos[(v_2-v_1)/2]\cos[(E_2-E_1)/2]\} \quad \text{(A8)}$$

This can be written as

$$y^2 = m/(l+x) \quad \text{(A9)}$$

where

$$l = \{r_1+r_2/4\sqrt{r_1r_2}\cos[(v_2-v_1)/2]\} - ½$$

$$m = \mu\tau^2/\{2\sqrt{r_1r_2}\cos[(v_2-v_1)/2]\}^3$$

$$x = ½\{1-\cos[(E_2-E_1)/2]\}$$

Equation (A9) is known as the First Equation of Gauss. It can be seen that l and m can be determined immediately since r_1, r_2, and the angle between them are known. x is the only variable not known because the difference in the eccentric anomalies is not known. The time of flight is what determines E_2-E_1, and since the time of flight is chosen, E_2-E_1 cannot be any arbitrary value.

Using additional substitutions and trigonometric identities, other equations are developed and finally

$$X = E_2-E_1-\sin(E_2-E_1)/\sin^3[(E_2-E_1)/2] \quad \text{(A17)}$$

then

$$y^2(y-l) = mX \quad \text{(A18)}$$

This is the Second Equation of Gauss. By combining the First and Second Equations of Gauss, then

$$y = l + X(l+x) \quad \text{(A19)}$$

The method assumes an initial value of y in (A9), after calculating l and m, and proceeds to (A19) where a new value of y is found. Iteration continues until $\Delta y = 0$, whereupon the semimajor axis and the Lagrange-Gibbs functions, f, g, and $\dot{g}$, are calculated and utilized to determine the necessary departure and arrival velocities, $\dot{r}_1$ and $\dot{r}_2$.

Method 1B: Lambert-Euler Preliminary Orbit Determination

This method works for radius vector spreads up to but not including $\pi^{(2)}$. It does not converge as fast as the Gaussian method. Consequently, this method was used only when the Gaussian method would not converge to a solution.

The Lambert-Euler method iterates the semimajor axis until the calculated time between the starting and end points is the same as the desired time.

Referring again to Fig. 2, where Gauss related the sector to triangle ratio to the difference in eccentric anomalies, Lambert related the chord length c to the difference in eccentric anomalies.

Using algebra, trigonometry, and geometry, two expressions containing the eccentric anomalies are derived and two angles, ϵ and δ, are defined.

$$\epsilon = \upsilon + [(E_2-E_1)/2]$$

$$\delta = \upsilon - [(E_2-E_1)/2]$$

The limits for these variables are as follows

$$0 \le (E_2-E_1)/2 \le \pi \qquad 0 \le \upsilon \le \pi$$
$$\sin(\epsilon/2) \ge 0 \qquad \cos(\delta/2) \ge 0$$

The value and sign of $\sin(\delta/2)$ can be determined uniquely but not so for the sign of $\cos(\epsilon/2)$; hence a sign must be assumed. This means that two different orbits must be tried to find the right one.

Since $\epsilon-\delta = E_2-E_1$, one can arrive at $\sqrt{\mu}\ \tau_c/a^{3/2} = (\epsilon-\sin\epsilon)-(\delta-\sin\delta)$ where τ_c is the time based on the assumed semimajor axis. Solving the equation for τ_c, one seeks $\tau-\tau_c = 0$, which then yields the ellipse that has the proper value of "a."

The procedure is to

- Assume an initial guess for the semimajor axis
  $$a = (r_2+r_1)/2$$
- Calculate the chord length c
- Calculate the sines and cosines of the known half-angles
- Assume a sign for the value of $\cos(\epsilon/2)$ from
  $$\cos(\epsilon/2) = \pm\sqrt{1-\sin^2(\epsilon/2)}$$
- Calculate the difference between the desired and calculated times of flight from

$$F = \tau - \tau_c = \tau-(a^{3/2}/\sqrt{\mu})[(\epsilon-\sin\epsilon) - (\delta-\sin\delta)]$$

- Once "a" stops changing, calculate the departure and arrival speeds as before.

METHOD 2: LAMBERT'S SOLUTION[4]

Coplanar Solution

Let V_E be the orbital velocity of the Earth and let a departure velocity magnitude V_{RE} from the Earth's orbit be specified. Choose a value of θ_D for the heliocentric angle θ (Fig.3)

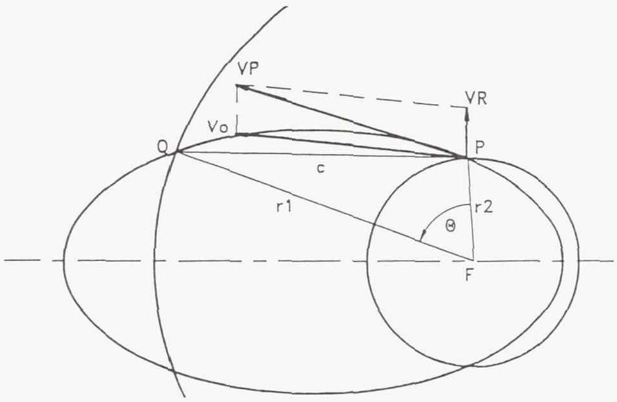

Fig. 3. Velocity Requirements for an Orbit to Orbit Voyage

between the point of departure on the Earth's orbit and the point on the martian orbit at which we intend to intercept Mars. Define the quantity delE = $(V_{RE}/V_E)^2$ where delE is the amount of energy needed at point P to transfer from an assumed circular orbit to an elliptical orbit for a voyage to Q. This energy amount can also be written as

$$\frac{\text{delE} = 3-(r_1/a)-(r_2/c)\sqrt{2r_1}\,\sin\theta}{\sqrt{(1/(s-c))-(1/2a)\ \pm/(1/s)-(1/2a)]}} \qquad \text{(C1)}$$

where $s = (r_1+r_2+c)/2$.

Equation (C1) is solved for the semimajor axis of the transfer ellipse using Newton's Method. It holds only for positive values of sin θ. Note that equation (C1) may have two roots, each of which corresponds to a satisfactory solution to the problem.

The next step was to compute the time T required for the journey from Earth to Mars. The following formula is valid if θ is not an integral multiple of π

$$T = (P/2)\{2N+1+(\text{sgn}(\sin\theta)/\pi)[\pm(\alpha-\sin\alpha-\pi) - (\beta-\sin\Upsilon\beta)]\} \qquad \text{(C2)}$$

where N is the integral part of $\theta/2\pi$ and $\alpha = 2\sin^{-1}\sqrt{s/2a}$ and

$$\beta = 2\sin^{-1}\sqrt{(s-c)/2a} \qquad \alpha,\beta>0$$

The positive or negative sign was used, respectively, according to whether the root a was obtained from the delE_+ or the delE_- branch of the curve. The function *sgn* was defined as +1,0,−1 according to whether the argument is respectively positive, zero, or negative.

With the time for the trip from Earth to Mars determined, the location of Mars at the time of departure is fixed. Therefore, the relative velocity V_{RM} of the spacecraft with respect to Mars can be calculated at the point of intersection with the martian orbit by

$$V_{RM}^2 = V_M^2[3-(r_2/a_D)-2(l_D/r_2)]$$

where V_M is the orbital velocity of Mars and l_D is the semilatus rectum of the departure orbit.

The procedure for determining an appropriate Mars-to-Mars and Mars-to-Earth trajectory is the same as used in obtaining tne departure trajectory. The magnitude of the relative velocity with which the ship leaves Mars is the same as that with which it arrived, regardless of the perturbations induced by the contact. For the return trajectory for example, the heliocentric angle θ_R was selected and measured from the intercept point on the Martian orbit to a point on the Earth's orbit. Equation (C1) was used with delE = $(V_{RE}/V_M)^2$ and with r_1 and r_2 now taken as the radii of the orbits of Mars and Earth, respectively, to solve for the semimajor axis a_R of the return orbit. If a solution existed, equation (C2) was used to determine the time for the return trip.

By iteration of the angle θ and repetition of the procedure above, it was determined whether or not a sufficient trajectory existed. Assuming a sufficient trajectory was found, it was then necessary to determine whether the gravitational field of Mars was sufficient to accomplish the transfer of the spacecraft from the departure orbit to the intermediate orbit, and from the intermediate orbit to the return orbit. Referring to Fig. 4, the turning angle δ was computed from equation (C4) by selecting d and knowing μ_M and V_{RM}

$$d = \frac{\mu(\csc\delta - 1)}{V_{RM2}} \qquad \text{(C4)}$$

Noncoplanar Solution

The geometry of the three-dimensional model of the orbits of Earth and Mars is shown in Fig 5.

The position of Earth at any given time is specified by the coordinates x, y, and z, where the x and y axes are in the plane of the ecliptic, and the positive x axis is in the direction of the vernal equinox. The ascending node, AN, is the point at which Mars crosses the ecliptic with a positive component of velocity in the z-direction.

To specify the position of Mars, the α, β, and δ axes are used. The α and β axes are selected in the martian orbit plane

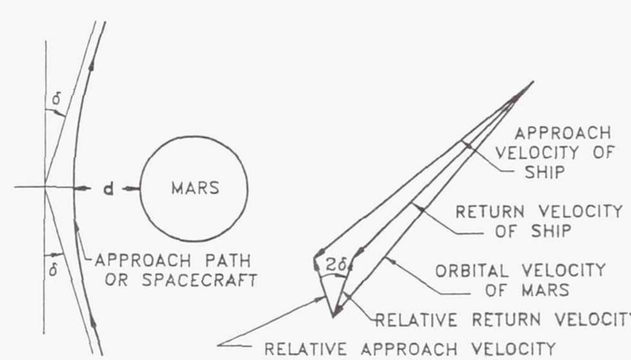

Fig. 4. Motion of Spacecraft in Vicinity of Mars

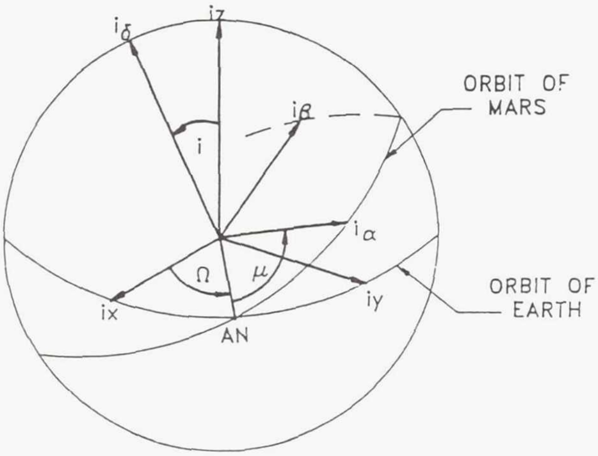

Fig. 5. Fixed Heliocentric Rectangular Coordinates for Earth and Mars Orbits

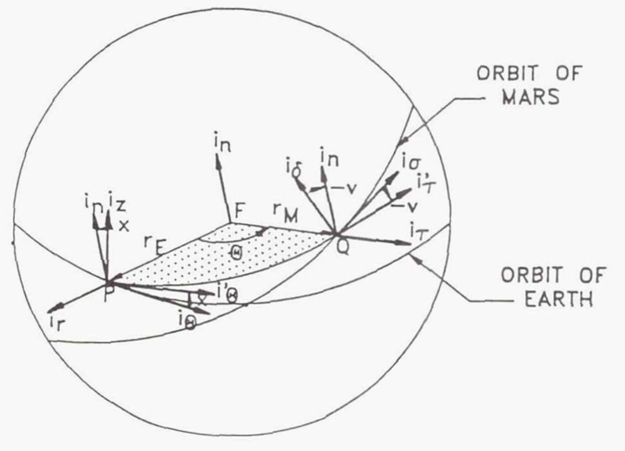

Fig. 6. Local Polar Coordinate Systems for Earth, Mars, and the Spacecraft's Orbit

with positive a in the direction of the perihelion of the martian orbit.

The mean anomalies of Earth and Mars are given by

$$M_E = 2\pi T + \Sigma_E - \Gamma_E \tag{C5}$$

$$M_M = (2\pi T/P_M) = \Sigma_M - \Gamma_M \tag{C6}$$

where T is time in years from epoch, Σ is the mean longitude of the planet at epoch, Γ is the longitude of perihelion of each planet, and P_M is the period of Mars in years.

From the mean anomalies, the eccentric anomalies E can be found using Newton's Method.

Referring to Fig. 6, r_E and r_M represent the position vectors of P and Q.

3-D Procedure

1. A departure time, T_D, is specified that is measured in years from the epoch.
2. The mean anomaly of the Earth at the point of departure, $M_E(T_D)$, is computed from equation (C4) and the corresponding eccentric anomaly of the Earth, $E_E(T_D)$, is obtained. Then the vector position of the Earth at the time of departure $r_E(T_D)$ is computed.
3. The vector velocity of the Earth at time T_D is then computed.
4. An estimate of the time T_{EM} in years required for the voyage from Earth to Mars is made and the mean anomaly of Mars, $M_M(T_D+T_{EM})$ for the point at which contact with the spacecraft will occur is computed from equation (C5). The corresponding eccentric anomaly, $E_M(T_D+T_{EM})$, and vector position, $r_M(T_D+T_{EM})$, are then obtained from Newton's Method.
5. The heliocentric angle θ_D, through which the spacecraft moves on the departure orbit, is calculated. From that the linear distance c, measured from the point of departure P to the point of arrival Q at Mars, is obtained.
6. From the time-of-flight equation, with $T = T_{EM}$, the semimajor axis a_D of the departure orbit is obtained. Then the semilatus rectum l_D is computed.
7. The vector i_n normal to the plane of the departure trajectory is computed and the result used to obtain the inclination angle X.
8. The velocity vector V_{PE} of the spacecraft at the point of departure is then calculated.
9. The vector velocity V_{RE} of the spacecraft relative to the Earth at the point of departure P may then be computed as the vector difference $V_{RE} = V_{PE} - V_E(T_D)$.
10. The magnitude of the relative velocity V_{RE} may now be compared with the prescribed value. If the two differ by more than a tolerable amount, a new estimate for T_{EM} must be made and steps 4 through 9 repeated.
11. When an Earth-to-Mars orbit has been found that satisfies the initial departure conditions, we may then determine the relative velocity of the spacecraft at Q, the point of contact with Mars. Finally, the relative velocity V_{RM} is computed as the vector difference $V_{RM} = V_{QM} - V_M(T_D+T_{EM})$.
12. To obtain an intermediate and return trajectory, the procedure is essentially the same. The spacecraft departs from Mars at time T_D + TE_M arrives at Mars again at T_D + T_{EM} + del T where del T is a time interval of between 15 and 180 days. The time for the trip from Mars to Earth is a result of the iteration process used for determining a trajectory whose relative velocity magnitude V_{RM} at Mars is prescribed.

RESULTS OF METHOD 1 (A&B)

For illustrative purposes, trajectory data has been presented for a starting data of JD 2447500.5 (Dec. 5, 1988) in Figs. 7-15.

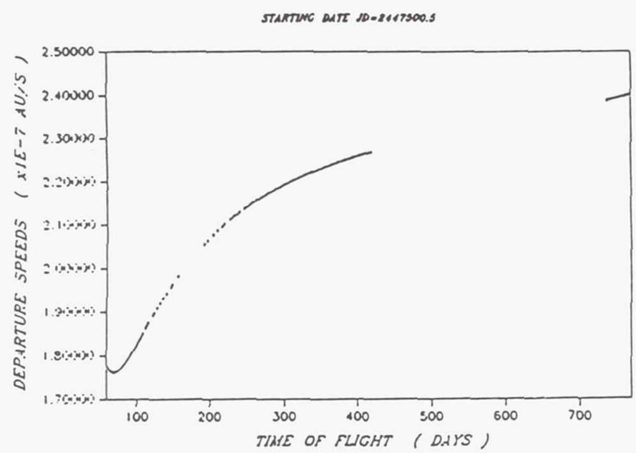

Fig. 7. Earth-Mars Trajectory Departure Speeds

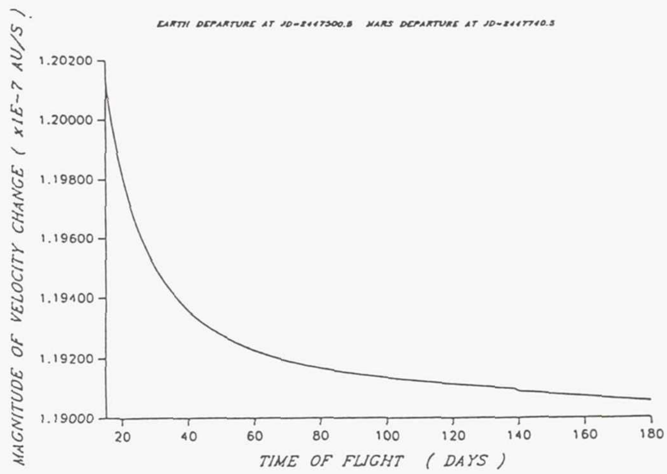

Fig. 10. Velocity Changes Necessary for Second Martian Encounter

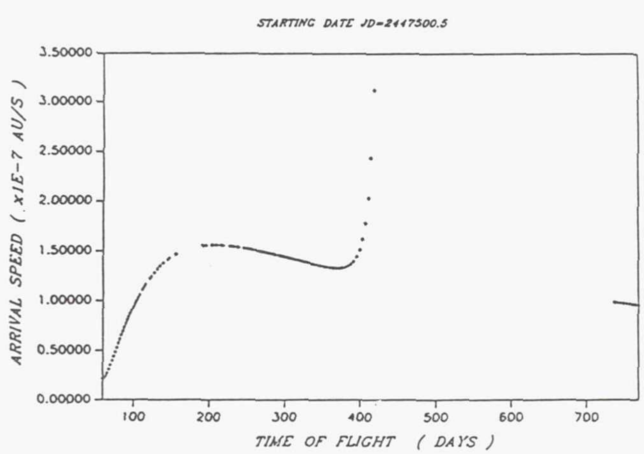

Fig. 8. Earth-Mars Trajectory Arrival Speeds

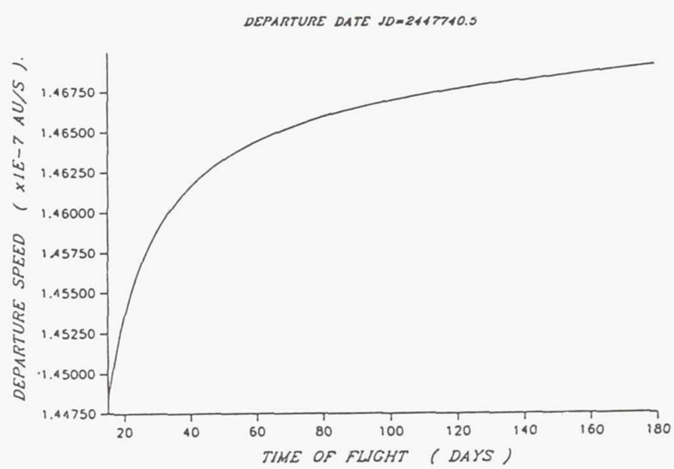

Fig. 11. Inter-Martian Trajectory Departure Speeds

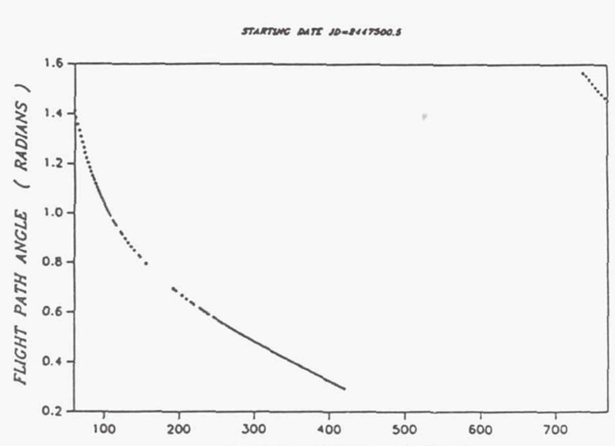

Fig. 9. Flight Path Angles for Earth-Mars Trajectory

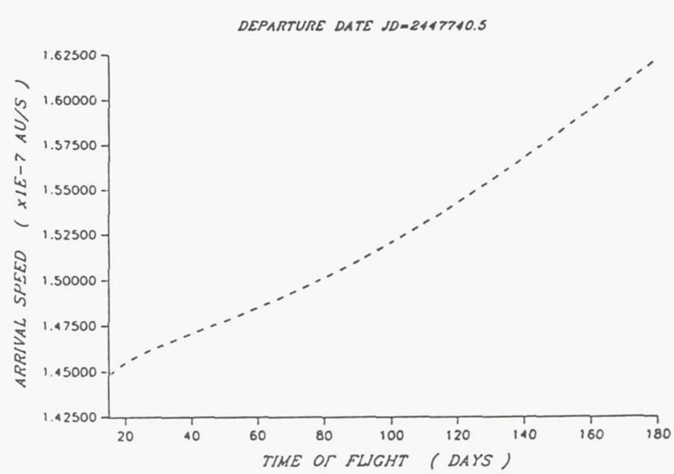

Fig. 12. Inter-Martian Trajectory Arrival Speeds

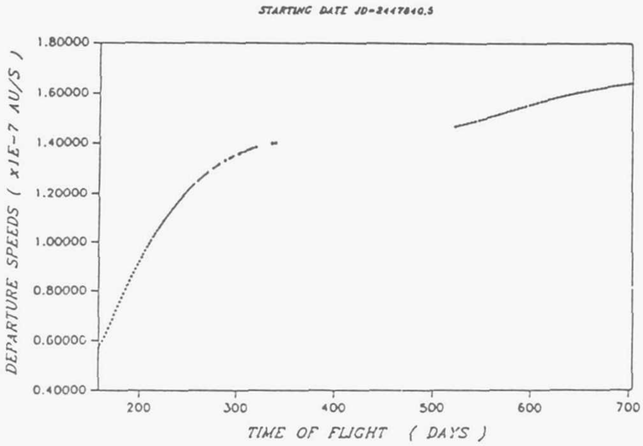

Fig. 13. Mars-Earth Trajectory Departure Speeds

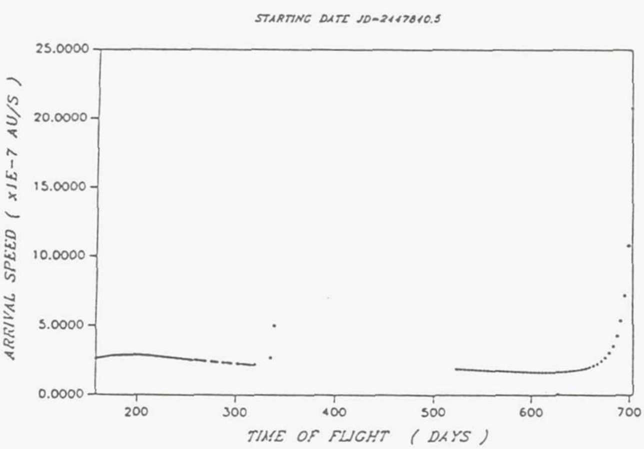

Fig. 14. Mars-Earth Trajectory Arrival Speeds

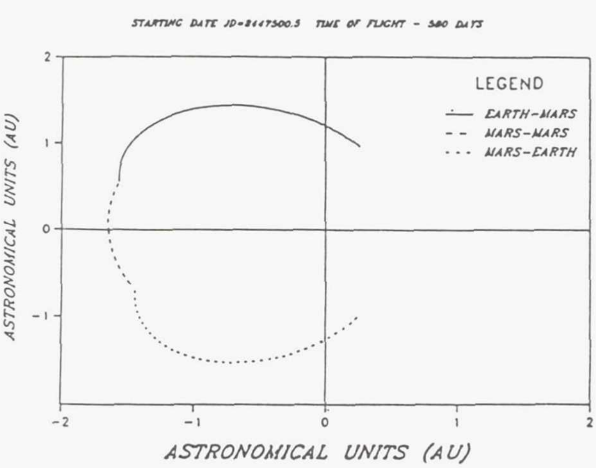

Fig. 15. Mars Trajectory Results—Complete Sample Mission

Figure 7 is a graph of Earth/Mars trajectory departure speeds, and shows the necessary departure velocities given a del t of 60 to 770 days (for a departure on JD 2447500.5). The graph can be explained as follows. At low times of flight, the speeds are decreasing. If the graph were extended from 0 to 770 days, it would be seen that the speeds approach infinity asymptotically. As the time of flight decreases, the speeds become hyperbolic. Such speeds coincide with an immense amount of energy and therefore were not considered. After reaching a minimum, the speeds necessary for longer transfers become steadily greater.

The large interval represents times where r_1 and r_2 were greater than π radians apart. These angles were not considered.

The small interstice represents orbits where Method 1B (Lambert-Euler) could not converge on a solution within a limited number of iterations. Consequently, Method 1A (Gaussian) was applied and was able to converge to a solution up to 184 days. In an additional effort to fill the interstice, the iteration limit was increased resulting in several more orbits. However, the interstice still remained and it was henceforth concluded that this was a result of the inability of the Methods to converge on a solution and not that the orbits did not exist. Figure 8 represents the Earth/Mars arrival speeds and is based on the same information as Fig. 7. The same explanation of the two interstices applied to this graph as in Fig. 7.

Figure 9 is the Flight-Path angle for Earth/Mars trajectories. This graph reveals prima facia that when the time of flight is small, the difference in true anomalies is small, and therefore the flight path angle approaches $\pi/2$. As the difference in true anomalies increases, the flight path angle approaches 0.

The next three graphs are all for proceeding from Mars to Mars after a specified 15-180 day time period.

Figure 10 represents velocity changes necessary for second martian encounters. It can be seen that high-velocity changes are required for short time intervals and lower velocity changes are required for high time intervals. These velocity changes represent only magnitude changes and do not give any information on direction. No plots were made of example trajectories because on the plot, the trajectory cannot be distinguished from the martian orbit.

Figure 11 represents intermediate martian departure speeds. It can be seen a priori that the greater the time of flight, the greater the initial velocity. If Mars traveled in a circular orbit, this line would be straight.

Figure 12 is the graph of the intermediate martian arrival speeds. Because the eccentricity of the orbit is very small, the variation is small. If the orbit were a circle, the graph of Fig. 12 would be a straight line and would match the graph of Fig. 11.

Figures 13 and 14 represent the Mars-to-Earth trajectory departure and arrivals, respectively. The large interstice in both plots represents flight path angles that were not considered. In Fig. 14, as the flight path angle approaches π and 2π, the arrival speed approaches hyperbolic speeds asymptotically.

Figure 15 represents a plot of a complete sample trajectory that departs from the Earth's orbit on JD2447500.5 and has a time of flight of 580 days.

ACKNOWLEDGMENTS

Principal authors M. Blake, K. Fulgham, and S. Westrup were assisted by faculty advisor Professor Stan H. Lowy.

REFERENCES

1. Nautical Almanac Office, *Planetary and Lunar Coordinates,* United States Naval Observatory, Washington DC, 1983.
2. Escobal P. R., *Methods of Orbit Determination,* Wiley & Sons, Inc., New York, 1965.
3. Estes R. H. and Lancaster E. R., *A Universal Solution of Lambert's Problem,* Goddard Space Flight Center, Greenbelt, Maryland, 1970.
4. Altman S. P., *Orbital Hodograph Analysis,* AAS Science and Technology Series, Vol. 3, American Astronautical Society, 1967.
5. Anthony M. L., *Space Flight Mechanic Specialist Symposium,* AAS Science and Technology Series, Vol. 2, American Astronautical Society, 1967.
6. Bate R. R., Muelles D. D., and White J. E., *Fundamentals of Astrodynamics,* Dover Publication, Inc., New York, 1971.
7. Battin R., *An Introduction to the Mathematics and Methods of Astrodynamics,* AIAA Education Series, AIAA, Inc., New York, 1987.
8. Battin R., *Interplanetary Space Probe,* Massachusetts Institute of Technology, Cambridge, Massachusetts, 1959.
9. Burgess E., *Report Developments in Space Flight Mechanics,* AAS Science and Technology Series, Vol. 9, American Astronautical Society, 1967.
10. Escobal P. R., *Methods of Astrodynamics,* John Wiley & Sons, Inc., New York, 1968.

N94- 71290

1994004535
382697

DESIGN OF A DIRECT NUCLEAR PROPULSION SYSTEM FOR A RESUPPLY MISSION TO PHOBOS

S23-20
160649
p- 6

TEXAS A&M UNIVERSITY
DEPARTMENT OF NUCLEAR ENGINEERING

For a long-term mission in space, a propulsion system with a high specific impulse and low mass must be designed. The system must also be safe in terms of human lives and must be cost efficient to a degree. The main focus of this study is to design a direct nuclear propulsion system for a resupply mission to Phobos from an orbiting Earth space station and return. The design considered is an annular, packed particle bed nuclear reactor with hydrogen used as the reflector, moderator, coolant and propellant. The use of hydrogen in all these areas helps reduce the total mass, since the amount of hydrogen required is only that needed for propulsion. The mass of hydrogen required for propulsion is reduced by using a direct nuclear propulsion system with a high specific impulse relative to a hydrogen oxygen system. Certain calculations were not looked at in great detail. This included the aerospace details of the mission. Most of the numbers for this section were found in tables and taken to be correct without extensive calculations. The main objective of the project was to study the thermohydraulic and neutronic aspects of the reactor.

INTRODUCTION

The space program will soon be attempting to explore the planets of our solar system. In order to do this we must have the ability to reach these planets in a vehicle that is safe and has the power capabilities to get us there and back. Several forms of propulsion are being researched and developed each with its own advantages and disadvantages. The method used for this study is a direct nuclear propulsion system. This system uses a nuclear reactor to heat hydrogen which exits a nozzle for propulsion. Due to its inherently higher specific impulse, this system does not need nearly the amount of propellant used in conventional propulsion systems. This cuts down on the mass needed and allows for a broader spectrum of uses in terms of mission length and payload size. This study investigates the use of direct nuclear propulsion for a round-trip, unmanned resupply mission to Phobos from an orbiting Earth space station. This resupply mission is based on a potential Phobos industrial production and supply base as investigated by the University of Texas, Department of Aerospace Engineering and Mechanical Engineering. The focus of this study is on the high-temperature gas-cooled packed particle bed reactor rather than the mission itself or the remaining vehicle components.

MISSION

The mission considered for this study is a resupply venture from a preexisting space station orbiting Earth to Phobos, the closest moon to Mars, and return to the space station at Earth. The initial calculations for the mission are aerospace in nature, calculating the ΔV for the mission and calculating masses of the various components of the spacecraft. Certain values were assumed to begin the calculations: a specific impulse equal to 1000 seconds, a payload mass of 25,000 lbs. and a mass ratio of 0.2. The specific impulse allows for the calculation of the outlet temperature of the propellant. From this temperature the materials are determined. In order to find the exhaust velocity, V_e, the specific impulse, I_{sp}, was considered to be 1000 seconds, which is reasonable for a direct nuclear propulsion system. The exhaust velocity is found using the formula

$$I_{sp} = V_e/g$$

The outlet temperature is then found using V_e and varying γ, which equals the ratio Cp/Cv. The ΔV was found by calculating the escape velocity using a Hohmann-type transfer from Earth orbit to Mars orbit and summing the ΔV's of the escape from a low Earth orbit, the travel to Phobos, the inception of an orbit about Phobos and back to the Earth space station. This value was multiplied by an error factor in case any midflight course adjustments are necessary.

Propulsion system considerations for the mission include the thrust chamber nozzle. A pertinent nozzle dimension is the throat which determines the convergent section leading to the nozzle exit diameter that would result in an appropriate geometry. The area of the throat is easily determined from the expression

$$F = P_c A_t C_f$$

where F is the desired thrust, A_t is the throat area, and C_f is the nozzle thrust coefficient. The system masses and power consumption were calculated using equations from *Fundamentals of Nuclear Flight* by Brussard. The propellant tanks were calculated using

$$M_{st} = (C_{st} M_p)/\rho^{0.66}$$

where C_{st} is 0.25 lbs/ft^3, M_p is the mass of the propellant, and ρ is the density of hydrogen. The mass of the propellant tanks was found to be 37,326 lbm. The mass of the rocket engine was found using

$$M_r = C_r F I_{sp} \pi_r$$

Table 1.

Payload Mass	25,000 lbs	11,364 kg
Specific Thrust		1000 sec
Thrust	126,000 lbs	57273 kg
Propellant Flowrate	126 lbs/sec	57.27 kg/sec
ΔV	50,000 ft/sec	1,524 m/sec
Mass Ratio		0.2
Exhaust Velocity	32,200 ft/sec	9814 m/sec
Exit Temperature	4910°F	2728 K
Propellant Mass	376,190 lbs.	170,995 kg
Final Mass	100,000 lbs	45455 kg
Reactor Mass	14,000 lbs	6364 kg
Reactor Power		3820 MW

where F is the thrust, I_{sp} is the specific impulse, C_r is 2.2×10^{-5}, and π_r is 8.3 lb/MW. The rocket engine mass was found to be 23,000 lbm. The mass of the propellant feed system was calculated using

$$M_{pe} = (C_p F P_d^{0.6})/(\rho I_{sp})$$

where C_p is 3 lb/(ft^3/sec-atm)$^{0.6}$ and P_d is the thrust chamber pressure in atmospheres. The M_{pe} was found to be 3200 lbms. The power consumption was calculated using

$$P_r = -(0.5\ n_j)\ dm/dt\ V_e^2$$

where dm/dt is the propellant flow rate, V_e is the exhaust velocity, and n_j is the overall system efficiency. The power was calculated to be 3820 MW. Table 1 shows other pertinent values used for the mission analysis that were found using formulae from *Fundamentals of Nuclear Flight*.

DIRECT NUCLEAR PROPULSION

Direct nuclear propulsion consists of a nuclear reactor that heats propellant to be used for exhaust, as seen in Fig. 1. In this design, a packed particle bed, annular reactor is used in which the hydrogen passes directly through the core region and exits through the inner region of the annulus, as seen in Fig. 2. The hydrogen propellant also works as a reflector, coolant, and moderator. This cuts down the need for more materials. The hydrogen outside the core is in liquid form and acts as a reflector to improve the reactor neutronic efficiency. As it enters the core, the hydrogen passes through a cold frit which is used to distribute the coolant evenly throughout the core region. Within the core and up to the nozzle throat, the hydrogen is a supercritical fluid and acts as a moderator and a coolant. Passing the hydrogen through the core allows for better heat transfer as it interacts directly with the small spherical fuel particles thus allowing a greater exit temperature for a given maximum fuel temperature. It also allows for moderation effects of the hydrogen, an advantage in this case. The hydrogen passes through hot frit and exits the system as the propulsive hot gas. The frits consist of tungsten because of its high melting point. The fuel element consists of a UO_2 kernel of radius 25.5 mm and a graphite cladding of width 4.5 mm. The cladding is small in order to reduce graphite's moderating effect. In the core, the volume of the fuel elements is equal to the volume of the moderator (void fraction of 0.5). The control of the reactor is accomplished by boron in control rods. Boron acts as a poison and reduces the k_{eff} of the reactor.

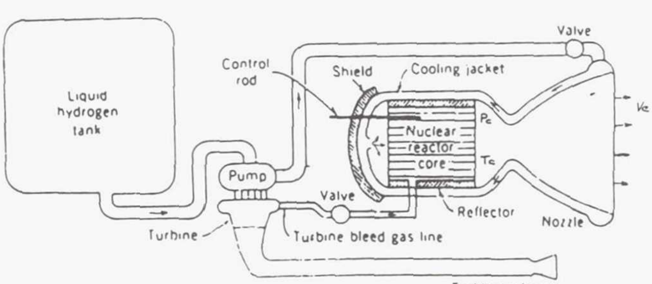

Fig. 1. Schematic Diagram of Nuclear Rocket Using Solid-core Fission Reactor

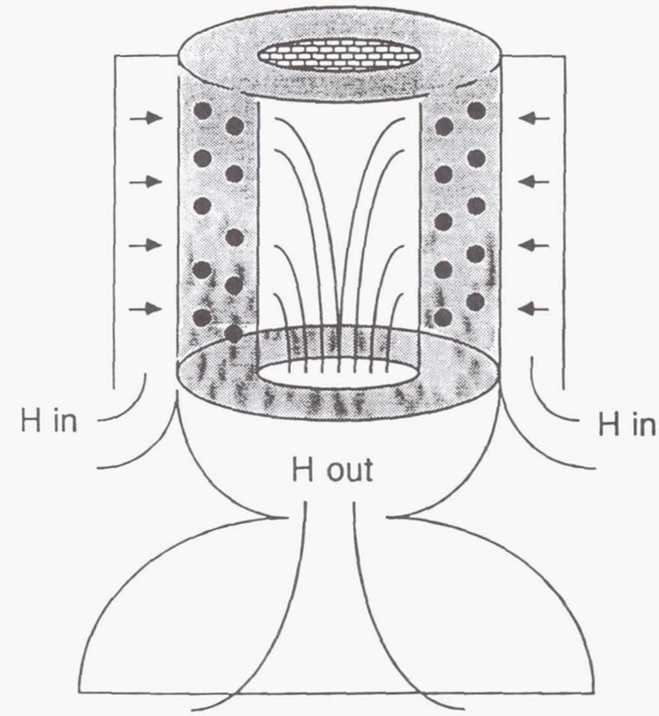

Fig. 2. Particle Bed Design Using an Annular Reactor Design

SYSTEM ANALYSIS

In order to analyze the system, considerations for both thermohydraulics and neutronics must both be satisfied. To do this, an iterative process is necessary. The thermohydraulic analysis is completed and produces a group of values to use in the neutronic analysis. The neutronic analysis then gives new numbers which go back for use in the thermohydraulic analysis. This process is repeated until both sides have been reasonably satisfied in the most efficient manner. Thermohy-

draulic considerations consist of the temperature distribution throughout the core and the high temperature location. This temperature has to be maintained reasonably below the melting points of the materials considered. The neutronics analysis must assure that the reactor will attain criticality. These calculations consist of many other numbers which must be recalculated for each iteration until the system has been optimized. The thermohydraulic analysis has been done using English units while the neutronic analysis was done in metric units. This is due mainly to the convention of the analytical techniques.

Neutronic Analysis

The neutronic calculations were performed by a code called DIF2DK that calculates the k_{eff} and radial flux distribution in a slab, cylinder or sphere, for multiregions. The code calculates these values by using two-group diffusion equations

$$-D_1\nabla^2\phi_1 + \Sigma_{R1}\phi_1 = \Psi_1(\nu\Sigma_{f1}\phi_1+\nu\Sigma_{f2}\phi_2)$$

$$-D_2\nabla^2\phi_2 + \Sigma_{a2}\phi_2 = \Psi_2(\nu\Sigma_{f1}\phi_1+\nu\Sigma_{f2}\phi_2) + \Sigma_{s12}\phi_1$$

where Ψ is the fission spectrum, Σ_{R1} is the removal cross-section for group 1, Σ_{a2} is the absorption cross-section for group 2, Σ_{s12} is the slowing down cross-section from group 1 to group 2, Σ_f is the fission cross-section for each group, and ϕ is the flux for the respective groups. The cross-sections for the two-group equations were calculated from a six-group cross-section collapse for hydrogen and three-group cross-section collapse for uranium. The formulae for these calculations are expanded versions of the formulae above. Figure 3 shows both the fast flux and thermal flux distributions as a function of the distance from the center.

In order to treat the core for analysis certain assumptions had to be made:

- The hydrogen is liquid while in the reflector region and is gaseous in the core region. This was justified by setting the reflector hydrogen temperature just below the boiling point so as it passes through the cold frit it changes phase into gas. This assures that there is no phase change in the core region or the reflector region.
- The graphite cladding moderating effects are assumed to be negligible. This is justified by the fact that the cladding has a negligible volume compared to that of the hydrogen and the fuel. Also graphite is a weak moderator compared to hydrogen.
- The reactor is considered to be symmetric. This allows for only half of the reactor to be analyzed with the other half of the reactor taken into account by the appropriate boundary conditions.
- The reactor is considered to be quasi-homogeneous. This is justified by the fact that the neutron mean free path is large compared to the size of the fuel element (which ultimately was found to be 600 μm in diameter). This allows for volume averaging of the cross-sections of the fuel and moderator in the core.

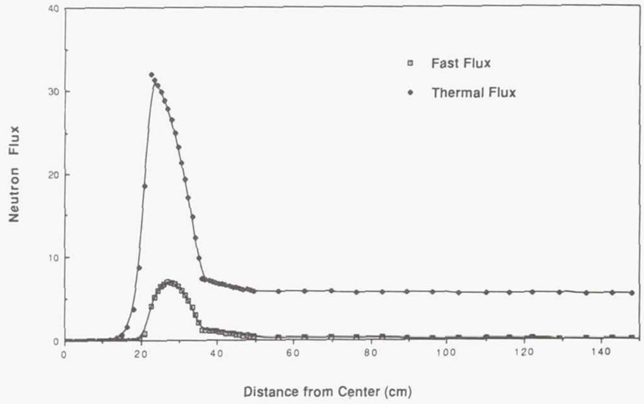

Fig. 3. Flux Shape

The code used treats the reactor for a large number of regions. For this analysis the reactor was divided into four regions: reflector region (liquid hydrogen), outer core region or inlet channel (UO_2 fuel and cold hydrogen gas), inner core region (UO_2 fuel and hot hydrogen gas), and inner annulus or exit channel (hot hydrogen gas). The core region was divided into two sections because the density of hydrogen changes as it is heated, so the changes in cross-sections of hydrogen across the core were taken into account.

From the initial thermohydraulic analysis, the ratio of height to density was given to be 1.0, the inner radius of the annulus was half the outer radius, and the void fraction was set at 0.5. After running calculations to find the k_{eff} of the system it was determined that the inner radius would have to be set at 0.45 times the outer radius. This calculation was performed while holding the volume and void fraction constant so there would be as little change in the thermohydraulics calculations as possible. The k_{eff} found for this geometry is 1.0802. The addition of boron into the core should be used to control the system while in use. Boron is a neutron poison that lowers the reactivity of the core. Owing to time constraints, neither the development of the control system nor the calculations of the neutronic effect of the boron were possible. For shutdown, all that is needed is to cut off the flow of hydrogen. The loss of moderator and reflector will cause the reactor to go subcritical. The case of submersion in water is not of importance due to the fact that this is a space-only vehicle and threat of submersion is not present.

Another factor to be determined is the burnup rate of the fuel. If this value is too high it can cause great deviations in how the neutronics calculations are made by changing flux shapes. The burnup rate is given by:

$$\text{Burnup Rate} = PA/E_r \text{ g/day}$$

where P is the thermal power, A is the atomic weight of the fissile material, and E_r is the recoverable energy per fission. Since burn time is 50 minutes, the fuel burnup is 0.1671 kg of fuel, which is negligible compared to the original mass of the fuel. The final dimensions of the core are outer radius of 48.98 cm, an inner radius of 2.04 cm, a height of 97.96 cm,

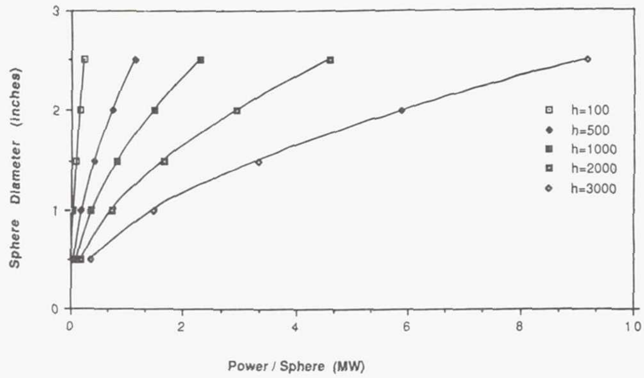

Fig. 4. Sphere Diameter vs. Power (=3820 MWt)

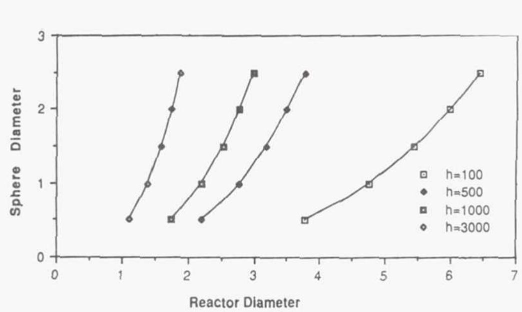

Fig. 5. Sphere Diameter vs. Reactor Diameter; Power = 3820 MWt

and a reflector width of 100 cm. The reflector is set at a large value in order to assure that it is considered an infinite reflector. Table 3 summarizes the reactor design specifications.

Thermal Hydraulics

To get a feel for a relationship between h, the heat transfer coefficient, sphere diameter, reactor size (diameter), and power per sphere, Figs. 4 and 5 were developed. These figures indicate that a small reactor diameter requires high h's and small sphere diameters. The diameter of the sphere would dictate the power per sphere and thus the relationship between the gas bulk temperature and fuel temperature. The data from the figures was used to indicate the direction one should take in selecting a "reasonable" reactor size vis-a-vis the sphere diameter to be used. The sphere diameter selected would then influence the reactor size and thus the resultant hydraulic parameters and attendant heat transfer relationships, i.e., Prandtl and Nusselt numbers. The "reasonable" reactor size would have to be within the projected weight constraint of 23,000 lbs, the goal being to design an annular particle bed gas cooled reactor with a gas exit temperature less than 1000°R from the melting point of uranium, 5630°R.

The design selection is based strictly on several iterative processes that led to a converging reactor size. With the reactor size constant, the sphere size was iterated to result in the final selection of a diameter equal to 600 micrometers or 0.152 inches. The converging reactor dimensions of 3.3 feet outside diameter, 1.65 feet inside diameter and a height equal to the outside diameter were finalized based on neutronics requirements, resulting in a reactor with an outside diameter of 3.214 feet, an inside diameter of 1.446 feet and a height of 3.214 feet. With these dimensions in the core, the following were found: an exit temperature of 4910°R, a fuel center temperature for the hot sphere of 4985°R, a fuel weight of 7114 lbs and a pressure drop of 23 psia. Since the fuel center temperature is below its melting point of 5630°R, the fuel weight is below the projected number and the hydrogen exit temperature is within 58°R of the desired value; the design was deemed acceptable but not optimal.

Table 2. Hydrogen Gas Properties at 3800°R

Heat Capacitance (K)	4.15 btu/hr-ft-°F
Density	0.024 lbs/ft^3
Viscosity (μ)	0.8 lbm/hr-ft
Heat Capacity (C_p)	3.85 btu/lb-°R
Prandtl ($Pr = C_p\mu/K$)	0.742

The initial calculations consisted of gathering the necessary factors/parameters and establishing the necessary assumptions to get the iteration started. The hydrogen gas properties used for the design are found in Table 2 from *Fundamentals of Nuclear Flight* by Brussard.

The following analysis of the fluid flow was based on formulae from *Heat Transfer and Flow in Nuclear Systems* by Henry Fenech. Initial calculations for temperature began with Newton's law of cooling

$$Q = Ah\Delta T_{ln}$$

where Q is the expected heat rate from the reactor of 3820 MW(t) or 1.200893×10^{10} btu/hr, h is the heat transfer coefficient, A is the heat transfer area and the ΔT was treated as a log mean temperature difference between fuel and coolant. The log mean ΔT addressed the hot channel concept as a circular pipe with the higher temperature difference (4968-4938°R) at the outside diameter and the lowest temperature difference (5630-4930°R) at the end of the hot channel, i.e., the inside diameter. The highest temperature of the gas was set at 90% of melting, thus leaving an extra 500°R of safety margin between the fuel melting point and the neutronics design gas temperature of 4500°R. Thus

$$\Delta T_{ln} = (4968\text{-}4938) - (5630)/(\ln 4930/600) = 2056°R$$

Figure 4 indicated that a 1.00-inch sphere would result in a power to sphere ratio of approximately 0.1 MW if an h equal to 150 btu/hr-ft^2-°R was used. This size sphere was then used to initiate the reactor sizing analysis, starting with a reactor outside diameter of 4.4 feet and a void fraction of $\epsilon = 0.5$. With this size reactor and sphere diameter, hydrogen average velocities and resultant Reynolds numbers were calculated. From these values, the Nusselt number can be calculated using

$$Nu = f_\epsilon Nu_s$$

where

$$f_\epsilon = 1 + 1.5(1 - \epsilon) = 1.75$$

where ϵ is given to be 0.5 and Nu_s is the Nusselt number for a sphere and is given as

$$Nu_s = 2 + (Nu_l^2 + Nu_t^2)^{0.5}$$

where Nu_l is the laminar Nusselt number and Nu_t is the turbulent Nusselt number given as

$$Nu_l = 0.664(Re/\epsilon)^{0.5}(Pr)^{0.33}$$

$$Nu_t = [0.037(Re/\epsilon)^{0.8}(Pr)]/[1+2.443(Re/\epsilon)^{-0.1}(Pr^{0.67} - 1)]$$

where Pr is the Prandtl number and Re is the Reynolds number. From these calculations, a new heat transfer coefficient was found to be 4906 btu/hr-ft^2-°R, which then allowed for the calculation of a new total heat transfer area.

Setting this transfer coefficient as a constant, calculations were made to find the sphere diameter that would best fit this heat transfer area converted to a reactor diameter equal to 4.4 feet. A 4.4-ft-diameter reactor with a void fraction of 0.5 would result in a fuel volume of approximately 25 cubic feet. This volume of fuel would result in a fuel weight of 17,100 lbs high, but still within the design goals, that serves as a guide for a high point limit. The calculations showed that a sphere diameter of 2.35 inches would be acceptable for this size reactor. The value for h was calculated to be 7564 btu/hr-ft^2-°R.

Having found the maximum point with respect to size (weight), a search began for a size closest to the design goal. Previous calculations indicated that a sphere diameter of 1.52 inches would result in a fuel volume of 13.65 cubic feet and a starting reactor diameter of 3.6 ft. Subsequent iterations resulted in a fuel volume of 10.4 cubic feet and a reactor volume of 20.8 cubic feet with a resultant outside diameter of 3.3 feet. The h was rather high at 11,745 btu/hr-ft^2-°R.

The reactor volume of 20.8 cubic feet was used to initiate the neutronics calculations necessary to establish the proper geometry to attain criticality. Criticality was reached theoretically with a reactor of outside diameter 3.214 ft and an inside diameter equal to 0.45×3.214 ft and a height of 3.214 ft.

The hot channel temperature distribution along the annulus radius was defined as

$$Tc = T_{in} + q'''/mc_p \int J_o \pi/2 dV + (q'''/A_{ht}h)\int \pi/2 J_o dA + (S_{no}R_f/6k_f + 3/10 + S_{no}R_c/3k_c(1+3/5))\int \pi/2 J_o dA$$

where S_{no} is the individual sphere power, R_f is the radius of the fuel sphere, R_c is the radius of the cladding, k_f is the fuel thermoconductivity, k_c is the cladding thermoconductivity, T_c is the sphere center temperature, T_{in} is the inlet temperature, the first integral is T_{bulk}-T_{in}, T_{bulk} is the hydrogen temperature, the second integral is T_{cl}-T_{bulk}, T_{cl} is the clad surface temperature, and the third integral is T_c-T_{cl}; the limits of integration being always between 3.214 and 0.45×3.214 ft. The average core power, q''', and core average flux, q'', are given as

$$q''' = 1.200893\times10^{10} \text{ btu/hr}/20.8 \text{ ft}^3 = 5.773524\times10^8 \text{ btu/hr-ft}^3$$

$$q'' = 1.200893\times10^{10} \text{ btu/hr}/498 \text{ ft}^2 = 2.4125459\times10^7 \text{ btu/hr-ft}^2$$

Since $V_r = \pi(0.1988)D_r^3$ and $dV_r = r\, 3\pi(0.1988)D_r^2 dD_r$,

$$T_{bulk} - T_{in} = 309.717 \int D_r^2 dD_r J_o$$

With the limits of integration being 3.214 ft and 1.45 ft and the J_o limits being between 2.405 and 1.2025, the calculation results in a T_{bulk}-T_{in} = 4872.8°R. This gives a T_{bulk} = 4873+38 = 4910°R.

The sphere diameter of 1.52 inches resulted in a cladding surface temperature of 6145°R. This temperature was considered to be unacceptable; therefore the sphere diameter was reduced to 0.1525 in or 600 m. The reactor size was held at 3.3 ft outside diameter, 1.65 ft for the inside diameter, H/D = 1 and the iteration resumed. The final dimensions, as previously discussed, came from neutronics considerations and were 3.214 ft outside diameter, a height of the same dimensions and an inside diameter of 1.45 ft.

The 600-m spheres with their small unit volume resulted in multiplying the heat transfer area almost an order of magnitude to 4903.726 ft^2. The total number of spheres came to 9.677 million. The Reynolds number was reduced dramatically resulting in a lower Nusselt number with a subsequent increase of h to 34,090 btu/hr-ft^2-°R.

In solving for T_{cl}-T_{bulk}, the heat transfer area, $A_{ht} = \pi D^2/2$ was used to put A_{ht} in terms of D in the integral $\int dA$. Thus

$$T_{cl} - T_{bulk} = (q'''\pi^2)/(2A_{ht}) \int D dD J_o$$

$$= 69.97 = 70°R \text{, thus}$$

$$T_{cl} = 70 + 4910 = 4980°R$$

using the *Transport Phenomena* expression and applying the F factors

$$T_c - T_{cl} = 5°R$$

$$T_c = 4985°R$$

which gives a 635°R safety margin. *Transport Phenomena* by Bird, Stewart, and Lightfoot was consulted to develop an approach that would result in credible pressure drops between the outside and inside diameters of the annulus reactor; that is, pressure drops resulting from hydrogen gas flowing across the reactor radius at relatively high velocities. Using pressure drop equations such as found in "Heat Transfer and Flow in Nuclear Systems" by Henry Fenech and in "Particle Fuel Bed Test" by F. L. Horn et al., Chapter 38, *Space Nuclear Power*

Table 3. Summary of Design Specifications

Specific Impulse	1000 sec
Delta V	50,000 ft/sec
Exhaust Velocity	32,200 ft/sec
Total Mass	476,190 lbm
Final Mass	100,000 lbm
Reactor Power	3820 MW
Reactor Height	97.96 cm
Reactor Outer Radius	48.98 cm
Reactor Inner Radius	20.40 cm
Reflector Width	100 cm

Systems 1985, resulted in extremely high pressure drops, thus the *Transport Phenomena* consultation.

Since the gas velocity was calculated using an average gas flow area equaling 5.0487 ft^2 (and attendant Re calculations), it was deemed proper to use the pipe pressure drop equations corrected for friction factors due to flow around spheres and further corrected to account for the particle bed void fraction

$$\Delta P = (f(0.5r)V^2)/[0.25(D/L)((1-\epsilon)/\epsilon^3)]$$

where $f = 0.44$ and $\epsilon = 0.5$. This expression gave a $\Delta P = 23$ psia, which, if it is off by a factor of 10 (230 psia), would still be a credible number.

FUTURE WORK

Because of the time constraints in this project, certain aspects were either overlooked or just lightly touched upon. One of these aspects concerns the properties of hydrogen. Hydrogen's density changes radically as it increases through the temperatures that were used in this project. Even though the neutronics calculations touched upon this by calculating the cross-sections at a hot and cold temperature, a more thorough and time-consuming effort is needed to actually attain the proper values as hydrogen heats up across the core. A possibility in solving this problem would be to set up a finite-difference scheme for the density of hydrogen as it increases in temperature. These numbers could then be used to calculate more accurately the cross sections in the core. This would mean treating the core in as many regions as were used in the finite-difference calculations. This change in hydrogen would also have to be taken into account for the thermohydraulic calculations.

Another consideration is the boron poison. Future work would have to entail the use of boron gas as the reactor-controlling poison. Boron is considered to be a better controlling agent than the use of control rods since boron use would neither change the geometry of the system nor disrupt the placement of the spheres in the reactor as would control rods. Further research into this area would entail the calculation of the negative reactivity effects on the system and the method of controlling the use of the bleed line. Since it would enter and exit with the hydrogen, mass considerations would also have to be taken into account. This is dependent on the amount of boron that would be needed for control and shutdown of the reactor.

One factor not included in the neutronic analysis is the appearance of decay heat as the moderator is removed. In this project, it is assumed that the loss of moderator would be sufficient to shut down the reactor; however, a method for cooling the reactor to limit decay heat would have to be considered. The presence of decay heat could cause problems in the overall analysis of the reactor.

Aside from the factors that could affect the reactor's performance, there is need for electrical power on the vehicle. One possibility is to bleed off hot hydrogen into a cycle for the production of electrical power. Since the reactor is only operable for about 50 minutes on this mission, there would be a need for battery cells that would be recharged when the reactor is brought into use and would provide a constant source of power at all other times.

ACKNOWLEDGMENTS

Principal authors R. Frymire and R. Martinez were assisted by faculty advisor Professor Fred Best.

MOON BASE REACTOR SYSTEM

TEXAS A&M UNIVERSITY

DEPARTMENT OF NUCLEAR ENGINEERING

The objective of our reactor design is to supply a lunar-based research facility with 20 MW(e). The fundamental layout of this lunar-based system includes the reactor, power conversion devices, and a radiator. The additional aim of this reactor is a longevity of 12 to 15 years. The reactor is a liquid metal fast breeder reactor that has a breeding ratio very close to 1.0. The geometry of the core is cylindrical. The metallic fuel rods are of beryllium oxide enriched with varying degrees of uranium, with a beryllium core reflector. The liquid metal coolant chosen was natural lithium. After the liquid metal coolant leaves the reactor, it goes directly into the power conversion devices. The power conversion devices are Stirling engines. The heated coolant acts as a hot reservoir to the device. It then enters the radiator to be cooled and reenters the Stirling engine acting as a cold reservoir. The engines' operating fluid is helium, a highly conductive gas. These Stirling engines are hermetically sealed. Although natural lithium produces a lower breeding ratio, it does have a larger temperature range than sodium. It is also corrosive to steel. This is why the container material must be carefully chosen. One option is to use an expensive alloy of cerbium and zirconium. The radiator must be made of a highly conductive material whose melting point temperature is not exceeded in the reactor and whose structural strength can withstand meteor showers.

NEUTRONICS

The neutronics for a compact core design are particularly important in that a small change in reactivity can cause a rapid change in reactor power that could lead to an accident if the core is poorly designed. In addition, a small core allows one the opportunity to explore innovative means of reactor control that take advantage of distinctive material properties. The property that this project took advantage of as a means of reactor control was a small core's high leakage, in that control reflectors are used instead of control rods or discs. A control reflector has the advantages of economizing neutrons, which are expensive to produce, and allowing the production of smaller, lighter cores. Another advantage of a control reflector is that it helps to reduce the power peak to the average ratio by causing a thermal peak and thus increases the fission rate at the core peripherally as shown in Fig. 1. This effect is not duplicated by control rods, and rods create severe flux perturbations that require transport theory to solve for; in addition, a control rod's absorbing action is a waste of a valuable resource, namely neutrons.

Our core design was initially to be a Clinch River breeder reactor core clone using gallium as a primary coolant due to concerns with the positive reactivity insertion caused by sodium voiding. The use of gallium as the primary coolant was canceled due to its high cost at \$3/g. The second coolant considered was lithium, which is much less expensive than gallium and still had a high enough boiling point to make the possibility of coolant voiding inconsequential relative to the fact that the core would be molten at that point. Another departure from the Clinch River design was a solid BeO fuel rod with uranium suspended in the matrix. This design was used in order to operate the reactor with a higher outer surface temperature and thus increase its efficiency. The solid rod concept was used to eliminate the cladding gap conductance losses and the cladding pellet interaction. In addition,

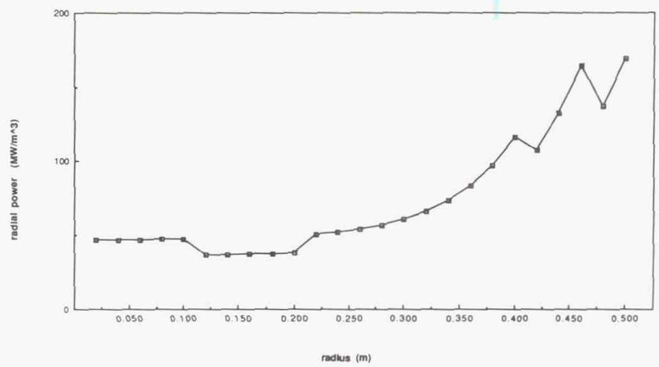

Fig. 1. Peak to Average Ratio (Power)

the conductance of BeO is five orders of magnitude higher than that of UO_2, which leads to lower fuel centerline temperatures. Moreover, the BeO undergoes a phase change at 1244°C from a body centered cubic lattice structure to a face centered cubic structure, which increases the pin volume by approximately 6%. This increase in volume decreases the macroscopic fission cross-section in the middle of the core and increases the leakage at the top of the core. The combination of these two negative reactivity effects serves to shut the reactor down. A 16-group neutronics calculation was performed using the approximations of diffusion theory. In order to perform these calculations a computer code called 2DB was created and used and the cross-section's flux was weighted. The code was then run for the case of no reflectors in the core and yielded a k_{eff} of 0.65.

This showed that the reactor was safe to travel without any reflectors present. However, when all the control reflectors were flooded with lithium the k_{eff} went up to 0.96, which is marginal although still subcritical. The case for the reflectors

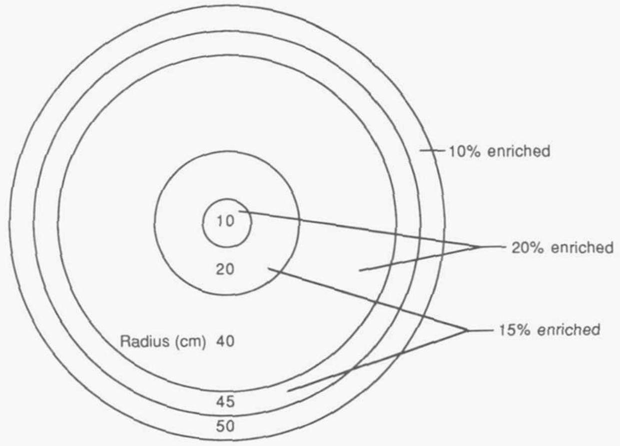

Fig. 2. Cross-section of the Core

halfway up and the void still intact failed to run in the given amount of computer time. Moreover, the case similar to the previous one, but with the reflector compartments flooded, yielded a k_{eff} of 1.29.

Finally, the case with the reflectors fully up yielded a k_{eff} of 1.31. This shows that the core possesses much excess reactivity for a long-running operation and can still be considered a subcritical assembly when the reflectors are removed. In addition, the conversion ratio is high, approximately 0.9; however, the burnup calculator on the code written is marginal and the calculation was done without including Pu-241. Also, the plutonium breeding would take place preferentially in the lower enriched bands of the reactor and in areas with a peak in resonance energy neutrons. Figure 2 shows an enrichment cross-section of the core. Figure 3 shows the resonance energy flux with increasing radius. The Pu breeding would serve to flatten the power profile and reduce the peak to the average ratio across the core as time progressed. This would enable the core to be run at a higher total heat generation without stressing the components beyond their design limits. An advantage of this system is that the plant can generate more electricity by simply adding more Stirling

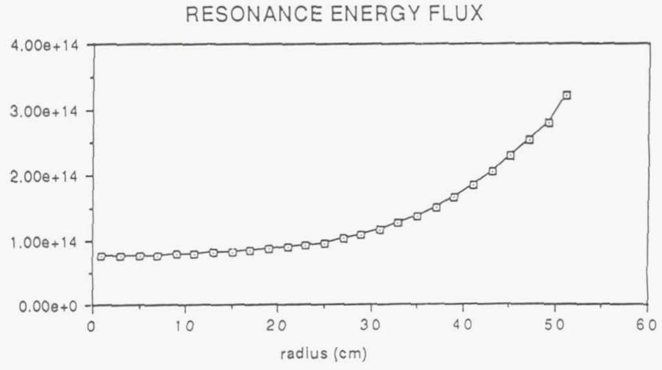

Fig. 3. Resonance Energy Flux

engines. This is critical in space applications in that the less mass that needs to be transported, the more economically feasible the mission.

THERMOHYDRAULICS, THERMODYNAMICS, AND OTHER SIGNIFICANT CORE ANALYSIS

Initially, the designed output expected was 20 MW(e), but because of the thermal design limits set by the fuel and coolant, only 15 MW(e) were obtained. The thermal limitations were the melting point of the fuel (2822 K) and the boiling point of the coolant (1600 K). The calculations were geared to obtain an exit temperature of 1200 K and an inlet temperature of 500 K. With these parameters in mind, after consulting *Nuclear Power Plant* by James Rust, we found that the hot channel of the core exceeds the thermal limitation of the coolant. The peak to average heat flux is approximately 2.27, which caused a great deal of problems.

$$q'''_{max}/q'''_{ave} = 2.27$$

For this design, the fuel has no cladding and, therefore, has no gaps. Cladding is used to prevent corrosion by the coolant and retention of fission products since it is made of nonfissionable material. The cladding may exert restraining forces that help to prevent distortion of the fuel during operation. We first assumed that BeO was strong enough to avoid any serious distortion, but Tang et al. clearly state in "Thermal Analysis of Liquid Metal Fast Breeder Reactors" that oxide fuels crack during irradiation. This may need to be explored in the future. Also, lithium can be corrosive to stainless steel and so other container materials such as Cb-Zr alloys must be looked into, as discussed in Benjamin Ma's work, *Nuclear Reactor Materials and Applications.*

The diameter of the BeO fuel rod is 0.5 cm and its length is 100 cm. This material will bend under extreme temperatures due to the nature of its structure. Both BeO and lithium are good conductors. There is little difference between the temperatures of the centerline and the bulk fluid. The pitch is 1.0 cm and the pitch-to-diameter ratio is 2.0, as shown in Fig. 4. To find the flow area, as indicated by the shaded area, the triangular area was found and then the pin area was subtracted from it.

Triangular Area = 0.4330127 cm^2
Pin Area = 0.19635 cm^2
Flow Area (channel) = 0.236663 cm^2

The core is 100 cm in height and has a height-to-diameter ratio of 1.0.

Core Area = 7853.9816 cm^2

Therefore, the number of triangles is Core Area/Triangle Area = 18138

Total Flow Area = 4292.6 cm^2

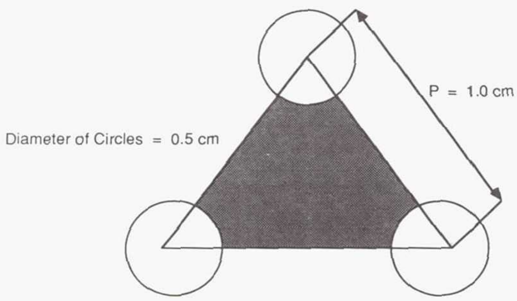

Fig. 4. Lattice Space

After analyzing the neutronics data we found that axially both the maximum heat flux, $q'''_{max}(z)$, and the average heat flux, $q'''_{ave}(z)$, were cosine shaped as expected. We modeled these shapes using a curve fit routine.

$$q'''_{max}(z) = 64.81 + 384.6z - 336.64z^2 - 37.158z^3$$

$$q''_{max}(z) = \int_0^z q'''_{max}(z)\, dz$$

$$= 64.81z + 192.3z^2 - 112.21z^3 - 9.29z^4$$

$$q'''_{ave}(z) = 34.734 + 110.89z - 73.129z^2 + 301.32z^3 - 806.12z^4 + 480.73z^5$$

$$q''_{ave}(z) = \int_0^z q'''_{ave}(z)\, dz$$

$$= 34.734z + 55.445z^2 - 24.376z^3 + 75.33z^4 - 161.224z^5 + 80.122z^6$$

The equivalent diameter of the channel was also calculated:

$$D_e = 4(\text{flow area})/\text{wetted perimeter} = 0.2651096 \text{ cm}$$

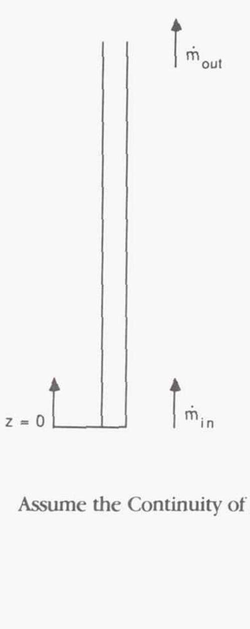

Fig. 5. Assume the Continuity of Mass

Beginning with the energy equation, we referred to *Fundamentals of Classical Thermodynamics* by Gordon Van Wylen and Richard Sonntag to derive all necessary equations in order to find the bulk fluid temperature and fuel centerline temperature. Initially, we assumed the continuity of mass applied, as shown in Fig. 5.

$$\frac{d}{dt}\int_V \rho\left(u + \frac{v^2}{2} + gz\right) dV =$$

$$-\int_A \left(u + p\nu + \frac{v^2}{2} + gz\right)\rho^{(vn)} dA + Q - W - \Psi$$

The following assumptions were made:

at steady state, $d/dt = 0$

kinetic and potential energy is negligible, $\frac{1}{2}(v^2) = 0$, $gz = 0$

$$h = u + p\nu$$

no work is being done by or to the system, $W = 0$

no dissipation is occurring, $P = 0$

$$Q = m\,(h(z) - h_{in})$$

and, if the fluid is single phase, we may appropriately substitute

$$Q = mc_p(T_b(z) - T_{in})$$

where

$$Q = \int_0^z q'''(z)\pi R_{Fs}^2\, dz$$

$$= \dot{m}c_p(T_b(z) - T_{in})$$

Thus, the expression for T_{bulk} is

$$T_b(z) = T_{in} + \frac{\int_0^z q'''(z)\pi R_{Fs}^2 dz}{\dot{m}c_p}$$

For convection, we found that the flow is so slow that the convective heat transfer coefficient is very small compared to the conductive properties of the coolant. Hence,

$$h_c \sim k/D_e$$

So, from Newton's Law of Cooling we have

$$Q = h_c A_s (T_{Fs} - T_{bulk})$$

but

$$Q = q'''\pi R_{Fs^2}\, l$$

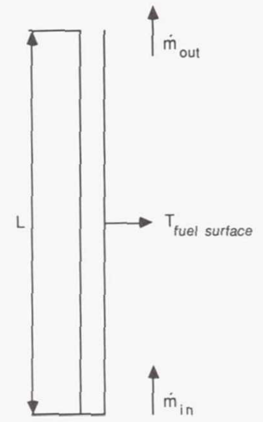

Fig. 6. Coolant Flows Along Pin

and

$$A_s = 2\pi R_{Fs}\, l$$

Then

$$q'''R_{Fs} = 2k/D_e(T_{Fs} - T_{bulk})$$

where T_{Fs} is depicted in Fig. 6. The expression for $T_{fuel\ surface}$ is

$$T_{Fs} = T_{bulk} + q'''R_{Fs}D_e/2k$$

Finally, from fuel centerline to fuel surface (without cladding), using the microscopic equation

$$\rho c_p \frac{DT}{Dt} = \vec{\nabla}\cdot k(r,T)\vec{\nabla}T(r) + q'''(r)$$

The following assumptions were made: at steady-state, d/dt = 0; the velocity field for a solid fuel pin = 0; we can neglect the axial condition; the pin is azimuthally symmetric; and conductivity, k, is not a function of temperature

$$-q'''(r) = k\,\nabla^2 T$$

Integrating this expression, we find

$$k\int \frac{d}{dr}\left(r\frac{dT}{dr}\right) dr = -\int q'''r\, dr$$

$$kr = -q'''r^2/2 + C_l$$

$$\text{at } r = 0,\ C_l = 0$$

$$\int_{T_{Fs}}^{T} dT = -\int_{R_{Fs}}^{r} \frac{q'''r}{2k} dr$$

$$T(r) - T_{Fs} = \tfrac{1}{4}k_{fuel}\,(q'''(R^2_{Fs} - r^2))$$

$$\text{at } r = 0,\ T(r) = T_{cl}$$

$$T_{cl} = T_{Fs} + \tfrac{1}{4}k_{fuel}\,(q'''(z)\,R^2_{Fs})$$

so the expression for fuel centerline is

$$T_{cl} = T_{in} + \frac{\pi R^2_{Fs}}{\dot{m}c_p}\int_0^z q'''(z)\,dz + \frac{q'''(z)}{2k_{coolant}} R_{Fs}D_e + \frac{q'''(z)R^2_{Fs}}{4k_{fuel}}$$

As stated above, the aim of the reactor was to change the bulk temperature from 500 K to 1200 K. In the hot channel, however, voiding will occur under these parameters. Also, the mass flow rate of the channel equals 8.65E-04 kg/sec due to the inconsistencies of the core. Although our aim was to produce 60 MW(t), the reactor output under these conditions was only 21.364 MW(t).

$$Q = \dot{m}c_p(T_{out} - T_{in})$$

$$= 18138\ (3.65\text{E-}04\ \text{kg/s})(4.61\ \text{kJ/kg-K})(700\ \text{K})$$

$$= 21.364\ \text{MW}$$

Since the flow rate is so slow, the only pumping consideration looked into for this system was the drop in pressure along the pipe lines. Since we consider the coolant incompressable, we may use the fact that work into the pump is given by

$$W = m\nu\,(P_2 - P_1)$$

where

P_2 = the pressure that needs to be maintained
P_1 = the pressure that occurs after the pressure drops
$P_2 - P_1 = \Delta P$ = pressure drop in the system
$\nu = 1/\rho$
ρ = density of the fluid
$\dot{m}$ = mass flow rate

We allow one MW of power for two pumps in the reactor system, one pump in operation and another used as a backup system. A hermetically sealed centrifugal pump driven by this power is used for the liquid metal loop. The power conversion devices are free piston Stirling engines (FPSE). Out T_{hot} input will be 1200 K and T_{cold} will be 300 K.

$$\eta_{Stirling} = 1 - T_c/T_h = 0.75$$

Since the efficiency of our Stirling engine is about 75%, the coolant temperature leaving the Stirling engines will be about 675 K. The output of the Stirling engine is given by

$$W_{Stirling} = Q_{li}\eta_{Stirling}$$

$$W_{Stirling} = 16.023\ \text{MW(e)}$$

Table 1. Thermohydraulic Characteristics

Power Output	21.364 MW(t)
Core Volume	0.7854 m^3
Core Height	1.0 m
Core Diameter	1.0 m
Pitch	0.001 m
Fuel Diameter	0.0005 m
Fuel Type	BeO enriched with U-235, U-238
Coolant Type	Lithium
Power Density	53.35 MW/m^3
Inlet Temperature	500 K
Exit Temperature	1200 K
Mass Flow Rate	6.62 kg/s

Table 2. Thermodynamic Characteristics

Direct Cycle	
Stirling Cycle Efficiency	75%
Carnot Efficiency	58.334%
Cold Temperature	500 K
Hot Temperature	1200 K
Thermal Efficiency	43.75%
Radiator Mass	2400 kg

Ideally

$$Q_{before} - W_{Stirling} = 5.341 \text{ MW of waste heat}$$

To power the facility, we will use 15 MW and keep one MW to power the pumps and for emergency power.

If $Q_{after} = 5.341$ MW, then using the expression

$$Q_{after} = \dot{m}c_p\,(T - 500\text{ K})$$

$$T = 675\text{ K}$$

Now, we must get rid of this waste heat through a radiator as discussed in detail in the next section.

Finally, the thermal cycle is evaluated using *Fundamentals of Classical Thermodynamics* by Van Wylen and Sonntag.

Carnot cycle:

$$\eta_{carnot} = 1 - T_c/T_h = 58.33\%$$

Thermal cycle:

$$\eta_{thermal} = h_{carnot} \times \eta_{Stirling} = 43.75\%$$

Table 1 summarizes the thermohydraulic characteristics and Table 2 summarizes the thermodynamic characteristics of the system. Table 3 gives the data used in the plots of temperature and flux vs. distance found in Figs. 7 through 10.

RADIATOR

Space nuclear power plants must reject their waste heat by thermal radiation. The amount of waste heat that can be radiated to space by a given surface area is determined by the Stefan-Boltzmann law and is proportional to the fourth power of the radiating surface temperature. The surface area and mass of the thermal radiator are very sensitive to the heat rejection temperature. Higher heat rejection temperatures correspond to smaller radiator areas and thus lower radiator masses. Radiator

Table 3. Data for Figures 7-10

	axial distance(m)	q'''_{avg}	T_{bulk} avg.(K)	T_{cl}avg.(K)	q'''_{max}	T_{bulk} max.(K)	T_{cl}max(K)
1							
2							
3	0.000	34.734	500.000	505.035	64.810	500.000	509.395
4	0.050	40.128	521.852	527.670	83.194	543.259	555.320
5	0.100	45.317	546.787	553.356	99.866	596.746	611.224
6	0.150	50.367	574.707	582.009	114.800	659.456	676.098
7	0.200	55.261	605.531	613.679	127.967	730.364	748.916
8	0.250	59.915	639.145	647.831	139.339	808.433	828.633
9	0.300	64.194	675.373	684.679	148.889	892.606	914.191
10	0.350	67.934	713.949	723.797	156.588	981.813	1004.514
11	0.400	70.960	754.507	764.794	162.409	1074.966	1098.510
12	0.450	73.099	796.580	807.177	166.324	1170.960	1195.073
13	0.500	74.202	839.605	850.362	168.305	1268.677	1293.076
14	0.550	74.163	882.944	893.696	168.324	1366.978	1391.380
15	0.600	72.935	925.915	936.489	166.353	1464.711	1488.828
16	0.650	70.547	967.827	978.054	162.365	1560.708	1584.246
17	0.700	67.123	1008.035	1017.766	156.331	1653.783	1676.446
18	0.750	62.904	1045.999	1055.118	148.224	1742.733	1764.222
19	0.800	58.258	1081.355	1089.801	138.015	1826.343	1846.351
20	0.850	53.706	1113.999	1121.785	125.678	1903.377	1921.596
21	0.900	49.934	1114.177	1151.416	111.183	1972.585	1988.703
22	0.950	47.815	1172.590	1179.521	94.504	2032.700	2046.400
23	1.000	48.425	1200.505	1207.525	75.612	2082.440	2093.402

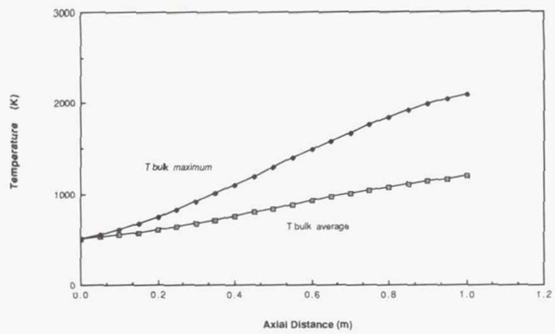

Fig. 7. Bulk Temperatures vs. Axial Distance

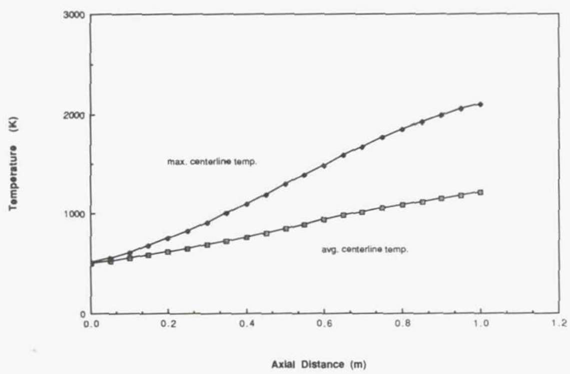

Fig. 8. Centerline Temperatures vs. Axial Distance

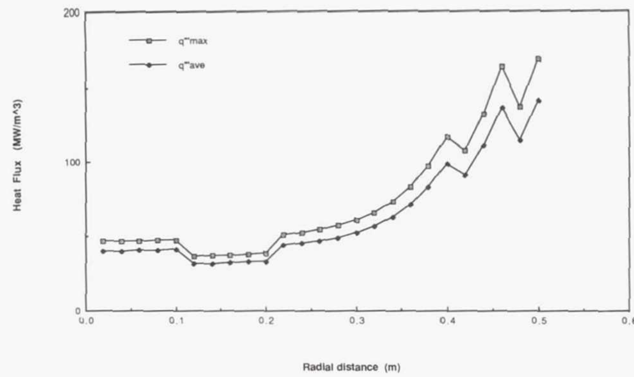

Fig. 9. Heat Flux vs. Radial Distance

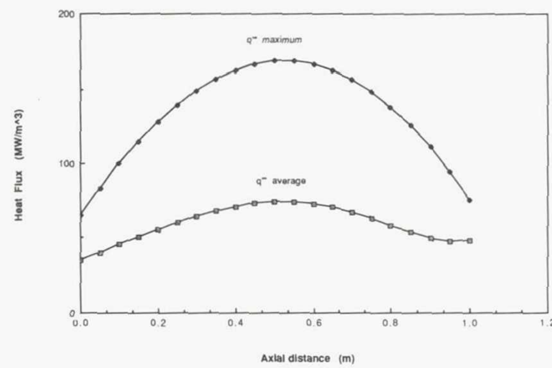

Fig. 10. Heat Fluxes vs. Axial Distance in the Core

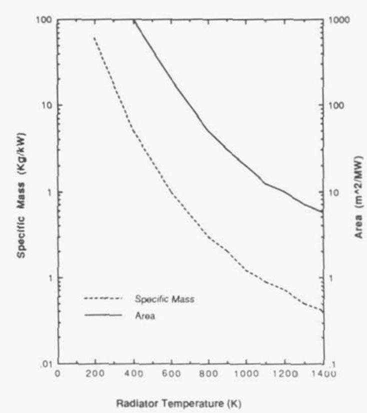

Fig. 11. Radiator Area and Mass as a Function of Temperature

area and mass as a function of temperature are shown in Fig. 11.

Using the Stefan-Boltzmann expression

$$Q_{after} = Q_{radiator} = [\epsilon\sigma(T^4_s - T^4_c) - I]A$$

or

$$A = Q_{radiator}/[\epsilon\sigma(T^4_s - T^4_c) -]$$

where A is the area of the radiator, $Q_{radiator}$ equals the waste heat of 5.341 MW, ϵ is the emissivity of the radiator surface (0.9), σ is the Stefan-Boltzmann constant (5.67E-08 W/m^2-K^4), T_s is the entering temperature (675 K), T_c is the sink space temperature (0 K) and I is the solar flux (1371 w/m^2). Then

$$A = 579.125 \text{ m}^2$$

or

$$A = 24.1 \text{ m} \times 24.1 \text{ m}$$

This area seems fairly small but this occurs if the radiator is 100% efficient.

Radiator materials should also be considered with the following general characteristics: high strength-to-mass ratios so that the radiator structure is able to survive the launch environment while minimizing its mass; high thermal conductivity; compatibility with working fluid or coolant; and high emissivity and good structural integrity. The efficiency of the radiator is also an important consideration. Efficient radiators should have a high emissivity and a low solar absorptivity to minimize the area and mass needed to accomplish the heat rejection necessary. For this project, a

radiator with carbon-carbon composite material is used because it has a high emissivity (approximately 0.85) at 800 K. For the area to extract the dumped heat, a square 24.1 × 24.1 m is recommended, placed in the horizontal direction since this area is not too large. Since the area is put in the horizontal direction all the calculations of the view factor are simplified.

CONCLUSIONS

A liquid metal fast breeder reactor was designed for a lunar-based research facility. The fuel was solid rods of BeO enriched with varying degrees of uranium. The core reflector was of beryllium, and natural lithium was chosen as a coolant. Stirling engines serve as the power conversion devices. A carbon-carbon composite radiator was also designed.

The fuel must be carefully examined to ascertain whether or not the cladding is nonessential. The obvious drawback to this design is the hot channel temperatures, which are dependent on high heat flux at the hot channel's position due to the core's design. Also, we did not include in our design any type of shielding, which is important for the safety of the research facility's personnel. There is a need for additional detail in the materials specified in our design. The Stirling engines were treated as black boxes because our design was primarily aimed at the neutronics and thermalhydraulics of the core rather than the associated thermodynamics of the power conversion devices. Finally, the radiator may also need to be examined further. If the core was redesigned to limit the heat flux at the hot channel, it would prevent voiding at this point. The peak to average ratio was much too high ($q'''_{max}/q'''_{avg} = 2.27$) and needs to be brought down to about 1.1-1.5 so that the temperatures do not get outrageously high.

ACKNOWLEGDMENTS

Principal authors H. Chavez, J. Flores, M. Nguyen, and K. Carsen were assisted by faculty advisor Professor Fred Best.

N94- 71292

1994004537
382699

525-66
160651
p-2

PROJECT LONGSHOT

UNITED STATES NAVAL ACADEMY

For centuries man has gazed skyward wondering, "What is out there?" In the 1960s man took the first step in answering this question by exploring near-Earth space through the Mercury, Gemini, and Apollo programs. The expanding technology of the 1970s brought more ambitious exploration of the solar system with Pioneer and Voyager. The space shuttle, in the 1980s, has shown man's resolve for a continuing presence in space. Looking forward, man will soon see the solar system more closely with Magellan and Galileo, and see much further with the Hubble Space Telescope. In all this history of exploration, no program has been developed to explore beyond the solar system. Project Longshot is proposed to meet this need.

Project Longshot is an unmanned probe to our nearest star system, Alpha Centauri, 4.3 light years away. The Centauri system is a trinary system consisting of two central stars (A and B) orbiting a barycenter, and a third (Proxima Centauri) orbiting the two. The system is at a declination of -67°.

The goal is to reach the Centauri system in 50 years. This time span was chosen because any shorter time would be impossible because of the relativistic velocities involved, and any greater time would be impossible because of the difficulty of creating a spacecraft with such a long lifetime (see Fig. 1). Therefore, the following mission profile is proposed: (1) spacecraft is assembled in Earth orbit; (2) spacecraft escapes Earth and sun in the ecliptic with a single impulse maneuver; (3) spacecraft changes declination to point toward Centauri system; (4) spacecraft accelerates to 0.1 c; (5) spacecraft coasts at 0.1 c for 41 years; (6) spacecraft decelerates upon reaching Centauri system; and (7) spacecraft orbits Centauri system, conducts investigations, and relays data to Earth. The total time to reach the Centauri system, taking into consideration acceleration and deceleration, will be approximately 50 years.

Navigation will be two-part. While the spacecraft is accelerating and decelerating, navigation information will be provided by inertial measuring units. During the coast phase, information will come from star trackers to keep Longshot on course.

Reaching the Centauri system requires a large amount of energy. Several systems were reviewed as possible means of propelling Longshot to its destination. These include solar sail, laser-pumped sail, nuclear fusion, and magnetic-field propulsion. None of these were feasible for our mission. To cross this 4.3-light-year distance in a time span of 50 years, a new means of propulsion is proposed: antimatter annihilation propulsion.

Antimatter is matter with opposite charge. When a matter particle combines with its antimatter equivalent, the two annihilate each other, converting their mass to energy. The current trend in antimatter technology points toward the possibility of using this energy to propel a spacecraft.

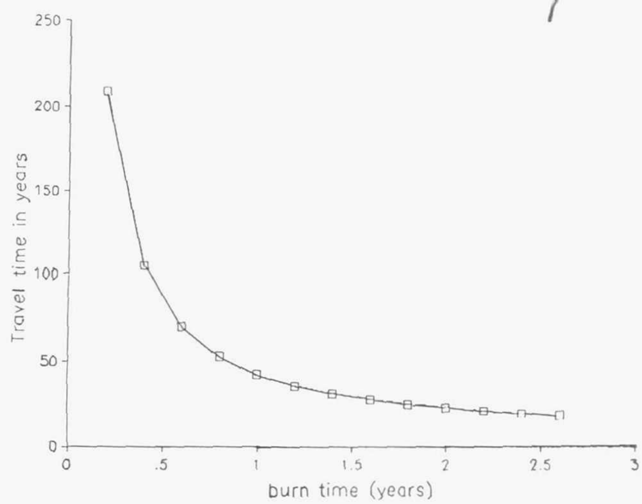

Fig. 1. Total Travel Time vs. Burn Time

The antimatter reaction does not instantaneously annihilate both particles, but does so in stages. Several highly energetic intermediate particles are produced in the reaction. By directing these particles through a magnetic nozzle, their momentum can be transmitted to the spacecraft. This method is highly efficient but not very powerful. The thrust from this method is expected to be only of the order of hundreds of newtons.

Another more promising method of using annihilation energy is to use it to heat a plasma and direct the plasma through a magnetic nozzle. The plasma will have to be of a heavy element to carry the necessary momentum to transfer to the spacecraft. This method will produce thrust in the hundreds of thousands of newtons, but is not as efficient. It also requires the production and confinement of heavy element plasmas, which have not yet been achieved.

Antimatter is currently being produced, but only in small quantities. Production needs to be boosted to the order of kilograms before this system is feasible. An effective means of isolating antimatter is also necessary to allow its use for propulsion (for more information, see ref. 1).

Providing power for a mission of such long duration is another problem. Fifty years is beyond the lifetime of fuel cells of radioisotope thermal generators; therefore, a nuclear fission reactor will be used to provide electrical power for Longshot. The reactor will use a core of low critical mass to minimize required fuel weight. It will use heat pipes to transfer the heat of the nuclear reaction to the working fluid, which will be liquid lithium. Heat pipes were chosen because they are lightweight and can be started from the frozen state. Electricity

PRECEDING PAGE BLANK NOT FILMED

PAGE 208 INTENTIONALLY BLANK

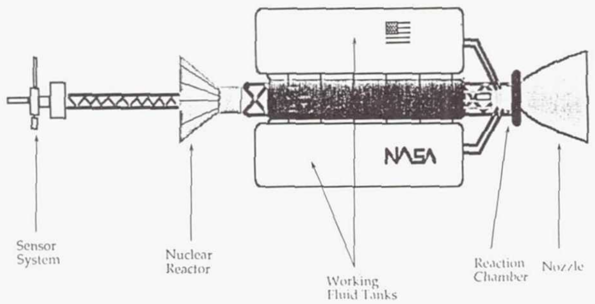

Fig. 2. System Configuration

will be generated by a thermionic conversion system. Waste heat will also be carried by heat pipes to radiators. The expected output of this reactor will be 3 MW, and it will have a mass of 10,700 kg.

Longshot will conduct a variety of scientific investigations. It will collect information about the interstellar medium in transit to the Centauri system, but will conduct the bulk of its investigations when it reaches its destination. Longshot will carry infrared detectors to detect the infrared emissions of possible planets in the Centauri system, and ultraviolet detectors will reveal information about planetary bodies in the system and possibly find stellar sources too weak to be seen from Earth. Photopolarimeters will analyze any planetary atmospheres. Longshot will conduct several particle investigations, including cosmic-ray particles, low-energy particles, and solar-wind plasma particles. Magnetometers will study planetary magnetic fields and interplanetary fields. Longshot will also conduct radioastronomical observations. The selection of experiments for Longshot was based on the assumption that the Centauri system is similar to our own solar system, since there is no other model to follow.

Communications is another system that is complicated by the long distance between the Centauri system and Earth. Both radio frequency and laser communications were studied to determine the best system. The system proposed is a laser communications system that will employ four relay stations spaced evenly between Earth and the Centauri system to carry information back to Earth. For a bit frequency of 1000 bits/sec, 153 kW of power are required, which is a large power requirement, but small for the distance it covers.

Longshot is clearly an ambitious project for any space program. Before it can be possible, tremendous advances in antimatter technology, reactor technology, and laser technology must be realized. Should these advances be realized, Fig. 2 shows what a possible Longshot configuration might look like. Project Longshot is a future step in man's quest for the stars.

ACKNOWLEDGMENTS

Project Longshot team members were J. Curtis West, Sally A. Chamberlain, Robert Stevens, and Neftali Pagan. Faculty advisors were Professor George F. Pieper and Assistant Professor Walter Daniel.

REFERENCES

1. Robert L., "Antimatter Propulsion." *J. Brit. Interplan. Soc., 35,* 391-395.

N94-71293

1994004538

382700

S26-16

160652

LUNAR SHUTTLE

UTAH STATE UNIVERSITY

p. 4

BACKGROUND

Current plans for the extension of human presence into the solar system include the establishment of a permanently occupied base on the Moon for use as a source of raw materials, a transportation node, a facility for the fabrication and launch of elements of the space exploration infrastructure, and a base for scientific investigation and astronomical observatories. All of the aforementioned uses of a lunar base foresee the requirement for a lunar shuttle to operate from the lunar surface to one or more orbiting space stations located in low lunar orbits (LLO).

The Utah State University lunar shuttle design is baselined for implementation after a mature lunar base has been established. The shuttle is designed to operate between the lunar base and a space station located in a 400-km-altitude orbit. This orbit was chosen with reference to Apollo experience, which has indicated that very low orbits, on the order of 100 km, may be unstable over periods of many months.

DESIGN REQUIREMENTS

After a thorough investigation of the anticipated needs and production capabilities of a lunar base, several design requirements were placed upon the shuttle. These requirements are (1) maximum use of lunar-derived propellant; (2) modularity and payload versatility; (3) two-way transport of 25-metric-ton cargo; (4) human transport capability; (5) satellite servicing; and (6) 3000-kg mass budget.

UNMANNED SHUTTLE VS. MANNED SYSTEM

Using these requirements as a baseline, the first major decision encountered was whether the lunar shuttle (LS) should be manned or fully automated. A decision matrix was created to aid in making the appropriate selection. Mass efficiency, flexibility, mobility, improvisation capabilities, safety, human time utilization, and complexity were given weighting factors and were considered in the selection. The decision favored a fully automated shuttle. Figure 1 shows the decision matrix used.

	MASS EFFICIENCY	FLEXIBILITY/MOBILITY	IMPROVISION CAPABILITIES	SAFETY	HUMAN TIME UTILIZATION	
WT. FACTOR	10	7	7	10	8	TOTAL
MANNED	5	5	10	5	6	309
AUTO	8	5	7	8	4	352

Fig. 1. Decision Matrix for Manned vs. Unmanned Shuttle

MAXIMIZING THE USE OF LUNAR DERIVED PROPELLANT

The first requirement listed is maximization of the use of lunar-derived propellant. One of the primary reasons given for returning to the Moon is to make use of its resources. The elemental concentration of oxygen on the Moon is nearly 50%. Gibson and Knudsen of Carbotek, Inc.[1] and other scientists and engineers have designed facilities for the annual production of 1000 metric tons of oxygen (or 83.3 metric tons/month). We chose to baseline our design assuming that this was a reasonable production rate. This assumption is key for the design of the LS, as the design requirements are based upon the oxygen production rate and the supply needs of the lunar base.

Our design allows for 25,000 kg of this oxygen to be transported on a monthly basis to a LLO space station where an Earth-to-Moon Orbital Transfer Vehicle (EMOTV) will leave supplies for the lunar base and will pick up the oxygen and transport it to the low Earth orbit (LEO) space station to be used to refuel space exploration and servicing vehicles.

Oxygen will also be used as the oxidizer for the lunar shuttle LH_2/LOX propulsion system and the hybrid Al/LOX attitude control system. To minimize the use of hydrogen as the fuel, two staging options were considered.

Magnetic Levitation and Acceleration

The first option considered was a magnetic levitation and acceleration system. As shown in Fig. 2, this concept considers magnetically accelerating the shuttle to a given velocity and then launching it off a ramp. The initial acceleration is created by an electromagnetic force between a rotor and stator of a linear synchronous motor and track system, as is being done in new railroad systems in Germany, Japan, and France.

Figure 3 illustrates the problem with using this system. The length of the track required to obtain a significant velocity is

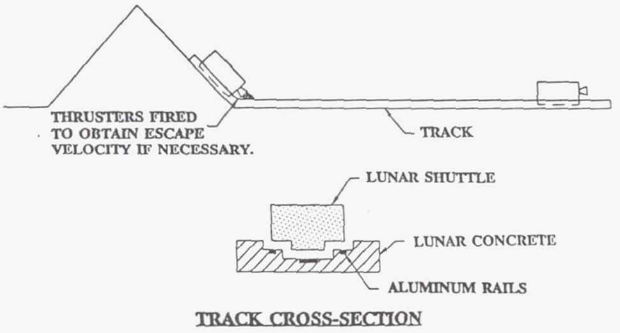

Fig. 2. Magnetic Levitation and Acceleration System

clearly excessive; thus, the concept of using the track was abandoned. However, due to the modular design of the shuttle, the magnetic levitation and acceleration system could be incorporated as the lunar base matures and the track is constructed.

Boosters

The second option considered was that of using boosters as done on the space shuttle. Aluminum/liquid oxygen hybrid boosters were studied as a possibility for reducing the amount of hydrogen required. Since it is elementally abundant on the lunar surface, 3000 kg/month of Al may be extracted. Using this Al in the form of hybrid boosters reduces the 6171 kg of LH_2 required by 654 kg, which is about an 11% savings; however, there are two significant disadvantages encountered when using this staging option.

The first of these is that reusable boosters require a considerable amount of refurbishment that would have to be done on the Moon, consuming valuable man hours. The second disadvantage concerns the boosters' consumption of all the processed Al that otherwise could be used in the construction of equipment and future spacecraft. Therefore, it was determined that the use of boosters would be more costly than advantageous.

SINGLE STAGE LH_2/LOX PROPULSION SYSTEM

The benefits of a single stage LH_2/LOX propulsion system far outweigh the penalties. The principal benefit is the total reusability of the single stage, which cannot be achieved with boosters.

The complexity of pump-fed engines coupled with a human transportation mission dictates that at least two engines be used so that a single engine failure will reduce the probability of loss of life.

Three engines have been considered for the LS's propulsion system. Each of these engines produces a maximum thrust of 100-kN and is designed to operate at an estimated I_{sp} of 465. The detailed design of these engines is beyond the scope of this study; however, it appears that a scaled down SSME would be a good candidate. Prior to the selection of any system for final design, the 100 kN thrust engines should be studied to determine the development costs. The cost of the new engines and their technical advantages should then be compared with the current technology adaptable engines.

MODULARITY AND PAYLOAD VERSATILITY

The second requirement, modularity and versatility, deals with building a reusable lander, suitable for minimizing the transportation cost to and from a permanent base. The concept of payload versatility and modularity inherently avoids the need for a fleet of several different kinds of shuttles to perform the various types of anticipated missions. This capability will result in a savings of billions of dollars.

The Utah State University LS module systems has been designed with three primary mission plans. These missions are (1) cargo transport; (2) human transport; and (3) satellite servicing.

Two-way Transport of 25 Metric Tons

The cargo transport mission consists of transporting 25 metric tons of LOX from the lunar surface to the LLO space station. The propulsion system's oxygen tank has been oversized to accommodate the 25,000 kg of oxygen being transported, thus avoiding the excessive mass of two tanks.

The EMOTV will bring up to 25 metric tons of equipment and supplies from LEO when it comes to pick up the oxygen. The requirement of transporting up to 25 metric tons of supplies to the lunar base was placed upon the shuttle after reports written by Eagle Engineering[2], the University of Texas at Austin[3], and several others were studied.

After transferring the oxygen to the EMOTV, the LS will then be loaded with the equipment and supplies for delivery to the lunar base.

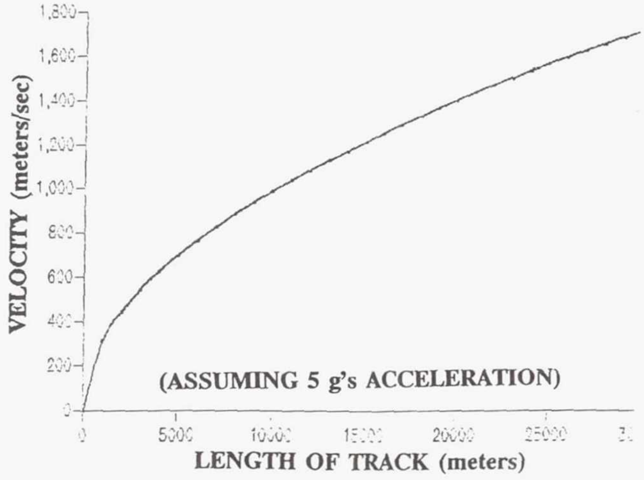

Fig. 3. Length of Track vs. Velocity

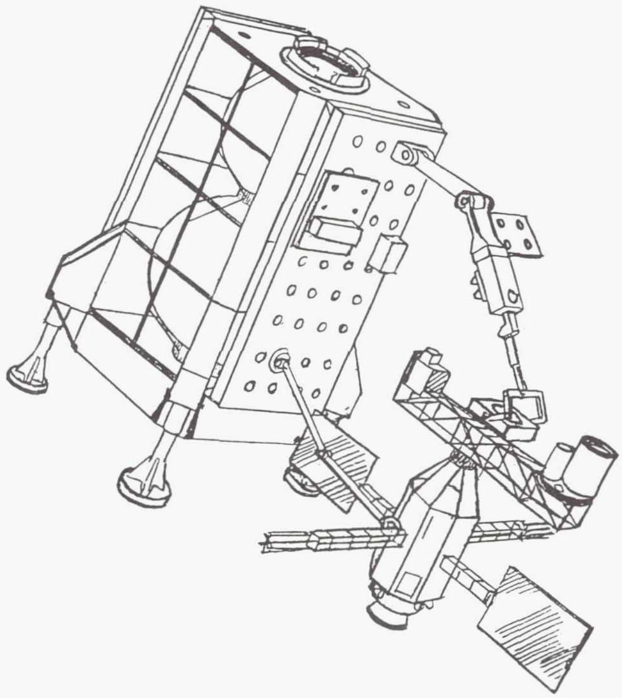

Fig. 4. Docking and Servicing Scenario

Human Transport

The second mission scenario is a human transport mission to be used every 90 days for the rotation of lunar base personnel. The preliminary investigation completed on the systems level indicated that a mature lunar base will require a staff of 20 to 30 people. Each member of the staff will work for approximately one year on the Moon before being transferred back to Earth and replaced by a new staff member.

To accomplish this rotation scheme, a human transport module has been designed to mount symmetrically on two sides of the shuttle. The transport module has been designed so that up to eight lunar base personnel can be transported in a single mission. The module consists of two pressurized cabins that will be mounted symmetrically about the spacecraft. Four people will be placed in each of these cabins. An oxygen and nitrogen resupply system will be coupled with CO_2-absorbing lithium hydroxide beds to maintain life support for the passengers.

Space Satellite Servicing

The third mission scenario incorporates the use of a modified version of the Flight Telerobotics Servicer (FTS) coupled with a utillity arm for space satellite servicing as shown in Fig. 4.

Goddard Space Flight Center provided USU with a copy of its report[(4)] on the FTS that will eventually be placed on the LEO space station. It seems prudent to make use of an existing design for the robotic servicing requirements of the LS; however, due to the differences in working scenarios, some modifications were necessary.

The body parts of the FTS were resized to handle a maximum acceleration of 2 m/sec^2 and a mass of 200 kg. This is larger than the space station FTS design. The reason for this is that the satellite servicing mission will be used only on rare occasions. When the service module is not being used on the shuttle, it will be used on the lunar base to perform programmed routines, freeing up the base personnel for scientific research. This will be in a $\frac{1}{6}$-g environment, which is more than the microgravity environment for which the LEO space station FTS was designed.

The FTS will service a satellite after a docking procedure is performed. A seven degree of freedom arm with a total length of 7.3 m has been designed to dock with satellites and to maneuver them into servicing position for the FTS.

3000-kg MASS BUDGET

Although a 3000-kg mass budget was specified, we wanted to reduce it if possible. A truss-type frame coupled with high mass-efficient systems such as lithium-titanium disulfide batteries and phased array antennas resulted in an inert mass of approximately 2800 kg.

In addition to minimizing the inert mass of the shuttle, we wanted to minimize the amount of propellant required to perform the most common mission, cargo transport. To accomplish this, an iterative procedure was used to determine near optimum trajectory.

SUMMARY

The final Utah State University lunar shuttle design succeeded in meeting all its design requirements. Lunar-derived propellant is used in the propulsion system (O_2) and the attitude control system (Al/LOX). Modularity and payload versatility were achieved through use of a central structural truss system designed to accommodate modules for cargo, humans, and servicing satellites. The entire system is designed to provide a two-way, 25-metric-ton transportation capacity. The final inert mass projection fits nicely within the 3000-kg budget.

ACKNOWLEDGMENTS

Principal authors were P. Voyer, M. Garcia, D. Higham, D. Spackman, J. Garcia, T. Chapman, M. Cook, J. Jelke, G. Slingerland, K. Anderson, B. Edwards, A. Jaber, M. Hall, K. Potter, T. Olsen, O. Monje, J. Watterson, S. Reel, J. Cantrell, and C. Christensen. Faculty advisor was Dr. Frank J. Redd; teaching assistant, K. Adams.

REFERENCES

1. Gibson M. A. and Knudsen C. W., Lunar Oxygen Production from Ilmenite. In *Lunar Bases and Space Activities of the 21st Century.* (W. W. Mendell, ed.), pp. 543-550. Lunar and Planetary Institute, Houston, 1985.

2. Stecklein J. M. et al., Lunar Lander Conceptual Design. In *Lunar Bases and Space Activities in the 21st Century.* In press, 1990.
3. Fowler W., *Moonport,* University of Texas at Austin, May, 1987.
4. Goddard Space Flight Center, *Final Report Flight Telerobotic Servicer (FTS) Tinman Concept In-House Phase B Study,* September 9, 1988.

N94- 71294

1994004539
382701
S27-66
160653
p. 4

A LUNAR VENTURE

UNIVERSITY OF VIRGINIA

INTRODUCTION

As the Earth's space station is in its final stages of design, the dream of a permanent manned space facility is now a reality. Despite this monumental achievement, however, man's quest to extend human habitation further out into space is far from being realized. The next logical step in space exploration must be the construction of a permanent lunar base. This lunar infrastructure can, in turn, be used as a staging ground for further exploration of the remote regions of the solar system.

As outlined by the National Aeronautics and Space Administration, the lunar base program consists of three exploratory and implementation phases. In response to the technological and facility requirements of Phase I and II of this program (Fig. 1), the Aerospace Vehicle Design Program of the University of Virginia (UVA) is proud to present a preliminary design for such a lunar infrastructure. This study is a comprehensive evaluation of the mission requirements as well as the design criteria for space vehicles and facilities. The UVA Lunar Venture is a dual system that consists of a lunar space station and a fleet of lunar landers/transporters. With such a design, it will be demonstrated that all initial exploratory and construction requirements for the lunar base can be efficiently satisfied. Additionally, the need for such a dual system will be justified both from a logistic and economic standpoint.

THE LUNAR LANDER

As part of a program to return to the Moon, a lunar lander will be needed for the establishment and operation of a manned surface base on the Moon, and for support of the lunar space station. Such a lander will be dedicated to transporting cargo and ferrying crew to and from the lunar surface and low lunar orbit. In a 1988 Lunar Base Systems Study, NASA outlined three phases for development of a manned lunar base. During Phase I, three years would be set aside for unmanned exploration of the Moon using orbiting satellites and surface probes. Phase II would span approximately 10 years and would be devoted to establishing a surface base ready for a permanently manned presence, at which time Phase III operations would commence. The lunar lander presented here was designed to meet the requirements for Phase II.

Realizing that a manned lunar base will require extensive equipment, the lander was designed for transporting maximum payload. The lander's engines will use liquid oxygen and hydrogen fuel to provide high performance. The vehicle will be able to operate automatically, but manual override control was incorporated into the guidance system for crew rotation missions. Simplicity and reliability were important design aims so that each lander would have twice the needed lifespan. To lessen the need for space maintenance, the engines must be reusable for the 30-mission vehicle life. Each lander will be taken to the Moon using the Advanced Launch System and the Orbital Transport Vehicle, both expected to be operational by the year 2000. The lander will be capable of transporting 15 metric tons to the surface and returning unloaded, ferrying a minimum of four astronauts to and from low lunar orbit and the surface base, and transporting up to 5 metric tons of lunar raw materials a year to the lunar space station. The largest payload expected for a reusable lander would be a 15-metric-ton LOX pilot plant. A maximum payload of 39 metric tons can be carried down without the lander returning to orbit unless it is refueled; a 20-metric-ton habitation shack, similar to a space station module, along with construction equipment would constitute the payload for initial base establishment on such a nonreturn lander.

Each lander, of a 5-lander fleet, will be staggered into operation and will complete an average of 15 missions during the Phase II period, which begins in the year 2000. The first year of Phase II will be dedicated to manned exploration of lunar base sites selected during Phase I. The years 2001 and 2002 will be cargo-intensive periods in which 12 missions will involve transporting equipment to the surface. Either seven or eight missions will be executed each year starting at 2002, with a total payload capability of 880 metric tons, half of which will be utilized by 2010; the payload reserves add flexibility for altering mission profiles and provide a buffer for contingencies during manned missions. The next four years will be personnel-intensive, in which 20 of the 30 missions will be dedicated to crew rotation. From 2007 to 2010, the lander will transport cargo and crew in preparation for a permanently manned presence on the Moon.

The lander will operate between a 200-km orbit inclined 20° to the lunar equator and the lunar surface. Operating from the lunar station's inclined orbit, the lander will reach a surface base located within 20° of the lunar equator by executing missions when the surface base passes underneath, thereby eliminating the need for plane-change maneuvers. However, in case of an emergency, a lander with a crew module will be able to evacuate the crew of the lunar space station to the surface base regardless of the exact orbit location. As an additional safety precaution, one lander will always be in orbit with the lunar space station in order to provide an escape vehicle should problems arise.

The structural mass of the lander will be 13.5 metric tons, and the propellant mass will be 35 metric tons. With a 15-metric-ton payload, the lander's stack mass would be 63.5 metric tons. The lander will be approximately 10 m in height and 9.1 m in diameter. The lander will be supported by four aluminum alloy landing legs, each 10.4 m in length, that incorporate spring-rachet mechanisms to absorb landing impacts. The vehicle will be able to land on slopes of up to 10° and negotate 5-ft-high obstacles. A crew module and

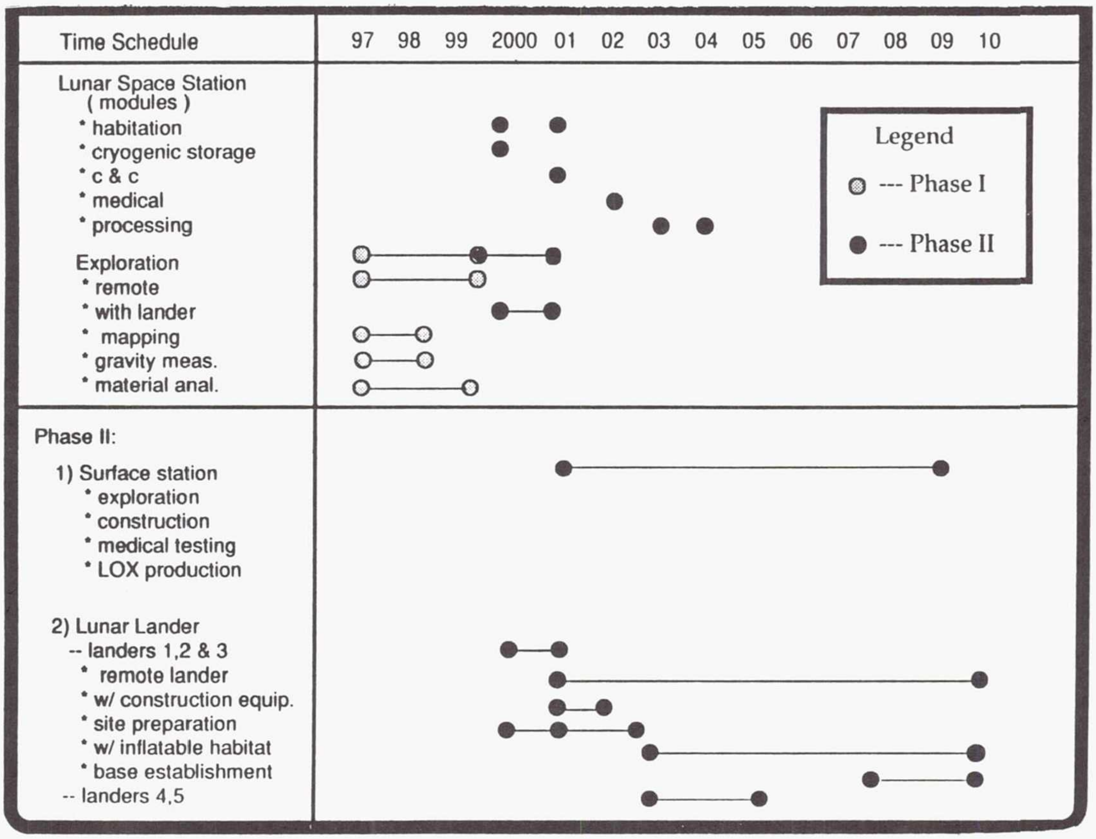

Fig. 1. Lunar Infrastructure Evolution

various payloads will be attached to the cargo pallet, which will be covered by a wire mesh that serves as a walkway for astronauts and provides multiple cargo attachment points. The cargo and an engine pallet will sandwich four propellant tanks. Both pallets will have an octagonal frame with I-beam members formed from aluminum-lithium alloys. The engine pallet will support four regeneratively cooled rocket nozzles and the necessary engine components.

Four engines allow for single engine failure since the remaining three can carry out the mission. The engines will gimbal 5° in any direction from the vertical. The engines are fed from two liquid hydrogen tanks, measuring 4.45 m in diameter, and from two liquid oxygen tanks, measuring 2.80 m in diameter. The propellants can approach an I_{sp} of 450 sec. The tanks are covered by 12 cm of multilayered insulation to reduce boiloff. The engines can be throttled from 500-18,000 lb thrust, and the total dry engine mass will be 1 metric ton. Maximum deceleration will be 2.7 m/sec^2, and maximum acceleration will be 1.8 m/sec^2.

Four clusters of four reaction-control thrusters will handle attitude control. The system will use monomethylhydrazine and nitrogen tetroxide as fuel. With an I_{sp} of 280 sec, each thruster will be capable of 125 lb of thrust. The total attitude system, including the propellants, will be approximately 200 kg. An open-loop system will be used for the environmental control and life support of the crew module. The crew module will be able to provide emergency life support for 24 hours. The landing and ascent sequences will require approximately an hour and a half to complete. Guidance, navigation, and control equipment will be located on the lander and could function autonomously so as to be able to land the spacecraft within 2 m of the destination. However, remote control will be possible from the crew module or from the lunar space station. Although each system will be multiply redundant, an abort system will automatically land or return the lander in case of redundancy failures.

S-band and Ku-band transmitters will provide communications between the lander, other elements in the lunar infrastructure, and Earth-based communications. The lander will have continuous contact with the lunar space station during each mission. A modified space shuttle fuel cell system will supply electrical power for up to 2 weeks for a total output of 720 kW-hr at an average draw of 2 kW.

THE LUNAR SPACE STATION

As part of the ambitious space exploration program that has been proposed for the end of this century and into the next,

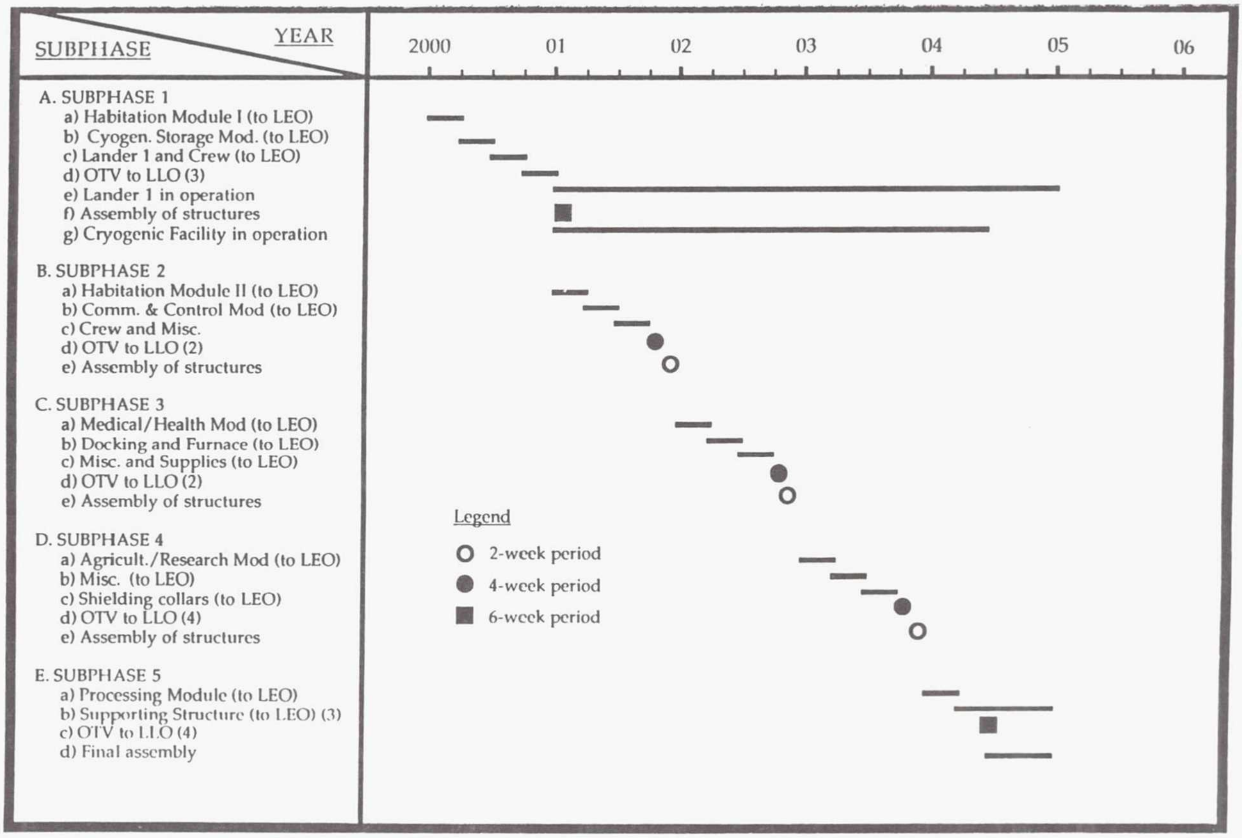

Fig. 2. LSS Deployment and Construction

the return of humans to the Moon is one of the primary objectives. In order to accomplish the goal of a permanent Moon base, a large support structure must be developed to provide the lunar residents all the materials and equipment that they will need to properly use the abundant natural resources. Our design team feels that one of the essential elements of this support structure is an orbiting lunar station similar to the Space Station *Freedom*. With the above considerations, we are proud to propose a space station concept for the low lunar orbit.

The lunar space station (LSS) is a complete support facility that will have the ability to provide the surface base with fuel, water, and equipment ferried from Earth. An added purpose of the station will be to experiment with manufacturing using lunar materials. Taking advantage of the zero-*g* environment, this facility will produce a superior grade of GaAs crystals for the construction of semiconductor devices. The abundance of silicon oxide and other silicates also allows for the mass production of fiberglass at a high profit margin. Additionally, vegetation of various kinds will be grown onboard, and will have an active role in the air and food cycles of the life support system. These, along with other minor experiments, will attempt to demonstrate the commercial applications of space exploration.

The obvious design problems, in this case, are the power requirements, space hazards, profitability of the industrial processes, and the prolonged zero-*g* effects. Our project will attack these problems with design concepts and solutions that are feasible with today's technologies. The single obstacle in realizing this project is the high cost of today's space transportation system. Our project will entail a trip from the ground to low Earth orbit via a system such as the space shuttle. Using a fleet of three or four orbital transfer vehicles (an assumed technology), semifabricated components of the lunar space station will be transported to a low lunar orbit. At this point, the remaining construction tasks will be completed in conjunction with the start up of the lunar lander program.

The LSS is an integral part of our proposed lunar venture. As a result, the design of the LSS system must satisfy all requirements envisioned by the lunar lander program as well as NASA. With this in mind, the following set of system requirements can be established for a standard mission scenario.

Structural Requirements

1. There will be a total of eight modules (by the completion of station buildup in the year 2005): one smelting furnace, one

processing module, one reasearch and agricultural module, two habitation modules, one internal storage module, one control and communication module, and one medical/health module. Also attached to the truss superstructure will be two liquid hydrogen tanks, one liquid oxygen tank, and a docking facility.

2. Each module must physically fit within the space shuttle cargo bay.

3. Hatch configuration for docking and module connection must be compatible with NASA standards for docking hatches; this includes outside and inside dimensions as well as the geometries of the mating surfaces and the access ways.

4. There will be sufficient structural shielding on all modules to protect the station from meteorites of up to 1 cm in diameter, traveling as fast as 75 km/sec.

5. There will be sufficient shielding in safe-haven areas of the habitation modules that crew members can remain safely (exposure of less than 5 rem) in these modules during periods of intense solar flares (up to 500 rad/day).

Power Systems

1. Power requirements will be rated at a peak of 250 kW with the following distribution: (1) industrial processing, 100 kW; (2) life support, 10 kW/module; (3) communication and electronics, 20 kW; and (4) miscellaneous, 10 kW. With the current station geometry of 8 modules, the total power requirement is 250 kW with 40 kW allowed for future expansion.

2. Power will be supplied by ten solar dynamic generators, rated at 25 kW each.

3. There will be sufficient thermal radiators or heat-sinking devices so that thermal radiation from power generation will not affect the station or any spacecraft in rendezvous with the LSS.

4. Backup power will be available in the form of rechargeable fuel cells. Rated power for the backup system will also be 250 kW.

Material Processing

1. There will be a smelting facility that will suport both fiberglass production and processing of GaAs crystals.

2. The formation and processing of semiconductive crystals will be done in a zero-*g* and zero-pressure environment.

3. Both processes will depend on only lunar raw materials.

4. Both processes will be sufficiently automated that only remote monitoring will be necessary.

5. Operating capacity will be 9 metric tons per year. This operating requirement will be met by three separate resupply missions for the lunar lander, each of 3 metric tons.

Orbital Considerations

1. The LSS will be placed in a low lunar orbit of approximately 200 km altitude.

2. At this time, the orbit inclination will be in agreement with the mission profile of the lunar lander, which is at 28°.

Life Support

1. Each module will have its own life-support system. This will eliminate multiple module failures.

2. Operating cycles for the air, water, and solid waste loops are as follows: (1) Air cycle will be closed-loop and regenerative; (2) water cycle will be semiclosed with 50% regeneration; and (3) solid waste cycle will be open-loop. Its byproducts will be used as fertilizers and plant nutrients.

3. Designed capacity for each ecological system will be for a maximum of 12 crew members.

4. The overall resupply cycle will be 90 days.

The above requirements outline in detail the design and implementation of our LSS. In order to properly coordinate our efforts with the lunar lander program, steps are also taken to lay out the deployment scheme and construction schedules. The construction of the LSS consists of five subphases that fall under Phase II of the NASA lunar base program. These are presented in Fig. 2.

ACKNOWLEDGMENTS

Authors Joo Ahn Lee and Lu X. Trinh were assisted by faculty advisor Professor Kenneth Haviland.

N94-71295

382703

19940045410

S28-16

160654

p. 14

LASER POWERED INTERORBITAL VEHICLE

VIRGINIA POLYTECHNIC INSTITUTE AND STATE UNIVERSITY

INTRODUCTION

This report presents a preliminary design of a low-thrust Laser Powered Interorbital Vehicle (LPIV) intended for cargo transportation between an Earth space station and a lunar base. The selected mission utilizes a spiral trajectory, characteristic of a low-thrust spacecraft, requiring eight days for a lunar rendezvous and an additional nine days for return. The ship's configuration consists primarily of an optical train, two hydrogen plasma engines, a 37.1 m box-beam truss, a payload module, and propellant tanks. The total mass of the vehicle, fully loaded, is 63,300 kg.

A single plasma, regeneratively cooled engine design is incorporated into the two 500 N engines. These are connected to the spacecraft by turntables that allow the vehicle to thrust tangential to the flight path. Proper collection and transmission of the laser beam to the thrust chambers is provided through the optical train. This system consists of a 23-m-diameter primary mirror, a convex parabolic secondary mirror, a beam splitter, and two concave parabolic tertiary mirrors.

The payload bay is capable of carrying 18,000 kg of cargo and is located opposite the primary mirror on the main truss. Fuel tanks carrying a maximum of 35,000 kg of liquid hydrogen are fastened to tracks that allow the tanks to be moved perpendicular to the main truss. This capability is required to prevent the center of mass from moving out of the thrust vector line.

The laser beam is located and tracked by means of an acquisition, pointing, and tracking system that can be locked onto the space-based laser station. Correct orientation of the spacecraft with the laser beam is maintained by control moment gyros and reaction control rockets. In addition, an aerobrake configuration was designed to provide the option of using the atmospheric drag in place of propulsion for a return trajectory.

Project Requirements

Requirements and objectives for the preliminary design of the LPIV have been established in consultation with NASA Langley Research Center. Power will be provided via two iodide laser stations (1.315 μm wavelength), one being a direct solar-pumped laser orbiting the Earth and the other a nuclear-powered laser placed on the lunar surface. The maximum beam power provided by the laser stations is 15 MW. The LPIV is to be capable of transporting payloads of 16,000 to 18,000 kg on each leg of its mission. The LPIV is to be reusable with allowances for periodic maintenance and component refurbishment. An aero-assisted version utilizing a rigid aeroshell is to be considered along with an all-propulsive version. The technology level for the LPIV construction is assumed to be one projected for the 2010-2020 time frame. The important design objectives for the LPIV are as follows: (1) minimize propellant requirements and vehicle dry mass, (2) minimize size of laser stations, and (3) minimize trip times.

Configuration

The general configuration of the LPIV is represented in Fig. 1. To capture the incoming laser and to align the thrust vector with the trajectory path, the vehicle utilizes a control moment gyro/reaction control rocket system for synchronized turntable rotation of the engines. This engine rotation provides the LPIV with thrust vectoring capabilities.

An aerobraked option of the LPIV is shown in Fig. 2. The advantage of an aerobrake is the use of the Earth's atmosphere to create drag on the vehicle, decelerating the vehicle without expending propellant in retro burns. Unfortunately, the addition of this feature onto the LPIV increases the vehicle dry mass and subjects it to extensive thermal and gravitational loads, requiring additional support structure. By choosing a symmetric geometry of the aerobrake, difficulties in maintaining a stable center of mass were alleviated and the benefits obtained by the LPIV's fixed mirror design were not sacrificed. Table 1 gives a mass breakdown of the nonaerobraked LPIV.

General Mission Scenario

The mission is assumed to begin in Low Earth Orbit (LEO), with a final destination being a Low Lunar Orbit (LLO). The initial orbit is oriented with the proposed Earth-orbiting space station. The LPIV is powered by the solar-pumped laser station and respective relay stations, which orbit the Earth in the equatorial plane at an altitude of one Earth radius. The payload it will handle consists primarily of maintenance supplies and provisions on the outbound mission, and oxygen manufactured at the lunar base on the return trip.

The mission scenario is broken into three phases: departure, coast, and capture, for both the aeroassisted and the nonaerobraked versions. The trajectory for departure follows a low-thrust spiral, taking into account the neccessary condition of intermittent power as a result of laser station solar occultation. A coast period will begin at an altitude of approximately 100,000 km with enough total energy to reach the Moon's orbit. A third phase is initiated near the Moon in order to match the spacecraft's velocity with the specified LLO circular speed; this is followed by an appropriate docking procedure. The return flight follows a similar outline except for the aerobraked version, which utilizes an aeroassisted passage before returning to LEO.

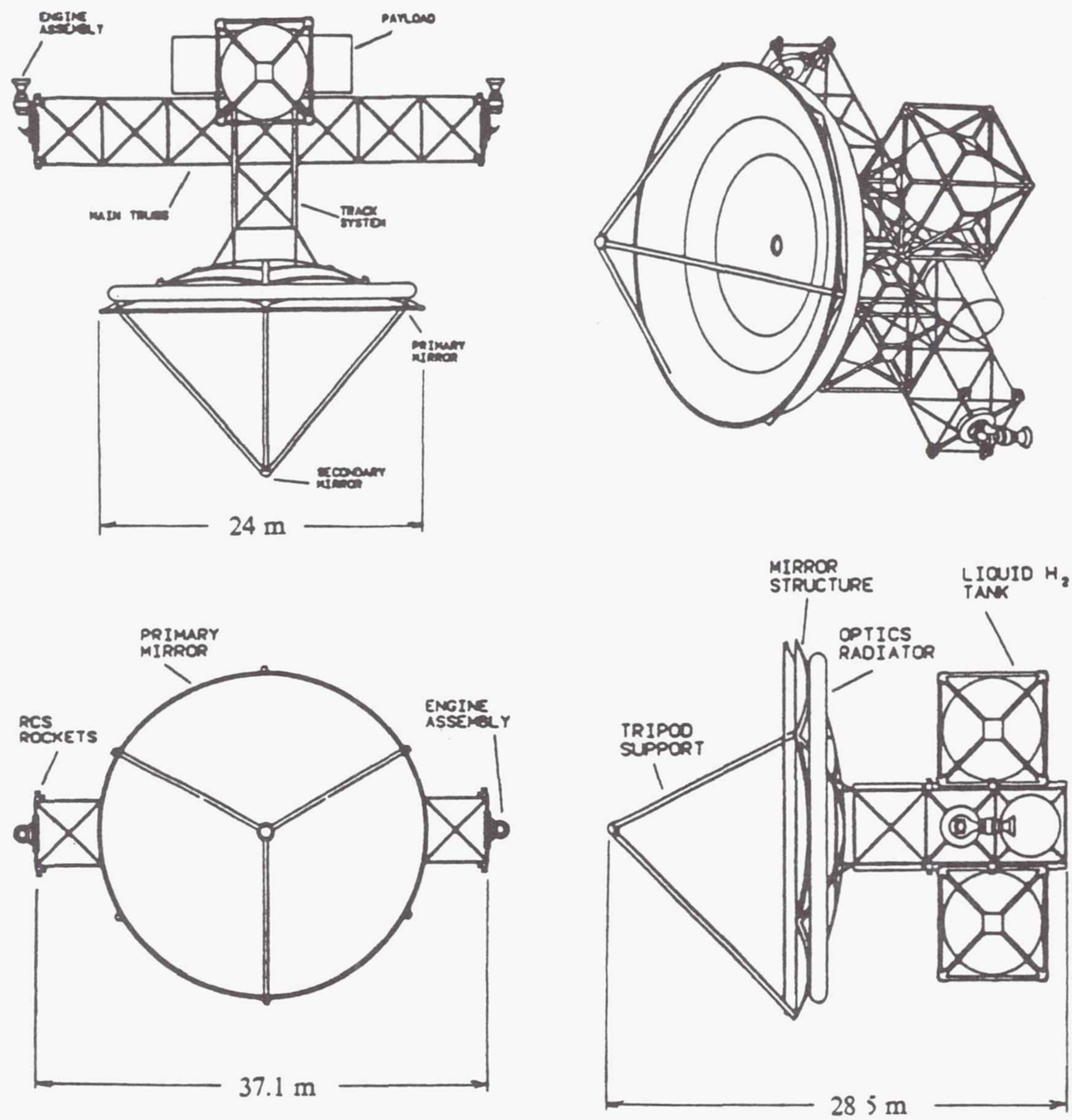

Fig. 1. All-Propulsive LPIV Configuration

ORBITAL MECHANICS AND TRAJECTORY ANALYSIS

Orbital mechanics and trajectory analysis were performed using a multifunctional mission simulation and analysis system named SIGHT (Simulated Interactive GrapHical Trajectory system) that provides real-time three-dimensional analysis of the orbital paths and rotations of multiple bodies. The system uses a numerical solution to the restricted three-body problem and introduces algorithms for guidance and navigation. The system was developed in conjunction with the LPIV design project.

As the Earth-orbiting laser station will be in an equatorial plane[1], it cannot provide continuous energy to the LPIV due to the passage of the station through the Earth's shadow. This station-solar occultation exists for 17% or 40 min out of the 240-min orbital period of the laser power station. Whenever the spacecraft is not in line of sight with the orbiting power station because of Earth interference, one of two optical relay stations are used. Designed to reflect and redirect the beam, the relays are placed in the same reference orbit at 115° lead and 115° lag with respect to the power station.

The first phase of the mission, an outward spiral departure, involves the time from the beginning of the mission leaving LEO to a point 94,000 km from the Earth, where the spacecraft achieves enough energy to enter a translunar trajectory. For the low-thrust propulsion system, the spiral orbit gives the

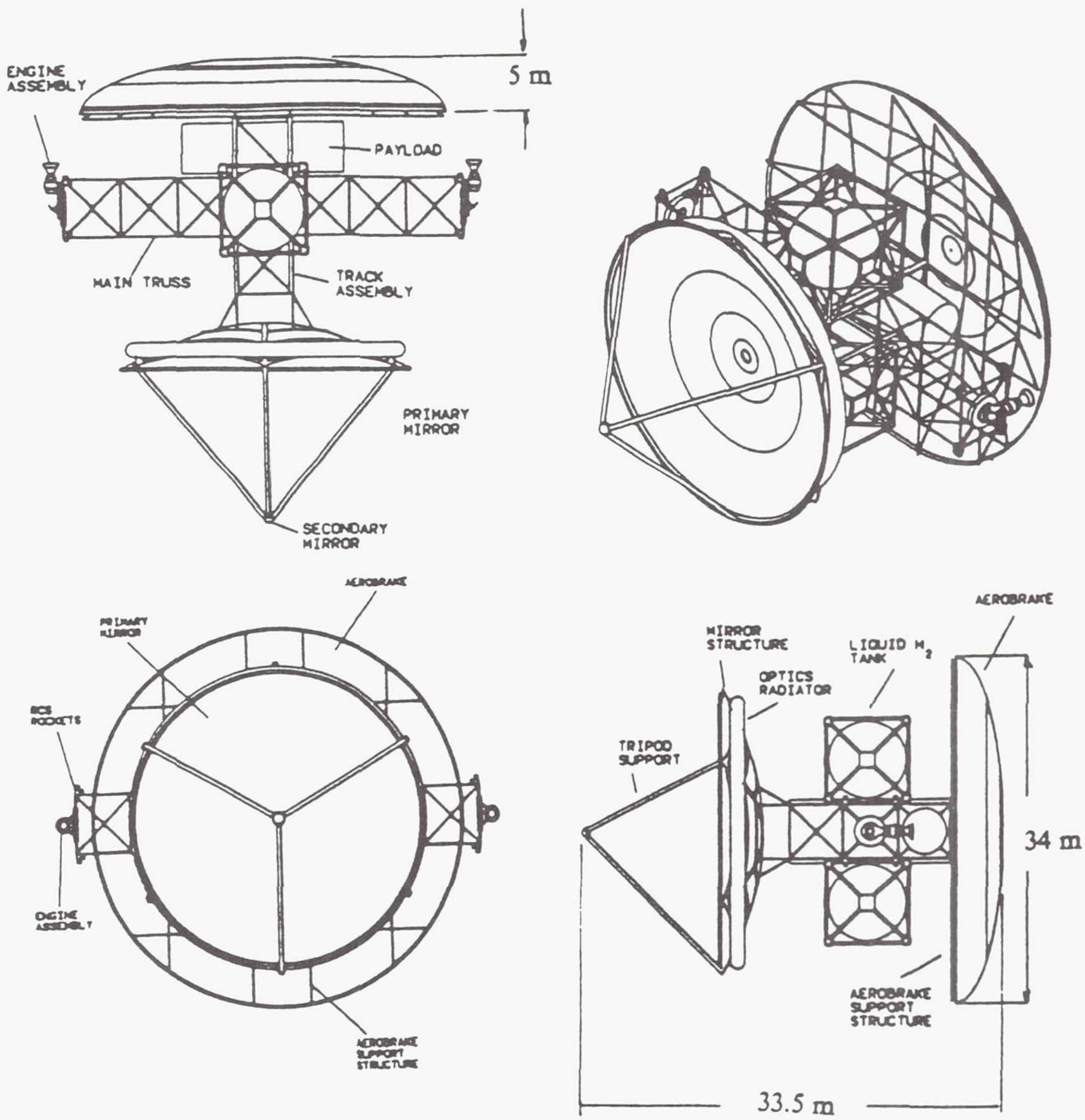

Fig. 2. Aeroassisted LPIV Configuration

maximum increase in velocity in the shortest possible time. In addition, a small portion of the thrust will be dedicated to plane-change since the LPIV must precess about 47° throughout its journey. Figure 3 is an isometric view of the orbital trajectory in the first phase. The change from continuous to dashed line in the spacecraft trajectory indicates the transition between thrust and coast periods. The beam path algorithm allows monitoring of the angle of orientation that the LPIV must maintain for laser beam capture. This information enables us to establish estimates for the reaction control system and moment gyros necessary for spacecraft pointing and tracking.

The second phase is an elliptical coasting period during which only small control rockets are required to navigate. During the final phase of the flight, the vehicle will perform appropriate navigational maneuvers (possibly involving a short decelerating spiral) in order to intercept the Moon's orbit and finally rendezvous with LLO. Navigation and rendezvous are accomplished through utilization of the laser propulsion system. Figure 4 displays key phases of the LPIV trajectory.

The aforementioned scheme is applicable for the return flight from LLO, a distance of 100 km above the lunar surface, to the space station orbiting at LEO. Relatively small modifications are necessary in terms of the time and position that the laser engines fire. Specifications of the outbound and return trajectories are given in Table 2.

Table 1. LPIV Total Mass Breakdown

Subsystem	Mass (kg)
Main Truss	734
Propellant Tanks	1293
RCS and CMGs	1022
Engines	200
Turntables	547
Docking Mechanism	90
Optical System	5400
Acquisition, Pointing and Tracking (APT)	105
Communications	70
Payload Module	649
Vehicle Dry Mass	12,300
Propellant Mass	35,000
Payload Mass	16,000
Total Vehicle Mass	63,300

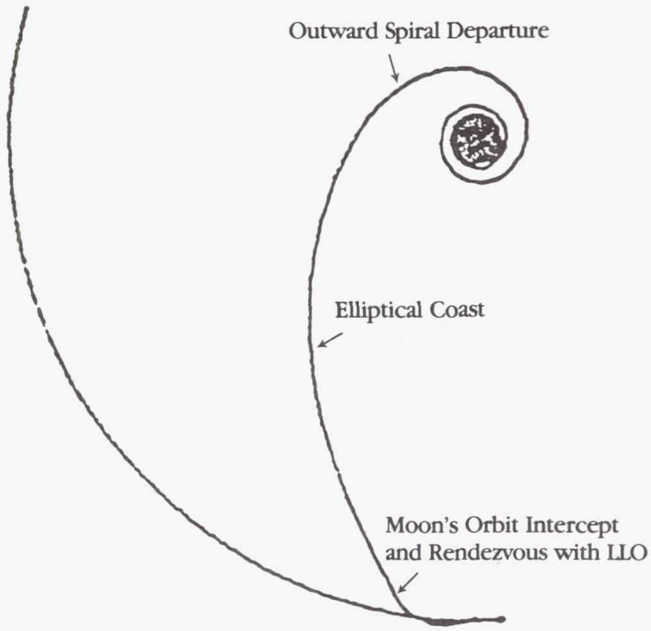

Fig. 4. Key Phases of LPIV Trajectory

Table 2. Outbound and Return Trajectories

	Phase I Initial	Phase II Injection	Phase III Rendezvous
		Outbound	
Mass (kg)	59,000	43,145	41,784
Radial Distance (km)	6,859	94,000	384,400
Velocity (km/sec)	7.624	2.524	1.01
Inclination (deg)*	28.5	5.12	5.12
Thrust (N)	1,000	0	1,000
Time of Flight (hr)	0	77.5	165
		Return	
Mass (kg)	41,784	40,242	26,903
Radial Distance (km)	384,400	94,000	6,859
Velocity (km/sec)	1.01	2.62	7.624
Inclination (deg)*	5.12	5.12	28.5
Thrust (N)	1,000	1,000	0
Time of Flight (hr)	0	127	201

*w.r.t. Earth's equator

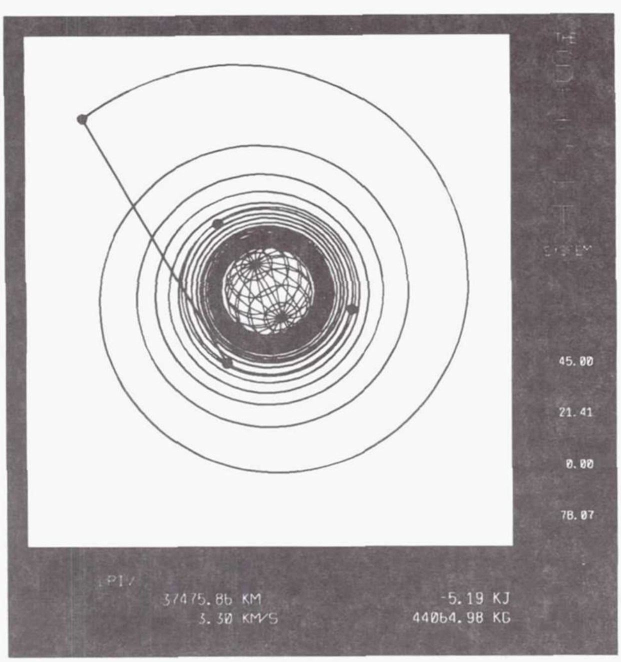

Fig. 3. Isometric View of Outward Spiral Trajectory

OPTICS

The function of the optical system is to intercept the laser beam, which may be as much as 24 m wide, and focus the beam to a few centimeters in the plasma chamber of the engines.

The selected configuration (Fig. 5) comprises the primary and secondary mirrors arranged into a Cassegrain configuration, with the secondary mirror suspended in front of the primary mirror by means of a tripod support structure. Since two engines are used, the power of the laser beam must be split and transferred to two different focusing points. The division of the power requires the use of a beam splitter.

Important factors that may effect the efficiency of beam transmission throughout the optical train are (1) degradation of the reflecting surfaces due to the space enviroment and (2) thermal cycling, which is induced as the vehicle travels in and out of the shadow of the Earth, causing structural fatigue. The LPIV's optical train is expected to operate unrefurbished for approximately two years with a maximum power loss of 10% through the entire laser path; therefore, possible surface degradation and thermal cycling effects must be taken into serious consideration when selecting mirror surface materials

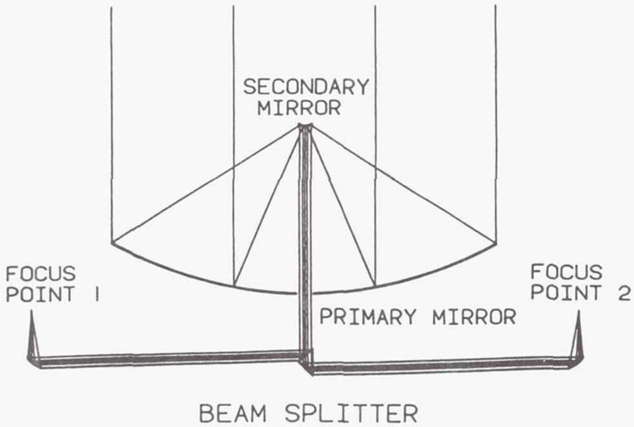

Fig. 5. LPIV Optical System

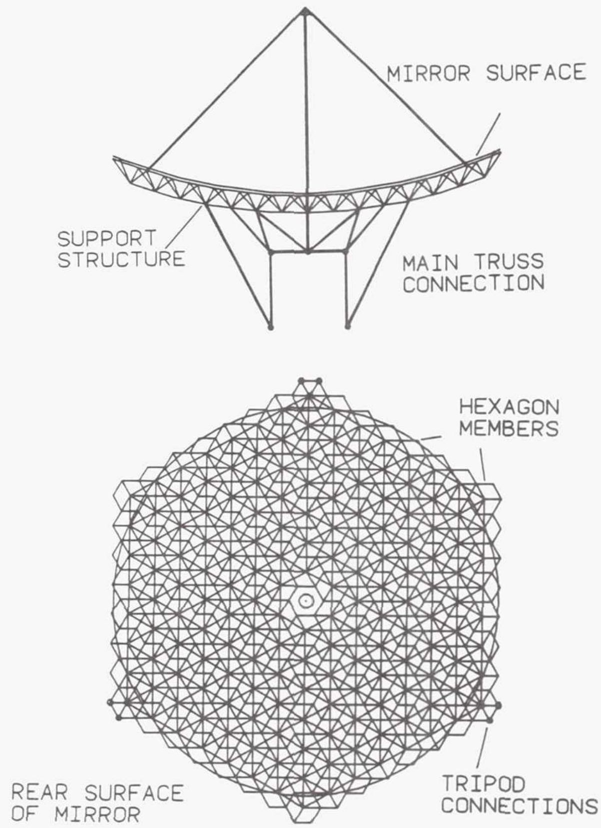

Fig. 6. Primary Mirror

and finish. The parabolic primary mirror selected for our vehicle has a reflective surface using dielectric coatings. The main advantage of a dielectric mirror is its high degree of reflectivity for a narrow range of wavelengths, possibly as high as 99.9+%. Dielectrics employ alternating layers of high and low refractive-index materials that provide multiple reflections, all in phase. For our application, a scheme of 10 dielectric layers, 0.3 μm thick, will be used to produce a high degree of reflectivity, reducing the heat absorbed by the mirror, and alleviating the need for cooling.

The diameter of the primary mirror was established on the basis of the maximum distance at which the beam would be received, beam divergence, wave front error, and beam jitter. The maximum distance of 110,000 km was determined from the maximum separation between the laser (or relay) and vehicle thrusting operations. The wave front error is caused by imperfections of the laser transmitting mirror. The beam jitter is caused by fluctuations in the emission intensity produced by nonlinearity in the refractive index of the laser's active medium. It should be emphasized that for most of the thrusting operation, the spot diameter will be smaller, or even significantly smaller, than 24 m due to the focusing ability of the laser transmitting system. Sizing of the mirror was based on the spot diameter, the minimum acceptable power requirements, and the amount of offset necessary to make use of the peak intensity of the beam. After examining these factors, a mirror diameter of 24 m was decided upon. Figure 6 shows a diagram of the main mirror. Initially, dielectric coatings offer a 99.9+% reflective surface, but over the two-year life cycle of the coating, degradation causes losses in reflectivity on the order of 2.0%. After this time, the mirror surface will have to be refurbished. The selection of the facesheet material is critical because the dielectrics must be applied in vapor form to the facesheet. The beryllium was chosen because of its low density and high specific heat. The structure consists of two perforated graphite epoxy, hexagonal panels (Fig. 7) connected with the surface layer by fused silica pegs. The panels can be assembled before being launched into orbit. Each panel will be fastened to six small angular C-beams using two spring pins in each C-beam. These pins will allow easy removal and replacement of panels having suffered damage or degradation during service. To allow for transporting in the space shuttle payload bay, the entire mirror assembly will be broken down into six identical subassemblies and assembled in space. The remaining C-beams will be connected along those six joints by a latch jaw assembly. The surface area of the primary mirror requires 126 hexagon panels. The mass of the surface of the primary mirror was calculated to be 2730.9 kg, resulting in a surface mass density of 6 kg/m^3. The mirror support structure is designed to allow for a maximum error in the mirror surface of $\pm$0.01 m from the prescribed contour. A truss system (Fig. 6) is used for supporting individual hexagonal panels and is made of graphite epoxy with a chromatic anodized aluminum foil coating.

The secondary mirror redirects the converging light rays from the primary mirror in paraxial fashion toward a circular hole at the center of the primary mirror. In order for the beam reflected from the secondary mirror to be paraxial, the primary and secondary mirrors must share a common focal point. Therefore, a convex, parabolic surface was employed. The secondary mirror has a diameter of 1.2 m and is mounted 12.13 m from the primary mirror at the end of a tripod support structure. The secondary mirror consists of 10 dielectric layers coated on a 2.5-cm thick beryllium slab that serves as a

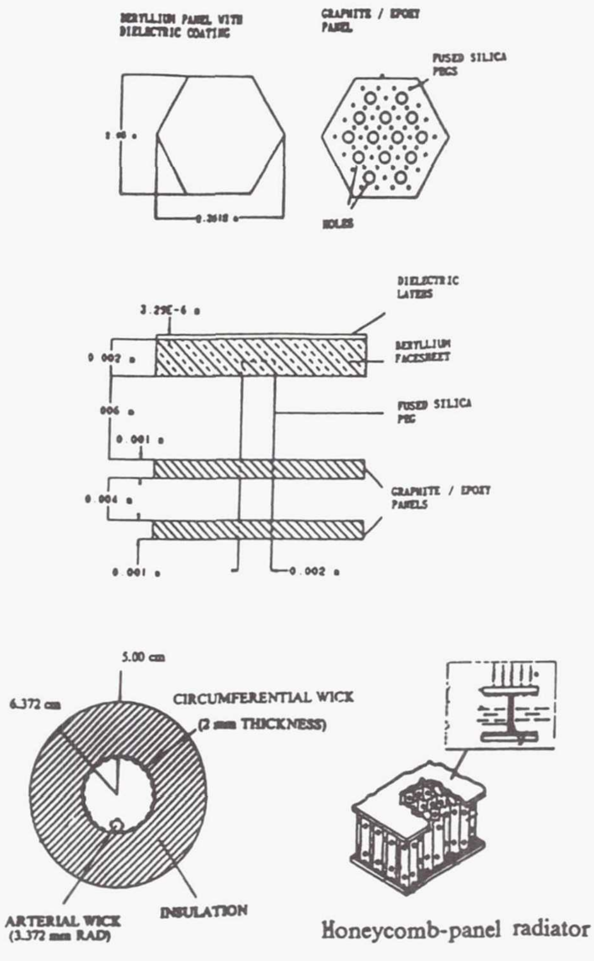

Fig. 7. Structure and Cooling Details

facesheet, housing of the cooling passages, and structural support for mounting. Since dielectrics were chosen for the reflective surface, the secondary mirror has an initial reflectivity of 99.9%. However, due to degradation it is assumed that the reflectivity will decrease to 98.5% during its service life.

The beam splitter is located in the center of the main truss. It consists of two mirrors joined at a right angle, the first being a slotted 50% open surface (Fig. 5) to reflect exactly one half of the incident radiation toward one engine. The second, aft surface reflects the remaining half of the laser beam toward the second engine. The assembly is adjusted to an angle of 0.749°. This rotation is needed to ensure symmetric positioning of the two tertiary mirrors.

The design of the tertiary mirrors was critical since each will converge and direct its incident beam into the plasma chamber of the engine. An offset parabolic, adaptive optics mirror having a diameter of 1.3 m was chosen for this reason. The dielectric layers for these mirrors are coated on a 2.5-cm beryllium facesheet that serves as both a substrate, housing for the cooling passages, and a mounting surface. The use of adaptive optics in the tertiary mirrors is an attractive option in that it allows for an accurate focusing of the beam in the plasma chamber.

Table 3. Optical Train Masses

	Mass (kg)
Primary Mirror	2730.9
Primary Mirror Support Structure	1200
Secondary Mirror with Tripod	350
Beam Splitter	80
Tertiary Mirror	110
Heat Pipe Cooling	700
Total	4170.9

Mirror Cooling

From a simple thermal analysis (radiation energy balance) of the beam splitter, secondary mirrors, and tertiary mirrors, it was concluded that these components require cooling to prevent excessive surface degradation.

The secondary mirror will be cooled by a heat pipe system consisting of (1) an evaporator on the back of the mirror, (2) a ring-shaped, honeycomb-panel heat-pipe radiator mounted behind the primary mirror (Figs. 1 and 2), and (3) three cylindrical pipes with arterial wicks (Fig. 7) mounted inside tripod legs and providing two-way passage between the evaporator and the radiator. A second wick is used around the heat pipe's inner wall near the evaporator, enabling liquid to be distributed evenly around the heat pipe. The beam splitter and both tertiary mirrors will be cooled by the propellant on the way from the propellant tanks to the engines.

Masses of the main components of the optical train are given in Table 3.

STRUCTURES

Due to the strict rigidity requirements of the optical system for the LPIV, proper material selection satisfying the structural integrity requirements of the spacecraft plays a key role in the development of the truss structure. The primary requirement for the structure of the LPIV is that it should be able to withstand all inertial, thermal, aerobraking, and docking loads while keeping the structural mass and deformations at a minimum. Static analysis performed on several truss structures indicated that the truss shown in Fig. 8 will adequately satisfy the LPIV requirements. Data obtained from the static analyses was combined with the data obtained from the simple thermal analyses in order to determine total displacements of the truss nodes. The results indicated maximum displacements of less than 2 mm. The graphite epoxy material selected for the structure meets the rigidity criteria while minimizing overall mass. Stress analysis was performed using the SSAM program(2). This program determined that the maximum stress the truss encounters is 138.4 kPa, which falls well under the critical stress value. The maximum stress occurs in a vertical member in the first cubical area past the center structure.

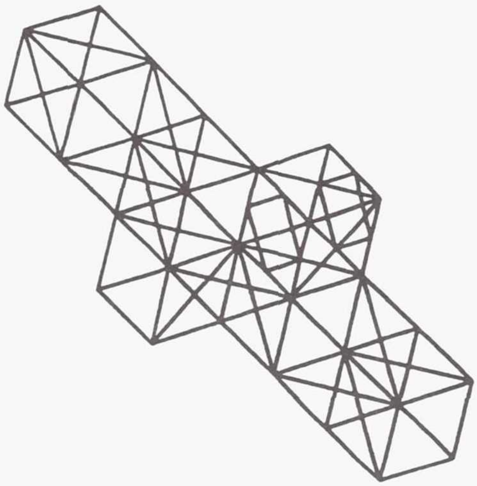

Fig. 8. Main Truss Configuration

A detachable payload module is required to provide the LPIV with the flexibility to carry a variety of cargo. The shape that best meshed with the LPIV configuration was a cylinder. The radius of the payload module is 2.6 m because it is the largest radius that could be integrated with the placement of the module on the LPIV. The module is constructed of boron/aluminum or its future derivative. The payload module is wrapped with aluminum bands to allow for easy attachment and added structural support. The payload module is attached to the LPIV inside the box truss, which extends out from the main truss opposite the mirror.

PROPULSION

The concept of a laser-powered interorbital vehicle rests on the technology to produce engines that will transfer laser power to the propellant. Depending on the optical arrangement, a single plasma or an array of plasmas may be created in the engine chamber. The engines will be of the single-plasma type because their small size does not justify the complexity of a multiplasma system, and most of the present knowledge of the plasma system is based on single plasmas. While multiplasmas may help to increase the heating of the hydrogen, their stability characteristics are obscure. Also considered was the fact that the primary mirror captures the beam off-center, possibly leading to an uneven temperature distribution between the plasmas of a multiplasma system. This effect is diminished by the use of a single-plasma engine. The scheme selected for our engines makes use of a stationary laser-sustained plasma in a steady flow of hydrogen gas to convert laser energy into the thermal energy of the hydrogen, which is then expanded through a propulsive nozzle. This energy conversion occurs via the inverse Bremsstrahlung (IB) mechanism, which requires the presence of free electrons, i.e., hydrogen in an ionized state (plasma). After the plasma is initialized (by means of injection of easily ionizable particulates), the IB and hence energy absorption process can be self-sustained with the plasma location being controlled by flow configuration and optical arrangement.

Table 4. Basic Data and Assumptions

Power of incoming laser (P)	15 MW
Optical train efficiency (η_{opt})	0.948
Thermal conversion efficiency (η_{th})	50%
Specific Impulse (I_{sp})	1500 sec

Initially, a hybrid system including a chemical rocket for injection from Earth or Moon orbit to the Earth-Moon transfer orbit was planned. The spiral orbit adopted later made this unnecessary because the nearly continuous laser engine burn was found to be adequate. The engine parameters have been established on the basis of the assumptions listed in Table 4.

From the energy equation, the thrust of each laser engine is 483.2 N and the propellant mass flow rate is 0.033 kg/sec. Chamber pressure and bulk temperature have been obtained from approximate 1-D calculations of nonequilibrium flow through a nozzle having an area ratio of 36 and producing a specific impulse of 1500 sec with a thermal efficiency of 50%. Initial calculations indicated the values as follows: chamber temperature, $T_o = 4500$ K, chamber pressure, $P_o = 6.8$ atm. Because the absorption of laser energy is strongly dependent on the laser wavelength and gas pressure, it was necessary to examine the absorptivity of the hydrogen plasma at the pressure of 6.8 atm. Based on the studies done on radiant energy absorption, the absorption due to electron-ion and electron-neutral IB was calculated. It was found that by increasing the chamber pressure to 10 atm, the absorption coefficient at 1.315 μm can be raised to values ranging from 0.28 cm^{-1} to 0.34 cm^{-1} at temperatures ranging from 17,000 K to 20,000 K. This will be sufficient to accomplish full absorption in a short distance inside the plasma. To keep the specific impulse of 1500 sec while the pressure is increased to 10 atm, the chamber temperature should be lowered to about 4400 K.

The size of the laser-sustained, hot plasma (>14,000 K) depends on the laser power, flow velocity, and chamber pressure. From published data, it has been estimated that at a pressure of 10 atm and a velocity of 20 m/sec, the laser intensity required for sustaining a plasma will be around 3.2×10^5 W/cm. The corresponding diameter of the highly absorbing plasma will be about 5 cm. The maximum diameter of the chamber and the throat diameter have been established from calculations based on high-temperature hydrogen data reported by Patch. The main engine parameters are summarized in Table 5.

A schematic of the proposed engine is shown in Fig. 9. The engine configuration has been selected from evaluation of various options that differed primarily in optical arrangement for the laser beam entry. A rear entry has been chosen over a side one because it eliminates possible impacting on the opposite wall, which might cause a serious wall overheating problem. An initial configuration using a focusing lens as a window to the engine was rejected in favor of an arrangement consisting of a parabolic focusing mirror (tertiary mirror) and

Table 5. Engine Characteristics

Laser power entering each engine	7.11 MW
Thrust	483 N
Propellant mass flow rate	0.033 kg/sec
Nozzle inlet stagnation temp	4400 K
Chamber pressure	10 atm
Average chamber flow velocity	20 m/sec
Chamber diameter (max)	30 cm
Throat diameter	2 cm
Nozzle area ratio	36

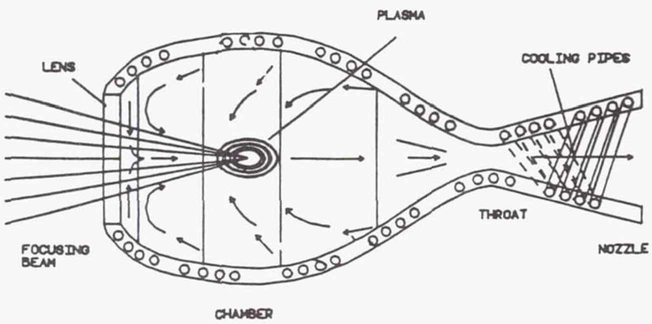

Fig. 9. Engine Schematic

a flat window. Such an arrangement results in longer focal lengths, which tend to improve plasma stability and allows more flexibility in focusing by using adaptive optics for the tertiary mirror. Also, the size of the window can be somewhat reduced. A possible candidate for the window material is sapphire, recommended for its high strength and high transmissivity (>99%).

Since the high-temperature plasma leads to an intense, mostly radiative heat transfer to the chamber walls, regenerative cooling combined with possibly high reflectivity of the internal chamber surface will be necessary to preserve the integrity of the chamber walls. About 20% of the hydrogen delivered to the engine will be injected directly to cool the window. The rest (80%) will be passed through four helical coils to cool the chamber and nozzle walls. The propellant is then injected into the engine chamber through rings stationed at various locations along the flowfield. The wall temperature on the gas side is limited by the material properties. Tungsten, considered for this design due to its relatively high ultimate strength at high temperatures and its good heat transfer properties, was assumed to have an upper operational temperature of about 2800 K. Preliminary calculations of the regenerative cooling system have been carried out with the following assumptions: Temperature of hydrogen entering the cooling system is 407 K, maximum temperature of the hydrogen entering the chamber is 2300 K, maximum temperature of the chamber internal wall is 2800 K, pressure at the entrance to the cooling system is 20 atm, and pressure at injectors to the engine chamber is 12.5 atm. The results have indicated the following parameters for the four helical cooling pipe systems: The length of each helical tubing is 7.5 m and the diameter of tubing is 15 mm.

CONTROL MOMENT GYROS/REACTION CONTROL SYSTEM

For a vehicle such as the LPIV, attitude control is crucial because of the necessity of maintaining continuous contact with the laser power system. The Reaction Control System (RCS) provides the LPIV with attitude control and translational mobility. It is required that the RCS provide attitude control during burns of the main engines without generating plumes that might interfere with the optical train. The Control Moment Gyros (CMGs) are used to rotate the LPIV's main mirror into alignment with the incoming laser beam. For those periods when attitude adjustment is needed and the main engines are not firing, small attitude control rockets are fired to generate the necessary torques. Larger rockets are used to adjust for orbital errors and to provide mobility when docking.

Since the LPIV has two planes of symmetry, only rotations about two-body axes are required to achieve any desired orientation in receiving the power beam. This reduces the number of gyros necessary to provide three-dimensional control of attitude from three to two. Using the global radius vectors of the LPIV and the laser power station (LPS), it is possible to determine the pitch and yaw angles the LPIV has to assume in order to track the LPS. Using the roll and yaw angles (Fig. 10), and the angular accelerations about the roll and yaw axes, the required torque values and maximum precession angles of gyros can be established. The LPIV moments of inertia and maximum precession angles are given in Table 6. The gyro specifications shown in Table 7 represent projections expected for an improved version of the Sperry M225 CMG.

Low Thrust RCS

Low-thrust rockets of the RCS are used to desaturate the CMGs whenever the LPS is in the Earth's shadow and therefore unable to provide power to the LPIV. During this time, the

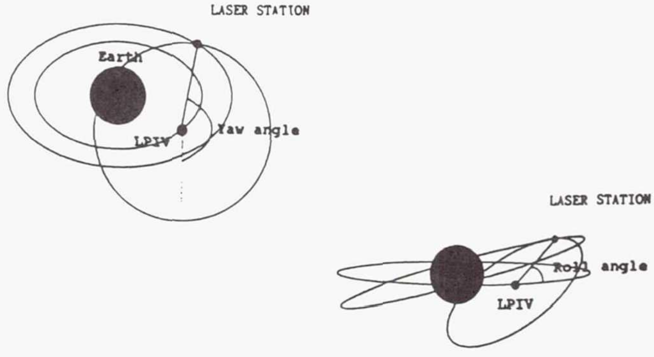

Fig. 10. Roll and Yaw Representation

Table 6. Moments of Inertia

	Non-Aerobraked LPIV	Aerobraked LPIV
Ix =	1.689×10^6kg m^2	1.921×10^6kg m^2
Iy =	1.309×10^6kg m^2	1.507×10^6kg m^2
Iz =	1.450×10^6kg m^2	1.648×10^6kg m^2
	Maximum Precession Angle of Gyros	
	Precession	Angular rate
Roll	0.22323 rad	0.00372 rad/sec^2
Yaw	0.11649 rad	0.00194 rad/sec^2

Table 8. Low-Thrust RCS Rockets and Desaturization Requirements

Thrust per rocket	5 N
Specific Impulse	230 sec
No. of rockets (roll)	4
No. of rockets (yaw)	4
Time of burn (roll)	71.18 sec
Time of burn (yaw)	104.3 sec
Mass propellant burned (roll)	0.7 kg
Mass propellant burned (yaw)	0.9 kg
Total propellant mass/ desaturization	1.6 kg

desaturization rockets will be fired to generate a torque equal in magnitude and opposite in sign to that necessary to reverse the precession of the CMGs. Thrust and propellant requirements given in Table 8 were derived from the shadow time for the power satellite, angular acceleration, and torque required to desaturate the gyros.

Since the desaturization rockets also provide fine translational control during docking, it is required that they be capable of delivering thrust along all three axes. To achieve this, clusters of rockets are attached to each of the four corners at either end of the main truss. In this manner, four rockets may be fired in any direction to translate the LPIV. Compressed hydrazine is stored in propellant tanks attached to each pod. Total propellant mass needed is determined by the number of desaturizations to be performed and the amount of maneuvering necessary for docking. During the thrusting period for escape from the Earth's gravitational pull, there are over 50 shadow periods within which it is possible to desaturate the CMGs. Of these, it is considered reasonable that no more than three periods will actually be used to desaturate. Because of the low thrust levels of the desaturization rockets, they are useful for only the finest control in docking. Using a 20-sec burn of all four engines parallel to an axis, and assuming an approximate mass of 40,000 kg at lunar capture, the desaturization rockets only provide a velocity change of 0.01 m/sec. This, however, is the type of maneuverability desired for fine control in docking.

Medium-Thrust RCS

For orbit corrections, aerobraking maneuvers, and initial docking operations, medium-thrust level RCS rockets are needed. These rockets may be used as backup engines should the laser engines fail. Pairs of nozzles are fixed to the truss at the midpoint of each side at each end of the truss. One nozzle points upward while the other is aimed outward from the truss to which it is attached. The rockets most crucial in the event of an emergency during aerobraking will be the two pointing in the negative x direction, toward the aeroshell. These rockets, as well as the other primary RCS rockets, are used for translational mobility and to correct orbital errors, mainly prior to rendezvous operations. Thrust sizing is based on the most critical backup propulsion requirement that concerns the postaerobraking maneuver.

After the aerobrake assists the LPIV in being "captured" by the Earth, the LPIV's orbit is circularized into LEO. Normally, this is performed by the laser engines. In the event that the laser engines should fail, however, it is up to the RCS system to apply enough impulse to prevent the LPIV from reentering the Earth's atmosphere. The Earth's atmosphere extends approximately 6500 km from the Earth's center, while the LEO orbit lies 6750 km from the center. In the event of an emergency, however, the transfer is into an orbit for which perigee lies just at 6500 km, barely avoiding the effects of atmospheric drag. The velocity change needed to execute this emergency maneuver is 90 m/sec, which is what must be delivered by the primary RCS within 2600 sec. Another sizing constraint is that the thrust of the RCS rockets should not be much greater than that of the laser engines since the truss structure is designed for a total force of 2000 N. There is a factor of safety associated with this limitation so it is reasonable to increase the thrust slightly, particularly for a system that is not expected to be used frequently, if ever.

Table 7. CMG Specifications

Angular momentum	305 N m sec
Output torque	305 N m sec
Mass	52.2 kg
Power	
Standby	15 W
Quiescent	50 W
Torquing (peak)	250 W

PROPELLANT TANK AND SUPPORT SYSTEM

The LPIV has two cryogenic tanks containing a total of 35,000 kg of liquid hydrogen propellant. Since the mass of the propellant takes up a large amount of the total vehicle mass as a whole, the tanks must be moved strategically so that the center of mass of the LPIV will remain at the same location (midpoint between the turntable centers) as the propellant is depleted. This is done by placing the tanks on tracks that move the tanks along the secondary truss. Due to the translation of the tanks with respect to the entire LPIV, a propellant line

system using flexible propellant hoses must be devised in conjunction with cryopumps to deliver propellant to the engines. Consideration must be given to the harsh environment of space, specifically the cyclic temperature fluctuations. Thermal effects and launch loads must be dealt with by proper material selection and structure design.

After detailed consideration of various tank configurations, two spherical tanks were decided upon. Such a choice satisfies symmetry requirements of the LPIV, minimizes shifting of the center of mass, and may reduce propellant sloshing. The LPIV tanks will be fabricated from a new low-density aluminum-lithium alloy, 2090 series (or its future derivative) developed by Alcoa. The technique of forming the tank is accomplished by spin forming a disc into a one-piece hemisphere. Two hemispheres will then be joined by a major weld. The interior is designed such that it will support slosh baffles in order to minimize sloshing loads. All support structures will be built, the tank assembled, and the insulation applied as a complete process because the tank is an integrated structure. The tanks will be carried to orbit by a second-generation shuttle requiring a larger payload area than the present shuttle. The aluminum tanks are supported by S-glass/epoxy composite struts that are in turn connected to the graphite/epoxy frames. The struts are attached to the tanks by a step-chem milling pattern combined with welding techniques. The other ends of the struts are connected to the tank structure using titanium rod-end fittings allowing movements of the struts as the tanks contract or expand due to thermal effects or pressurization. Struts and frame members utilize the same materials as members of the main truss. An MLI/foam system was selected for insulation of the propellant tanks because of greater potential for future improvement. The thickness of the MLI/foam required for the tank was determined by allowing 1% boiloff. The MLI is made of alternating layers of metallized Kapton film and Dacron net spacers. Between the MLI and the foam is a gas-impervious barrier film made of aluminized Kapton bonded over the outside of the foam. This barrier entraps in the foam volatile materials that could escape into the MLI and degrade its performance. The Rohacell 31 foam (or its future derivative) is adhesively bonded to the tank surface. The foam insulation around the tank mounting supports must allow for movement of the support struts. These movements are caused by thermal contraction and expansion of the tank and supports, tank pressurization, and vibration due to launch loads. An 8-mil-thick YB-71 paint is sprayed on top of the MLI to provide a reflectance of 94%. Finally, a layer of Mylar is applied to protect the paint surface from micrometeorite collisions. For the duration of the LPIV mission of 15 days, approximately 350 kg of liquid hydrogen will be lost or vented due to the assumed 1% boiloff.

Track System

The track system (Fig. 11) of the propellant tanks uses two T-tracks extending along the secondary track that will support the tanks and their structures. The tanks will be moved along the tracks by means of a center screw track with an actuator connected to the propellant tank support platform. The T-track

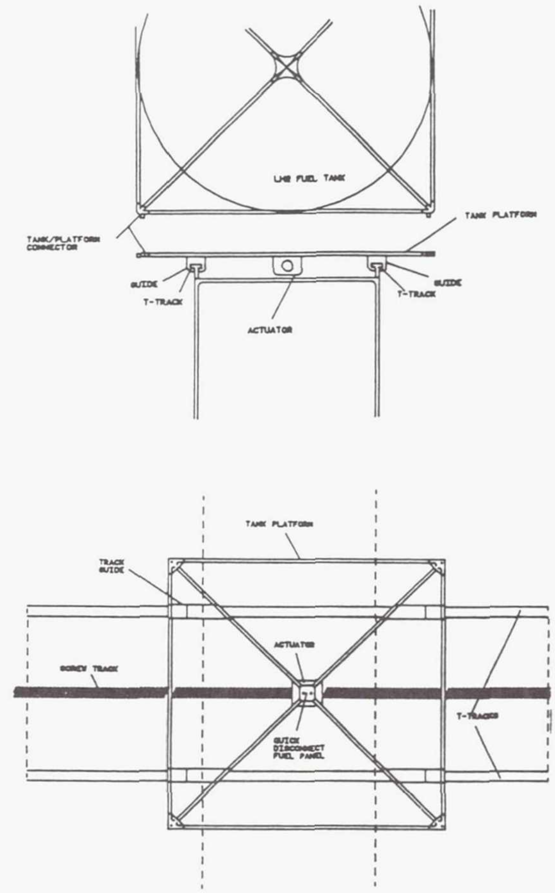

Fig. 11. Tank Track System

is connected to the LPIV along the secondary truss at the joints used to connect the truss members. The actuator designed for the LPIV is made from a combination of cams, rollers, and gears providing very accurate positioning. The maximum power requirement for each actuator is 5 W, or 10 W for both actuators. The propellant tank platform serves as a propellant tank holder and is permanently attached to the tracks. The platform is attached to the screw track and T-tracks by the actuator and four guides, respectively, and will be made of tubes connected by fittings at the corners. Each fitting contains a male-female latch devised to lock the tank in place after attachment. These latches can be operated by electrical pulses to either a closed or open position to attach or release the propellant tank from the platform. The platform will also have

Table 9. Masses and Key Dimensions of the Tank System

	Masses (kg)		Dimensions (mm)
Dry mass of both tanks	1025	Tank diameter	7800
		Wall thickness	1.17
Insulation	268	MLI thickness	18.4
Track system	2190	Foam thickness	1.84

a quick disconnect panel for propellant flow between the tank and the LPIV. The four guides on the platform will hold the platform and tank to the T-tracks. These guides will require a rolling and braking mechanism so that they can move freely when the actuators are activated and clamp to the T-tracks when the actuators stop. Key dimensions and masses of the tank system are listed in Table 9.

Propellant Feed System

The propellant feed system is responsible not only for necessary and precisely controlled supply of the hydrogen to the laser engine but also for the cooling of the engine walls, beam splitter, and tertiary mirrors. A turbopump powered by the hot hydrogen bled from the cooling system has been selected over an electrically driven pump under the assumption that improvements in technology over the next 20 years will greatly enhance the reliability of the rotating turbomachinery. The LPIV will use two turbopumps, one for each engine. The use of two pumps simplifies operation of the cooling system. Propellant will be fed to the pumps from the pressurized tanks. The propellant inside the tanks will be maintained at low pressure presently determined to be 5 psia since this is known to be the lowest practical pressure while still providing a net positive suction head at the pump inlet. The turbopumps must increase the pressure of the propellant from 5 psia (0.34 atm) to about 367 psia (25 atm). This will be the pressure required for the propellant to overcome the friction in going through the cooling and injection into the engine. An electric motor will be used to initiate the rotation of the pump until the operational speed is achieved. The required pumping power is 1.34 kW. The turbine is driven by a small fraction (5%) of hydrogen diverted from the engine cooling system at a location where the hydrogen temperature is around 1050 K. The hydrogen discharged from the turbine is reintroduced back to the cooling system. While no detailed configurations are presented, approximate estimates of the turbopump systems have indicated that both the turbine and the pump will be very small and will have to operate at very high speeds. The single-stage turbine will use a rotor with the blade tip and blade root diameter of approximately 2 and 1.5 cm, respectively, and the operational speed may be around 80,000 rpm. A small centrifugal pump will have an impeller designed so as to optimize the suction specific speed. A near 1:2 speed reduction gear may be required for matching of turbine and pump. Since the propellant tanks will be moving along the tracks, it is necessary to devise a scheme to install flexible propellant lines between the tanks and the laser engines. The proposed design requires that the hose material retains flexibility at 21 K without degradation and that the hose will be kept out and away from the laser beam. All slack must be taken up by spring mechanisms. Total mass for the propellant feed system is 135 kg.

ACQUISITION, POINTING, AND TRACKING (APT) SYSTEM

Laser-powered vehicles place stringent demands on the acquisition, pointing, and tracking (APT) system. The APT system must not only maintain the laser beam on target throughout the LPIV's period of powered flight, but must also be able to locate and acquire the beam prior to thrusting. The APT system relies heavily on three other systems of the craft, the communication system, the on-board computer, and the RCS system. The communication system is used to establish an initial link between the LPIV and the Laser Power Station (LPS). The computer is used to calculate the positions of the LPS and LPIV given the orbital data. The RCS system is used to maneuver the vehicle into a position from which it can receive the power beam. The other primary components of the APT system consist of the optical receiver, the optical transmitter, the fine pointing gimbal assembly, and several photodetectors.

Link

Working to establish the link are the communication system, the optical transmitter, and the optical receiver. The communication system is employed only in the initial stage of acquisition to instruct the LPS to emit its pilot beam and begin its search pattern. The optical transmitter and receiver are located on the back of the secondary mirror and share the same optics (Fig. 12). The transmitter is a Nd:YAG laser with a frequency doubler. Doubling the frequency accomplishes three goals: First, it reduces noise and interference by increasing separation from the iodide power beam (1.315 μm); second, the smaller wavelength allows the optics themselves to be smaller, which cuts down on mass; finally, the smaller wavelength boosts the antenna gain, which lowers the power requirements[3]. At the specified wavelength and with the antennas on the LPS and the LPIV, the Nd:YAG laser needs only 40 W of power. The receiver is effectively a simple 20-cm reflector telescope of the type designed by Eastman Kodak[4]. It must be modified only slightly to allow for the quadrant photodetector to be placed in the proper position behind the primary mirror. A dichroic beam splitter is located in the path of the oncoming beam that allows most of the radiation incoming at 1.315 μm to pass through while reflecting most of the outgoing radiation at 0.532 μm.

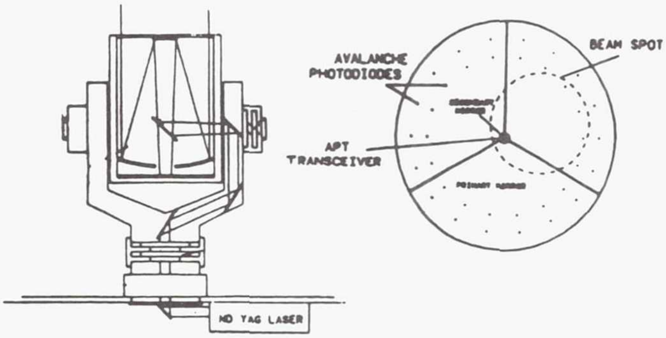

Fig. 12. APT System

Aim

The telescope is mounted on a gimbal assembly with two degrees of freedom about the azimuth and elevation. This gimbal assembly, along with the photodetectors and the RCS system, make up the aiming portion of the APT system. The gimbal assembly is used for the fine pointing of the optical receiver and consists of an azimuth motor and an elevation motor, each with its own induction angle sensor. The azimuth has full 360° mobility and the elevation has a field of view of just over 30°. Both the azimuth and elevation are controlled by induction motors, which consume 12 W each, built into the gimbal assembly. The quadrant photodetector located in the telescope operates on the principle that when the beam is on center, the radiation in each quadrant will be equivalent. They are constructed of four independent avalanche photodiodes (APDs). In order to locate the beam vertically, the energy in the lower two quadrants is subtracted from that of the upper two quadrants and the difference is divided by the total energy. For horizontal location, the same is done between the right and left quadrants. Coordinates are then relayed to the computer, which may then instruct the RCS system or the LPS of the appropriate action to take to center the beam. There is a system of photodetectors in addition to the quadrant photodetector in the telescope that work together to ensure proper beam alignment. They are located around the periphery of the primary mirror in two rings at 20° intervals. The outer ring is located 2 m from the edge of the primary mirror and the inner ring is located 2 m inside of the outer ring. The photodetectors in each ring are APDs covered by a dielectric filter tuned to a wavelength of 1.315 μm corresponding to the wavelength of the power beam. APDs were selected for the photodetectors because of their small size of close to 1 in, their high reliability, and their compatibility with light at the given wavelength[4]. If the beam is properly offset, at least one of the photodetectors on the inner ring will be activated and none of those on the outer ring will be activated. This dictates that at least one edge of the beam spot is between the two rings (Fig. 12). This beam position is maintained by the RCS system.

Computer

The on-board computer is used to calculate the position of the power station from which the LPIV will receive the beam. A modified SIGHT program will be used to control and manipulate the LPIV. The computer must be given the complete orbital data for all the power and relay stations and be able to solve for their position at any time using the data from the on-board clock. In order to correct for small errors and to account for orbital variations, this data is automatically updated every time the APT system locks onto the LPS, and it can be directly changed using the communication system from the space station or from the mission control.

The Lead Ahead Problem

Due to the finite speed of light and the long distances that may exist between the LPS and the LPIV, it is necessary to calculate the angle by which the LPS must lead the LPIV when sending the beam so that it is received on target. In order to estimate this lead-ahead angle, we need to know the velocities of both objects. The LPS is in a circular orbit at one Earth radius and its velocity is 5.59 km/sec.

The main case which deserves consideration here is when the LPIV is farthest (100,000 km) from the LPS during powered flight and the signal travel time is the longest (0.33 sec). Assuming that the velocities are linear (this is a good approximation within a small time step) and also assuming that the response times of the vehicles are negligible (much less than 0.33 sec), the change in relative position, perpendicular to the line of sight, may be as large as 1.863 km. This corresponds to a lead-ahead angle of 37.3 μrad showing that lead-ahead angle must be accounted for. In order to calculate the lead angle, the computer uses the preprogrammed orbital data to calculate the position and velocity of the LPS. The LPIV knows its own velocity from the data provided by the accelerometers and its position is determined by the star trackers. Given this data, the computer can calculate the relative angle between the transmitter and the receiver and adjust the APT system accordingly. Because of the APT's importance, reliability and accuracy have been the two primary considerations in its design. Individual components have been selected for their high durability and projected long life. Secondary considerations included mass and power requirements. A list of mass and power specifications for the APT system is given in Table 10.

Table 10. APT Mass and Power Specifications

	Masses (kg)		Power (W)
Telescope	4.5	Laser	40
Laser	4.5	Gimbals	24
Gimbals	65		
Mount	10		
All APDs	6.5		
Totals	105		64

COMMUNICATION SYSTEM

The communication system of the LPIV has three basic functions: telemetry, tracking, and command (TTC). Telemetry is used to monitor the vehicle's status during the course of its mission. The on-board computer continuously gathers information regarding the health of the LPIV and sends it back to either the Earth-based mission control station or the space station to be analyzed. The TTC system assists in tracking the vehicle by establishing an initial link with the laser power station for the purposes of course pointing. TTC may also be used to command the vehicle for manuevering during docking or initial firing, to update the orbital flight data, or to change orbits. For the LPIV to be able to establish a link directly with the space station or mission control it would have to be equipped with at least two antennas in order to avoid blocking the transmission by another part of the vehicle. It would also

require a completely separate APT system for use by the TTC system. In order to avoid such problems, it is necessary for the laser station to have the capability of serving as a repeater station for satellite transmission from either the space station or mission control. Because the laser station will be continuously tracking the LPIV and the space station will be tracking the laser station, a separate APT system is not needed. It also enables the communication link to be uninterrupted for a much longer period of time because the antenna will not fall into the shadow of the vehicle. The repeater at the laser station is only employed during powered flight of the LPIV. During the coasting stage, the LPIV may orient itself to point in the direction of transmission. The links from the laser station to the space station and to mission control are left out with the assumption that current communication satellites such as INTELSAT (INternational TELecommunications SATellite) can be used to establish these links. Only the link between the repeater at the laser station and the LPIV is discussed here.

For digital data transmission, the LPIV will use directional antennas. A frequency-division multiple access (FDMA) technique will be employed to allow for the number of subsystems of the LPIV to communicate on the same bandwidth. For representing a digital signal with an analog wave, a Quaternary Phase Shift Keying (QPSK) modulation technique will be used similar to the one recommended for the space station. To reduce the noise in the signal and provide more accurate data transmission, convolution coding with a constraint length of around 7 and a rate of 1/2 will be employed. The LPIV will use two small omnidirectional antennas weighing up to 4 kg placed at each end of the truss for making initial contacts between the directional antennas. Since antenna gain is inversely proportional to the wave length, we have selected for the LPIV frequencies of 40 GHz for receiving and 60 GHz for transmitting on the assumption that frequencies in the 40 to 60 GHz range will be in common use in the 21st century. The directional antenna will be of the asymmetric or offset type to minimize the problems due to the central obstruction of the axisymmetric type. It should be located at the periphery of the primary reflector at 90° from the main truss, as shown in Fig. 13. By placing the antenna at this point we are getting it as close to the primary mirror as possible without blocking the power beam and as far as possible from the engines to minimize blockage of the signal and deterioration of the antenna by exhaust particles. The reason for this is so that when the APT system has properly aligned the craft for powered flight, the antenna will be aligned as close to boresight as possible with that of the laser station.

Aerobraked LPIV Design

The aerobraked configuration of the LPIV uses an aerobraking passage through the Earth's atmosphere in order to achieve a velocity decrement without the costly expenditure of propellant, thereby reducing the necessary amount of hydrogen. The design of the aerobrake must take into consideration the following goals: First, the mass of the added aerobrake structure possibly should not exceed the mass of the propellant that would be saved by the aerobrake procedure; second, the structure should be able to withstand both the forces and thermal loadings that the vehicle would encounter during atmospheric entry; third, the aeroshell should adequately protect the existing LPIV vehicle from excessive heating; and finally, the aerobrake should be refurbishable if damage should occur, with the requirement that the entire structure be designed for transport into and assembly in a space environment.

Originally, a raked elliptical cone geometry was considered due to its excellent aerobraking and aeromaneuvering capabilities. However, by using an asymmetrical shape for the aeroshell, a stable center of mass is difficult to maintain upon rotation of the engines. Therefore, a nonraked elliptical conic was selected instead. Its surface geometry is given by $x^2/25 +$

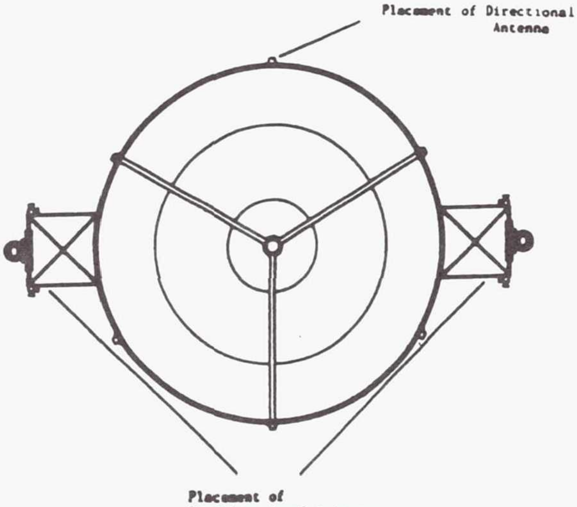

Fig. 13. Communication System

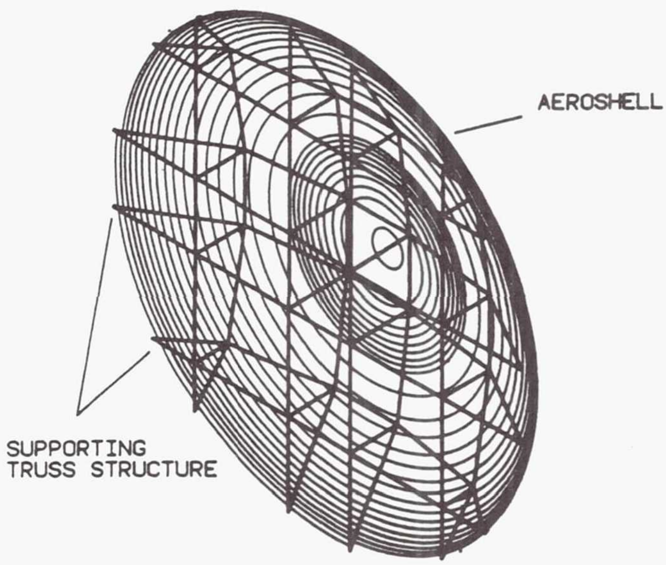

Fig. 14. Aerobrake Shell and Truss Structure

Table 11. LPIV Electrical Power Requirements

	"Semi-constant" Power (W)
Gyroscopes	250
APT system	200
Turntable motor	15
Receiver/Preprocessor	25
Track actuator	5
Central processor	20
Comm. system	70
Aero. telescoping motors (4)	32
Range/Range Rate System	25
Truss telescoping motors (4)	7
Tracking sensors	20
Total	769 W

$y^2/289 + z^2/289 = 1$. Sizing analysis resulted in selecting a diameter of 34 m and a depth of 5 m. The aerobrake will need slight tilting abilities to generate nonzero L/D values. The main characteristics of the aerobrake are as follows: $C_D = 1.48$; ballistic coefficient $m/C_DA = 19.83\ kg/m^2$; $C_{Y\beta} = -0.0050/°$; $C_{n\beta} = 0.0023/°$; and $C_{l\beta} = 0.0030/°$.

The truss structure supporting the aeroshield (Fig. 14) is similar to the one proposed previously[5]. The symmetrical features associated with this design allow for the support truss to be made up of only two different frames, which are then repeated in a cross hatched pattern. The truss is constructed of graphite/epoxy tubular members that are connected by means of titanium fittings. The joints are basic revolute pin joints that allow one degree of freedom. The structure supporting the aerobrake shell was made deep enough so that a payload bay could be located inside the aerobrake itself, thereby helping to reduce the required diameter of the aerobrake. With this configuration, however, comes the problem of payload recovery once docked at the space station. The problem is remedied by using a telescoping truss that can be extended once docked at the space station, or in orbit about the Moon. The four central support truss members are made up of two concentric cylinders equipped with motor/piston assemblies allowing the aerobrake structure to be pushed out and away from the rest of the LPIV. A mass breakdown of the aerobrake is as follows: aeroshield (TPS tiles and ribbing) = 2700 kg; supporting truss = 800 kg; total mass = 3500 kg.

Table 12. Characteristics of the All-Propulsive LPIV

Propulsion	
Laser power	15 MW
Laser transmitter aperture	30 m
Optical train efficiency	94.8
Thermal conversion efficiency	50%
Specific impulse	1500 sec
Propellant flow rate	2 at 0.033 kg/sec
Thrust	2 at 483 N
Masses (kg)	
Vehicle dry mass	25,000
LEO to LLO payload	18,000
Initial propellant at LEO	35,000
Overall vehicle loaded	63,300
Initial propellant at LLO	17,784
Propellant used for LEO-LLO trip	17,216
Propellant used for LLO-LEO trip	14,881
Performance	
LEO-LLO trip time	8 days
LLO-LEO trip time	9 days
LEO-LLO payload mass ratio	0.338
LLO-LEO payload mass ratio	0.532
Overall structural coefficient	0.26

ELECTRICAL POWER SYSTEMS

The basic LPIV power requirements are listed in Table 11.

In addition, a short-duration 3000-W power will be required for start-up of the turbopump motors. This power will be provided by a short-duration, secondary, rechargeable battery system. Consideration of various potential candidates for the LPIV power source resulted in selection of a propellant cell system as the main power source. Newly developed hydrogen/oxygen cells provide an efficient, reliable and long-lifetime energy source. Table 12 presents the key characteristics of the all-propulsive LPIV.

ACKNOWLEDGMENTS

Design team members M.T. Clarke, J.J. Cooper, G.P. Eggleston, M.A. Farkas, D.C. Hunt, J. King, H. Nguyen, G. Rahal, K. Saw, R. Tipton, J.P. Tirone, and H. Vu were assisted by Project Advisor Dr. A.K. Jakubowski.

REFERENCES

1. DeYoung, R. J., Walker, G. H., Williams, M. D., Schuster, G. L., and Conway, E. J., "Preliminary Design and Cost of a 1-Megawatt Solar-Pumped Iodide Laser Space-to-Space Transmission Station," NASA Langley Research Center, Hampton, Va., *NASA Technical Memorandum 4002,* Sept. 1987.
2. Korites B. J., *Structural Analysis Software for Microcomputers,* 2nd ed., Kern International, Inc., Pembroke, Ma., 1987.
3. Hacker, G., "System Considerations for an Optical Intersatellite/Interorbit Link Based on ND:YAG Laser Technology," *Optical Systems for Space Applications,* 810, April, 1987.
4. Katman, M., Ed., *Laser Satellite Communications,* Prentice-Hall, Englewood Cliffs, New Jersey, 1987.
5. Aerospace Senior Students, "Aeroassisted Manned Transfer Vehicle (TAXI) for Advanced Mars Transportation," Dept. of Aerospace and Ocean Engineering, Virginia Polytechnic Institute and State University, Blacksburg, Va., 1987.

19940004341
383651
12p

N94-71296

ADVANCED SOLAR-PROPELLED CARGO SPACECRAFT FOR MARS MISSIONS

UNIVERSITY OF WASHINGTON

S29-16
160655
p. 11

At the University of Washington, three concepts for an unmanned, solar powered, cargo spacecraft for Mars-support missions have been investigated. These spacecraft are designed to carry a 50,000-kg payload from a low Earth orbit to a low Mars orbit. Each design uses a distinctly different propulsion system: a solar radiation absorption (SRA) system, a solar-pumped laser (SPL) system, and a solar powered magnetoplasmadynamic (MPD) arc system. The SRA directly converts solar energy to thermal energy in the propellant through a novel process developed at the University of Washington. A solar concentrator focuses sunlight into an absorption chamber. A mixture of hydrogen and potassium vapor absorbs the incident radiation and is heated to approximately 3700 K. The hot propellant gas exhausts through a nozzle to produce thrust. The SRA has an I_{sp} of approximately 1000 sec and produces a thrust of 2940 N using two thrust chambers. In the SPL system, a pair of solar-pumped, multi-megawatt, CO_2 lasers in sun-synchronous Earth orbit converts solar energy to laser energy. The laser beams are transmitted to the spacecraft via laser relay satellites. The laser energy heats the hydrogen propellant through a plasma breakdown process in the center of an absorption chamber. Propellant flowing through the chamber, heated by the plasma core, expands through a nozzle to produce thrust. The SPL has an I_{sp} of 1285 sec and produces a thrust of 1200 N using two thrust chambers. The MPD system uses indium phosphide solar cells to convert sunlight to electricity, which powers the propulsion system. In this system, the argon propellant is ionized and electromagnetically accelerated by a magnetoplasmadynamic arc to produce thrust. The MPD spacecraft has an I_{sp} of 2490 sec and produces a thrust of 100 N. Various orbital transfer options are examined for these concepts. In the SRA system, the mother ship transfers the payload into a very high Earth orbit and a small auxiliary propulsion system boosts the payload into a Hohmann transfer to Mars. The SPL spacecraft releases the payload as the spacecraft passes by Mars. Both the SRA-powered spacecraft and the SPL-powered spacecraft return to Earth for subsequent missions. The MPD-propelled spacecraft, however, remains at Mars as an orbiting space station. A patched conic approximation was used to determine a heliocentric interplanetary transfer orbit for the MPD propelled spacecraft. All three solar-powered spacecraft use an aerobrake procedure to place the payload into a low Mars parking orbit. The payload delivery times range from 160 days to 873 days (2.39 years).

INTRODUCTION

With the renewed interest in planetary exploration, the United States has been considering a manned Mars mission. Such a mission should be different from the Apollo mission to the Moon in that it should establish the initial elements of a long-term outpost that would be utilized and expanded by subsequent manned missions over a period of several decades. A substantial amount of supplies and equipment will be needed. As we have learned from the Skylab, Salyut, and Mir long-duration manned Earth-orbital missions, long-term exposure to zero gravity has adverse effects on human physiology; therefore, the transfer time for a manned Mars mission should be as short as possible. To facilitate a rapid transfer, all supplies and equipment not essential to the crew need to be transported on a separate cargo vehicle. The substantial payload masses envisioned for such a mission will require the utilization of advanced propulsion systems capable of I_{sp}s well in excess of the levels characteristic of chemical propulsion systems. Nuclear-thermal, nuclear-electric, and solar-electric propulsion schemes, the latter two involving ion propulsion, have been suggested for such missions during the past three decades(1).

Students at the University of Washington have designed three new approaches for an Earth-to-Mars cargo transport utilizing solar energy for propulsion. Mission assumptions include that the U.S. manned space station is operational and that the vehicle components are transported to low Earth orbit (LEO) by the space shuttle and assembled by a crew from the space station. The payload consists of supplies and equipment with a mass of 50,000 kg, which is within the range of payload masses that have been considered by others. The cargo ferry would be launched long before the manned mission, so that the success of the supply mission can be ascertained before the manned mission begins its journey. The three concepts include a solar radiation absorption (SRA) propulsion system, a solar-pumped laser (SPL) propulsion system, and a solar-powered magnetoplasmadynamic (MPD) propulsion system. All three concepts offer specific impulses well in excess of those achievable by chemical propulsion systems.

The SRA propulsion system (Fig. 1a) employs direct conversion of solar energy to thermal energy in the propellant using a novel process developed at the University of Washington(2). Solar energy is concentrated using erectable reflectors and is directed through a sapphire window into an absorption chamber. Hydrogen propellant, seeded with an alkali metal (potassium), absorbs the incident radiation, and the heated propellant exhausts through a nozzle to produce thrust.

In the SPL propulsion system (Fig. 1b), the thruster aboard the cargo vessel is powered by a remote, Earth-orbiting laser system. The laser itself is powered by concentrated solar radiation using a blackbody pumping concept capable of 15% efficiency(3). The laser beam is transmitted to the spacecraft, where the energy is focused into an absorption chamber in which the hydrogen propellant is heated through a plasma breakdown process. The heated propellant expands through a nozzle to produce thrust.

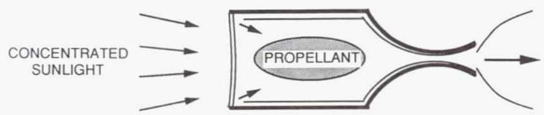

Fig. 1a. Solar Radiation Absorber Thruster

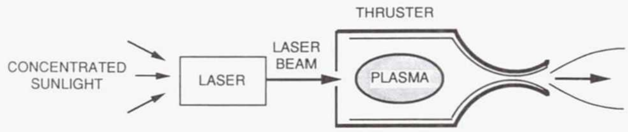

Fig. 1b. Solar-Pumped Laser Thruster System

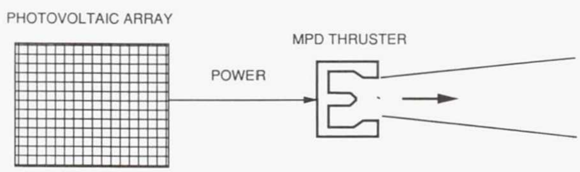

Fig. 1c. Magnetoplasmadynamic Thruster System

The MPD propulsion system (Fig. 1c) uses advanced solar cell technology (indium phosphide) to convert sunlight to electricity, which powers the magnetoplasmadynamic propulsion system. In this system, the argon propellant is ionized in a diffuse electric arc and electromagnetically accelerated to produce thrust.

This report presents a summary of the three propulsion systems separately. Within each propulsion system section is a review of the propulsion theory, a description of the spacecraft structure, a summary of the orbital mechanics particular to each propulsion design, and a summary of the key elements and performance characteristics.

SOLAR RADIATION ABSORBER PROPELLED SPACECRAFT

The solar radiation absorber (SRA) propelled spacecraft, shown in Fig. 2, utilizes directly a flowing gas volume absorber to convert solar energy to thermal energy in the propellant[2]. The SRA propulsion system circumvents the material limitations of conventional surface absorbers, as well as the erosion problems and inefficient heat transfer encountered by particulate volume absorbers.

Propulsion

The SRA thruster is depicted in Fig. 3. Solar radiation enters the thrust chamber through a transparent window and transfers its energy to the propellant, which consists of gaseous hydrogen seeded with potassium vapor. The potassium serves as a broadband absorber of the solar spectrum[4] and transfers energy to the hydrogen through the process of collisional quenching[5]. The heated propellant is exhausted through a nozzle set at right angles to the chamber axis. This configuration was chosen to simplify the solar collection optics.

In the present design the chamber pressure is 100 atm and the mixture ratio of hydrogen to potassium is 9:1 by mass. The chamber has a diameter of 0.64 m and a length of 0.8 m. As the propellant travels through the chamber, its temperature increases due to the volumetric absorption of the solar energy, as shown in Fig. 4. Since the propellant is a broad band absorber, the cooler propellant in the vicinity of the window absorbs the reradiation from the hotter propellant deeper inside the chamber. This process, known as radiation trapping, results in much higher conversion efficiencies (90% in the present case) than are possible with solid surface absorbers[2]. The present SRA thruster provides 1470 N of thrust with an I_{sp} of 1000 sec. Two units are required for the mission.

The hydrogen propellant and the potassium vapor require independent storage systems. The 39,600 kg of hydrogen required for this mission are stored cryogenically in spherical storage tanks, shown in Fig. 5. The tanks are 4.4 m in diameter,

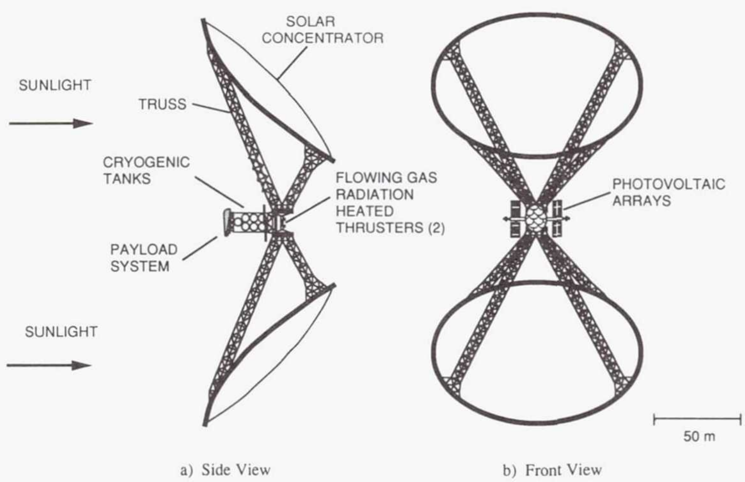

Fig. 2. Solar Radiation Absorber Propelled Spacecraft

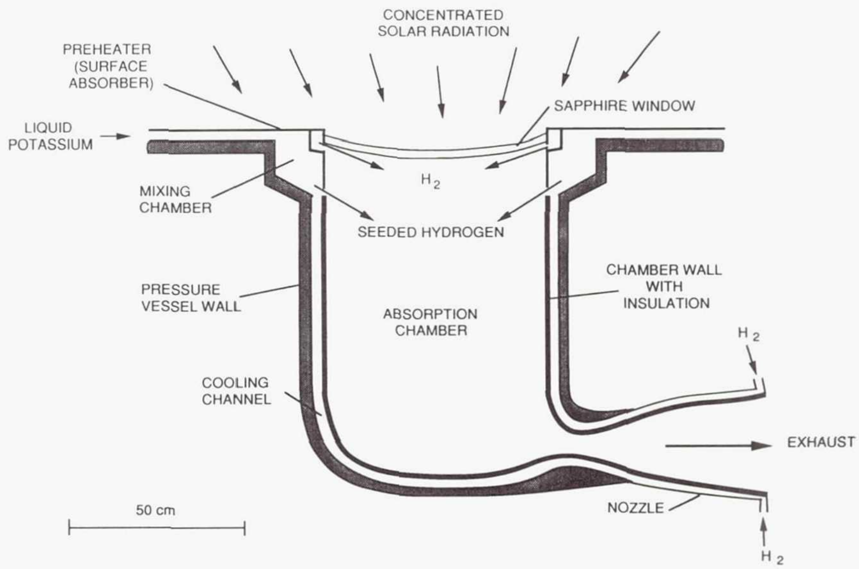

Fig. 3. Schematic of the Solar Radiation Absorber Rocket

and are delivered to LEO in the form of pairs of hemispherical shells. Interlocking continuous flanges are located along the open end of each hemispherical shell. The shells are assembled and filled with hydrogen propellant in LEO. A total communication liquid acquisition device, consisting of channels within the storage tank walls and lined with a fine wire mesh, delivers the hydrogen to the SRA thruster.

The potassium storage tank is also spherical in shape. The 4400 kg of liquid potassium is stored in a single spherical tank with a diameter of 2.18 m. The potassium is stored at 420 K. It is kept at this temperature by a small electrical heater on the tank wall. The liquid potassium is extracted by means of capillary tubes and pumped to a solar heater to be vaporized prior to combination with the preheated hydrogen. The hydrogen/potassium propellant mixture is delivered to the SRA thruster at a mass flow rate of 0.15 kg/sec.

Both the transparent window and the walls of the absorption chamber are subject to high heat-transfer rates. The window temperature is maintained at 400 K by passing a pure hydrogen cooling film over the surface of the window. The absorption chamber is surrounded by a cooling jacket through which the hydrogen propellant is passed. This preheats the hydrogen, prior to its entering into the thrust chamber.

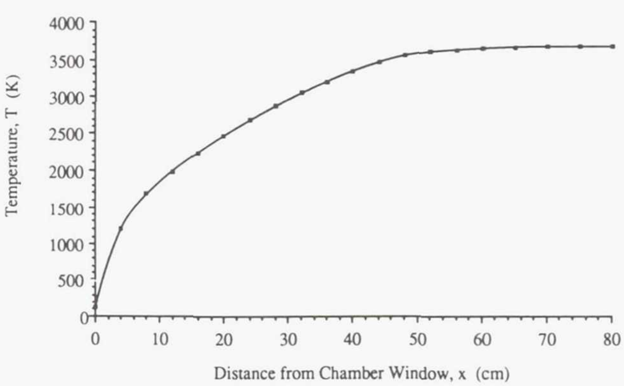

Fig. 4. Computed Absorption Chamber Temperature Profile

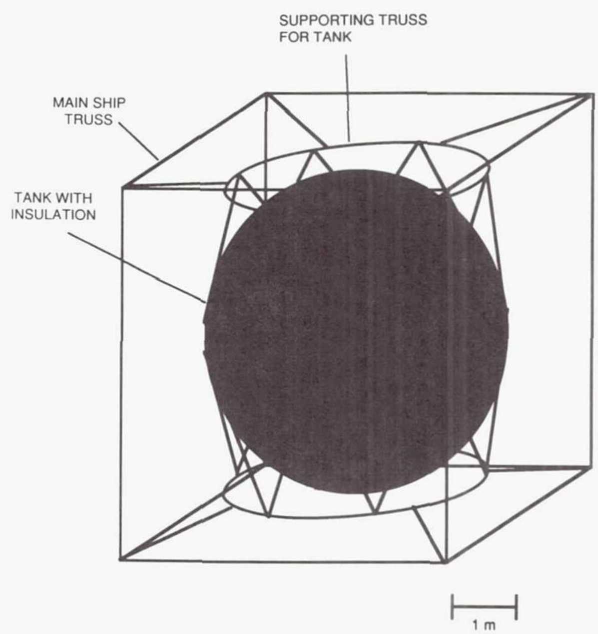

Fig. 5. Tank Truss Configuration

Solar Collectors

The SRA propulsion system uses two solar concentrators (Fig. 2) to capture incoming solar flux. Two off-axis paraboloid sections comprise the concave light amplification mirror (CLAM) system. The CLAM system concentrates the solar intensity of 1.33 kW/m^2 available in the vicinity of the Earth, to a maximum intensity of 24 MW/m^2, the intensity necessary to provide sufficient energy to the SRA propulsion system. The CLAM system operates at a concentration ratio of 7350 and produces a nearly circular image with a diameter of approximately 1.25 m. The intensity at the center of the image peaks at 24 MW/m^2, while the average image intensity is 8.3 MW/m^2. The SRA thruster operates at a maximum thermal efficiency by utilizing the higher intensities at the central regions of the image. The outer regions of the image are used to vaporize the potassium and preheat the hydrogen in a surface absorber.

The CLAM optical system uses two inflatable solar reflectors supported by a rigidified torus. Inflatable reflectors offer a minimal specific mass ranging between 0.02 and 0.1 kg/m^2. The reflectors are inflated while in LEO. The surface area of each CLAM reflector is 11,300 m^2, and each one is pressurized to 5×10^{-4} Torr. Consequently, a negligible amount of inflatant is lost due to leakage over the duration of the mission(6). The total mass of the CLAM system is approximately 900 kg.

The transparent window in the thrust chamber is composed of sapphire and has a thickness of 2.5 cm and a diameter of 0.64 m. Sapphire is a good transmitter of the solar radiation within the wavelength range of 0.25 to 6.0 μm. By coating the window with a dielectric anti-reflection material, the reflection losses can be reduced to 1%. Approximately 2.5% of the incident solar flux is absorbed in the window. As noted above, this heat is removed through hydrogen film cooling.

Structures

The support structure for the SRA-propelled spacecraft is composed of graphite/epoxy composite tubes clad with aluminum. The tubes form truss elements, interconnected with titanium fittings, threaded for ease of assembly in orbit. The main truss configuration consists of four triangular trusses that extend to the edges of each of the inflatable reflectors. The reflectors are maintained in a fixed orientation toward the sun through rotational joints(7), which allow the reflectors to rotate about one axis.

The mass of the spacecraft at the beginning of the mission is 135,500 kg. The total propellant mass required is 43,400 kg. The resulting payload mass fraction is 37%, more than twice that achievable with a chemical propulsion system.

Orbital Mechanics

The orbital mechanics of the SRA-propelled spacecraft initially consists of a series of perigee burns, as shown in Fig. 6, that place the spacecraft into successively larger elliptical orbits about the Earth. As the apogee increases, the velocity at perigee increases. The payload is released from the mother spacecraft at a point where the velocity of the spacecraft is 0.7 km/sec below the hyperbolic excess speed required to enter a Hohmann transfer to Mars. A small chemical propulsion system imparts the necessary velocity increment to insert the payload into a Hohmann transfer to Mars, where an aerobrake procedure places it into a low Mars parking orbit. After releasing the payload, the mother spacecraft reverses its thrusting to return to the initial LEO for subsequent missions. The payload release occurs 21 days after launch and the mother spacecraft arrives back in LEO 2 days later. The payload take 258 days to reach Mars.

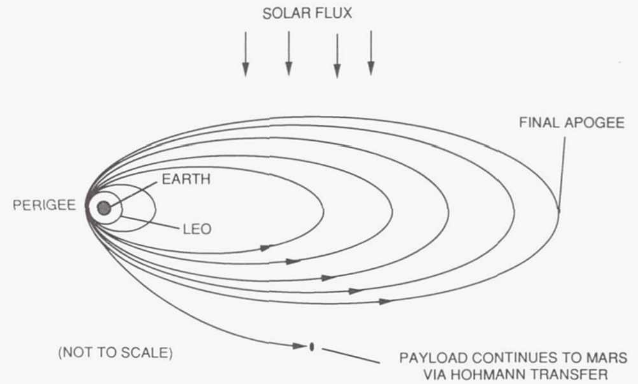

Fig. 6. Earth Orbits Heated Thrust Chamber and Injection Trajectory to Hohmann Transfer for Solar Radiation Absorber Spacecraft

SOLAR PUMPED LASER-PROPELLED SPACECRAFT

The search for high-performance propulsion techniques for interplanetary transport has stimulated research into the feasibility of laser propulsion(8,9). The principle behind laser propulsion is to beam energy from a separately stationed laser to a spacecraft; the laser beam received by the spacecraft serves as the primary energy source for the propulsion system. The significant advantage of laser propulsion over other advanced propulsion techniques is that the energy source is not aboard the spacecraft, and thus, it does not add to the mass of the ship.

Two types of lasers are suitable for laser propulsion: continuous wave (CW) and repetitively pulsed (RP). In the CW laser thruster (Fig. 1b), a continuous laser beam is directed into an absorption chamber, where a propellant is heated and then expanded through a nozzle(8). In the RP laser thruster, a solid propellant is bombarded with a train of pulses of laser energy(9). Because of the inherent complexities of the RP laser thruster, the CW laser thruster was chosen for this design study.

Propulsion

Conceptually, the CW laser thruster design presented in this report is fairly straightforward (Fig. 7). Laser energy is beamed

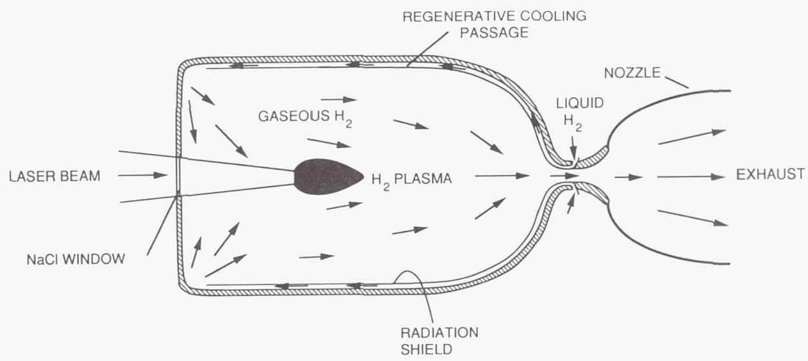

Fig. 7. Schematic of Laser Heated Thrust Chamber

to a collector aboard the spacecraft and is directed to the thruster by an optical train. A window in the thruster allows the laser beam to pass into the absorption chamber, where it is absorbed by a plasma discharge in the propellant gas. This plasma transfers energy to the surrounding propellant flow by radiation and convection. The heated propellant is expanded through a nozzle to produce thrust. Hydrogen was chosen as the propellant because its low molecular weight results in the highest possible I_{sp}. Hydrogen's low density presents a storage problem, but the advantages of hydrogen were determined to outweigh its disadvantages[10].

Absorption of the laser energy by the propellant takes place by way of the inverse Bremsstrahlung process[9]. A plasma is initiated in the center of the absorption chamber and the free electrons in the plasma absorb the incoming photons of the laser beam. Through collisions, the electrons raise the thermal energy of the propellant flow.

The chamber pressure was chosen to be 10 atm to make the nozzle area large enough to prevent the laser beam from damaging it during the first 150 nsec of startup. Using a 2-D axisymmetric model[11] to analyze the heat transfer within the absorption chamber, the peak plasma temperature was found to be 18,000 K and the propellant temperature at the entrance to the nozzle was determined to be 4300 K, for a propellant mass flow rate of 0.036 kg/sec and a laser input power of 5.4 MW. Taking into account frozen flow losses, the exit velocity was determined to be 12,600 m/sec. Under these conditions, each thruster produces 600 N of thrust at a I_{sp} of 1285 sec.

The thruster is constructed of molybdenum alloy because of the high temperatures the walls must endure; the temperature of the propellant flow along the walls is on the order of 4000 K. The thruster is regeneratively cooled by incoming propellant flowing between the thruster wall and an inner radiation shield. Another critical design concern relating to the thruster is the window. Excessive absorption of incoming laser energy would reduce the overall efficiency of the laser propulsion system and affect the integrity of the window itself. The window material chosen for the proposed design is Polytran NaCl, which absorbs only 1% of the incoming 10.6-μm radiation[12].

Solar-Pumped Laser

The spacecraft's two thrusters receive energy from two solar-pumped laser systems in solar synchronous orbit around the Earth (Fig. 8). Solar pumping is achieved by concentrating solar energy into blackbody cavities that serve to excite the lasing medium in tubes lining the blackbody cavity[3]. The output beam of each laser is transmitted and directed by a system of mirrors and laser relay units to a receiver on the spacecraft.

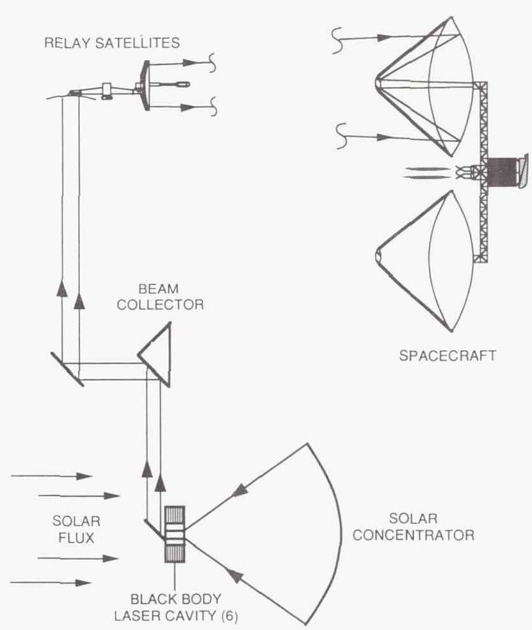

Fig. 8. Schematic of Solar-Pumped Laser Propulsion System

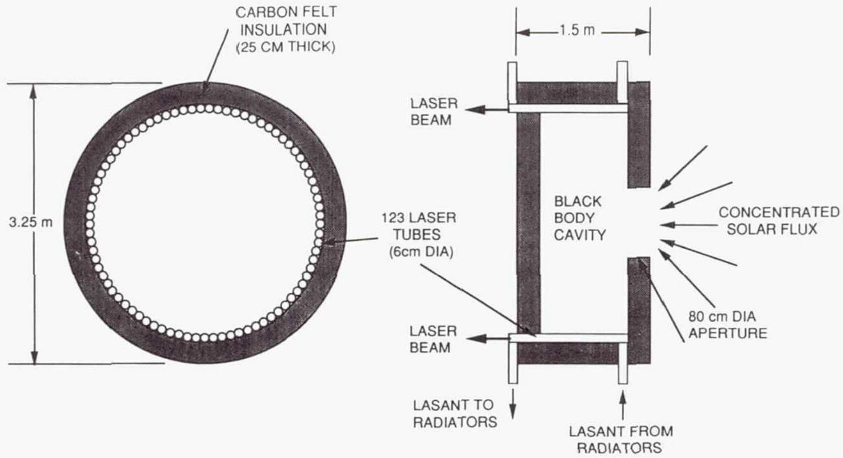

Fig. 9. Blackbody Solar-Pumped Lasers

To meet the propulsion requirement of 5.4 MW for each thruster, each laser system must generate approximately 6 MW to compensate for the losses at the reflecting surfaces and the losses due to diffraction. The proposed 6 MW are obtained from six 1-MW solar-pumped lasers. A 15% efficiency is projected for solar-to-laser power conversion(3). Given a solar flux of 1.33 kW/m^2 at LEO, a solar collector area of 5155 m^2 is required for each MW of laser output. In the proposed design, each laser system has six solar collectors. Each of the collectors concentrates the solar flux directly into one of the six blackbody cavities. The reflective surface of the collectors is fabricated of aluminized Kapton to provide high reflectivity over a broad band of wavelengths.

Each of the blackbody cavities is lined with 123 laser tubes (Fig. 9). The laser tubes are 1 m in length and 6 cm in diameter. Although cesium iodide, CsI, is a good candidate for the laser tube material because it is highly transparent to the 2000 K radiation in the blackbody cavity, other, stronger materials, such as ZnSe, may have to be used even though they may only be moderately transparent(3). The blackbody cavity material is carbon, in order to withstand the 2000 K equilibrium temperature. This temperature is a good choice in terms of cavity efficiency and total laser mass(3). Approximately 25 cm of carbon felt surrounding the blackbody cavity serve to insulate the cavity and limit the heat losses that would otherwise reduce the efficiency of the laser(3).

The CO_2 lasing medium must be kept at approximately 300 K to reach threshold in a blackbody cavity at 2000 K(3). Accordingly, inside each laser tube is a coolant tube that serves to keep the lasant temperature low enough to lase well. The cooling tubes have a diameter of 2 cm and circulate a coolant through the laser to a radiator and back to the laser. The CO_2 also circulates slowly through the tubes to a radiator to further assist in keeping itself cool. Further analysis into the exact cooling requirements and methods is required.

Laser Relay Units

Several laser relay units (LRUs) in orbit around the Earth continuously direct the laser beam to the spacecraft during the thrusting phase of the mission. The relay system consists of six separate units in a circular, equatorial orbit. The number of LRUs depends on the desired altitude and the minimum beam approach to the Earth's atmosphere. A beam approach altitude of no less than 250 km must be maintained to prevent excessive atmospheric absorption of the laser energy. For the proposed system, with two space-based laser systems, six relay units at an altitude of 3,000 km are sufficient for continuous transmission of the laser energy to the spacecraft.

A critical area of concern that requires further investigation is the tracking and aiming system. Both tracking and accurate aiming require knowledge of the instantaneous locations of the spacecraft, the laser platform, and the laser relay units. External influences on the system, including thermal shocks due to day-night cycling, atmospheric drag in LEO, which is greatly influenced by sun-spot activity, and gravity gradients induced by variations of the Earth's surface height, all contribute to the tracking and aiming problem.

Laser-Propelled Spacecraft

The 100-m-diameter laser receivers on the spacecraft are inflatable optics in order to reduce the mass of the spacecraft. The transparent balloon material is polyphosphazene with an aluminized reflective side. Argon was chosen to inflate the receiver because it has no absorption at the 10.6 μm wavelength of the laser, it will not react with the shell materials, and storage and leakage do not present significant problems(13).

Once the laser beam has been received by the spacecraft, an optical train directs the beam from each receiver to its

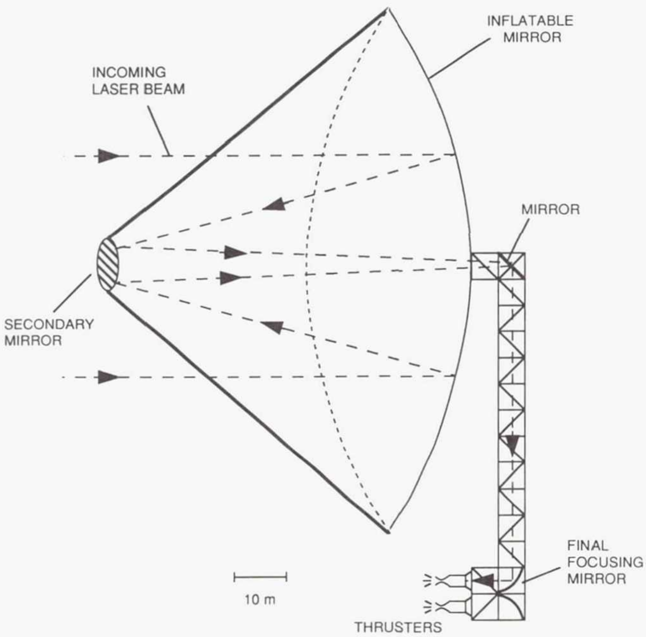

Fig. 10. Optical Train of the Laser-Propelled Spacecraft

corresponding thruster window. Figure 10 illustrates how the Cassegrainian receiver passes the laser beam to the optical train within the receiver support structure. The receivers are able to rotate 360° around the support structure through the use of solar α joints[7]. The mirrors of the optical trains are driven by motors to adjust to every movement made by the receivers and to continuously deliver the beam to the thruster windows. The directing mirror, at the top of each of the structures, moves with its receiver in order to keep the beam directed down through the center of the structure. At the bottom of each support structure, a second directing mirror rotates with the engine as it moves around the support structure and focuses the laser beam into the thrust chamber.

In the preliminary design of the spacecraft, the primary concerns were to minimize the mass and to ensure alignment of the optics. Varying thermal gradients in the spacecraft structure could distort the position of the laser receivers and the mirrors of the optical train, which could potentially impair the thruster performance. The spacecraft, as shown in Fig. 11, consists of four main parts: the collectors with their surrounding structure, the propellant tanks and associated structures, the payload and aerobrake, and the thruster.

The two laser collectors are each located at the end of a 100-m truss. The propellant tanks are clustered in a 10 × 10 × 25 m box truss (made up of individual 5 m boxes) that can accommodate up to 64 tanks (192,000 kg of propellant). For this mission, only 39 tanks, holding 117,000 kg of propellant, are required. The payload and aerobrake are placed at the front of the spacecraft for easy jettisoning. The thrusters are positioned to direct thrust through the center of mass of the spacecraft.

Structures

The main truss elements of the proposed design are 5-m hollow rod elements that have an outer diameter of 4.11 cm, and a wall thickness of 2.2 mm. Each element is fabricated of graphite/epoxy with a coating of anodized aluminum on the inner and outer surfaces. These dimensions and materials were selected primarily for the following reasons: (1) similarity to the elements that will be used in the space station: (2) compatibility with space shuttle payloads; (3) lower mass than conventional metals; (4) greater stiffness than conventional metals; (5) lower cost through fewer parts than a truss structure with smaller elements; and (6) compatibility to grow in three dimensions when needed.

To combat the problem of exposure to thermal fluxes, multilayer insulation is applied to all necessary members of the structure. An anodized aluminum foil layer, 0.1 mm thick, is wrapped around the trusses to further maintain the temperature of the graphite/epoxy within allowable limits. The overall effect is to reduce the thermal cycling distortion of the structure, thereby increasing its stability.

The total mass of the structural design, not including receiver supporting truss, is 2000 kg. The overall vehicle mass of the laser-propelled spacecraft is 204,900 kg, and the payload mass ratio is 24%.

Orbital Mechanics

The orbital mechanics of the SPL-powered spacecraft consists of a constant thrust spiral around the Earth to achieve

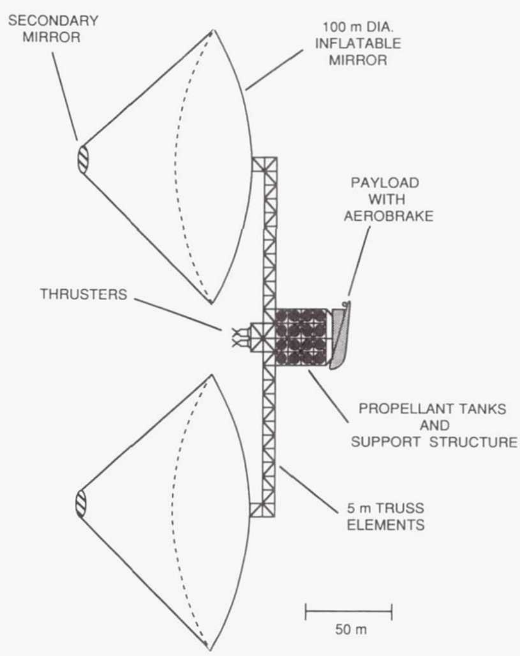

Fig. 11. Solar-Pumped Laser Propelled Spacecraft

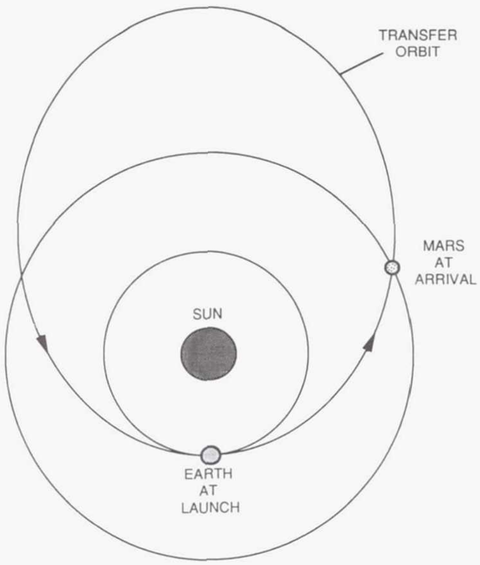

Fig. 12. Mars Fly-by Trajectory

the required hyperbolic excess speed to enter a Mars fly-by transfer. The Mars fly-by transfer is an elliptical transfer that intersects the orbit of Mars along its outbound leg (Fig. 12). Upon approach to Mars, the payload assembly is released to follow an aerobrake maneuver into a low Mars parking orbit. The mother spacecraft continues along the elliptical orbit to return to Earth. Further investigation, however, indicates that a quasi-impulsive transfer may be a better orbital maneuver. Such a transfer would use a series of perigee burns to produce increasingly larger elliptical orbits, similar to the orbital transfer scheme of the solar radiation absorber-propelled spacecraft described earlier.

MAGNETOPLASMADYNAMIC-PROPELLED SPACECRAFT

The magnetoplasmadynamic (MPD) propelled spacecraft, shown in Fig. 13, provides a third method of solar-powered cargo transport to Mars. Since Ducati reported the first successful MPD thruster in 1964, this propulsion system has become a viable alternative to ion propulsion for interplanetary travel[14-16]. In comparison with the SRA spacecraft and the SPL spacecraft described above, the MPD-propelled spacecraft operates at the lowest thrust level, 100 N, but with the highest I_{sp}, 2490 sec. Also, contrary to the SRA and the SPL spacecraft, the MPD-propelled spacecraft remains at Mars and provides an orbiting station to support future manned Mars missions.

Propulsion

The main component of the propulsion system is the MPD thruster, shown in Fig. 14. This device consists of a central cathode surrounded by a coaxial anode. A voltage difference of 75 V across the electrodes results in the development of an 8.1 kA diffuse arc current, which generates a self-induced, azimuthal magnetic field. Incoming propellant is ionized and accelerated through the $j \times B$ interaction of the diffuse arc current and the azimuthal magnetic field. Each thruster produces a thrust of 20 N at a propellant mass flow rate of 0.82 g/sec.

After prolonged operation, however, the cathode fails through erosion, rendering the thruster useless. The lifetime of an individual MPD thruster is approximately 2000 hours, or 83.3 days[16]. Consequently, since this mission necessitates 664 thruster burn days, multiple thrusters are required. A total of 43 thrusters are configured in a concentric circle array. Thrusters are fired in combinations of five, to the full extent of their lifetime. This configuration not only allows the sequential firing of series of thrusters to maintain a constant thrust level, but also provides replacements in the event of a thruster malfunction. Multiple thrusters also allow efficient use of the decreasing solar power as the spacecraft travels away from the sun. The total mass of the thrusters is 1700 kg.

The characteristics of the MPD propulsion system require a gaseous propellant. A minimum storage volume, however, suggests transporting the propellant as a liquid and vaporizing the liquid as needed. Consequently, an ideal propellant has a high liquid density, as well as a low vaporization energy. Argon, with a liquid density of 1.42 g/cm^3 and a vaporization energy of 157 J/g, was selected. The 170,000 kg of argon required to complete this Mars mission are stored in a cryogenic ellipsoidal propellant tank, as depicted in Fig. 15.

Surface tension of the liquid propellant forces a vapor bubble with a diameter equal to the minor axis of the ellipsoidal propellant tank to reside at the center of the tank[17]. Under the low accelerations of the MPD-propelled spacecraft, this vapor bubble remains at the center, allowing a vapor probe to extend into the bubble and extract only gaseous argon[17]. A series of heaters within the vapor bubble maintains a sufficient supply of argon vapor for the thrusters. The argon vapor is delivered to the MPD thrusters at a mass flow rate of 4.1 g/sec.

Each MPD thruster accumulates 15% of the electrical energy at the anode in the form of thermal energy. This heat is

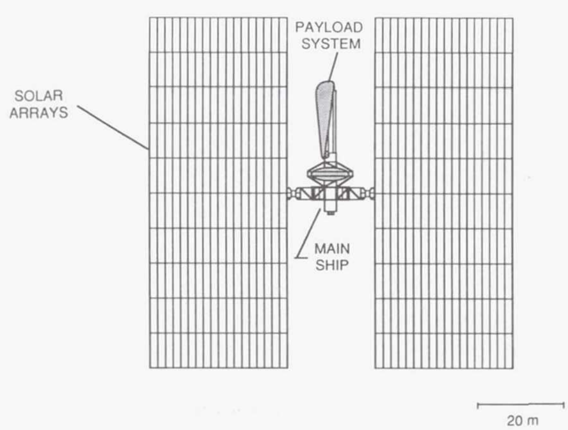

Fig. 13. MPD-Propelled Spacecraft

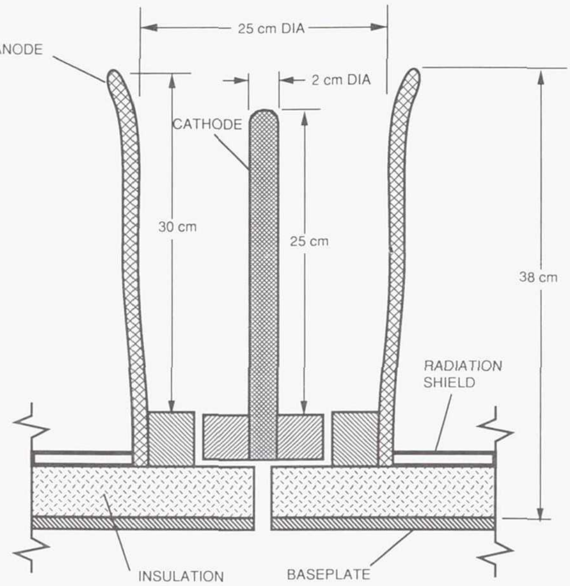

Fig. 14. Cross-section of MPD Thruster

radiated into space, resulting in an equilibrium anode temperature of 2000 K. Heat transfer to the main body of the spacecraft is minimized through a tungsten radiation shield and a layer of insulation. The solar heat flux into the cryogenic propellant tank is attenuated by covering the propellant tank with a multilayer insulation.

Power Supply

The power to operate the MPD thrusters is supplied through solar photovoltaic arrays. Two solar arrays, with a total solar cell area of 11,100 m^2 are placed on either side of the MPD-propelled spacecraft and combine to produce 3.21 MW of electrical power in the vicinity of Earth. As the spacecraft ascends from the initial LEO, it travels through the Van Allen radiation belts, encountering intense electron and proton radiation. Consequently, the solar cells must minimize the amount of degradation damage suffered as a result of this radiation and maintain a sufficient level of power input to the MPD thrusters. Indium phosphide solar cells were selected to circumvent this problem. These solar cells are capable of a process known as self-annealing, which allows the cells to return to their initial level of performance after suffering radiation damage[(18)]. The self-annealing process draws current from functional cells through forward-biased diodes within damaged cells. Through this procedure, the degradation effects of the Van Allen radiation belts can be reversed.

Solar cell efficiencies of 21% are required to successfully complete this mission, while indium phosphide solar cells have achieved experimental efficiencies of only approximately 13.6%. Although gallium arsenide solar cells, the most advanced solar cells to date, have achieved efficiencies of 20%, they suffer considerable amounts of degradation through the Van Allen belts[(18-20)]. Gallium arsenide solar cells also degrade with age and do not provide an optimum selection for long-term use in martian orbit. Therefore, in the interest of extended life of the spacecraft, indium phosphide solar cells appear to be the most suitable alternative. The use of indium phosphide solar cells, however, hinges upon anticipated increases in efficiency and production level[(20)]. The overall mass of the solar array system is 28,000 kg.

The solar arrays supply electrical power at a current of 16.4 kA and a voltage of 200 V to prevent any arcing between adjacent solar cells[(21)]. These current and voltage levels must be conditioned to the corresponding requirements of the MPD thrusters (75 V at 8.1 kA). The power conditioning equipment consists of a DC to AC converter, a constant voltage transformer, and a rectifier. The total efficiency of the power conditioning components is 95%.

The solar arrays also provide power to stationkeeping systems throughout the mission. Stationkeeping equipment consists of navigation and guidance controls, thruster management systems, and array alignment controls. Stationkeeping operations must be maintained constantly throughout the mission. Consequently, during the travel time spent within the shadow of the Earth (i.e., during parts of the escape spiral), where solar energy is unavailable, an alternate power source is necessary. Nickel hydrogen batteries, with a specific power of 100 Whr/kg, are used to power the stationkeeping equipment when in the shadow[(22)].

Engine start-up and control systems also function through power delivered from the solar arrays. Power is accumulated as electric charge across a small capacitor bank. At the beginning of the mission, as well as after each coast phase, the capacitor is discharged, resulting in a 500-V pulse across the electrodes within each MPD thruster, which is sufficient to initiate the arc[(16)].

Structures

The support structure of the MPD-propelled spacecraft requires a material with a high tensile strength to provide a rigid structure, as well as a low density to minimize the total

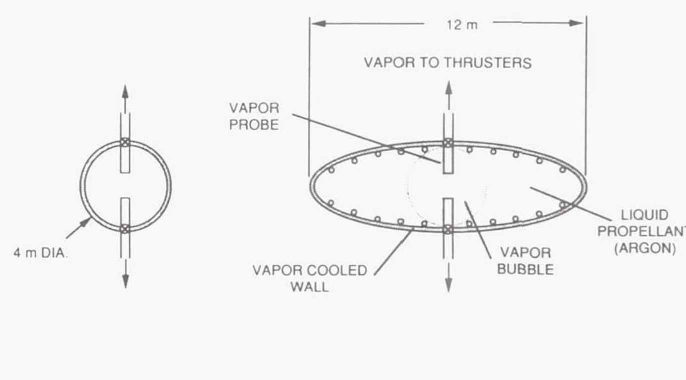

Fig. 15. Propellant Storage Tank for MPD Propulsion System

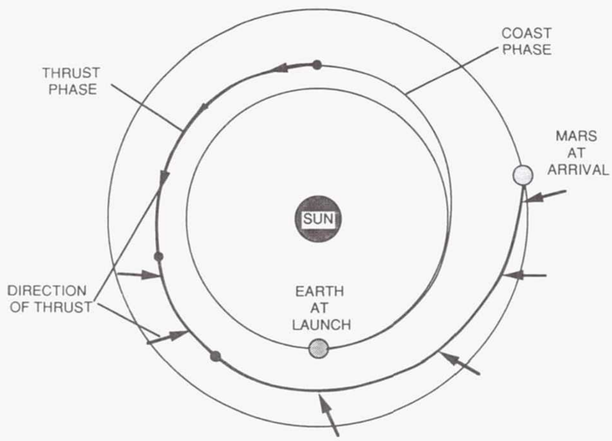

Fig. 16. Earth to Mars Spiral Trajectory (Spiral Escape from Earth Not Shown)

vehicle mass. A graphite/epoxy material with a tensile strength of 1.34×10^9 N/m^2 and a density of 1490 kg/m^3 was selected as a suitable structural material. The graphite/epoxy is fabricated into truss elements of hollow cylindrical tubes. Support trusses for the MPD-propelled spacecraft consist of both tetrahedral truss configurations and box truss configurations.

Contiguous truss elements are interconnected through titanium fittings and titanium nodes(23). The titanium fittings are threaded to provide a functional method of assembly in LEO, as well as a minimal chance of separation between adjacent truss members. Each solar array is attached to the main body of the spacecraft through a solar α joint(7). This joint allows each array to rotate about one axis and transmits electrical power from the solar arrays to the power conditioning components within the main body of the spacecraft. The total structural mass of this MPD-propelled spacecraft is approximately 8700 kg. The overall mass of the spacecraft, including the propellant, is 265,000 kg, indicating a payload mass ratio of 19%.

Orbital Mechanics

The orbital mechanics of the MPD-propelled spacecraft first involves a constant thrust maneuver to escape the gravitational influence of the Earth. Upon exiting the Earth's sphere of influence, the spacecraft assumes a heliocentric orbital transfer, which includes a coast phase, followed by acceleration and deceleration phases to match the velocity of the spacecraft with the orbital velocity of Mars around the sun. The interplanetary trajectory of the MPD-propelled spacecraft is shown in Fig. 16. As the distance of the spacecraft from the sun increases, the power available for the MPD thrusters decreases. To maintain thruster efficiency, the number of operating thrusters is decreased to match the available power. At Mars only two thrusters can be used. Upon approach to Mars, the payload is released to follow an aerobrake maneuver to a low Mars orbit, while the mother spacecraft follows a spiral maneuver into a high Mars parking orbit. The total time of transfer to Mars is approximately 2.39 years.

CONCLUSIONS

Each propulsion system collects and exploits solar energy in very different ways. The spacecraft designs are unique according to the individual requirements of the propulsion system. The solar radiation absorber (SRA) system directly concentrates the solar radiation into two chambers where it is absorbed by alkali metal vapor that transfers the energy to the primary component of the propellant, hydrogen. The solar-pumped laser (SPL) system uses concentrated solar energy to pump two 6 MW CO_2 lasers located on two platforms in sun-synchronous orbit around the Earth. The resultant laser beams are directed and transmitted to receivers on the spacecraft, which relay them to two thruster chambers, where the laser beams generate a hydrogen plasma. The magnetoplasmadynamic (MPD) system converts solar energy to electricity that is used to ionize argon and accelerate the resultant plasma by electromagnetic body forces. Specific impulses vary from 1000 sec for the solar radiation rocket to 2450 sec for the magnetoplasmadynamic thruster.

The SRA system offers the largest payload mass fraction (37%) and the lowest initial mass (135,500 kg). The latter is an important parameter because all of the components, materials, and propellant necessary for the Mars cargo mission must originally be brought up from Earth to LEO. Thus, even with anticipated reductions in the cost of lifting payloads to LEO, there is a great premium on minimizing the initial mass of the interplanetary spacecraft. The SRA system presents a number of important technological problems, however. Although experimental proof of concept has been demonstrated, much work remains to be done on the physics of the interaction of solar energy with the alkali-seeded hydrogen, on the handling of the high-temperature corrosive potassium, on the design of a suitable window, and on the problems of heat transfer and erosion in the thrust chamber. Research in these areas is currently under way at the University of Washington.

Although the SPL system offers a payload mass fraction of 24%, it requires a complex infrastructure of space-based lasers and relay units, as well as extremely stringent tracking capabilities. The latter could be ameliorated by using an orbital mechanics scenario similar to that of the SRA system. Many additional problems also need to be resolved before the laser propulsion concept can be implemented. The required CW laser power levels have not yet been attained on Earth. Additional research is needed in the areas of plasma stability, reradiation losses, and cooling requirements. Even tor an optimal orbital transfer scenario, the complexity and cost of the entire system is likely to make it impractical.

The MPD propulsion system appears to be the most technologically feasible at this time; however, its implementation is predicated on the availability of indium phosphide photovoltaic cells of 20% efficiency. Even so, its payload mass fraction (19%) appears to be only marginally better than that which might be achieved using a shuttle-derived chemical

propulsion system. Optimization studies need to be performed to enhance the payload mass fraction and to reduce the initial mass of the solar-MPD system.

The propulsion concepts presented here use the most abundant source of energy available in space: the sun. However, much further research is required if this resource is to be effectively exploited to transport large payloads to Mars and other planets within the solar system.

ACKNOWLEDGMENTS

Authors were J. Auzias de Turenne, M. Beall, J. Burianek, A. Cinniger, B. Dunmire, E. Haberman, J. Iwamoto, S. Johnson, S. McCracken, M. Miller, N. Phelps, A. Prochko, M. Rhodes, T. Schmitt, J. Slostad, R. Teeter, J. Thorpe, T. Tran, T. Unger, and J. Wornath. Faculty advisors were Professors Adam Bruckner and Abraham Hertzberg.

REFERENCES

1. Sutton G. and Ross D., *Rocket Propulsion Elements,* John Wiley & Sons, New York, 1976.
2. Mattick A. T. et al., "High Temperature Solar Photon Engines." *J. Energy, 3,* 30-39, 1979.
3. Taussig R. et al., "Solar-Pumped Lasers for Space Power Transmission." AIAA Paper No. 79-1015, June 1979.
4. Rault D. F. G., "Radiation Energy Receiver for High Performance Energy Conversion Cycles." Ph.D. dissertation, University of Washington, 1983.
5. Mattick A. T., "Coaxial Radiative and Convective Heat Transfer in Gray and Nongray Gases." *J. Quant. Spectrosc. Radiat. Transfer, 24,* 323-334, 1980.
6. Thomas M. and Friese G. J., "Pressurized Antennas for Space Radars." AIAA Paper No. 80-1928, 1980.
7. Mikulas M. and Bush H., "Design, Construction, and Utilization of a Space Station Assembled From a 5 Meter Erectable Truss." NASA TM-89043, October 1986.
8. Kantrowitz A., "Propulsion to Orbit By Ground-Based Lasers." *Astronaut. Aeronaut., 10,* 74-76, May 1972.
9. Glumb R. J. and Krier H., "Concepts and Status of Laser-Supported Rocket Propulsion." *Astronaut. Aeronaut., 21,* 70-79, August 1983.
10. Eskridge R. H. et al., "An Experimental Study of Laser Supported Plasmas for Laser Propulsion." NASA TM-86583, Marshall Space Flight Center, Huntsville, Alabama, January 1983.
11. Keefer D. R. and Crowder H., "A Two-Dimensional Model of the Hydrogen Plasma for a Laser Powered Rocket." AIAA Paper No. 82-0404, January 1982.
12. The Harshaw Chemical Company. "High Power Laser Optics." TP120478.
13. Allcock H. R., "Polyphosphazenes: New Polymers with Inorganic Backbone Atoms." *Science,* 193, September 24, 1976.
14. Cassady R. J., "An MPD Thruster Driven Cargo Ferry for Support of the Manned Mars Mission." AIAA Paper No. 88-2896, July 1988.
15. Jahn R. G., *Physics of Electric Propulsion.* McGraw-Hill, New York, 1968.
16. Coomes E. P. et al., "The Pegasus Drive - A Multimegawatt Nuclear Electric Propulsion System." In *Space Nuclear Power Systems 1986,* pp. 365-373, Orbit Book Co., Malabar, Florida, 1987.
17. Carney M. J., "Liquid-Vapor Interface Locations in a Spheroid Container Under Low Gravity." NASA N86-23854, April 1986.
18. Brinker D. J. and Weinberg I., "Indium Phosphide Solar Cells — Status and Prospects for Use in Space." NASA TM-87315, Lewis Research Center, Cleveland, Ohio, 1986.
19. Hess W. N., *The Radiation Belt and Magnetosphere.* Blaisdell Publishing Co., New York, 1968.
20. Weinberg I., Personal Communication, February 1989.
21. Stella P., Personal Communication, February 1989.
22. Faymon K. A., "Space Power Technology to Meet Civil Mission Requirements." AA420 Guest Lecturer, University of Washington, January 31, 1989.
23. Franz J. and Laube J., "Design and Manufacturing Aspect of Tubular Carbon Fiber Composite/Titanium Bonded Joints". In *Composite Structures,* Elsevier Applied Science Publishers Ltd., United Kingdom, 1986.

19940454Z
383652
2P
Swp

N94- 71297

530-66
160656
p. 2

SUMMARY OF ACTIVITIES

UNIVERSITY OF WISCONSIN, MADISON

MARS PENETRATOR DRILLING MECHANISM

Design work on the Mars Penetrator Project, in cooperation with the NASA Ames Research Center, is being continued. This semester's efforts are focused on the drilling mechanism which must penetrate the martian subsurface soil to collect and retrieve an uncontaminated sample. It is also desired that the sample acquisition process be repeated several times throughout the mission. The previous design concept established in the Fall '88 semester has raised much skepticism concerning both its ability to cut into the hard soil repeatedly and the effectiveness of the sample retrieval concept it employed. (Refer to the NASA/USRA 1988 Mars Penetrator Report). Analytical as well as experimental investigations have found the design to be insufficient for the performance level required by the mission. A new design to collect martian soil samples more efficiently is recommended. The new design consists of a rotary-percussive drill mechanism. This mechanism is optimum for dry drilling, necessary to avoid contamination of the soil sample, in many different soil types. In order to incorporate the rotary-percussive drill into the system, a redesign of the entire drive mechanism is in progress. This was necessary since the motor will now rotate the bit as well as deliver an axial impulse. The vibrational motion of the drill bit allows for a much more effective means of retrieving the soil sample. Inclined planes (much like saw teeth) will be put in the hollow drill bit. The pulses of the bit will stimulate a vibrational conveyor and cause the sample particles to migrate back into the penetrator. This method will eliminate the need, as in the previous design, for the additional inner bit to move the sample.

THE MARTIAN EGG SAMPLING DEVICE

The need for a small, relatively inexpensive device to study the chemical structure of the martian soil was established. The egg design was chosen for its low cost compared to other systems and potential for a large number of eggs to be deployed on the martian surface.

The design process included analysis of the dynamics of reentry, dissipation of heat during reentry, impact with the surface, access to undisturbed soil samples, and ability to gather samples from the soil at three depths. The egg consists of the reentry systems, soil probe lifting system, soil probe package, gas chromatograph, transmitter, and battery power supply. The egg must function only once, but is designed to withstand one martian year.

Initially, the probe is protected by an ablative aeroshell, which dissipates most of the heat generated by friction with the atmosphere. A ballute and parachute system are used as a first and second stage in slowing the probe during descent. The aeroshell is released when the parachute is deployed. The probe impacts the surface at 10 m/s to minimize the impact crater depth. The soil probe package is lifted out of the impact crater by an inflating polymer balloon. The soil probe falls to the side, out of the crater, in the correct orientation. A porous, telescoping tube is inserted into the soil. The force required to insert the probe is calculated to be 7N. Gases from the soil are evolved by heating the soil at the specified depths. They are drawn into the probe and analyzed by the gas chromatograph.

MARTIAN MOLE SAMPLING DEVICE

The Mars Mole is designed as a rover-based device which penetrates the martian soil to a depth of up to 10 m, obtains a sample of soil, and returns it to the surface for analysis. Samples from that depth will provide valuable information about the history and geology of Mars, possibly including evidence of past life forms. The device was designed to meet the following specifications: (1) Weight <10 kg; (2) Size <20×20×30 cm; (3) Power <1000 W; (4) Ability to obtain sample of at least 5 cc; (5) Ability to penetrate fine, loose sand; and (6) Need to obtain at least one sample.

The design chosen was one which uses one front auger-like drill to move the soil from in front of the mole and eight side augers which move the soil along the outside of the mole. The side augers also provide downward force as well as directional control. The mole will operate in this manner: (1) Rover arrives at suitable site; (2) Rover's robotic arm deploys the mole and provides initial push into ground; (3) Mole digs to required depth, steering around obstacles; (4) Sampling device takes sample into mole; (5) Mole returns to surface by reversing side auger motion and is retrieved by a tether; and (6) Removal of sample and analysis of specimen are accomplished on rover. The mole will need approximately four days to complete its mission at a site.

SPACE STATION UMBILICAL CONNECTOR PROJECT

This project is a device which provides the translational motion of the connectors on the Space Station *Freedom* to allow engagement for power and data transfer. The design is capable of delivering a 20-lb force within the necessary tolerances and will operate reliably in the space environment. In providing this motion, restrictions include a predetermined size, engagement forces, and reactionary force. The device designed uses two linear motors incorporating two latches which limit the resulting external force. The motors move the latches into the proper engagement position. The latches are released into a neutral position, accounting for any misalignment. With the latches in position, the motors' relative directions are reversed and a plug is drawn into a receptacle. The plug is rigidly fixed to the platen of the motor which is

PRECEDING PAGE BLANK NOT FILMED

PAGE 344 INTENTIONALLY BLANK

fixed to the envelope by a motion restricting device. The plug and receptacle use a pin and cone alignment device to adjust their positions in the lateral and cone. The movement is reversed for disengagement.

1994004543
383653
10p

N94-71298

PROPELLANT RESUPPLY OF ORBITING SPACECRAFT

S31-66
160657

WORCESTER POLYTECHNIC INSTITUTE

p. 10

The technology to transfer safely and easily fluids in microgravity is necessary to extend the duration of future space missions. The absence of gravity in space causes fluids to behave much differently than on Earth, making propellant resupply extremely difficult. The Gamma Ray Observatory (GRO) is one of the satellites being designed for refueling. The GRO's thrusters are fueled by the monopropellant hydrazine that as a vapor is unstable above 200°F. This has a major impact on refueling system design and operation. A system using high pressure gas and flexible diaphragms to transfer propellant from a supply vehicle to the GRO was proposed and designed. A ground-based system utilizing the transfer technique of ullage recompression was built to investigate the process.

INTRODUCTION

The number of satellites orbiting the Earth is steadily increasing to meet the demand in areas such as telecommunication, Earth imaging, military surveillance, and astronomy. Many of these satellites are positioned in low Earth orbit (LEO) and experience a slight amount of atmospheric drag, tugging them Earthward. Thrusters are used to maintain the altitude of a satellite and as a result mission length for many of these satellites is limited by the amount of fuel carried on board. When the propellant tanks are empty, the satellite no longer has the ability to maintain orbit or maneuver. After a period of time, the orbit decays to the point where the satellite enters the atmosphere and disintegrates. Refueling satellites in orbit with either storables or cryogenics would eliminate the need to replace those satellites that consume all of their propellant.

In addition to propellants, many satellites require cryogenic liquids to cool instrumentation. When these coolants are exhausted, the ability to control temperatures is drastically decreased.

There are several benefits to developing a fluid transfer system. The first is that orbital resupply of satellites will substantially increase their productive life. While it may be possible to retrieve these satellites, this would be costly and the satellites are at greater risk during launch. Therefore, it is more effective to refuel these satellites in orbit. Another benefit of refueling satellites in orbit is that their structural weight could be considerably reduced if they were launched with minimal fuel. This would permit greater design flexibility in future satellites[1].

This design effort focused on refueling the Gamma Ray Observatory (GRO), which is one of the few satellites designed for refueling. The thrusters it uses for altitude adjustment are fueled by the liquid propellant, hydrazine. Since hydrazine is a monopropellant, no oxidizer is necessary for ignition. However, its vapor is volatile and may decompose at temperatures above 200°F. This has a major impact on on-orbit refueling system design.

In space the effects of gravity are almost nonexistent, causing fluids to behave much differently than they normally do on Earth. The interface between liquids and gases becomes spherical in reduced gravity. Additionally, a gas bubble may occupy random locations in a liquid because the difference in densities of liquid and gas has no effect in microgravity. Because of this behavior, liquids and gases in storage tanks are separated by a flexible diaphragm. This is the case with the GRO's storage tanks where hydrazine and pressurant are separated by a diaphragm. This is not possible with cryogens because the extremely low temperatures cause cracking of the diaphragm.

In addition to designing the refueling module that performs the actual resupply, consideration was given to the types of satellites to be refueled; the vehicle to launch the refueling module; and its compatibility with the space shuttle, space station, or Orbital Transfer Vehicle (OTV).

Once the overall resupply system was designed, a small-scale fluid transfer system was built to test the transfer process. During the fluid transfer, temperature, pressure, and flow rate were measured. The results aided in making certain design decisions.

GAMMA RAY OBSERVATORY

There are several satellites that might benefit from the development of an orbital refueling system, including the GRO, which will be fueled by the storable monopropellant hydrazine. The use of hydrazine simplifies propulsion system design because no oxidizer is required for ignition and since it is a liquid at nominal conditions as compared to cryogens, only limited thermal control is necessary.

The GRO is a low Earth orbiting satellite equipped with scientific instruments designed to gather information on gamma rays that are high-energy photons produced by astronomical events. Because gamma rays are relatively sparse, large instruments are necessary. The main body of the GRO measures 25 ft long, 15 ft high, and 15 ft wide. With propellant, it weighs approximately 35,000 lbm. The four large instruments alone weigh 12,000 lbm[2].

In 1990 the GRO will be launched by the shuttle into an orbit 160 miles above the Earth at an inclination of 28.5°. It will then move to an altitude of 250 miles using its propulsion system, which contains a maximum of 4240 lbm of hydrazine when all four of its tanks are full (1060 lbm per tank). On the GRO's 24-month basic science mission, the propellant will serve three purposes: (1) ascent from or descent to the shuttle; (2) periodic reboost to compensate for orbital decay due to

drag; and (3) controlled deorbit to provide safe reentry into the Indian Ocean.

The GRO will have the capability to be refueled when necessary. However, the fuel carried at launch should last for the GRO's two-year mission. It may then be refueled to extend its life in orbit or be permitted to reenter the atmosphere and fall into the Indian Ocean.

The GRO's propulsion system consists of several major subassemblies including tanks, piping, thrusters, and instrumentation. The four diaphragm propellant tanks are capable of supplying up to 4240 lbm of hydrazine to an orbit adjust thruster module (OATM) consisting of four 100 lbf thrusters. Two thruster isolation valves limit the amount of hydrazine in the feed lines between the valves and engines. The thrusters are able to adjust the GRO's orbit altitude. Four dual thruster modules, each consisting of two 5 lbf thrusters, are used for attitude control. The two propellant distribution modules (PDM) contain feed system filters, propellant pressure transducers, and latching isolation valves. Also, there are two propellant and pressurant fill-and-drain modules (FDM) and the satellite's portion of refueling coupling.

The GRO propellant tanks are conoellipsoidal in shape and are built by welding together two nearly symmetrical titanium alloy shells. The tanks have a 36-in internal diameter and a 47-in internal length. An elastomeric diaphragm is attached at the tank equator by a welded retaining ring. The purpose of the diaphragm is to separate the liquid propellant and the pressurant. However, small amounts of hydrazine may cross the diaphragm to the pressurant side. The tanks weigh 95 lbm each and have a minimum usable volume of 36,626 in^3. The maximum operating temperature of the tank is 102°F with a maximum operating pressure of 465 psia and a minimum burst pressure of 800 psia. The expulsion of the fuel is performed by blowdown from a pressure of 400 psia to 84 psia at a design temperature of 45°F[2].

When fuel is needed for propulsion, it is expelled from the tanks using a blowdown system. It passes through the PDM that controls the propellant flowpath (to the OATMs or DTMs). The PDM can also control the quantity of propellant in each tank through the use of its crossover isolation valves.

The GRO is resupplied through the NASA standardized refueling coupling. The two fill-and-drain modules containing the eight propellant and pressurant fill-and-drain valves can then be utilized to resupply the fuel (hydrazine) and at the same time restore the pressurant (nitrogen) through ullage recompression.

REFUELING MODULE REQUIREMENTS

With the GRO identified as the initial user of a propellant transfer system, the refueling module that will perform the orbital fluid resupply was considered. The refueling module had to be flexible enough to operate from the shuttle, the space station or an OTV and to accommodate launch by either the shuttle or an Expendable Launch Vehicle (ELV). The purpose of this refueling module was to resupply systems operating on storable monopropellants such as the GRO. Martin Marietta has designed a monopropellant refueling module to resupply satellites such as the GRO (Fig. 1). It consists of the four major subsystems listed below with the key features of each[1].

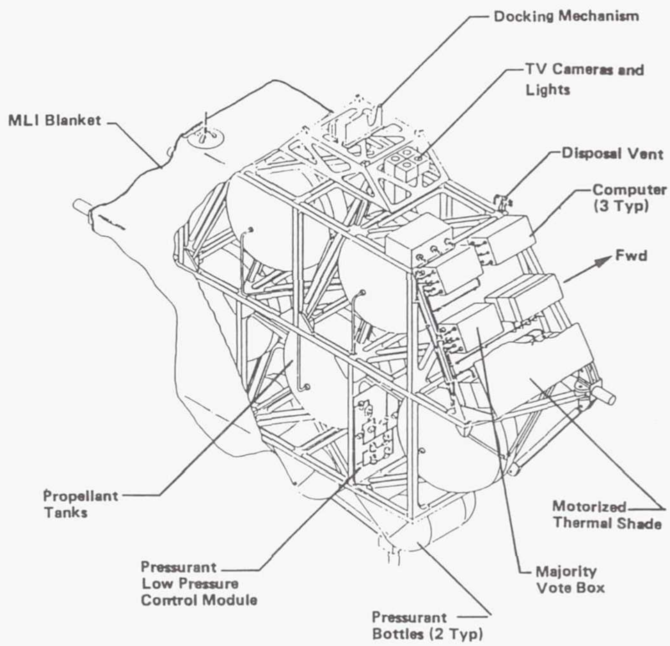

Fig. 1. Proposed Storable Monopropellant Refueling Module[1]

Fluid System	• five hydrazine storage tanks with maximum propellant capacity of 4850 lbm
	• mass fraction (payload/total weight) of 0.66
Structural	• bolted aluminum structure,
	• maximum total weight of 7850 lbm
Avionics	• two-fault tolerant majority vote for data handling and control,
	• third computer capable of providing control and monitoring should two fail
Thermal Control	• external multi-layer insulation blanket

Two options are available for placing such a refueling module into space, either in the shuttle or an ELV. Launching the refueling module in the shuttle would allow the module to perform resupply operations directly from the payload bay without removal. The refueling module could also be removed from the shuttle and docked with the space station or an OTV. The module could later be loaded into the shuttle for return to Earth if necessary.

Launch on an ELV is also possible. The ELV must be able to transport the refueling module to a proper orbit for retrieval by an OTV. An ELV currently being designed by NASA is the Titan IV. It offers the largest payload fairing diameter (5 ft) for an ELV, which is comparable to the shuttle's. Either launch

system could be used to transport the same refueling module without major modifications.

The ELV could deliver the refueling module into orbit, but then an OTV would have to intervene and transport the module from this point. An OTV would be able to deliver payloads through major orbit changes such as from LEO to geosyncronous orbit or from one inclination to another. Such a vehicle would be launched by either the shuttle or an ELV assembled at the space station, and remain there when not in use(3). For refueling operations, an OTV should be space based, reusable, have a manned capability, and be able to carry enough payload to refuel the satellite with the largest propellant capacity designed for refueling.

There have been several designs for OTVs in recent years. One design that utilizes aerobraking was developed by NASA(4). This OTV includes an aerobraking device that acts as a heat shield and "forms the basis of the support structure of the propulsion system and other systems" of the vehicle(3). This OTV is able to carry a crew and place a payload of 29,800 lbm into GEO or carry 15,700 lbm from LEO to GEO and back.

Once the refueling module is successfully placed into orbit, it can perform resupply operations from the shuttle cargo bay, from a docking area on the space station, or directly from an OTV. Once operational, the refueling process could be performed either by a crew member or robotically.

While the subsystems of the refueling module and all the possible scenarios are extremely important to the success of the refueling process in space, the major aspect of the design focused on the fluid subsystem.

PROPELLANT AND PRESSURANT TRANSFER PROCESS

Numerous propellant transfer methods and scenarios have been proposed for the on-orbit propellant resupply of satellites. The various methods depend upon the type of tank being resupplied, the type of tank being used to supply propellant, and the type of propellant being resupplied (cryogen or storable). Most of the methods can be placed into one of three general categories: ullage recompression, ullage vent, or ullage exchange. Ullage is the combination of pressurant and any residual vapor (hydrazine) present. A summary of their key advantages and disadvantages is shown in Table 1.

Since the most promising user of expendable resupply is the GRO, the transfer system was designed to be compatible with this satellite.

The ullage recompression method of propellant transfer was chosen to resupply the GRO propulsion system because of its operational and mechanical simplicity. Venting pressurant should be avoided because pressurant resupply would be necessary. Also, volatile and corrosive hydrazine vapor may be mixed with the pressurant, and venting the combination could expose hardware and personnel to it. Ullage recompression involves forcing liquid into a tank containing low pressure gas and possibly some liquid. As the volume of liquid in the receiving tank increases, the gas is compressed. This method is compatible with either screen, vane, or diaphragm tanks with cryogens or storables. The resupply would "ideally be performed from a system pressure regulated at a pressure equal to or greater than the maximum initial blowdown pressure in the receiver system (typically about 350 psia)"(2). The major advantages to ullage recompression are its simplicity and that pressurant resupply of the receiving tank is not required.

Table 1. In-orbit Propellant Transfer Options(4)

Options	Advantages	Disadvantages
Ullage recompression	• Mechanical simplicity; no provisions required for purging and repressurizing tank ullage	• Requires large heat dissipation and resulting long transfer time
	• Operation simplicity; only propellant transferred	• Pressure of refueling supply must be higher than beginning of life propellant tank pressure
	• Propellant flowmeters not required. PVT data can be used to measure fuel load	
	• Refueling/repressurization accomplished simultaneously	
Ullage vent/ repressurization	• Low pressure propellant supply	• Mechanically and operationally more complex than ullage recompression
	• Lower heat of compression than ullage recompression during repressurization	• Propellant metering required
Ullage exchange	• Constant pressure propellant transfer	• Mechanically and operationally more complex than ullage recompression
	• Lowest compression heating	• Propellant metering required
	• Operationally less complex than ullage vent	• Requires ullage positioning acquisition device in receiver
	• Simultaneous tank fill possible	

The recompression process produces an increase in pressurant temperature in the receiving tank. Small amounts of hydrazine may be present on the gas side of the diaphragm due to the permeability of the diaphragm or leaks. If the temperature of the ullage reached 200°F because of rapid filling, ignition could occur.

Since hydrazine can decompose at 200°F, the substantial increase in temperature may be hazardous. Therefore, the heat generated during the resupply process must be dissipated to the liquid hydrazine and tank walls to ensure the vapor temperature does not exceed design temperatures. This dissipation is difficult because although conduction in microgravity is the same as on Earth, free convection in microgravity is much less than on Earth. Thus the flowrate at which the transfer takes place must be restricted to ensure adequate time for heat dissipation.

FLUID TRANSFER SYSTEM REQUIREMENTS

The fluid transfer system is at the center of the orbital refueling system. It is within the fluid transfer system that the pressurant and the propellant to be resupplied are contained. The primary requirement of the fluid transfer system is the ability to deliver fuel to satellites on-orbit. After the refueling module docks with a satellite, the propellant can be transferred to the satellite. Many satellites use a blowdown system to deliver fuel to their thrusters. A blowdown system uses high-pressure gas to push fuel through a series of valves and pipes to the thrusters.

Another important requirement for the fluid transfer system is the ability to contain and control an emergency situation caused by either component failure or human error. Redundancy and backup systems are necessary to protect against accidents. This is important because hydrazine is volatile and extremely corrosive to many materials. Safety is a vital concern in space. It is important that a system be able to handle a worst case scenario.

Martin Marietta has designed a monopropellant refueling system to resupply satellites such as the GRO. The system provides the propellant tankage, pressurant storage, control valving, and vent provisions required to safely transfer hydrazine to appropriate satellites. It consists of four major elements: pressurization subsystem, catalytic vent subsystem, propellant storage subsystem, and propellant distribution subsystem. After careful review of the Martin Marietta design, a simplified transfer system was designed to test the concepts established by Martin Marietta engineers. This simplified prototype system aided in identifying the critical needs of the fluid transfer system.

INVESTIGATION AND ANALYSIS OF THE FLUID TRANSFER PROCESS

Introduction

Once a preliminary design was proposed for the orbital fluid transfer system, an engineering simulation approach[5] was chosen to provide design and operational data for on-orbit heat transfer analysis. By using an engineering simulation approach, a small scale, ground-based transfer system could be used to aid in determining design parameters for an actual orbiting fluid transfer system. Tests could be run at conditions similar to those expected for the full-scale system. This approach assumed that the transfer process was too complex to understand from basic principles, therefore the total process was studied and the results were scaled.

Heat Transfer in Microgravity

There are three modes of heat transfer to be considered in analyzing any heat transfer problem: conduction, convection, and radiation.

Convective heat transfer may be in the form of either forced convection or free convection. In orbit, forced convection is significant in fluids moving at high velocities such as pipe flow. Natural convection, which is caused by density gradients within a fluid, can be significant on Earth, but it will have a much smaller effect in microgravity.

Radiation heat transfer is frequently important in space design, but it should not be in the fluid transfer system design. Because the transfer system will be thermally insulated from the environment and inside the propellant tanks temperature differences are relatively small, thermal radiation can be assumed to be negligible when analyzing ullage recompression.

Conduction heat transfer is always present except when no mass is present such as in a vacuum. Limiting heat transfer to conduction provides a lower bound for heat transfer where convection could occur. Following NASA guidelines, calculations based on conductive heat transfer should be used to determine only conservatively low heat transfer rates in orbit[5]. To estimate expected heat transfer rates, both convection and conduction must be considered.

Scaling Consideration

Some interesting implications arose regarding scaling to larger tank sizes. "At constant fill rates, the maximum temperature rise is proportional to the absolute pressure and the flowrate, but is inversely proportional to the diameter-length product for cylinders. For constant percentage flowrates, the temperature increase is proportional to the diameter to the first power for cylinders"[6]. Convection is proportional to the temperature difference, surface area, and gravity level, and has a major impact on maximum temperature.

Experiment Design

In the design of the experimental system, there were several factors that had to be investigated before selecting and purchasing materials and hardware for the overall system including: (1) choice of working fluids (pressurant gas and transfer liquid) for ease of handling and low cost; (2) calculation of maximum expected internal tank pressure to determine material necessary for tank fabrication; (3) tank sizes and gas supply pressures that would produce suitable timelines and temperature rises; (4) calculation of the maximum velocity through the transfer piping to select a suitable flowmeter; and (5) theoretical analysis of temperature and pressure during the transfer resulting from compression and heat transfer.

The choice of working fluid and pressurant was based on safety and cost, resulting in the selection of water as the transfer liquid and a regulated air supply in the laboratory as pressurant.

Prior to fabrication of the experimental transfer system, it was necessary to calculate the maximum internal pressure. This pressure was equal to either the pressure produced by an instantaneous transfer of the entire volume of liquid from the supply tank to the receiver tank or to the maximum pressure of the pressurized air supply, whichever was more. The maximum volume of liquid was equal to twice the volume of the rolling diaphragm (4.44 l).

Since the transfer was assumed to be instantaneous, the process was both adiabatic and isentropic. Given that the initial pressure in the receiving tank was 14.7 psia and utilizing isentropic relationships, a maximum pressure of 77.42 psia was calculated. For safety reasons, supply pressure was never allowed to exceed 50 psia.

Safety was a major concern when working with high pressures. To calculate the stress limits of the storage tanks, an analysis of the cylindrical structure and its associated hoop stress was performed. The tubing used had an inside diameter of 6 in and a 0.25-in wall thickness. Since the diameter was 24 times greater than the wall thickness, it was treated as a thin-walled pressure vessel. According to the supplier, the acrylic tubing was rated to approximately 90 psid. Based on the equation for hoop stress, it was determined that the tubing was rated for a hoop stress of approximately 900 psi while the maximum hoop stress expected was 753 psi.

The maximum velocity through the piping connecting the supply and receiving tanks was required to select a flowmeter with the correct operating range. The maximum velocity was calculated based on the initial pressures in each tank, the length and diameter of piping, and the number of piping components. This was assumed to be the maximum velocity because as the transfer continues, the pressure in the receiving tank increases and the supply pressure remains constant, resulting in a lower pressure difference between the tanks.

A computer program was written to model the entire ground-based fluid transfer experiment. The algorithm calculated values of pressures and temperatures in the receiving tank as well as flow rates at incremental time steps during the transfer process.

The program initially calculated a flow rate based on the pressure difference between the two tanks. Isentropic relations were used to determine changes in receiving tank temperature and pressure resulting from compression caused by the small volume change. The small volume change was based on a small time interval and the flow velocity at the start of the time step. The second part of the program calculated new temperatures and pressures due to heat transfer from the gas to the tank walls and across the diaphragm to the liquid. The process was repeated until the transfer process was complete.

Another computer simulation utilized to model the ullage recompression process was developed at Johnson Space Center. ORSCOMP simulates a NASA space flight experiment, the Orbital Refueling System (STS 41-G), which transferred hydrazine between tanks using pressurized nitrogen. It incorporates unsteady fluid flow and heat transfer calculations for every component of the system[6]. The program calculated pressures, temperatures, and flow rates for comparison with laboratory data. There was also an option for normal Earth gravity or microgravity, which affect convection heat transfer.

The major elements of the experimental system represent the propellant storage subsystem, the propellant distribution subsystem, the pressurant distribution subsystem, and the vent system (Fig. 2).

The experimental system was designed to be easily built, to withstand expected pressures and temperatures, to accommodate the diaphragm flange retention method, and to be sized for bench-top use. Clear plastic tubing with aluminum endplates was used for the fabrication of the storage tanks because of its compatibility with these two fluids. Clear plastic made it possible to observe the system during operation.

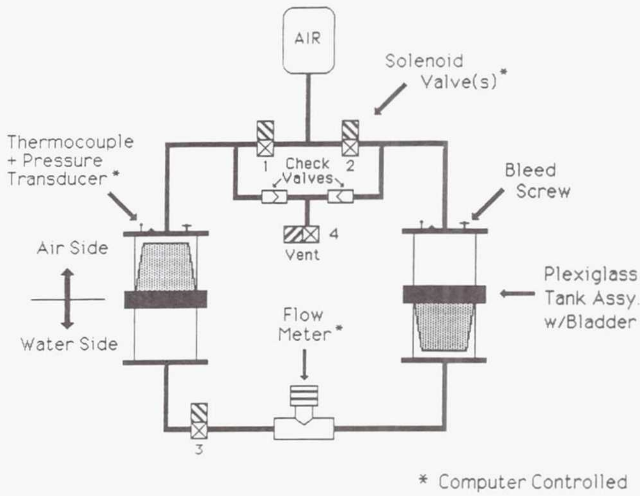

Fig. 2. Ground-based Fluid Transfer Experiment

The size of the storage tanks was determined based on several design considerations including accommodations for the diaphragm, ease in handling, the ability to fabricate using standard flanges, and ensuring the tanks would withstand system pressures.

The expulsion system was designed to utilize rolling diaphragms. The particular diaphragm was chosen because of its flat gasket-type edges that made it compatible with the available flanges and because it provided a highly reliable seal.

In order to accommodate the installation of the rolling diaphragm, the storage tanks were fabricated in two sections with the diaphragm situated in the center, allowing the diaphragm to move in either direction. The stroke length governed the amount of fluid transferred. Flanges were epoxied to the cylinder ends and were either used as the clamping hardware for the diaphragms or were bolted to aluminum plates which served as endcaps.

The fluid distribution subsystem was designed to provide a flowpath for transfer from supply to receiving tank. The subsystem also was required to permit flow in both directions. The hardware includes 0.5-in steel tubing, a solenoid valve, and a paddlewheel flowmeter. The selection of the flowmeter was based upon calculations of the maximum velocity through the system.

The pressurant distribution subsystem provided a regulated supply of air to the storage tanks for fluid transfer. This subsystem caused the diaphragm to deflect, forcing liquid from one tank to the other and compressing the pressurant side of the receiving tank. It also vented the system, allowing the tanks to return to atmospheric pressure. This subsystem insured that flow in both directions was possible. The piping components consisted of three solenoid valves, two check valves, 0.375-in

aluminum tubing, and connectors for the high pressure air supply. Also, on the pressurant side of each tank, accommodations were made for pressure transducers and thermocouples.

The control portion of the on-ground experiment was developed to control the operation and to be an intricate part of the data acquisition system. These two purposes were combined to control the experiment and record the data simultaneously using one computer. The control of the fluid flow and the pressurant supply was accomplished through the use of solenoid valves and a specially designed driver circuit that acted as an interface between the computer and the valves, allowing the computer to operate the valves when necessary.

In addition to controlling the process, the computer program handled data acquisition. The information produced during the experiment was stored by the computer. Temperature was measured by two thermocouples, one in the pressurant side of each tank. Pressure transducers were situated on the pressurant side of the receiving tanks to measure pressure. Flow data was collected from a paddlewheel-type flowmeter. The oncoming flow rotated the paddlewheel, producing a sinusoidal signal whose amplitude was proportional to the flow velocity.

Theoretical Results

The purpose of the computer model was to predict the operation of the experiment before it was performed and to aid in its design. It helped determine if the experiment would proceed within the design boundaries and also allowed for comparison with experimental data.

Review of the output for the various supply pressures yielded important information regarding the behavior of the various parameters during the transfer process. There are four groups of output for supply pressures of 25, 30, 35, and 40 psia. During the simulation, these supply pressures were kept constant. For each of the four different supply pressures, temperature, pressure, and flow rate were calculated as a function of time.

The plots for the supply pressures of 25 and 30 psia revealed a steady rise in temperature early in the transfer process. Once the temperature peaked, it slowly decreased toward the ambient temperature. The pressure curve showed the pressure in the receiving tank increasing steadily at a rapid pace toward the supply pressure. As the pressure approached the supply tank pressure, the curve leveled off and remained constant for the remainder of the fluid transfer. This leveling off was reflected in the flow rate curve, where at approximately the same time, the flow rate curve also leveled off. After the expected initial sharp increase in flow rate, it slowly decreased due to the minimal pressure differences between the supply and receiving tanks.

As the supply pressure was increased, variations were observed in the plots for the supply pressures of 35 and 40 psia. For these supply pressures, the temperature rose steadily throughout the transfer and did not peak until the latter stages of the process as heat was transferred to the surroundings. The pressure curves showed a steady increase during the process with the pressure not equal to the supply pressure until the end of the transfer.

These plots demonstrate that as the supply pressure increases, the fluid transfer rate will increase, which will cause increased temperatures.

Experimental Results

The experimental data was obtained by transferring liquid using the supply pressures used in the computer simulation (between 20 and 40 psia). There are four groups of output for the supply pressures of 22, 28, 32.5 and 37 psia. As in the computer simulation, temperature, pressure, and flow velocity were plotted vs. time.

The temperature and pressure curves for the receiving tank at the various supply pressures were all very similar in shape. In each case, the temperature rose at a fairly constant rate for about 10 sec, then increased at a slower rate until the maximum temperature was reached at about 15 sec. After the point of maximum temperature, the curves steadily decreased until they approached the ambient temperature. The pressure plots showed the pressure increasing at a constant rate for about 10 sec and then increasing at a slower rate until the maximum value was attained at 25 sec. The pressure remained at its maximum value for the remainder of the process with slight variations.

Unlike the temperature and pressure curves, which are plotted until the temperature in the receiving tank returns to ambient temperature, the flow curves are only plotted until the actual transfer process is complete (flow rate equals zero). The curves for the flow velocity indicate a sharp rise for the first 2 or 3 sec at which point the maximum value was reached. From there, the flow steadily decreased until the 10-sec mark and then decreased at a slower rate until the transfer ended.

Comparison of Theoretical and Experimental Results

When comparing the theoretical and experimental results there is a noticeable similarity. The plots for the theoretical model at supply pressures of 25 and 30 psia are very similar to those for the experimental model at supply pressures of 22 and 28 psia (Fig. 3). Had the computer simulation been allowed to continue until reaching ambient temperature, the curves for the higher pressures (35 and 40 psia) would also have been similar.

The most apparent difference between the two models was the time needed to reach the maximum flow velocity. In the theoretical model the flow was at the maximum value almost instantaneously, but experimentally it took nearly 3 sec. This may explain why, experimentally, the time required to reach the maximum temperature and pressure was longer. The less dramatic temperature rise in the experiment as compared to the computer model was probably due to the time necessary for the thermocouples to respond to temperature changes in their surroundings.

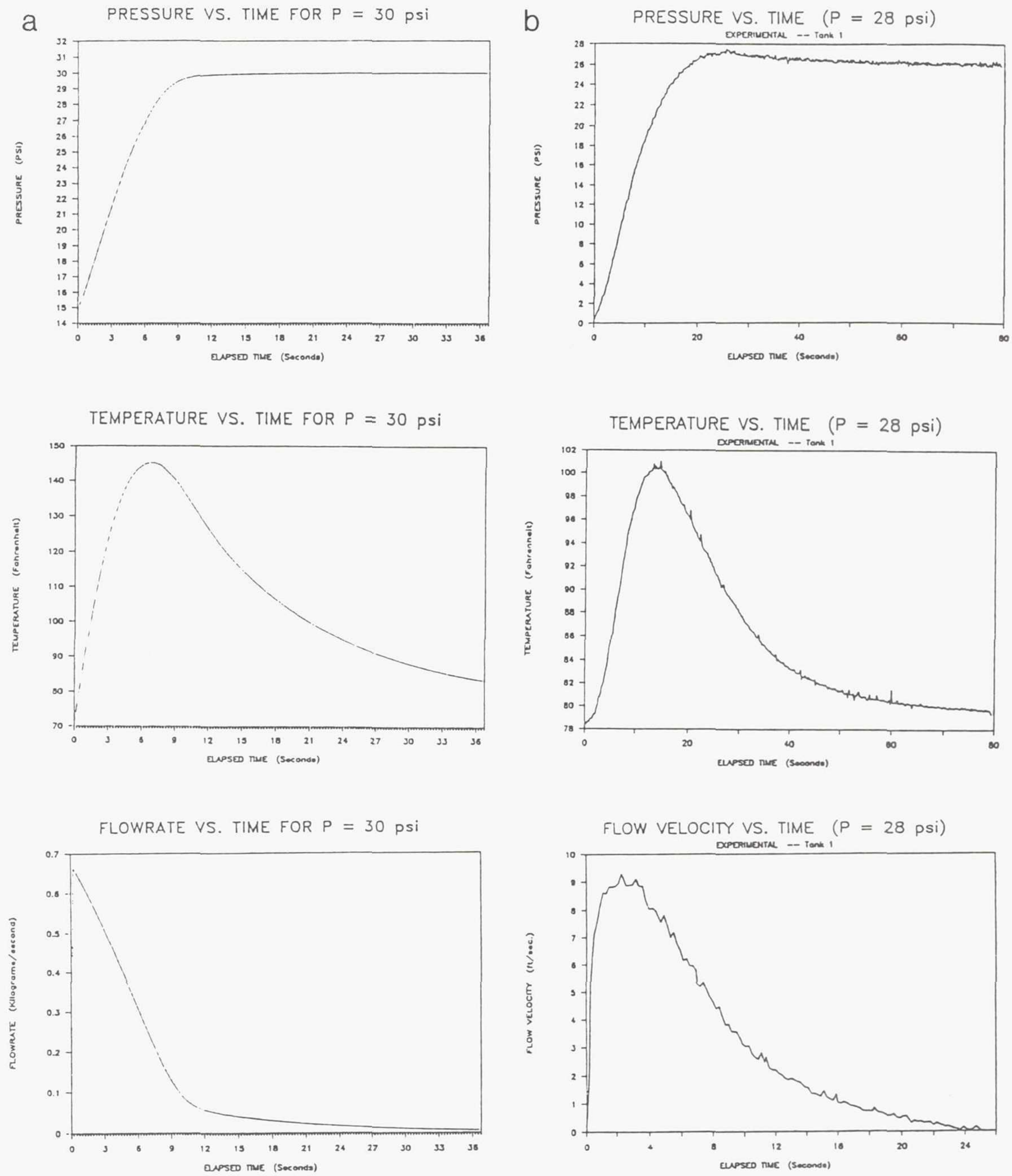

Fig. 3. Pressure, temperature, and flow rate as a function of time during fluid transfer. (a) Computer simulation (supply pressure of 30 psia). (b) Laboratory experiment pressure of 28 psia.

ORBITAL REFUELING SYSTEM DEVELOPMENT

Introduction

The experimental model formed the groundwork for the development of an orbital refueling system. It demonstrated the basic design concepts, operational guidelines, and operational procedures for handling fluids in microgravity.

Several concepts have been developed for refueling satellites on-orbit. Most proposals use existing technology. This design was based on technology and hardware requirements associated with monopropellant resupply of the GRO using

ullage recompression. Modularity was emphasized in the design, which would allow the resupply of other satellites with various consumables, and stationing in the shuttle, an OTV, or at the space station.

Fluid Transfer System Design

The fluid transfer system includes the propellant supply tanks, pressurant storage, control, and vent provisions required to permit safe hydrazine transfers to the GRO.

Consideration was first given to the propellant storage subsystem and capacity required to resupply a depleted GRO propulsion system. The GRO's propulsion system is made up of four propellant tanks having a combined capacity of 4240 lbm. It was decided that a transfer system having four propellant storage tanks operating individually or in combination would satisfy the refueling requirements of the GRO. The option of an additional propellant tank was also provided to expand the capability of the transfer system for refueling larger satellites.

After a review of existing tanks, the GRO propellant tanks were chosen. Each tank is constructed of two symmetrical titanium alloy shells with a diaphragm separating propellant and pressurant attached at the tank equator. Diaphragms provide mechanical and operational simplicity and work well with storables. Each tank has a minimum usable volume of 36,626 in^3 (1060 lbm), a 36-in diameter, a 47-in length, and weigh 95 lbm each. The minimum burst pressure is 800 psia(2).

The second design element required of the fluid transfer system was the pressurization subsystem. Since the transfer process operates in a blowdown mode, the pressurization subsystem was required to provide regulated gas pressure equal to, or greater than the maximum initial blowdown pressure in the satellite's propulsion system (approximately 350 psia for the GRO)(2).

The pressurization subsystem consists of three high-pressure nitrogen storage tanks, pressure regulators, control valves, and check valves. The major functions of the subsystem include: (1) to provide pressurant to the propellant storage tanks to permit pressurized propellant transfer; (2) to provide a pressure relief system isolation from the propellant storage system; and (3) to allow emergency propellant tank pressure reductions in the event of excessive system pressure or temperature.

A purge capability was designed into the pressurant subsystem because of the numerous concerns associated with propellant and ullage leaks, spills, and venting. Pressurant, passing through the propellant and ullage transfer lines, would clear all refueling disconnects and adjoining pipes of residual propellants prior to disengaging the resupply and receiver vehicles(4). The provision of these propellant and ullage transfer purge lines will help minimize the possibility of a leak emanating from propellant transfer.

The design of the propellant distribution subsystem was partially determined by the transfer process selected. A schematic of the system is shown in Fig. 4. Ullage recompression was chosen because of its mechanical and operational simplicity. The hardware for this subsystem consists of control

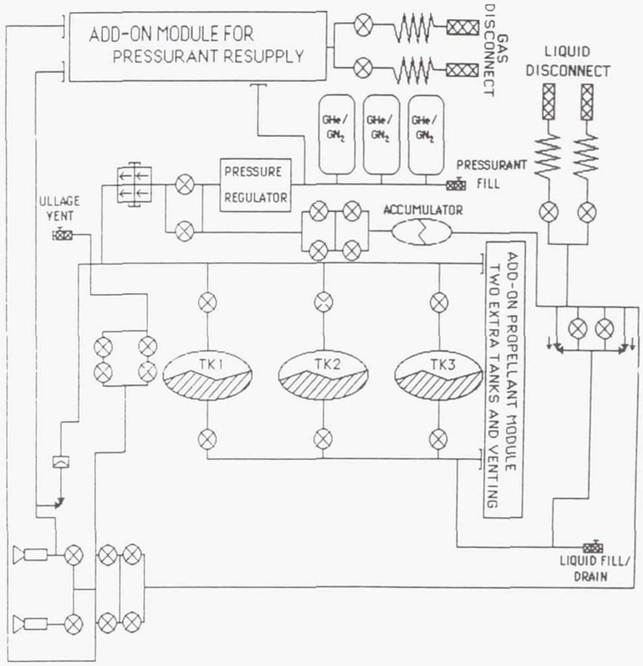

Fig. 4. Schematic of Orbital Hydrazine Transfer System

valving, service couplings, and flow meters required to control the propellant flow.

Each component in this design is required to provide tolerance to insure safety and guard against propellant leakage. Valves and couplings are critical in preventing losses in hydrazine systems. The results of a TRW study indicated that whereas gas leaks were a strong function of the inlet pressure, hydrazine leaks were not strongly affected by inlet pressure(2). The liquid servicing couplings were recommended to provide two-failure tolerance against leakage. The pressurant couplings need only be single-failure tolerant, since the tank diaphragms must fail in order to expose these couplings to propellant.

The estimated weight of the Fluid Transfer System is given in Table 2(7).

Refueling Module Design

It was necessary to develop a refueling module that provided structural, avionic, and thermal support to the fluid transfer system. Also identified was the need to develop an automatic

Table 2. Estimated Weight of the Fluid Transfer System

Nitrogen tanks (3)	165
Propellant tanks (4)	380
Piping, valves, and fittings	336
Gaseous nitrogen supply	211
Propellant	4260
Total	5362 lbm

Table 3. Estimated Weight of Refueling Module

Structure	3,190
Thermal control	273
Avionics	644
Electrical power system	516
Space maintenance provisions	476
Fluid transfer system (dry)	1,102
Refueling module	6,201 lbm
Gaseous nitrogen supply	211
Propellant	4,260
Total payload	4,471 lbm
Refueling module with payload	10,672 lbm

mating mechanism capable of performing both docking and coupling mating functions.

The major design requirement of this refueling module was to provide the flexibility necessary to service a wide range of users and to be adaptable to operation from the space station, the shuttle or an OTV. The approach to the design of the refueling module consists of a bolted aluminum structure, a two-fault tolerant/majority vote avionics subsystem for data handling and control, and a multilayer insulation blanket in combination with tank heaters for thermal control. The resupply module is capable of accommodating the design of the monopropellant fluid transfer system. An estimate of the weight of the module is given in Table 3[7].

ON-ORBIT REFUELING SCENARIO

On a mission to refuel the GRO with hydrazine the shuttle lifts off with a refueling module in the cargo bay. After the shuttle docks with the space station, the refueling module is removed from the cargo bay by a robotic arm and is attached to an OTV. The orbit necessary for the OTV to intercept with the GRO is programmed into the OTV's flight software. The crew then fire the OTV's thrusters. Several hours later the OTV moves alongside the GRO and docks with it. Two astronauts perform an EVA to connect the refueling module to the GRO's propellant tanks. Pressurant forces hydrazine from the tanks of the refueling module to the GRO propellant tanks. Gas temperature in the GRO's propellant tanks is monitored to ensure it does not rise above the design temperature (102°F). Eight hours later the propellant transfer is complete and the OTV returns to the space station.

The refueling module's empty hydrazine tanks are loaded into the shuttle for return to Earth. Subsequent shuttle flights will bring tanks full of hydrazine or other fluids for attachment to the refueling module.

The multifunctionality of the refueling module configuration provides the flexibility of launching by the shuttle or an ELV and performing refueling from the space station, OTV or the shuttle. It also serves as a common structure for various transfer systems. Flexibility in both launch and operations is provided in the refueling module's design to accommodate different users and refueling scenarios with a minimum number of modifications.

CONCLUSIONS

Based on the laboratory results, there are several observations that can be made. From analysis of the data, it was determined that for a system where the pressurant is supplied to the transfer tank abruptly, the temperature increase is dramatic and sudden. This temperature change is dangerous for hydrazine systems. Therefore, during operation of a hydrazine transfer system, the supply tank pressure should be restricted.

Instead of applying a constant pressure throughout the transfer, the pressurant supply should be regulated based on the temperature of the compressed pressurant on the receiving side. A pressure can be applied that maximizes the flowrate yet keeps the temperature of the compressed gas within safe limits. It should allow the same volume of fluid to be transferred, over only a slightly longer time span. However, it will have a stabilizing effect on the temperature profile for the transfer period.

Since the fluid transfer will be decreased, the temperature rise will not be sudden, as was the case with the experiment. Instead, the temperature will rise more slowly during the transfer and result in a lower maximum temperature. Since the duration of the transfer will be longer, the heat generated can dissipate to the surroundings and the system temperature will be lower, avoiding the high temperatures experienced with a constant pressure system.

Overall, it is important that the propellant resupply system be modular with respect to both its transportability and fluid transfer subsystem. The overall system should be flexible enough to be used in several different scenarios, such as launch by either the shuttle or an ELV, and operation from the space station, the shuttle, or an OTV with minimum modifications. Also, the refueling module itself should have interchangeable subsystems enabling it to handle various storable or cryogenic propellants, coolants, and other consumables when necessary.

ACKNOWLEDGMENTS

Principal authors P.J. Bloznalis, teaching assistant; R. Lupien, M. Sudbay, M. D'Angelo, B. Perry, and M. Vidal were assisted by faculty advisor Dr. William Durgin.

REFERENCES

1. Dominick S. M., Eberhardt R. N., and Tracey T. R., *Orbital Spacecraft Consumables Resupply,* AIAA/ASME/SAE/ASEE 24th Joint Propulsion Conference, July 11-13, 1988, Martin Marietta Space Systems, Denver, CO, AIAA-88-2922.
2. Carlson R. A., Hevert S. C., and Weatherly J. A., *The Gamma Ray Observatory (GRO) Propulsion Subsystem.* AIAA/ASME/SAE/ASEE 24th Joint Propulsion Conference, July 11-13, 1988, TRW Space and Technology, Redondo Beach, CA, AIAA-88-3051.
3. *Design of an Integrated Aerobraking Orbital Transfer Vehicle,* NASA Paper #N85-21262, 1985.
4. Chandler F. O., *Expendable Resupply Fluid System Design Issues,* Rockwell International, Downey, CA, A86-42831.

5. Boyd W. C., *Orbital Refueling Demonstration System Description*, NASA Johnson Space Center, 1983.
6. Boyd W. C. and Kauffman D., *An Analysis of Ullage Heat Transfer in the Orbital Refueling System*, NASA JSC, 1985.
7. Woodcock G. R., *Space Stations and Platforms*, Orbit Book Company, 1986.

omit

Aeronautics Projects

19940045443836548P

N94-71299

AERODYNAMIC CONTROL, RECOVERY, AND SENSOR DESIGN FOR A FIRST STAGE FLYBACK BOOSTER

S32-05
160658
P 7

UNIVERSITY OF CALIFORNIA, LOS ANGELES

The Advanced Aeronautic Design Program at UCLA for 1988-1989 consists of two projects, the flyback of the first stage of a winged air-launched booster, and the design of an adiabatic wall temperature sensor for the hypersonic regime.

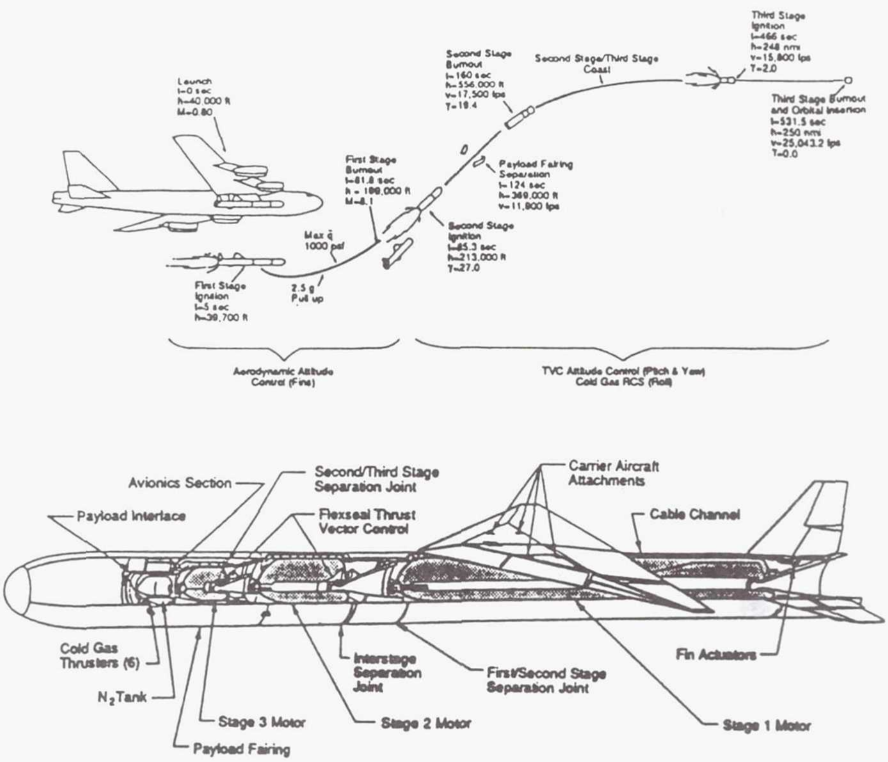

Fig. 1. Mission Profile and Geometry

FIRST STAGE FLYBACK

The mission of the flyback group is to control and recover the first stage of a commercially developed winged booster launched from a B-52 at 40,000 ft and Mach 0.8. First-stage separation occurs at 210,000 ft and Mach 8.7; the second and third stages will continue deployment of their 600 lb payload into low Earth orbit (Fig. 1). The job of the flyback group begins at this point, employing a modified control system developed to stabilize and maneuver the separated first-stage vehicle to a suitable landing site approximately 130 miles from the launch point over the Pacific Ocean.

This multidisciplinary design was accomplished by four subgroups: aerodynamic design/vehicle configuration (ADVC), trajectory optimization, controls, and thermal management.

ADVC: Aerodynamic Design/Vehicle Configuration

The primary responsibilities of the ADVC subgroup were the (1) determination of aerodynamic coefficients and stability derivatives for the proposed vehicle; (2) specification of vehicle redesign constraints; (3) recommendation of means by which stability and range could be augmented; and (4) recommendation of final landing modes.

The accomplishments of the first of these tasks was facilitated by the use of â code—APAS (Aerodynamic Preliminary Analysis System)—developed by Rockwell International for NASA. Through APAS, a database was developed that characterized the behavior of the vehicle over a series of points along its flight profile. The issue of nonlinearity in hypersonic flow was dealt with through an assumption of piece-wise

PRECEDING PAGE BLANK NOT FILMED

PAGE 258 INTENTIONALLY BLANK

linearity between points in the database, and a redefinition of these points so they would best meet the linear assumption. Software developed by ADVC was used in accessing the database, in calculating the stability derivatives, and in generating the (B) matrix required by the guidance and controls subgroup in their state-space analysis.

A comparison of the APAS results to existing hypersonic databases, including the GHAME and HCV models developed at the NASA Dryden Flight Research Center, a set of Navier-Stokes solutions for a Lockheed X-series aircraft, and a set of four models tested by AGARD in hypersonic windtunnels, served as the basis of our validation of the APAS runs. Traditional subsonic-flow textbooks supplemented the evaluation of the APAS UDP (subsonic) data.

The decisions made in completing the second of the ADVC tasks, the determination of constraints on modifications to the first stage, were governed by the premise that the launch vehicle could not be reproduced. To ensure the continued commercial viability of the launch vehicle, it was felt that the mass of the payload could reasonably be reduced between 50 and 70 lb, which in turn translated into a 900-1260 lb addition of weight to the first stage (an 18:1 ratio). Lacking the time and resources to conduct a fine analysis on the effects of adding surfaces to the launch vehicle, ADVC decided that any surfaces added could enter the free-stream only after separation.

Once the aerodynamic database had been established, it became apparent that the flyback vehicle was inherently statically stable for Mach numbers greater than 1.2. Stability in this range was largely a result of the lifting contribution of the two horizontal fins stationed near the exit nozzle. A cursory review of the database indicated that stability in yaw and roll was satisfied.

The margin of static instability below this speed increased as the vehicle approached its landing velocity of 50 ft/sec. Given the predominance of subsonic flight in the flight profile established by the trajectory optimization group, several means by which stability could be augmented were considered, including the repositioning of the wing aft upon separation, the utilization of a reaction-controls system stationed in the nose cone of the vehicle, and parasails. However, it was felt that the static instability of the vehicle could be compensated for by a guidance and control system, and that such measures would be unnecessary.

The determination of the landing mode for the vehicle, the fourth and final task of the ADVC, was governed largely by the aforementioned constraints. Limited space, restricted weight, and the proscription against endangering the basic mission of the launch vehicle all contributed to the final decision to land the vehicle with a parachute placed in the nose. Current estimates show that approximately 11 ft^3 of space are required to store a parachute of sufficient strength to bring back the first stage. This requires 1 ft^3 more volume than the nose allows. Nevertheless, the plan to land the first stage by parachute remains viable, provided a smaller parachute of adequate strength can be found. If this is later found to be unworkable, the wing will be detached from the fuselage shortly before landing, and recovered with a smaller parachute loaded in the hollow wing.

Trajectory Optimization

The objective of the trajectory optimization group was to determine the optimum path and landing site for the first stage of a three-stage winged booster, without jeopardizing the original mission of the entire vehicle. Since the inspection of the recovered vehicle can reveal valuable hypersonic flight data, a maximum hypersonic flight time is a secondary consideration to recovering the booster. In conjunction with the ADVC, controls, and sensors technology groups, the trajectory group determined the optimum flight path given the existing aerodynamic data control power of the first stage as well as the capabilties of the sensors presently being designed.

The first stage's original mission profile requires an air launch from a B-52B at 36.5°N, 123°W (approximately 50 miles west of Monterey, California, over the Pacific Ocean), with an initial heading due south. However, this initial launch point can be moved south depending on the mission and range requirements. The trajectory optimization begins when the first stage separates from the second and third stages.

Given the conditions after separation, the possible landing sites for the first stage include Vandenberg Air Force Base, which requires a range of 130 miles, or a Santa Barbara Channel Island such as San Nicolas, which is 225 miles away from the point of separation. Although Vandenberg is closer to the separation point, the first stage must make a larger turn to reach it compared to San Nicolas (Fig. 2).

In order to devise a trajectory suitable for these purposes, a computer code was written to simulate the flight of the first stage. Given the constraints and the conditions at separation, the objective of the code is to determine the altitude, velocity, and flight path angle for each increment of sampling time. From the data points generated, a flight profile can be constructed and studied.

The trajectory was subdivided into five phases. Since the initial flight path angle of the vehicle is 25.9° above the horizon, the first stage will continue to ascend after separation. In this phase, the vehicle is assumed to fly ballistically until it reaches its peak. Afterwards, the descent phase will also be ballistic until a suitable dynamic pressure is attained. At this point the first stage will fly at a constant dynamic pressure until the flight becomes very steep (approximately 45°). The vehicle will then be required to make a pull-up maneuver, which is the fourth phase of the trajectory. Once the pull-up maneuver has been completed, the vehicle will fly the remainder of the path with a constant flight path angle.

The governing equations of motion used in the computer code were derived from a summation of forces on the vehicle assuming that the first stage is a point mass. The wind axis is used as the coordinate reference system. Furthermore, the atmospheric winds have been included in the analysis.

Since the governing equations are nonlinear and cannot be solved explicitly, the code generates the results by numerical methods. The initial inputs for the code include the initial flight path angle, altitude, and velocity. Then, for a small increment of time, the program calculates the new values for the altitude, velocity, flight path angle, and the ground distance traveled during that interval, and the code uses these new

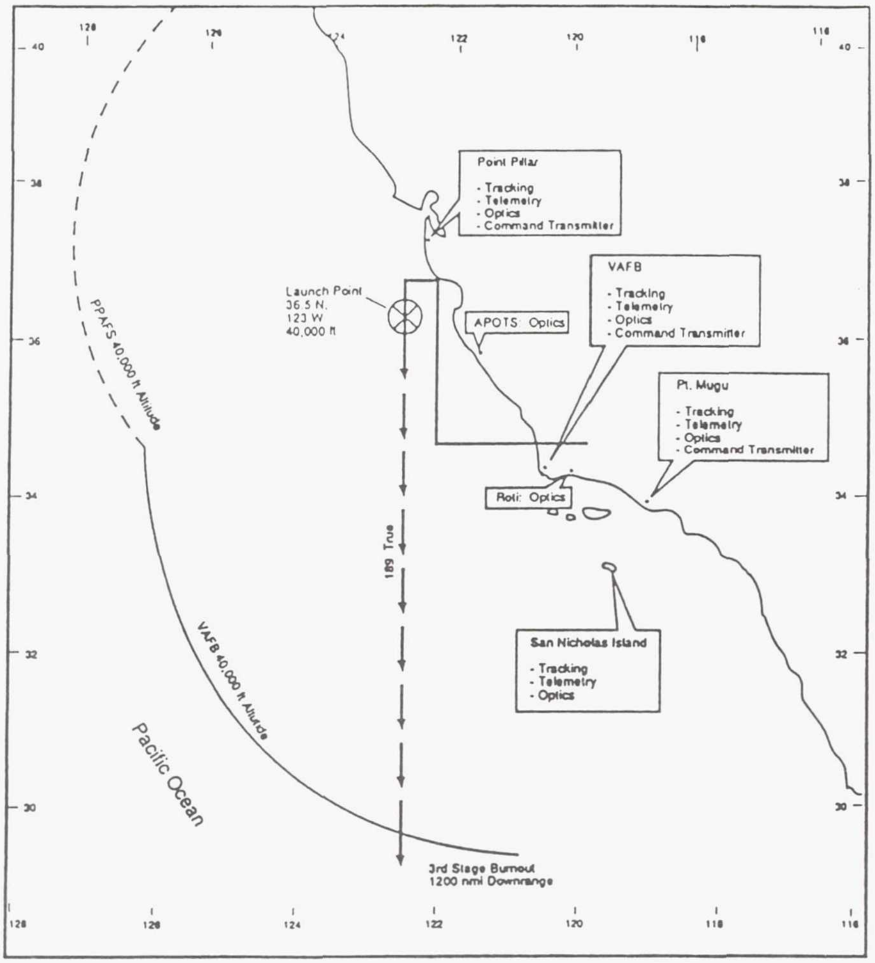

Fig. 2. Candidate First Stage Landing Sites

values as initial conditions for the next time step. This process continues until the vehicle has landed.

The parameters that the trajectory group can control during these calculations are time increments between each calculation, the constant dynamic pressure with which to fly, and the aerodynamic coefficients provided by APAS. By selecting a certain lift-to-drag ratio at a given velocity, the trajectory group is indirectly specifying the control system necessary to follow the specified trajectory.

Due to the time limitations, the trajectory has not incorporated the Earth's rotation. At the equator, for example, the Earth is rotating away from the vehicle at 28.7 miles per minute. Hence, the vehicle will require more range than that specified to compensate for the Earth's turning. Also, the flight path angle for the glide and pull-up phases of the trajectory will not be finalized until the control power of the vehicle is determined.

Controls

The control systems subgroup for the hypersonic vehicle flyback group concerned itself with the stability and trajectory analysis of a booster segment after its separation from the mother vehicle. The majority of the analysis for the vehicle involved using the state-space approach. The states of the aircraft, including dynamic response and trajectory motion, are represented in the state vector with the stability derivatives as its coefficient matrix, (A). The stability derivatives are the results of the aerodynamics group's work on a software simulation program. The control vector includes the control surface deflection terms, and its coefficient matrix, (B), consists of control derivatives also obtained by the aerodynamics group. The command reference inputs for feedback analysis are the result of trajectory optimization done by the trajectory group.

In the analysis of vehicle stability, it was determined that the first stage of the vehicle, the segment that is being recovered, is statically unstable in the subsonic regime and only marginally stable in the hypersonic regime. That is, the poles of the system with no feedback applied in the subsonic regime occupied the right side of the complex plane, and it was decided that feedback of the appropriate state variables to the control system would resolve the instability by moving the poles to the desired locations in the left side of the plane.

The initial assumption that facilitated analysis was that the longitudinal and lateral components of motion could be decoupled and analyzed independently of one another. Making the assumption that the vehicle maintains stability in the lateral direction, the focus became the longitudinal stability. The state variables used to represent the longitudinal system for the purpose of stability analysis were the angle of attack (α) and the pitch rate (q). Concentrating on the short-period poles, which are the eigenvalues of the (A) matrix, pitch rate feedback was applied to move the poles from the right side of the complex plane, where they existed without feedback, to the left side. Feedback of state variables involved additions in the (A) matrix of feedback gain terms and the corresponding control derivatives from the (B) matrix.

However, it was found that pitch rate feedback alone would not be sufficient to adequately move the poles, so α was also introduced as a feedback element. The result was that, given a desired location for the short-period poles of the system, the respective feedback gain coefficients could be determined using state-space techniques.

The static instability of the vehicle was resolved by applying feedback with not one, but two variables. Although utilizing α in the feedback loop facilitated the movement of the poles, it had a drawback. Alpha is a difficult quantity to measure unless a Flush Air Data System (FADS) is used, so the advantage of using α in feedback for theoretical purposes is balanced by the additional equipment required onboard. The stability implementation gave a good foundation for the trajectory analysis because the method of feedback paralleled that for controlling dynamic response. It was important that stability was achieved since it would be impossible to execute maneuvers for the desired trajectory with an unstable vehicle.

Trajectory analysis involved augmenting the state-space system used above in 12 states including longitudinal, lateral, and inertial quantities. They consisted of the angular and translational velocities in the aircraft axis frame plus the directional angles and the distance traveled along each axis. The control vector was augmented to include aileron, elevator, and rudder deflections. The assumption was made that the trajectory devised by the trajectory group was optimized by considering aerodynamic and inertial forces so the vehicle would follow the predetermined flight path with occasional correction for disturbances by the control system. These corrections required feedback gain values that were not as critical as those for achieving stability, and served only to maintain the vehicle on course.

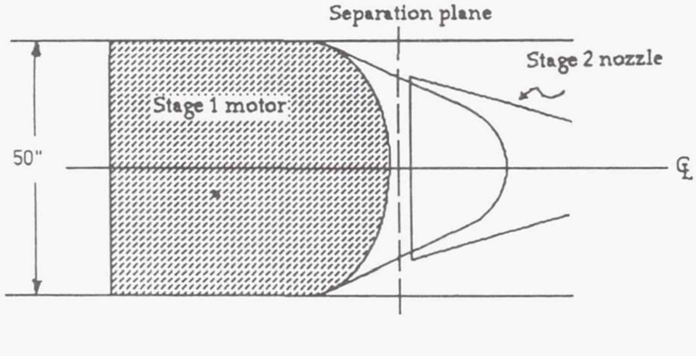

Fig. 3. Nose Attachment to First Stage

The state variables that needed to be fed back for trajectory were the forward velocity (V), the angle of attack (α), the angle of sideslip (β), the flight path angle, and the heading angle. The pitch rate, which was also fed back for stability, completed the set of states that were fed back. The autopilot was then designed by determining the gain by which each feedback state variable is scaled before it is fed back. The task then was to determine if the autopilot could perform the given trajectory, which consisted of only two maneuvers, a heading angle change and a flight path angle change. A steady-state assumption was used to determine if the maneuvers requested by the trajectory group were physically realizable, since analyzing a general trajectory would require a general nonlinear simulation.

The final effort of designing feedback gains for the 12-state control system has been completed and resolved so that the design trajectory is viable and the vehicle can perform within the bounds of stability. The control law now can be implemented by a computer code stored as firmware in the onboard control system unit. Accepting measurements from the onboard inertial measurement unit, the control system can determine the required response to assure both stability and the maintenance of trajectory.

Thermal Management

The purpose of the thermal management group was to assess vehicle thermal loads during return flight, and to make sure that the vehicle can withstand these loads. The nose and wing leading edge were identified as critical heating regions, and the nose was selected as an area of study. Wingshock impingement was also studied. The unmodified vehicle uses a spray-on ablative heat shield, and it was originally hoped that such a thermal protection scheme could be studied and designed, with an emphasis on calculating additional heat shield weights. This was not possible, so a broader approach was taken.

As the first stage lacked a nose cone, one was designed. The major design limitation was one of space, so it was designed to fit into the second-stage exhaust nozzle (Fig. 3). This limited us to a 25° half-angle cone. Several additional factors influenced the design. First, sharper cones experience higher heating rates, but lower overall stagnation heating rates, due to their reduced frontal area. Sharp cones also result in weaker shock, preserving the hypersonic flow we wish to study (Fig. 4). However, it was undesirable to have a nose that protruded too far into the nozzle, and we hoped to minimize wing shock impingement. A bluntness ratio (frustrum-base-radius-to-apex-radius ratio) of 0.3 was finally selected. The nose cone's addition also has the benefit of adding about 10 ft^3 of usable space to the vehicle (Fig. 5).

The flight under study consists of an ascent stage, where the nose is assumed to be at a constant temperature of 25°F. Upon separation, the nose is exposed to the outside air at no angle of attack. Stagnation-point heating rates were then calculated

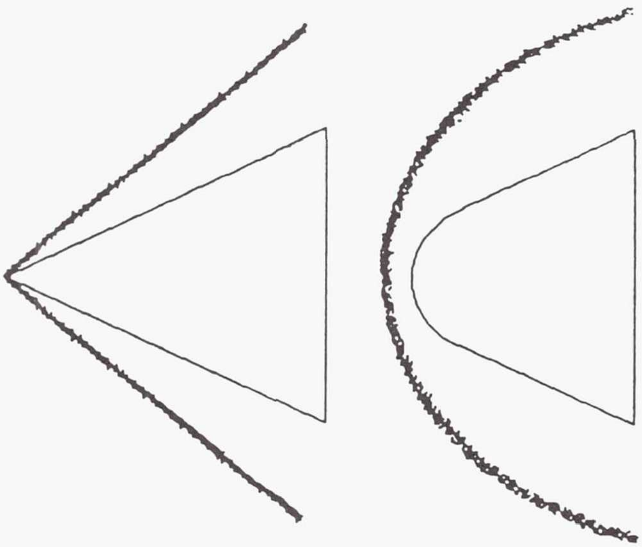

Fig. 4. Hypersonic flow interactions as a function of geometry. (a) Sharp cone: high heating rate, attached shock; (b) Blunt cone: lower heating rate, detached shock.

for a trajectory provided by the trajectory optimization group. These rates were calculated by a FORTRAN code using Lees' approximate method, where

$$q_s = 21\left(\frac{\rho_\infty}{R_o}\right)^{1/2}\left(\frac{V_\infty}{1000}\right)^3\left(1 - \frac{h_w}{h_s}\right)\ \text{Btu/ft}^2\ \text{sec} \qquad (1)$$

where R_o is the radius of the nose spherical portion, V_∞ and ρ_∞ are the free-stream velocity and density, and h_w and h_s are the wall and free-stream enthalpies.

Two variations were tried. A cold wall assumption, where the nose was kept at 25°F, and a hot wall assumption, where the wall surface temperature was allowed to increase, were calculated to provide an upper and lower bound for the thermal loads. These were integrated over the trajectory to find the overall heat transferred to the vehicle nose. This was then compared to a reference ascent trajectory to determine whether these loads were acceptable and what kinds of thermal protection schemes were needed. The heating turned out to be a third of that sustained on the ascent, allowing additional spray-on ablative heat shielding for sufficient thermal protection. The original composite structure should also perform adequately for the nose cone.

In addition to the stagnation region, the wing leading edge region was studied. Although CFD codes to give the local flow properties and shock geometry were not available, some analysis of the bow shock/wing interaction could be done using the hydraulic analogy. A two-dimensional model was run on a water table at an elevated Mach number to simulate the three-dimensional shock geometry. In an impingement region, heating rate is tied to the pressure in that local flow separation can cause heating rates to increase by several orders of magnitude. Although large impingement regions were observed, the vehicle is traveling in a region of relatively low dynamic pressure for a short period of time. While the possibility of a leading-edge burnthrough seems likely, it is probably not critical and will not result in the loss of the vehicle. Wind tunnel tests should be performed to analyze this more closely.

SENSOR TECHNOLOGY

The mission of the sensor group was to design a sensor that measures the adiabatic wall temperature in the hypersonic ascent of the winged air-launched booster and to verify predictions used in CFD modeling codes for future application to the hypersonic regime. In order to demonstrate the technology, a proof-of-concept version was built at UCLA and will be tested in the supersonic regime of the Flight Test Fixture of an F-104 at the NASA Dryden Flight Research Center.

The design was conducted by mechanical and electrical engineering students split into two subgroups, a mechanical/thermal group and an electrical design group.

Mechanical/Thermal Group

The purpose of the design project was to develop a sensor that would allow the adiabatic wall temperature to be determined. More precisely, the sensor would determine the appropriate correlation to use for the recovery factor (r) in equation (2) below.

$$T_{aw} = T_e + r\,\frac{U_e^2}{2C_p} \qquad (2)$$

T_{aw} is the adiabatic wall temperature, T_e is the ambient air temperature, U_e is the free-stream velocity, and C_p is the heat capacity of air. T_{aw} can be determined from the sensor output and, from this, the recovery factor (r) can be inferred from equation (2).

Several assumptions were made for the thermal design of the sensor. First, r was correlated as $Pr^{1/3}$ (for a turbulent boundary layer) and the calculations followed. Other assumptions included that there was a one-dimensional heat flux, that the flow was over a flat plate, and that there was no heating due to shock waves at the sensor location.

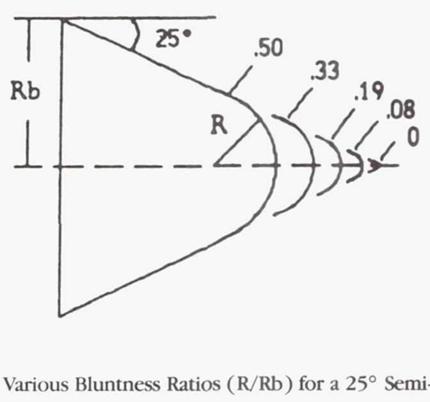

Fig. 5. Various Bluntness Ratios (R/Rb) for a 25° Semi-apex Cone

Fig. 6. Heat Transfer Nodes

The sensor considered was based on the idea of having two surfaces, one exposed to the air flow and the other on the inner side of the skin. A heater mounted at the inner surface would raise its temperature to match that of the top surface. When a zero temperature gradient is achieved between the two surfaces, adiabatic conditions could be assumed. This temperature is the "radiation equilibrium temperature" from which T_{aw} and r can be determined.

An energy balance at the surface indicated that a sensor pair would be needed to eliminate the unknown convective heat transfer coefficient (h). The pair consists of one sensor with a high emittance surface and one with a low emittance surface. Thus, by simply measuring the surface temperature of each sensor, T_{aw} can be found. Preliminary results of the surface temperatures determined from equation (2) and the energy balance at the surfaces indicated temperatures in the range of 2000°C. Due to materials limitations, the flow conditions were modified to give a 500°C maximum temperature for the final design of the device.

Once the surface temperature was obtained, a transient analysis revealed that if conductive heat transfer were the mode used to obtain a flux from the top to the bottom surface, then either a slow response was expected or a very powerful heater was needed. Figure 6 illustrates the conductive and radiative modes of heat transfer. As seen, the conductive method requires a thick slab that introduces slow transient responses as well as two-dimensional heat flow.

While the conductive heat flux arrangement seemed impractical, a radiative heat flux design offered more flexibility. The new design called for two plates, one at the surface and the other below it, separated by a layer of air. The new mode offered several advantages over the original system. These advantages are as follows: (1) a lumped capacitance method could be used, thus simplifying the calculations; (2) the lower thermal mass of the plates gave faster transient response for the system; (3) the bottom plate thickness could be minimized, thus allowing the use of a low-power heater; and (4) two-dimensional conduction effects could be safely neglected, due to the reduced thickness.

Next, the plate and heater geometries and physical properties were considered (Fig. 7). The material chosen for the sensor plug and the lower plate was AISI 309 stainless steel. Its main advantages are that (1) it is a very common material, (2) it is machinable down to 0.001 in, (3) it remains strong at elevated temperatures, and (4) it has a fairly low thermal coefficient of expansion. The material chosen for the heater was 80-20 Ni-Cr wire because of its wide use as a heating element. Aluminum oxide was chosen as the material to electrically insulate the heater from the lower plate. To achieve the different emittances at the sensors' surfaces, two coatings were chosen. A gold coating vapor deposited on one sensor would give an emittance of about 0.03, while black paint on the other surface would yield emittance values of about 0.97.

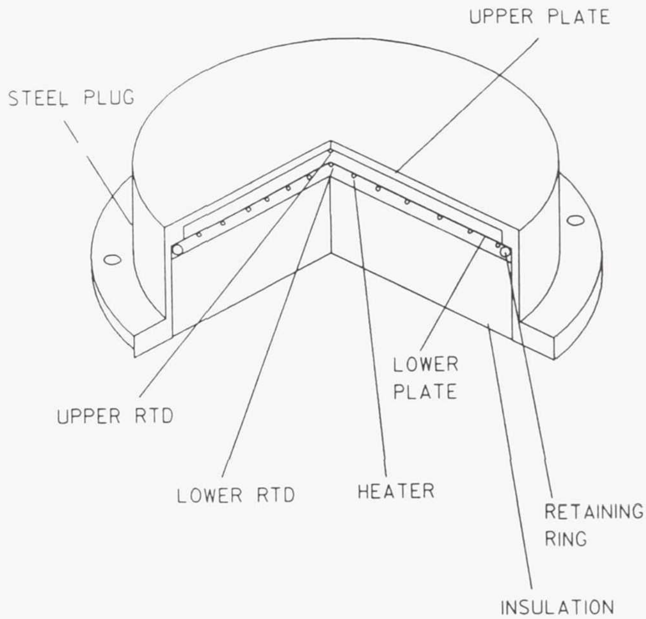

Fig. 7. Sensor Geometry

Finally, heat loss at the back of the heater had to be minimized. This was accomplished by packing a slab of Manville molded Min-K super-insulation behind the heating element. Specifications of the sensor are shown in Table 1. An illustration of one of the sensor pairs is shown in Fig. 8.

Table 1. Sensor Specifications

Plug Material:	AISI 309 Stainless Steel
Plate Diameter:	0.04 M
Plug Height:	0.0191 M
Top Plt. Thickness:	7.62 E-04 M
Bot. Plt. Thickness:	1.27 E-04 M
Al. Oxide + Adhes.:	4.00 E-08 M
Maximum Temp:	500°C
Heater:	80-20 Ni-Cr Wire
Gauge:	30 (2.54 E-04 M)
Length:	0.63 M
Output:	5.00 W
Volts:	8.40 V
Current:	0.595 A
Adhesive Type:	High-temperature Ceramic
Minimum Time Response of Sensor:	0.74 sec
Sensor Emissivity Coat:	High: Black Paint $\epsilon = 0.97$ Low: Vapor-deposited Gold $\epsilon = 0.03$

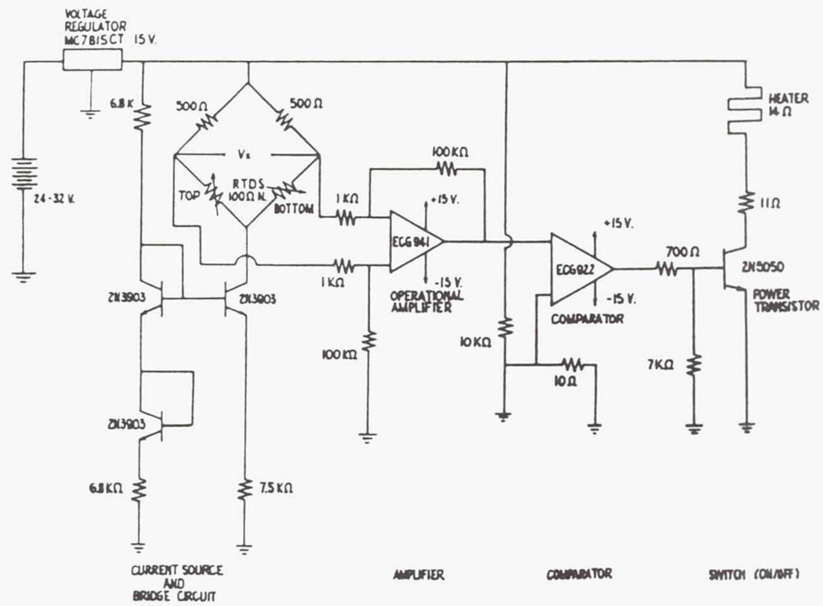

Fig. 8. Sensor Schematic

Electrical Design Group

The sensor, from an electrical perspective, involves maintaining the balance of a bridge circuit containing resistance temperature devices (RTDs). The RTDs chosen have a nominal resistance of 100 Ω. Basically, an RTD is a conducting material whose resistance depends, roughly linearly, upon temperature. Therefore, supplying a constant current to the bridge generates resistance-dependent voltages. These signals are then used to measure the temperature surrounding each RTD. Furthermore, to reduce the effect of self-heating, the current is held to a minimum of 1 mA, or approximately half that value for each branch of the bridge, through the use of bipolar junction transistors (BJTs).

Creating a balanced bridge translates into effecting a minimum differential voltage, V_x. Given fixed resistance of 500 Ω in the upper portion of each branch, the current divides equally when both RTDs sense the same temperature. Initially, the ascent of the test vehicle will increase the temperature surrounding the RTD mounted on the top surface. Hence, a nonzero differential voltage, V_x, is produced since the bottom RTD remains at the initial, cooler temperature. For a constant current of 1 mA into the bridge, a difference of 1° between the temperatures of both RTDs produces a differential voltage of +35.3 μV.

To effectively handle such accuracy, an op-amp with a gain of 100 is included in the design to amplify the signal. The comparator then compares its input voltage to a reference of 15 mV set by a voltage divider. Whenever the absolute value of the input voltage rises above the reference, the output switches to the positive or negative supply of 15 V, depending on its true polarity.

Finally, to control the heater, a power transistor is selected to provide a collector current of 0.5 A, delivering 5 W of power to the 14 Ω heater. The 700-Ω resistor at the base guarantees an active transistor when the input rises to the positive supply. Similarly, the 7-kΩ resistor provides a path to ground for a large negative input, safeguarding against burnout. Thus, an NPN bipolar junction transistor in common-emitter configuration was chosen for these reasons. Since the heater is physically attached near the bottom RTD, current supplied to the heater raises the temperature of the RTD until it matches, within 1°, that of the upper surface.

Thus, this circuit will compare the signals generated by the two RTDs and control the heater to create a zero heat flux condition between the two opposite plates in the sensor.

It is clearly evident that the completion of this project has reemphasized the successful combination of electrical and mechanical engineering concerns and abilities within an aeronautical design effort.

1994004545
383655
CoP

N94-71300

AIR TRANSPORTATION IN THE CALIFORNIA CORRIDOR OF 2010

CALIFORNIA POLYTECHNIC STATE UNIVERSITY, SAN LUIS OBISPO

S33-03
160659
P. 5

The topic of the 1988-1989 NASA/USRA Advanced Design Project at California Polytechnic State University, San Luis Obispo, was the development of an air transportation system to meet the needs of the California Corridor for the year 2010. As aircraft design is taught by two instructors having different philosophies about the teaching process, the two classes took different approaches to address the problem. The first part of this summary (California Air Transit System) represents the work done by the students of Professor A. E. Andreoli, who followed a systems approach, emphasizing the determination of the proper mission. The second part of the summary (Four Aircraft to Service the California Corridor) contains the four aircraft designed by Dr. D. R. Sandlin's class based on specifications determined from work done in previous years.

Fig. 1. California Air Transit System

CALIFORNIA AIR TRANSIT SYSTEM

The California Corridor Air Transit System (CAT) is composed of three types of vehicles and a new "superhub" airport located in the San Joaquin Valley. This hub, known as the Corridor Access Port, or CAP, acts as a mode mixer for most of the flights within California, as well as the interstate and international flights. "Mode mixer" refers to the changing of vehicles, in that the passenger flies from his origin to the CAP, then changes flights to the one bound for his destination. The proposed vehicles for the system are a 31-passenger electric-powered conventional takeoff and landing aircraft, a magnetically-levitated train, and a 40-passenger vertical takeoff and landing (VTOL) tilt rotor aircraft. All these vehicles are well within the reach of current technology.

Due to the ground congestion problems in California, generally over half the time associated with trips within the state is spent on the ground; therefore, the main goal of the proposed system is to get the people out of their cars and into the air en route to their destination. Because people prefer different modes and because everyone's priorities are not the same, the three different vehicles are required. The passengers will board the vehicle near their home and will be transported by it to the CAP, where they will switch to the vehicle that which will take them to their destination. The system allows for a higher level of service, i.e., directly from the passenger's local community, because the CAP serves as a hub (Fig. 1). For instance, assume that a resident of San Bernardino wishes to travel to Concord, California. At any given time of the day, there are probably not enough people in San Bernardino wishing to go to Concord to fill a direct flight, however, there are most likely enough people in San Bernardino at that time who need to travel to some destination by air to fill a 30- or 40-passenger vehicle. Thus, the flight to the CAP operates near capacity, which makes it a profitable venture for the airline. Naturally, the same is true for the flights departing the CAP to the suburban communities.

The concept of the CAP is similar to the Wayport idea proposed by James Sheppard of the Federal Aviation Administration, although the Wayport is not integrated with any corridor-type transportation. Our analysis shows that the Wayport idea is inefficient unless it is structurally integrated with a corridor transportation system. This is because although it shares many of the benefits of the CAP, the traveler must still go to the major metropolitan airport to get into the system, so he has increased his overall trip time, for in addition to the ground time at each end of the trip, he has an additional ground-time segment in the middle. Those going through the CAP will naturally also have this ground time; however, they will have reduced the ground time on each end such that the overall trip time is reduced.

The proposed site for the CAP is in the Tulare Dry Lake Bed southeast of Kettleman City, California, just east of Interstate 5. The site was surveyed, and the approximately 40,000 acres that would be required were found to have little elevation change, and there is virtually no agriculture on the site. The location near Highway 5 provides for easier construction, since roads will not have to be built. The location is also near the California Aquaduct which would provide water during construction and for operation of the CAP. The ten 14,000-ft runways are linked to the vertiport by an

PRECEDING PAGE BLANK NOT FILMED

PAGE 266 INTENTIONALLY BLANK

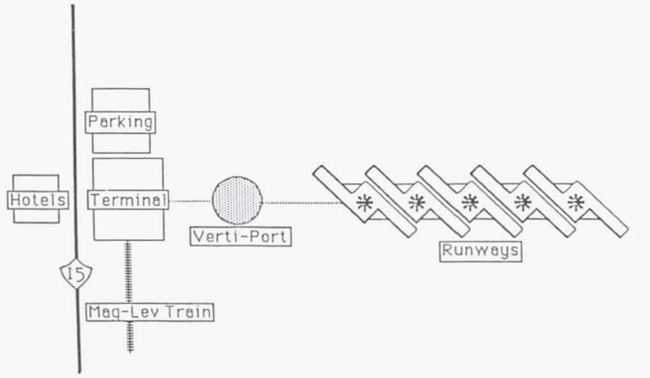

Fig. 2. Corridor Access Port (CAP)

underground rail system to provide efficient passenger handling. A schematic of the CAP facility is shown as Fig. 2.

Because passengers have different needs and priorities, it was necessary to design three vehicles to serve all the markets, and a plan of integration needed to be developed. The Mag-Lev train (Fig. 3) has been shown to be the most cost effective mode of travel for the Corridor; however, in order to achieve this, it must be heavily used, and only stop in a few locations. This makes it rather inconvenient for those not living close to the stations. The Mag-Lev travels at speeds of around 300 kts as it serves passengers traveling within the Corridor as well as those making connections to outbound flights at the CAP. If passenger volume were high enough, it is estimated that fares could be as low as 11 cents per mile. This would mean that a trip from Los Angeles to San Francisco would be about $33;

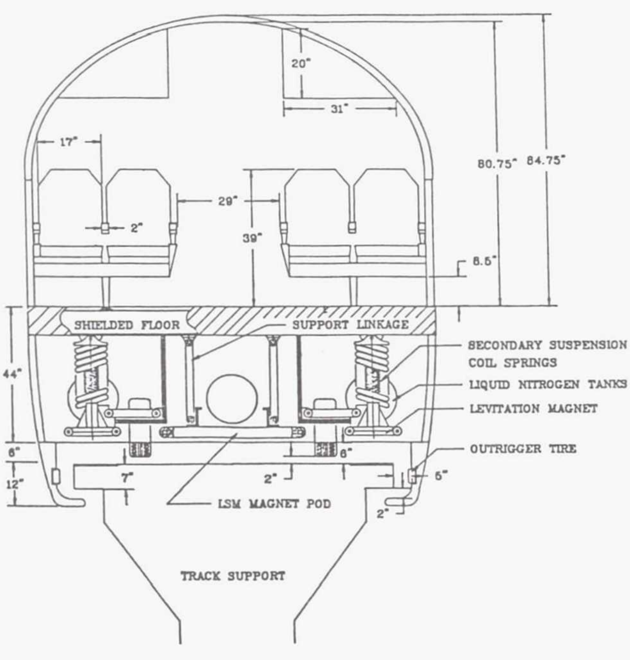

Fig. 3. Mag-Lev Train

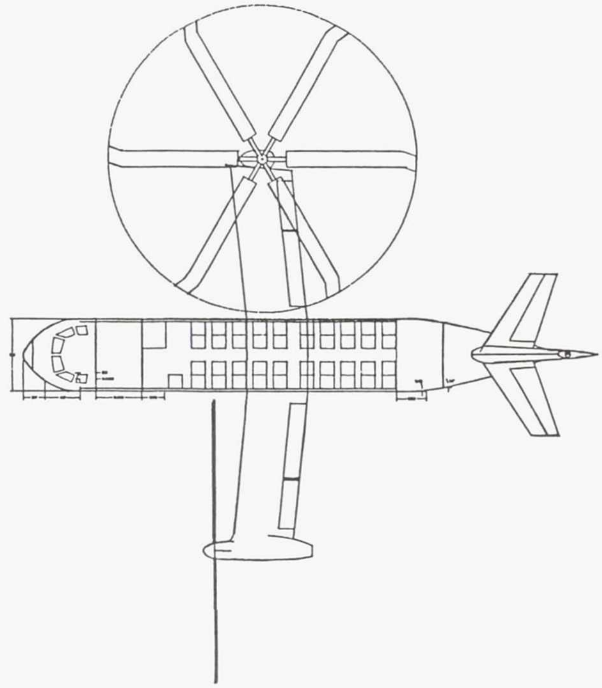

Fig. 4. Wildcat Tilt Rotor

however, as was mentioned earlier, if the traveler's origin and destination are not near the train station, he has gained little. Also, there are doubts that the system would be able to transport the volume of passengers that would be required for this fare; a more likely Los Angeles to San Francisco ticket price would be $45.

The second vehicle designed is the Tilt Rotor VTOL aircraft, named the Wildcat, which is shown in Fig. 4. In addition to cost and convenience, the design of this vehicle concentrated on reduced air and noise pollution. The aircraft burns liquid hydrogen as fuel. This immediately draws concerns about safety, but several studies have shown that hydrogen fuel is actually safer in accidents than conventional hydrocarbon aircraft fuels. The Wildcat will land at community vertiports, where it will load passengers bound for the CAP. At the CAP, it will refuel and load passengers bound for the community vertiport. Since refueling for the Wildcat can be centralized, hydrogen containment facilities are not required at each vertiport. Therefore, the vertiports need to be little more than paved landing sites, each with a small terminal. Because of the high load factors (the percentage of seats filled per flight) anticipated, the ticket cost for the Wildcat is calculated to be around 20 cents per mile. This puts the Los Angeles to San Francisco fare at about $60. This is significantly higher than the Mag-Lev, but a great deal of trip time is saved by using the Wildcat.

The final vehicle design is the most evolutionary type. It is an electric-powered conventional takeoff and landing aircraft, called the ECTOL (Fig. 5). Similar to the Wildcat, the ECTOL operates out of suburban communities, although it requires a

C-4.

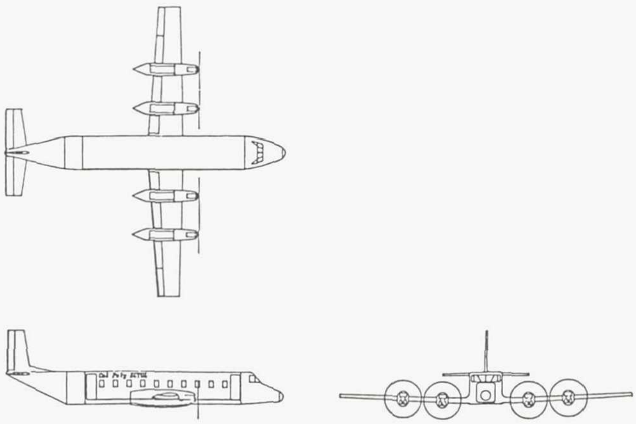

Fig. 5. ECTOL Electric-Powered Aicraft

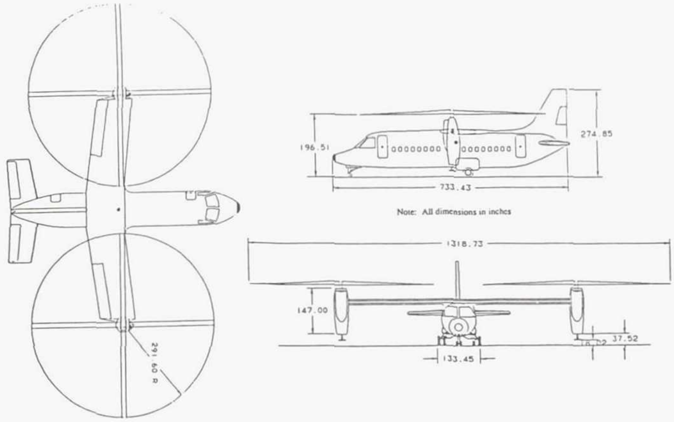

Fig. 6. Transit Tilt Rotor (all dimensions in inches)

4,000-ft runway. It operates under the same premise as the tilt rotor, except that it does not always fly to the CAP. As time progresses and the system continues to grow with the population of California, it may become apparent that some routes receive enough demand that going to the CAP would be unnecessary. In this case, direct routes would be established. The ECTOL was also designed to be low in air and noise pollution. The reaction that creates the electric power produces a solution of lithium hydroxide that is stored on the aircraft and recycled. Because it is propelled by an electric motor, the only detectable noise is the aeroacoustic noise of the propellers. The Los Angeles to San Francisco ticket price is estimated to be about $57.

In order for the system to be accepted, a careful plan of integration must be developed. Because of its evolutionary nature, the ECTOL should be implemented initially. It will service smaller airports as commuter airlines do now. At the same time, construction would begin on the Mag-Lev track. This will face stiff political opposition, for legislators will be opposed to it going through their districts if it does not stop there. The Mag-Lev will be the second vehicle to come on line. The study has shown that there is currently sufficient demand to warrant this system. At this point, construction would begin on the CAP facility and the community vertiports. It is important that these vertiports be located in urban or industrial environments, far away from the residential neighborhoods to limit opposition due to the associated noise, but close enough to be convenient. The last stage of the implementation is the opening of the CAP and the start of the tilt rotor service. At this point, much of the air traffic would be diverted away from the overcrowded major metropolitan airports.

Unless something is done about the state of transportation in California, it will continue to deteriorate until it reaches unbearable levels. The proposed system is certainly not the only solution; however, it is believed that any solution that adequately addresses the problem must be a revolutionary and large complete system, not merely a series of patches to keep the current system together.

FOUR AIRCRAFT TO SERVICE THE CALIFORNIA CORRIDOR

Transit

The population in California is projected to reach 36 million by the year 2010. This increase will cause a major impact on the present transportation system. Therefore, new transportation systems must be incorporated to accommodate the needs of the expanding population.

To achieve the portal-to-portal service that will make VTOL aircraft cost-competitive with other means of transportation, vertiports must be incorporated into the present transportation system to allow VTOL access close to a traveler's destination. Examples of potential vertiport locations are above freeways, on top of buildings, on waterfront property, or at existing airports.

Transit was designed to fulfill the VTOL requirements for the California Corridor. The tilt rotor aircraft has many advantages that make it the best VTOL configuration for the given mission. The advantages include VTOL and STOL capabilities, less noise, lower weight, flexibility in operation, and marketability for other missions. The 40-passenger Transit configuration shown in Fig. 6 has a cruise speed of 325 kts at 16,000 ft and a design range of 375 n.m.

California Condor

California is currently one of the fastest growing states in the United States and its population trends are expected to continue. The major metropolitan areas within the state are already saturated, causing many other developing areas to take the inflow of people and industry. By the year 2010, it is foreseen that there will be a need for necessary changes in air transportation within the California Corridor. Cities such as Bakersfield, Fresno, Ventura, Santa Barbara, San Luis Obispo, Salinas, Stockton, and Tracy have high growth potentials. These cities often have airports much smaller than those of San

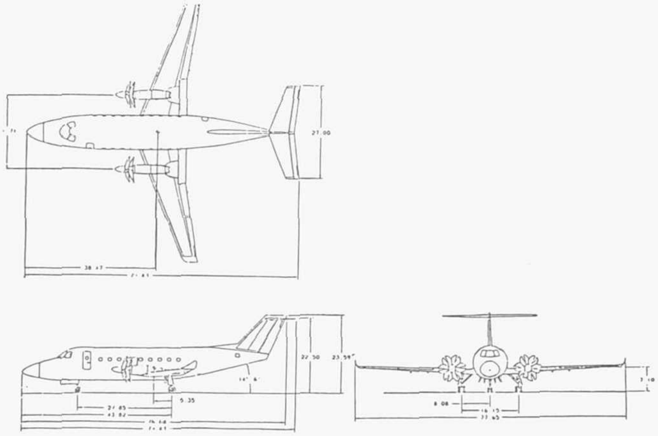

Fig. 7. The California Condor (CC-38)

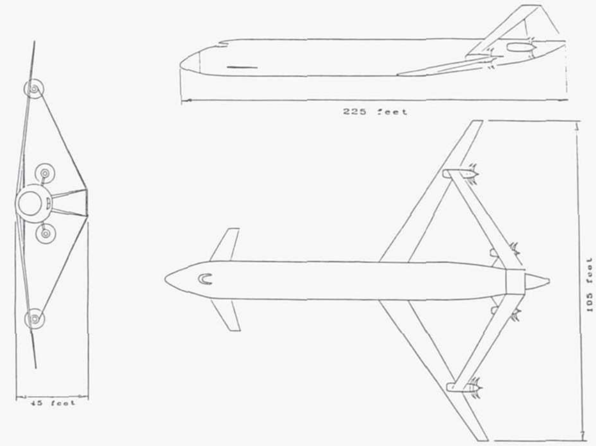

Fig. 9. HCRST Joined Wing Aircraft

Francisco and Los Angeles. The California Condor (CC-38) was designed so that airports such as these can be accessed.

The CC-38, whose geometry is shown as Fig. 7, is a partial solution to the problems associated with the current air transportation. Accommodating 38 passengers, it is twice the size of the commuter aircraft that currently serve the same market. This increased size will reduce the number of flights required, helping to reduce the congestion at the major airports. The aircraft cruises at a velocity of 348 kts (Mach = 0.57 at 20,000 ft) and has a landing field length of 4000 ft. This runway length allows the aircraft to land at all the cities currently served by commuter airlines.

Sky Hopper

The California Corridor is defined as the air traffic within California to the cities between San Diego and San Francisco. This traffic is expected to increase significantly by the year 2010 to the extent that our current transportation system will be insufficient to handle the increased traffic volume.

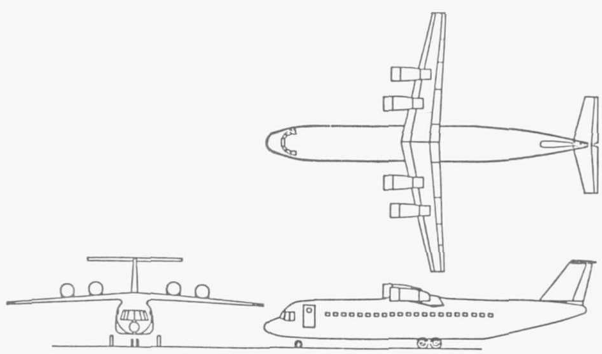

Fig. 8. The California Sky-Hopper

The primary purpose of our aircraft mission is to fly short-range connecting and commuting flights into the major airports without adding congestion to the already overcrowded airspace. This can be achieved by installing small, short takeoff and landing runways (STOL ports) at the existing international airports.

The California Sky-Hopper, shown in Fig. 8, is a 40-passenger STOL aircraft using upper surface blowing to achieve the necessary high lift coefficients. It has a 500-n.m. range, with a cruise speed of 450 kts at 25,000 ft. The landing field requirement is set at 2500 ft.

HCSRT

The California Corridor is one of the most heavily traveled airways in the world. Air traffic is increasing at an alarming rate, with California's population growth rate being one of the highest in the nation. The current system is operating at its capacity and will be unable to meet the transportation needs for the year 2010.

It was considered that the most effective way to reduce the traffic at the hubs was to reduce the number of aircraft in service by increasing the passenger capacity per aircraft. A large high-capacity aircraft would result in fewer aircraft needed to accommodate a given number of passengers. These large aircraft were found to improve all aspects of airport and airspace overcrowding. The air traffic control system is already overstressed and any reduction in the volume of air traffic would be beneficial.

The High Capacity Short Range Transport (HCSRT), shown in Fig. 9, carries 600 passengers and has a design range of 870 n.m. The joined wing configuration cruises at Mach = 0.80 at 30,000 ft, and has a minimum landing field length of 8600 ft.

ACKNOWLEDGMENTS

Principal authors of the California Air Transit System project M. Cameron, K. Mahaffy, G. Yanagi, L. Lechmanski, and T. Riddle

were assisted by faculty advisor Professor A.E. Andreoli and graduate assistants M. Esty and R. Wynne.

Principal authors of the design project of four aircraft to serve the California corridor were K. Howard, C. Chan, M. Gorman, and B. Bauer. They were assisted by faculty advisor Dr. D.R. Sandlin and graduate assistants M. Esty and R. Wynne.

1994004546
383656
12P

N94- 71301

HIGH ALTITUDE RECONNAISSANCE AIRCRAFT DESIGN

CALIFORNIA STATE POLYTECHNIC UNIVERSITY, POMONA

S34-05
160660
p- 11

A Universities Space Research Association (USRA) sponsored (undergraduate) study is presented on the feasibility and design of a high altitude reconnaissance/research aircraft. The aircraft mission was to carry 1,000-3,000 lb of atmospheric pollutant monitoring equipment for 1-5 hr at an altitude of 100,000-130,000 ft. Three configurations subject to the same mission requirements were studied in detail. The three designs analyzed were the tandem-wing-twin-boom, joined wing, and conventional twin-boom configurations. The performance of the three proposed configurations is presented and shows that high altitude flight is possible with current technology. Different possible propulsion systems were investigated and suggestions are made for further investigation and better optimization of the designs.

INTRODUCTION

Recent discovery of the ozone hole above the North Pole has generated much concern in the worldwide scientific community for the effect of solar radiation on the planet's ecology system. Ozone serves as a protective shield against harmful radiation. Currently, NASA is employing ER-2 research aircraft for the investigation of the ozone layer above Antarctica at altitudes of about 70,000 ft. However, at latitudes closer to the equator the ozone layer is located at higher altitudes ranging from 80,000 to 100,000+ ft, which is outside the operating envelope of ER-2 aircraft. This prompted NASA to start an investigation of the design requirements for a subsonic aircraft that would have the capability of achieving altitudes in excess of 100,000 ft. As part of this investigation and the NASA/USRA design project, California State Polytechnic University, Pomona has been involved in the design of aircraft that would meet these high altitude cruise and payload requirements.

DESIGN PROCESS

This high altitude research design project was made a part of the senior aerospace design course sequence at California State Polytechnic University, Pomona. The design project was started in the fall quarter of 1988. During the fall quarter the class was divided into three major groups: Propulsion, Aerodynamics, and Structures.

Each group investigated the problem areas within their domain of interest and formulated possible solutions associated with their particular problem areas. The mission requirements were identified and a request for proposal was developed. The preliminary design evaluation yielded eight design configurations from which three were selected for further study. The initial vehicle configurations included conventional (tail aft), canard (wing aft), three surface (canard, wing, tail), dual wing (wing, wing, tail), flying wing, biplane, and joined wing aircraft designs, as well as a high altitude blimp design. After some detail analysis the eight configurations were reduced to the three that were analyzed in considerable detail.

The propulsion group investigated alternate propulsion systems. By the end of the fall quarter the possible propulsion systems were reduced to two that were further analyzed during the second phase (winter and spring quarters) of the design process.

During the second (winter) quarter the class was realigned into three groups to investigate the three different configurations of interest. In the process of realignment, a matrix management system was employed. Three new group leaders were chosen. One configuration was assigned to each of the new groups. The new groups were composed of individuals from the initial propulsion, structures, and aerodynamics groups. An effort was made to provide each of the new groups with at least one member from each of the initial groups. The initial group leaders retained their respective responsibilities for propulsion, aerodynamics, and structures, and served as consultants to the new configuration groups throughout the winter and spring quarters of the 1988-1989 academic year. The consultants were also responsible for designing certain components to be used by all the configuration groups.

Trade studies were made by each of the three configuration groups during the second (winter) quarter. Complete conceptual designs were finished during the spring quarter of 1989.

DESIGN SPECIFICATIONS

A common request-for-proposal (RFP) was developed from the very general mission requirements provided by NASA. The RFP was for a complete aircraft that meets the requirements shown in Table 1.

At latitudes closer to the equator, the ozone layer is located at altitudes above 80,000 ft. Therefore, a minimum cruise

Table 1. RFP Specifications

1. The aircraft cruise altitude should be at least 100,000 and preferably 130,000 ft.
2. The aircraft should be capable of carrying payloads of 1000 to 3000 lb.
3. The design cruise Mach number should be 0.7.
4. The cruise time should be one to three (preferably) hours, which will allow sufficient time for data acquisition.
5. The aircraft shall be piloted.
6. Design the aircraft with present technology.

PRECEDING PAGE BLANK NOT FILMED

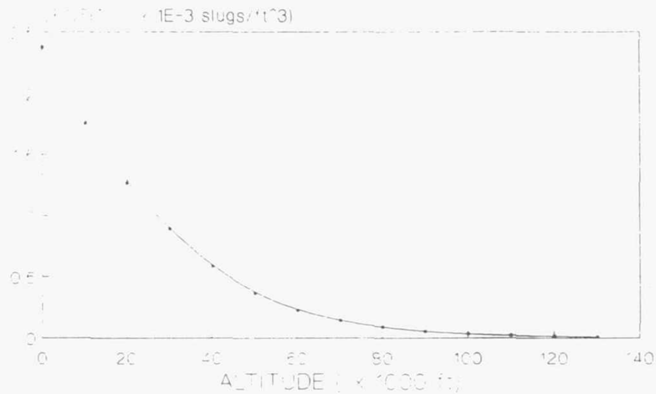

Fig. 1. Air Density Variation with Altitude

altitude of 100,000 ft was chosen. The payload carrying capability of the aircraft was suggested by NASA personnel[1].

Several major factors were involved in the determination of the cruise Mach number. Sufficient speed was required for fast collection of air samples from different locations without entering the transonic and supersonic speed regions. At transonic and supersonic speeds the temperature rise and possible dissociation in the flow would interfere with accurate analysis of air samples. On the other hand, lower cruise speed would become a major engineering obstacle since at those altitudes the air density is approximately 0.00003211 slugs/ft^3, as can be seen in Fig. 1. This low density at high altitude results in a very low dynamic pressure ($q_\infty < 8.0$ psf), generating small lift per unit area and thereby requiring prohibitively large wing surface areas.

Since the area of investigation is fairly new and probably full of surprises, it was decided that the presence of a human should be required. This was a major factor in the decision for having a piloted vs. a remotely piloted vehicle. Also, since the ozone layer problem currently gets worse with time, the technological level was taken to be currently available technology.

With these mission requirements the mission profile shown in Fig. 2 was prepared. This is a generic mission profile that was used for all three configurations. This generic profile provided a common basis for comparison.

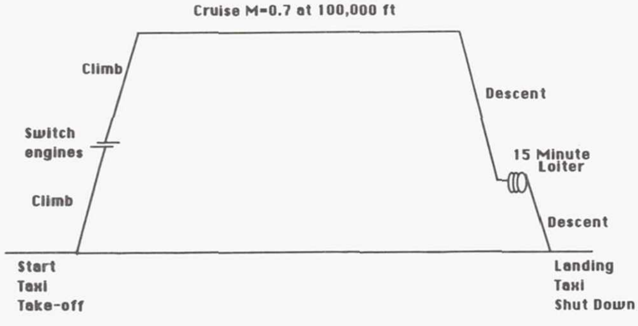

Fig. 2. Mission Profile

PROPULSION SYSTEMS

Due to the high altitude cruise requirement, conventional propulsion systems were not considered appropriate. Figure 3, adopted from Nicolai[2], illustrates the propulsion requirements for the mission compared to conventional propulsion systems.

It can be seen that many systems will not be able to operate at the desired altitudes. As a result, several conventional and nonconventional propulsion systems were investigated to determine the best system for operation at altitudes above 100,000 ft. The following propulsion systems were investigated: turbofan/turbojet, nuclear, laser, microwave, monopropellant reciprocating engines, and fuel cells.

Turbofan/Turbojet

Turbofan and turbojet engines were analyzed to determine the maximum possible operating altitude for these propulsion systems at subsonic speeds. Figures 4 and 5 show the altitude performance of ideal turbojet and turbofan engines that were designed to produce 17,000 and 15,000 lb, respectively, of static sea level thrust.

For both engines, the thrust is reduced to almost zero at 100,000 ft. Since the density at 100,000 ft is very small, the required cruise thrust at those altitudes (approximately 7000 lb) required an inlet that was over 20 ft in diameter. The corresponding sea level static thrust would be close to 90,000 lb. Engine size and large sea level thrust values effectively eliminated the use of turbojets or turbofans as propulsion means for altitudes above 60,000 ft.

Nuclear

A nuclear propulsion system would certainly meet range and endurance requirements set forth in any flight plan. An almost

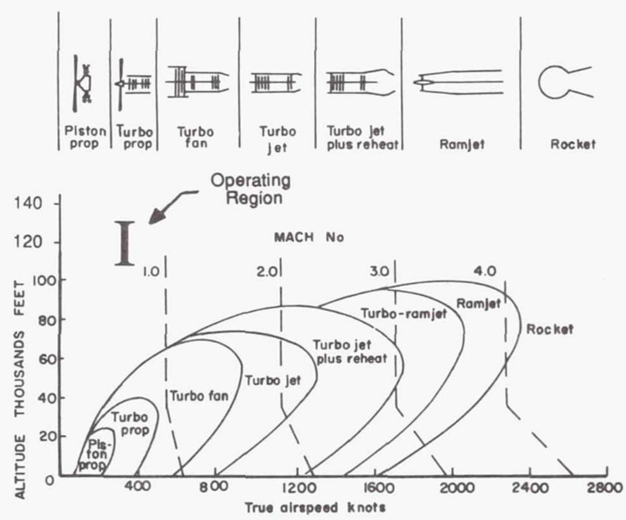

Fig. 3. Propulsion Systems

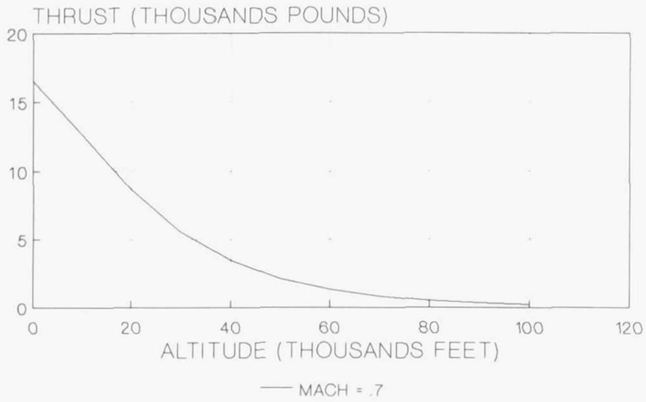

Fig. 4. 17,000 lb Thrust Turbojet Performance vs. Altitude

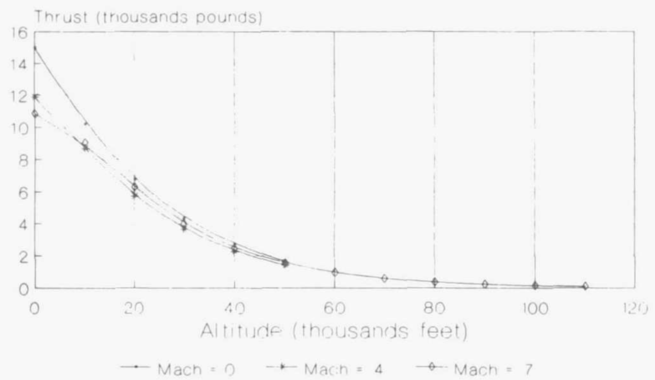

Fig. 5. Thrust vs. Alt and Mach Number, 15,000 lb Thrust Turbofan

unlimited supply of energy can be achieved from this system. However, there were several major factors that prevented this system from being seriously considered. Because of the neutrons, gamma rays, and other products present in nuclear fission, the pilot and instruments must be shielded. The shielding requirements would greatly increase the aircraft weight. Also, the political overtones and the technological design level of such a system would be major obstacles.

Laser

Another alternative propulsion concept for the proposed high altitude aircraft is that of laser power. This would consist of an aircraft flying at altitude with a receiving surface atop its fuselage to collect laser beams from satellites. Essentially the energy produced by the laser would be used to heat a fluid used to power the turbine of a turbofan engine. Although this propulsion system would result in a lighter propulsion system than would otherwise be possible, there are several obvious obstacles for this type of system. First, proven system technology, which would require very accurate tracking systems and high powered laser satellites, is currently not available. Secondly, the cost of such a system would be extremely high.

Microwave

A microwave-powered propulsion system for high altitude aircraft was suggested by Morris[3]. Using ground-based microwave stations, microwave beams would be directed toward the aircraft that would collect the energy and convert it into electrical power; an electrical motor would drive propellers. This is probably the lightest propulsion system that could be used. However, there are several drawbacks to this system. First, the microwave beams may interfere with the sampling instruments. Secondly, the microwave beam may alter the chemical composition of the ozone layer. Also, the cost of maintaining different ground based power stations would be prohibitive.

Fuel Cells

The use of fuel cells as a propulsion unit was investigated. The principle of conversion of energy is the foundation for the fuel cell concept. The fuel cell converts the chemical energy, created by the interaction of two reactants, to electrical energy by way of electrodes. The fuel cell differs from a battery in that the reactants of the fuel cell are kept away from the electrode housing and are brought together only when electric energy is required. Because of the proposed altitude at which the aircraft will operate, the best reactants for a low temperature fuel cell system are oxygen and hydrogen. The oxygen-hydrogen reaction also has one of the largest energy discharge values per unit mass. The main drawback with this type of system is that the reactants need to be kept in a liquid state to conserve volume. This would require extra apparatus that would increase the propulsion weight.

Reciprocating Engines

Finally, reciprocating engines provide an effective means of propulsion for high altitude flight. Although the availability of air at high altitudes causes a major obstacle for piston engines, this can be overcome by using monopropellants as fuel. Analysis indicated that a reciprocating engine powered by hydrazine fuel would produce the required thrust for high altitude cruise. Hydrazine is currently being used by the space shuttle and F-16 to produce maneuvering thrust and as an auxiliary power unit, respectively. A hydrazine engine was used for the Mini-Sniffer high altitude aircraft design project[4,5]. The major drawback to the use of hydrazine is that it is extremely toxic. However, the usage of hydrazine in the space shuttle and F-16 indicates that the technology for handling hydrazine safely is available.

PROPULSION SYSTEM SELECTION

It was decided that two propulsion systems would be used to propel the aircraft. A turbofan engine will be used at low

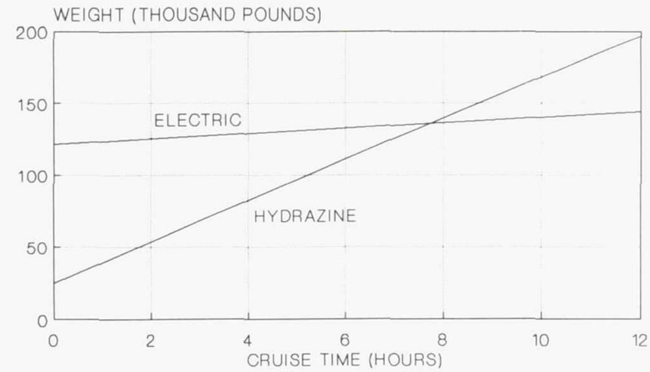

Fig. 6. Hydrazine and Electric Systems, System Weight vs. Cruise Time

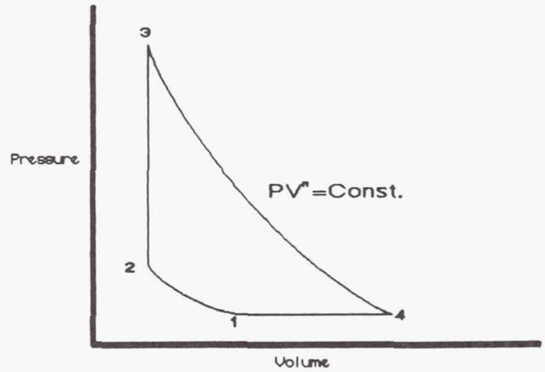

Fig. 8. Ideal Expansion Cycle

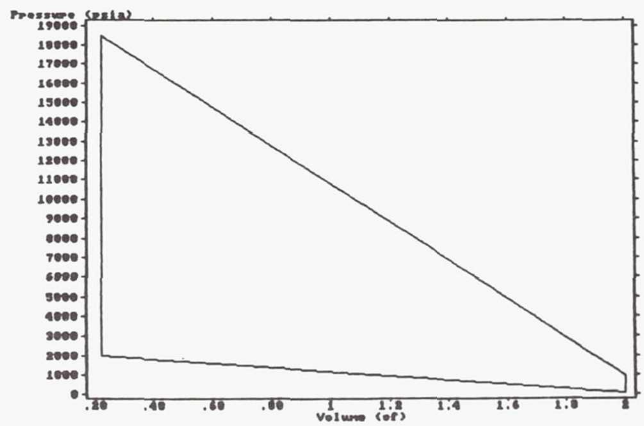

Fig. 9. Cycle Analysis for H2 Engine

altitudes and a reciprocating (monopropellant) engine will be used at high altitude.

Trade-off studies between the fuel cell and the hydrazine powered engine (Fig. 6) indicated that for low cruise time requirements the hydrazine system would result in a lighter overall weight. Due to the high fuel consumption rate, the hydrazine engine was not practical for the whole mission. Therefore, an afterburning turbofan engine was chosen as a first stage propulsion system. The turbofan engine was used for take-off and climb up to between 50,000 to 60,000 ft at which point the hydrazine engine was activated for climb to 100,000+ ft of altitude.

The hydrazine engine that was utilized for the high altitude propulsion system was a scaled version of the engine used in the Mini-Sniffer design project. A hydrogen scavenging system was added to it (Fig. 7) to lower the sfc.

The by-products of the hydrazine engine are nitrogen and hydrogen. The hydrogen is combined with oxygen and burned as a secondary fuel system to achieve higher efficiency. The cycle analysis for both the ideal hydrazine engine and the secondary hydrogen/oxygen systems are shown in Figs. 8 and 9, respectively. Figure 10 shows the hydrazine engine weight as a function of shaft horsepower.

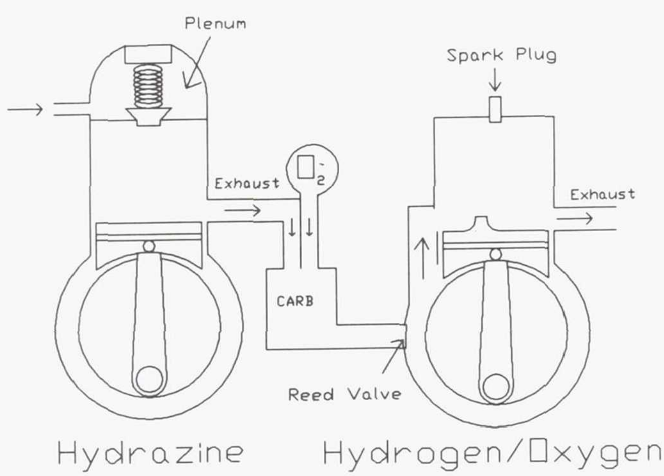

Fig. 7. Hydrogen Scavenging System

The ACSYNT computer code[(6)] was used to design the turbofan engine. It was designed so that the engine would produce 4500 lb of thrust at 50,000 ft altitude. This resulted in an engine that would produce 30,000 lb of static thrust at sea level. Figures 11 and 12 show the performance of the turbofan engine at sea level and at 50,000 ft for different power settings. It can be seen that the thrust-producing capability of the engine is reduced at the higher altitudes.

The required propeller diameter for the reciprocating engine was determined after extensive trade-off studies were made between the propeller diameter and the aircraft gross take-off weight. Figure 13 shows the efficiency of the propeller at different altitudes. It can be seen that, with a 42-ft-diameter propeller, 80% efficiency can be achieved at an altitude of 100,000 ft.

CONFIGURATIONS

Initially eight configurations were investigated. These configurations are given in Table 2.

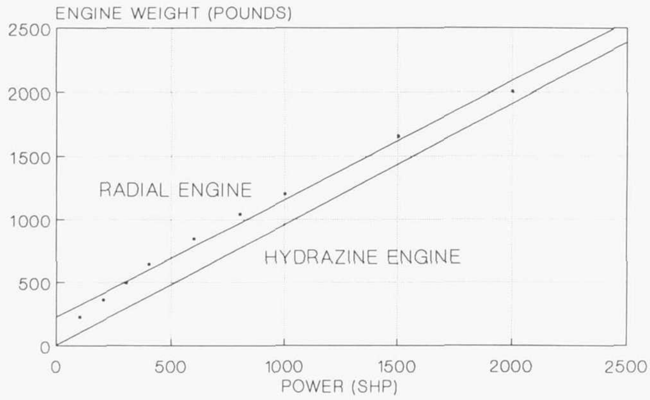

Fig. 10. Piston and Hydrazine Engines

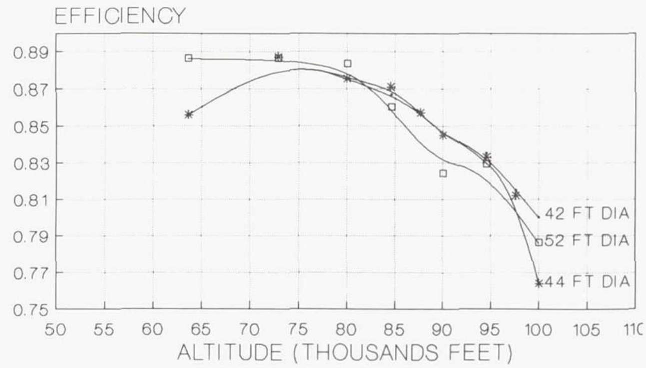

Fig. 13. Four-bladed Propeller Efficiencies: ACSYNT Results

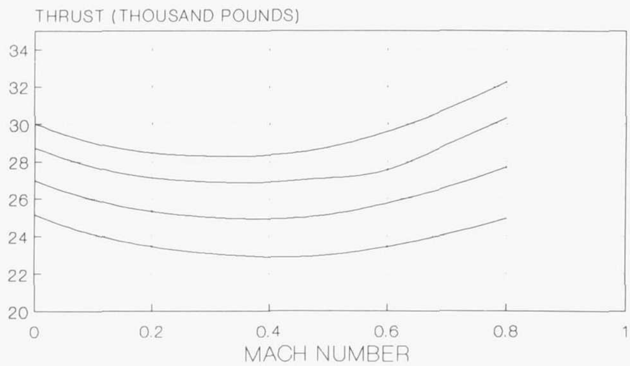

Fig. 11. 30,000-lb Thrust Afterburning Turbofan Performance at Sea Level

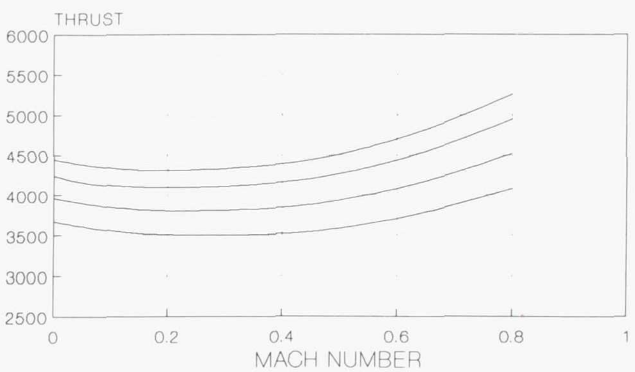

Fig. 12. 30,000-lb Thrust Afterburning Turbofan Performance at 50,000 ft

Table 2. Candidate Configurations

1.	Conventional (tail aft)
2.	Flying wing
3.	Three surface (small canard-wing-h. tail)
4.	Tandem wing (wing, wing, tail)
5.	Joined wing
6.	Canard (wing aft)
7.	Biplane
8.	High Altitude Blimp

Preliminary analysis indicated that the flying wing configuration is very unstable at high altitudes. Despite the flying wing's higher possible efficiency at the altitudes in question, a straight wing is desirable. This was not possible with the flying wing. The flying wing design would require sweep for stability, which would have drastically reduced the lift and resulted in a prohibitively large wing surface area. In addition, a stability augmentation system would drive up the aircraft cost.

The three surface configuration was rejected because the slight gain in the lower induced drag was offset by the lower stability in the system. Also, initial calculations indicated that to have a favorable affect from the canards, the canards would have to be very large. This would have resulted in a tandem wing configuration that was already chosen as one of the configurations for detailed consideration.

The canard design was eliminated because a paper by Cronin and Selberg[7] showed that a canard configuration has a lower L/D than a conventional design. There are also stability problems if maximum efficiency is the primary goal.

The biplane design can yield a lower induced drag if set up with the correct stagger and spacing[8]. Also, Gall and Smith[8] indicate that for high efficiency the wings should be close to each other. However, this design was eliminated because of the difficulty in keeping the high aspect ratio wings from flexing and hitting each other without excessive bracing, which would negate any aerodynamic benefits. In addition, if shock waves (transonic flow) were to form on the two wing surfaces it would have increased the interference drag.

The blimp becomes impractical due to the enormous sizes involved. Table 3 and Fig. 14 show the blimp weights and volumes involved in climbing to 100,000 ft.

As a result of the above evaluation, three configurations were chosen for detail analysis. The three configurations selected were the twin-boom tandem wing, the joined wing, and the

Table 3. Blimp Data at 100,000 ft

Weight (lb)	Vol. (ft^{3}E-6)	Radius (ft)	Length (ft)
1,000	0.967	40	200
5,000	4.836	65	360
10,000	9.672	85	425f
50,000	48.359	140	780
100,000	96.717	180	950
200,000	193.434	230	1,150
300,000	290.152	260	1,300
400,000	386.869	290	1,450
500,000	483.586	310	1,600

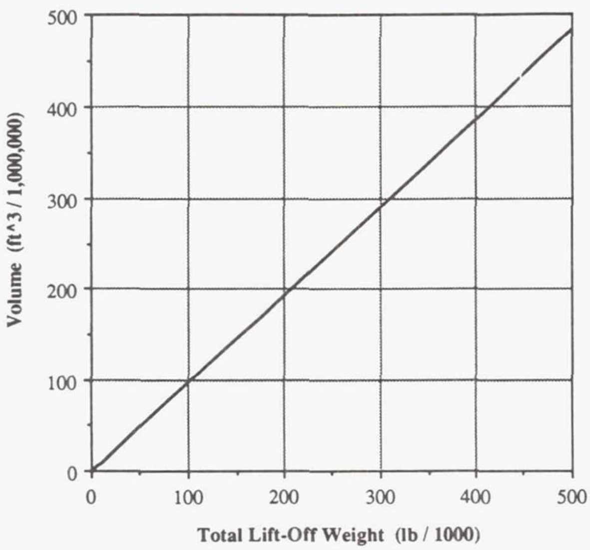

Fig. 14. Volume of Blimp Required for Various Weights at 100,000 ft

conventional twin-boom configurations. The tandem wing and joined wing designs should have higher efficiencies than conventional configurations, as well as some structural reinforcing capabilities.

Twin-Boom Tandem Wing

The twin-boom tandem wing configuration is shown in Fig. 15. It has a front wing aspect ratio of 8.86 and a rear wing aspect ratio of 11 with an overall wing loading of 3.0 psf at altitude. The main advantage of the tandem wing is that high aspect ratios can be achieved with each wing, with shorter span, than a single wing, and yet maintain the large surface area that is required. The twin booms provide the necessary structural strength.

Table 4 shows a summary of the geometry and weight data for the tandem wing design.

Joined Wing

The joined wing configuration is shown in Fig. 16. The advantage of the joined wing is twofold. The anhedral of the rear wing and the dihedral of the front wing provide good lateral stability characteristics. Also, because the two wings are joined together, the aircraft is structurally very strong, which is a desired quality in aircraft with large wing spans. The wings were joined at the 70% span position for maximum structural efficiency[9]. The major problem with the joined wing configuration is that it is not a proven technology.

Table 5 shows a summary of the performance and weight data for the joined wing design.

Conventional Twin-Boom

The conventional twin-boom configuration is shown in Fig. 17. This configuration was designed for a higher wing loading (compared to the other two configurations) at cruise conditions (W/S = 6.0 psf) at the cost of a lower (compared to the other two configurations) stall margin during cruise. The higher wing loading was chosen because it is not well supported structurally and a larger wing surface area would have resulted in heavier wings. The twin booms were used to provide structural strength to the large horizontal tail and space for landing gear retraction. The advantage of this somewhat conventional configuration is that it is a simple system and has proven to be reliable over the years. This

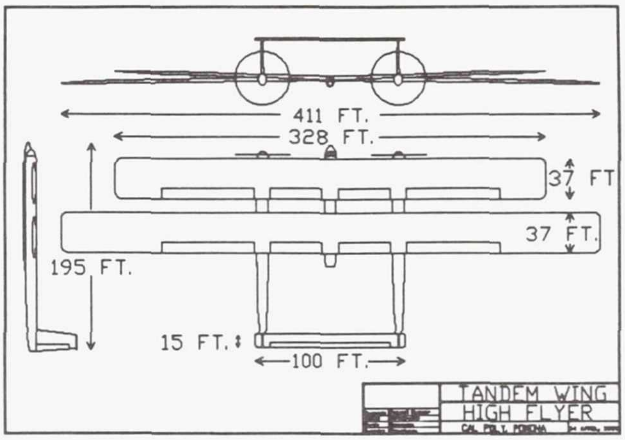

Fig. 15. Twin-boom Tandem Wing Configuration

Table 4. Tandem Wing Configuration Design Data

Parameter	Value
Front wing area	12,062 ft^2
Rear wing area	15,352 ft^2
Front wing span	328 ft
Rear wing span	411 ft
Front wing aspect ratio	8.96
Rear wing aspect ratio	11.0
Fuselage length	96 ft
Boom length	195 ft
Gross take-off weight	104,500 lb
Cruise weight (initial)	79,500 lb
Empty weight	54,000 lb

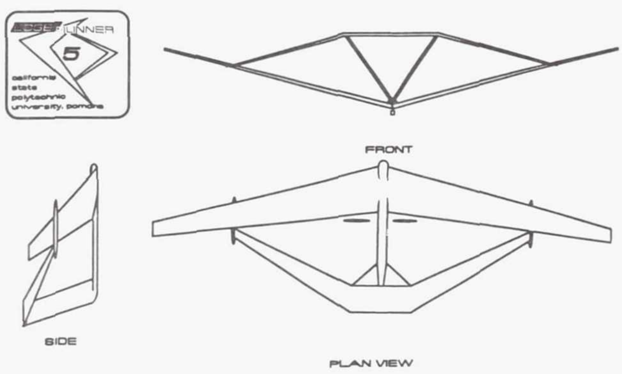

Fig. 16. Joined Wing Configuration

Table 5. Joined Wing Configuration Data

Parameter	Value
Front wing area	16,250 ft^2
Rear wing area	7,875 ft^2
Front wing span	500 ft
Rear wing span	375 ft
Front wing aspect ratio	15.3
Rear wing aspect ratio	15.4
Fuselage length	160 ft
Boom length	195 ft
Gross take-off weight	137,000 lb
Cruise weight (initial)	105,000 lb
Empty weight	82,000 lb

conventional configuration was also used as a basis for comparison of the tandem and joined wing designs.

Table 6 shows a summary of the performance and weight data for the conventional configuration.

AERODYNAMICS

The aerodynamic characteristics of the three configurations were evaluated using the methods outlined by Nicolai[(2)]. The major problem in the aerodynamic analysis was the selection of an airfoil that would provide the required lift without having shock waves (transonic flow) on the surface.

Airfoil Design

The airfoil selection criteria included high lift at cruise conditions (100,000 ft, Mach 0.7, Re = 2 million), low shock

Table 6. ConventionalTwin-Boom Configuration Design Data

Parameter	Value
Wing area	13,454 ft^2
Aspect ratio	8.0
Fuselage length	60 ft
Boom length	69.6 ft
Gross take-off weight (ACSYNT results)	95,000 lb
Cruise weight (initial)	71,000 lb
Empty weight	51,333 lb

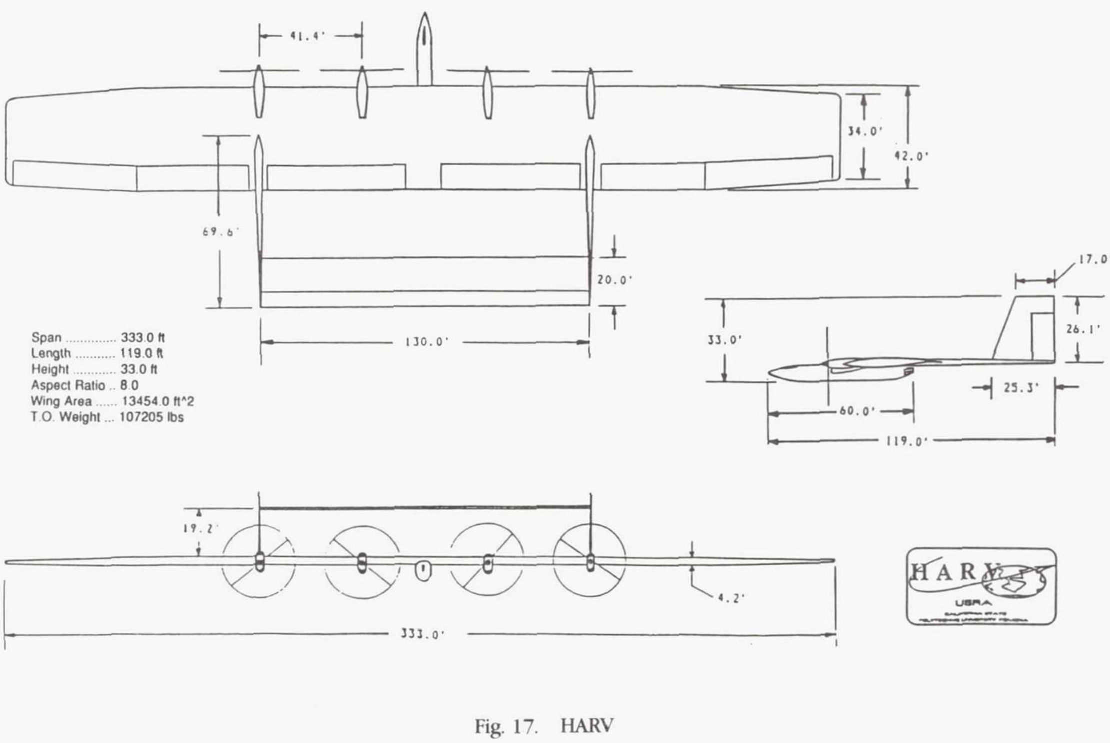

Fig. 17. HARV

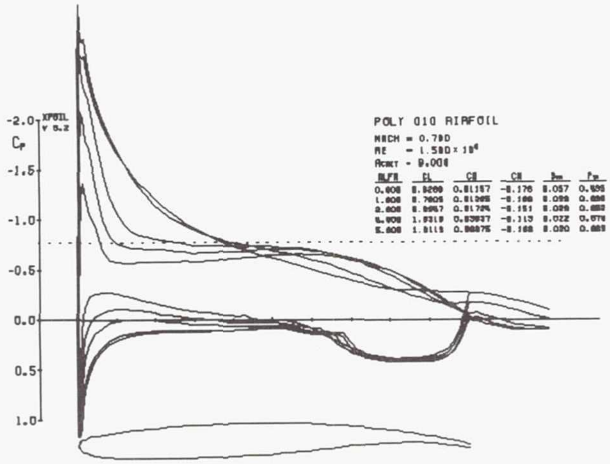

Fig. 18. XFOIL Pressure Distributions

losses, and low drag. Two methods for choosing an airfoil were available. A suitable airfoil could have been picked and available data extrapolated to our extreme flight conditions, or a new airfoil could have been designed utilizing various software available. The compromise chosen started with a known reasonable airfoil. It was modified slightly and reanalyzed. This permitted a check of the analysis for order of magnitude errors.

The computer code called XFOIL written by Mark Drela(10) was used to modify the airfoils. The base airfoil is that used on the MD-80 aircraft. This was used because it is a supercritical airfoil and should minimize shocks. In order to increase the lift of this airfoil the XFOIL code was used to tailor the pressure (C_p) distribution. This yielded an airfoil with more trailing edge reflex, higher lift, and no greater shock losses (Fig. 18). The negative result was a large negative pitching moment coefficient, C_m. This was not a problem on the dual and joined wing aircraft since the lift between the two wings can be tailored for trim. The large negative C_m was unacceptable on the conventional design, however, since the large trimming forces negate so much of the added lift and increase trim drag significantly. Therefore some of the trailing edge reflex was removed from the airfoil for the conventional design.

The XFOIL program is subject to limits of integration errors. These manifest themselves in the "peakedness" of the C_p distributions near the leading edge of the airfoil (Fig. 18). This has been ascertained by comparing experimental data to the program results for an unmodified MD-80 airfoil. This means two things. First, the lift estimates will be slightly high. Second, the shock waves will not be as strong as indicated by these peaks.

PROPELLERS

For the propeller analysis two methods were employed. Initially, the standard Hamilton Propeller Charts(11) and the ACSYNT computer program were used to design the general size of the propellers and determine their performance. The second program used to analyze the propellers was the computer program called XROTOR, another program supplied by Mark Drela(10). This program solves for the helically symmetric potential flow about a rigid helicoidal wake. This takes into account hubs and nacelles. Due to the cruise conditions this program designs propellers that are ideal. The program yields a propeller with a 20-ft radius (acceptable) and a root chord of 30 ft (obviously unacceptable). However, if the design is used as a starting point, modified to have a constant chord, and reanalyzed, the performance is acceptable and the planform is more realistic. These problems stem from designing a propeller to work efficiently in a very rarified atmosphere.

Based on the specific configuration, different propeller diameters, ranging from 40 to 50 ft, were obtained. For the conventional configuration, a 42-ft propeller diameter was obtained, producing 4000 lb of thrust at an altitude of 100,000 ft.

WEIGHT AND STRUCTURAL ANALYSIS

For all three configurations the structural analyses were performed using the NASTRAN structural analysis program(12). Figure 19 shows the NASTRAN model of the joined wing configuration and the resulting deflections. Maximum deflection was determined to be approximately 68.6 in. For the conventional configuration the wings had to be strongly reinforced in order to keep the maximum deflection small

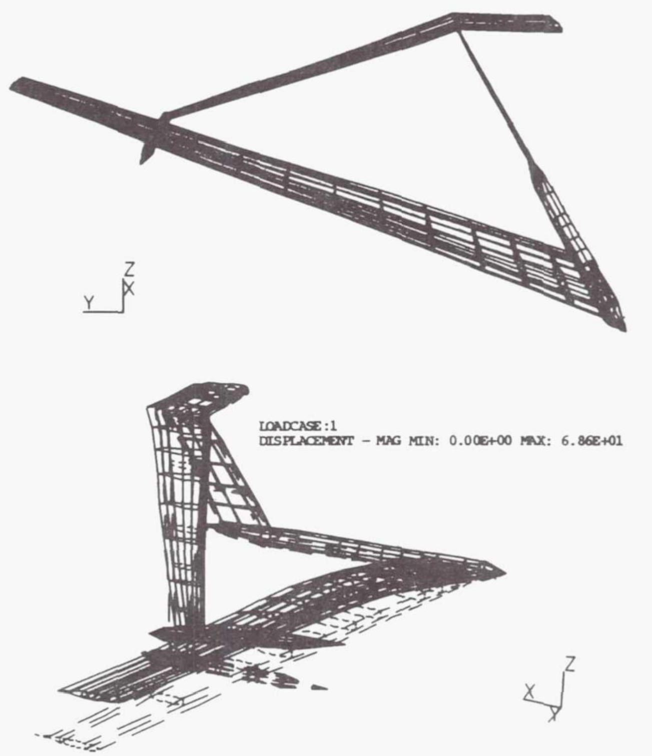

Fig. 19. Structural Configuration of the Joined Wing

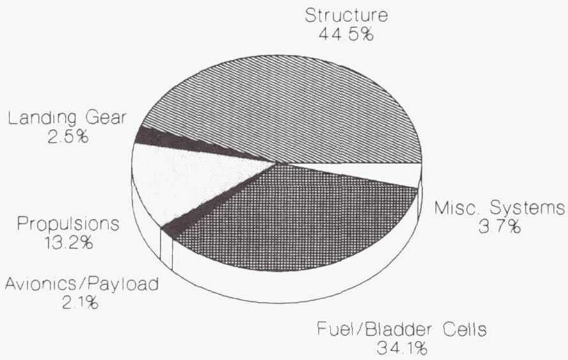

Fig. 20. Weight Breakdown

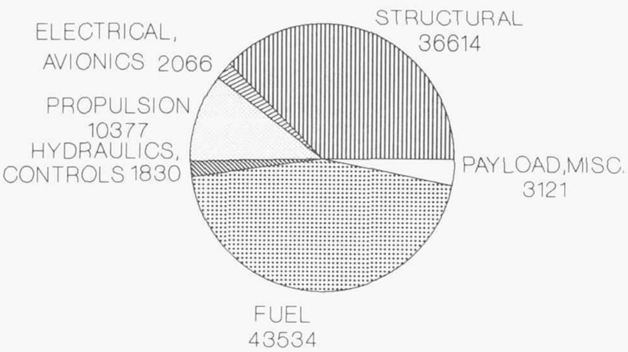

Fig. 21. Weight Distribution Calculated by ACSYNT

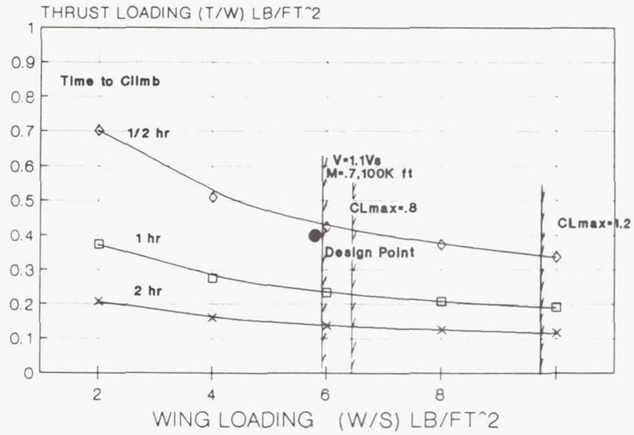

Fig. 22. Sizing Chart (Sea Level)

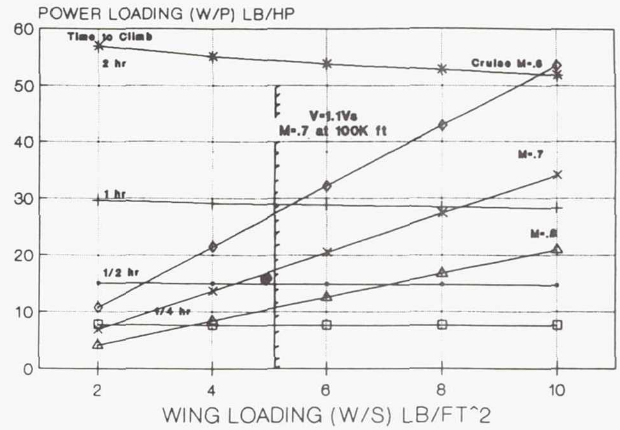

Fig. 23. Sizing Chart (50,000 ft)

(maximum deflection was 37 in). This resulted in slightly heavier wings.

The component wing weights were calculated using the methods outlined by Nicolai[2]. For the nonconventional designs, the weight equations were modified to achieve reasonable results.

Figures 20 and 21 show the weight distribution for the conventional configuration by two different methods. In Fig. 20 Nicolai's methods were used. In Fig. 21 ACSYNT was used to calculate the weight of the components. The results agreed within 10%. The gross take-off weight predicted with Nicolai's methods was 105,000 lbs and with the ACSYNT program, 95,000 lbs.

PERFORMANCE

The three configurations were designed using the generic sizing chart shown in Fig. 22. With the sizing chart, initial power and wing loadings were determined.

Figure 22 was based on the discussion in Roskam[13] and allows take-off, landing, and cruise conditions to be examined on one chart. Since two propulsion systems were utilized, initially two different sizing charts were prepared. One sizing chart was prepared for the 50,000-ft altitude (Fig. 23) utilizing the hydrazine engine, and the second one created for sea level utilizing the turbofan engine.

These two sizing charts were later combined into one sizing chart at sea level, as shown in Fig. 22, and the design points were chosen so that at least 20% stall margin will be maintained at cruise speed and altitude for the joined wing and tandem wing. For the conventional configuration the stall margin was lower (10%).

The take-off distance is proportional to the wing loading and inversely proportional to the aircraft thrust-to-weight ratio. A maximum take off distance was chosen to be 5000 ft, in compliance with FAR 25 requirements. As shown in Fig. 24 for the tandem wing, and similarly for the other configurations, the aircraft take-off distance was within the required field length.

The climb performance utilizes the minimum fuel consumption path to achieve the required cruise altitude. As shown in Fig. 25, the rates of climb for the aircraft decrease with altitude up to 50,000-60,000 ft. In this altitude range the hydrazine engine is activated to take the aircraft up to cruise altitude.

Depending on the configuration, the different aircraft were able to cruise at different altitudes. Figure 26 shows the power available and required curves at a cruise altitude of 110,000

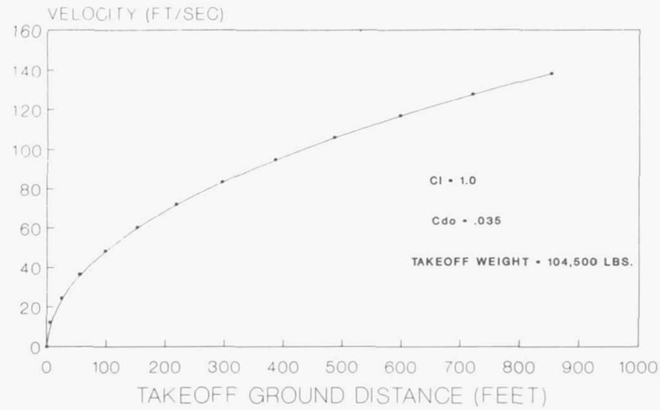

Fig. 24. Velocity vs. Distance (Take-off Roll)

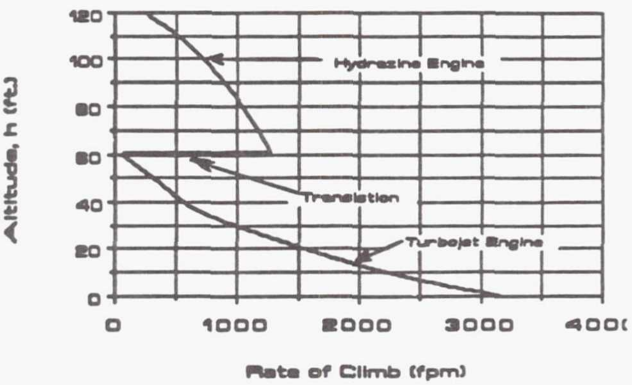

Fig. 25. Maximum Rate of Climb vs. Altitude

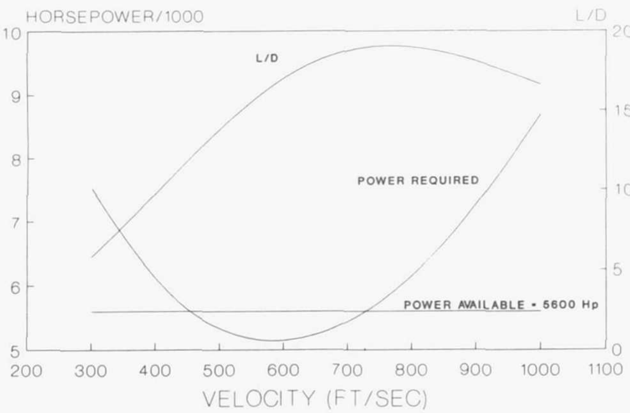

Fig. 26. Cruise Performance (110,000 ft)

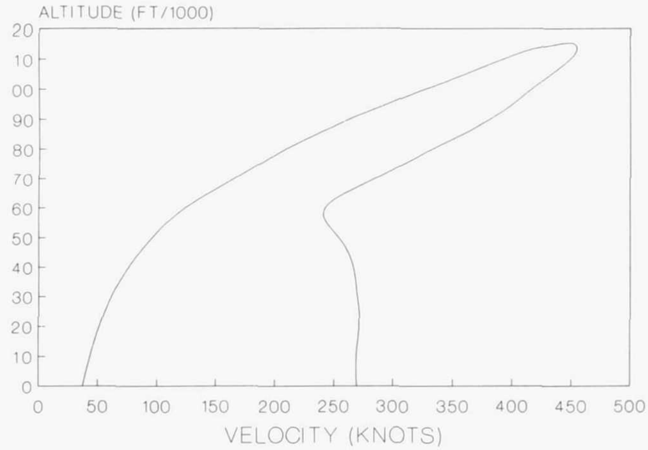

Fig. 27. Flight Envelope (Tandem Wing)

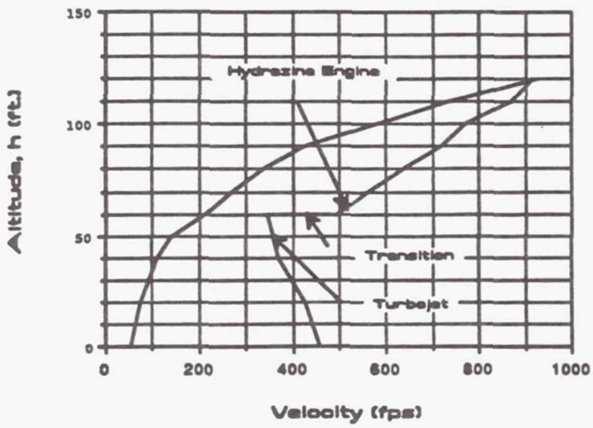

Fig. 28. Flight Envelope (Joined Wing)

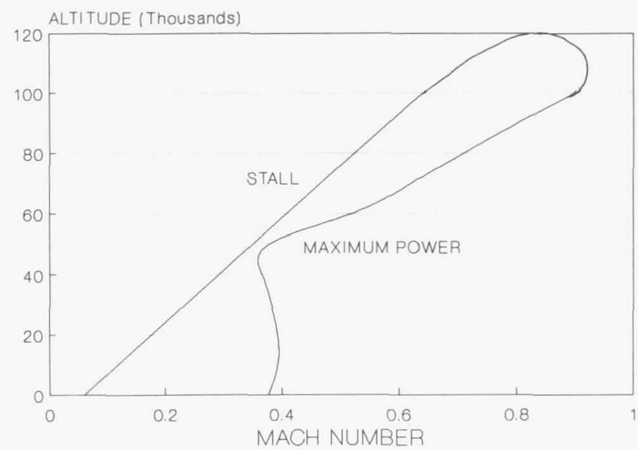

Fig. 29. Flight Envelope (Conventional Wing)

ft for the tandem wing configuration. From the Figure it can be seen that the cruise condition was achieved at maximum lift-to-drag ratio, which insured maximum cruise efficiency.

The performance analysis of the three configurations indicates a very narrow flight envelope in the 50,000-100,000 ft altitude range. Figures 27, 28, and 29 show the operating envelopes for the tandem wing, joined wing, and conventional configurations, respectively. At altitudes between 50,000 and 60,000 ft, the turbofan engine will be turned off and the reciprocating engine will be turned on. The exact altitude for changeover is configuration dependent.

Table 7. Configuration Performance Summary

Parameter	Joined Wing	Tandem Wing	Conventional
Service Ceiling	113,000 ft	112,300 ft	110,000 ft
Absolute Ceiling	119,000 ft	116,000 ft	120,000 ft
Cruise Altitude	112,000 ft	110,000 ft	100,000 ft
Cruise Speed	0.7 Mach	0.7 Mach	0.7 Mach
Cruise Range	568 NM	568 NM	406 NM
Take-off Distance	1453 ft	990 ft	3800 ft
Landing Distance	2142 ft	1400 ft	1120 ft

Table 7 provides a summary of the performance data for the three configurations.

CONCLUSIONS

1. It is possible to achieve the required cruise altitude utilizing conventional technology. With an appropriate propulsion system, altitudes of 130,000 ft can be achieved. It is suggested that further study be conducted in the area of propulsion. If the propulsion systems can be combined into one unit, it will greatly reduce the weight.

2. Further iterations of the design are needed to reduce the weight and improve the performance. With better airfoil designs higher lift coefficients can be achieved.

3. Further studies should consider supercharging an existing turboprop propulsion system to determine if such a system will operate at altitudes above 100,000 ft. If a conventional turboprop system is possible it would greatly reduce the propulsion weight.

ACKNOWLEDGMENTS

The authors, D. Poladian and D.J. Reinhard, acknowledge the contributions to this paper by Demetrius T. Griffin, Linda J. Gutierrez, Eric J. Raymundo, Jeffrey E. Peltz, and Melvin B. Desembrana, who served as group leaders of various design teams associated with this project. We also acknowledge the contributions of the individual members of the project design teams. Without their efforts this paper would not have been possible. We appreciate the efforts of George Kidwell of NASA ARC for his guidance in this effort. We also appreciate the efforts of John Sevier, Carol Hopf, and their staff at Universities Space Research Association (USRA) for their constant encouragement and support. We especially thank Dr. Conrad F. Newberry for his immeasurable support and patience.

REFERENCES

1. George Kidwell, personal communication, NASA Ames Research Center, Fall, 1988.
2. Nicolai L. M., *Fundamentals of Aircraft Design.* METS Inc., San Jose, 1975.
3. Morris C. E. K., Jr., Parametric Study of Microwave-Powered High-Altitude Airplane Platforms Designed for Linear Flight, NASA Technical Paper 1918, 1981.
4. Reed R. D., "High-Flying Mini-Sniffer RPV: Mars Bound?", *Astronaut. Aeronaut., 16, no. 6,* 26-39.
5. Akkermann J. W., Hydrazine Monopropellant Reciprocating Engine Development. ASME Preprint, ASME Annual Winter Meeting, December 10-15, 1978.
6. Bruflat A. B., *User's Manual for ACSYNT - A Computer Program for Aircraft Synthesis.* Naval Postgraduate School, December, 1977.
7. Cronin D. L. and Selberg B. P., *Aerodynamic-Structural Study of Canard, Dual Wing and Conventional Wing Systems for General Aviation Applications.* NASA CR-172529, February, 1985.
8. Gall P. D. and Smith H. C., "Aerodynamic Characteristics of Biplanes with Winglets", *J. Aircraft, 24, no. 8,* 518-522.
9. Wolkovitch J., "The Joined Wing: An Overview", *J. Aircraft, 23, no. 3,* 161-178.
10. Mark Drela, personal communication, MIT, Fall, 1988.
11. *Generalized Method of Propeller Performance Estimation.* PDB 6101, Revision A, Hamilton-Standard (United Aircraft Corporation), June, 1963.
12. Gockel M. A. (ed.), *MSC/NASTRAN, Hand-book for Dynamic Analysis (Version 63).* The Macneal-Schwendler Corporation, June, 1983.
13. Roskam J., *Airplane Design Part 1: Preliminary Sizing of Airplanes,* Roskam Aviation and Engineering Corporation, Ottawa, Kansas, 1985.

1994004547
383657
98

N94- 71302

A SECOND-GENERATION SUPERSONIC TRANSPORT

CASE WESTERN RESERVE UNIVERSITY

S35-05
160661
P. 7

INTRODUCTION

Ever since the advent of commercial flight vehicles, one goal of designers has been to develop aircraft that can fly faster and carry more passengers than before. After the development of practical supersonic military aircraft, this desire was naturally manifested in a search for a practical supersonic commercial aircraft. The first and, to date, only supersonic civil transport is the Concorde, manufactured by a consortium of British and French aerospace companies. Unfortunately, due to a number of factors, including low passenger capacity and limited range, the Concorde has not been an economic success. It is for this reason that there is considerable interest in developing a design for a supersonic civil transport that addresses some of the inadequacies of the Concorde.

For the design of such an aircraft to be feasible in the near term, certain guidelines must be established at the outset. Based upon the experience with the Concorde, whose 100-passenger capacity is not large enough for profitable operation, a minimum capacity of 250 passengers is desired. Second, to date, because of the limited range of the Concorde, supersonic commercial flight has been restricted to trans-Atlantic routes. In order to broaden the potential market, any new design must have the capability of trans-Pacific flight. A summary of the potential markets involved is presented in Fig. 1. Also, because of both the cost and complexity involved with actively cooling an entire aircraft, an additional design constraint is that the aircraft as a whole be passively cooled.

One additional design constraint is somewhat less quantitative in nature but of great importance nonetheless. Any time a new design is attempted, the tendency is to assume great strides in technology that serve as the basis for actual realization of the design. While it is not always possible to avoid this dependence on "enabling technology," since this design is desired for the near term, it is prudent, wherever possible, to rely on already existing technology. This is of particular importance with respect to support technology such as airport terminals and runways.

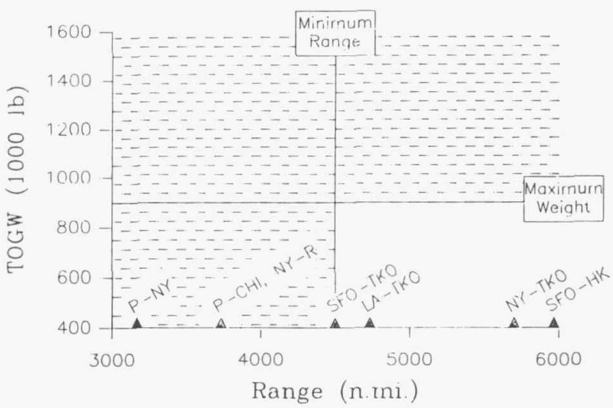

Fig. 1. NASA HSCT Study

Based on the above introductory remarks, a possible approach to the design of a second-generation supersonic civil transport is presented below. The design Mach number for this aircraft is 3.5. This value was chosen as it represents the limiting Mach number in the absence of active cooling. The ensuing design attempts to deal with the particular problems that are the most demanding, while relying on proven technology where it is adequate. The report clearly does not solve, or even deal with, every aspect of the aircraft design. Rather, a general direction is suggested and supported with initial, approximate calculations.

DESIGN CHALLENGES

One practical difficulty with any supersonic civil transport is the effect it has on the environment; specifically, the issue of sonic boom must be addressed. Due to the shock waves generated by an aircraft flying supersonically, sonic boom is generated at ground level. Present regulations prohibit the generation of sonic boom over populated areas beyond a certain minimal level. In addition, at present there is no way to eliminate the sonic boom through the design of the aircraft. As a result of this constraint, the craft will be required to fly at subsonic speeds for much of the overland portions of its flights. This presents the designers with the challenge of finding a design that is effective under both supersonic and subsonic conditions. This dual flight envelope is most problematic in the areas of aerodynamics and propulsion.

In addition to this difficulty, there are some specific problems associated with flight at Mach 3.5. These include high wave drag, low lift-to-drag ratio and stagnation pressure losses through the propulsion system. Although all these problems have been dealt with in previous supersonic aircraft, both civil and military, because all the above phenomena are strong functions of Mach number, the increase to Mach 3.5 magnifies these difficulties considerably.

In the area of materials and structures, the primary challenge is in the selection of materials that will be able to withstand the considerable aerodynamic heating without requiring global active cooling. In addition, as with any aircraft, it is of crucial importance that the weight of these materials be kept as low as possible. Since a long-range supersonic aircraft requires that a large fraction of the TOGW (take-off gross weight) be fuel and since a reasonable payload fraction is necessary for economic viability, the empty weight of the vehicle must be a smaller than usual fraction of the maximum TOGW. This

PRECEDING PAGE BLANK NOT FILMED

284 INTENTIONALLY BLANK

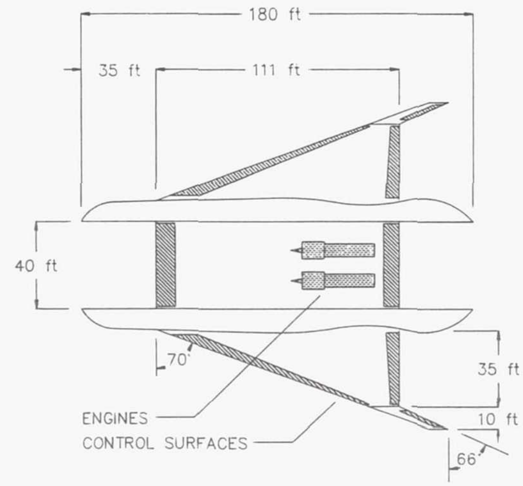

Fig. 2. Planform View

reduction in the empty weight can come from two areas, materials selection and efficient structural design.

DESIGN

Because of the tendency of supersonic aircraft to require very large, and therefore, heavy, wings for a given fuselage, the decision was made to employ a twin-fuselage, "flying wing" type planform. A dimensioned sketch of the planform appears in Fig. 2 and a comparison of overall dimensions between this design and a Boeing 747 in Fig. 3. There are several advantages to this approach. First, preliminary data[1,2] suggest that a twin fuselage configuration with a center lifting surface reduces wave drag, thereby increasing cruise lift-to-drag ratio. Second, since a single fuselage would have to be quite a bit larger to carry the same number of passengers, the overall length of the plane is reduced through the use of two fuselages. This may also lead to a decrease in empty weight since a smaller fuselage requires less structural reinforcement. Twin fuselages also allow a significant portion of the wing area to be located between the fuselages, reducing the size, and, most importantly, the root bending moment, of the outboard wings. Estimated empty weight is 240,000 lb, with a gross takeoff weight of 750,000 lb.

A biconvex airfoil with a cranked-arrow planform and a maximum thickness of 6% was chosen for the wings. This airfoil and configuration has shown high lift at supersonic speeds as well as adequate performance at subsonic conditions[3] when flaps and slats are employed. One difficulty with the wing design is the desire for a rounded leading edge at subsonic speeds and for a sharp one at supersonic cruise conditions. A possible solution is a dual geometry leading edge as pictured in Fig. 4. Figure 4a indicates the wing configuration at cruise conditions. For takeoff, landing, and low speed flight, the sharp leading edge segments are retracted into the wing and slats and flaps are deployed as indicated in Fig. 4b. Although this arrangement is somewhat complicated from a kinematic standpoint, it does not appear to be much worse than many of the flaps that are presently employed.

The choice of materials for the aircraft was primarily motivated by the desire to avoid global active cooling, and, naturally, to minimize weight. At the cruise speed of Mach 3.5, the stagnation temperature is 885°F. Since the nominal skin temperature will not exceed the stagnation temperature, this value was chosen as the design skin temeprature. In actuality, the highest radiation equilibrium temperature occurs at the fuselage apex, and is calculated to be 855°F[4]. There are several materials that maintain the necessary strength and ductility at this temperature. One such material, already in use in the aircraft industry is Ti_3Al. This titanium-aluminum alloy, developed by Pratt and Whitney, is ductile and can be used at temperatures up to 1300°F without losing its strength. While Ti_3Al exhibits a very high strength-to-weight ratio in addition to its high-temperature properties, it is also difficult to work and very costly; thus, other materials, such as high-temperature composites are also being investigated for use in the primary structures of the craft.

	SST–II	Boeing 747
Span (ft)	160	196
Length (ft)	180	230
Wheelbase (ft)	60	84
Wing Area (ft^2)	9040	5500

Fig. 3. Dimensions

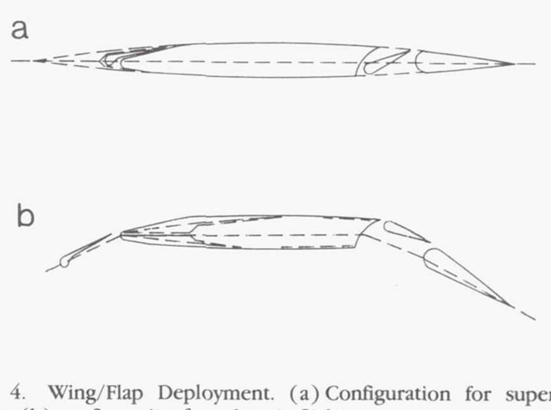

Fig. 4. Wing/Flap Deployment. (a) Configuration for supersonic flight; (b) configuration for subsonic flight.

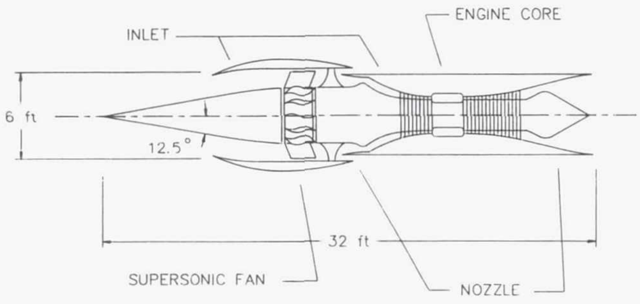

Fig. 5. Supersonic Through-Flow Turbofan Engine

The propulsion system consists of four supersonic through-flow turbofan engines, shown in Fig. 5. These will be mounted on the center surface between the two fuselages, with two engines above and two below the surface. An unusual example of propulsion-airframe integration is the "D"-shaped cross-section of the fuselages. This allows a more uniform flow to reach the engines. The center lifting surface is used to provide some compression of the flow before it reaches the engine inlets. The flow is compressed and slowed from the free-stream Mach number of 3.5 to a Mach number of 3.2 at the engine inlets. A schematic diagram of this compression is found in Fig. 6. The choice of this type of engine is motivated by two major factors. First, due to the relatively low stagnation pressure loss and fuel consumption associated with these engines[5,6], it is anticipated that they will be more efficient than conventional turbojets. In addition, because these engines do not require a large, complex inlet system, a substantial weight savings is expected.

In the following sections, specific aspects of the design will be discussed in relation to various regions of the flight envelope. These will be presented in order of interest.

SUPERSONIC CRUISE

During the supersonic cruise phase, the sharp leading edge is extended and the flaps are completely retracted to yield a configuration that is efficient at supersonic speeds (Fig. 4a).

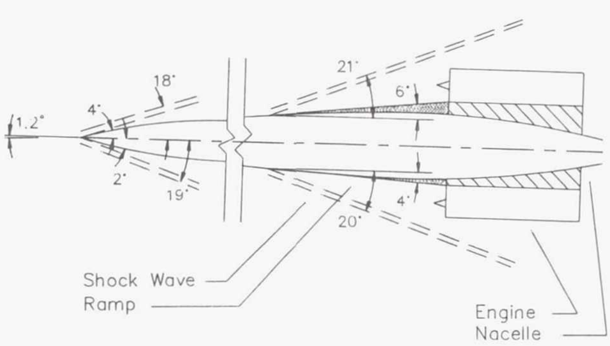

Fig. 6. Compression Surfaces

From the calculations presented in Appendix A, the following average values can be determined:

$$\alpha = 1.2^\circ$$
$$C_L = 0.0759$$
$$C_{DW} = 0.0084$$
$$C_{DS} = 0.0052$$

where α is the angle of attack, C_L is the lift coefficient, C_{DW} is the wave drag coefficient and C_{DS} is the skin-friction drag coefficient. Although there are other components of the total drag at cruise, the skin-friction and wave drag components comprise the bulk of the total drag and, for the purposes of a first approximation, the other components are neglected. These coefficients result in the following forces on the aircraft:

$$L = W = 700{,}000 \text{ lb}$$
$$\begin{aligned} D &= D_{wave} + D_{skin\ friction} \\ &= 77{,}500 \text{ lb} + 48{,}000 \text{ lb} \\ &= 125{,}500 \text{ lb} \end{aligned}$$

This results in an average cruise lift-to-drag ratio of 5.5. It should be noted that these values represent the initial design attempt. Based upon subsequent analysis, it is anticipated that they may increase by up to 7% (i.e., TOGW = 800,000 lb maximum).

The required thrust of 125,500 lb is supplied by the four supersonic through-flow turbofan engines. These engines are twin-spool turbofans, with the conventional fan stages replaced by a single-stage fan with supersonic axial flow. The maximum thrust capacity of these engines at the cruise conditions is 41,250 lb per engine (165,000 lb total), providing a thrust margin in excess of 25%. The thrust specific fuel consumption (TSFC) of the engines at the design point is calculated as 1.397 lbm/lbf/hr. At the design point, the Mach number at the face of the six-foot diameter fan is 3.0. The initial compression of the flow, shown in Fig. 6, is discussed above. The remaining compression is accomplished by a conical centerbody with a 12.5° half-angle at the engine inlet.

The performance values for the propulsion system have been calculated with an assumed bypass ratio of 0.5. This results in a fan pressure ratio of 1.364 in order to match the required core inlet flow. Since a supersonic fan is expected to achieve pressure ratios on the order of 3[5], a greater bypass ratio is possible. Increasing the bypass ratio will increase thrust while decreasing TSFC.

SUBSONIC CRUISE

Due to the fact that at the present time it is impossible to eliminate the sonic boom associated with supersonic flight, the portion of the flight path over populated areas must be flown at reduced speed. It is hoped that flight at supersonic Mach numbers up to 1.4 will be possible with only minimal sonic boom. Present regulations, however, forbid any supersonic flight over land (south of the Arctic Circle) and it is therefore necessary to fly portions of the flight in subsonic cruise. Although this does not represent a significant fraction of the

overall flight path for most of the routes in question, aircraft performance is so fundamentally different at subsonic conditions that it is important to study this regime as well.

During subsonic flight, including takeoff and landing, the biconvex airfoil shape is augmented with high-lift devices. These include a trailing edge, double-slotted flap and a leading edge extensible slat. The angular displacement of these surfaces can be controlled from the cockpit with the result being a variable camber wing. During the subsonic portion of the flight, the two half-wedges that provide a sharp leading edge in supersonic cruise are retracted into the wing. The subsonic wing configuration is pictured in Fig. 4b. Comparison of the two wing configurations shown in Fig. 4 indicates that the total chord is not drastically changed by the deployment of the flaps and slats as opposed to the sharp leading edge, and for design calculations, chord is taken as unchanged for all flight regimes.

Based on the calculations of Appendix B, relevant average values are:

$$\alpha = 4.1^\circ$$
$$C_L = 0.2932$$
$$C_{DI} = 0.0146$$
$$C_{DS} = 0.0072$$

where α is the angle of attack, C_L is the lift coefficient, C_{DI} is the coefficient of induced drag, and C_{DS} is the skin-friction drag coefficient. Here, too, there are other components of drag that have been neglected in comparison to the induced and skin-friction components of drag. It should be noted that the seemingly low lift coefficient is not in error, but is a result of the oversized wings. Resultant forces based upon these coefficients are:

$$L = W_{\text{take-off}} = 750{,}000 \text{ lb}$$
$$D = D_{\text{induced}} + D_{\text{skin friction}}$$
$$= 37{,}300 \text{ lb} + 18{,}000 \text{ lb}$$
$$= 55{,}300 \text{ lb}$$

This results in a subsonic lift-to-drag ration of 13.6, which is consistent with present technology.

Because of the fact that the supersonic through-flow turbofan engine is still in its developmental stages, the performance of the propulsion system at subsonic conditions remains unknown. The most difficult aspect in question is how the supersonic single-stage fan will perform at low speeds. Although reliance on technological advances was avoided where possible, the propulsion system remains an area where some enabling technology is required in order to meet the mission specifications.

TRANSONIC REGION

The primary challenge in the transonic region of the flight envelope is in the realm of propulsion. There is no difficulty in maintaining sufficient lift, and retaining positive control of the craft is relatively easily accomplished. The wave drag coefficient, however, is three times as large transonically

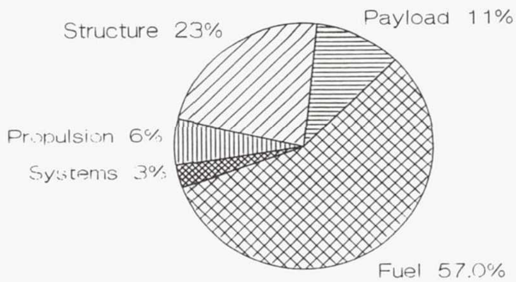

Fig. 7. Weight Breakdown

($M_\infty \approx 1$) as it is at cruise ($M_\infty = 3.5$) (see Appendix C). In addition to this effect, spillage drag and nacelle afterbody drag contribute to a decline in available thrust. The increase in drag and decrease in thrust combine to drastically cut the thrust margin of the aircraft (the proverbial "sonic barrier").

Preliminary analysis of the performance of the supersonic through-flow fan engine indicates that, due to the elimination of complex inlets that must be "started" and the inherently variable bypass ratio, the decrease in performance will be, at worst, comparable to that experienced by conventional systems. Since conventional systems do get through the transonic region, we can, at this point in the study, assume that no unsurpassable problems will be encountered.

WEIGHT BREAKDOWN

Although the gross takeoff weight is an important factor in determining the viability of the aircraft, it is also instructive to examine how this weight is apportioned between the various subsystems. An indication of this weight breakdown is presented in Fig. 7. The fuel fraction is derived from the

	SST-II	747-200B	Concorde
Range (n.mi.)	6100	6150	3900
T.O G.W. (1000's lbs)	750	775	389
Fuel (%)	57	44	53
Structure (%)	32	46	44
Payload (%)	11	10	3

Maximum range configurations

Fig. 8. Aircraft Comparison

calculated TSFC of the propulsion system and the desired range of the aircraft. The payload fraction is based upon a passenger load of 250. The remaining 32% is divided between primary structure, propulsion system weight and other systems based, in part, upon analysis by the WAATS weight analysis program(7).

A comparison between the weight breakdown of this aircraft and those of the Boeing 747-200 and the Concorde (maximum range configurations)(8) is found in Fig. 8. It is useful to note that the fuel fraction of the new design far exceeds that of the 747, but not that of the Concorde. This is consistent with the expectation that a supersonic aircraft requires more fuel than a subsonic one. However, the structure fraction of this design is about 30% lower than that of either of the other aircraft. This requires a great increase in overall structural efficiency, as well as new, lighter materials. Possible areas of weight savings are, as alluded to previously, the twin fuselage design and the supersonic through-flow fan engines.

CONCLUSIONS

This report summarizes the conceptual design of a Mach 3.5, 250-pasenger aircraft with trans-Pacific range. While many of the issues have been addressed, there is clearly a great deal of additional work needed before the design is anywhere near complete. Primarily, the supersonic through-flow fan engine is a technology that still must be validated. Further, the enormous improvements needed in structural efficiency require great strides in the areas of materials science and structural design.

One obvious option, if these technological advances cannot be totally realized, is to lessen, somewhat, the demands that the aircraft must meet. One example of this approach can be seen by referring to Fig. 1. While the initial objective called for a range of 6000 n.m., in order to service the San Francisco to Hong Kong route, the aircraft could be designed for 5000 n.m. and still be able to fly several trans-Pacific routes. Clearly, a good deal more work must be done to see if this compromise is necessary or if the initial demands for a more aggressive design can be met. This additional study merely represents the next step in the long and complicated design process.

APPENDIX A

The lift coefficient for a biconvex airfoil at supersonic speed is given by

$$C_L = 2C_1\alpha - \frac{16C_2(T_U^2 - T_L^2)}{3}$$

where

C_1 = first-order Busemann coefficient
C_2 = second-order Busemann coefficient
T_U = maximum upper-surface thickness as a fraction of chord
T_L = maximum lower-surface thickness as a fraction of chord
α = angle of attack (in radians)

The relevant Busemann coefficients are

Center Body	*Wings*
$C_1 = 0.5963$	$C_1 = 3.0151$
$C_2 = 1.2450$	$C_2 = 8.3074$

From these values, the following expressions for the lift coefficients can be generated

$$\text{Center Body:}\quad C_{LC} = 1.1926\,\alpha - 0.00976$$
$$\text{Wings:}\quad C_{LW} = 7.190\,\alpha - 0.0163$$

The value of α can then be calculated by equating the total lift with the weight

$$W = \tfrac{1}{2}\gamma p_\infty M_\infty^2\,[C_{LW}S_W + C_{LC}S_C]$$

where S_w and S_c are the wing and center-body surface areas, respectively. These values are

$$S_w = 4620\ \text{ft}^2$$
$$S_c = 4420\ \text{ft}^2$$

Using this equation along with the above expressions for the lift coefficients, the calculated angle of attack is

$$\alpha = 0.0206\ \text{radians} = 1.2°$$

An average lift coefficient is then given by

$$C_L = \frac{C_{LW}S_W + C_{LC}S_C}{S_W + S_C}$$

with the resulting value

$$C_L = 0.0759$$

The total lift is then given by

$$L = \tfrac{1}{2}C_L\gamma p_\infty M_\infty^2\,(S_W + S_C)$$

which, as expected, gives a value of

$$L = 700{,}000\ \text{lb}$$

A similar calculation for the wave drag coefficient is possible using the expression

$$C_{DW} = \frac{16C_1(T_U^2 + T_L^2)}{3} + 2C_1\alpha^2 - 16C_2\alpha(T_U^2 + T_L^2)$$

with the resulting average value of the wave drag coefficient

$$C_{DW} = 0.0084$$

The magnitude of the wave drag is calculated in the same manner as the lift, replacing the lift coefficient with the drag coefficient, resulting in

$$D_{wave} = 77{,}500 \text{ lb}$$

In order to calculate the skin friction drag coefficient, the skin friction coefficient must first be found. This coefficient is found in McCormick[9] as a function of Reynolds number. For cruise conditions

$$Re = 2.03 \times 10^8$$

which gives

$$C_f = 0.0013$$

This is related to the skin friction drag coefficient, C_{DS}, by the ratio of the total wetted area to the reference surface area.

The skin friction drag coefficient is then

$$C_{DS} = 4\ C_f$$
$$= 0.0052$$

From the coefficients given above, forces on the aircraft at supersonic cruise are

$$L = 700{,}000 \text{ lb}$$
$$D_{wave} = 77{,}500 \text{ lb}$$
$$D_{skin\ friction} = 48{,}000 \text{ lb}$$

APPENDIX B

For the purposes of these calculations, it is assumed that subsonic cruise occurs at Mach 0.9 at an altitude of 35,000 ft. The lift coefficient is then calculated by equating the lift force with the maximum weight of the aircraft, 750,000 lb. This is expressed

$$C_L = \frac{W}{\frac{1}{2}\gamma p_\infty M_\infty^2 S}$$

The resulting value of lift coefficient is

$$C_L = 0.2932$$

This value can then be used to calculate the coefficient of induced drag using the expression

$$C_{DI} = \frac{C_L^2}{\pi AR}$$

where AR is the aspect ratio as given by

$$AR = \frac{b^2}{S}$$

where b is the span. Here, the span is 130 ft, which gives

$$AR = 1.87$$
$$C_{DI} = 0.0146$$

Although this calculation of the induced drag coefficient is only strictly correct for elliptic lifting surfaces, it is assumed to be valid to the degree of accuracy of this first design.

In order to calculate the angle of attack, the two-dimensional lift coefficient must first be calculated. This is done with the expression

$$C_{L,\infty} = C_L \left[1 + \frac{2}{AR} \right]$$

which gives a value

$$C_{L,\infty} = 0.6068$$

The angle of attack is then calculated from

$$C_{L,\infty} = 2\pi \sin \left(\frac{h}{c} + \alpha \right)$$

where the ratio of h/c is the ratio of wing thickness to chord and is equal to 0.0243. The resultant value for the angle of attack is

$$\alpha = 0.0724 \text{ radians}$$
$$= 4.1°$$

The skin friction drag coefficient is calculated in the same manner as in Appendix A. Here, the skin friction coefficient from McCormick is

$$C_f = 0.0018$$

for

$$Re = 2.15 \times 10^8$$

The skin friction drag coefficient is then

$$C_{DS} = 4\ C_f$$
$$= 0.0072$$

From the coefficients given above, forces on the aircraft at subsonic cruise are

$$L = 750{,}000 \text{ lb}$$
$$D_{induced} = 37{,}300 \text{ lb}$$
$$D_{skin\ friction} = 18{,}000 \text{ lb}$$

APPENDIX C

Liepmann and Roshko[10] have developed a transonic similarity relationship of the form

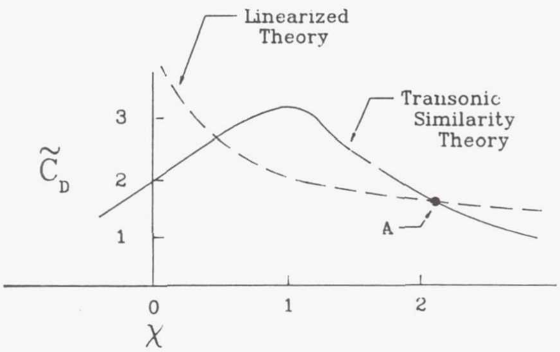

where the parameters are expressed

$$\tilde{C}_D = \frac{[(\gamma+1)M_\infty^2]^{1/3}}{\left[\frac{t}{c}\right]^{5/3}} C_D$$

$$\chi = \frac{M_\infty^2 - 1}{\left[(\gamma+1)\left(\frac{t}{c}\right)M_\infty^2\right]^{2/3}}$$

where t/c is a thickness ratio. In this particular case, the curve must be shifted to compensate for the arc-airfoil shape as opposed to the wedge geometry for which the relation was derived.

Point A represents the point at which the wave drag coefficient predicted by transonic similarity coalesces with that predicted by linearized theory. For the relevant airfoil, t/c is taken as 0.06 (since the maximum thickness is 6%), which gives values at point A

$$\chi = 2.2 \rightarrow M_l = 1.39$$
$$\tilde{C}_D = 1.6 \rightarrow C_D = 0.0088$$

However, the calculated value for C_D from linearized theory is

$$C_D = 0.005$$

In order to achieve this value the similarity curve is shifted along the ordinate axis, yielding

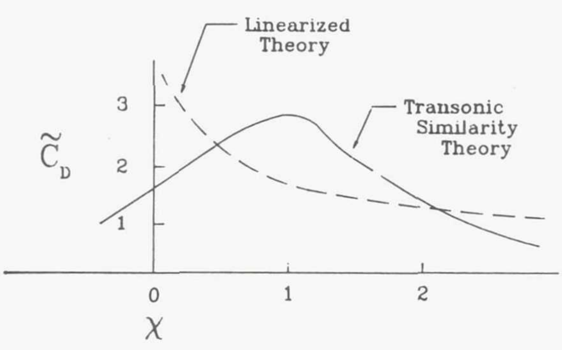

From the new curve, the maximum value of wave drag occurs at

$$\chi = 1 \rightarrow M_l = 1.12$$
$$\tilde{C}_D = 2.8 \rightarrow C_D = 0.018$$

The skin friction drag is calculated as before. The Reynolds number at these conditions is

$$Re = 1.33 \times 10^8$$

which, from McCormick, gives a skin friction coefficient of

$$C_f = 0.0019$$

which gives

$$C_{DS} = 0.0076$$

From the coefficients calculated above, the drag force values are

$$D_{wave} = 35{,}000 \text{ lb}$$
$$D_{skin\ friction} = 15{,}000 \text{ lb}$$

ACKNOWLEDGMENTS

Principal authors were W. Humphrey, G. Grayson, J. Gump, G. Hutko, R. Kubicko, J. O'Brien, R. Orndorff, R. Oscher, M. Polster, C. Ulrich, M. Wheatley, and K. Wooddell. They were assisted by faculty advisor Professor E. Reshotko.

REFERENCES

1. McMillin S. N. and Wood R. M., "Planform Effects for Low-Fineness-Ratio Multibody Configurations at Supersonic Speeds." AIAA Paper 86-1799, August 1986.
2. Nielsen J. N., "Arrays of Bodies of Revolution for Minimum Wave Drag." AIAA Paper 85-0449, January 1985.
3. Bruckman F., Radovcich N. A., and Wright B. R., "Arrow Wings for Supersonic Cruise Aircraft." AIAA Paper 78-151, January 1978.
4. Cohen C. B. and Reshotko E., "Heat Transfer at Forward Stagnation Points of Blunt Bodies." NASA TN-3513, July 1955.
5. Franciscus L. C., "Supersonic Through-Flow Fan Engines for Supersonic Cruise Aircraft." NASA TM-78889, 1978.
6. Franciscus L. C., "The Supersonic Through-Flow Turbofan for High Mach Propulsion." NASA TM-100114, AIAA Paper 87-2050, 1987.
7. Glatt C. R., "WAATS — A Computer Program for Weights Analysis of Advanced Transportation Systems." NASA CR-74-35289, 1974.
8. Taylor J. W. R. (ed.), *Jane's All The World's Aircraft.* McGraw-Hill, New York, 1974.
9. McCormick B. W., *Aerodynamics, Aeronautics, and Flight Mechanics,* p. 319. John Wiley and Sons, New York, 1979.
10. Liepmann H. W. and Roshko A., *Elements of Gas Dynamics.* John Wiley and Sons, New York, 1957.

19940045 48
383658
10P

N94-71303

PRELIMINARY DESIGN OF A FAMILY OF CLOSE AIR SUPPORT AIRCRAFT

UNIVERSITY OF KANSAS

S36-05
160662
P- 10

A family of three Close Air Support (CAS) aircraft is presented. These aircraft are designed with commonality as the main design objective to reduce the life cycle cost. The aircraft are low wing, twin-boom, pusher turbo-prop configurations. The amount of information displayed to the pilot was reduced to a minimum to greatly simplify the cockpit. The aircraft met the mission specifications and the performance and cost characteristics compared well with other CAS aircraft. The concept of a family of CAS aircraft seems viable after preliminary design.

NOMENCLATURE

AC	Aerodynamic Center
BL	Buttock Line
CAS	Close Air Support
CG	Center of Gravity
LE	Leading Edge
FS	Fuselage Station
HUD	Heads-up Display
MGC,$\bar{c}_w$	Mean Geometric Chord
SL	Sea Level
TO	Take-off
WL	Water Line

INTRODUCTION

In the event of a Warsaw Pact-NATO confrontation, the main attack by the Warsaw Pact forces will most likely focus on the Fulda Gap in West Germany. This predicted attack will be spearheaded by the Soviet ground forces stationed in East Germany. The attack force could consist of as many as 90+ divisions with each division containing roughly 300 main battle tanks and 1000 other tracked vehicles[1]. To prevent such an assault from succeeding, a means of destroying Soviet battle tanks must be introduced.

There are three weapons available to perform the anti-tank mission: (1) tank against another tank, (2) a well trained soldier armed with anti-tank weapons, and (3) Close Air Support (CAS) aircraft (both helicopters and fixed-wing aircraft).

Using a NASA/USRA grant for aeronautics engineering design projects, a team of students concluded that a family of three CAS aircraft is needed to help perform the anti-tank missions[2]. The aircraft are as follows:

1. An aircraft to take out advancing armor and highly defended targets (such as fuel or ammunition depots, enemy headquarters, etc.) in all weather conditions.
2. An aircraft with reduced capabilities from the aforementioned aircraft (less range and less payload) but with a lower cost that can attack tanks in fair weather and night/day conditions.
3. A very low cost aircraft that, through sheer numbers, halts the advancing tank formations in fair weather conditions.

A team of 16 students at the University of Kansas has completed the preliminary design of the three aircraft[3]. To reduce the life cycle cost, these aircraft were designed to employ technology commonality.

MISSION SPECIFICATIONS

The mission specifications for the three aircraft are presented in Table 1. These specifications are a result of

Table 1. Mission Specifications for a Family of Close Air Support Aircraft

Crew:	One Pilot, full military gear One Martin/Baker ejection seat
Armament:	One internal GPU-13A 30-mm cannon (A) 1200 rounds of ammunition (B) 400 rounds of ammunition (C) 400 rounds of ammunition
Payload:	(A) Total payload of 10,000 lbs to include laser and infrared guided weapons, free-fall weapons, and rocket pods. (B) Total payload of 4100 lbs to include laser and infrared guided weapons, free-fall weapons, and rocket pods. (C) Total payload of 2,000 lbs to include free-fall weapons and rocket pods.
Performance:	(A) Maximum speed of 350 kts at SL, fully loaded. Cruise speed of 250 kts at 5000 ft. Service ceiling of 15,000 ft. Combat radius of 400 n.m. Sustained 5 *g's* at 150 kts at SL, fully loaded. One hour endurance at 5000 ft. (B) Maximum speed of 350 kts at SL, clean. Cruise speed of 250 kts at 5000 ft. Combat radius of 120 n.m. Sustained 5 *g's* at 125 kts at SL, fully loaded. Four hours of endurance at 5000 ft. (C) Maximum speed of 350 kts at SL, clean. Cruise speed of 250 kts at 5000 ft. Combat radius of 100 n.m. Sustained 5 *g's* at 125 kts at SL, fully loaded. Two hours of endurance at 5000 ft.
Groundrun:	(A) 2000 ft on steel planking (B) 1200 ft on soft field (C) 1000 ft on soft field
Powerplant:	(A) Twin engine advanced turboprop with one counter-rotating propeller. (B) Twin engine advanced turboprop with one counter-rotating propeller. (C) Single engine advanced turboprop.
Certification:	Military

PAGE 292 INTENTIONALLY BLANK

PRECEDING PAGE BLANK NOT FILMED

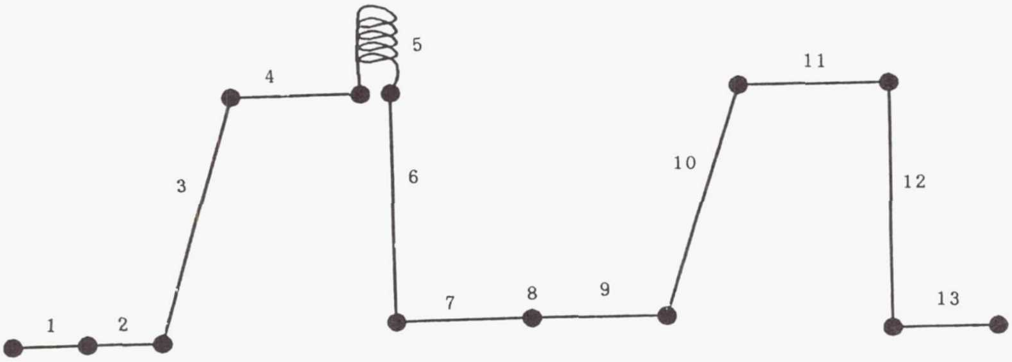

1) Start-up and taxi
2) Take-off
3) Climb to 5,000 ft
4) Cruise out at 250 kts at 5,000 ft for
   A) 350 nm
   B) 70 nm
   C) 50 nm
5) Loiter at 5,000 ft for
   A) 1 hr
   B) 4 hrs
   C) 2 hrs
6) Descend to SL
7) Dash-in 50 nm at
   A) 350 kts
   B) 250 kts
   C) 250 kts
8) Attack
9) Dash-out for 50 nm
10) Climb to 5,000 ft
11) Cruise in at 250 kts at 5,000 ft
12) Descend to SL
13) Land, taxi, and shutdown

Fig. 1. Mission Profile

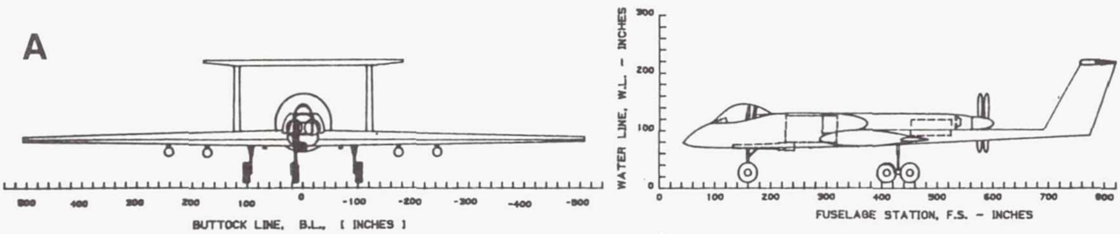

	Wing	Horizontal Tail	Vertical Tail
Area(ft^2)	890	160	2*60
Span(ft)	84.0	33	9.7
MGC(ft)	11.8	5.5	6.25
Aspect Ratio	8.0	6.8	1.6
LE Sweep(deg)	12.5	0	30
Taper Ratio	0.25	1	.7

Weight	
Take-off (lb)	39,725
Empty (lb)	20,726
Fuel (lb)	10,200
Payload (lb)	10,000
TO Power (hp)	12,000
TO Wing Loading (lb/ft^2)	44.6
TO Power Loading(lb/hp)	3.31

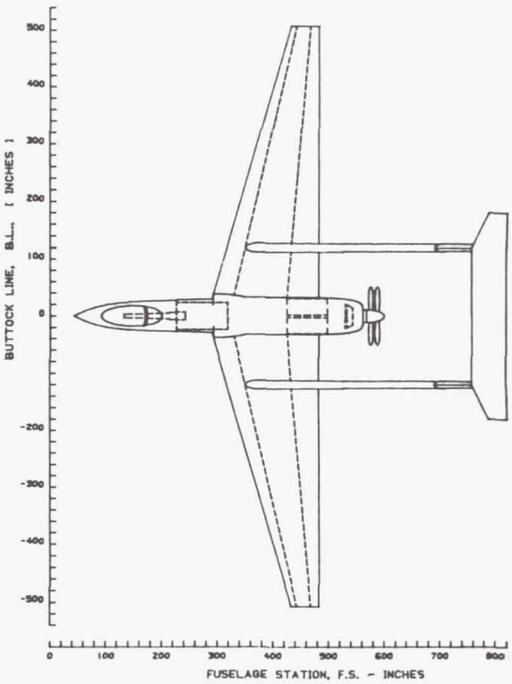

Fig. 2. Three Views and Characteristic Data

B

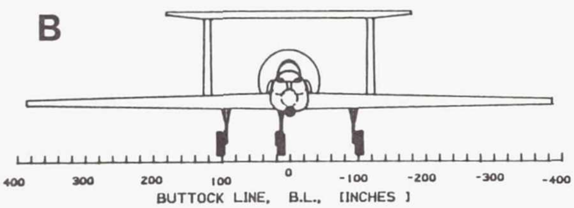

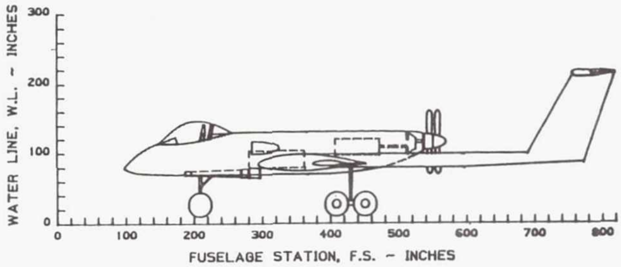

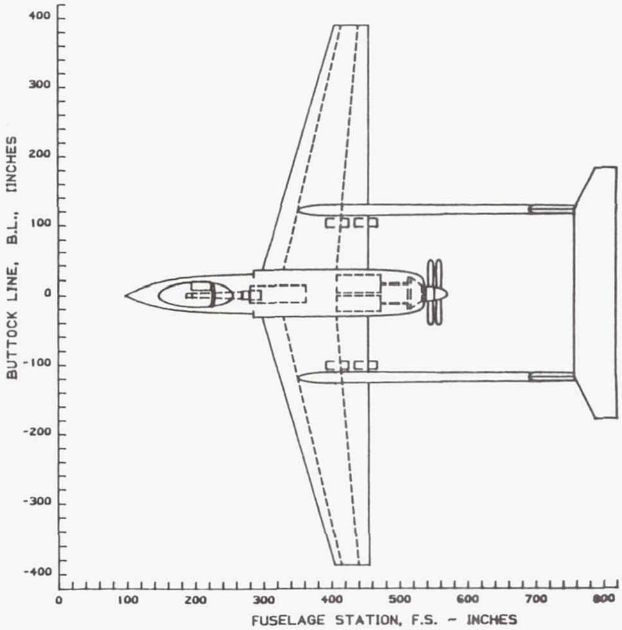

	Wing	Horizontal Tail	Vertical Tail
Area(ft^2)	577	160	2*60
Span(ft)	64.0	33	9.7
MGC(ft)	9.8	5.5	6.25
Aspect Ratio	7.2	6.8	1.6
LE Sweep(deg)	12.5	0	30
Taper Ratio	0.31	1	.7

Weight	
Take-off (lb)	22,289
Empty (lb)	12,457
Fuel (lb)	5,030
Payload (lb)	4,100
TO Power (hp)	5,000
TO Wing Loading (lb/ft^2)	38.6
TO Power Loading(lb/hp)	4.46

C

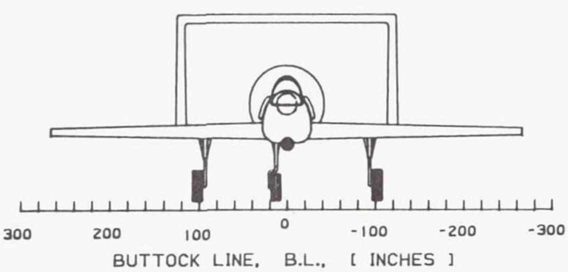

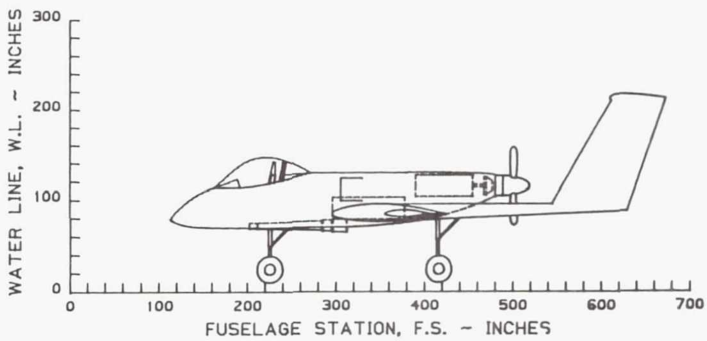

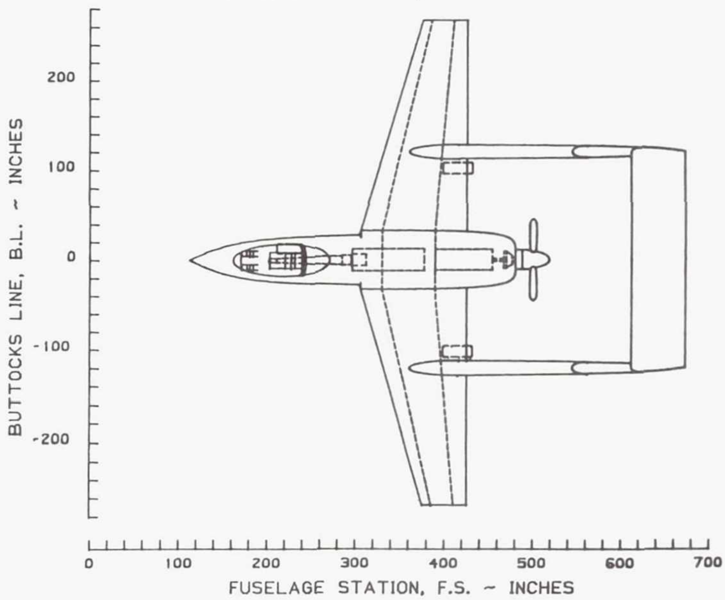

	Wing	Horizontal Tail	Vertical Tail
Area(ft^2)	335	110	2*60
Span(ft)	44.0	20	9.7
MGC(ft)	8.0	5.5	6.25
Aspect Ratio	5.9	3.6	1.6
LE Sweep(deg)	12.5	0	30
Taper Ratio	0.39	1	.7

Weight	
Take-off (lb)	10,935
Empty (lb)	7,237
Fuel (lb)	1,750
Payload (lb)	2,000
TO Power (hp)	2,000
TO Wing Loading (lb/ft^2)	32.6
TO Power Loading(lb/hp)	5.46

battlefield scenario studies performed by the class[2]. The mission profile for the aircraft is shown in Fig. 1. The three aircraft were designed with commonality as a prime objective.

Commonality has several distinct advantages:

1. Reduced procurement cost per aircraft due to common components. Commonality reduces the individual component cost by increasing the number of each component produced.
2. Reduced direct operating cost, since there are fewer components which must be kept on hand for spares (overhead).
3. Reduced indirect operating cost because the logistics of maintaining spares for the three aircraft will be simplified, due to fewer different components. Battlefield maintenance will also be improved, since parts from battle-damaged aircraft may be used on three different aircraft as required.

CONFIGURATION DESCRIPTION

The three aircraft are low wing, twin-boom, pusher-propeller configurations. The reasons for this type of configuration are:

1. The engine(s) can be mounted closer to the center of gravity of the aircraft, giving more favorable weight and balance characteristics.
2. A pusher configuration provides excellent forward visibility, compared to a tractor configuration. This is an important consideration for a ground attack aircraft.
3. A pusher configuration allows nearly 100% commonality in the cockpit section, which accounts for much of the cost and weight of a ground attack aircraft.
4. The twin-boom empennage structure allows for a high degree of commonality in the empennage surfaces.

The three-views of the three aircraft are shown in Fig. 2. The characteristic data of the aircraft is also shown.

Commonality was achieved in the components listed in Table 2. The forward fuselage, wing, and propulsion system will be discussed in more detail.

Table 2. Common Components between the Three Aircraft

(1) Forward Fuselage	Martin/Baker ejection seat
	Canopy
	Structure
	Instrument panel
(2) Wing Components	
(3) Landing Gear Components	Tires and wheels
	Brakes
(4) Empennage Surfaces	Vertical tail
	Horizontal tail
	Boom structure
(5) Engine Systems	

Forward Fuselage Design

The forward fuselage was designed to obtain the highest degree of commonality between the three aircraft as possible. The forward fuselage is shown in Fig. 3. The structure was designed to meet the specified needs of each aircraft. For instance, Aircraft A and B have an attack radar, while Aircraft C does not. The nose cone for all three aircraft had to be capable of carrying that radar. The three aircraft have the GPU-13A 30-mm cannon internally installed offset to the left side

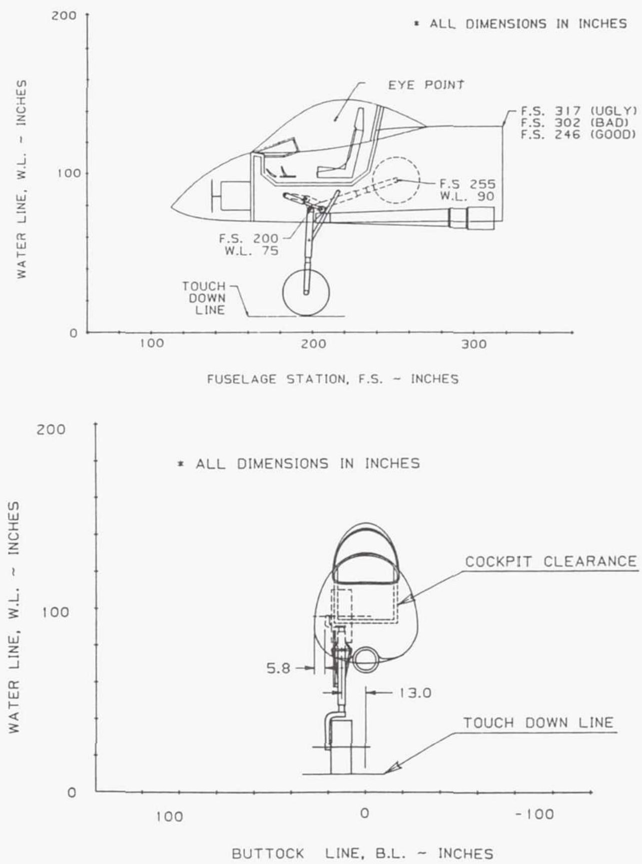

Fig. 3. Forward Fuselage Layout

to allow room for the nose gear to be retracted. The firing barrel of the cannon is on the centerline to prevent any adverse yawing moment and to improve accuracy. This configuration is similar to the Fairchild A-10[4].

The cockpit was designed to give the pilot good visibility, which is crucial in a ground attack aircraft. The pilot has the following visibility:

- 20° down over the nose
- 45° down over the sides
- 5° down over the rear fuselage
- unlimited visibility above

The design of the instrument panel incorporates the idea of simplicity. The pilot should be shown only the information required to complete the mission or to evaluate actions to be taken after a failure. Thus, the amount of information presented to the pilot was reduced to a minimum, greatly simplifying the cockpit. The proposed cockpit for the aircraft is shown in Fig. 4. This cockpit consists of a heads-up display (HUD), an 8 in × 8 in CRT for map presentation, and an 8 in × 8 in CRT for relevant information presentation (such as weapon status).

Wing Design

To attain commonality, the wings were designed such that the wing of Aircraft C is incorporated in the wing of Aircraft

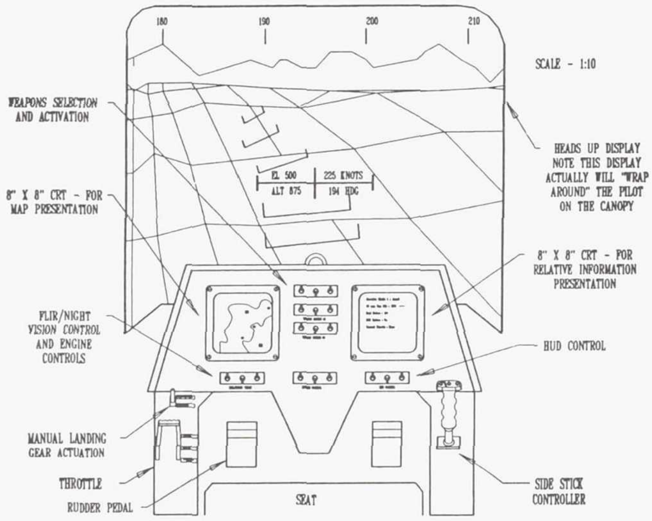

Fig. 4. Proposed Cockpit of the Aircraft

B, and the wing of Aircraft B is incorporated in the wing of Aircraft A. An extension is connected to the wing of Aircraft C to obtain the wing of Aircraft B, and an extension is connected to this wing to obtain the wing of Aircraft A. This yields commonality in the spars, ribs, skins, and control surfaces. The wings are shown in Fig. 5.

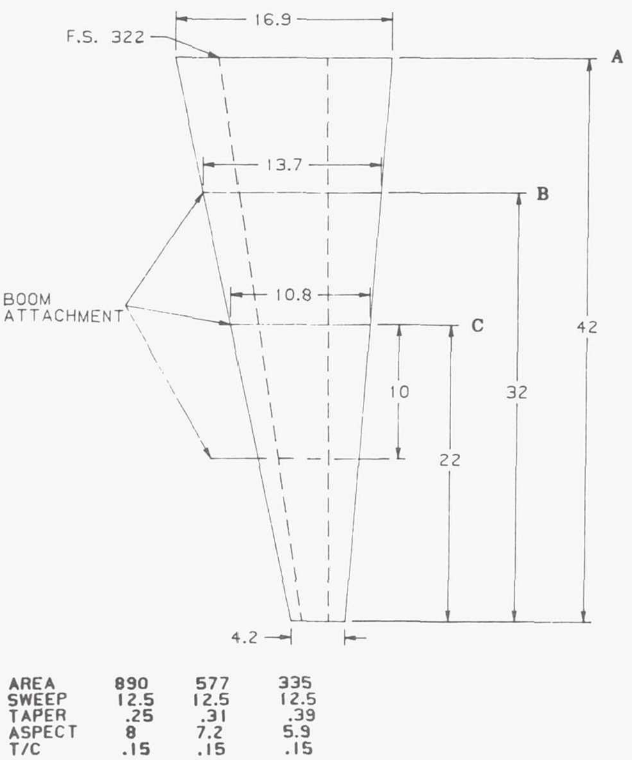

Fig. 5. Wing Layout

Propulsion System Design

From preliminary sizing calculations[6] it was determined that the aircraft required the following installed powers at take-off: (1) 12,000 hp, (2) 5000 hp, and (3) 2000 hp.

To provide a measure of commonality in the design, it was decided that Aircraft B and C would have the same powerplant and Aircraft A and B would use the same type of installation. The size of the powerplants are (1) two engines each producing 6000 shp, (2) two engines each producing 2500 shp, and (3) 1 engine producing 2500 shp (de-rated to 2000 shp).

The propulsion system installations for the aircraft are shown in Fig. 6. Note that the installation of the two larger aircraft has two engines driving one gearbox. This system is similar to the Fairey Gannett[7].

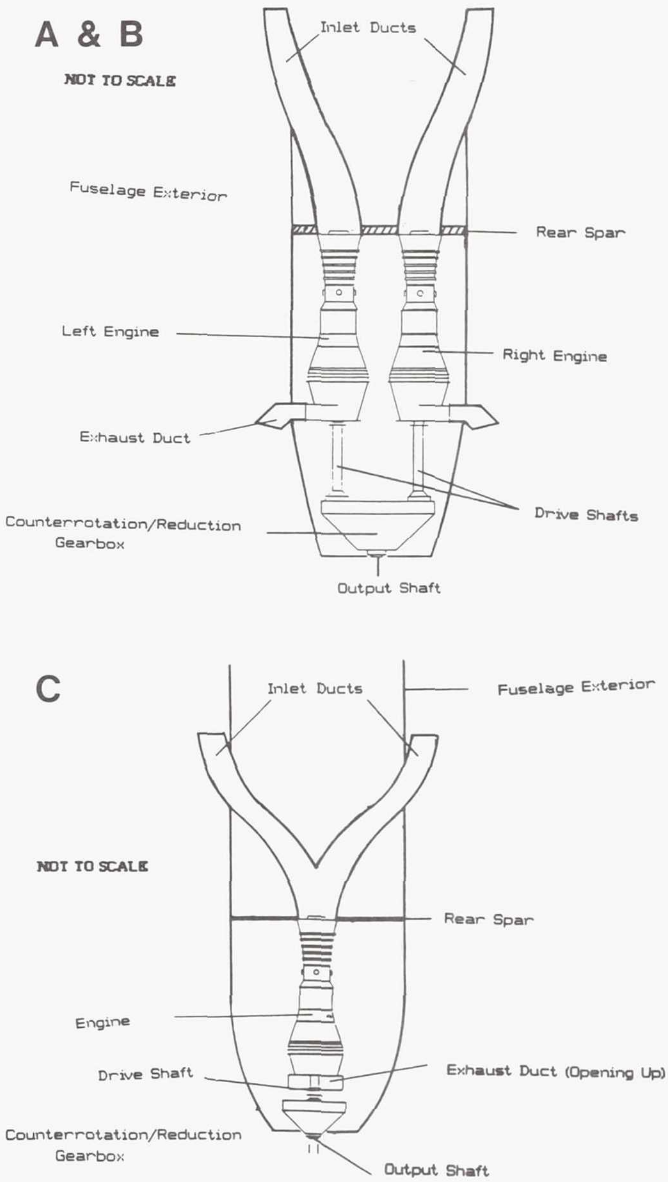

Fig. 6. Propulsion Installation

WEIGHT AND BALANCE

The aircraft incurred a weight penalty due to commonality caused by the common components being designed to meet the needs of all three aircraft. To estimate this penalty, the weights of the aircraft were estimated without any commonality effects included. Then, the weight of the common components were estimated[3]. The difference between the two is the weight penalty due to commonality. The basic weights of the aircraft, including the effects of commonality, are listed in Table 3. The weight penalties due to commonality are also shown. The weight-c.g. excursion diagrams are shown in Fig. 7.

Table 3. Basic Weights of the Aircraft

Weight(lb)	A	B	C
Structural	11,197	6,605	3,220
Powerplant	6,490	3,734	1,615
Fixed Equipment	3,956	3,035	2,402
Empty	20,726	12,457	7,237
Operating Empty	21,149	12,791	7,517
Take-off	39,725	22,289	10,935
Penalty due to Commonality	614	652	1,050

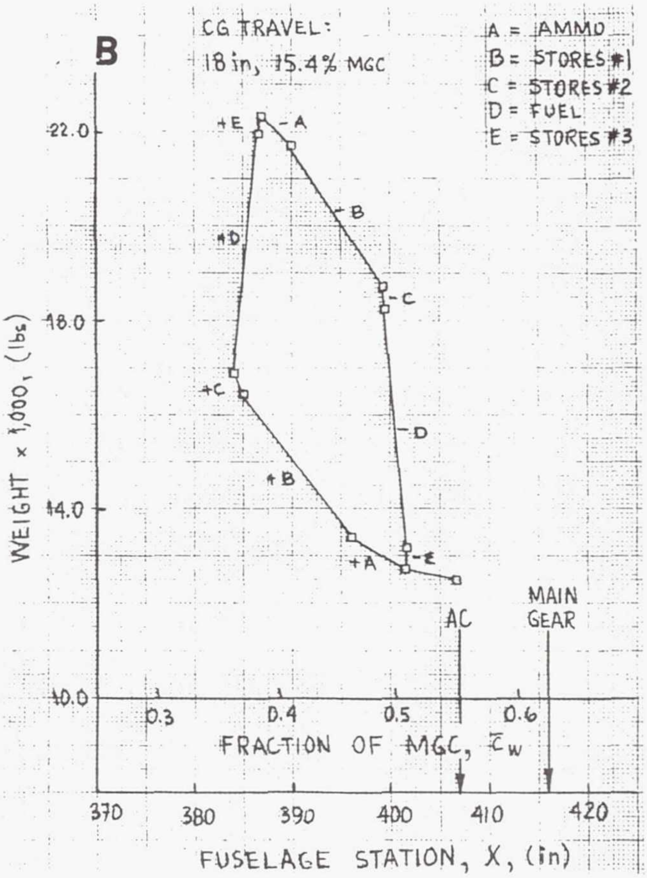

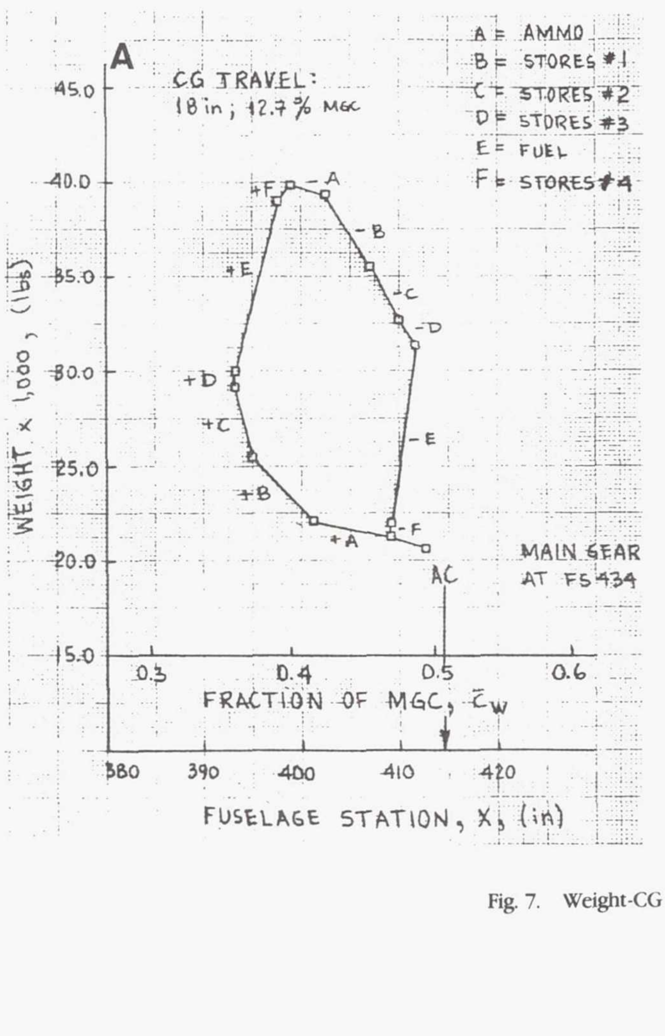

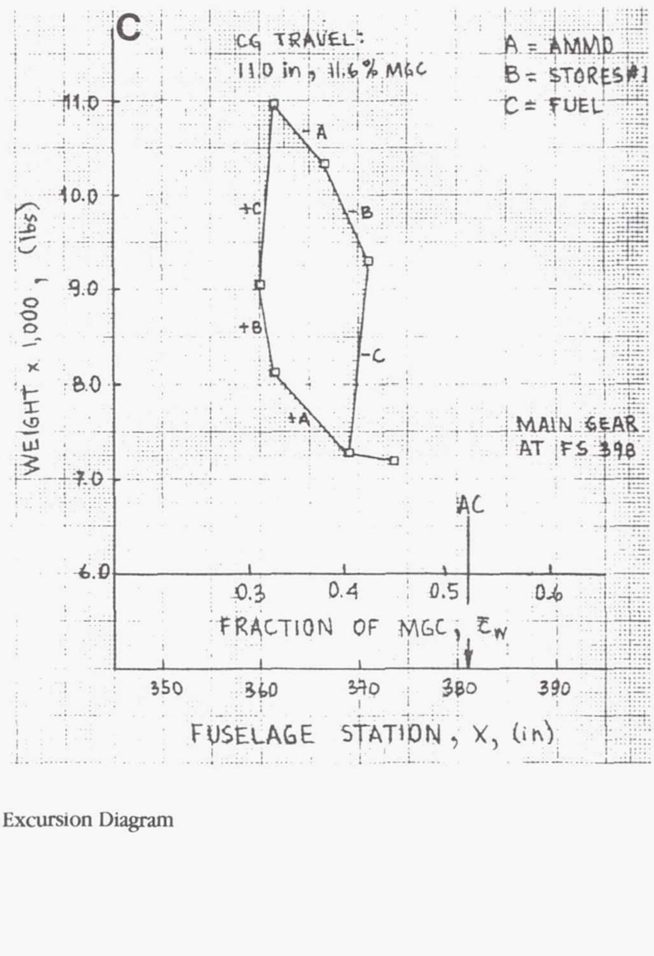

Fig. 7. Weight-CG Excursion Diagram

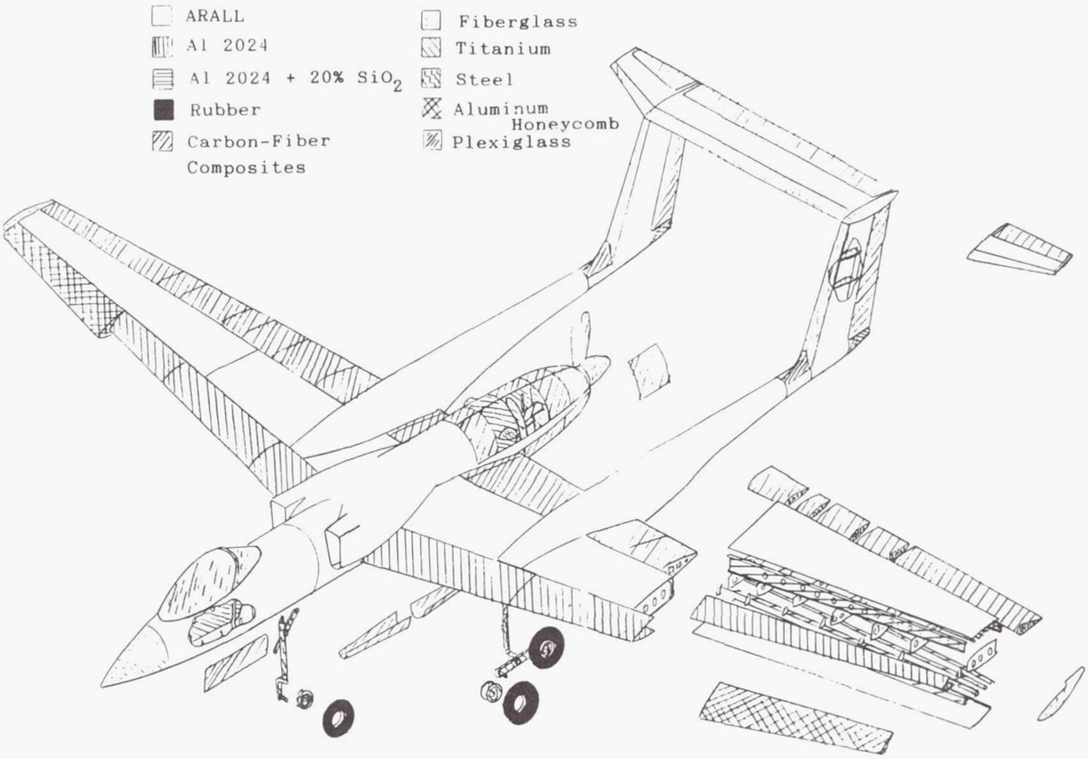

Fig. 8. Material Selection for Aircraft A

MATERIAL SELECTION

The materials selected are shown in Fig. 8. Advanced materials are used wherever possible to reduce the weight of the structure.

STABILITY AND CONTROL

A detailed stability and control analysis was performed on Aircraft A only. The derivatives were calculated for eight flight conditions that were used to determine the natural frequencies, damping ratios, and time constants. The military specifications (MIL-F-8785C) were used to determine the handling qualities of the aircraft. The results of this analysis are shown in Table 4. It is seen that this aircraft meets Level 1 requirements except in six cases. An investigation as to whether to fix this by aerodynamic design adjustments or by stability augmentation needs to be conducted.

Table 4. Handling Qualities of Aircraft A

		Longitudinal							
Variable	Units	Take-off	Cruise		Loiter	Dash-in	Maneuver	Dash-out	Landing
Weight:	(lbs)	39,508	39,508	20,932	39,508	39,508	30,220	20,932	20,932
Speed:	(kts)	106	250	250	150	350	220	350	106
Mach number:		0.16	0.385	0.385	0.23	0.53	0.33	0.53	0.16
Altitude:	(ft)	0	5,000	5,000	5,000	1,000	1,000	1,000	0
Load Factor:		1	1	1	1	1	5	1	1
I_{yy}	(slugs.lbs)	94,773	94,773	80,854	94,773	94,773	8 7,813	80,854	80,854
CATEGORY		C	B	B	B	A	A	A	C
Phygoid mode damping ratio:									
$zeta_p$		-0.336	0.202	0.391	0.088	0.304	1.417	0.576	-0.055
LEVEL		?	1	1	1	1	1	1	?
Undamped short period natural frequency:									
$w_{n_{s.p}}$	(rad/sec)	1.557	3.595	3.501	2.285	5.251	3.133	5.351	1.563
n/a	(g's/rad)	3.565	23.06	43.51	8.370	57.06	20.15	107 .7	6.645
LEVEL		1	1	1	1	1	1	1	1
Short period damping ratio:									
$zeta_{S.P}$		0.827	0.906	1.235	0.819	1.116	1.053	1.451	1.0 93
LEVEL		1	1	1	1	1	1	2	1

Lateral-Directional

Variable	Units	Take-off	Cruise		Loiter	Dash-in	Maneuver	Dash-out	Landing
Weight:	(lbs)	39,508	39,508	20,932	39,508	39,508	30,220	20,932	20,932
Speed:	(kts)	106	250	250	150	350	220	350	106
Mach number:		0.16	0.385	0.385	0.23	0.53	0.33	0.53	0.16
Altitude:	(ft)	0	5,000	5,000	5,000	1,000	1,000	1,000	0
Load factor:		1	1	1	1	1	5	1	1
CATEGORY		C	B	B	B	A	A	A	C
Dutch roll damping ratio:									
$zeta_D$		0.222	0.209	0.214	0.208	0.225	0.213	0.230	0.228
LEVEL		1	1	1	1	1	2	1	1
Dutch roll undamped natural frequency:									
w_{n_D}	(rad/sec)	1.917	4.667	4.365	2.905	6.960	4.244	6.510	1.798
LEVEL		1	1	1	1	1	1	1	1
$zeta_D\ w_{n_D}$		0.425	0.977	0.934	0.604	1.565	0.905	1.498	0.411
LEVEL		1	1	1	1	1	-	1	1
Roll mode time constant:									
T_R	(sec)	0.168	0.064	0.059	0.112	0.034	0.061	0.031	0.156
LEVEL		1	1	1	1	1	1	1	1
Spiral stability - time to double amplitude:									
$T_{2,}$	(sec)	4.92	31.28	36.55	12.65	61.99	38.36	67 .78	68.27
LEVEL		3	1	1	2	1	1	1	1

Table 5. Performance Characteristics of the Aircraft

	Aircraft A		Aircraft B		Aircraft C	
	REQUIRED	ACTUAL	REQUIRED	ACTUAL	REQUIRED	ACTUAL
Maximum Speed (kts)						
Sea level, fully loaded	350	364	250	299	250	281
Stalling Speed (kts)						
Sea level, Wto + stores		100		93.6		86.1
Take-off, Wto + stores		96.9		90.2		77.6
Landing, 90% Wto		88.9		75.5		62.8
Maneuvering						
150 kts, SL, fully loaded	5 *g's*	5.2 *g's*	5 *g's*	4.99 *g's*	5 *g's*	5.2 *g's*
Take-off Groundrun (ft)	2,000	1,810	1,200	1,120	1,000	710
Landing Groundrun (ft)	2,000	1,130	1,200	816	1,000	560
Endurance at 5,000 ft (hrs)	1.0	1.33	4.0	5.16	2.0	3.37
Combat Ceiling (ft)	15,000	34,300		31,000		32,500
Combat Radius (n.m.)	400	560	120	168	100	157
Military Climb Requirements						
Take-off min. RC, OEI (fpm)	500	726	500	645	500	759
Take-off CGR (rad)	0.005	0.067	0.005	0.064	0.005	0.108

Table 6. Performance comparison of the Aircraft with Other CAS Aircraft

	1	2	3	4	5	6	7	8	9	10	11
Aircraft A	20,726	39,725	10,000	364	560	1.3	5.2	34,300	1,810	1,130	10.9
Aircraft B	12,791	22,289	4,100	299	168	5.2	5.0	31,000	1,120	816	7.1
Aircraft C	7,517	10,935	2,000	281	157	3.4	5.2	32,500	710	560	2.8
A-10	24,918	50,000	14,638	368	250	1.8	3.2	—	4,000	2,000	7.5(9)
Pucara	10,022	14,991	3,307	270	189	—	—	32,800	985	656	—
Frogfoot	20,950	42,330	9,920	530	300	—	—	—	—	—	—
AMX	14,770	27,558	8,377	550	280	—	—	42,600	2,461	2,400	—
A-1	10,550	25,000	9,000	216	1,300	4.0	—	25,000	—	—	—
Enforcer	7,885	14,000	5,680	300	400	—	6.0	25,000	1,730	1,580	—
AH-64	10,760	21,000	1,700	160	260	3.2	3.5	21,000	0	0	9.8(10)

(1) Operational Weight Empty (lbs)
(2) Take-off Weight (lbs)
(3) Payload Weight (lbs)
(4) Maximum Speed(kts)
(5) Combat Radius (n.m.)
(6) Endurance (hrs)
(7) Sustained *g's*
(8) Combat Ceiling (ft)
(9) Take-off Groundrun (ft)
(10) Landing Groundrun (ft)
(11) Cost in Millions of Dollars (1989)

PERFORMANCE

The performance capabilities of the three aircraft are shown in Table 5. The values are compared to those required by the mission specifications, all of which are met. The capabilities of these aircraft are compared to other CAS aircraft in Table 6, and are found to be comparable. In comparing Aircraft A with the A-10, while both have roughly the same maximum cruise speed and endurance, the lower cost A-10 can carry more payload. However, the A-10's take-off and landing groundruns are longer, its combat radius is lower, and it can sustain fewer *g's* than Aircraft A.

COST ANALYSIS

The life cycle cost of an aircraft consists of research and development cost, acquisition cost, and operating cost. Methods exist to calculate these costs[8], but the cost savings due to commonality needs to be included. The savings were calculated by using the following method:

1. The cost per pound of producing N aircraft is estimated using the standard methods without avionics and engines.
2. The cost per pound of producing $3 \times N$ aircraft is estimated without avionics and engines ($3 \times N$ of the common parts will be produced).
3. The weight of the common components is multiplied by the difference between the values obtained in (1) and (2), which is the cost savings due to commonality per aircraft. Note that the cost of research and development is spread out over the entire production run.

Table 7 shows the unit cost of the aircraft, both with and without the commonality savings included, when 250, 500, 750, and 1,000 aircraft are produced. The savings due to commonality ranges from 0.9% to 8.3% of the cost of the aircraft. These savings are lower than what was expected, and more advanced methods should be used to better determine the cost savings. The operating cost is also shown in Table 7.

For a fleet of 100 aircraft, a comparison of the research and development cost, acquisition cost, and operating cost is shown in Fig. 9. These data are for a service life of 20 years flying 300 hours per year. The acquisition cost is based on production of 500 aircraft.

Table 7. Acquisition and Operating Cost

#	Aircraft A NC	Aircraft A C	Aircraft B NC	Aircraft B C	Aircraft C NC	Aircraft C C
	Unit Acquisition Cost in Millions of Dollars					
250	11.80	11.61	7.80	7.58	3.26	2.99
500	11.00	10.87	7.28	7.13	2.98	2.80
750	10.67	10.57	7.05	6.93	2.87	2.72
1000	10.47	10.38	6.92	6.82	2.80	2.67
	Unit Operating Cost per Year in Dollars					
	$413,000		$311,000		$278,000	

# = Number of aircraft produced.
NC = Unit cost without commonality.
C = Unit cost with commonality.
Costs are in 1989 dollars.

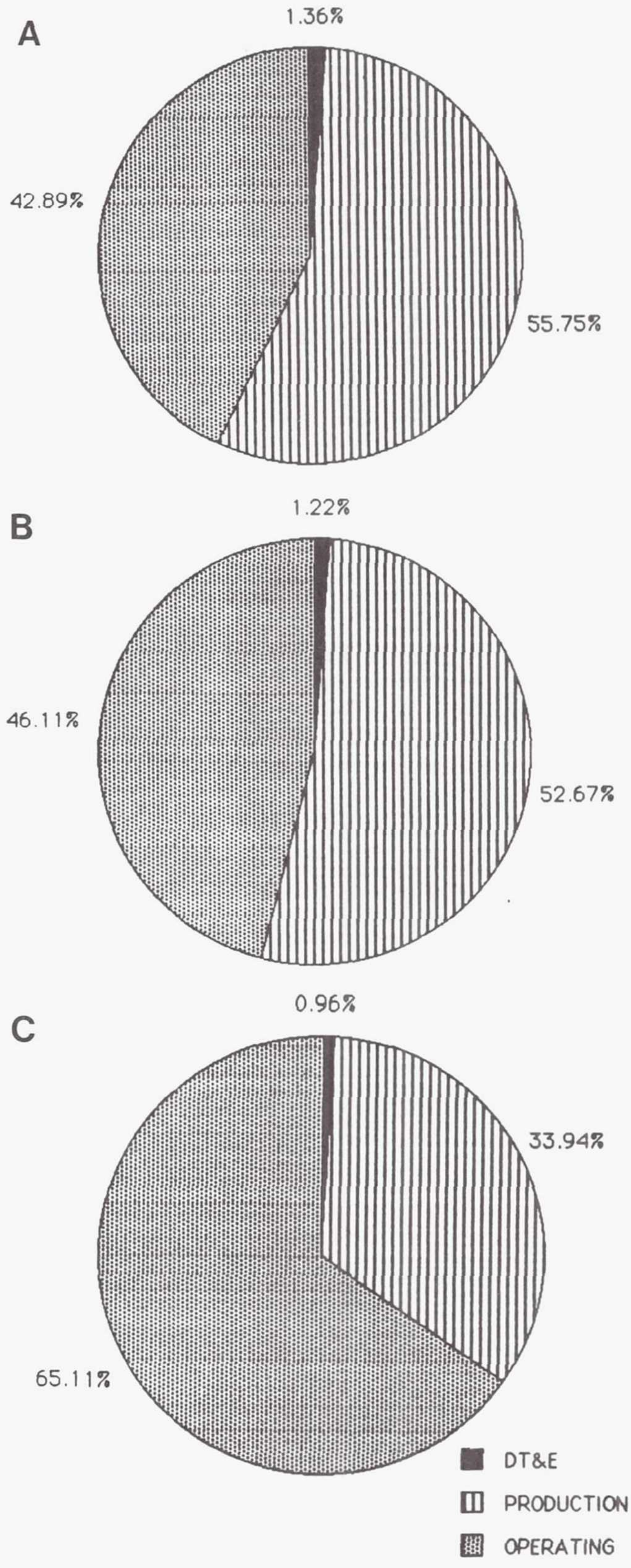

Fig. 9. Comparision of Research and Development, Acquisition, and Operating Cost for a Fleet of 100 Aircraft

CONCLUSIONS AND RECOMMENDATIONS

The family of CAS aircraft was designed with commonality as a prime design goal. The low wing, twin-boom, pusher turbo-prop configurations met all the mission specifications. The aircraft have Level 1 handling qualities except for six cases, which should be corrected with either aerodynamic design adjustments or stability augmentations. The performance and cost characteristics of these aircraft are comparative to other CAS aircraft.

A family of CAS aircraft seems viable after preliminary design. The configurations should be taken through more advanced design stages to better determine the viability of this concept.

ACKNOWLEDGMENTS

Principal author Jeff Tuschhoff was assisted by design team members Rudy Bartel, Brian Cox, Paul Darrah, Ty Drake, Louis Hendrich, Robin Hicks, Mark Holt, Mark Hoyle, Brian Kerns, Wayne Lussier, Doug May, Nikos Mills, Pete Stonefield, John Valasek, and Linda Witt. Dr. Jan Roskam provided guidance and support to the design team, while Shelby J. Morris of NASA Langley Research Center was the technical monitor for the project. Finally, USRA gave us the opportunity to participate in the Advanced Design Program.

REFERENCES

1. Berry Jr., C. "Defeating Red Armor," *Air Force Magazine,* Oct. 1988, pp. 94-99.
2. Tuschhoff, J., Bartel, R., Cox, B., Drake, T., Hendrich, L., Hicks, R., Holt, M., Hoyle, M., Kerns, B., Lussier, W., May, D., Mills, N., Stonefield, P., Witt, L., and Valasek, J., "Battle Scenario and Mission Specifications for Three Close Air Support Aircraft," University of Kansas, Lawrence, KS, Oct. 18, 1988.
3. Tuschhoff, J., Cox, B., Lussier, W., and Mills, N., "Preliminary Design of a Family of Close Air Support Aircraft," University of Kansas, Lawrence, KS, May 17, 1989.
4. *The Great Book of Modern Warplanes,* Portland House, New York, 1987, pp. 10-72.
5. Kerns, B. and Valasek, J., "Instrumentation Design and Analysis for the Advanced Close Air Support Aircraft," University of Kansas, Lawrence, KS, November 21, 1988.
6. Tuschhoff, J., Bartel, R., Cox, B., Drake, T., Hendrich, L., Hicks, R., Holt, M., Hoyle, M., Kerns, B., Lussier, W., May, D., Mills, N., Stonefield, P., Witt, L., and Valasek, J., "Initial Design of a Family of Close Air Support Aircraft," University of Kansas, Lawrence, KS, December 21, 1988.
7. Taylor, J.W.R., *Jane's All the World Aircraft,* Jane's Publishing Company, London, England, 1954-55, pp. 70-71.
8. Nicolai, L.M., *Fundamentals of Aircraft Design,* METS, Inc., City, Cal., 1975, pp. 24-1 - 24-35 .
9. Stuflesser, G., "The Cheaper Strike Aircraft: A valid concept," *Si vis pacem Para Bellum,* December 1977.
10. McDonnell Douglas Advertisement, *Aviation Week & Space Technology,* November 1988.

1994004545 383659 12P

N94-71304

DESIGN OF UNMANNED FLIGHT VEHICLE SYSTEMS FOR AERODYNAMIC DATA ACQUISITION

UNIVERSITY OF NOTRE DAME

S37-05 160663 P. 11

A series of design studies was conducted in order to develop flight vehicle concepts for remotely piloted vehicles intended for aerodynamic data acquisition with particular emphasis on the low Reynolds number flight regime. Five different concepts were developed as part of the senior level Aerospace Systems Design course at the University of Notre Dame. The systems were designed to provide surface pressure and component force measurements on specially instrumented lifting-surface test specimens which were to be carried aloft by a base flight vehicle. The project included the fabrication of subscale, remotely piloted technology demonstrators to validate the base vehicle flight worthiness.

INTRODUCTION

The wind tunnel has traditionally been the primary source of basic aerodynamic data such as surface pressure measurements or component force and moment measurements. It is also used extensively for flight vehicle development. There are many obvious reasons for using the wind tunnel and it has evolved into the most useful of all aeronautical research tools. Unfortunately there are certain situations in which wind tunnel testing is limited. Matching the critical scaling parameters, Mach number and Reynolds number, is not always possible. Of particular concern in the commercial aircraft community is the lack of adequate high Reynolds number testing facilities for the next generation of commercial transports. Presently, there are no wind tunnel facilities available for the level of production testing needed to develop these new aircraft. One option is to explore alternate testing methods to complement the present wind tunnel facilities.

During the past few decades there has been been steady development of a special class of flight vehicle systems referred to as Unmanned Air Vehicles (UAVs) or Remotely Piloted Vehicles (RPVs). Though much of this development has focused on the military applications of these flight vehicles[1], the potential for nonmilitary and commercial application has been shown[2,3]. The NASA/Air Force HiMAT program was one of the first major programs in which a remotely piloted vehicle was used to validate a number of advanced vehicle technologies[4,5]. As developments in remotely piloted or autonomous vehicle technologies continue, there will be other opportunities for similar applications. These could include validation of numerical methods[6], application to hypersonic flight testing[7], or possibly the use of subscale vehicles at relatively low altitudes with which both Mach and Reynolds number for the next generation transports could be matched[8].

The application of RPVs to the acquisition of aerodynamic data on components or complete configurations was the focus of this study. A number of successful applications of similar efforts have been documented[9,10]. Because this study was conducted as part of a senior level, undergraduate engineering design course, its scope was limited by the expertise of the student members of the design teams. For this reason it was decided that the integration of instrumentation and flight vehicle and system control were the most critical basic issues and could be addressed with an application in a "less hostile" flight regime. Therefore the low Reynolds number testing problem was considered. This appeared to be well suited to the RPV application and also provided a realistic design challenge.

REQUEST FOR PROPOSALS

The project was defined using three different requests for proposals (RFPs). These identified concepts which could be used to collect surface pressure data, as given below in the Blue Mission, or to collect component force and moment data in the Gold Mission, or a special application for a high aspect ratio delta wing in the Green Mission. The Blue Mission specification is included (see next section) to provide basic mission specifications although the design groups were allowed to take exception with different aspects of the mission definition if justification could be provided.

The mission outlined in the RFP was very general and may have provided an almost unrealistic challenge to the design teams, considering the single-semester timeframe for the project. Unlike some undergraduate aircraft design studies, this project required consideration of the entire system including instrumentation, data telemetry, and system operation and control. These areas are not traditionally considered in an undergraduate curriculum and required independent study on the part of the students. One other aspect of the project was the requirement that the technologies included in the systems be such that the final designs could actually be fabricated in a university laboratory environment for "reasonable" costs. Though the design groups were developing preliminary concepts rather than final designs, if promising designs did evolve, some consideration would be given to performing detailed design studies and actual system fabrication.

The basic organization of the course and the requirements imposed on the students have been described in detail[11]. One of the aspects of this course is the requirement that the design teams actually fabricate a technology demonstrator for their aircraft concept. This technology demonstrator is to be used to validate the basic flightworthiness of the configuration and is not intended to perform the actual design mission. These aircraft which are remotely piloted and fabricated using conventional "modeling" techniques are developed during the

last three weeks of the course. This requirement introduces the students to a wide range of additional problems and often influences decisions in the conceptual design phase.

The fabrication of prototypes has proven to be a very positive aspect of the course though it requires significant additional effort. Although the time constraints often limit the success of all of the technology demonstrators, the experience of transforming ideas to "hardware" is very beneficial. This approach has been successfully applied in other undergraduate design programs(12) and the RPV applications are well suited to this type of project.

BLUE MISSION RFP

Opportunity

The wind tunnel has served as the primary source of aerodynamic data for flight vehicle configurations. The wind tunnel is used to test subscale models of flight vehicles or to collect basic aerodynamic data. Within the wind tunnel, certain flow conditions such as model position and flow speed can be accurately controlled, but other influences such as wall interference and free stream turbulence are more difficult, if not impossible, to control. Wind tunnel testing can also be limited by the ability to achieve dynamic similarity between the test and actual flight conditions. Remotely piloted vehicles have been used for testing technology demonstrators, but their use in collecting in-flight aerodynamic data has not yet been fully exploited. The use of an RPV for the collection of aerodynamic data at low Reynolds numbers will be the goal of this design effort.

Objectives

1. Develop a proposal for an aircraft and associated flight control and data acquisition system with the following characteristics:

a. Usable as an airborne aerodynamic data acquisition system for collecting surface pressure distributions and other appropriate near field flow information on "two-dimensional" or "three-dimensional" lifting surfaces. The lifting surfaces must be able to be tested at angles of attack from -20° to +40° over a Reynolds number range (based on chord) of 4×10^4 to 1×10^6.

b. Lifting surfaces ranging in size from chords of 4 in to chords of 16 in.

c. Three-dimensional wing configurations with wing spans from 1 to 5 ft should be considered and wing sweep angles from -20° to +30°.

d. An instrumentation system capable of collecting all necessary associated data such as airspeed, angle of attack, etc., with sufficient accuracy in order to provide useful aerodynamic information.

2. Take full advantage of the latest technologies associated with lightweight, low cost radio controlled aircraft and propulsion systems. Since this system may be expected to operate in a wide variety of climates and test locations, the safety of the system will be of critical importance. All possible considerations must be taken to avoid damage or injury in case of system malfunction.

3. Develop a flying prototype for the system defined above. The prototype must be electric powered and should be capable of demonstrating the flight worthiness of the basic vehicle and feasibility of the flight control and data collection system. A basic test program for the prototype must be developed and demonstrated with flight tests.

System Requirements and Constraints

The system design shall satisfy the following:

1. All basic operation will be line-of-sight although automatic control or other systems can be considered.

2. Takeoff and landing must be accomplished in a circular area with no greater than a 150-ft radius (50-ft object clearance). Any special landing or takeoff equipment must be considered as part of the system. For repeated flights, system turnaround must be able to be accomplished in 15 min.

3. Only clear weather capabilities need be considered.

4. All airborne instrumentation and associated flight control systems must be included in the design.

5. Two people must be able to accomplish ground handling and system operation.

6. The complete system should be portable in a conventional pickup truck.

7. Noise nuisance must be a consideration both for the operator and the region in which the aircraft operates.

CONCEPT DESCRIPTIONS

This section briefly describes each of the concepts that resulted from the design studies. These descriptions focus on special considerations associated with each design and the manner in which the individual missions would be performed. The concepts are identified by the group names. The Sky Shark and the SPiRiT were designed to satisfy the Blue Mission, surface pressure measurements. The Air Rhino and the MANTA were designed in response to the Gold Mission RFP, component force or moment measurements, while the Delta M was designed for highly swept delta wing applications.

Each of the design groups developed detailed technical proposals which presented information on all aspects of the design concepts. The following is a synopsis from the executive summary that was included in each proposal. This paper is not intended to provide in-depth technical detail on each aircraft but to describe those features considered most important in the development of the concept.

The Sky Shark

The aircraft designed to meet these requirements, the Sky Shark, is shown in Fig. 1. The aircraft's basic specifications are given in Table 1. In the design of this aircraft, accurate data acquisition and aircraft control (in the context of varying test configurations) were decided to be the most important design considerations. To ensure accurate aerodynamic data, the test specimen should be situated on the craft such that it

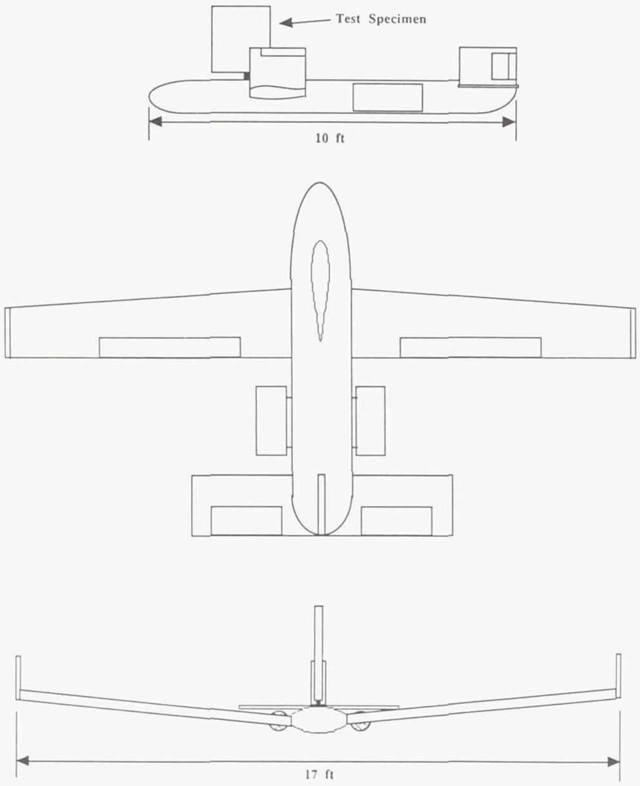

Fig. 1. Sky Shark

experiences the least amount of aerodynamic interference from other parts of the plane. The Sky Shark has the test specimen mounted vertically on top of the fuselage, near the nose. The vertical mounting was chosen to reduce interference from the wing. The section is mounted forward, near the center of gravity, for two reasons. First, near the nose of the craft, proper design of the fuselage can minimize aerodynamic interference with the test specimen. Second, by locating the section near the center of gravity, the forces created by the specimen will not induce large moments.

As Fig. 1 shows, the Sky Shark has a forward, mid-mounted wing with dihedral. From the standpoint of stability, a forward-mounted wing allows the c.g. to be positioned at the front of the aircraft, near the test specimen, as desired. The wing is mid-mounted in order to move it down and away from the test specimen. The dihedral will provide roll and lateral stability which is needed to counteract the destabilizing effects of the test specimen.

The design includes conventional horizontal stabilizers with oversized elevators for longitudinal stability and control. For lateral stability and control, a single vertical tail with oversized rudders will be used. The control surfaces are oversized in order to correct for any moments created by the test specimen. Roll control will be provided by ailerons on the wings. In order to balance the side forces created by the test specimen, winglets have been positioned on the the wing tips. These active and all-movable winglets are considered rather unconventional and are the result of the requirement to carry an additional lifting surface which will experience high angles of attack. The winglets will be used to balance the side force without creating large yaw moments that would result if the vertical stabilizer were used.

The aircraft will be powered by two ducted fans, mounted on the fuselage behind the wing. It is hoped that proper positioning and integration of the ducted fans will also allow for reduced interference with the test specimen and thus, more accurate data acquisition.

The Sky Shark is capable of meeting most of the mission requirements. For chord lengths of .8 ft to 1.4 ft, the Sky Shark allows testing for the Reynolds number range, 4×10^4 to 1×10^6. If it is desired to test smaller chords, only Reynolds numbers up to 5×10^5 can be achieved. The required angles of attack and sweep can be attained in flight by the aircraft.

The Sky Shark will start its mission on the ground, where it will be fueled, and a test specimen attached. The aircraft will be launched by means of a catapult system. Once in the air, it will cruise at altitudes of 100-3000 ft, where data acquisition will occur. The Sky Shark will fly a rectangular pattern, 1200 ft long by 500 ft wide. The pressure data will be taken for a specific test specimen during steady level flight along the length of the rectangular pattern and stored on board. The craft will allow 20 minutes of testing, with a maximum mission endurance of 45 minutes. The Sky Shark will land on conventional landing gear, which have been retracted up to this point.

The design of the Sky Shark appears to present no significant technical problems. However, some potential trouble spots should be pointed out. Although the greatest effort has been expended in making this aircraft as stable as possible, destabilizing forces and moments from the test specimen may cause problems. This design proposal has assumed that an automatic control system will be incorporated into the aircraft. Such advanced control systems are essential to the success of the Sky Shark.

Table 1. Basic System Parameters

	Weight (lb)	Span (ft)	Length (ft)	Wing Area (ft2)	Aspect Ratio
Air Rhino	35	9.7	6.7	15	6.3
MANTA	30	15.2	6.7	23	10
Sky Shark	60	17.5	10	34	9
SPiRiT	30	17	10.8	29	13
Delta M	25	14	5.2	14	14

SPiRiT

The Surface Pressure Readings and Testing (SPiRiT) aircraft is designed to measure the surface pressure distributions about a two- and three-dimensional lifting surface at Reynolds numbers ranging from 4.0×10^4 to 1.0×10^6. The RPV will be able to accommodate lifting surfaces with spans ranging from 1 to 5 ft and chords ranging from 4 to 16 in. The test specimen

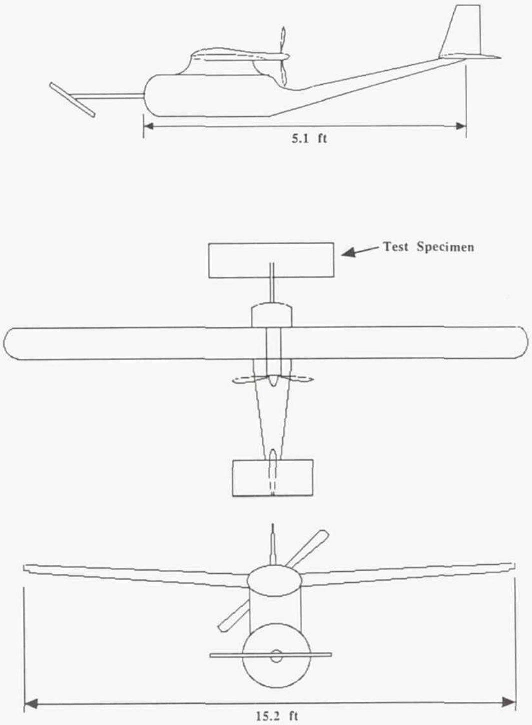

Fig. 2. SPiRiT

itself will be able to rotate in flight to angles of attack ranging from -20° to 40°.

The primary goal of this design is to be able to make accurate measurements of the pressure distribution on the test specimen. Because of anticipated problems with attitude control for extended periods of time, it would be desirable to measure all points of the pressure distribution simultaneously (or as close to simultaneously as possible). Assuming that this can be accomplished, the next important consideration is the influence the RPV has on the flow around the test specimen. To minimize the disturbance, a pusher-propeller, high-wing configuration was selected. Furthermore, the test specimen was mounted as far forward as possible to reduce the interference effects of the wing and propeller. The final configuration is shown in Fig. 2.

The secondary design goals generally involved evaluation of the performance parameters, estimation of stability and control characteristics, and reduction of the weight to improve performance. To maximize the amount of time-on-station data, it is necessary to reduce the drag and weight of the RPV. These goals led to a high aspect ratio wing. The test specimen is mounted forward of the main fuselage and will create large aerodynamic forces which significantly alter the stability and control characteristics. Thus, in order to control these high forces, a large tail and control surface will be required. At the same time, because an automatic flight-control system will be incorporated into the design, it is felt that the RPV should be statically and dynamically stable. This will reduce the workload of the flight-control system.

The actual test specimen itself should be easily interchangeable with other test specimens. This will make the entire RPV a more versatile and easy-to-use experimental tool. For ease of operation, two people at most should be needed for operation. One person controls the data acquisition and the other person controls the flight systems.

The current design has met all these goals. The A/D system collects one complete pressure distribution in 0.2 seconds and stores the data on board for later processing. The RPV will fly for a maximum of thirty minutes and collect data for twenty minutes. It can be operated by two people from a 45.7-meter-(150-foot) radius area.

The design itself, however, is incomplete in several key areas. Preliminary analysis indicated that for the high α conditions and the largest possible test specimen, the main wing would be required to carry a significant download. Thus, basic trim and trim drag considerations must be considered in greater detail. One possible design concept to correct this is to have the wing rotate on its pylon so as to produce a downward force without significant rotation of the fuselage. This wing rotation will be coordinated with the test specimen angle of attack and flight velocity to ensure steady level flight of the aircraft. This will be accomplished by the automatic flight control system. Perhaps a simpler solution would be to invert the specimen for positive angle of attack testing, although such a strategy means that positive and negative angle of attack tests must be completed in separate missions.

There are other considerations that must be addressed in order to evaluate this concept. The proposed data-acquisition system uses four parallel-processing A/D converters to increase the sample rate. This type of parallel processing is complicated and very expensive, and details for such a system have not been addressed. Similarly, the Automatic Flight Control System utilizes a closed-loop feedback system to regulate the airspeed and angle of attack of the test specimen. To save space and weight, the RPV was not equipped with this processing capability. The pertinent information must be radioed to the ground and the correction signals radioed back to the RPV. It is possible that the telemetry system will take too long to encode, transmit, and decode the data. If the telemetry system does take too long, the controls will not respond to the changing environment as desired and the acquired data will be useless.

It is generally recognized that the design of this RPV is still in its preliminary stages. Another iteration of the design process should bring the final design of this concept into a much sharper perspective.

MANTA

This remotely piloted vehicle was designed to collect aerodynamic data on airfoil test specimens at low Reynolds numbers. The aircraft test section is located forward of the aircraft to reduce aerodynamic interference between the flight vehicle and the test section. Its name is the result of its "manta ray" appearance. The aircraft has a 19.4-ft wingspan, an aspect ratio of 13 and a fuselage length of 11.8 ft. The aircraft is fitted with twin 3-hp engines mounted on either wing. Data will be

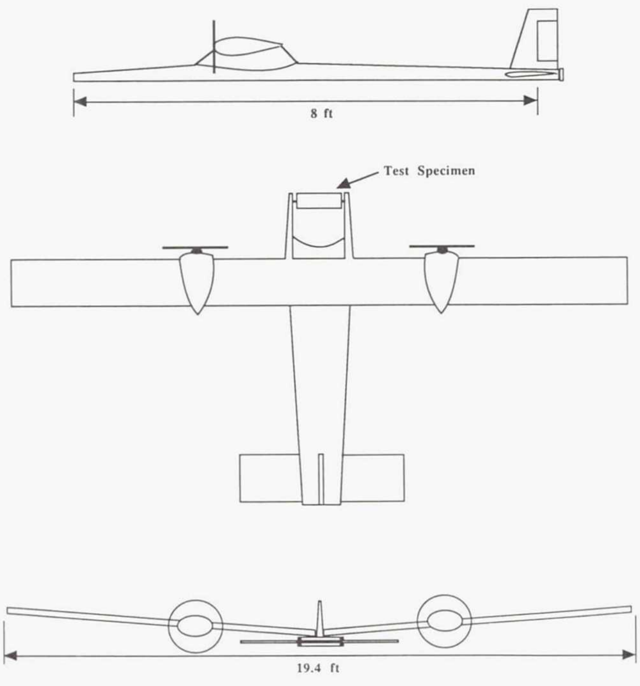

Fig. 3. MANTA

taken using a force-balance system and then radioed to a ground receiver. The MANTA incorporates an automated control system which will control the craft during the data acquisition phase of the flight.

The goal of the MANTA vehicle is to collect actual flight load data for primarily two-dimensional airfoil sections. The variation in test-section angle will be from -20° to 40° with the Reynolds number varying in a range from 4×10^4 to 1×10^6.

The MANTA aircraft is designed for flight under clear weather conditions only. It is operated under line-of-sight conditions due to the nature of the remote control system and the two man limitation of the ground operations team. The amount of wind in which the MANTA can safely operate and the effect of wind gusts on the aircraft still need to be determined. The MANTA is designed to take off using a conventional landing-gear arrangement. Two wheels are located on either side of the fuselage beneath the wing, and the third wheel is a steerable tail wheel located just beneath the vertical stabilizer.

A study of the priorities yielded the following design goals: (1) Wide range of test conditions; (2) Accurate data collection; (3) Good durability; (4) Efficient cruise performance; (5) Cost; (6) Ease of use; and (7) Ease in manufacturing. Based on these, many designs were proposed and evaluated. The resulting concept places the test section forward of the aircraft fuselage and wing. The test section is supported by two booms which are located on either side of the fuselage with a constant separation distance of 2 ft. This allows a maximum test section span of 2 ft. Twin 3-hp engines are mounted on either wing 4 ft from the fuselage centerline. The empennage is located 7 ft from the aircraft center of gravity. The vertical tail has been sized to provide directional stability and to allow a safe landing under one-engine-out conditions. The horizontal tail is sized to ensure longitudinal stability throughout the Reynolds number range and the test specimen angle-of-attack range. The final specifications of the MANTA vehicle can be seen in Table 1 and a schematic of the design is given in Fig. 3.

One of the most difficult tasks involved the proper sizing and movement of the horizontal stabilizer. Large amounts of lift will be generated by the test section at the high angles of attack. At present the horizontal tail is sized so as to allow full test section angle-of-attack range. However, this will sometimes dictate that the aircraft itself must actually fly at a negative angle of attack to achieve steady level flight. Data collection while the aircraft is in a steady maneuver should be investigated to determine feasibility and possible benefits over straight-and-level flight data collection.

Another potential problem that was identified and was not resolved was the difficulty in determining the lift effects of the fuselage. In order to support the booms, the proposed fuselage is very wide and rather thin. Its contributions to the total vehicle aerodynamics could not be determined with the analytical tools at hand. The actual effect must be studied in order to ensure that desirable stability and handling characteristics are obtained during flight.

Air Rhino

The Air Rhino is a remotely piloted "airfoil test platform" airplane. It is designed to measure the component forces on easily interchangeable test airfoils for low Reynolds numbers and varying angles of attack. A three-view drawing and specifications summary are given in Fig. 4 and Table 1.

The data will be gathered in a steady flight environment. The flight plan calls for ascending to cruise altitude and, once there, flying a series of straight, level, unaccelerated test runs where data will be taken. The flight path is controlled by an autopilot system. While the plane is circling back for another test run, the pilot may make adjustments in test airfoil angle of attack or autopilot-programmed flight velocity. Fig. 5 is a schematic of a proposed data sampling mission.

Measurements of the lift, drag and moment on the vertically mounted test airfoil will be made using a specially designed force balance. Other measurements to be taken include the static pressure, the dynamic pressure, the temperature, the plane angle of attack, and the test airfoil angle of attack. These data are sent back to a ground-based receiver, where the data are processed and stored by microcomputers.

The propulsion system consists of a pusher propeller mounted behind the test airfoil and the fuselage to avoid flow interference on the test section. The three-bladed propeller is powered by a reciprocating gas engine capable of producing 8 hp at 8000 rpm. The three-bladed propeller was chosen for efficiency and noise reduction. Endurance, range, rate of climb, and rate of descent are all excellent for the Air Rhino, because its propulsion system is designed for the top velocity of 200 ft/s, so the engine is overpowered for the middle speed ranges.

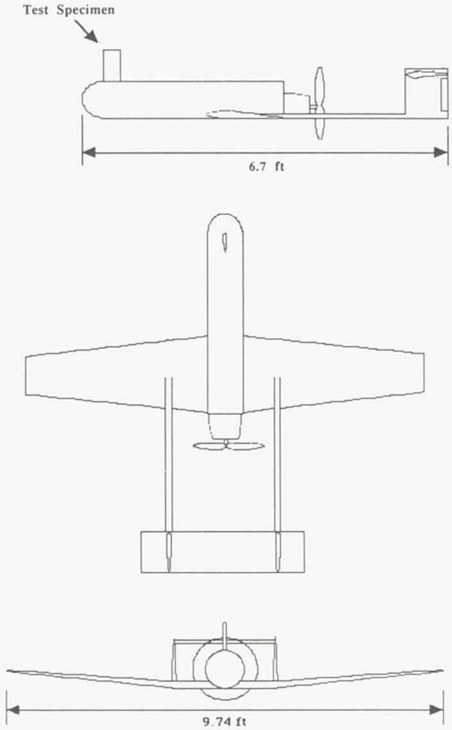

Fig. 4. Air Rhino

Air Rhino wing has a 9.8-ft span, 1.5-ft mean chord wing with spar-and-rib construction. The tail and horizontal stabilizer are located at the end of long twin composite booms mounted aft of the propeller. Three control surfaces are used: ailerons, rudder and a stabilator. These surfaces are actuated by independent servos, as are the flaps, the landing gear and the throttle.

Since this was a preliminary concept study, there are some areas that will require future study. These include development of control to compensate for both the moment and the force of the test airfoil and a more detailed evaluation of the aerodynamic interference between the test specimen and fuselage surface flow and propulsion system.

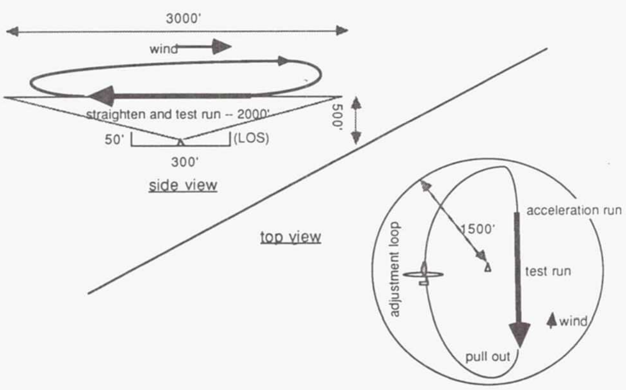

Fig. 5. Typical Data Collection Mission Flight Plan

Delta M

The mission requirements for the performance of aerodynamic tests on a highly swept delta wing planform posed some unique problems. These included aerodynamic interference, structural support, data acquisition and telemetry, aircraft stability and control, and propulsion system integration. However, since the overall integrity of the aircraft is of primary importance, the preliminary concept was selected in order to arrive at a basic design suitable for further development.

The proposed aircraft is a testbed for a class of highly swept, delta wing planform models used in aerodynamic testing. The overall aerodynamic configuration of the proposed aircraft incorporates twin tail booms, a low horizontal tail, twin vertical tails, a fuselage "pod," and a low-mounted, rectangular-planform wing (Fig. 6). With the exception of the twin tail booms, which are the result of concerns over the aerodynamic interference with the wake of the delta wing model, all of the configurational components are relatively conventional.

The data acquisition system incorporated in this design has the advantage of being extremely fast. It is designed for the rapid sampling of up to 100 pressure ports. During each test flight the test engineer will be able to test any of 20 angles of attack in the Reynolds number range of 5.5×10^5 to $1.65\text{x}10^6$. A typical mission would allow for 28 tests during each flight with an average flight duration of 30 minutes.

This aircraft will be catapult launched in order to reduce fuel requirements and to limit takeoff distance. Once in the air the aircraft will be remotely controlled by the ground-based pilot until the test altitude is reached, at which time control will be transferred to a computer-based, automatic control

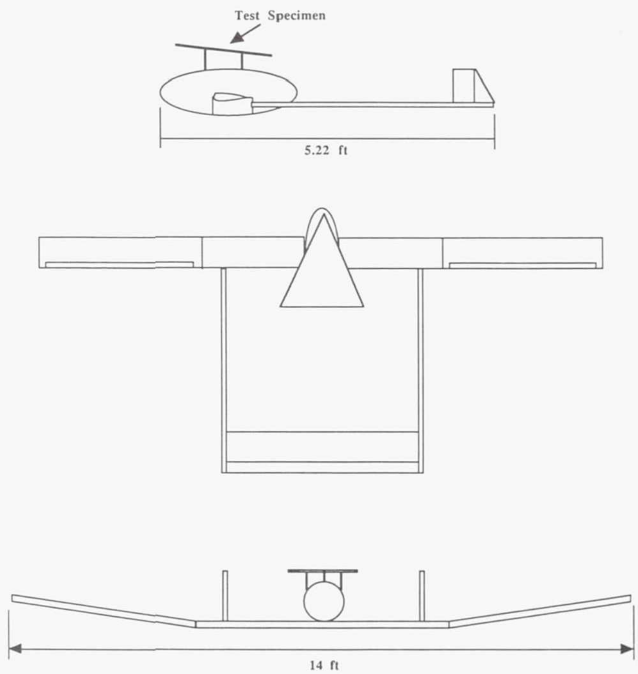

Fig. 6. Delta M

system. This will allow for the standardization of the data acquisition procedure. As a safety feature, the test engineer always reserves the right to override the automatic system and resume manual control. After the flight, the proposed aircraft will land on the deployed spring-loaded landing gear.

The propulsion system proposed for this design uses a ducted fan unit housed in the rear of the fuselage. This system was chosen because of concerns about interference between the propulsion system and the test specimen. By locating the inlets away from the upper surface of the aircraft (wings, forward end of fuselage, rear end of fuselage, etc.), good flow quality should be ensured. Because of the twin tail boom configuration, potentially disrupted flow from the test model will not be allowed to impinge upon the vertical control surfaces. Also, the model will be mounted in a region above the fuselage outside the boundary layer.

Stability and control considerations are very important for a remotely piloted vehicle. Due to the placement and size of the tail surfaces, sufficient static stability is assured. Though maneuver performance is not critical, adequate controllability must be achieved. Due to the placement of the delta wing test specimen above and slightly aft of the aircraft center of gravity, the pitching moment created by the lift and drag on the model will work to cancel each other at the extreme angles of attack.

Although this aircraft was designed as a "work-horse," it has good performance characteristics. The typical flight duration will allow for the collection of significant amounts of data and a wide range of test conditions. Particular concerns which must still be addressed include details on the inlet design and ducted fan integration, landing gear installation, and details of the automatic flight control system.

SYSTEM DESIGN CONSIDERATIONS

The concepts defined above were the result of a series of preliminary design studies. The primary design goals of each concept were defined by the design teams; thus, the emphasis of each team was somewhat different and each encountered different problems. It should be stressed that this project considered the design of a complete system, not simply an airframe. Therefore, the potential success of the entire system rested upon the successful integration of the individual subsystems. The following is a brief summary which addresses each of the primary technical areas and highlights methods used in the design process and problems encountered.

Data Acquisition and Flight Control

The design of the data acquisition system and the integration of the instrumentation into the flight vehicle was the most difficult aspect of the design project[13]. Since only a general description of the test specimen was provided, detailed definition of the instrumentation was difficult. In this low Reynolds number range, component forces are usually relatively low, requiring a rather sensitive balance. On the other hand, the flight testing and ground handling requirements dictate a durable and robust system. A similar dilemma is encountered in conducting surface pressure measurements, since the low speeds result in rather low pressure differences which establish a need for rather large, heavy transducers.

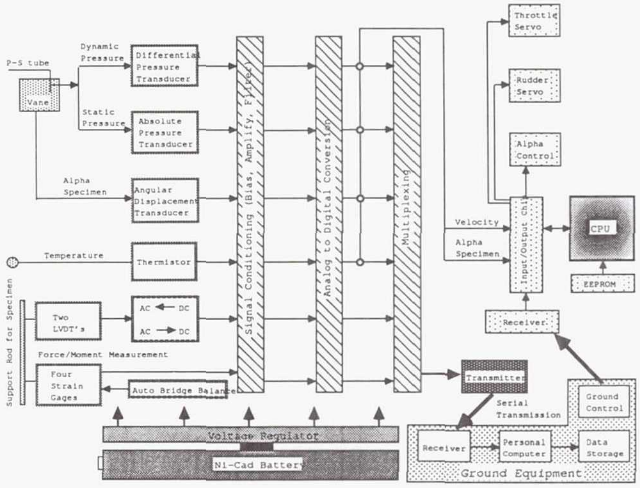

Fig. 7. Schematic of Data Acquisition System

Defining onboard data processing and storage as well as the data telemetry requirements for these systems was equally complex. Purdue University[14] has been developing an RPV-based flight test program and provided useful input based on their experiences. The accuracy of onboard instrumentation and the design of an automated flight planning system are well beyond the scope of this preliminary concept study, but considerations of each were made by the design teams. Fig. 7 illustrates the proposed system for the Air Rhino, which included the aerodynamic and flight data acquisition systems, data processing, and transmission equipment.

Aerodynamics

The aerodynamic design of the vehicles was rather straightforward. In each case relatively simple, conventional designs proved adequate for the mission. Since neither range nor endurance, typical aircraft design parameters, was considered critical, there did not appear to be an overwhelming need to "optimize" the aircraft aerodynamics.

The overriding concern was the placement of the test specimen so that it would encounter as close to free stream conditions as possible. This resulted in the placement of the test specimen as discussed above. Unfortunately, the tools available to predict the three-dimensional flow fields associated with the base vehicle and the test specimen were quite limited. Simple vortex models were used but more analysis using interfering lifting surface methods would be required. Fig. 8 illustrates the type of results achieved with these simple methods. It shows the induced velocity at the test specimen resulting from lift generated by the main wing for a single flight condition. This type of data was used to determine the wing/test specimen spacing. Table 2 contains a comparison of some of the basic aerodynamic parameters for the five concepts.

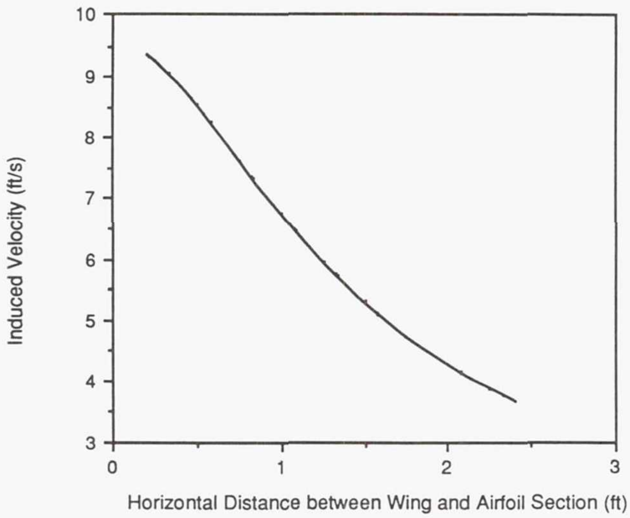

Fig. 8. Induced Velocity at Test Specimen due to Wing Lift

Table 2. Basic Aerodynamic Parameters

	Airfoil (main wing)	C_{Do} (Aircraft)	Taper (wing)	Dihedral (wing)
Air Rhino	Wortmann FX63-137	.015	0.6	5°
MANTA	NACA 23012	.0115	0.5	—
Sky Shark	NACA 1408	.023	0.8	10°
SPiRiT	Gottigen 797	.027	1.0	3.5°/5.8°
Delta M	NACA 4415	.015	1.0	8°

Airfoil Selection. Since the test specimen is flown in the low Reynolds number regime, the primary lifting surfaces and control surfaces must also operate in this regime. There are numerous problems associated with low Reynolds number airfoil performance such as reduced C_{lmax}, increased sensitivity to surface roughness and nonlinear or hysteretic behavior of C_l. Since flight performance was not considered to be the most critical aspect of these systems, some of the groups selected rather conventional (NACA) airfoils where others used newer, low Reynolds number airfoils.

An additional problem is the availability of adequate aerodynamic data. There is a limited number of sources[(15)] that can be used to provide airfoil data, but, considering the rather wide Reynolds number range in which these vehicles operate, reliable data was difficult to find. This was particularly true in drag prediction, since much of the component drag data and traditional drag buildup methods are not well-suited for this low Reynolds number range.

Complex high-lift devices were not used on any of the concepts since most felt that takeoff performance was not critical and the mechanical complexity associated with them would be unwarranted for this mission.

Wing Planform. Rather conventional wing planforms were selected by each group. Each had a rather high aspect ratio, although induced drag was not considered a significant design influence. Wing loading ranged from 1.0 to 2.3 lb/ft^2 which is very low by most flight vehicle standards, but is consistent with large-scale, radio-controlled aircraft operating in this speed range.

The design teams did have access to a simple lifting surface analysis procedure developed by Kroo[(16)] which proved quite useful in preliminary planform selection. Figure 9 illustrates the results of a trade-off study which investigated the influence of taper and sweep on spanwise c_l distribution. This particular program is an extended lifting line method for which the students have the necessary theoretical background. Therefore, they are better able to interpret the results than if a much more sophisticated method were used.

Fuselage. In each case the fuselage was intended to carry the data acquisition systems, telemetry and control equipment, and fuel. For the Delta M it was also intended to house the ducted fan engine. Since the test specimen was mounted near the fuselage in each case, aerodynamic interference with the fuselage was considered important, but prediction of this interaction was limited by the available tools.

Contribution of the fuselage to the aircraft drag was estimated using component drag buildup methods, but the results were considered approximate at best since the empirical data base from which the component contributions were determined was developed at a larger Reynolds number.

Propulsion

In order to achieve the low cost goals of each of the design groups, off-the-shelf propulsion systems were proposed for each concept. There are a number of two-cycle and four-cycle internal combustion engines which are available for this type of application. Primary design considerations were engine placement, propeller design, and aerodynamic interference of the propulsion system with the test specimen. Table 3 summarizes some aspects of the propulsion systems for each concept.

In an attempt to reduce the interference with the test specimen, two of the concepts proposed ducted fan engines

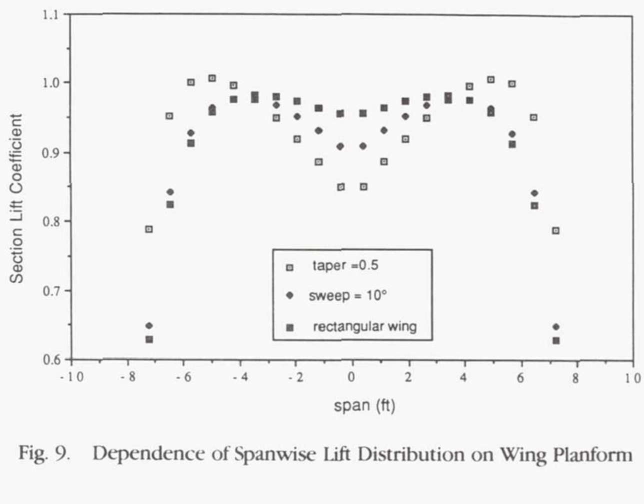

Fig. 9. Dependence of Spanwise Lift Distribution on Wing Planform

Table 3. Propulsions Systems

	Type	Prop	BHP (at rpm)	Weight Fraction (%)
Air Rhino	Internal Combustion (IC)	3-blade pusher	8.0 (8,000)	39.7
MANTA	IC-twin	3-blade tractor	6.0 (7,900)	16.7
Sky Shark	IC	ducted fans	3.0 (16,000)	23.8
SPiRiT	IC	3-blade pusher	7.5 (11,000)	29.4
Delta M	IC	ducted fan	5.0 (19,500)	11.0

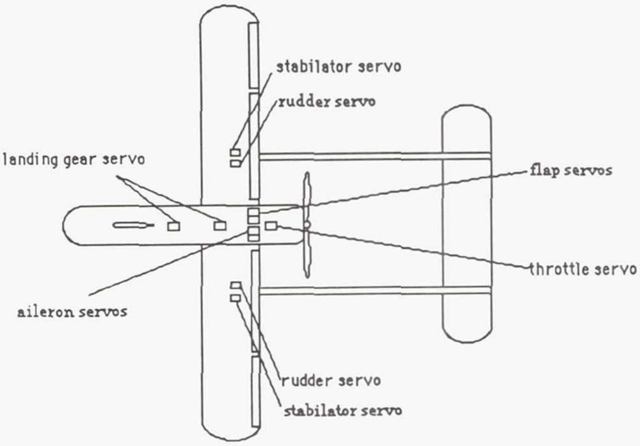

Fig. 10. Control System Actuator Location

which are available in this power range. There is little detailed technical information available on these power plants; therefore, inlet design and the actual influence on the flow field about the body could not be determined at this stage of the design. Two of the other groups selected pusher configurations in order to reduce interference and the third selected a twin-engine design with the engines placed well outboard on the wings. Prediction of the aerodynamic or acoustic interference for these engine placements was not accomplished during this study.

The power requirements and weight fractions for each of the configurations were not critical elements in the design.

Stability and Control

Inherent static and dynamic stability were very important design considerations because of the remote operation of these vehicles. Each group assumed that the vehicle would be piloted by a ground-based pilot during launch and landing phases of a mission and by some form of automatic system during the flight data acquisition phase. A stable platform would also help during the ground pilot phase and aid in consistent test conditions for data acquisition phase. Each group attempted to establish a design which satisfied basic longitudinal static stability with adequate static margins.

Dynamic stability and handling qualities were not addressed in this phase of the design. Handling qualities present a problem with remotely piloted vehicles since accepted standards similar to those for piloted aircraft do not exist. Additional problems related to instrumentation for the ground-based pilot and basic aircraft visibility were also encountered.

Details of the automatic flight control system were beyond the scope of this effort, but other considerations such as required instrumentation, control surface sizing, and certain aspects of the mechanical installation were briefly considered. Figure 10 is a schematic of the actuator locations required for the Air Rhino.

Structures and Materials

Since low cost was one of the primary design drivers for each of these systems, materials selection and structural design were based on existing technologies, many of which are used by the aviation hobbyist. These include wood and fiberglass construction although numerous applications of other composites were included. These materials actually simplify the manufacturing process and maintain reasonable costs.

Preliminary structural analyses were performed for most of the lifting surfaces, which were of semi-monocoque construction. Finite-element analysis using a recently developed design program was conducted in order to establish the validity of a number of the designs and to establish spar locations and allowable deflections[17].

Weight estimation was performed for each of the concepts and this presented some additional problems. Weights data and weight fraction information are not readily available for a large number of aircraft in this class. This limited the reliability of the initial weights data, but since these were rather simple systems, the component weights could be developed. Table 4 illustrated the system weights of the major components for the Air Rhino.

Table 4. Component Weights—Air Rhino

Component	Center of Gravity Locations: Center Gravity location (ft)	Weight (lbs.)
Fuselage hull	1.85	5.0
Booms	4.85	1.4
Horiz. stabilizer	6.25	1.2
Vert. stabilizer	6.35	0.4
Battery	0.583	1.5
Autopilot	1.0	1.0
Test airfoil & force balance	0.167	2.5
Circuit boards & instruments	1.67	0.5
Wing	2.675	5.4
Fuel	3.0	2.0
Engine & Propeller	4.0	8.0
Total accountable weight:		28.9

Table 5. Basic Performance Parameters

	Maximum Range (miles)	Maximum Endurance (min)	R/C Maximum (ft/s)	V Maximum (ft/s)
Air Rhino	100 at 80 ft/s	101 at 55 ft/s	73	200
MANTA	40	30	—	—
Sky Shark	47	40	36	190
SPiRiT	—	30	75	150
Delta M	202 at 100 ft/s	180	33.5	150

Performance

Only preliminary performance estimates were performed for each of the systems. Of primary concern was predicting the time on station as related to the amount of data that could be collected on a single flight. Table 5 summarizes some of the performance characteristics for each of the aircraft. Typical mission times of approximately 30 minutes were established based on onboard data storage limitations and were satisfied by each of the concepts. These would not be considered high performance aircraft. The most limiting performance requirement appeared to be the need for a rather wide, steady, level-flight speed range. This was imposed by the Reynolds number range required for the test specimen. Since the aircraft were not required to perform extensive maneuvers and would operate at low altitude, none of the concepts appeared to be performance limited.

TECHNOLOGY DEMONSTRATOR DEVELOPMENT

Each of the design teams completed a flight-worthy technology demonstrator. The total fabrication time for each was approximately three weeks. The technology demonstrator was required to establish the viability of the basic configuration. It was not required that it include the instrumentation or data acquisitions systems, and it would be controlled by a ground-based pilot.

The design teams were provided with remote-control radio systems and propulsion systems and were responsible for the acquisition of all other materials and complete system fabrication. For reasons of safety and ease of operation, the groups were requested to use a specific electric powered propulsion system for the technology demonstrator. This system produced about 0.2 hp at 6000 rpm and created problems in "scaling" as groups attempted to fabricate the technology demonstrators. They were then forced to build subscale versions of their actual designs which increased problems with low Reynolds number airfoil performance. The electric propulsion systems were also significantly heavier than those proposed for their actual concepts and even though they were not required to carry all of the data collection instrumentation, the weight fractions for the electric propulsion and flight control system exceeded those for the propulsion, control, and instrumentation systems for the actual design. Thus, the technology demonstrators were overweight and underpowered, a situation that should be avoided.

The flight test program consisted of one 2-hour period during the last week of the semester. All of the aircraft launched or took off on their own power and maintained sustained flight for some period of time. The Sky Shark performed a very successful flight and landing and received high marks from the two test pilots. The MANTA provided the most eventful flight when the vertical stabilizer failed due to flutter and separated from the aircraft resulting in loss of control and catastrophic crash. The other three aircraft did fly, although each encountered a pilot control or inadequate power problem on takeoff and therefore "landed" very shortly thereafter. Each incurred damage that could not be repaired within the two-hour period.

Due to the very limiting time constraints placed on the course, the modifications required to continue the flight tests were not performed and the aircraft were retired to the museum. The experience gained by the student designers was not "retired" and demonstrated the challenges associated with successful development of flight vehicle systems.

CONCLUDING REMARKS

The systems described in this paper were conceptual designs resulting from a single-semester undergraduate course. The purpose of the course is to provide the students with design experience at the systems level and to introduce parametric trade-off studies and optimization techniques. This is accomplished by performing design studies on realistic aircraft systems. The mission used for this project involved the design of unmanned flight-vehicle systems for aerodynamic data acquisition. This was a rather complex mission, even though the application involved low-speed subsonic flight.

Five concepts were proposed in order to satisfy this mission. Each was the result of approximately eight weeks of effort. These primary studies indicated that the critical considerations were the data acquisition and instrumentation systems, the flight control systems, and the integration of the test specimen onto the base vehicle. Each of these was addressed by the design teams and a number of solutions were proposed.

The designs illustrated the feasibility of developing a rather low cost flight-test system, but the concepts presented in this paper are preliminary. Additional design studies would be required prior to actual system development.

ACKNOWLEDGMENTS

The project reported here was supported by the NASA/Universities Space Research Association (USRA) Advanced Aeronautics Design Program. The project was directed by Dr. Stephen M. Batill, who served as course instructor, and Messrs. Walt Howard and Daniel Jensen, who served as project teaching assistants. Technical coordination was provided by the Boeing Commercial Airplane Company, and the authors wish to thank Mr. Cal Watson and Dr. John McMasters of the Boeing Company for their support and assistance. Segments of this

paper have been edited from the final design proposals submitted by the student design teams.

We particularly wish to acknowledge the efforts of all of the students in the AE441 Aerospace Systems Design course in the Spring 1989 for their enthusiasm and hard work. Each should be considered as co-author in this effort and we acknowledge efforts of the group leaders Messrs. Robert Ziemba, Tyrus Soares, Paul Bielski, Mark McLaughlin, David Condron and Andrew Shearon. We also wish to acknowledge the contribution of Dr. Patrick Dunn who had co-responsibility in presentation of this course and Mr. Joseph Mergen whose technical consultation and advice was invaluable to the students.

REFERENCES

1. Lowndes, J., (ed.), "Aerospace America", Vol.27, No. 2, Feb. 1989.
2. Aderhold, J.R., Gordon, G., and Scott, G.W., "Civil Uses of Remotely Piloted Aircraft," NASA CR-137894, July 1976.
3. "RPV's - Aerodynamics and Related Topics", Vols. I and II, vonKarman Institute for Fluid Dynamics, Lecture Series 101, May 1977.
4. Kehoe, M.W., "Highly Maneuverable Aircraft Technology (HiMAT) Flight-Flutter Test Program," NASA TM-84907, May 1984.
5. Putnam, T.W., Robinson, M.R., "Closing the Design Loop on HiMAT (Highly Maneuverable Aircraft Technology)," NASA TM-85923, Sept. 1984.
6. Stollery, J.L., Dyer, D.J., "The Flight Performance of an RPV Compared with Wind Tunnel and Theoretical (CFD) Results," Paper ICAS-88-4.9.2, *Proceedings of the 16th Congress of the International Council of the Aeronautical Sciences,* Israel, pp. 1392-1401, Aug. 1988.
7. Holmes, B.J., Smith, R.H., "Hypersonic Flight and Instrumentation Research Experiments," Paper No. 84, Third NASP Technology *Symposium*, NASA Ames, *June* 1987.
8. McMasters, J.H., "The Possible Use of Remotely Piloted Vehicles (RPV's) for High Reynolds Number Configuration Validation Testing," Private Communication, April 1988.
9. Jenkins, M.W.M., "Free Flight Research at Lockheed-Georgia," SAE Paper 810567, Business Aircraft Meeting, April 1981.
10. Yip, L.P., Robelen, D.B., and Meyer, H.F., "Radio-Controlled Model Flight Tests of a Spin Resistant Trainer Configuration," AIAA Paper 88-2146, 4th Flight Test Conference, San Diego, May 1988.
11. Batill, S.M., Nelson, R.C., and Dunn, P.F., "Unmanned Flight Vehicles - From Concept to Prototype: An Undergraduate Design Experience," AIAA Paper 88-4414, AIAA Aircraft Design, Systems and Operations Conference, Sept. 1988.
12. Perkins, J., Mitcheltree, R., and Vess, R., "Aircraft Design Education at North Carolina State University," AIAA Paper 89-0649, 27th Aerospace Sciences Meeting, Jan. 1989.
13. "Basic Principles of Flight Test Instrumentation Engineering," Pool, A. and Bosman, D. (eds.) AGARD-AG-160, Vol.1, April 1974.
14. Andrisani, D., Private Communication, Purdue University Department of Aeronautics and Astronautics, Feb. 1989.
15. Miley, S.J., "A Catalog of Low Reynolds Number Airfoil Data for Wind Turbine Applications," NTIS Document DE82-021712, Feb. 1982.
16. Kroo, I., "LinAir for the Macintosh," Desktop Aeronautics, Stanford, CA, 1987.
17. Swift, R.A., "Application of Finite Element Methods to the Preliminary Structural Design of Lifting Surfaces," M.S. Thesis, Department of Aerospace and Mechanical Engineering, University of Notre Dame, May 1989.

1994004550

383660

8P

N94- 71305

A HYPERSONIC EXECUTIVE TRANSPORT

538-05

160664

p. 7

OHIO STATE UNIVERSITY

Four teams of seven students each developed conceptual designs for a hypersonic executive transport. The specifications called for a 10-passenger jet that had a range of 6000-nm while cruising at a Mach number between $M=4$ and $M=6$ and was capable of operating from 10,000-ft runways. The configurations produced by the student design teams varied significantly in both planform and propulsion, but all met the mission requirements. A methane-fueled, variable-cycle turbofan-ramjet powered, double-delta transport was the most conventional design; a second aircraft having variable sweep canards utilized hydrogen-fueled turbofan-ramjet engines and laminar flow control on its delta wing. Two configurations were derived from waverider concepts, analytically shaped flying wings that exploit an $M=6$ shock wave for efficient lift-to-drag ratios. One of the waveriders uses a liquid, noncryogenic fuel—methylcyclohexane—to power separate turbofan and ramjet engines. The second waverider initially operates its turbofan-ramjet engine with liquid JP-X for take-off and flight to $M=3$, then switches to liquid hydrogen for the ramjet high Mach number cycle. The design studies include the effects of aerodynamic heating, environmental concerns, and operating and production costs of each hypersonic transport.

INTRODUCTION

The Ohio State University (OSU) design task for the past two years has focused upon hypersonic trans-Pacific passenger flight. Take-off weight for 250-passenger transports capable of $M=6$ flight for 6000-nm ranges were determined to be in excess of one million pounds; further, operating and production costs were exorbitant, so the possibility of early practical hypersonic flight was remote. Therefore, the design task for the present year was altered; the project was to be a 10-passenger, executive class, hypersonic aircraft. The smaller payload allows a lighter, lower-cost vehicle with more flexible operation allowing an early in-service date, thereby providing valuable practical experience in the hypersonic flight regime. A multimission capability could also be built into the small transport by replacing the 10 passengers with 2500 lb of electronic sensors, thus providing an incentive for military support for a portion of the research and development costs.

Four preliminary design teams responded to the aircraft specifications set down in Table 1. While each group developed airplanes that satisfied these requirements, each design team had its own unique approach. The aircraft all weighed about 200,000 lb; three teams used turbofan-ramjet engines, and one team chose separate turbofan and ramjet engines. The four aircraft used four different fuels for propulsion: liquid hydrogen, methane, JP-X, and an endothermic, noncryogenic fuel, methylcyclohexane. One aircraft used boundary layer suction to maintain laminar flow while two other designs employed waverider concepts to improve lift-to-drag ratios at cruise.

A description of the four concepts and their propulsion systems follows. Key elements of the design process are touched upon, and the performance characteristics and costs of the four aircraft are reviewed.

Table 1. Aircraft Requirements

Range	6000 nautical miles
Payload	10 passengers
Cruise Speed	4 < Mach < 6
Takeoff and Landing	10,000 ft

DESCRIPTION OF THE AIRCRAFT

The XHT-2 Laser shown in Fig. 1 is a modified delta wing airplane designed to fly at Mach 5. It is powered by three turbofan-ramjets that run on liquid methane. The Laser has a pair of forebody strakes that can be deflected individually or in tandem. These strakes are used as control surfaces by modifying the vortex lift. Pertinent specifications are given in the accompanying legend.

Figure 2 illustrates the Hypercanard, a high wing aircraft designed to cruise at Mach 6. Its fuel is liquid hydrogen and it uses two turbofan-ramjets. This plane uses canards to

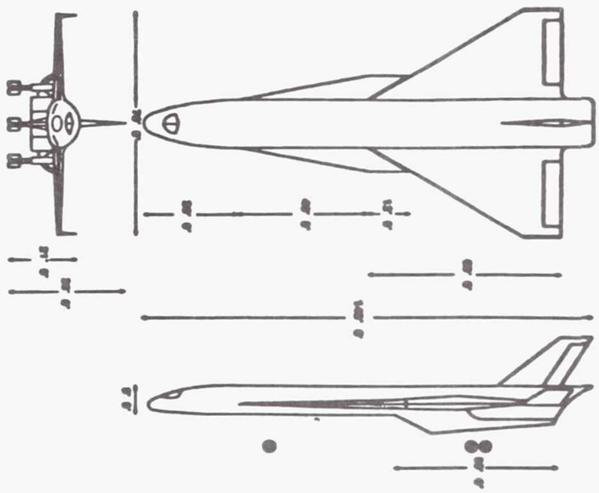

Fig. 1. XHT-2 Laser. Weight: 256,920 lb; area: 3000 sq ft; length: 140 ft; span: 70 ft; W/S: 85.6 psf; T/W: 0.58; cruise Mach: 5; cruise alt: 90,000 ft; engines: 3 turbofanramjets; fuel type: liquid methane; fuel weight: 165,000 lb; special features: deflectable strakes.

PRECEDING PAGE BLANK NOT FILMED

PAGE 314 INTENTIONALLY BLANK

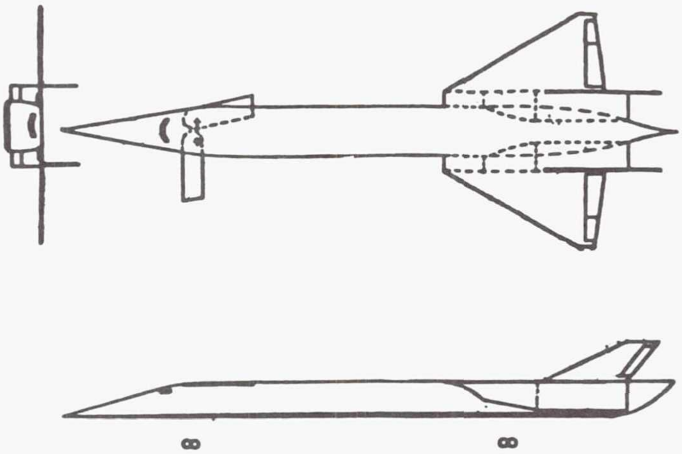

Fig. 2. Hypercanard. Weight: 201,730 lb; area: 2625 sq ft; length: 190 ft; span: 73 ft; W/S: 76.9 psf; T/W: 0.60; cruise Mach: 6; cruise alt: 100,000 ft; engines: 2 turbofanramjets; fuel type: liquid hydrogen; fuel weight: 82,000 lb; special features: boundary layer control and movable canards.

generate additional lift for take-off and to trim the aircraft subsonically. For supersonic flight the canards are swept back into the fuselage. Also, the Hypercanard uses a hybrid laminar flow control (HLFC) system to reduce friction drag. The power to run the HLFC system comes from an auxiliary power unit (APU).

The HyBuJET of Fig. 3 is a waverider designed to cruise at Mach 6. It is powered by three turbofan-ramjets. The turbofans, which are fueled by JP-X, are used to take off and accelerate to Mach 3. The ramjets burn liquid hydrogen and are used for the high Mach number portion of the flight.

The SR-89 Stingray is another of the waverider configurations and is designed to cruise at Mach 6. It is powered by two turbofans and four ramjets. The fuel chosen was methylcyclohexane (MCH). MCH is an endothermic fuel that breaks down into hydrogen and toluene. As shown in Fig. 4, the Stingray is a modified waverider with the analytically derived planform altered by the cockpit, the contoured engine box, and the vertical stabilizers.

The selection of the engine for an aircraft is always important and for hypersonic flight the need for an efficient and highly integrated propulsion system is vital. Before making a choice, the design teams examined several advanced engine systems currently under development including the turbine bypass engine, the turbofan-ramjet, the supersonic through-flow fan engine, and the scramjet. The teams determined that both the turbine bypass engine and the supersonic through-flow fan engine were not optimum for the high cruise speed requirement; in addition, the cruise speed was not high enough to warrant a scramjet engine. Based on this reasoning, three design teams (Laser, Hypercanard, and HyBuJET) decided to use the turbofan-ramjet engine. The fourth design team (Stingray) chose to use a system of two turbofans and four ramjets. This team was influenced by safety concerns; in the event of an engine failure, loss of a ramjet would not affect the turbofans. The General Electric Aircraft Engine Business Group provided data on the turbofan-ramjet engine operating at different speeds and altitudes using several different fuels. A picture of a turbofan-ramjet and typical data are shown in Fig. 5.

Selection of the fuel to be used was a key element for all the designs. Hydrogen is the most energetic of the potential fuels. The heat of combustion for hydrogen is about 50,000 Btu/lb compared to around 20,000 Btu/lb for the others. However, as shown in Fig. 6, hydrogen is a very low density fuel and so its volumetric energy release is lower than

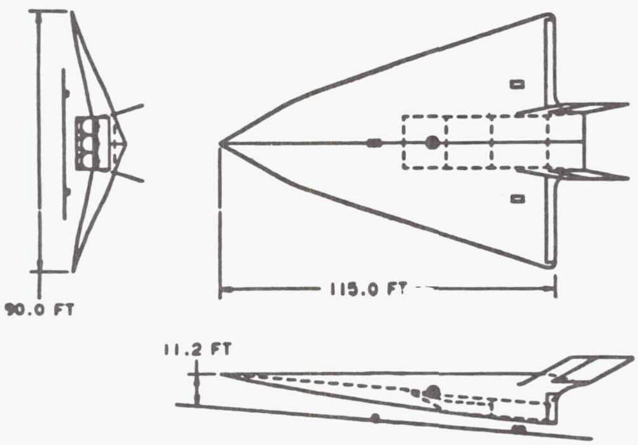

Fig. 3. HyBuJET. Weight: 171,300 lb; area: 5661 sq ft; length: 115 ft; span: 90 ft; W/S: 29.8 psf; T/W: 0.44; cruise Mach: 6; cruise alt: 100,000 ft; engines: 3 turbofanramjets; fuel type: liquid hydrogen and JP-X; fuel weight: 36,854 lb and 40,924 lb; special features: pure waverider.

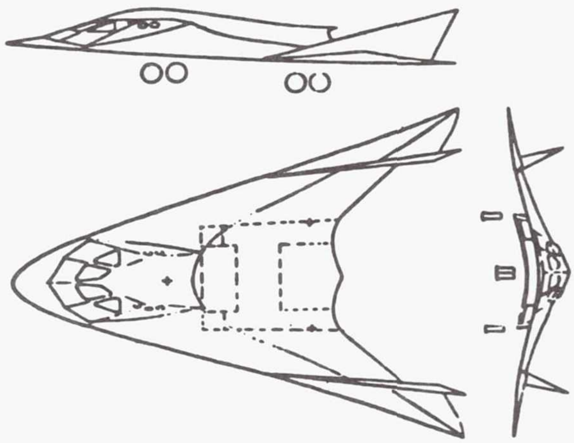

Fig. 4. SR-89 Stingray. Weight: 233,600 lb; area: 2000 sq ft; length: 104 ft; span: 82 ft; W/S: 116.8 psf; T/W: 0.47; cruise Mach: 6; cruise alt: 100,000 ft; engines: 2 turbofans/4 ramjets; fuel type: MCH; fuel weight: 148,102 lb; special features: modified waverider.

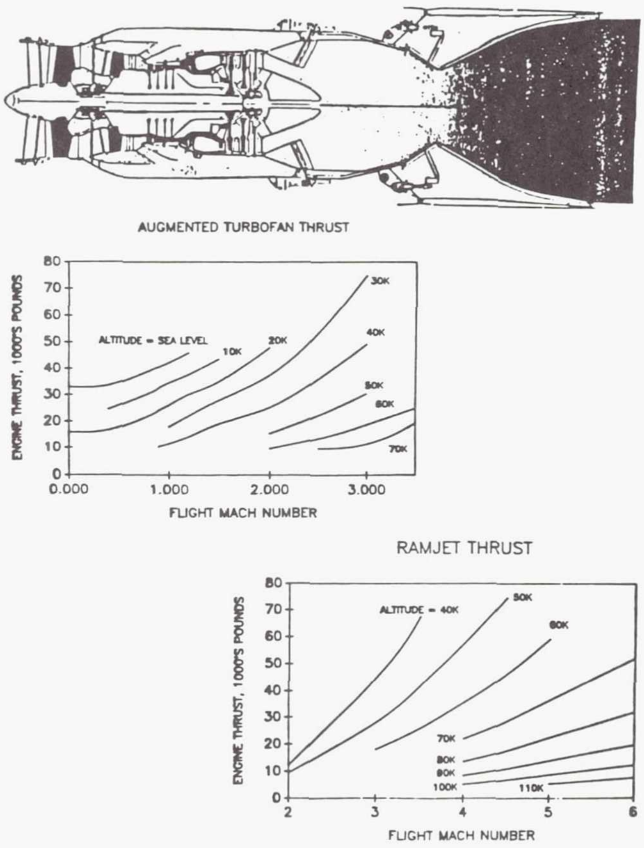

Fig. 5. Turbofanramjet

other fuels. Other factors of concern are the fuel's capability as a heat sink and its cost. Based on these parameters, the four design teams chose the fuel for their planes and, surprisingly, all four teams chose different fuel combinations. The Laser uses liquid methane as a compromise among the various fuel properties. The Hypercanard team chose liquid hydrogen because of its value as a heat sink and its high heat of combustion. MCH is used in the Stingray because it has the most energy per unit volume; it is also cheaper and easier to handle than the cryogenic fuels. The design team for the HyBuJET chose to use two fuels, hydrogen and JP-X, so that the total fuel volume and the total fuel cost is less than using hydrogen alone.

DESIGN PROCESS

All four design teams followed the same process in developing their aircraft. Each team started with an initial concept for the plane, and then used prior history to develop a plot of thrust loading vs. wing loading and a preliminary weight estimate. With this information the size of the aircraft is known. Next the configuration is analyzed and modified as necessary to meet the mission requirements. Then the teams use this iterative process to arrive at an optimum aircraft.

As the designs became firmer, the weight estimation for all four planes was performed by the WAATS computer code for advanced weight analysis. The WAATS program uses empirical methods to estimate the weight of each component in the aircraft, then it generates a composite weight for each system and an overall gross weight. To improve the accuracy of the estimate, specific weight information was input when it was

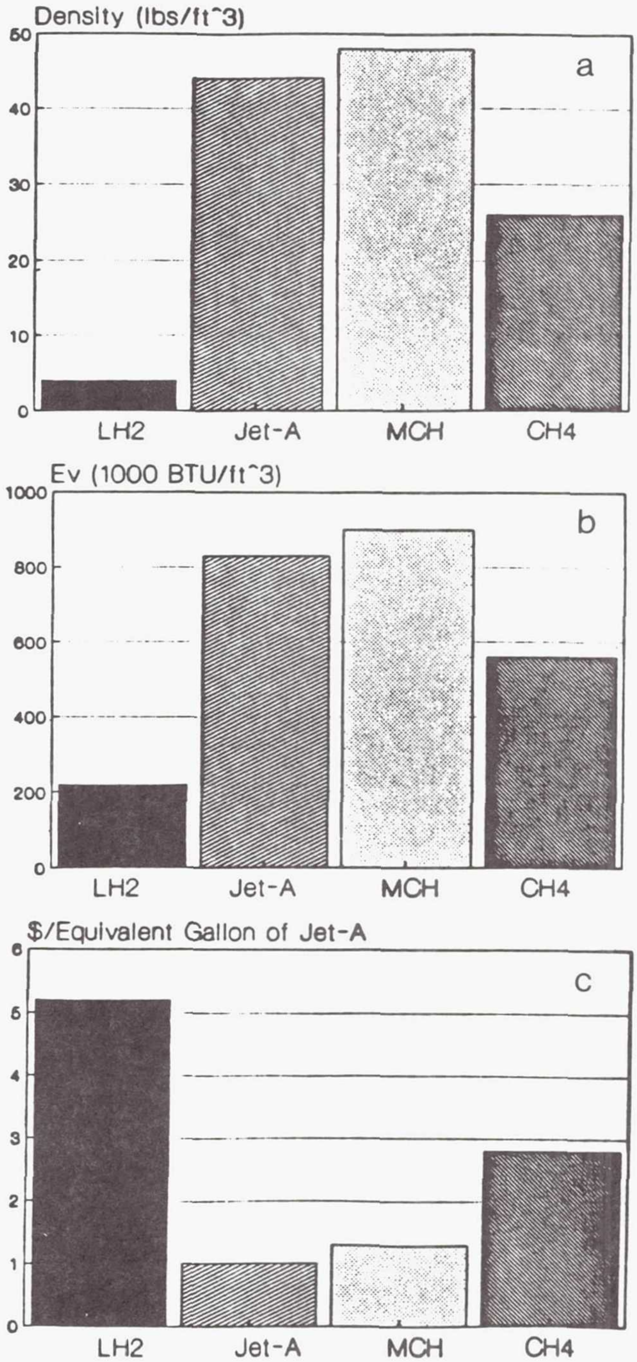

Fig. 6. (a) Densities of selected fuels. (b) Volumetric energy release. (c) Comparison of fuel costs.

Table 2. Weights

	XHT-2 Laser	Hypercanard	HyBuJET	SR-89 Stingray
Takeoff	256,920 lb	201,730 lb	171,3000 lb	233,500 lb
Empty	89,420	117,230	91,022	82,998
Fuel	165,000 (CH_4)	82,000 (LH_2)	77,778 (LH_2 + JP-X)	148,102 (MCH)

available from engine data or technical reports. A breakdown of weights for the four aircraft is given in Table 2.

The subsonic and supersonic aerodynamic analyses were performed using the methods described by Nicolai[1]. The teams had available the Harris Supersonic Wave Drag program for low supersonic analysis and an in-house shock-expansion code for additional supersonic information. For the hypersonic aerodynamic prediction, the Laser design team used the method presented by Williams[2]. The Hypercanard continued to use shock-expansion methods for the hypersonic aerodynamics.

The two waverider configurations were developed using the Maryland Axisymmetric Waverider Program (MAXWARP)[3]. The MAXWARP program takes a specified flow field and superimposes a power law body on this flow field. A leading edge shape is then superimposed on the shock surface and the streamlines are traced back to determine the upper and lower surfaces. The upper surface is defined as a freestream surface.

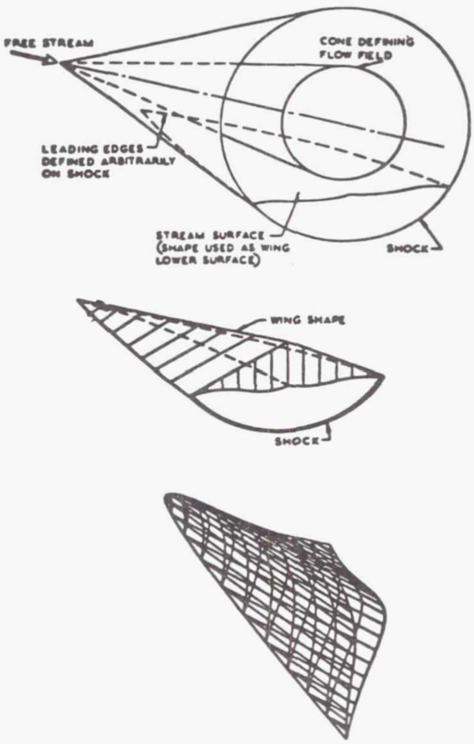

Fig. 7. Cone-Flow Wing. Top view shows construction from known flow field; middle view shows resulting wing and shock; and bottom view shows MAXWARP output.

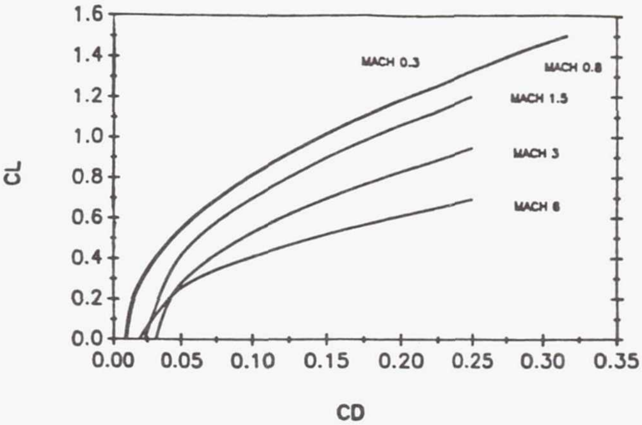

Fig. 8. Drag Polars of the SR-89 for Various Mach Numbers

An example of a waverider body is given in Fig. 7. In addition to the geometry of the waverider, MAXWARP determines the aerodynamic coefficients for cruise including C_M, C_D, and C_L. Figure 8 shows the drag polars of the Stingray for several Mach numbers.

With the refined aerodynamic analysis, the design teams often had to modify the aircraft to improve performance. The Hypercanard, for example, elected to use a hybrid laminar flow control system to improve the plane's lift-to-drag ratio. The potential benefits of this HLFC system and its layout are given in Fig. 9. The Stingray design team had to modify the analytical MAXWARP planform into a practical configuration by adding engines and fins. The engine box and two vertical fins were created by following different stream surfaces back from the shock in the same manner as the waverider itself was generated.

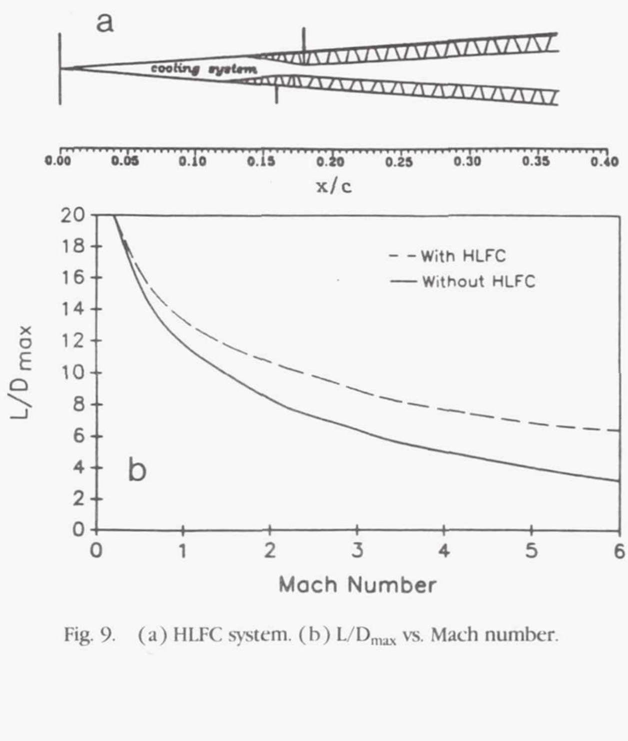

Fig. 9. (a) HLFC system. (b) L/D_{max} vs. Mach number.

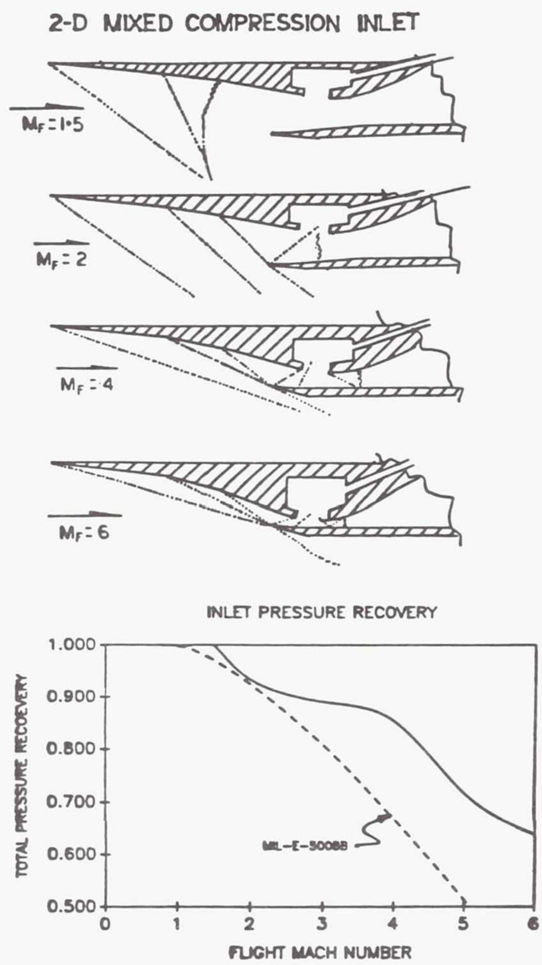

Fig. 10. Mixed Compression Inlet

mission profile for their aircraft. Figure 12 shows a typical mission profile; this one is for the waverider HyBuJET. Figure 13 shows the thrust available and the thrust required for the Stingray as a function of Mach number; the altitude dependence is prescribed by its mission profile. Note in Fig. 13 that there exists a thrust "pinch" at Mach 2. At this Mach number and altitude, the available turbofan thrust is decreasing, which requires the ramjets to be started. Because of potential problems with vehicle acceleration during climb, the Stingray group used an energy-state method analysis to develop a minimum fuel climb (Fig. 14). The constant excess specific power contours are plotted on the altitude vs. speed diagram. Coupled with the aircraft's performance characteristics, these specific power contours define a climb trajectory that uses minimum fuel.

In addition to these classic performance problems, the teams investigated the sonic boom characteristics of their aircraft. Figure 15 presents the sonic boom overpressure as a function of altitude for the HyBuJET aircraft. Above 90,000 ft the

Other important issues addressed at this time by the teams include landing gear, inlet systems, heat transfer and skin temperature, and cooling systems. A typical inlet showing the required variable geometry necessary to handle the engine air flow as the Mach number increases and a graph of the total pressure recovery through the inlet are given in Fig. 10.

The equilibrium skin temperature distribution and the cooling system schematic for the HyBuJET are shown in Fig. 11. The equilibrium temperature was determined by balancing the convective heat input with the radiation from the skin as its temperature increased. Calculation of turbulent heat transfer coefficients was done by using the Von Karman form of the Reynolds analogy in conjunction with Spalding and Chi's skin friction coefficients[4]. It was assumed that the flow was fully turbulent and that there was no heat conduction through the skin.

PERFORMANCE

Takeoff, climb, cruise, and landing performance used the methods presented by Nicolai[2]. Each team developed a

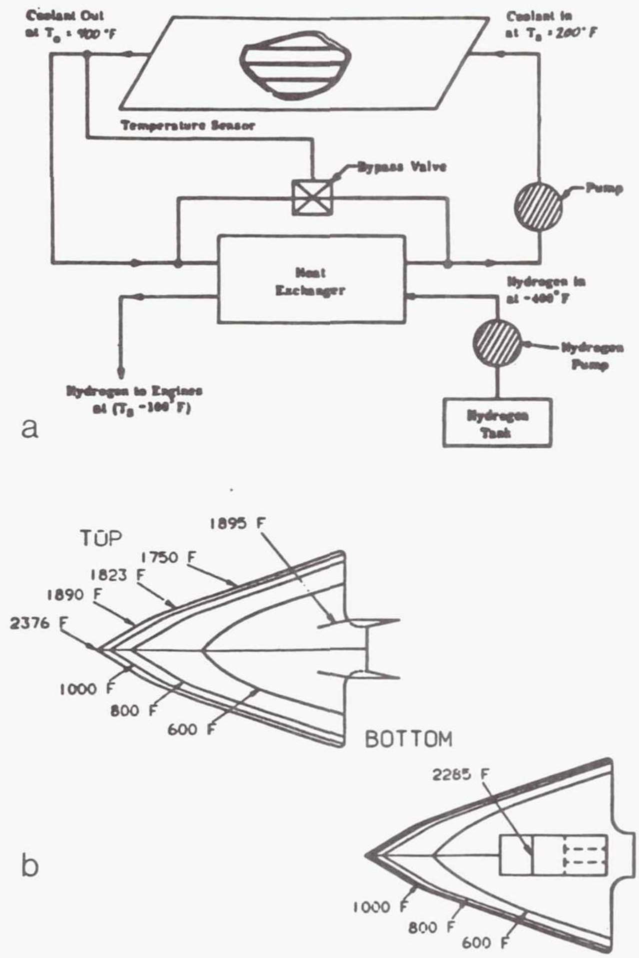

Fig. 11. (a) Cooling system schematic. (b) Skin temperature distribution.

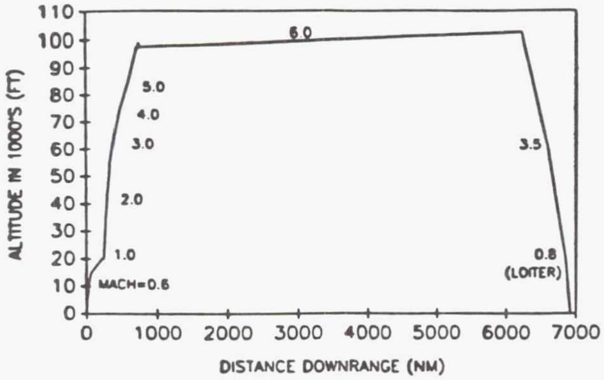

Fig. 12. Mission Profile

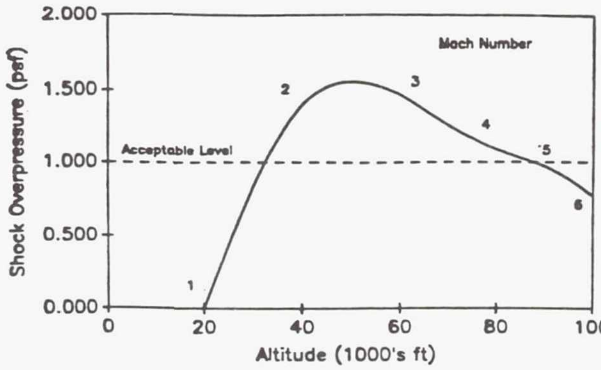

Fig. 15. Shock Overpressure vs. Altitude

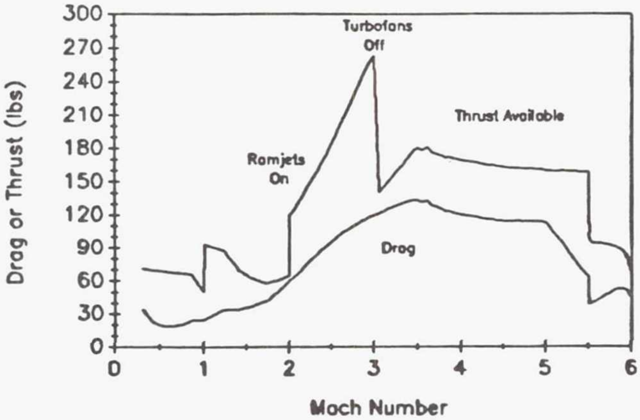

Fig. 13. Thrust Pinch of SR-89 Stingray

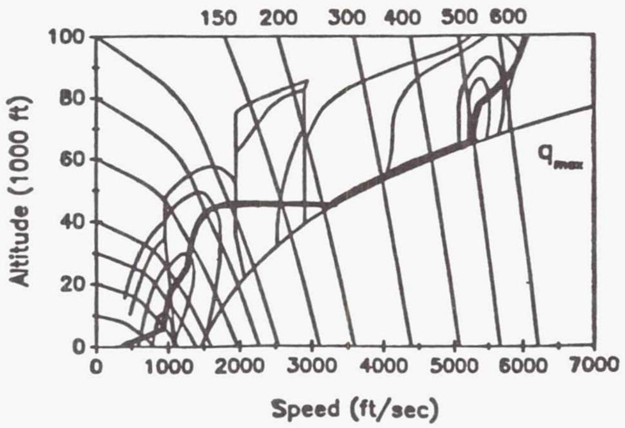

Fig. 14. Constant Energy Contours for the SR-89 Stingray

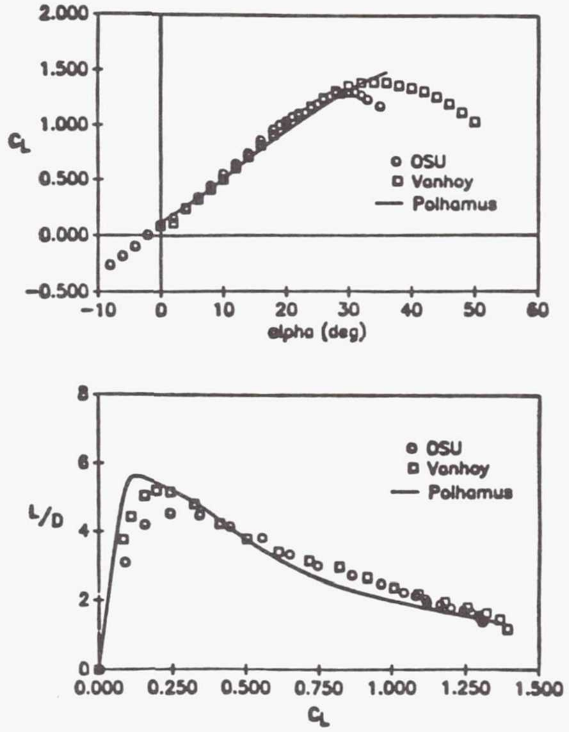

Fig. 16. (a) C_L vs. alpha. (b) L/D vs. C_L

overpressure is less than 1 lb/sq ft. This value has been suggested as an acceptable boom pressure limit. If this is true, then supersonic flight over land by this aircraft may be permissible.

The teams built models of their aircraft for testing in the OSU $3' \times 5'$ subsonic wind tunnel in an effort to verify a portion of the aerodynamic analysis. Typical lift coefficient vs. angle of attack and lift-to-drag ratio vs. lift coefficient curves for the HyBuJET waverider are shown in Fig. 16. The square symbols are experimental results from a 70° delta wing tested by Vanhoy[(5)], and the solid line is the theory for the aerodynamic performance of a 70° delta wing by Polhamus[(6)]. The circles represent the data taken by the OSU students. These experiments confirm the low speed predictions of the HyBuJET team. A small steel model of the HyBuJET is in fabrication; designed by the students, this model will be tested in the OSU hypersonic wind tunnel at M = 6 later this year.

Table 3. Aircraft Costs for 75 A/C Production (in Millions of Dollars)

	Laser	Hypercard	HyBuJET	Stingray
Dev., Test & Eval.	8,619	10,206	9,217	8,434
Production	5,601	6,947	4,355	5,347
Total	14,220	17,152	13,572	13,781
Cost per A/C	189.6	217.1	171.8	174.4

Note: 10% Profit on DT&E and Production

ECONOMICS

The cost of producing 75 aircraft was estimated using the method outlined by Nicolai[1], adjusted for the 1989 price index. The estimated cost of building four prototypes of each aircraft and then performing test and evaluation of the prototypes nears $10 billion as shown in Table 3. When the production run is completed in approximately five years, the cost per aircraft varies from $172 million for the lightest, the waverider HyBuJET, to $217 million for the Hypercanard.

Direct operating costs (DOC) were estimated using the methodology developed at Battelle Memorial Institute by Mr. James Loomis, head of the High Speed Commercial Transport Division. Table 4 presents these costs, which emphasize the impact of fuel cost on DOC. The Hypercanard, using liquid hydrogen fuel, will use more than $157,000 of fuel per hour. Use of cheaper methane in the Laser reduces fuel cost to $25,400 per hour, while the Stingray's MCH costs are less than $14,000 per hour. Ticket prices for a 6000-nm trip range from almost $50,000 in the Hypercanard to a mere $8160 in the Stingray.

Table 4. Direct Operating Costs (in $/hour)

	Laser	Hypercanard	HyBuJET	Stingray
Insurance(1)	1,833	1,540	1,500	2,333
Depreciation(1)	3,420	6,540	5,100	6,600
Land. Fees/ Crew	350	350	350	350
Maintenance(2)	5,000	5,000	5,000	5,000
Fuel	25,430(3)	157,250(4)	74,000(5)	13,965(6)
DOC	36,033	170,680	86,130	28,248
Costs per Avail. Seat. n.m.	1.80	8.26	3.75	1.36

(1) 1,500 flight hours/year
(2) Maint. at $50/hr × 100 hours
(3) CH_4 costs at $1.64/gal
(4) LH_2 costs at $3.00/gal
(5) JP-X costs at $1.00/gal
(6) MCH costs at $1.60/gal

SUMMARY

Four design teams have developed conceptual designs for a 10-passenger, hypersonic transport. Each design had a different configuration and utilized different fuels, but all met the airplane requirements listed in Table 1. Table 5 summarizes major characteristics of the four aircraft. The Laser was the heaviest, had the most conventional approach, had the lowest lift-to-drag ratio, and burned relatively low-cost methane. The Hypercanard employed laminar flow control on flying surfaces to increase its lift-to-drag ratio and used liquid hydrogen increasing the necessary volume to carry its fuel. Both HyBuJET and Stingray were waverider designs with analytically developed planforms. They had the highest lift-to-drag ratios and the lowest wing loading. The two had different fuel systems—the Stingray noncryogenic MCH, and the HyBuJET a combination of JP-X and liquid hydrogen.

Table 5. Summary of the Four Configurations

	Laser	Hypercanard	HyBuJET	Stingray
Weight (lbs)	256,900	201,700	171,300	233,600
L/D	4.4	5.9	6.6	6.1
C_L	0.11	0.14	0.04	0.09
Trip Time (min.)	183	130	143	121
Cost ($M)	74.7	92.6	58.1	71.3
Fuel	LCH4	LH2	LH2 + JP-X	MCH

Of interest are the estimated costs of the aircraft, and whether the government should underwrite the initial research and development costs. As shown in Table 5, the HyBuJET cost is reduced to $58 million, which is quite reasonable for an aircraft with its capabilities in light of present day transonic business jets that can cost $20 million.

ACKNOWLEDGMENTS

Principal authors were J. DeBonis, J. Bruns, M. Detelich, A. Wiederkehr, T. Woodrow, T. Ramsey, B. Collet, K. Igar, D. Kendall, D. Miklosovic, R. Reuss, M. Ringer, T. Scheidt, J. Smolko, C. Dever, L. Dudzinski, R. Fritsch, B. Stevens, T. Uhase, J. Higgins, J. Negro, N. Machi, B. Theiss, D. Blum, and K. Ruffing. Faculty advisor was Dr. Gerald M. Gregorek; teaching assistant, P. Weissman.

REFERENCES

1. Nicolai L. M., *Fundamentals of Aircraft Design*. San Jose, CA: METS, Inc., 1974.
2. Williams L. J., *Estimated Aerodynamics of All-Body Hypersonic Aircraft Configurations*. NASA TM-X 2091, 1971.
3. Bowcutt K. G., Anderson J. D., and Capriotti D., *Viscous Optimized Hypersonic Waveriders*. University of Maryland, 1987.
4. Spalding D. B. and Chi S. W., "The Drag of a Compressible Turbulent Boundary Layer on a Smooth Flat Plate with and without Heat Transfer". *J. Fluid Mechanics*, January 1964.
5. Vanhoy D., *Low Speed Wind Tunnel Testing of a Mach 6 Viscous Optimized Waverider*. University of Maryland, 1988.
6. Polhamus E. C., *Prediction of Vortex Lift Characteristics by a Leading-Edge Suction Analogy*. NASA Langley, 1971.

1994004551
383661
6P

N94- 71306

DESIGN OF A SPANLOADER CARGO AIRCRAFT

S39-05
160665
p. 5

PURDUE UNIVERSITY

INTRODUCTION

With a growing demand for fast international freight service, the slow-moving cargo ships currently in use will soon find a substantial portion of their clients looking elsewhere. One candidate for filling this expected gap in the freight market is a span-loading aircraft (or "flying wing") capable of long-range operation with extremely large payloads. This report summarizes the design features of an aircraft capable of fulfilling a long-haul, high-capacity cargo mission.

During the academic year 1988-1989 a total of eight groups worked on the design of this type of aircraft. The Request for Proposal was developed in cooperation between NASA Langley Research Center (LaRC) and Purdue University. The principal architects of this proposal were Professor T. A. Weisshaar of Purdue and Dr. Vicki Johnson of NASA/LaRC. Assistance was received from Mr. Jeffrey Layton (the NASA/USRA Teaching Assistant at Purdue) during his tenure at NASA/LaRC during the summer of 1988.

During Mr. Layton's time at NASA/LaRC he developed a database for weight estimation of flying wings and spanloaders from reports and papers written on the subject. These included Northrop's early flying wings.

The spanloader seeks to gain advantage over conventional aircraft by eliminating the aircraft fuselage and thus reducing empty weight. The primary disadvantage of this configuration is that the cargo-containing wing tends to be thick, thus posing a challenge to the airfoil designer. It also suffers from stability and control problems not encountered by conventional aircraft. The result is an interesting, challenging exercise in unconventional design.

The report that follows is a student written synopsis of an effort judged to be the best of eight designs developed during the year 1988-1989. Each of the eight design teams prepared a 100-page document detailing their design, the design process, and recommendations for the future. The present report was prepared by a team of Purdue seniors consisting of Ronald Henderson, Timothy Ventimiglia, Jeffrey Focke, David McGruder, and Scott Bravard. This report was presented at the NASA/USRA Student Design Conference during 1988-1989.

The Request for Proposal provided to the class[1] and attached as an Appendix to this report is summarized as follows:

Range: 6000 n.m.
Payload: 300,000 lb, plus 30 first-class passengers
Crew Size: 6 (includes two flight crews)
Cruise Mach Number: 0.7 minimum
Cargo Compartment Size: Sufficient to handle 8′ × 8′ × 8′ standard cargo containers

The aircraft must meet all FAR requirements and be able to operate from international airports. The design will take advantage of technology available for production in the year 2000. The projected market for this aircraft is transportation of freight from Europe and the U.S.A. to countries in the Pacific Basin.

DESIGN OVERVIEW

The result of this design study, encompassing 14 weeks of effort by a team of five students, was the **Bisonaire Buffalo**, shown in Fig. 1. This aircraft is a spanloader with a payload capability of 300,000 lb plus 30 first class passengers, well within the range of a useful spanloading aircraft. For structural efficiency, the cargo distribution within the wing is balanced by the aircraft lift distribution. This efficiency results in an aircraft operating empty weight of 457,300 lb. and a maximum take-off weight of 1,131,500 lb.

The propulsion unit consists of six turbofan engines to take advantage of turbojet speed and economy. Aerodynamic design takes advantage of thick supercritical airfoils, low-aspect ratio wings, and end plates (winglets) to combine performance and sufficient wing volume for the cargo. A detailed study of the stability of the aircraft for both normal operation and off-design conditions was done to ensure proper handling qualities and adherence to FAR requirements.

AERODYNAMICS

The final design evolved from simple concepts, to which were gradually added more complex components; the final aircraft design is the result of compromises between the ideal design and restrictions imposed by operational reality. For example, since this aircraft carries its payload in the wing,

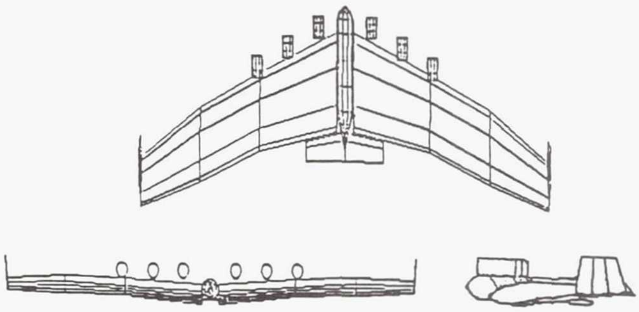

Fig. 1. The Bisonaire Buffalo Spanloader Transport

PRECEDING PAGE BLANK NOT FILMED

PAGE 322 INTENTIONALLY BLANK

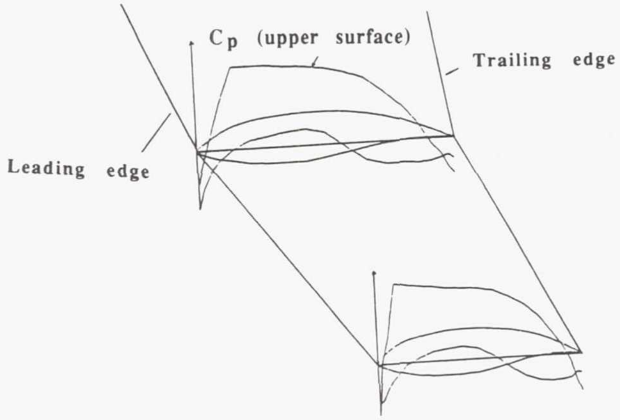

Fig. 2. Airfoil Cross-sections with Calculated Pressure Distributions

relatively thick airfoils must be used to accommodate the volume requirements. This creates drag at transonic Mach numbers, placing a restriction on the cruise Mach number. Also, winglets were necessary to improve lift and to provide yaw control.

To achieve an operational cruise Mach number of 0.75, while minimizing drag and providing the largest airfoil cross-section possible, new supercritical airfoil designs were developed using the PANDA airfoil design program[2]. PANDA uses an analytical method based on superposition of sources and vortices; once the pressures have been calculated, the boundary layer properties can be computed and the total drag estimated using the Squire-Young formula. These cross-sections, together with their predicted surface pressure distributions during cruise and respective placement on the wing, are shown in Fig. 2.

The wing design effort was also aided by the use of a computer code developed for the MacIntosh computer. This code, LinAir, is a program capable of modeling multielement, nonplanar lifting surfaces[3]. This code allowed the proper selection of wing sweep and jig shape to improve the cruise configuration and allow for trim.

For design purposes, the aircraft was modeled using three wing sections (each with variable sweep and incidence to optimize local Mach number and thickness requirements). The effects of winglets and a small horizontal surface mounted flush with the trailing edge of the main wing were also accounted for. Based on ref. (4) a winglet surface area of 15% of the wing semispan was chosen. The total wing area is 15,180 sq ft. The wing span is 278 ft, a span that is restricted by requirements that the plane fit on existing runways.

By varying flight parameters, such as angle of attack and Mach number, a detailed analysis of the wing performance was constructed. Figure 3 shows the predicted drag polar for this design. Figure 4 gives L/D values for various angles of attack at the cruise Mach number. Several projected high-technology applications were included in this design (see Table 1).

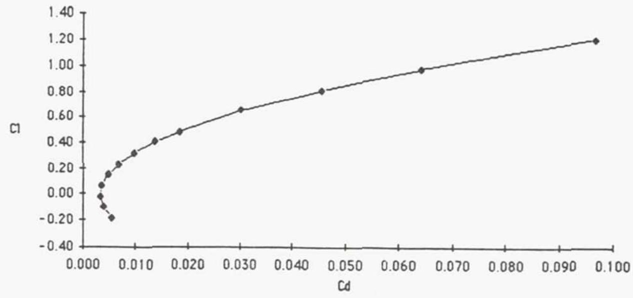

Fig. 3. Drag Polar for the Buffalo

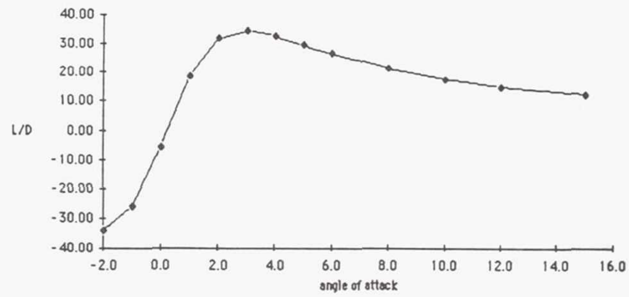

Fig. 4. L/D vs. Aircraft Angle of Attack

STRUCTURES

The flying-wing design provides several challenging structural problems, while at the same time offering such sought-after advantages as cargo arrangement that balances the lift distribution. The primary benefit of the design is a significant reduction in overall structural weight.

The initial design efforts focused on an all-flying-wing structure. However, such designs were aerodynamically unstable. This problem was solved by adding a small fuselage section. Figure 5 shows a top view of the final design. This arrangement allowed the movement of passengers, cargo, and fuel forward to produce a statically stable aircraft.

The aerodynamic center was calculated using methods from Roskam[5]. Using this data, together with center-of-gravity data,

Table 1. Aerodynamic Features and Benefits

Feature	Benefit
Low Wing Loading	• Improved Take-off/Landing
Supercritical Airfoils	• Thicker Cross-sections • Lower Drag • Higher Cruise Mach Number
Winglets	• Improved L/D (3.4%-6.2%)
Swept Wings	• Delayed Drag Rise
Laminar Flow Control	• Decreased Drag (up to 80%)
Vortex Management	• 50% (Targeted) Decrease in Landing/Take-off Separation

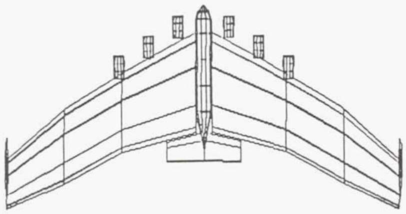

Fig. 5. Planform View of Design

Engine Weights Summary

Engine Weight	9232.37 lbs
Nacelle Weight	1963.80 lbs
Thrust Reverser Weight	1759.92 lbs
Total Misc Propulsion Weight	563.56 lbs
Total Prop. Plumbing Weight	757.82 lbs
Total Engine Weight	**14277.47 lbs**

Fig. 7. Engine Component Weights

the static margin was computed for all flight segments. The aircraft was stable with a minimum stability margin of 5.44% during landing. The weight breakdown used in all calculations was obtained from the flight optimization program FLOPS[6], modified for use at Purdue on the Engineering Computer Network.

The wing loading at maximum gross weight is 74.54 lb. Design analysis included the determination of shear and bending moments for a wing constructed of T300/5208 graphite/epoxy composite skin material[7].

For the aircraft to be commercially feasible, it must use available, standardized cargo containers now in use by Federal Express. Using two different size containers, the AYY and the M3[8,9] and a payload density of 9.2 lb/ft^3, this design can carry a payload of 327,500 lb.

Construction of the flight deck and landing gear was modeled after the Boeing 757[10]. This creates an aircraft that fulfills both the RFP and FAR requirements.

PROPULSION

The propulsion system provides controlled thrust as well as power for the accessory equipment. It can be broken down into four subsystems: the engine, lubrication subsystem, engine controls, and accessory drives. This design uses six turbojet engines. This number was chosen by carefully considering reliability, maintainability, and weight. Engines were sized using fuel data and operational characteristics for a hypothetical engine provided by NASA/LaRC.

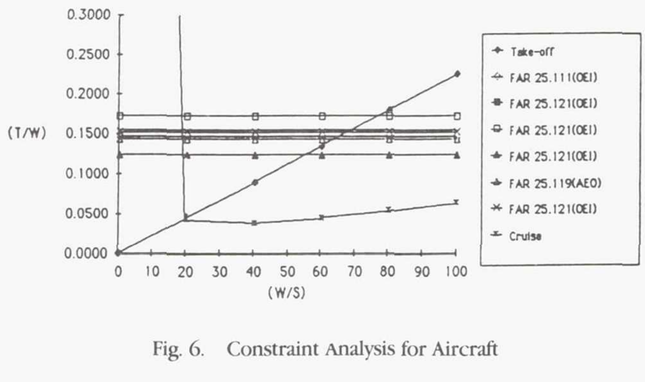

Fig. 6. Constraint Analysis for Aircraft

A major consideration in engine sizing is the amount of thrust necessary at take-off and at cruise. Figure 6 shows the results of a constraint analysis considering required thrust-to-weight vs. wing loading for the aircraft design. Based on this analysis, a sea-level value of engine thrust-to-weight ratio of 0.23 was chosen. To produce this amount of thrust, 6 engines will be needed, each producing 45,000 lb of thrust. Prohibitive size ruled out fewer engines, while the use of more than six engines would result in excessive maintenance cost.

As mentioned previously, NASA/LaRC provided the engine deck used to size the engines and to provide performance estimates. An engine deck gives net thrust and fuel flow for selected Mach numbers and altitudes. Using this engine deck, a scaling program was developed and was used to adjust the engine to meet the required thrust level. The scaled-up engine will have a total length of 19.1 ft and a maximum diameter of 11.8 ft, with a total engine weight of 14,280 lb. The breakdown of the engine component weights is given in Fig.7.

PERFORMANCE

Performance analysis will define an aircraft's capabilities and limitations for specific tasks that it must accomplish. This discipline takes a set of physical characteristics for an aircraft and determines various parameters, such as how high, how far, how fast, and how well the aircraft accomplishes its mission.

The Request for Proposal required this aircraft to fly a 6000-n.m. flight in 16 hrs or less. Given the requirements for payload and range, a climbing-cruise profile was utilized to maximize the range for a minimum amount of fuel. This cruise schedule is permissible since the aircraft will be operating primarily over the Pacific Ocean.

This aircraft is designed to cruise at a Mach number of 0.75. Cruising at a higher Mach number leads to transonic flow conditions over the wing and an associated drag rise. Cruise at a lower Mach number reduces engine efficiency and increases trip time. The aircraft has a maximum service ceiling of 46,000 ft. By using a cruise-climb schedule between 35,000 ft and 39,200 ft, the aircraft has a range of 6184 n m fully loaded and completes its mission in less than 15 hours.

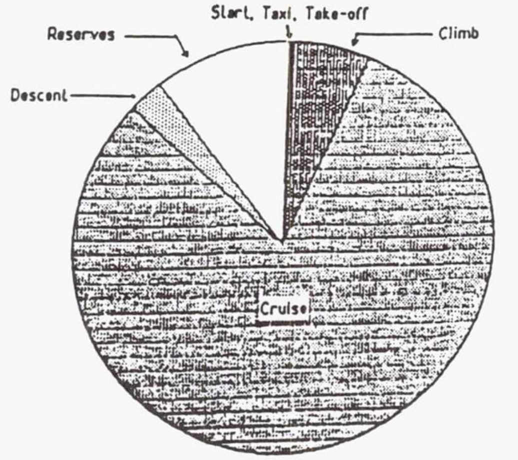

Fig. 8. Fuel Requirements to Complete Mission

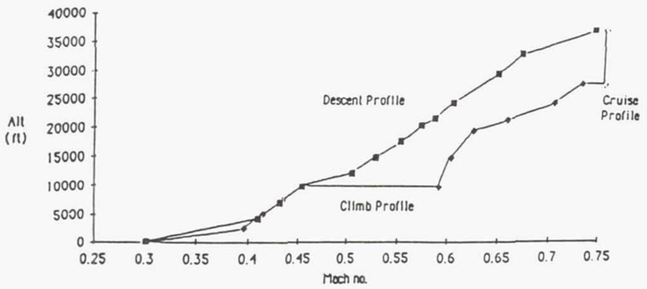

Fig. 9. Altitude-Mach Number Schedule for Efficient Flight

Calculations from FLOPS[6] show that, fully loaded, this aircraft can lift off in 7215 ft and land in 9567 ft. The stall speed is 115 knots with an approach speed of 150 kts, which complies with FAR 25.119[10]. Also, the one-engine-inoperative characteristics (OEI) meet FAR 25.111 and 25.121 requirements[11].

Figure 8 shows the fuel requirements for each segment of the mission. With a total fuel capacity of 56,600 gal, a diversion to an alternate airport still leaves the aircraft with 2600 gal in reserve.

Figure 9 shows altitude vs. Mach number for the most efficient flight, as determined using the FLOPS code mentioned previously.

STABILITY AND CONTROL

Leonardo da Vinci wrote, "A bird is an instrument working according to mathematical law . . . it is within the capability of man to reproduce its movements." However, a bird has greater flexibility than an aircraft and this gives rise to movable control surfaces. In fact, the feathering structure on some birds' wings was the inspiration for some multielement airfoil designs[12].

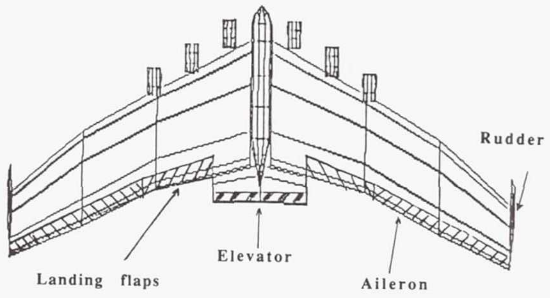

Fig. 10. Planview of Control Surface Layout

In flight tests both stability and control have been demonstrated to be difficult, though obtainable, with a spanloader configuration[13]. A pure flying wing is desired as the aerodynamically optimum vehicle, but a trade-off is encountered between efficiency and static stability. In this aircraft, some of that aerodynamic efficiency had to be sacrificed to include a small fuselage section and tail surfaces, resulting in a spanloader as opposed to a true "flying wing."

Two fundamental problems were encountered during the design of stabilizing surfaces for this aircraft. The first of these, mentioned previously, was positioning the center of gravity relative to the aerodynamic center to produce a positive static margin. The combined effect of adding a fuselage and horizontal tail resulted in a static margin ranging from 6-15% for the entire mission. The second problem was the size and position of the vertical tail surface.

To examine static stability of the aircraft, two computer codes were available, LOPROG (longitudinal) and LAPROG (lateral-directional)[14]. Using results from LAPROG, vertical winglets were designed to act as rudders with sufficient control deflection to provide lateral stability.

Control surfaces were sized based on studies of other aircraft of similar gross weight[15]. A plan view of these surfaces is presented in Fig. 10. The greatest area of concern for the design and placement of the control surfaces occurs during landing. The final design is stable and controllable about all three axes during all phases of the mission.

ECONOMICS

It is estimated that a fleet of 100 aircraft would cost $95 million per aircraft. From the manufacturer's point of view, there are two basic goals of a cost analysis. One is to estimate the development cost of the project. The other is to estimate probable operating costs, for this is the primary factor upon which the potential buyer will base his purchase decision.

It is this analysis that will probably determine whether or not the preliminary design becomes a full-blown project.

In 1982, the Office of Technology Assessment estimated the development costs of a major new aircraft at $6 billion[16]. For example, the Boeing 767 is estimated to have cost somewhere between $2 billion and $10 billion dollars to develop[17]. It

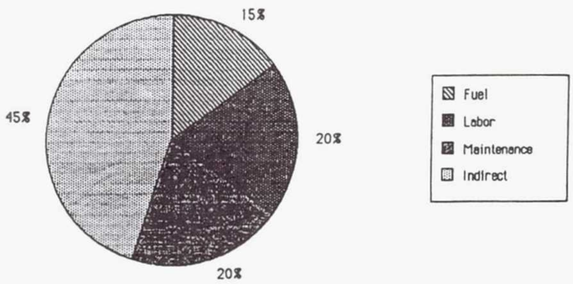

Fig. 11. Operational Costs

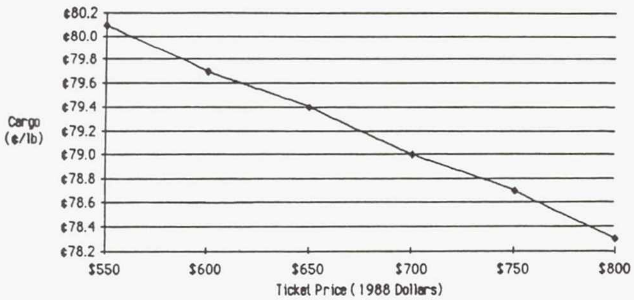

Fig. 12. Ticket and Cargo Prices

follows from this that market conditions at the time of the sale will determine the selling price of an airplane. This often requires selling below cost, or making promises that, in the long run, cannot be kept[17].

While presumably not as interesting to the manufacturer as development costs, operating costs are easier to estimate. If the manufacturer can promise a more financially efficient product than his competitor, he will have a better chance at making the sale. A breakdown of operating costs for this aircraft is shown in Fig. 11.

Figure 12 shows the price for tickets and cargo that must be charged by the operator to make a profit. To calculate these costs, the following assumptions were made: (1) fuel costs over a period from July 1987 to June 1988 were averaged to obtain a fuel cost of $0.62 per gallon[18]; (2) the load factor (ratio of passengers to seats available) was set at 70%; (3) cargo hold was fully loaded at 300,000 lb; and (4) the profit margin was set at 10%.

These prices are very competitive: a one-way ticket from Los Angeles to Tokyo (November 1988) cost $760, and overseas shipping rates are consistently greater than $1/lb.

CONCLUSION

An initial design study of a spanloading air freighter has been completed. The analysis of this design shows that an aircraft of this type is feasible, both to build and operate. Utilizing existing technology and technology anticipated to be available in the near future, the aircraft can be manufactured, flown, and should make money for its operators.

REFERENCES

1. Weisshaar T. A., "Request for Proposal: Design for a Spanloader Air Freighter." AAE 451, School of Aeronautics and Astronautics, Purdue University, 1988.
2. Kroo I., "PANDA - A Program for Analysis and Design of Airfoils," Version 1.3 User's Guide. Desktop Aeronautics, 1987.
3. Kroo I., "LinAir for the Macintosh," Version 1.2 User's Guide. Desktop Aeronautics, 1987.
4. Turriziani R. V., "The Effects of Advanced Technologies on the Weight and Range of YB-49 Configured Flying Wing Aircraft." *Kentron Memorandum 3-92000/4LRT-260,* PRC Kentron International, Hampton, Virginia, September, 1984.
5. Roskam J., *Airplane Flight Dynamics and Automatic Flight Controls.* Roskam Aviation and Engineering Corporation, Ottawa, Kansas, 1982.
6. McCullers L. A., "Flight Optimization System (FLOPS)," Release 2.0 User's Guide. PRC Kentron International, Hampton, Virginia, September, 1983.
7. Tsai S. W. and Hahn H. T., *Introduction to Composite Materials.* Technomic Publishing Company, Inc., Westport, Connecticut, 1984.
8. *Field Management Instruction Series: Container Density.* Federal Express Corporation, Memphis, Tennessee, 1988.
9. Tyler J. E. Jr., "Maximizing the Physical Capacity of a Fleet of Aircraft and Containers Handling Mixed Freight." SAE Technical Paper Series, Federal Express Corporation, 1986.
10. *General Description of the 757.* The Boeing Corporation, Seattle, Washington, 1982.
11. Roskam J., *Preliminary Sizing of Airplanes.* Roskam Aviation and Engineering Corporation, Ottawa, Kansas, 1985.
12. Kuethe A. M. and Chow C. Y., *Foundations of Aerodynamics,* Fourth Edition. John Wiley and Sons, New York, 1986.
13. Campbell J., "Wing Design." *Popular Mechanics,* January, 1987, 53-56.
14. Smetana F. O. , *Computer Assisted Analysis of Aircraft.* McGraw-Hill, New York, 1984.
15. *Jane's All The World's Aircraft.* 1986-1987 Edition, Jane's Publishing Company, London, 1986.
16. Drake J., *AAE 470: Air Transportation Economics.* School of Aeronautics and Astronautics, Purdue University, Fall, 1988.
17. Newhouse J., "The Sporty Game," Parts I-IV. *The New Yorker,* June 14-July 5, 1982.
18. Sharp I. P., *Aviation Daily,* August 10, 1988.

1994004552 383662 8P

N94- 71307

LASER-BOOSTED LIGHTCRAFT TECHNOLOGY DEMONSTRATOR

RENSSELAER POLYTECHNIC INSTITUTE

S40-05 160666 p- 7

The ultimate goal for this NASA/USRA-sponsored "Apollo Lightcraft Project" is to develop a revolutionary manned launch vehicle technology that can potentially reduce payload transport costs by a factor of 1000 below the space shuttle orbiter. The Rensselaer design team proposes to utilize advanced, highly energetic, beamed-energy sources (laser, microwave) and innovative combined-cycle (airbreathing/rocket) engines to accomplish this goal. This year's effort, the detailed description and performance analysis of an unmanned 1.4-m Lightcraft Technology Demonstrator (LTD) drone, is presented. The novel launch system employs a 100-MW-class ground-based laser to transmit power directly to an advanced combined-cycle engine that propels the 120-kg LTD to orbit, with a mass ratio of two. The single-stage-to-orbit (SSTO) LTD machine then becomes an autonomous sensor satellite that can deliver precise, high-quality information typical of today's large orbital platforms. The dominant motivation behind this study is to provide an example of how laser propulsion and its low launch costs can induce a comparable order-of-magnitude reduction in sensor satellite packaging costs. The issue is simply one of production technology for future, survivable SSTO aerospace vehicles that intimately share both laser propulsion engine and satellite functional hardware. A mass production cost goal of 10^3/kg for the LTD vehicle is probably realizable.

INTRODUCTION

In order for laser propulsion to enable a significant reduction in the cost of certain critical space systems, both launch and payload costs must be reduced by an order of magnitude or two. Canavan[(1)] was first to bring this fact to light, noting that a reduction in either category alone would have much less economic impact. This conclusion emerged from recent in-depth examinations of the economics for laser propulsion deployment of sensors, interceptors, and decoys[(1,2)]. Furthermore, Canavan affirms that the minimum effective system must be able to launch 60-100-kg payloads. After evaluating cost projections, he concludes that a system designed for payloads smaller than this could increase costs significantly, reducing laser propulsion's margin with respect to conventional chemical rocket alternatives[(1)].

Apparently, the true costs of building and launching today's large satellite platforms are not widely known, as discussed in a recent *Aerospace America* article[(3)]. For example, sensor hardware can cost upwards of \$200,000/kg (\$$10^5$/lb); and to boost that sensor into geostationary orbit (GEO) typically requires \$10,000/kg (\$4500/lb) of payload. Flying the shuttle orbiter to a 250-km low Earth orbit (LEO) may cost \$6600/kg (\$3000/lb), but the actual price is really almost twice that amount because the shuttle itself is not amortized against the payload[(4)]. The projected launch cost goal for the Advanced Launch System (ALS) is roughly \$660/kg (\$300/lb) to LEO. Hence, for laser propulsion to play a significant role in boosting future critical space systems, launch costs must fall to \$66/kg (\$30/lb), or at least below \$100/kg.

Canavan has raised the fascinating issue of whether and how laser propulsion and its low launch costs could induce a substantial reduction in satellite package costs[(1)]. In our opinion, such reductions could be facilitated by an exceptionally close integration of the laser-propulsive engine and satellite functional hardware. Pushed to the extreme, almost every vehicle component could be designed to serve multiple functions, in both transatmospheric and orbital flight modes.

Clearly, the final configuration of any laser-boosted machine will be strongly driven if not entirely dominated by the mission it must perform, be it interceptor, decoy, or sensor. A near-infinite number of successful configurations could be alleged to exist, but it is most instructive to select a specific mission, and then to explore a single configuration from the initial design concept through the preliminary engineering design process.

INITIAL LTD DESIGN CONCEPT

The advanced aerospace vehicle considered here is exemplary of a class of sensor machines that can be derived largely from an intimate integration of propulsion and sensor systems. The proposed design exploits the inherent advantages of advanced beamed-energy sources (i.e., high-power lasers) and innovative combined-cycle (airbreathing/rocket) engines to accomplish this goal. The authors believe that this unique approach could possibly enable a reduction in both launch and sensor package costs by two orders of magnitude below present levels. However, as pointed out by Canavan[(1)], the numbers of these sensor satellites may not be great enough to justify the expense of the entire laser launch facility for this application alone. Nevertheless, the laser launch facility is likely to be built for a completely different defense-related purpose, and amortized over a great number of users and dissimilar mission applications anyway.

GROUND-BASED LASER LAUNCH FACILITY

Portrayed in Fig. 1 is a 100-MW-class ground-based laser (GBL) that could be built with free-electron laser technology in the next five years, by assembling several (e.g., five) smaller units into an array. Redundant units could be built into the system so that inoperative modules could be dropped out, with no loss in system utility during a boost. As shown in Fig. 1, a beam combiner could then be invoked to link all the output beams together.

PRECEDING PAGE BLANK NOT FILMED

328

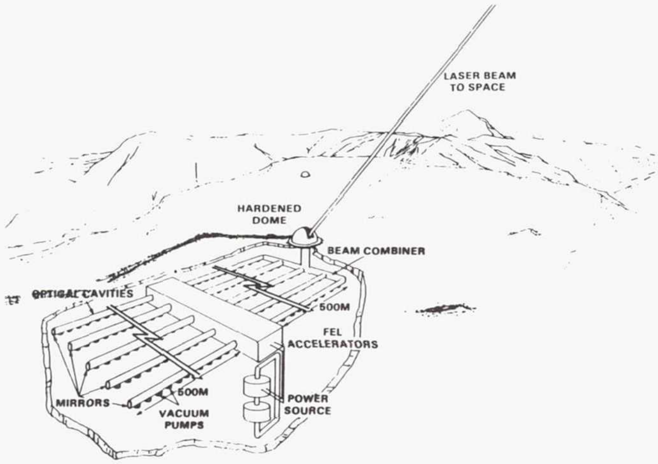

Fig. 1. Ground-based FEL Laser Launch Facility

All the units could be fired simultaneously to give the lowest pulse repetition frequency (PRF) of perhaps several hundred Hz at the highest pulse energy (E_p); at the other extreme, each unit could be triggered sequentially to yield the lowest E_ps and PRFs up to 10 kHz. Near-term pulsed laser propulsion engines can be designed around whatever laser pulse durations are available (e.g., from 40-400 nsec).

Configured in this manner, the GBL facility can be programmed to deliver a complicated pulse train sequence of PRFs, E_ps, and t_ps with the utmost ease. This pulse train can be calculated to exactly match what a laser propulsion engine will need along a given launch trajectory, i.e., normally a direct function of flight Mach number and altitude. The goal is to produce an efficient thruster without introducing too much flight hardware, which has added so much to the cost of chemical rockets, as Kantrowitz(4) has observed.

The essential point of this advanced launch scheme is to place as much of the laser power transmission system complexity as possible on the ground (where there is no weight penalty) so that it can be serviced easily. With this approach, laser-powered thrusters can be reduced to their simplest and most reliable configuration.

The "straw man" GBL facility suggested here is set at the 250-MW level (peak), which is adequate to launch a 120-kg (dry mass), 1.4-m-diameter Lightcraft Technology Demonstrator (LTD) to LEO. The range of laser pulse energies required by its combined-cycle (airbreathing/rocket) engine is $40\ \mathrm{kJ} < E_p < 70\ \mathrm{kJ}$; PRF varies from 200 Hz to 10 kHz, and t_p varies from 0.3 to 0.4 μsec, depending on the exact trajectory (i.e., Mach number vs. altitude) flown to orbit. With these parameters, the peak flux across the 1.0-m-diameter LTD primary optic will fall in the range of 13.0 to 30.0 MW/cm^2.

Kantrowitz(5) notes that the important costs for a GBL installation are for capital and operating expenses which might add another 20% of the capital cost per year (see ref. 5 for an in-depth accounting of the economics for a GBL launch facility). The Free Electron Laser (FEL) is the favored future GBL system due to its promise of high electric-to-laser conversion efficiency and reliability.

Kantrowitz(5) has noted that to make laser propulsion a serious contender for space transportation to LEO, it is necessary to develop propellants that can achieve high thruster efficiency at low incident laser flux levels. It is also apparent that atmospheric transmission problems must be considered, especially in the immediate vicinity of the vehicle where the beam must propagate unhampered through the thruster's rapidly expanding, and potentially absorbing, exhaust.

Adaptive transmitter optics can be invoked to successfully bring the power beam up through the atmosphere. The 10-m-diameter beam-director mirror would allow a 10 μm beam to be focused on a 1-m-diameter vehicle base, out to a range of about 800 km. This performance is, of course, close to the diffraction limit. With even shorter wavelengths (e.g., 1 μm), the transmitter diameter could be reduced to 4 m (and below).

THE LTD COMBINED-CYCLE ENGINE CONCEPT

The Lightcraft Technology Demonstrator (LTD) is a single-stage-to-orbit transatmospheric vehicle utilizing both airbreathing and rocket propulsion modes. The LTD will transition into the rocket mode at about Mach 5 and 30 km altitude.

The LTD advanced microspacecraft is, in several respects literally a "flying engine." The forebody aeroshell acts as an external compression surface, e.g., the airbreathing engine inlet. The afterbody has a dual function: it is the primary receptive optic (parabolic mirror) for the laser beam that provides power to the engine, and it is also an external expansion surface (plug nozzle) during the rocket engine

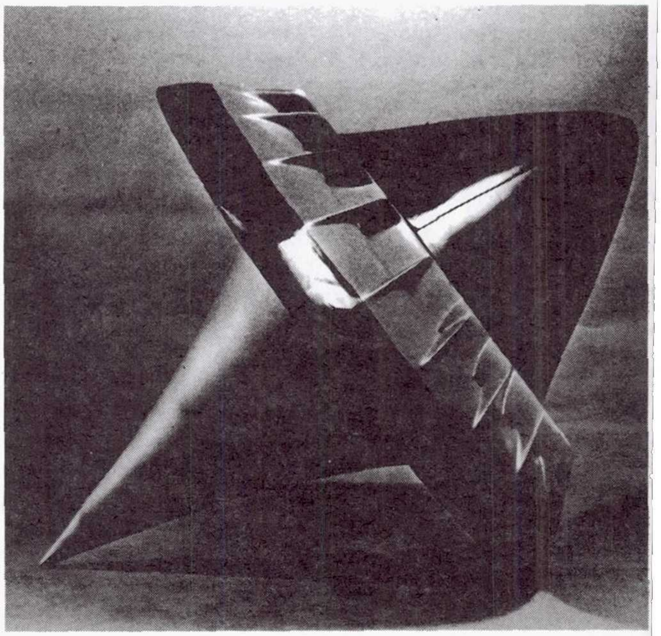

Fig. 2. Lightcraft Technology Demonstrator (1.4-m diameter)

mode. It is the opinion of the authors that focusing mirrors mounted on the laser-propelled vehicle is the most expedient way to permit both low flux levels in the atmospheric transmission link and elevated flux levels within the thruster (which are required for high propulsive efficiency). The reference "point design" for the LTD is configured around a 1-m-diameter parabolic receiving mirror, as shown in Fig. 2.

The primary thrust structure is the annular shroud. The shroud serves as both inlet and impulsive thrust surface during the airbreathing engine mode; at this time, the LTD centerbody is treated as the "vehicle airframe" component. In the rocket mode, the annular inlet is closed; the afterbody and shroud combine to form the rocket thrust chamber. The three primary structures: forebody, shroud, and afterbody, are interconnected by an internal support frame to which all internal subsystems are attached.

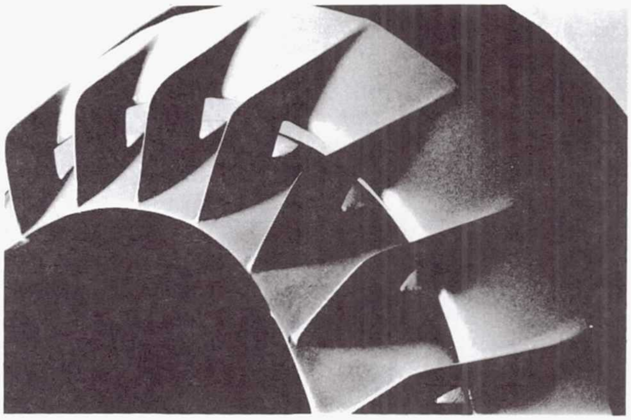

Fig. 3. LTD Shroud and Support Strut

FOCUS OF THE LTD DESIGN PROJECT

This year's efforts have been to develop a conceptual design for a small, 1.4-m-diameter Lightcraft Technology Demonstrator around components derived from current liquid propellant chemical rocket engines, advanced composite structures, and high power laser mirrors. Specific areas that were addressed by the design team included aerodynamics, propulsion, structures, propellant management, heat transfer, optics for sensor and propulsion missions, lightsat/microsat subsystems, mechanical subsystems, detailed LTD mockup construction, and finally, the definition of future experimental test facilities (for next year's effort).

Aerodynamics and Propulsion

In the area of aerodynamics and propulsion, first an analytical computer model of the airbreathing pulsejet cycle was developed, providing a database of engine performance characteristics. A vehicle aerodynamic drag model was then assembled. Next, an optimal trajectory analysis was performed using a computer code called SORT (Simulation and Optimization of Rocket Trajectories), which had previously been modified for lightcraft engines and aerodynamics.

The focus of the propulsion analysis was to model the laser-heated blast wave and impulse-generation process using an axisymmetric representation that excludes radiation and convection. For the most part, air within the laser-generated blast wave was modeled as an ideal gas throughout the expansion process. The engine inlet air state (i.e., pressure, temperature, density, etc.) prior to laser-heating, was a direct function of flight Mach number and altitude; hence, graphical results are presented vs. these flight variables. The equations developed by Raizer[6,7] to describe the initial state of the laser-induced blast waves, were used in modeling the "line-source" impulse-generation process.

The simple LTD inlet flow model predicted the state of the inlet air (pressure, temperature, velocity, etc.) that refreshes the lower annular shroud impulse surface. This aerodynamic model was needed not only for the refresh air state, but also for defining external drag characteristics of the entire vehicle. In the latter, it is important to distinguish between the drag produced by engine-related vs. airframe-related components, so as not to over penalize Lightcraft performance.

Trajectory Analysis

The trajectory analysis of any launch vehicle becomes a critical step in the overall system integration process. Many important engine/vehicle-related characteristics must come together for the final product: performance. Launch vehicle performance is typically measured by payload capability, which for the LTD is the entire dry mass and ullage gas, totaling 124 kg. The LTD must attain LEO with the available propellant, while minimizing total laser energy consumed along the launch trajectory.

The trajectory was evaluated using a computer tool called SORT that was written by McDonnell Douglas Astronautics Co. for NASA to design space shuttle trajectories[8]. The code is sufficiently general to analyze any trajectory and model all important environmental parameters that affect vehicle dynamics. Engine performance, vehicle aerodynamics, guidance algorithms, and mass histories interact with atmosphere and gravity models.

The capability of the SORT program is quite extensive by its use of these sophisticated vehicle and environmental models. The program can iterate on trajectory parameters to optimize performance, achieve a desired criteria, or constrain the solution to avoid some specified limit.

Even with all the generality built into SORT, certain modifications were required for the LTD. The most significant software modification involved the unique energy source, a laser. A new vehicle steering option was also encoded so that the LTD could always point at the ground-based laser station (or laser relay satellite). After these modifications were included, SORT was able to model Lightcraft performance to a high degree of accuracy.

Structural Design

Once the overall LTD vehicle structural configuration was defined, more detailed analysis of primary and secondary

structure subcomponents was carried out. Consideration was given to using state-of-the-art materials technology and mass production techniques for low unit cost (e.g., $\$10^5$/vehicle). A close integration of laser-propulsive engine and satellite functional hardware was necessary. Much emphasis was placed on the annular shroud structure, the primary impulsive thrust surface (see Fig. 3). A finite element computer code called CAEDS (Computer Aided Engineering Design System) was used to conduct both static and dynamic structural analyses and stress and modal behavior of the LTD shroud structure were extracted. This work will continue in the future as the LTD structural model becomes more elaborate.

Driving issues in the LTD structural design process were the component mass allowances and propulsion system requirements; aerothermal loads were also considered in a generic sense, to identify the current operating limits. Specific transatmospheric flight paths must be analyzed in future studies to assess their suitability for alternative engine and structures technology.

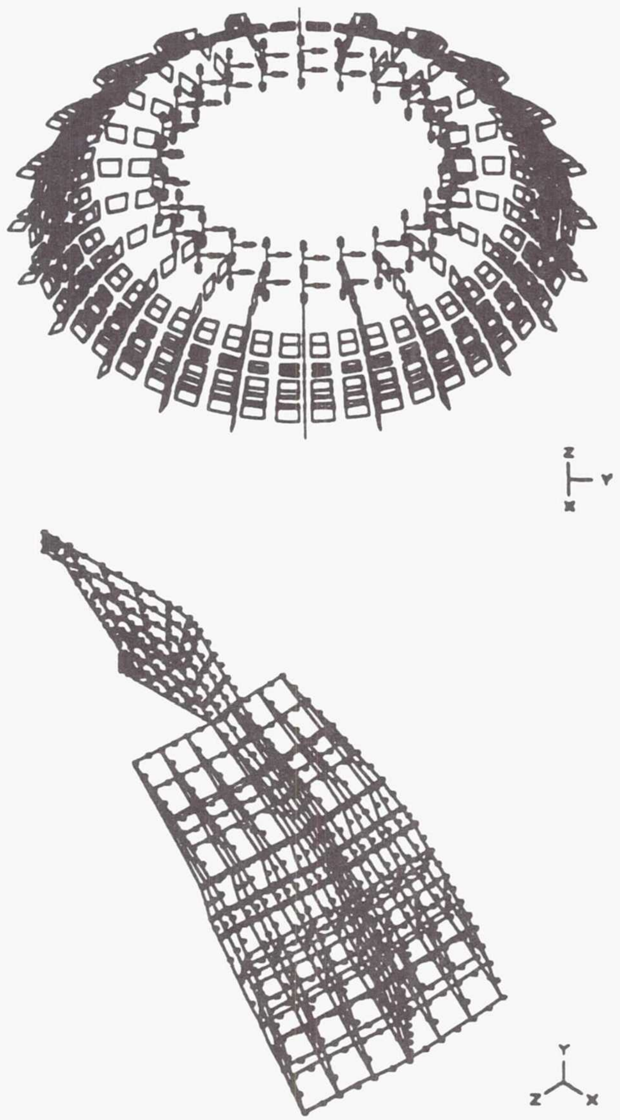

Fig. 4. Finite Element Models of Shroud and Strut

The LTD structure must meet the combined challenge of providing a lightweight, efficient airframe that can survive severe engine and aerodynamic heating, i.e., a "thermo-structural" viewpoint. Clearly, any successful thermo-structural concept must meet existing materials and manufacturing limitations.

The LTD primary structure is a large fraction of the vehicle's inert weight, yet this comprises a small structural weight fraction. Applied loads must be predicted to an accuracy that will allow knowledgable reductions in margins of safety, to eliminate every ounce of nonoptimum structure. A large experimental database of aerothermal loads must now be assembled for future detailed finite element structural and heat transfer analyses.

Structural Dynamic Analysis

Finite element modeling techniques were used to evaluate the annular shroud and support strut design proposed for the LTD (see Fig. 4). Both static and dynamic structural analyses were implemented to extract the stress and modal behavior. Pulsed airbreathing or rocket engines must avoid the natural frequencies of the vehicle structure, or catastrophic failure of the system will result. The present analysis concluded that the LTD shroud and support structure is able to withstand stresses of induced oscillations at the current engine design PRFs of 1-10 kHz. Even though resonant frequencies may be produced in flight, extremely small amplitudes (of displacement) will not cause damaging stress levels. The LTD structure seems to resonate at frequencies in the 10-100 Hz range.

The static stress analysis examined the integrity of the shroud/strut section, and revealed areas that needed further refinement. The shroud itself was found to be excessively strong and can easily sustain the applied loads; thus, some material can be removed from the shroud interior to permit further weight reduction. Also, the proposed strut mounting design provides sufficient strength for attaching the struts securely to the internal LTD support frame.

Propellant Management Systems Design

The LTD combined-cycle, laser-propulsion system employs onboard cryogenic fluids for reaction propellant, sacrificial coolant, and feed system pressurant. Liquid nitrogen has been chosen as the propellant for several reasons. Although liquid hydrogen would be the most desirable propellant because of its low molecular weight (and higher rocket specific impulse), only 14 kg would fit into the LTD's 28-in-diameter storage tank; in contrast, 140 kg of LN_2 would occupy the same volume (see Fig. 5). Heated to high temperature and pressure, nitrogen can produce specific impulses in the range of 725-1025 sec, depending on whether the exhaust gases are dissociated or not. (LN_2 is also favored because it is an inert and exceptionally clean coolant, a consideration that is especially important for high-power laser optics.)

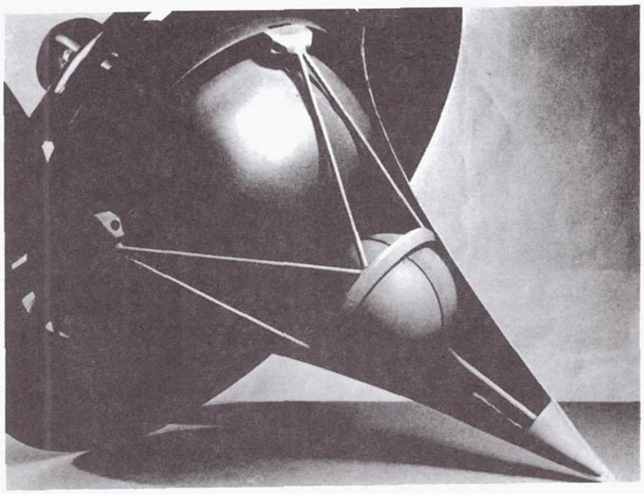

Fig. 5. Cutaway View of LTD Showing Storage Tanks for LN_2 and Helium

Several candidate injector designs have been identified for the rocket engine mode (see Fig. 6). The injector orifices are designed to act as "acoustic valves," to automatically deliver propellant into the rocket engine thrust chamber. Precise control of injector orifice pressure is necessary for optimum propellant utilization during flight.

High-pressure, super-critical helium was chosen for the pressurant because of its superiority as an inert agent with a very low boiling point. The LTD pressurant system is modeled after one flown on the Apollo lunar module descent rockets. Storing the helium at near liquid temperatures enables maximum pressurant density.

The computer-controlled propellant management system must (1) deliver the proper mass flow rate of liquid nitrogen coolant to critical actively-cooled engine components during the airbreathing propulsive mode and (2) provide uniform propellant mass flow during the rocket mode. Sensors distributed over the vehicle's outer skin and engine will

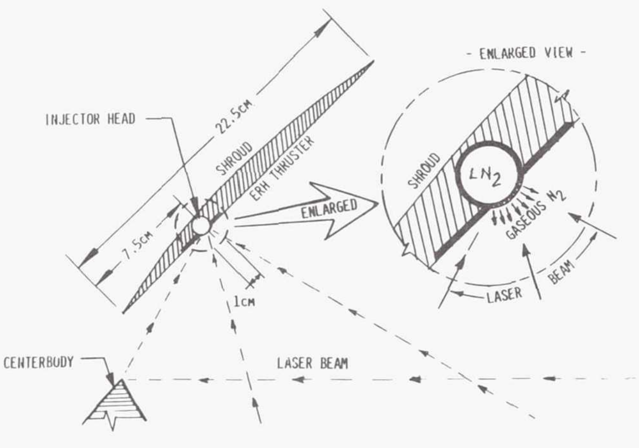

Fig. 6. Proposed LTD Injector Design

monitor surface temperatures. The mass flow rate of LN_2 coolant will be adjusted to compensate for variations in laser power absorbed by the primary mirror during the airbreathing mode. Laser power input is constant during the rocket mode.

The heat transfer analysis has focused upon active cooling of the LTD's engine hot structures, (i.e., mirror, shroud, and shroud support struts). Regenerative cooling will be employed by the primary mirror/plug nozzle and hot thruster impulse surfaces. The leading edges of the shroud support struts and the shroud will utilize transpiration cooling and platelet technology. The shroud thruster surface and propellant injector array will be film cooled. A thermal protection system (TPS) such as used on the space shuttle orbiter will cover the vehicle forebody.

Optics for Propulsion

The design and fabrication of the LTD primary receptive mirror has been investigated. Although some of the physics behind propagating the high-energy laser beam through the heated exhaust plume is not fully understood, the concept is shown to be within reach of current technology. The primary optic could be manufactured using existing diamond-turning lathe facilities. Development of multilayer high-reflectivity coatings and microchannel cooling systems are the main technical problems encountered. The mirror must exhibit high figure quality and minimal surface roughness throughout the launch trajectory. Calculations of beam divergence indicate that a 4-m diameter adaptive ground-based transmitter is entirely sufficient for a 1-μm wavelength. The effects of pointing error were evaluated using a computer ray trace routine; errors of 0.5° or less shift the focus asymmetrically on either side of the annular engine, but the effect is self-correcting and the LTD is therefore stable in this respect. At incident angles up to 1°, the power loss and spot size increase but do not cause a critical loss of thrust for near-, intermediate-, or far-field beam profiles. An adaptive pointing error correction system is proposed, using retroreflectors to sample the power beam edges (at 24 azimuthal locations) and feed data back to the ground power source via laser rangefinding.

Optics for Sensor Satellite Mission

The use of the LTD as a sensor satellite has been explored. The primary mirror could serve a dual purpose on each mission; however, since the mirror is designed primarily for propulsion applications, its performance in other respects is limited. A ray trace analysis of the primary optic indicates that it has superior light-gathering ability, but the angular field of view is limited to only about 0.5°. Coma is the dominant aberration over the entire field of view; a small amount of astigmatism is present for larger angles of incidence, while other aberrations are essentially negligible. Several candidate sensors, including CCD and CID technology, are commercially available and meet the requirements of the LTD retina.

A special mechanical subsystem was developed to deploy this advanced segmented photo-optic sensor (the "ring retina"), into the focal region of the primary mirror; in this

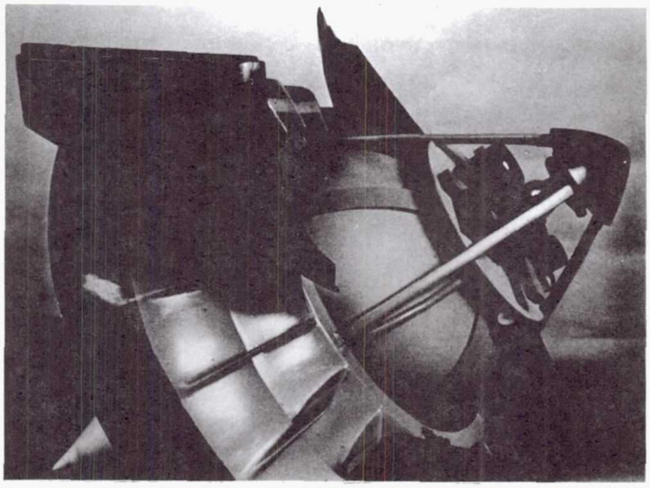

Fig. 7. LTD Satellite Functional Hardware, Located in Forward Payload Section of Vehicle

manner, the propulsive optics are transformed into a powerful 1-m-diameter telescope. Functional hardware necessary for the LTD to perform satellite functions is located in the forward (nose) payload section of the vehicle.

Lightsat Systems Design

Once in orbit, the LTD will function as a lightweight sensor satellite, complete with all the requisite onboard electronics, communications, and attitude control systems (see Fig. 7). The LTD senses its attitude with a sun sensor and an Earth horizon sensor. To change attitude, it uses a combination of cold gas jets and/or magnetic torque bars. It will be equipped with an erectable lightweight antenna for communicating with launch command, accessing the TRDSS (and STDN) network, and relaying data gathered from LTD sensors. An onboard computer will manage satellite electrical, mechanical and attitude control systems, coolant flow rates, and solar array actuators. The solar array is mounted on the inner forebody surface, which opens into four "petals" to collect solar energy for recharging onboard nickel-hydrogen batteries. The batteries are used primarily when the satellite traverses the Earth's shadow. This combination of satellite components is chosen for minimal cost and weight, so that the LTD can fulfill its primary objective of a self-launched lightsat.

FUTURE DIRECTIONS

In the upcoming year, efforts will be focused on the LTD's propulsion system and vehicle aerodynamics rather than on its

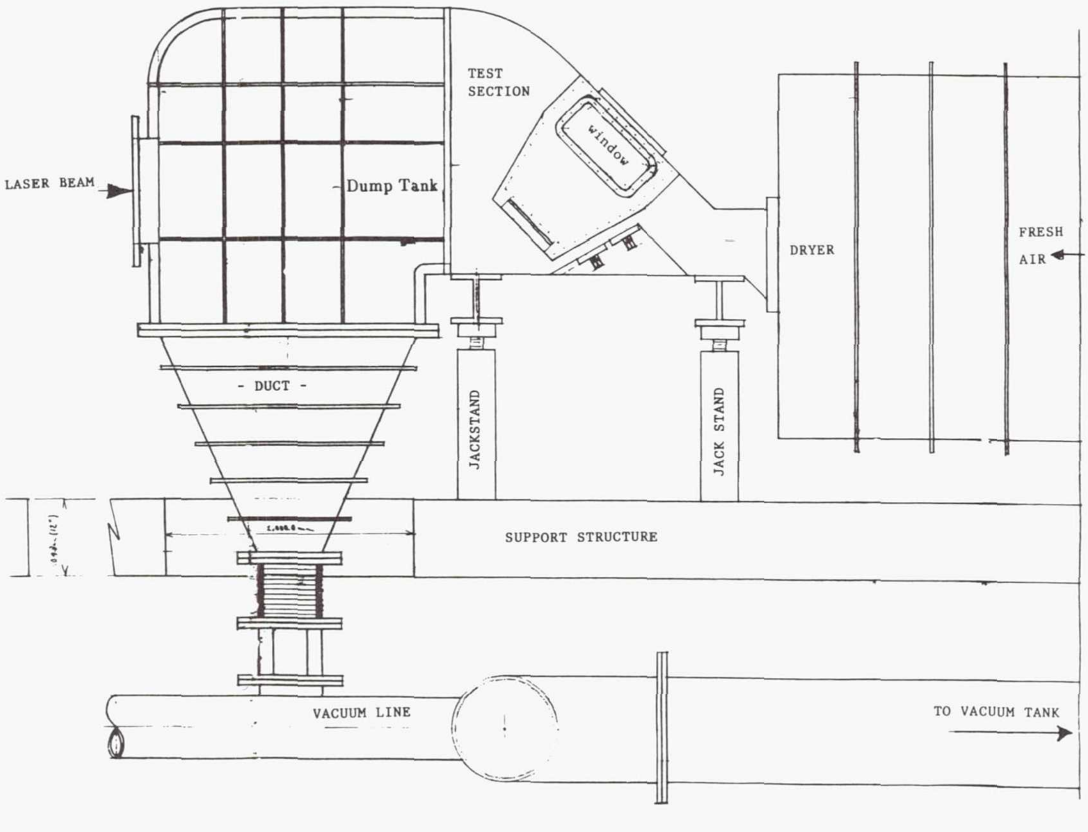

Fig. 8. LTD Wind Tunnel Laser Impulse Experiment

mission as a sensor satellite. A 3-D computational fluid dynamic (CFD) model of the LTD's external inlet will be assembled and run for a variety of different shapes and flight speeds. From these computer simulations, the boundary layer thickness, external surface pressure distribution, and transition point (from laminar to turbulent flow) can be determined. A Naval Research Laboratory (NRL) 2-D blast wave code may also be employed to model the impulsive thrust generated by laser-induced blast waves. In addition, a computer analysis of the radiation/convection heat transfer to the LTD will be conducted to find the engine/vehicle thermal profile. All of this will enable the choice of appropriate spacecraft materials (specifically tailored to withstand the hypersonic transatmospheric environment), and also to design active thermal cooling systems for the primary optic and engine hot-sections. Finally, a more detailed vibrational analysis will be performed that includes not only the shroud/strut assembly, but also the spacecraft internal support structure.

Several experiments will be performed to validate theoretical vehicle and engine performance simulations. Hot and cold flow wind tunnel tests are planned, with two different scale models, 5.5-in-diameter and 1.25-in-diameter. The air speeds will be varied from subsonic to hypersonic. Schlieren photographs and pressure data will be taken. Laser impulse experiments will also be performed with an exact 1/15 segment of the annular engine (see Figs. 8 and 9), in both static and dynamic wind conditions. These high-power laser experiments will yield engine impulse and heat transfer data to prove technical feasibility of the propulsion concept.

Finally, additional systems-integration questions that were not addressed in this final report, e.g., LTD range safety issues, manufacturing cost analyses, and high-power laser attenuation by the engine exhaust plume, may be explored.

SUMMARY

The research effort focuses on the concept of a 100-MW-class, laser-boosted Lightcraft Technology Demonstrator (LTD) drone. The preliminary conceptual design of this 1.4-m-diameter microspacecraft involved an analytical performance analysis of the transatmospheric engine in its two modes of operation (including an assessment of propellant and tankage requirements), and a detailed design of internal structure and external aeroshell configuration. The central theme of this advanced propulsion research was to pick a known excellent working fluid (i.e., air or LN_2), and then to design a combined-cycle engine concept around it. Also, a structural vibration analysis was performed on the annular shroud pulsejet engine. Finally, the sensor satellite mission was examined to identify the requisite subsystem hardware, e.g., electrical power supply, optics and sensors, communications, and attitude control systems.

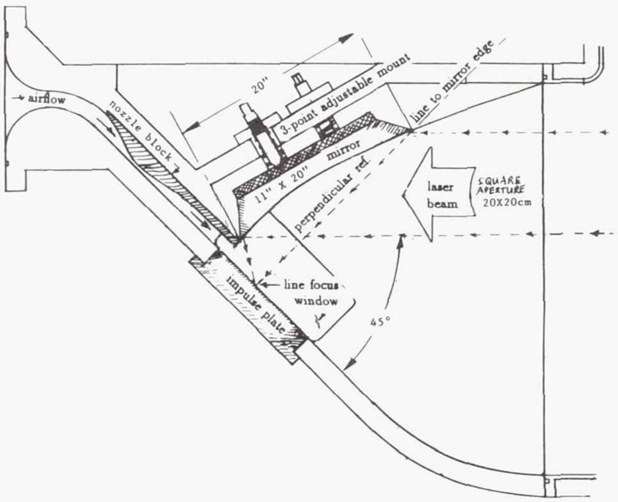

Fig. 9. LTD Laser Impulse Experiment Test Section (Side View)

ACKNOWLEDGMENTS

Principal authors M. Antonison and faculty advisor Dr. Leik Myrabo were assisted by S. Chen, C. DeCusatis, K. Kusche, M. Minucci, J. Moder, C. Morales, C. Nelson, J. Richard, S. Sarbacker. Additional assistance was provided by J. Burnett, M. Hulscher, V. Hurst, M. Knocken, E. Pavlovic, P. Post, W. Sheets, T. Sontrop, and H. Spyropoulos.

REFERENCES

1. Canavan G. H., "Laser Propulsion of Sensors and Interceptors." LA-UR-87-3208, Los Alamos National Laboratory, Los Alamos, NM, 1987.
2. Canavan G. H., "Decoy Development with Laser Propulsion." LA-UR-88-1246, Los Alamos National Laboratory, Los Alamos, NM, April 1988.
3. Fuhs A. E. and Mosier M. R., "A Niche for Lightweight Satellites." *Aerosp. Am.*, April 1988, pp. 14-26, p. 36.
4. Mozey R., "The Cost of Lifting Weapons to Space." Center for International Security and Arms Control, Stanford University, Stanford, California, October 1986.
5. Kare J. T. (ed.), *Proceedings of the First SDIO/DARPA Workshop on Laser Propulsion,* Lawrence Livermore National Laboratory, CONF-860778, Livermore, California, July 7-18, 1986.
6. Raizer Yu P., "Heating of a Gas by a Powerful Light Pulse." *Soviet Physics, JETP, Vol. 21, No. 5,* Nov. 1965.
7. Raizer Yu P., *Laser Induced Discharge Phenomena.* Consultants Bureau (Div. of Plenum Publishing), New York, 1977.
8. Berning M., "Version IV User's Guide for the Simulation and Optimization of Rocket Trajectories Program." McDonnell Douglas Astronautics Co., Houston, Texas, Transmittal Memo No. 1.2, TM-FM86028-53, December 1985.

omit

Invited Talks

PRECEDING PAGE BLANK NOT FILMED

PAGE 336 INTENTIONALLY BLANK

1994004553

383663

2p

N94-71308

S41-31

160667

p. 1

A MARS BASE

ECOLE POLYTECHNIQUE FEMININE
Veronique Soule

This study was initiated to provide an approach to the development of a permanently manned Mars base. The objectives of a permanently manned Mars base are numerous. Primarily, human presence on Mars will allow utilization of new resources for the improvement of the quality of life on Earth, allowing for new discoveries in technologies, the solar system, and human physiology. Such a mission would also encourage interaction between different countries, increasing international cooperation and leading to a stronger unification of mankind. Surface studies of Mars, scientific experiments in the multiple fields, the research for new minerals, and natural resource production are more immediate goals of the Mars mission. Finally, in the future, colonization of Mars will ensure man's perpetual presence in the universe.

Specific objectives of this study were:

(1) to design a Mars habitat that minimizes the mass delivered to the Mars surface, provides long-stay capability for the base crew, and accommodates future expansion and modification;

(2) to develop a scenario of the construction of a permanently manned Mars base;

(3) to incorporate new and envisioned technologies.

The one feasible scenario for the development of a Mars base utilizes robots entirely for base construction. Substantial astronaut EVA would increase the risk of serious crew injury by exposing the astronauts to the harsh Mars environment during hazardous construction operations. This approach would make transportation costs prohibitive since, in general, with each cargo mission there is an associated manned mission (it takes a minimum of nine months for the Earth-Mars one-way trip). Operational costs would also be increased due to the crew life support requirements.

This work represents my efforts in continuing further studies and improvements of a Mars base concept of a team of students at the University of Texas, Austin. This work also used previous studies of a Lunar Habitat developed by students at the University of Houston.

The purpose of the mission drivers is to establish the criteria and reasons for going to Mars. For long-range goals, human crews on Mars can do much better science than automated equipment because people have unique capabilities that are difficult or impossible to automate. One advantage of having people on the surface of Mars is that they can make decisions and respond immediately to a situation. Greater flexibility results because plans or emphasis can be adaptable to different situations. People can also analyze, synthesize, and reduce data instantaneously. In short, a human being is a stable, well-calibrated, mobile instrument. The best there is! Therefore, the use of humans in the exploration of Mars is the most cost-effective approach with respect to scientific results, even though manned missions require a high threshold funding level. There are actually five basic categories of reasons for going to Mars: (1) scientific research, (2) resource utilization, (3) settlement feasibility, (4) economics for future expansion, and (5) international involvement and shared costs.

The environment of Mars must be taken into consideration in determining base design. Aspects such as atmospheric disturbances, temperature changes, and dust storms will affect final base operations. Manufacturing facilities for basic life support requirements such as water, air, and space ship refueling are essential to base independence.

Human safety is one of the most important factors. The construction of a base on Mars is far too dangerous for humans. The use of advanced robotics for Mars base construction is a challenging engineering task, but is possible; therefore, robots will build the facility before crews set foot on the surface. These robots must be durable, efficient, and able to withstand the harsh environment. Great advances in technology will be necessary before robots of this sophistication will be ready to perform the complex tasks required to construct a Mars base. Once this plateau in robotics has been achieved, human resources may be diverted to other scientific endeavors.

The base configuration provides the minimum habitable volume required for the first six to eight crew members, but will be expandable. Additional reductions in mass delivered to the surface are realized since the base modules are to be covered by martian regolith. The initial design calls for five specific module types: Habitat, Science/Central Control and Command, Greenhouse, Medical Center, and EVA module. The Mars supporting infrastructure includes communication equipment, weather station, satellite network, and propellant plant.

International cooperation on a large-scale basis in the development of a martian base is also a necessity.

PRECEDING PAGE BLANK NOT FILMED

PAGE 338 INTENTIONALLY BLANK

19940004554
383664
4P

N94-71309

THE ROLE OF SOLAR SAILS IN THE INVESTIGATION AND EXPLORATION OF MARS

S42-18
160668
P 4

MOSCOW AVIATION INSTITUTE
Eugene Krivenchenko

INTRODUCTION

I represent "ISKRA" ("SPARK") Student Space Design Bureau of the Moscow Aviation Institute (MAI). I would like to express my gratitude to executives of Universities Space Research Association for giving me the opportunity to make a report at the Conference, and I hope that our collaboration will be fruitful and mutually beneficial.

MAI, included in the system of public education, is the largest Soviet academic university in the field of aerospace. More than 17,000 full-time students study at its nine colleges. Traditionally MAI's activity is directed towards training specialists for a single branch of industry. ISKRA Students Space Design Bureau is a special subdivision of the College of Astronautics and Automatic Spacecraft, and it is intended for practical student training in design of actual structures. Our design bureau specializes in making small artificial unpressurized Earth satellites designed for remote study of Earth and space exploration as well as for carrying out interregional amateur radio communication. Just when the design bureau was founded we succeeded in designing and launching several artificial Earth satellites named "ISKRA." Dozens of students took part in their creation which permitted the students to gain grounding in the field, as well as the experience of practical designing of complex cosmic objects. Participation in production of more complex space vehicles has become the next logical step on the road to the development of our design bureau. Nine departments of our college cover all the main applied problems in the process of designing space systems including life-support systems. It allows the design bureau to carry on operations dealing with a few independent projects simultaneously. A wide range of investigation permits every student to apply his skills.

One of the projects designed in the bureau is a space vehicle equipped with solar sails for stabilization and orientation control and, partly, as a propulsion unit. It was gratifying for us to have been invited to the international competition of vehicles with solar sails announced by the United States. This report is a summary of work done. Here we can express our own opinion on the role of vehicles with solar sails in the infrastructure of programs dealing with complex investigation and exploration of Mars. In the report we suggest some means of solving a number of problems including the problem concerning the development of "Columbus-500." Considering the possibility of solar sail vehicle application in the program of Mars investigation and exploration, we proceeded from the following premises:

1. The program provides for relatively large, regular, Earth-Mars freight traffic, excluding spacecraft for crew delivery. Time for freight transportation is not limited, which makes the idea of solar sails rather appealing.

2. The expenditure on creation and use of transport fleet should be minimum.

It is certain that this proposal is not original. Similar projects can be reasonable to produce unified freight modules and solar sail elements, whose structure would provide the following:

1. Solar sail module. The structure provides vehicle configurations assembly in the near-Earth orbit, which possesses a required solar sail area. After the payload delivery to Mars, there will be an opportunity to use solar sail modules and, perhaps, sail material in the orbit of Mars (in the design of orbital solar power plants, large-size space antenna reflectors, life support systems, etc.).

2. Cargo module. Module construction provides the deployment of payload of advisory mass and its delivery to Mars. After payload is delivered, the modules may be used as an orbital station element or a martian base.

3. Scientific module. The module separates from the cargo vehicle during its flight to Mars and continues its solo flight to the outer planets for further study. It is impossible to create large structures of the kind which are able to transport dozens of tons of payload without solving a series of technical problems, storing statistical data, and performing preliminary tests and experiments. The "Columbus 500" program could become an important stage in this field.

Let me remind you that three spacecraft, each weighing about 500 kg, are supposed to be launched to Mars in 1992. Each of them is expected to use solar sails as a propulsion system. In our design bureau preliminary analysis of possible constructive solutions was carried out together with other industrial specialists. The most advanced student groups were drawn into the work on the basis of competition. They had put forward their proposals concerning the spacecraft appearance. At the first stage of work we tried to appreciate the possibilities of producing spacecraft capable of reaching Earth escape velocity to Mars, so that the length of the geocentric path did not exceed one revolution around the Earth. According to methods described in the paper, sail area(s) necessary for its transfer to the parabolic orbit is solved by formula 1.

$$S_n = \frac{m_a}{2(1+\rho)\, Po\, a_o^2/K_\odot - \gamma_n} \qquad (1)$$

S_n - Area solar sail, m^2.
m - Spacecraft mass, kg.
ρ - Reflection coefficient;
P - Sunlight pressure on black body on Earth;
$P = 4.5\ 10^{-6}\ H/m^2$.

PRECEDING PAGE BLANK NOT FILMED

340 INTENTIONALLY BLANK

a - Astronomic unit of length, $a_o = 1.496\ 10^{11}$ m;
$K_\odot = 1.325\ 10^{20} m^3/s^2$, Sun's gravitational parameter
γ_n - relative mass of $1m^2$ of sail

$$O < \gamma_n < 3.04 \times 10^{-3}\ kg/m^2.$$

Analysis of this variant shows that it may be carried out only for construction perfection of solar sails lying in an interval from zero to 3.04: 10-3 kg/mm.

According to the information obtained, at the present stage lack of material of required quality makes it technically difficult. That is why the spacecraft should be accelerated to the escape velocity along the spiral trajectory around the Earth. This imposes certain requirements to the control system of the spacecraft being designed. Designs which have been considered as suitable for participation in the conference may be classified according to the following features: (1) by structure, (2) by deployment technique, and (3) by control method.

In practice, just after consideration, structures of "chute" type (low reliability), as well as structures of "balloon" type (considerable mass) were excluded. Great attention was paid to consideration of rotor structures in various versions. In considering proposals, special attention was paid to the following:

1. Minimum relative mass of the vehicle.
2. Time for 90° turn in regard to OY axis.
3. Reliability of vehicle structure.
4. Composite materials used.

DESIGN CONSIDERATIONS

Heliorotor and Its Versions

Since the heliorotor is a classical structure and is described in a series of papers, we see no need to elaborate further. This structure requires a careful approach to the choice of heliorotor blade geometrical parameters. For example, the optimal period of T_{opt} rotor motion is calculated by formula 2.

$$T_{opt} = \pi\ 1\ (\rho/2\sigma_\circ) \qquad (2)$$

π - 3.14
1 - Rotor blade length, m^2;
ρ - Blade's relative density, kg/m^3;
$\sigma_\circ$ - Blade's unfold centrifugal stress.

Thus, changing the blade length makes it possible to avoid the influence of undesirable perturbing forces caused by the gravity gradient which occurs with the proximity of the spacecraft's orbital motion period and its own rotation period. Further, blade geometrical parameters influence its inclination angle, which is 3 calculated by formula 3.

$$\theta = \frac{4\ P_n\ 1\ d}{\sigma_\circ\ b\ d} \qquad (3)$$

P_n - Sun force component normal to sail, H/m^2;
l,b,d - Blade's length, breadth, and thickness, m;
x - Displacement of center of pressure, m;
$\sigma_\circ$ - Centrifugal stress has by blade's, Pa.

For regulating the inclination angle, it is necessary to control flexural displacement of the center of solar light pressure, as well as blade mass center. Blade section temperature difference will also lead to its deformation. It may be prevented by means of application of struts to its deformation. It may be prevented by means of application of struts and rigid framework along the blade's longitudinal axis.

Frame Structures

Both frame-type bodies and inflatable tube frame structures made of polymer solidifying in outer space, were considered for square structures. The mass of vehicle in the first approximation may be represented by formula 4.

$$M_\Sigma = M_1 + 2\ \gamma_c\ 1 + 0.5\ \gamma_s\ 1^2 \qquad (4)$$

M_Σ - Spacecraft mass, kg.
M_1 - Payload mass, kg.
γ_c - Relative mass of girder constructions, kg/m;
γ_s - Relative mass of $1m^2$ of sail, kg/m^2;
1 - Length square's diagonal, m.

Knowledge of flight time, required sail area, and sail film mass characteristics make it possible to formulate requirements to frame structures. Control surface and spacecraft mass center displacement are the main methods for controlling these structures. When these estimations were carried out, the sail was considered absolutely rigid.

Figure A1 shows the dependence of solar sail deflection on the optimal deflection angle of control surface (1 α opt.) and (2 α opt.), that is schematically shown in Fig. A2. Figure A3 shows the dependence of low oscillation natural frequency of the whole system on solar sail position.

The vehicle center mass displacement shown in Fig. B1 is somewhat similiar to Figs. B2 and B3 which also show dependence for a control scheme.

It is obvious that for the first scheme, the law and the whole control system will be simpler because the law of change (ω) (φ) is similar to the linear one and the range of low oscillation natural frequency change is twice less than for the second scheme.

As for the deployment scheme, all the structures considered are automatic. Common feature for all the versions is working out Service System (SS) and scientific systems in an unpressurized manner. At present, we are completing the design of these variants for selecting basic structures to the conference.

But the way we see it, the final choice of arrangement and practical realization of the project are impossible without solving a series of technical problems. These problems are the development and comparison of algorithms of stabilization and controlling spacecraft gaining low acceleration, the

examination of methods for similar object tracking by ground station, and their position prediction. In addition to this, it is necessary to study thoroughly and to define frequency characteristics of large film structures, to analyze sail material property changes as a result of prolonged space stay, and to analyze these changes on flight performance.

Thus, for example, change of sail admission coefficient in connection with 4 metallized cover degradation and with microvents formation may influence T_{opt} spacecraft flight time according to formula 5.

$$T_f = \frac{2}{3} \frac{r_s^{2/3} - r_e^{2/3}}{a_o} \qquad (5)$$

$$\frac{g_\odot - \frac{a_n}{2}(1-\tau_1^1)\sqrt{(1+\rho-\tau_2^1)\cos^3\beta\,(1+\sin\beta)}}{2\,a_n\,(1-\tau_1^1)\,\rho\cos^2\beta\sin\beta}$$

r_s, r_e - Radius of initial first orbit and radius of final or both, km;

a_o - Astronomic unit, $a_o = 1.496\ 10^{11}$m

$g_\odot = 0.592$ sm/s^{-2}, acceleration due to Sun's gravity on the Earths

$a_n = 2\ P_o\ \Sigma$ - Sun's acceleration at a growing, m/s^2;

β - Angle between solar sail and Sun's direction, °;

τ_1^1 - Sail's transparent coefficient;

τ_2^1 - Sail's penetrate coefficient.

To gain data of that kind, it would be reasonable to launch small solar sail spacecraft. A vehicle powered with measuring equipment, different film samples, and the ability to function during a long period of time would make it possibile to get this information. In our design bureau such a vehicle was designed. This vehicle is able to make a stretched orbit flight with a pericenter altitude more than 5,000 km under active or passive stabilization conditions with the aid of solar pressure forces.

The vehicle is designed on the module principle and admits the most vital systems redundancy without equipment mass or volume limitations. The vehicle can be used for investigation of near-Earth and near-planet space during 5-10 years on high elliptical orbits. The main feature of the vehicle is that under active orientation conditions it has maximum controllability, and under passive stabilization conditions it has zero gravity and maximum recovering moment. In the design process factor (6) was formulated. If it is used, such a vehicle may be made. Characteristics obtained include mass geometric parameters of the sail and the central body formula (7) which permit prompt definition of sail parameters by changing central body parameters.

We believe this vehicle could be launched in two years if both sides have an interest in this. After working out the main principles of orientation and stabilization of the vehicle and after analyzing the results obtained, it would be possible to proceed to the second stage of the preliminary program of

$$a_o \leq \frac{J_{xo}}{J_{yo}} \leq 1{,}5 \qquad (6)$$

$$a_o = \begin{cases} 0 & \text{- The mirror sail;} \\ 0.145833 & \text{- The black sail.} \end{cases}$$

Jxo, Jyo - Moment of inertia relative to axis OX and OY;

$$\left.\begin{aligned} m &= f_1 \frac{J_{yo}}{r}, \\ 1 &= f_2 r, \\ \cos\alpha &= \frac{\sqrt{2}}{2} = \frac{d}{f_2} \end{aligned}\right\} \qquad (7)$$

m - A single solar sail's mass, kg;

l - Distance from setting its point of sasi to gravity, m

α - Angle between axis OY and Sun's direction, °;

r - Distance from the setting point of solar sail to axis OY, m;

f_1, f_2, f - Analytic function from variable

$$f_1 = \frac{(1-\sqrt{2f})^2}{2},$$

$$f_2 = \frac{\sqrt{2f}}{1-\sqrt{2f}},$$

$$f = E_1 + E_2 \frac{J_{xo}}{J_{yo}} - \sqrt{E_3 + E_4 \frac{J_{xo}}{J_{yo}}},$$

	E_1	E_2	E_2	E_2
The mirror sail	0.209335	0.435666	2.70928 10^{-2}	6.97038 10^{-2}
The black sail	0.10684	0.70761	7.6749 10^{-4}	0.29724

launching an artificial Moon satellite with a solar sail. At the moment, a rough design is being drafted. Besides lunar exploration, this vehicle would make it possible to work out solar spacecraft control methods, orbit maneuvering methods, etc.

Thus, preliminary elaboration has shown the following:

1. It is possible to build a 500 kg vehicle powered by a solar sail for a flight to Mars.

2. The necessary stages of elaboration are the building and testing of small spacecraft, particularly AES and AMS to corroborate the principles of solar sail spacecraft functioning and control.

3. The accelerating technical realization of the project can be clearly seen in wide cooperation, including an international one, that draws young specialists and students from aerospace universities of various countries to collaborations.

In conclusion, I would like to express my hope that our first meeting will serve as the beginning of a mutually beneficial collaboration between the U.S. universities and the Moscow Aviation Institute.

1994004555
383667
2P
N94- 71310

MODERN DESIGN METHODOLOGY AND PROBLEMS IN TRAINING AIRCRAFT ENGINEERS

MOSCOW AVIATION INSTITUTE
N. K. Liseitsev

S43-80
160669
P. 2

My brief report on the problem of the modern aircraft specialist education is devoted only to content and methods of teaching the course in "General Aircraft Design" in Moscow Aviation Institute. I have been lecturing on this theme for 15 years on the faculty of airplane and helicopter designs and construction.

In our opinion, this is the key course which crowns the special training of an aircraft design engineer. It combines all the preceding courses into a whole and supplements them with logic and methods of analysis and synthesis of complex technical systems. This allows a student to start an independent solution to aircraft design problems.

It is evident that not every graduate will be occupied with the problems of general aircraft design in his future work. Nevertheless, we believe that at least once in his life he should be a chief designer.

Aircraft design is a creative process, which, according to Dixon, includes analysis, synthesis, and decision making. Every constituent of this process has its own methods, techniques, and solutions of the arising tasks. It complicates the problem of training specialists.

Aircraft design as a scientific discipline first appeared in the late thirties and early forties. At that time, the subject problems and methods of this discipline were initially formulated. But since that time, they have changed greatly. The changes that have occurred in systems being designed over these fifty years are extensive, from the Wright brothers' airplane to modern complex transport planes, military aviation complexes and aerospace systems. While the first problem that the designer was to solve was once simply to create a stable flying airplane, now his task is to design an airplane whose parameters and performance are optimized for definitive purposes, taking into account, not only complex technical problems, but also economic, ecological, and other restrictions.

The complication of the design object and tasks is known to have led in the middle sixties to the so-called design "crisis". The attempt to modify the situation stimulated the development of new design technology, based on broad employment of computing techniques and computer graphic facilities. It demanded the creation of new design methodology, the main components of which were the principles of systems approach, the methods of mathematical simulation, and the mathematical instrument for the complex system optimization theory.

In this connection, changes have taken place since the 1970's, both in the theoretical design principles and in the methods and facilities of the design task solutions.

All this, naturally, has demanded changes in the institute's course "Aircraft Design" and its scientific and methodic support. In the manual, sections devoted to the theoretical basis of the complex systems design and computer-aided design methods have been added. The research system of the computer-aided aircraft design has been created as a basis for acquiring skills in solving design problems in the framework of new technology.

This system provides automation of the laborious calculating operations that accompany the process of airplane shape forming. It also gives the calculation results in a form convenient for the user. Within the limits set up by the conceptual design, the system carries out project scaling, its parameter optimization, the estimation of parameter, and restriction changes on the aircraft integral characteristics.

The system based on a block principle, includes:

1. The core of the system, intended for the airplane design parameter agreement (solution of an airplane existence equation).

2. A group of calculating blocks that determine the aerodynamic and mass characteristics of an airplane, the characteristics of an airplane power plant, and its guidance stability.

3. A group of estimating blocks that calculate the airplane performance and airplane effective indicators.

The content of this 60-hour course in aircraft design has been changed. Proceeding from the principle, formulated by Claude Helvetius, that "knowing the principles in some cases makes up for the ignorance of the facts," in this course we give only fundamental design principles that are common to all airplanes. They are the following:

The hierarchic structure of an airplane as an aviation complex system; from this may be drawn the following design problems and classification of the design variables and criteria.

Kinds and ways of the registering design restrictions.

The most important relations between the parameters and characteristics of an airplane.

Methods and algorithms of gross weight determination of an airplane and determination of its parameters that satisfy the design requirements.

The methods of an airplane layout and center-of-gravity position determination.

The students study the design pecularities of the different types of aircraft in courses which they choose themselves, taking into account the trends of the research institutes in which they will work.

One of the most important factors in training specialists is the student's practical activity in solving design problems. For this, students do design practice in the design organizations and write a course paper devoted to the study of the design parameter determination algorithms of an airplane of the stated purpose.

The graduation practice and 22 weeks of work experience crown the education. The main theme of the graduation paper is the advance project development of a new airplane. The graduation practice and work are carried out, as a rule, either at the research institute where the graduate will work, or at the student designers' office at the Moscow Aviation Institute. Light experimental airplanes are designed and built by the students at the designers' office.

The graduation papers are written both individually and in groups. The latter gives a more detailed study of the project and gives the student skills to work in a group.

Nowadays we are creating a base of knowledge and expert system on design. This is especially important since it is difficult to present in mathematical form most procedures of the design process. This is particularly true for the design of essentially new aircraft. The experience of the most skilled specialists, including specialists from industry, systematized in expert systems, will allow it to become the property of all students.

I believe that we share many common problems in the education of future aircraft specialists and in the development of design techniques, expert systems, and educational programs. We should very much like to discuss possible ways of attaining our goals through cooperative efforts.

1994004556
383668
2P

N94-71311

THE INTEGRATION OF EDUCATION AND RESEARCH

S44-80
160670
p. 2

MOSCOW AVIATION INSTITUTE
Vladimir K. Serdjuk

When I had conversations with American colleagues in Moscow last year, I would not have believed that I would be speaking here now. But, since it is true, I thank the USRA and Stan Sadin very much.

In speaking with many of you, I understand that we have some of the same problems in many fields, especially in education. Allow me to exchange with you some problems and some experiences in solving the problem of integrating education and research.

To our mind, scientific research and higher education are closely connected processes since any research is, first of all, a process of acquiring and storing knowledge. And the problem of integrating these two processes is a traditional one for higher educational institutions. There are a number of reasons for the urgency of this problem.

At present, new knowledge (in the sphere of physical principles, technologies, and the like) is known to grow rapidly, especially in aerospace engineering. For many reasons the period of study cannot be extended, and there is even a tendency to shorten it.

We cannot orientate our students to use their knowledge when they leave college. We find it very important to involve them in research and teach them to do research while they are students. Moscow Aviation Institute, like many other technical colleges, carries out a large amount of scientific research along with education. Some of the results are to be used in future long-term projects as well as in current programs.

Research is done by both the tutorial staff and by the scientific-engineering personnel which includes all categories of specialists typical for research and design bureaus. These two differ in their natural processes and approaches; the two corresponding perspectives ensure their fulfillment and predetermine differences in solving the above problem.

From the point of view of education and research, we do the following:

1. New subjects or new sections in a traditional course that cover new tendencies in science and engineering are introduced into the curriculum.

2. Scientists from the corresponding scientific centers, scientific workers from design bureaus and industrial enterprises are invited to lecture (and teach lab). These people are bearers of prospective scientific results and solutions that were realized in patterns of space techniques.

3. Students' pieces of research and their yearly projects, especially senior students' projects, are based on the design programs of sponsoring organizations. They do some of their research with these organizations, taking part in design and construction of current and advanced space vehicles.

4. According to the curricula which are uniform throughout the country, our students do practical work in the space industry and at the space center.

5. Last but not least, our students work on graduation projects at the places of their future work under the supervision of both the college and the enterprise. Within the bounds of scientific research, our students and some members of the tutorial staff do research under the supervision of design bureaus and industrial enterprises. A distinguishing feature of the students' participation in this work is that some of the students work as if they worked under a contract and some of them work on a voluntary basis. Let me remind you that research at higher educational institutions pursues a number of objects, the most important of which is the use of the scientific potential of a higher educational institution and growth of the scientific qualification of the tutorial staff.

There are two forms of student participation in scientific research. In the first form, a student joins a team of researchers as a junior colleague doing simple work at the beginning, and later, when he gets more experienced, he gets more complex and independent tasks. In the second form, the student works at the SDB or a similar organization. Here they are provided with every opportunity for study and rapid scientific growth. Objectives of their research are chosen with guidance from the tutorial staff. Such student organizations exist practically in every department, and they deal with the problems of their own departments. But there are also student research bureaus dealing with problems common to the whole faculty. In this case the objectives of their research are determined by the faculty; the responsibility for all aircraft design lies with the aeronautics faculty, while that for artificial earth satellites (AES), with our cosmonauts faculty.

Student SDB "ISKRA," which is represented by Mr. Krivenchenko at this conference, belongs to the student organization category. "ISKRA" works on problems sponsored by both industrial enterprise and by our college. He will present an account of the results of a study carried out.

To our mind, this is one of the most efficient forms of developing aerospace engineers. Those students who are interested in research and development, as a rule, make rapid progress when they come to work at plants, design bureaus, or research institutes.

At present, our faculty is looking forward to drawing these students to research work and research teams who give lectures.

We at MAI are planning to establish an educational research complex, the main objective of which is to join the effort of both groups, the tutorial staff and scientific-engineering personnel. This includes providing funding, research facilities,

and so on, to foster the improvement of education and increased volume of scientific development.

We are looking forward to international cooperation on the basis of student organizations, such as our SDS "ISKRA," which could develop "Initiatives" as required programs. It would lead to better understanding between our countries and may give an extra impetus and added quality to both our advanced programs as a result of intellectual and technological fusion.

In this connection, I would like to draw your attention to the evidence that prospective space programs are becoming more and more international. One of the main reasons for this is their high price.

The U.S. Space Station program, is underway with the participation of many countries of Western Europe, as well as Canada and Japan. The program of manned flight to Mars is being discussed on many different levels. We can safely say that complex and expensive advanced programs of the future will follow these examples of international cooperation.

Specialists from many countries will take part in the development of these projects, and each of these countries will do their best to make these programs economically moderate and technologically efficient.

It is here that the extensive experience of the USA and USSR in the sphere of space technology must give rise to new improved quality. Students of America, Soviet Union, and other nations are the people who will have to accomplish these projects; therefore, they need a basis of mutual understanding as quickly as possible.

Taking all these reasons into consideration, we would like to make a concrete suggestion for the establishment of an international educational center in space and aerospace research. The main task of this center would be the joint training and raising of the professional skills of young, beginning specialists as well as specialists with higher qualifications.

We would propose to locate its headquarters in both the USA and USSR. We propose to discuss at this conference this concrete proposal in the hope that we can develop a realized program for its organization. We would also like to share your and our ideas. Thank you.